MICROCOPY RESOLUTION TEST CHART

NATIONAL BUREAU OF STANDARDS-1963-A

①

UNITED STATES AIR FORCE

GRADUATE STUDENT SUMMER SUPPORT PROGRAM

1987

PROGRAM TECHNICAL REPORT

UNIVERSAL ENERGY SYSTEMS, INC.

VOLUME I of II

Program Director, UES
Rodney C. Darrah

Program Administrator, UES
Susan K. Espy

Program Manager, AFOSR
Major Richard Kopka

Submitted to

Air Force Office of Scientific Research

Bolling Air Force Base

Washington, DC

December 1987

DTIC
SELECTE
MAR 0 1 1988
H

TABLE OF CONTENTS

AFOSR·TR· 88-0209

88 2 23 173

REPORT DOCUMENTATION PAGE

Form Approved
OMB No. 0704-0188

1a. REPORT SECURITY CLASSIFICATION	1b. RESTRICTIVE MARKINGS
2a. SECURITY CLASSIFICATION AUTHORITY	3. DISTRIBUTION / AVAILABILITY OF REPORT
2b. DECLASSIFICATION / DOWNGRADING SCHEDULE	Approved for public release; distribution unlimited.

4. PERFORMING ORGANIZATION REPORT NUMBER(S)	5. MONITORING ORGANIZATION REPORT NUMBER(S)
	AFOSR-TR- 88-0209

6a. NAME OF PERFORMING ORGANIZATION	6b. OFFICE SYMBOL (If applicable)	7a. NAME OF MONITORING ORGANIZATION
Universal Energy Systems Inc.		AFOSR/XOT

6c. ADDRESS (City, State, and ZIP Code)	7b. ADDRESS (City, State, and ZIP Code)
4401 Dayton-Xenia Road Dayton, OH 45432	Building 410 Bolling AFB DC 20332-6448

8a. NAME OF FUNDING / SPONSORING ORGANIZATION	8b. OFFICE SYMBOL (If applicable)	9. PROCUREMENT INSTRUMENT IDENTIFICATION NUMBER
Same as #7		F49620-85-C-0013

8c. ADDRESS (City, State, and ZIP Code)	10. SOURCE OF FUNDING NUMBERS			
	PROGRAM ELEMENT NO.	PROJECT NO.	TASK NO.	WORK UNIT ACCESSION NO.
Same as #7	61102F	3396	D5	

11. TITLE (Include Security Classification)

USAF Graduate Student Summer Support Program - Volume 1 - 1987

12. PERSONAL AUTHOR(S)
Rodney C. Darrah, Susan K. Espy

13a. TYPE OF REPORT	13b. TIME COVERED	14. DATE OF REPORT (Year, Month, Day)	15. PAGE COUNT
Annual	FROM _____ TO _____	December 1987	

16. SUPPLEMENTARY NOTATION

17. COSATI CODES			18. SUBJECT TERMS (Continue on reverse if necessary and identify by block number)
FIELD	GROUP	SUB-GROUP	

19. ABSTRACT (Continue on reverse if necessary and identify by block number)

See Attached

20. DISTRIBUTION / AVAILABILITY OF ABSTRACT	21. ABSTRACT SECURITY CLASSIFICATION
☒ UNCLASSIFIED/UNLIMITED ☐ SAME AS RPT. ☐ DTIC USERS	UNCLASSIFIED

22a. NAME OF RESPONSIBLE INDIVIDUAL	22b. TELEPHONE (Include Area Code)	22c. OFFICE SYMBOL
LT. COL. CLAUDE CAVENDER	202-767-4970	XOT

DD Form 1473, JUN 86   Previous editions are obsolete.

I.   <u>INTRODUCTION</u>

Universal Energy Systems, Inc. (UES) was awarded the United States Air Force Summer Faculty Research Program on August 15, 1984. The contract is funded under the Air Force Systems Command by the Air Force Office of Scientific Research.

The program has been in existance since 1978 and has been conducted by several different contractors. The success of the program is evident from its history of expansion since 1978.

The Summer Faculty Research Program (SFRP) provides opportunities for research in the physical sciences, engineering, life sciences, business, and administrative sciences. The program has been effective in providing basic research opportunities to the faculty of universities, colleges, and technical institutions throughout the United States.

The program is available to faculty members in all academic grades: instructor, assistant professor, professor, department chairman, and research facility directors. It has proven especially beneficial to young faculty members who are starting their academic research programs and to senior faculty members who have spent time in university administration and are desirous of returning to scholarly research programs.

Beginning with the 1982 program, research opportunities were provided for 17 graduate students. The 1982 pilot student program was highly successful and was expanded in 1983 to 53 students; there were 84 graduate students in the 1984 program.

In the previous programs, the graduate students were selected along with their professors to work on the program. Starting with the 1985 program, the graduate students were selected on their own merits. They were assigned to be supervised by either a professor on the program or by an engineer at the Air Force Laboratories participating in the program. There were 92 graduate students selected for the 1985 program.

Again in the 1986 program, the graduate students were selected on their own merits, and assigned to be supervised by either a professor on the program or by an engineer at the participating Air Force Laboratory. There were 100 graduate students selected for the 1986 program.

Follow-on research opportunities have been developed for a large percentage of the participants in the Summer Faculty Research Program in 1979-1983 period through an AFOSR Minigrant Program.

On 1 September 1983, AFOSR replaced the Minigrant Program with a new Research Initiation Program. The Research Initiation Program provides follow-on research awards to home institutions of SFRP participants. Awards were made to approximately 50 researchers in 1983. The awards were for a maximum of $12,000 and a duration of one year or less. Substantial cost sharing by the schools contributes significantly to the value of the Research Initiation Program. In 1984 there were approximately 80 Research Initiation awards.

1

PREFACE

The ~~United States Air Force~~ *U.S. AF* Graduate Student Summer Support Program (USAF-GSSSP) is conducted under the United States Air Force Summer Faculty Research Program. The program provides funds for selected graduate students to work at an appropriate Air Force Facility with a supervising professor who holds a concurrent Summer Faculty Research Program appointment or with a supervising Air Force Engineer. This is accomplished by the students being selected on a nationally advertised competitive basis for a ten-week assignment during the summer intersession period to perform research at Air Force laboratories/centers. Each assignment is in a subject area and at an Air Force facility mutually agreed upon by the students and the Air Force. In addition to compensation, travel and cost of living allowances are also paid. The USAF-GSSSP is sponsored by the Air Force Office of Scientific Research, Air Force Systems Command, United States Air Force, and is conducted by Universal Energy Systems, Inc.

The specific objectives of the 1987 USAF-GSSSP are:

(1)   To provide a productive means for the graduate students to participate in research at the Air Force Weapons Laboratory;

(2)   To stimulate continuing professional association among the Scholars and their professional peers in the Air Force;

(3)   To further the research objectives of the United States Air Force; *and*

(4)   To enhance the research productivity and capabilities of the graduate students especially as these relate to Air Force technical interests.

During the summer of 1987, 101 graduate students participated. These researchers were assigned to 25 USAF laboratories/centers across the country. This two volume document is a compilation of the final reports written by the assigned students members about their summer research efforts.

1

LIST OF 1987 GRADUATE STUDENT PARTICIPANTS

NAME/ADDRESS	DEGREE, SPECIALTY, LABORATORY ASSIGNED	
Antoinne C. Able Meharry Medical College School of Medicine Nashville TN 37208 (615) 361-5303	Degree: Specialty: Assigned:	M.S., Biology, 1982 Biology SAM
Mark T. Anater Dept. of Polymer Science University of Akron Akron, OH 44311 (216) 434-1844	Degree: Specialty: Assigned:	B.S., Chemistry, 1986 Chemistry ML
Petar Arsenovic Dept. of Materials Science John Hopkins University Baltimore, MD 21218 (301) 338-8970	Degree: Specialty: Assigned:	M.S., Mechanical & Aerospace Sciences, 1985 Chemistry ML
Catherine Aubertin Dept. of Educational Psychology Southern Illinois University Carbondale, IL 62901 (618) 536-7763	Degree: Specialty: Assigned:	M.S., Environmental Design 1982 Environmental Design HRL/MO
David R. Bosch Dept. of Mechanical/Aero. Eng. Arizona State University Tempe, AZ 85287 (602) 965-3291	Degree: Specialty: Assigned:	B.S., Mechanical Engineering 1987 Mechanical Engineering APL
Steven W. Bucey Dept. of Physics Kent State University Kent, OH 44240 (216) 673-1255	Degree: Specialty: Assigned:	M.S., Physics, 1986 Mechanical Engineering ML
John N. Bullock Dept. of Electrical Engineering Univ. of Missouri-Rolla Rolla, MO 65401 (314) 341-3123	Degree: Specialty: Assigned:	B.S., Electrical Eng., 1987 Electrical Engineering APL

Robyn A. Butcher
Wright State University
Dept. of Biology
Dayton, OH 45435
(513) 886-1784

Degree: B.S., Biology, 1987
Specialty: Biology
Assigned: AAMRL

Kevin P. Cahill
Dept. of Electrical/Comp. Eng.
University of Cincinnati
Cincinnati, OH 45221
(513) 475-4461

Degree: B.S., Physics, 1987
Specialty: Physics
Assigned: AL

David C. Carpenter
Dept. of Nuclear Engineering
Texas A&M University
College Station, TX 77843
(409) 845-4161

Degree: M.S., Nuclear Eng., 1986
Specialty: Nuclear Engineering
Assigned: WL

Andrew D. Carson
Dept. of Educational Psychology
University of Texas-Austin
Austin, TX 78712-1296
(512) 471-4155

Degree: M.S., Human Development 1986
Specialty: Nuclear Engineering
Assigned: HRL/MO

Kyunam Choi
Dept. of Physics and Astronomy
University of New Mexico
Albuquerque, NM 87131
(505) 277-6317

Degree: M.S., Physics, 1984
Specialty: Physics
Assigned: WL

Otis Cosby Jr.
Meharry Medical College
School of Medicine
Nashville, TN 37208
(615) 321-6413

Degree: B.S., Natural Science, 1983
Specialty: Natural Science
Assigned: SAM

Richard B. Davidson
Dept. of Mathematics
University of Alabama
Birmingham, AL 35205
(215) 934-3720

Degree: B.S., Math & Computer Sci.
           1987
Specialty: Mathematics
Assigned: ML

Tamara Della-Rodolfa
Dept. of Psychology
Indiana Univ. of Pennsylvania
Indiana, PA   15705
(412) 357-2426

Degree: B.S., Psychology, 1986
Specialty: Psychology
Assigned: AAMRL

Steve Dixon   Degree: B.S., Chemistry, 1986
Dept. of Chemistry   Specialty: Chemistry
Wright State University   Assigned: AAMRL
Dayton, OH 45435
(513) 873-2855

James Drakes   Degree: B.S., Physics, 1987
Dept. of Physics   Specialty: Physics
Tennessee Space Institute   Assigned: AEDC
Tullanoma, TN 37388
(615) 455-0631

Susan M. Dumbacher   Degree: B.S., Aerospace Engr., 1986
Dept. of Aerospace Eng.   Specialty: Aerospace Engineering
University of Cincinnati   Assigned: FDL
Cincinnati, OH 45219
(513) 621-0095

Donna N. Edwards   Degree: M.S., Chemistry, 1982
School of Pharmacy   Specialty: Chemistry
Florida A&M University   Assigned: OEHL
Tallahassee, FL 32307
(904) 599-3302

Kathy S. Enlow   .   Degree: B.S., Community Health Care
Dept. of Healty, Physical Ed.   1985
University of Alabama   Specialty: Health Care
Tuscaloosa, AL 35487-1967   Assigned: SAM
(205) 348-6075

Thomas Enneking   Degree: M.S., Civil Eng., 1978
Dept. of Civil Engineering   Specialty: Civil Engineering
University of Notre Dame   Assigned: FDL
Notre Dame, IN 46556
(219) 283-1497

Gloria Fisher   Degree: M.S., Industrial/Org. Psych.
Dept. of Psychology   1987
University of Mississippi   Specialty: Industrial Psychology
University, MS 38677   Assigned: OEOMI
(601) 232-5077

Inge Ford-Belgrave   Degree: B.S., Biology, 1984
Texas Southern University   Specialty: Environmental Pollutants
University, MS 38677   Assigned: OEHL
(601) 232-5077

Beverley Gable
Dept. of Psychology
Ohio University
Lancaster, OH 43130
(614) 654-0602

Degree: M.S., Psychology, 1987
Specialty: Psychology
Assigned: AAMRL

Deborah Gagnon
Dept. of Psychology
State University of New York
Amherst, NY 14260
(716) 689-7553

Degree: B.S., Psychology, 1987
Specialty: Psychology
Assigned: AAMRL

Edward Gellenbeck
Dept. of Computer Science
Oregon State University
Corvallis, OR 97330
(503) 752-1977

Degree: M.S., Computer Science, 1985
Specialty: Computer Science
Assigned: SAM

James A. Gerald
Dept. of Electrical Eng.
University of Mississippi
University, MS 38677
(601) 232-3752

Degree: B.S., Electrical Engr., 1987
Specialty: Electrical Engineering
Assigned: WL

Maurice Gilbert
Dept. of Medicine
Meharry Medical College
Nashville, TN 37208
(615) 327-6111

Degree: M.S., Biomedical Sci., 1983
Specialty: Biomedical Sciences
Assigned: SAM

Jeffrey Girard
Dept. of Mechanical Eng.
Washington State University
Pullamn WA 99164
(509) 335-8654

Degree: M.S., Mechanical Engr., 1982
Specialty: Mechanical Engineering
Assigned: ESC

Beverly Girten
Dept. of Exercise Physiology
Ohio State University
Columbus, OH 43210
(614) 292-1223

Degree: M.S., Exercise Physiology
1983
Specialty: Exercise Physiology
Assigned: AAMRL

Laura Giusti
Dept. of Psychology
San Diego State University
San Diego, CA 92182
(412) 833-3912

Degree: B.S., Psychology, 1986
Specialty: Psychology
Assigned: AAMRL

Nadia Greenridge   Degree: M.S., Anthropology, 1984
Dept. of Anthropology   Specialty: Anthropology
New York University   Assigned: AAMRL
New York City, NY 07631
(212) 598-3258

Thomas Harkins   Degree: B.S., Mech. Engr., 1986
Dept. of Mechanical Eng.   Specialty: Mechanical Engineering
Louisiana State University   Assigned: AD
Baton Rouge, LA 70808
(505) 766-3671

Deborah Hollenbach   Degree: B.S., Biology, 1986
Dept. of Biology   Specialty: Biology
University of Dayton   Assigned: AAMRL
Dayton, OH 45432
(513) 259-2135

Adrienne Hollis   Degree: B.S., Biology, 1986
Dept. of Biomedical Sciences   Specialty: Biology
Meharry Medical College   Assigned: SAM
Nashville, TN 37208
(615) 327-6221

Stephen Huyer   Degree: B.S., Aerospace Engr., 1986
Dept. of Aerospace Engineering Specialty: Aerospace Engineering
University of Colorado   Assigned: FJSRL
Boulder, CO 80309
(303) 444-63-68

David James   Degree: B.S., Computer Sci., 1985
Dept. of Math   Specialty: Computer Science
Eastern Illinois University   Assigned: AEDC
Charleston, IL 61920
(217) 581-2028

George James, III   Degree: M.S., Aerospace Engr., 1986
Dept. of Aerospace Eng.   Specialty: Aerospace Engineering
Texas A&M University   Assigned: RPL
College Station, TX 77843-3141
(409) 845-3947

Stephen R. Jenei   Degree: B.S., Biology, 1986
Dept. of Biology   Specialty: Biology
University of Dayton   Assigned: AAMRL
Dayton, OH 45469-0001
(513) 229-2135

Kenneth Jenks
Dept. of Aero/Astronautical Eng.
University of Illinois
Urbana, IL 61801
(217) 244-0743

Degree: B.S., Computer Sci., 1985
Specialty: Computer Science
Assigned: WL

Michele Johnson
School of Electrical Engr.
Cornell University
Ithaca, NY 14853
(607) 255-4304

Degree: B.S., Electr. Eng., 1984
Specialty: Electrical Engineering
Assigned: RADC

Scharine Kirshoff
Dept. of Geology
University of Alaska
Fairbanks, AL 99503
(907) 474-7274

Degree: M.S., Geology, 1986
Specialty: Geology
Assigned: AFGL

Gary Lake
Dept. of Industrial Eng.
University of Houston
Houston, TX 77035
(713) 749-2538

Degree: M.S., Industrial Engr., 1985
Specialty: Industrial Engineering
Assigned: OEHL

David Landis
Dept. of Civil Engineering
Auburn University
Auburn, AL 36849
(205) 826-4320

Degree: B.S., Civil Eng., 1986
Specialty: Civil Engineering
Assigned: ESC

Sharon Landis
Dept. of Computer Sci./Eng.
Auburn University
Auburn, AL 36849
(205) 826-4330

Degree: B.S., Computer Engr., 1986
Specialty: Computer Engineering
Assigned: ESC

Craig Langenfeld
Dept. of Mechanical Eng.
Ohio State University
Columbus, OH 43210
(614) 268-2176

Degree: B.S., Mechanical Engr., 1986
Specialty: Mechanical Engineering
Assigned: APL

Christopher Leger
Dept. of Mechanical Eng.
Louisiana State University
Baton Rouge, LA 70893
(504) 334-2453

Degree: B.S., Mechanical Engr., 1986
Specialty: Mechanical Engineering
Assigned: AD

Bruce Liby
Dept. of Physics/Astronomy
University of New Mexico
Albuquerque, NM 87107
(505) 277-2616

Degree: M.S., Physics, 1984
Specialty: Physics
Assigned: WL

A. Jeannine Lincoln
Dept. of Biomedical Sciences
Wright State University
Dayton, OH 45435
(513) 873-2504

Degree: B.S., Biochemistry, 1987
Specialty: Biochemistry
Assigned: AAMRL

Yolanda Malone
School of Medicine
Meharry Medical College
Nashville, TN 37208
(615) 321-0939

Degree: B.S., Chemistry, 1985
Specialty: Chemistry
Assigned: SAM

Randal Mandock
Dept. of Mechanical Eng.
Georgia Institute of Tech.
Atlanta, GA 30332
(404) 894-3776

Degree: M.S., Atmospheric Sci., 1986
Specialty: Atmospheric Sciences
Assigned: OEHL

James W. Mattern
Dept. of Physics/Electr. Eng.
Oregon Graduate Center
Beaverton, OR 97005
(503) 690-1130

Degree: B.S., Computer Engr., 1986
Specialty: Computer Engineering
Assigned: AD

Matthew McBeth
Dept. of Elect./Biomedical Eng.
Vanderbilt University
Nashville, TN 37235
(615) 322-2767

Degree: B.S., Computer Sci., 1986
Specialty: Computer Science
Assigned: AEDC

Jennifer B. McGovern
Dept. of Psychology
University of Florida
Gainesville, FL 32611
(904) 392-0605

Degree: M.S., Psychology, 1987
Specialty: Psychology
Assigned: SAM

Roland Medellin
Dept. of Biology
Brown University
Providence, RI 02912
(401) 273-7646

Degree: B.S., Biology, 1987
Specialty: Biology
Assigned: OEHL

Otto M. Melko
Dept. of Mathematics
University of California
Santa Cruz, CA 95064
(408) 429-2085

Degree: M.S., Math, 1982
Specialty: Mathematics
Assigned: AD

Ethan S. Merrill
Dept. of Engineering
University of Mississippi
Greenville, MS 38701
(904) 283-2942

Degree: B.S., Civil Engr.
Specialty: Civil Engineering
Assigned: ESC

Veronica Minsky
Dept. of Computer Science
Middle Tennessee State Univ.
Murfreesboro, TN 37217
(615) 898-2669

Degree: B.S., Linquistics, 1978
Specialty: Linquistics
Assigned: AEDC

Frank W. Moore
Dept. of Computer Sci./Eng.
Wright State University
Dayton, OH 45435
(513) 873-3515

Degree: B.S., Computer Engr., 1986
Specialty: Computer Engineering
Assigned: AL

Stephen Morgan
Dept. of Psychology
Montclair State College
Upper Montclair, NJ 07043
(201) 893-4000

Degree: B.S., Psychology, 1984
Specialty: Psychology
Assigned: HRL/LR

Lisa Morris
Biology Department
University of Dayton
Physiology Laboratory
300 College Park Avenue
Dayton, OH 45469-0001
(513) 229-2135

Degree: B.S., Biology, 1985
Specialty: Physiology
Assigned: AAMRL

Conrad Murray
School of Medicine
Meharry Medical College
Nashville, TN 37208
(615) 321-5837

Degree: M.S., Biochemistry, 1986
Specialty: Biochemsitry
Assigned: SAM

Steven Naber
Dept. of Statistics
Ohio State University
Columbus, OH 43201
(614) 421-6647

Degree: M.S., Statistics, 1984
Specialty: Statistics
Assigned: OEHL

Jerome Nadel
Dept. of Psychology
University of Kansas
Manhattan, KS 66506
(913) 532-6850

Degree: B.S., Psychology, 1980
Specialty: Psychology
Assigned: HRL/OT

Victoria Nasman
Dept. of Psychology
Northwestern University
Evanston, IL 60201
(312) 491-7643

Degree: M.S., Psychology, 1984
Specialty: Psychology
Assigned: SAM

Mark Neumeier
Dept. of Mechanical Systems
Wright State University
Dayton, OH 45435
(513) 873-2476

Degree: M.S., Psychology, 1984
Specialty: Psychology
Assigned: SAM

Khan Nguyen
Dept. of Mechanical Eng.
University of Chicago-Illinois
Chicago, IL 60607
(312) 849-1362

Degree: M.S., Mathematics, 1984
Specialty: Mathematics
Assigned: APL

Wendy Nguyen
Dept. of Biology
Trinity University
715 Stadium Drive
San Antonio, TX 78284
(512) 736-7231

Degree: B.A., Biology, 1987
Specialty: Biology
Assigned: SAM

Bernadette Njoku
Dept. of Chemistry
Meharry Medical College
Nashville, TN 37208
(615) 327-4098

Degree: B.S., Chemistry, 1982
Specialty: Chemistry
Assigned: SAM

Charles Norfleet
Dept. of Civil Eng./Mechanics
Southern Illinois University
Carbondale, IL 62901
(618) 536-2368

Degree: B.S., Engineering Mechanics,
1986
Specialty: Engineering Mechanics
Assigned: ML

Douglas Phillpott
Dept. of Management
Auburn University
Auburn, AL 36830
(205) 887-3889

Degree: B.S., Chemical Engr., 1984
Specialty: Chemical Engineering
Assigned: LMC

Susan Poppens
Dept. of Computer Science
University of Missouri
Rolla, MO 65401
(314) 341-4491

Degree: B.S., Math/Comp. Sci., 1985
Specialty: Math/Computer Science
Assigned: ESMC

Mark Prazak
Dept. of Chemistry
Wright State University
Dayton, OH 45371
(513) 873-2855

Degree: B.S., Chemistry, 1986
Specialty: Chemistry
Assigned: ML

Mark Reavis
Aerospace Dept.
University of Colorado
College of Engineering
Campus Box 429
Boulder, CO 80309

Degree: B.S., Aerospace, 1987
Specialty: Aerospace
Assigned: FJSRL

Peter Riddiford
Dept. of Electrical Eng.
Ohio State University
Columbus, OH 43210
(614) 292-1752

Degree: B.S., Electrical Eng., 1987
Specialty: Electrical Engineering
Assigned: FDL

Keith Riese
Dept. of Electrical Eng.
University of Nebraska
Lincoln, NE 68588-0511
(402) 472-3771

Degree: M.S., Electrical Eng., 1972
Specialty: Electrical Engineering
Assigned: SAM

Mary Robinson
Dept. of Health
University of Alabama
Scottsboro, AL 35768
(205) 259-5342

Degree: B.S., Sociology, 1976
Specialty: Sociology/Psychology
Assigned: SAM

Filiberto Santiago
Dept. of Mechanical Eng.
University of Puerto Rico
Mayaguez, PR 00708
(809) 834-4040

Degree: M.S., Mechanical Eng., 1987
Specialty: Mechanical Engineering
Assigned: AEDC

Gregory Schoeppner
Dept. of Civil Engineering
Ohio State University
Columbus, OH 43210
(614) 436-3392

Degree: M.S., Civil Engr., 1984
Specialty: Civil Engineering
Assigned: FDL

James Seaba
Dept. of Mechanical Eng.
University of Iowa
Iowa City, IA 52242
(319) 335-5681

Degree: M.S., Mechanical Engr., 1986
Specialty: Mechanical Engineering
Assigned: APL

Jon Shupe
Dept. of Mechanical Eng.
University of Houston
Houston, TX 77004
(713) 749-7497

Degree: M.S., Mechanical Engr., 1985
Specialty: Mechanical Engineering
Assigned: ML

Christopher Sierra
Dept. of Mechanical Eng.
University of Iowa
Iowa City, IA 52241
(319) 337-6205

Degree: B.S., Mechanical Engr., 1986
Specialty: Mechanical Engineering
Assigned: FDL

Gregory Sloan
Dept. of Physics/Astronomy
University of Wyoming
Laramie, WY 82071
(307) 766-6150

Degree: B.S., Physics/Astronomy 1985
Specialty: Physics/Astronomy
Assigned: AFGL

Elisabeth Smela
Dept. of Electrical Eng.
University of Pennsylvania
Philadelphia, PA 19104
(215) 898-8548

Degree: B.S., Physics, 1985
Specialty: Physics
Assigned: ML

Rita Smith
Dept. of Mechanical Eng.
University of New Mexico
Albuquerque, NM 87111
(505) 275-2061

Degree: B.S., Mechanical Engr., 1979
Specialty: Mechanical Engineering
Assigned: WL

Brian Spielbusch
Dept. of Electrical Eng.
University of Missouri
Independence, MO 64050
(816) 476-1250

Degree: B.S., Electrical Engr., 1985
Specialty: Electrical Engineering
Assigned: WL

Louise Stark
Dept. of Computer Engineering
University of South Florida
Tampa, FL 33612
(813) 971-9625

Degree: B.S., Computer Engr., 1986
Specialty: Computer Engineering
Assigned: RADC

Steven Steinsaltz
Dept. of Math
John Hopkins University
Baltimore, MD 21218
(301) 338-8000

Degree: M.S., Mathematics, 1985
Specialty: Mathematics
Assigned: RADC

John Stewman
Dept. of Computer Sci./Eng.
University of South Florida
St. Petersburg, FL 33702
(813) 577-9029

Degree: B.S., Computer Engr., 1986
Specialty: History
Assigned: RADC

Tod Strohmayer
Dept. of Physics/Astronomy
University of Rochester
Rochester, NY 14608
(716) 325-3019

Degree: M.S., Physics, 1987
Specialty: Physics/Astronomy
Assigned: AFGL

Teresa Taylor
Dept. of Civil & Environ. Eng.
University of Washington
Pullman, WA 99164-2902
(509) 335-8546

Degree: M.S., Geological Engr., 1984
Specialty: Geological Engineering
Assigned: ESC

Tien Tran
Dept. of Electr. & Comp. Eng.
University of Cincinnati
Cincinnati, OH 45221
(513) 851-7350

Degree: B.S., Electrical Engr., 1980
Specialty: Electrical Engineering
Assigned: RADC

John Usher
Dept. of Industrial Eng.
Louisiana State University
Baton Rouge, LA 70816
(504) 388-5112

Degree: M.S., Industrial Engr., 1986
Specialty: Chemical Engineering
Assigned: ML

Pretta VanDible
Dept. of Chemical Engineering
Prairie View A&M University
Houston, TX 77446
(713) 857-2827

Degree: M.S., Chemical Engr., 1986
Specialty: Chemical Engineering
Assigned: RPL

William VanValkenburgh
Dept. of Computer Science
Western Michigan University
Kalamazoo, MI 49008
(616) 385-5961

Degree: B.S., Computer Science, 1986
Specialty: Computer Science
Assigned: AL

Joseph Varga
Dept. of Physics
Kent State University
Kent, OH 44242
(216) 672-2246

Degree: M.S., Physics, 1978
Specialty: Physics
Assigned: ML

Deborah Vezie
Dept. of Chemical, Biomedical
 Materials Engineering
University of Arizona
Tempe, AZ 85281
(602) 784-8221

Degree: B.S., Biomedical Engr., 1987
Specialty: Biomedical Engineering
Assigned: ML

James Wade
Dept. of Astronautical Eng.
University of Illinois
Urbana, IL 61801
(217) 244-0743

Degree: B.S., Physics, 1986
Specialty: Astronautical Engineering
Assigned: WL

Randall Westhoff
Dept. of Mathematics
Eastern Washington University
Cheney, WA 99004
(509) 359-6225

Degree: B.S., Mathematics, 1986
Specialty: Mathematics
Assigned: AD

Terri Wilkerson
School of Medicine
Wright State University
Dayton, OH 45324
(513) 873-2934

Degree: B.S., Electrical Eng., 1985
Specialty: Electrical Engineering
Assigned: AAMRL

Douglas Wise
Dept. of Mechanical Eng.
University of Dayton
Oakwood, OH 45419
(513) 298-9073

Degree: B.S., Mechanical Engr., 1986
Specialty: Mechanical Engineering
Assigned: ML

PARTICIPANT LABORATORY ASSIGNMENT

1987 USAF/UES GRADUATE STUDENT SUMMER SUPPORT PROGRAM

AERO PROPULSION LABORATORY (AFWAL/APL)
(Wright-Patterson Air Force Base)

1.	David R. Bosch	4.	Khan V. Nguyen
2.	John N. Bullock	5.	James P. Seaba
3.	Craig A. Langenfeld		

ARMAMENT LABORATORY (AD)
(Eglin Air Force Base)

1.	Thomas K. Harkins	3.	Otto M. Melko
2.	Christopher Leger	4.	Randall F. Westhoff

ARMSTRONG AEROSPACE MEDICAL RESEARCH LABORATORY (AAMRL)
(Wright-Patterson Air Force Base)

1.	Robyn A. Butcher	8.	Nadia C. Greenidge
2.	Tamara Della-Rodolfa	9.	Deborah E. Hollenbach
3.	Steve L. Dixon	10.	Stephen R. Jenei
4.	Beverley A. Gable	11.	A. Jeannine Lincoln
5.	Deborah Gagnon	12.	Lisa M. Morris
6.	Beverly E. Girten	13.	Terri L. Wilkerson
7.	Laura M. Giusti		

ARNOLD ENGINEERING DEVELOPMENT CENTER (AEDC)
(Arnold Air Force Station)

1.	James A. Drakes	4.	Veronica L. Minsky
2.	David L. James	5.	Filiberto Santiago
3.	Matthew B. McBeth		

AVIONICS LABORATORY (AFWAL/AL)
(Wright-Patterson Air Force Base)

1.	Kevin Cahill	3.	Frank W. Moore
2.	James W. Mattern	4.	William B. VanValkenburgh

DEFENSE EQUAL OPPORTUNITY MANAGEMENT INSTITUTE (DEOMI)
(Patrick Air Force Base)

1.   Gloria Z. Fisher

EASTERN SPACE AND MISSILE CENTER (ESMC)
(Patrick Air Force Base)

1.   Susan A. Poppens

ENGINEERING SERVICE CENTER (ESC)
(Tyndall Air Force Base)

1.	Jeffrey Girard	4.	Ethan S. Merrill
2.	David W. Landis	5.	Teresa A. Taylor
3.	Sharon K. Landis		

C. PARTICIPANT LABORATORY ASSIGNMENT (Page 2)

FLIGHT DYNAMICS LABORATORY (AFWAL/FDL)
(Wright-Patterson Air Force Base)
1. Susan M. Dumbacher
2. Thomas J. Enneking
3. Mark E. Neumeier
4. Bryan P. Riddiford
5. Gregory A. Schoeppner
6. Christopher Sierra

FRANK J. SEILER RESEARCH LABORATORY (FJSRL)
(USAF Academy)
1. Stephen A. Huyer
2. Mark A. Reavis

GEOPHYSICS LABORATORY (AFGL)
(Hanscom Air Force Base)
1. Scharine Kirchoff
2. Gregory C. Sloan
3. Tod E. Strohmayer

HUMAN RESOURCES LABORATORY/LR (HRL/LR)
(Wright-Patterson Air Force Base)
1. Stephen Morgan

HUMAN RESOURCES LABORATORY/MO (HRL/MO)
(Brooks Air Force Base)
1. Catherine A. Aubertin
2. Andrew D. Carson

HUMAN RESOURCES LABORATORY/OT (HRL/OT)
(Williams Air Force Base)
1. Jerome I. Nadel

LOGISTICS MANAGEMENT CENTER (LMC)
(Gunter Air Force Station)
1. Douglas E. Phillpott

MATERIALS LABORATORY (AFWAL/ML)
(Wright-Patterson Air Force Base)
1. Mark T. Anater
2. Petar Arsenovic
3. Steven W. Bucey
4. Richard B. Davidson
5. Charles W. Norfleet
6. Mark Prazak
7. Jon A. Shupe
8. Elisabeth Smela
9. John M. Usher
10. Joseph C. Varga
11. Deborah L. Vezie
12. Douglas L. Wise

OCCUPATIONAL AND ENVIRONMENT HEALTH LABORATORY (OEHL)
(Brooks Air Force Base)
1. Donna N. Edwards
2. Inge B. Ford-Belgrave
3. Gary F. Lake
4. Randal L. Mandock
5. Roland A. Medellin
6. Steven J. Naber

ROCKET PROPULSION LABORATORY (RPL)
     (Edwards Air Force Base)
     1.   George H. James, III
     2.   Pretta L. VanDible

ROME AIR DEVELOPMENT CENTER (RADC)
     (Griffiss Air Force Base)

1.	Michele E. Johnson	4.	John H. Stewman
2.	Louise Stark	5.	Tien N. Tran
3.	Steven J. Steinsaltz		

SCHOOL OF AEROSPACE MEDICINE (SAM)
     (Brooks Air Force Base)

1.	Antoinne C. Able	8.	Jennifer B. McGovern
2.	Otis Cosby, Jr.	9.	Conrad R. Murray
3.	Kathy S. Enlow	10.	Victoria T. Nasman
4.	Edward M. Gellenbeck	11.	Wendy T. Nguyen
5.	Maurice B. Gilbert	12.	Bernadette Patricia Njoku
6.	Adrieine L. Hollis	13.	Keith A. Riese
7.	Yolanda A. Malone	14.	Mary C. Robinson

WEAPONS LABORATORY (WL)
     (Kirtland Air Force Base)

1.	David C. Carpenter	5.	Bruce Liby
2.	Kyunam Choi	6.	Rita Smith
3.	James A. Gerald	7.	Brian K. Spielbusch
4.	Kenneth C. Jenks	8.	James W. Wade

RESEARCH REPORTS

RESEARCH REPORTS

1987 GRADUATE STUDENT SUMMER SUPPORT PROGRAM

Technical Report Number	Title	Graduate Researcher
Volume I		
1	Effect of Repeated Low Dose Soman On Acetylcholinesterase Activity *** Same Report as Prof. Maleque ***	Antoinne C. Able
2	Synthesis of an Aromatic Heterocyclic Terphenyl Monomer	Mark T. Anatar
3	Characterization of Graphite Fibers by X-ray Diffraction	Petar Arsenovic
4	An Eight-Domain Framework for Understanding Intelligence and Predicting Intelligent Performance ***Same Report as Prof. Dillon***	Catherine A. Aubertin
5	Configuration Factors for Spacecraft/ Expansible Radiator Interaction	David R. Bosch
6	Computer Evaluation of Ion-Implanted Dopant Profile Evolution During Annealing	Steven W. Bucey
7	The Interface Contribution to GaAs/Ge Heterojunction Solar Cell Efficiency ***Same Report as Prof. Wu***	John N. Bullock
8	Isolation of Osteogenic Cells From The Trauma-Activated Periosteum	Robyn A. Butcher
9	A Test Chip for Evaluation of MBE Epitaxial Layers for Novel Device Applications ***Same Report as Prof. Roenker***	Kevin Cahill
10	Preliminary Thermal Analysis of a Bimodal Nuclear Rocket Core	David C. Carpenter
11	Air Force Officer Selection Revisited: Entertaining The Possibilities for Improvement ***Same Report as Dr. Appel***	Andrew D. Carson

1987 USAF-UES SUMMER FACULTY RESEARCH PROGRAM

GRADUATE STUDENT SUMMER SUPPORT PROGRAM

Sponsored by the

AIR FORCE OFFICE OF SCIENTIFIC RESEARCH

Conducted by the

Universal Energy Systems, Inc.

FINAL REPORT

Effect of Repeated Low Dose Soman On Acetylcholinesterase Activity

Prepared by: Mohammed A. Maleque, Ph.D.
                          with Antionne Able and Otis Cosby, Jr.

Academic Rank: Associate Professor

Department: Pharmacology

University: Meharry Medical College
                        Nashville, Tennessee

Participants: Antoinne C. Able
                        Otis Cosby

Research Location: USAFSAM/RZB
                        Brooks AFB
                        San Antonio, TX 78235

USAF Researcher: Lt. Col. Stan L. Hartgraves

Date: 28 August 87

Contract No: F49620-85-C-0013

REFERENCE DR. MALEQUE

SFRP FINAL REPORT NUMBER 87

1987 USAF-UES SUMMER FACULTY RESEARCH PROGRAM

GRADUATE STUDENT SUMMER SUPPORT PROGRAM

Sponsored by the

AIR FORCE OFFICE OF SCIENTIFIC RESEARCH

Conducted by the

Universal Energy Systems, Inc.

FINAL REPORT

Prepared by: Mark T. Anater

Academic Rank: Bachelor of Science, Chemistry

Department and   Polymer Science

  University: University of Akron

Research Location: AFWAL/MLBP   WPAFB   Dayton, OH   45433

USAF Researcher: Dr. Fred Arnold

Date: 28 Sept 1987

Contract No: F49620-85-C-0013

FINAL REPORT SUBMITTED BY

MARK ANATER

NOT PUBLISHABLE AT THIS TIME

1986 USAF-UES SUMMER FACULTY RESEARCH PROGRAM

GRADUATE STUDENT SUMMER SUPPORT PROGRAM

Sponsored by the

AIR FORCE OFFICE OF SCIENTIFIC RESEARCH

Conducted by the

Universal Energy Systems, Inc.

<u>FINAL REPORT</u>

Prepared by: Petar Arsenovic

Academic Rank: Graduate Student

Department and   Materials Science

  University: Johns Hopkins University

Research Location: AFWAL/MLBP
                      Wright Patterson AFB
                      Dayton, Ohio 45433

USAF Researcher: Dr. W. W. Adams

Date: 24 July 1987

Contract No: F49620-85-C-0013

Characterization of Graphite Fibers by

X-ray Diffraction

by

Petar Arsenovic

ABSTRACT

Samples of different types of graphite fibers were
prepared for measurement in a Picker diffractometer. Young's
modulus and crystallite orientation measurements were made, as
well as equatorial and meridional scans on the fibers. The
results show that the higher modulus fibers have improved
crystallite orientation, and that applying tensile stress will
increase the orientation by a small amount. The diffraction
peaks become less sharp for fibers with a lower modulus.
This work was an important step toward the formulating of a
model that will explain the mechanical behavior of graphite
fibers in terms of their internal structure.

Acknowledgements

I. INTRODUCTION:

Carbon fibers have been known for many years, first being used as filaments for incandescent lamps in the late 19th century. Not until the early 1950s was the first major effort undertaken to develop high strength carbon fibers. These fibers are now important in many advanced technical applications, especially in aerospace composites for which the high specific modulus is valuable.

A thorough understanding of the properties of the fibers, as well as their internal structure, are vital in the design of composites in which these fibers are used. These considerations are important for structures ranging in size from space stations and aircraft to circuit boards.

Research has been conducted at the Johns Hopkins University on a series of pitch based graphite fibers. The Young's modulus was determined as a function of applied static tensile stress over a wide range of temperatures for different types of graphite fibers. Laser generated ultrasound was used to make these measurements. Fig. 1

SOUND VELOCITY MEASUREMENT SYSTEM

Fig. 1

Fig. 3

PITCH FIBERS

YOUNG'S MODULUS (GPa)

P120
P100
P 75
P 55
P 25

T (°C)

Fig. 2

T = ROOM TEMP.

P120
P100
P 75
P 55
P25

YOUNG'S MODULUS (GPa)

STRESS. (MPa)

3-5
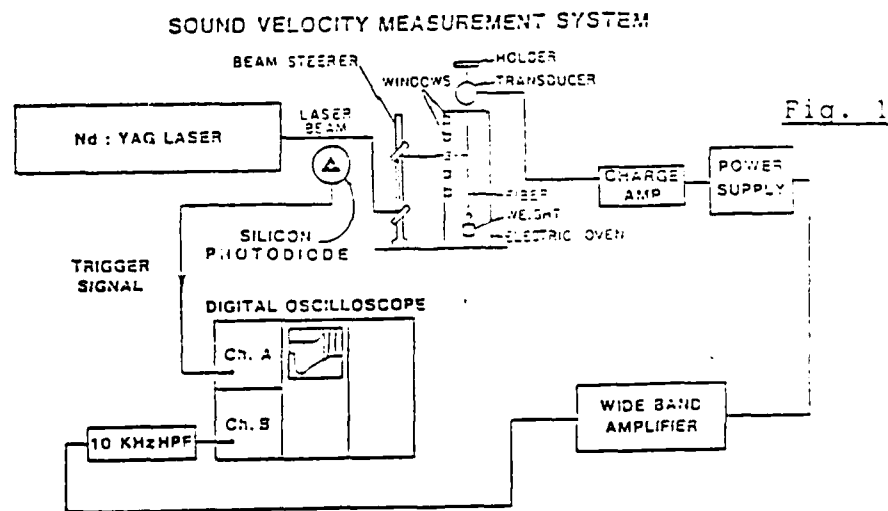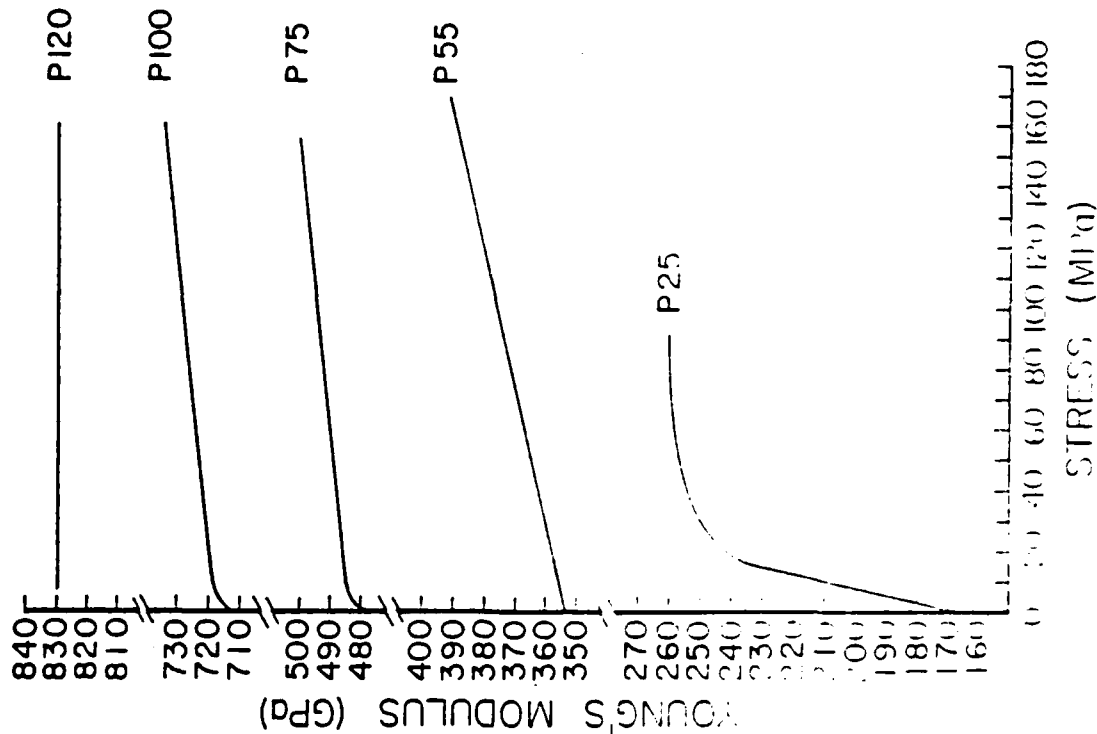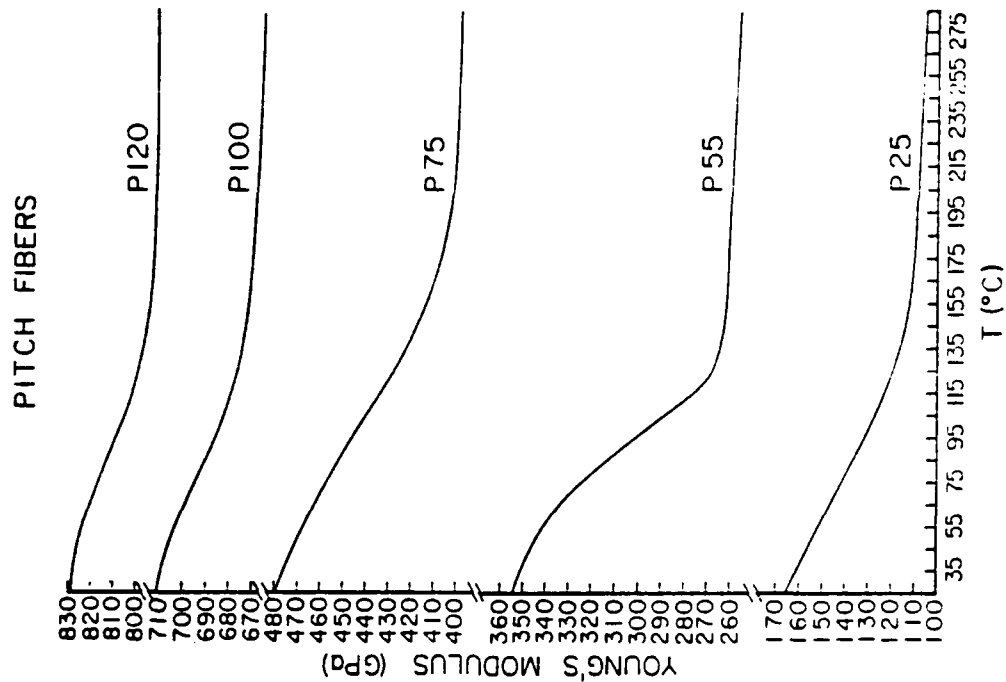
shows the experimental setup used.

Fig. 2 shows the modulus of five types of carbon fibers: P25, P55, P75, P100, and P120 as a function of applied tensile stress. The modulus increases with stress to different degrees in all cases, P25 showing the largest change, while P120 demonstrates almost no change at all. Fig. 3 shows modulus as a function of temperature. In all cases the modulus decreases with increasing temperature.

A major concern is to try to explain some of these effects in terms of the internal structure of the graphite fibers. The work conducted this summer at the Wright Patterson Air Force Base Materials Laboratory was the first step to proposing a model to explain the behavior of graphite fibers under various experimental conditions.

II. OBJECTIVES:

The structure of crystalline graphite is as shown in Fig. 4, with carbon atoms arranged in a hexagonal array.
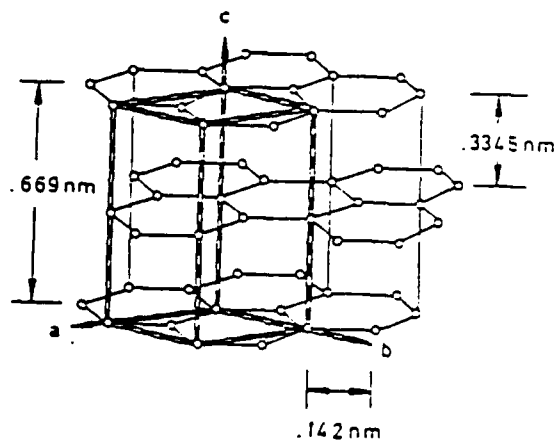
Fig. 4

microscope. The number of fibers can then be calculated by
the equation:

$$\text{number of fibers} = \frac{m}{P}\left[\frac{4}{\pi d^2 \ell}\right]$$

In this equation, m is the mass of the bundle, d is the dia-
meter of an individual fiber (always on the order of 10
microns), and P is the density of the fiber.

The samples are mounted in metal end pieces, and held
in the mounts by epoxy. The end pieces are inserted into a
fiber deformation device sample holder, which is mounted on
the chi circle of a Picker diffractometer. Various types of
x-ray scans can then be accomplished.

IV. ORIENTATION MEASUREMENTS:

Crystallite orientation in the graphite fiber samples
is expressed in terms of Herman's orientation factor. This
is calculated by measuring the intensity of the (002) equ-
atorial reflection as a function of the diffractometer angle
chi. The orientation factor is calculated by:

$$f = \frac{\sum I(3\sin^2 \chi - 1)\cos \chi \, \Delta \chi}{2\sum I \cos \chi \, \Delta \chi}$$

In this equation, I is the intensity, X is the diffractometer
angle, and ΔX is the step size. An orientation factor of
-0.5 would mean perfect orientation.

The conditions of the orientation experiments were as
follows: X-ray tube voltage 35 kV; tube current 40 mA;
(Except for P100: Volts = 40 mV; current = 60 mA); Cu Kα
radiation (1.54 angstroms); Nickel filter used; 1.5 mm

3-8

The graphite fibers being studied here consist of interlinked crystallites with the type of structure shown of the previous page. There are also regions of disorder, particularly at the crystallite boundaries; other imperfections such as voids, amorphous areas, and dislocations are present as well.

As noted earlier, the modulus of the fibers increases with applied tensile stress. Part of this effect is thought to be caused by improvement of the crystallite orientation with respect to the fiber axis. The study of this effect was one goal of the effort of this summer of 1987, as well as observing if fibers with a higher initial ultrasonic modulus (modulus at no stress) have an improved crystallite orientation.

Another goal was the determination of the X-ray modulus of some of the fibers and to compare them to the ultrasonic moduli obtained previously.

Finally, the running of equatorial and meridional scans of the fibers was accomplished to observe any changes in peak position, peak sharpness, and peak width at half height.

III. SAMPLE PREPARATION:

Each sample is a bundle of graphite fibers, with approximately 2000 fibers in a bundle. The exact number for each sample is determined by measuring the mass m of a known length l of fiber bundle. The density of each type of fiber is known, and their diameters were measured in an optical

incident beam collimator; 1.0 mm diffracted beam collimator.

When load is applied, it is measured in millivolts,
which is then converted to grams by the conversion factor
2665 gms = 1 mV.

Sample	# fibers	Load (mV)	Load (gms)	Stress (MPa)	Orient. Factor
P25	798	0.1	266.5	41.7	-0.3735
		0.8	2132.0	333.4	-0.3946
P55	1851	0.3	799.5	53.9	-0.4726
		1.5	3997.5	269.5	-0.4726
		3.0	7995.0	538.9	-0.4736
		4.0	10660.0	718.6	-0.4741
P75	1553	0.3	799.5	64.2	-0.4822
		1.5	3997.5	321.2	-0.4823
		3.0	7995.0	642.4	-0.4832
P100	1755	0.3	799.5	56.8	-0.4925

As can be seen from the above table, the orientation
factor improves significantly from the lowest modulus fiber
(P25) to the high modulus fiber (P100). The orientation
changes only slightly when stress is put on each fiber.
These changes can be seen in figs. 5 and 6, where fig 5
shows the orientation scan of P55 at 0.3 and 4.0 mV, where
only a small shift in the peak is seen. Fig. 6 shows the
scans of P55, P75, and P100 at 0.3 mV stress. A much larger
shift is observed. Crystallite orientation accounts for some
of the effects observed in the elastic tensile properties of
the fibers, but it is clearly not the only mechanism at work.

P55 ORIENT

Fig. 5

ORIENTATION (.3 MV)

Fig. 6

CHI (DEGREES)

REL. INTENSITY

P65

P75

P100
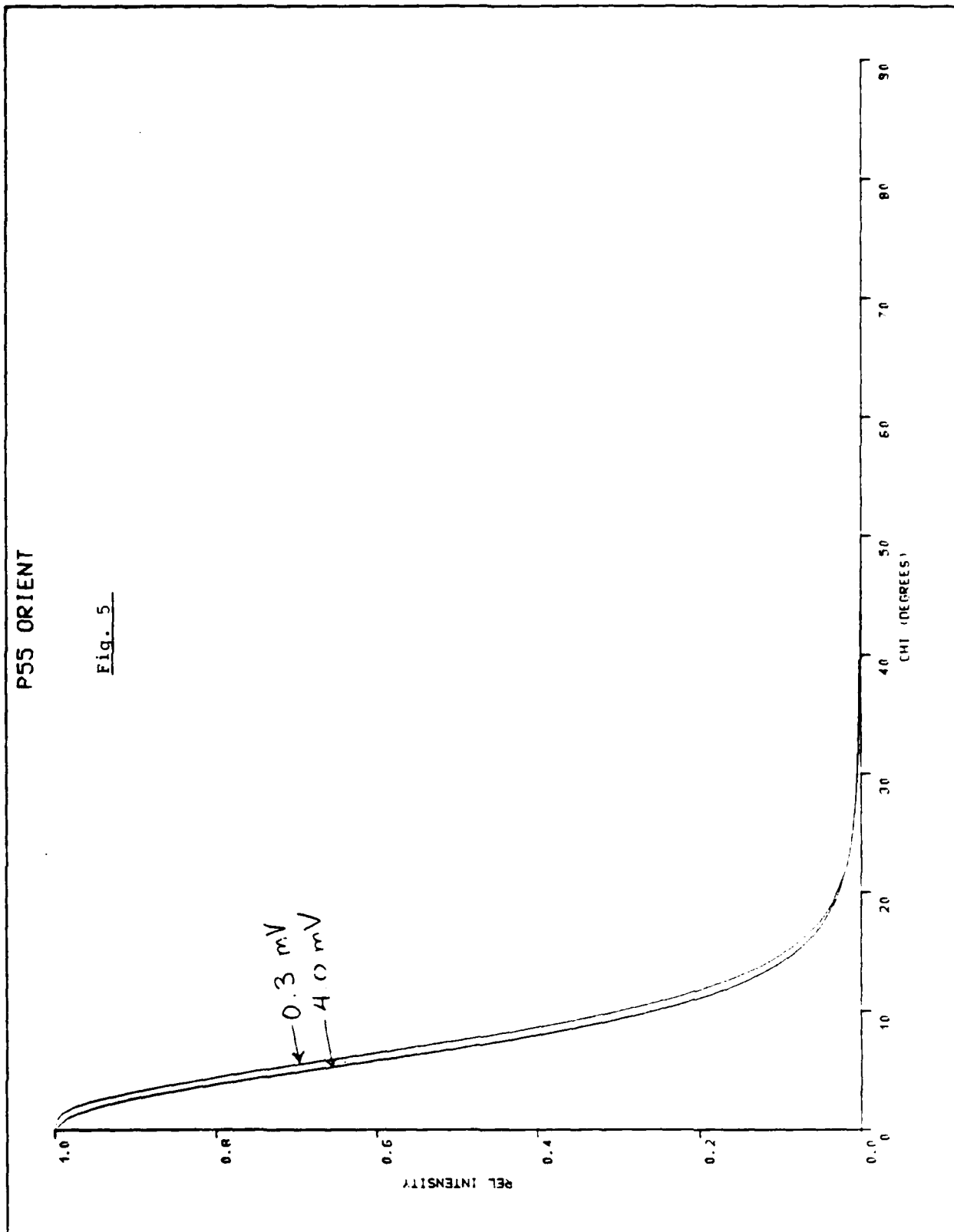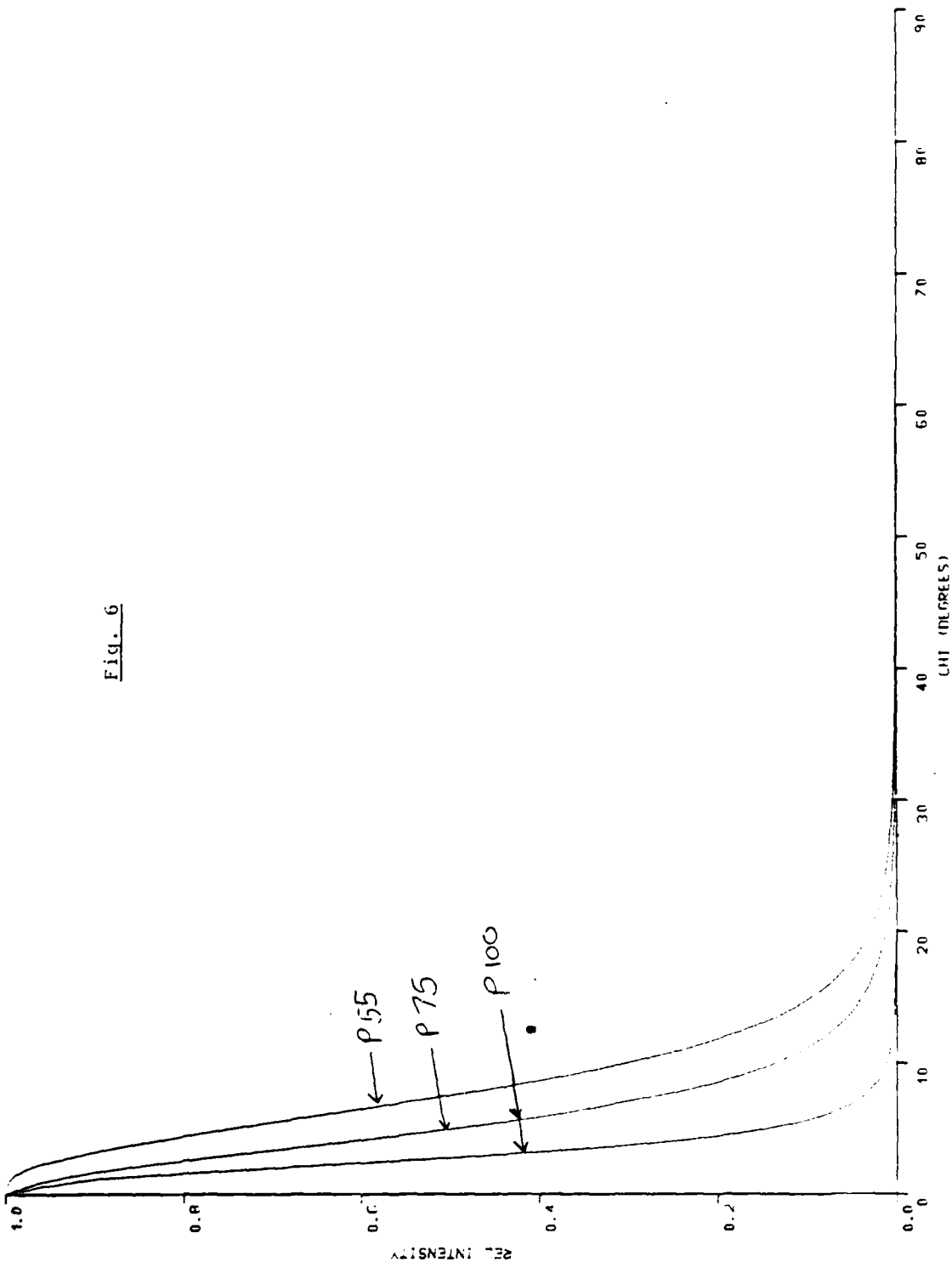
V. X-RAY MODULUS MEASUREMENTS:

X-ray modulus measurements were made on the samples P55 and P75. The modulus is determined by observing the shift in the two theta values of the (110) meridional reflection when different stresses are applied. The scan range consisted of 7 points located symmetrically on the peak. From the shifts in theta, changes in the interplaner d spacing are found, and a plot is made of tension vs. d spacing. Two theta values for each point are determined by a least squares fit of a Gaussian curve to the scanned points. A linear plot is fit to this data (Tension vs. d spacing). The modulus can then be determined by:

$$ Y = \frac{0.0882 d_c S p}{MDN} $$

Y is the modulus in Gigapascals, M is the slope of the d spacing vs. tension curve in angstroms/mV, d_c is the average lattice spacing (angstroms), p is the fiber density (gm/cm^3), S=2665 gm/mV, D= denier per fiber, and N is the number of fibers in the sample.

Accurate measurement of the X-ray modulus of these fibers was difficult because of the extremely small changes in two theta that needed to be observed. This is due to the high modulus of the fibers. In order to get reasonable shifts in two theta, extremely high loads had to be applied, often enough to break the sample. In addition, the samples had some translational motion in the sample holder when stress was applied, making measurements even more difficult.

These problems were tackled by using long counting times and trying to get the maximum load on the fibers without breaking them. Sample test conditions: Unfiltered Cu Kα radiation, tube current 40 mA, tube voltage 35 kV, diffracted beam aperture 3mm wide and 5 mm high. The modulus measurements were made twice, turning the fiber 180 degrees along the fiber axis. (motor "up" vs. motor "down").

Sample	Ultrasonic modulus (GPa)	X-ray modulus (GPa)	fiber orient.
P55	354	564.9+/-15.1	Up
		619.1+/-42.0	Down
P75	480	813.1+/-123	Up
		857.3+/-63.0	Down

Fig. 7 shows the plot of tension vs. interplanar spacing for P55 in the "motor up" orientation.

The x-ray modulus is higher than the ultrasonic modulus in all cases.

VI. EQUATORIAL AND MERIDIONAL TWO THETA SCANS:

The equatorial and meridional scans showed a sharpening and nerrowing of the diffraction peaks as the fiber modulus got higher. The P25 (lowest modulus fiber) scans showed in particular a very diffuse background and broad peaks, suggesting a higher degree of disorder. The crystallite orientation factor of P25 shown earlier is also significantly lower than that of the other fibers. Figs. 8 to 11 show some of these scans.

Fig. 7

d SPACING (Angstroms) $*10^{-2}$

TENSION (Newtons)
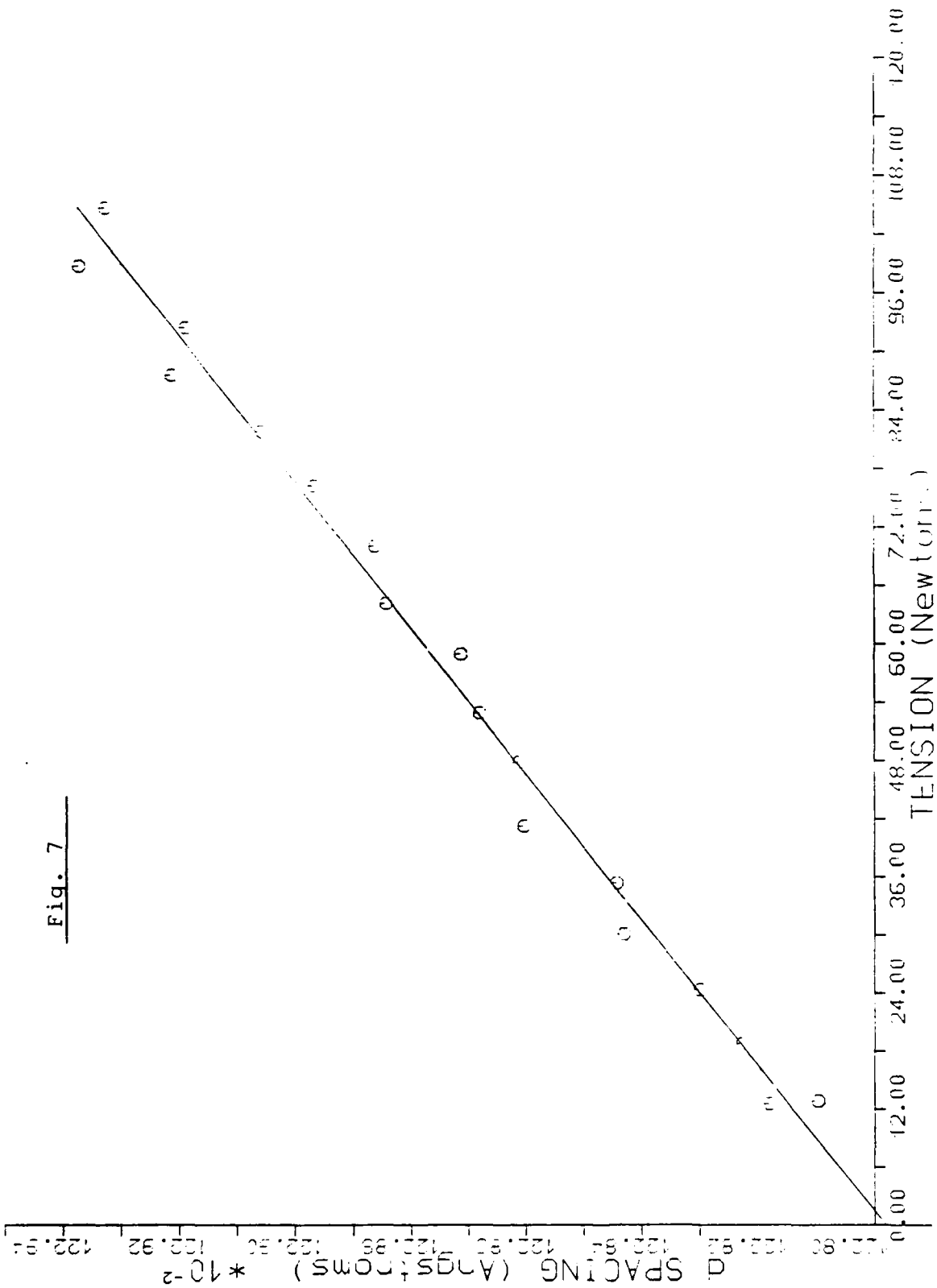
P25 MER NI FILTER

Fig 8

3-15

Fig. 9
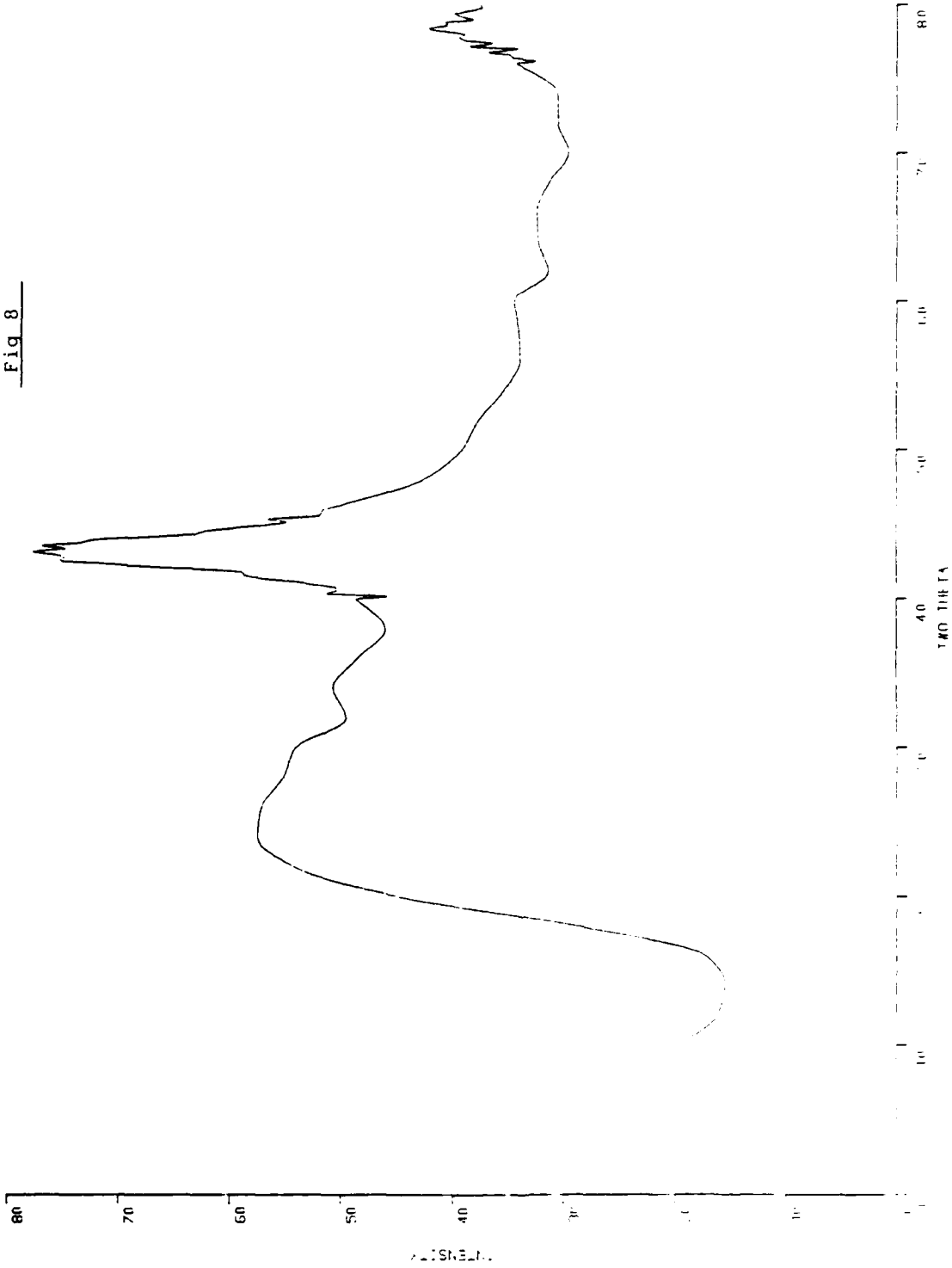
D55 MER NI FILTER

P25 EDU NI FILTER

Fig. 10

3-17

P55 EQU NI FILTER

Fig. 11

3-18
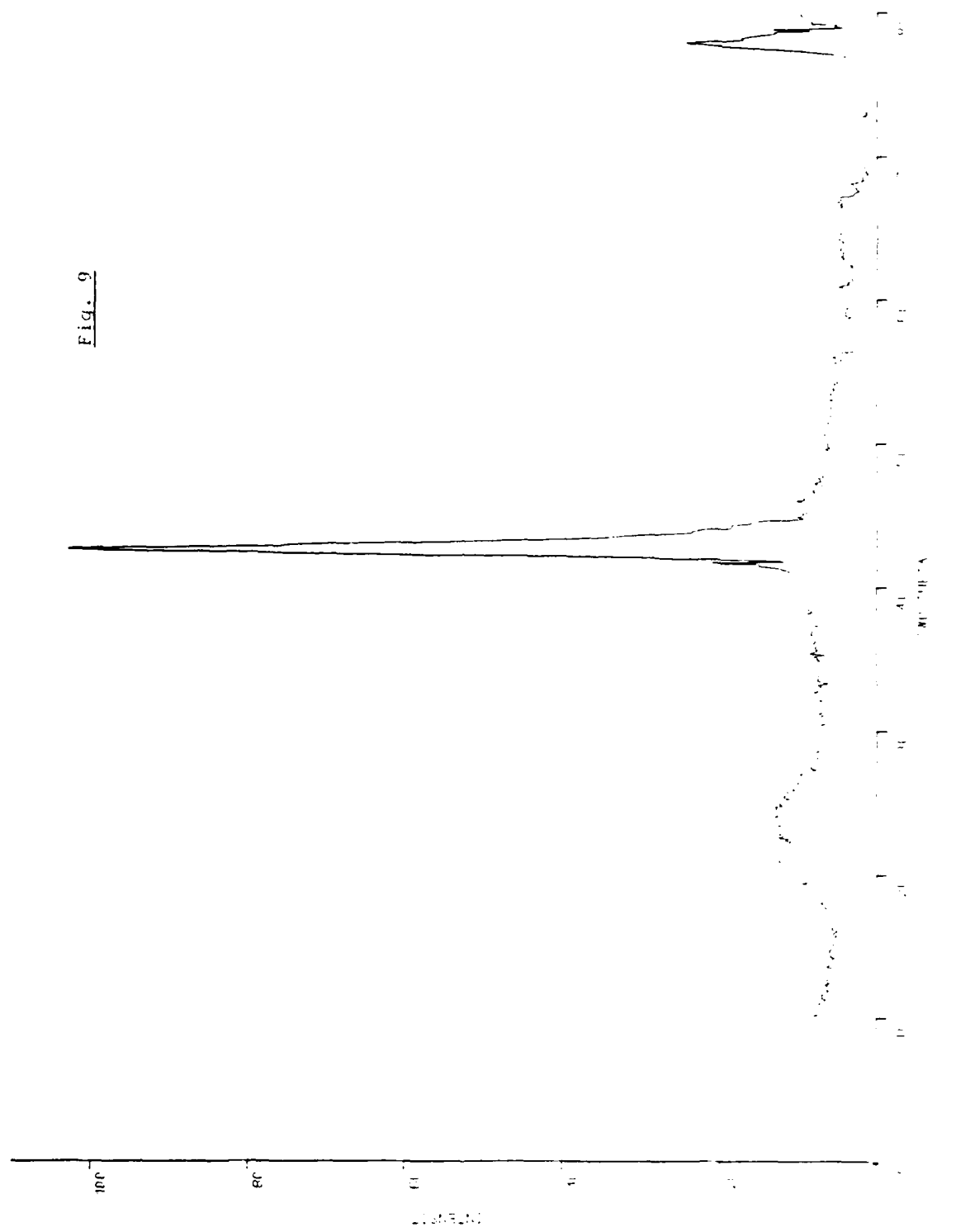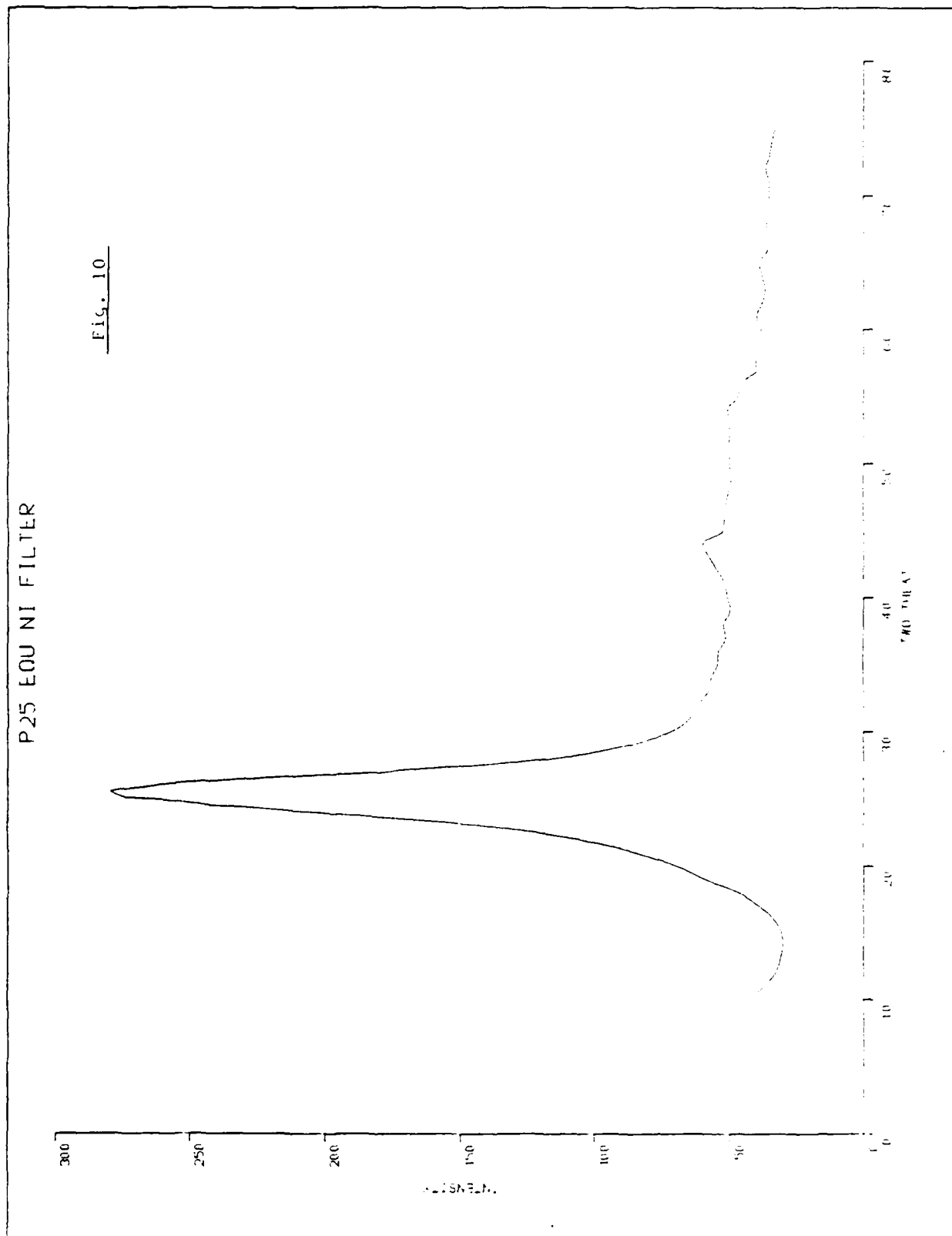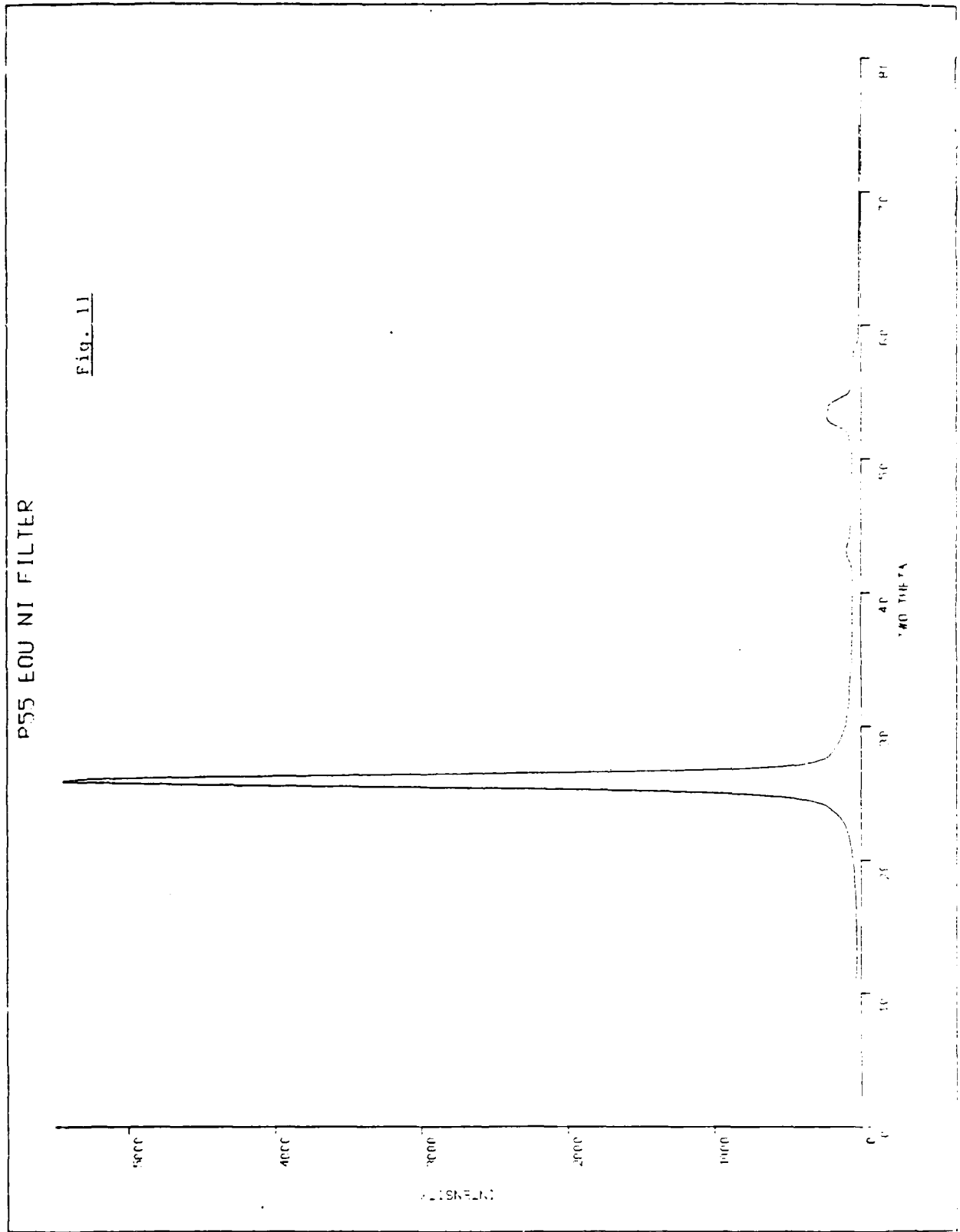
VII. RECOMMENDATIONS:

More work should be done on these graphite fibers.
The work done this summer with the Picker diffractometer
was only at room temperature. A temperature cell could be
constructed to obtain these measurements below and above
room temperature. More work also should be done to get
modulus data on the highest modulus fibers. (P100 and P120).
These fibers are the most difficult to get accurate modulus
data. Also, PAN (polyacrylonitrile) based graphite fibers
could be tested in addition to the pitch based fibers that
were experimented on here.

Finally, when enough results are known, a complete
model explaining the behavior of graphite fibers wii be
developed

REFERENCES

Donnet, J.B., and Bansal, R.C. Carbon Fibers. International Fiber Science and Technology/3. 1984

Lenhert, P.G. Report on X-ray Modulus Determination of Ordered Polymers. 1985

Lenhert, P.G., O'Brien, J.F., and W.W. Adams. A User's Guide to the Picker Diffractometer for Polymer Morphology Studies. AFWAL-TR-86-4024. 1986

Arsenovic, P., Eby, R.K., Jiang, H., and J.M. Liu. Characterization of the Nonlinear Elastic Properties of Graphite Fibers. 1987

Watt, W., and B.V. Perov. Strong Fibers. Handbook of Composites, Vol 1. 1985

1987 USAF-UES SUMMER FACULTY RESEARCH PROGRAM/

GRADUATE STUDENT SUMMER SUPPORT PROGRAM

Sponsored by the

AIR FORCE OFFICE OF SCIENTIFIC RESEARCH

Conducted by the

Universal Energy Systems, Inc.

<u>FINAL REPORT</u>

<u>AN EIGHT-DOMAIN FRAMEWORK FOR UNDERSTANDING INTELLIGENCE</u>

<u>AND PREDICTING INTELLIGENT PERFORMANCE</u>

Prepared by:	Ronna F. Dillon/Catherine Aubertin
Academic Rank:	Professor /Graduate Student
Departments:	Educational Psychology, Psychology,
	and Psychiatry
University:	Southern Illinois University
Research Location:	Air Force Human Resources
	Laboratory, Manpower and
	Personnel Division, Test and
	Training Branch (AFHRL/MOEL)
USAF Researcher	Dr. William C. Tirre
Date:	September 21, 1987
Contract No:	F49620-85-C-0013

REFERENCE DR. DILLON

SFRP FINAL REPORT NUMBER 37

1987 USAF-UES SUMMER FACULTY RESEARCH PROGRAM/

GRADUATE STUDENT SUMMER SUPPORT PROGRAM

Sponsored by the

AIR FORCE OFFICE OF SCIENTIFIC RESEARCH

Conducted by the

Universal Energy Systems, Inc.

PROGRESS REPORT

Configuration Factors for

Spacecraft/Expansible Radiator

Interaction

Prepared by:	David R. Bosch
Academic Rank:	Graduate Student
Department and	Mechanical Engineerint Department
University:	Arizona State University
Research Location:	AFWAL/POOS
	Wright Patterson AFB, OH 45433
USAF Researcher:	Tom Mahefkey
Date:	6 Nov 87
Contract No:	F49620-85-C-0013

Configuration Factors for

Spacecraft/Expansible Radiator

Interaction

by

David R. Bosch

ABSTRACT

The configuration factors for approximating the interaction between
a expansible radiator and a spacecraft body are needed to determine the
overall performance of the radiator. Research was done to determine the
availability of the needed configuration factors. They were not
available for the desired geometry. Therefore, the program called VIEW
(written under the supervision fo A.F. Emery of the University of
Washington in Seattle) was adopted to calculate them. Because of a
late start, and other problems, the work was not yet finished at the
time of this publication.

I. INTRODUCTION:

The calculation of the net radiant heat flux between a expansible radiator and a spacecraft's body is needed to determine what effect the spacecraft body will have on the radiator's overall performance.

Determining the interaction between one radiator and a spacecraft's body is the first step in the overall analysis. The determination of the interaction between multiple radiators and a spacecraft body would necessarily follow.

II. OBJECTIVES OF THE RESEARCH EFFORT:

Currently, there are no configuration factors available that are applicable for calculating the radiant heat exchange in the spacecraft/ radiator geometry being used.

After an extensive review fo the methods used to calculate configuration factors, it was determined that using numerical techniques in the form of available programs was the most appropriate method of calculating the needed factors.

The AFWAL/POOS-3 lab had a program called VIEW (written under the supervision of A.F. Emery at the University of Washington in Seattle) available for calculating configuration factors using a IBM/AT personal computer.

The objective of my research effort, as a participant in the 1987 Summer Faculty Research Program, was to become intimately familiar with using VIEW so that it could be used to approximate the configuration factors between one expansible radiator and a spacecraft body.

III. DISCUSSION:

The research was began by a thorough review of the basics of radiant heat transfer. This was necessitated by the lack of coverage of this subject in undergraduate heat transfer courses.

After completing the review, the integrals for two flat plates with a common edge, of equal length, different widths, and orientated at right angles to each other were written and evaluated analytically. From this exercise it was determined that the time to write and evaluate the integrals used in determining the configuration factors for the spacecraft/radiator combination was prohibitive. It was at this time that the decision was made to use VIEW to obtain the factors.

The first step in becoming familiar with VIEW's abilities was to study the user's manual. After this was done, several of the example problems included with the software were run to become familiar with the procedure of running the program.

Data was then written to define the flat plate problem described above. This data was run and the results correlated well with the analytical results.

The next step was to write data that would describe the spatial arrangement of two cylinders at right angle to each other, of equal

radius, and a distance apart. This arrangement was chosen because it coincided with geometries with known factors. Because the VIEW graphics software for use in generating surfaces was not yet available a short segment of code was written to accomplish the task. From this, results were obtained but determined to be unacceptable. This was as far as the work had proceeded at the time of this publication.

There are several reasons why this assignment was not accomplished in the ten weeks spent at Wright Patterson. First, I wasn't assigned to the project until almost half of the ten week period had elapsed. Until then I worked on other things that weren't associated with the configuration factor work. Also, there were problems encountered in using the VIEW software. Most of the problems involved difficulties getting the program to link after making changes in the code. Also, no manual was available for the PC version of the software. The manual used was intended for the main frame version and didn't include the changes make when adapting it for use on the PC.

IV. CONCLUSION:

This work will continue until the original objectives are achieved and the desired configuration factors are compiled and formally reported.

1987 USAF-UES SUMMER FACULTY RESEARCH PROGRAM/

GRADUATE STUDENT SUMMER SUPPORT PROGRAM

Sponsored by the

AIR FORCE OFFICE OF SCIENTIFIC RESEARCH

Conducted by the

Universal Energy Systems, Inc.

FINAL REPORT

Computer evaluation of ion-implanted

dopant profile evolution during annealing

Prepared by: Steven W. Bucey

Academic Rank: Graduate Student

Department and   Physics

University: Kent State University

Research location: AFWAL/MLPO WPAFB, Ohio

USAF Researcher: Dr. Patrick M. Hemenger

Date: August 10, 1987

Contract No: F 49620-85-C-0013

Computer evaluation of ion-implanted

dopant profile evolution during annealing

by

Steven W. Bucey

ABSTRACT

The project is to study the partial annealing of dopant implanted GaAs or silicon. Dr. David Moroi has developed an analyti al solution for the concentration profile during ion-implantation which had not been evaluated. A computer analysis was made to compare with a numerical solution. For the case of the linear dependence of the diffusion parameter excellent agreement was found between the solutions for a constant diffusion. but for a concentration dependence an overall relative error of about 5% is shown over the range of significant concentration.

Acknowledgments

I wish to thank the Air Force Systems Command and the Air Force Office of Scientific Research for sponsorship of this research and Universal Energy Systems for their help in the administrative and directional aspects of this program.

I also would like to thank the people of the materials Research Lab, Laser Physics, for their help and Dr. Patrick M. Hemenger for helping me find my way around. I most especially would like to thank Dr. David Moroi for allowing me to work on this project and helping me every step of the way.

I. Introduction

An understanding of the processes involved during ion-implantation and annealing of semi-conductors is required to be able to control the electrical properties of doped semiconductor material. These properties depend upon the kind of dopant, its implantation energy, and the final profile of the dopant.

Standard numerical procedures require extensive computer run time to produce usable analysis. These procedures suffer from instability problems and are costly in computer time.

Using judicious mathematical techniques, Moroi and Hemenger[1] developed an analytical solution for the dopant profile during annealing. This solution still required the use of a computer to be evaluated.

The goal of this report was to compare the analytic solution to a solution developed by a standard numerical procedure and determine the correctness and usefulness of the solution.

II. The Analytic Solution

Considering the dopant diffusion equation and the equations for the initial and boundary condition defined by

$$\frac{\partial C}{\partial t} = \frac{\partial}{\partial z}\left[D \frac{\partial C}{\partial z}\right] \qquad \text{for } z,\ t > 0 \qquad (1)$$

where

$$D = D[C(z,t)] \qquad (2)$$

$$C_0(Z) = C(Z,0) \qquad (3)$$

$$\left.\frac{\partial C}{\partial z}\right|_{z=0} = \qquad (4)$$

$$C(\infty,t) = 0 \qquad (5)$$

6-4

Moroi and Hemenger used new variables to produce a transformed set of equations which could easily be solved. By assuming that the diffusivity of a dopant is of the form

$$D = \beta \, C^{\gamma} \, (z,t) \qquad\qquad \gamma \neq -1 \qquad\qquad (6)$$

a solution for the dopant concentration profile is found to be

$$\eta(\zeta,\tau) = \frac{1}{2(\gamma+1)\sqrt{\pi \tau}} \left[\exp\left(\frac{-(\zeta-\zeta_0)^2}{4\tau}\right) \cdots \right]$$

$$+ \exp\left(\frac{-(\zeta+\zeta_0)^2}{4\tau}\right) \, \mathrm{erfc}\left(\cdots\right) \cdots \qquad (7)$$

where

$$\zeta = \left(\frac{\gamma+1}{2 S_0^2}\right)^{1/2} z \qquad\qquad (8)$$

$$\zeta_0 = \left(\frac{\gamma+1}{2 S_0^2}\right)^{1/2} z_0 \qquad\qquad (9)$$

(S_0 and Z_0 are constants in the assumed gaussian profile of the initial data).

and

$$\tau = \left(\frac{\gamma+1}{2 S_0^2}\right)^{1/2} \int D \left[\, C(z,t)\,\right] \, \cdots \qquad (10)$$

Note that the complimentary error function erfc(x) was approximated to be

erfc $(x) = (a\,y + b v_2 - c v^3 + d v^4 + e v^5) \exp(-x^2)$

where $y = 1/(1 + px)$

and a, b, c, d, e, p are constants.

To solve for the dopant profile at a given time t we must solve eq.
'10'for the time t. To do this we must subdivide the t from 0 to x_n and
add up the values of the Δt_i found in the numerical approximation to eq. 10
by

$$ x = \left[\frac{Y_i}{Y_{ij}} \right]^{i} \left[\frac{1}{2} c_i \Delta t_i + \sum_{i=1}^{n-1} c_i \Delta t_i + \frac{1}{2} c_n \Delta t_n \right] \quad (11) $$

Starting at n=1 we continue to add up the Δt_i found in eq. 11 until
they equal the total time desired.

To calculate the value of C needed for the value of D in equation 11
we use this equation to transform the variable:

$$ \pi(z_i, z) = \frac{1}{Y_{ri}} \, c^{-\gamma r_i}(z_i, z_n) \quad (12) $$

If Z represents the depth into a semiconductor wafer and t is the
time evolution of the dopant profile then the solution gives a dopant
concentration for any given Z point.

III. The Numerical Solution

The same system was also evaluated by using a finite differences numerical approximation, which was reduced to generating a solution based upon the following equation:

$$C(z, t+\Delta t) = C(z, t) + \ldots \Delta t [\ldots] + \frac{C(z,t) \Delta t}{2 \Delta z} [\ldots] \quad (13)$$

where GR (z,t) is the gradient of the diffusion parameter at z.

Now this method of solution is valid only if three criteria are met. The first is that the space time variables must be related by

$$\frac{\beta \Delta t}{(\Delta z)^2} \leq 1/2 \quad (14)$$

where ß is the coeficient of the diffusion parameter. In the solution this is set instead to equal 1/4.

The other two criteria are the boundary conditions. The model assumes that $Z = 1 \mu m$ and $t = 20$ seconds are near infinity. With this in mind a mesh size of $\Delta Z = 0.001$ is picked and then the code calculates the Δt need.

Since the method of solution requires the slope at a given point the new value at a given point depends upon its neighbor's values. This requires calculation of all points out to "infinity" and thus 1001 points are needed, with $C(1001,t)=0$ always. Also, since the slope of $C(o,t)$ is zero always this implies that $C(-\Delta z,t) = C(\Delta z,t)$ for calculation purposes only.

IV. Results

Two cases where considered:

$$\theta = \beta \quad (15)$$

6-7

$$D = BC(Z, t)$$ (16)

both with $Co(Z) = exp\left(- \dfrac{(Z-Zo)^2}{2\ So^2}\right)$

Figures 1 through 6 show the results for various time profiles. Figure one is this initial distribution for both cases. Excellent agreement is achieved throught the time considered. Figures 2-4 However, for the case of equation (16) the fit is poor at best but at least a general agreement between solutions is shown (figures 5 & 6).

V.   Recommendations

We are not sure why the second case gave a poor fit. Three possibilities suggest themselves. The first is that in one or both cases computer round off error accumulates with time. This is supported by the fact that in short time the fits are still good.

The second may be that the numerical solution is not sophisticated enough to handle the given conditions, and may require a more advanced treatment.

The third case, which we hope is not true, is that the analytic solution requires additional correction terms to be added.

References

1)   Moroi, D.S.; P.M. Hemenger, "Exact analytical solution to diffusion
     equation for ion-implanted dopant profile evolution during
     annealing." Applied Physics Letters, #50 Vol. 3, 19 January 1987.

2)   R. Ghez, A.S. Oehrlein, T.O. Sedgwick, F.F. Morehead, and Y.H. Lee,
     "Exact description and data fitting of ion-implanted dopant profile
     evolution during annealing," Appl. Phys. Lett. 45, 881 (1984).

Figure one
INITIAL DATA.
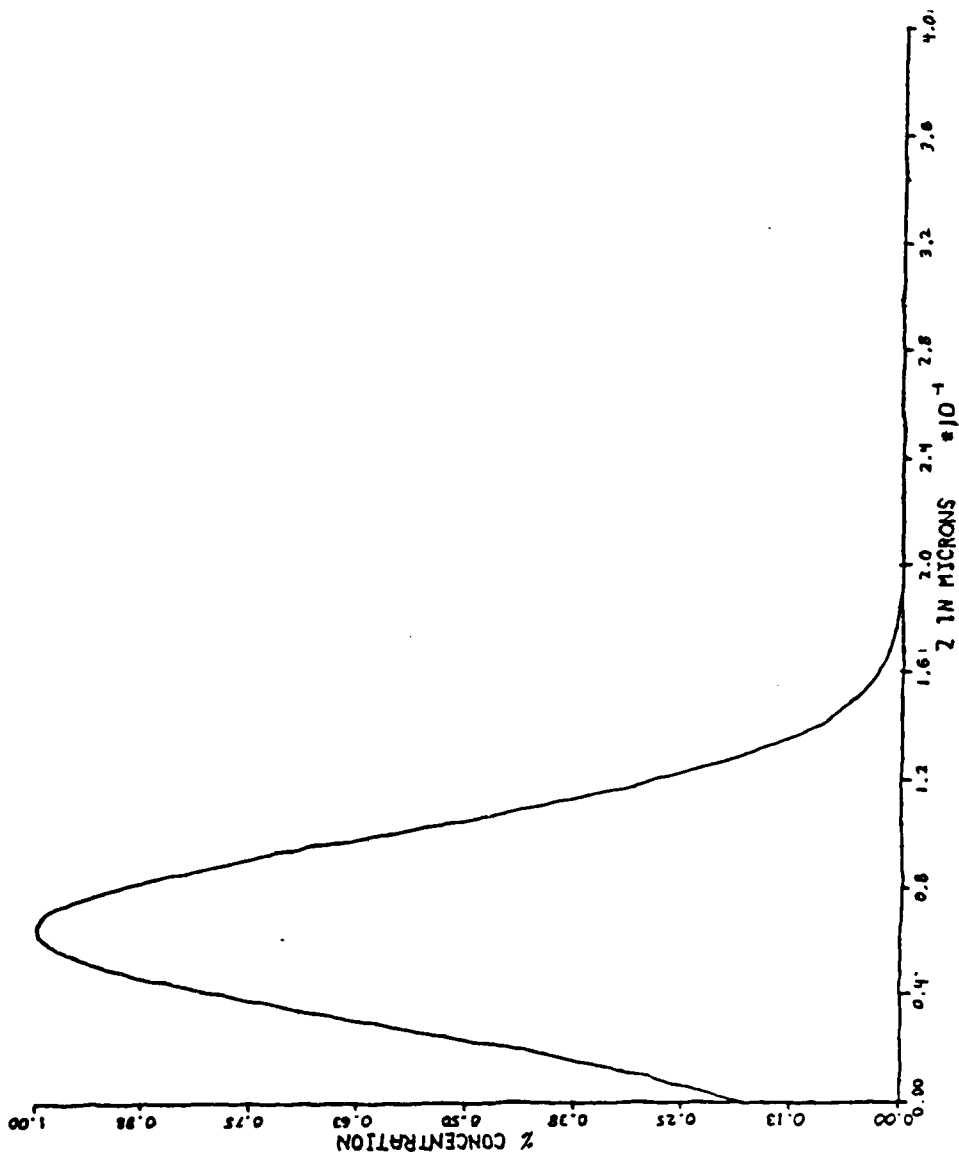
Figure Two
NUMERICAL AND ANALYTIC. I SECOND.

Figure Three
NUMERIC AND ANALYTIC. 20 SECONDS.
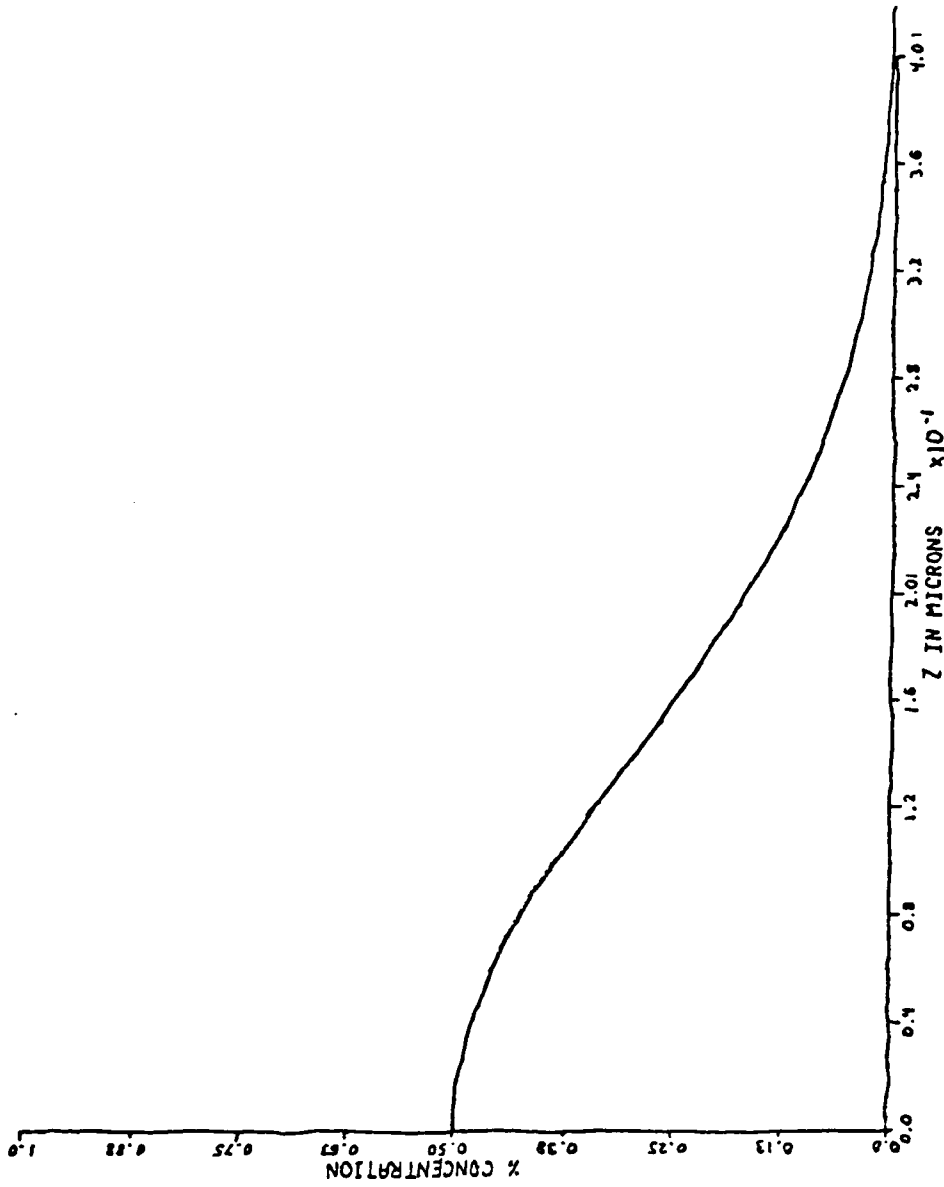
Figure Four
NUMERICAL AND ANALYTIC, 1 SECOND

6-13
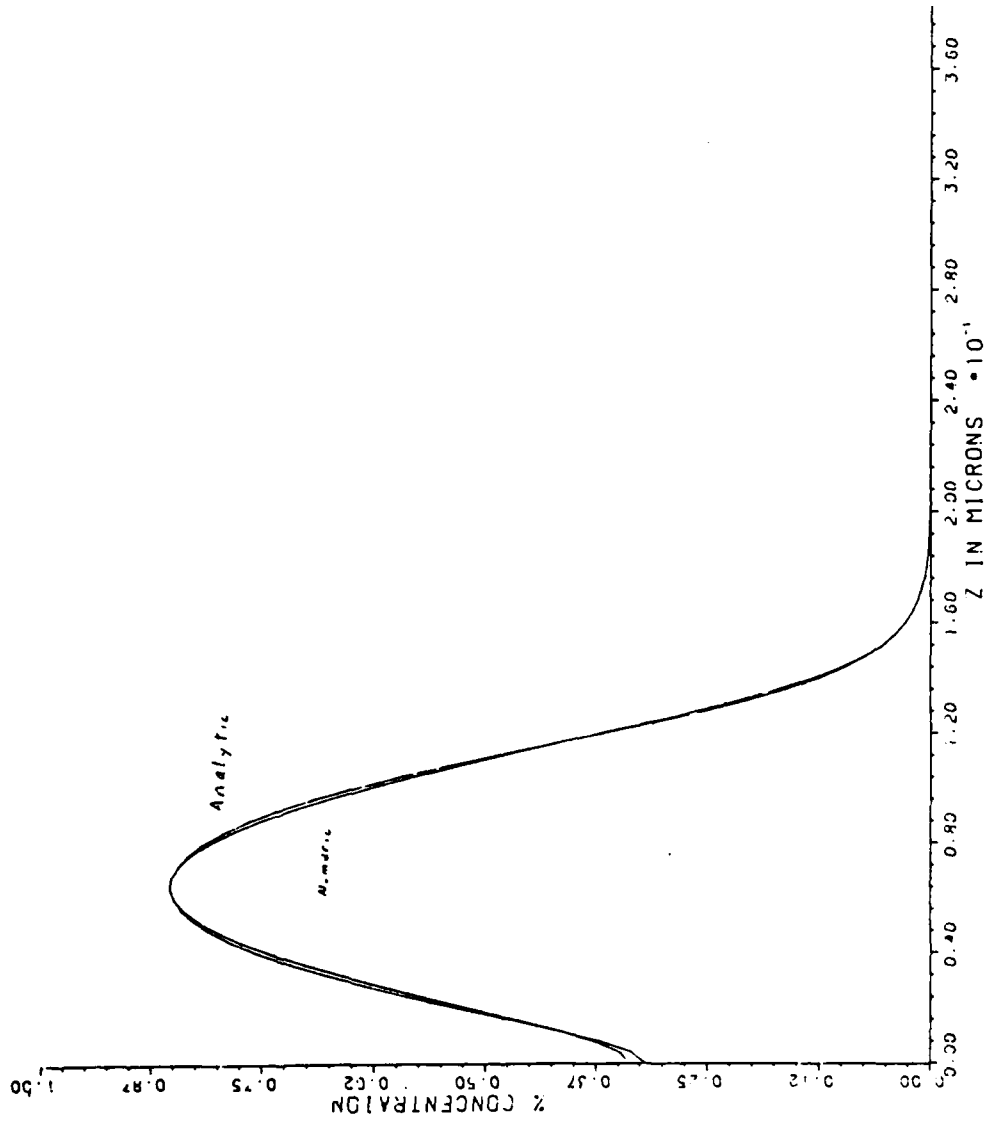
Figure Five
NUMERICAL AND ANALYTIC, 10 SECONDS
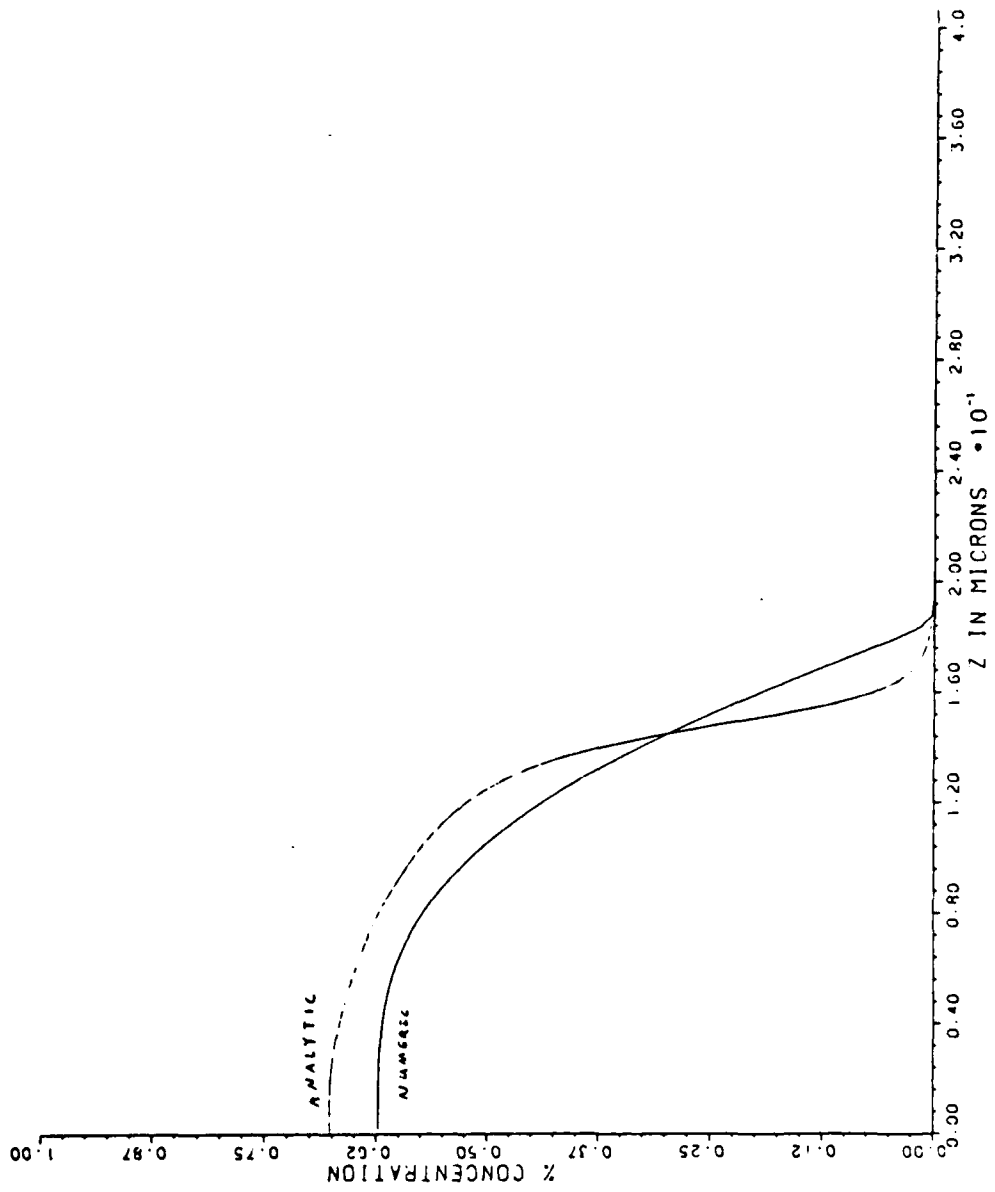
6-14

1987 USAF-UES SUMMER FACULTY RESEARCH PROGRAM

GRADUATE STUDENT SUMMER SUPPORT PROGRAM

Sponsored by the

AIR FORCE OFFICE OF SCIENTIFIC RESEARCH

Conducted by the

Universal Energy Systems, Inc.

FINAL REPORT

The Interface Contribution to GaAs/Ge Heterojunction Solar Cell Effeciency

Prepared by: Cheng-Hsiao Wu, Ph.D. and John Bullock

Academic Rank: Associate Professor, graduate student

Department and   Electrical Engineering Department

  University: University of Missouri-Rolla

Research Location: USAFWAL/POOC
                    Wright-Patterson AFB
                    Dayton OH 45433-6563

USAF Researcher: Joseph Wise

REFERENCE DR. WU

SFRP FINAL REPORT NUMBER 156

1987 USAF-UES Summer Faculty Research Program/
Graduate Student Summer Support Program
Sponsored By The
Air Force Office of Scientific Research
Conducted By The
Universal Energy Systems, Inc.

Final Report
Isolation of Osteogenic Cells From The
Trauma-Activated Periosteum

Prepared by: Robyn A. Butcher
Academic Rank: Graduate Student
Department and   Physiology and Biophysics
University: Wright State University
Research Location: Biodynamics Effects Branch,
                        Armstrong Aerospace Medical Research
                        Laboratory, W.P.A.F.B.
USAF Researcher: Dr. Noel S. Nussbaum
Date: August 22, 1987
Contract No.   F49620-85-L-0013

Isolation of Osteogenic Cells From The
Trauma-Activated Periosteum

By

Robyn A. Butcher

Abstract

Closed, greenstick type fractures were created in adult
male white New Zealand rabbits. After a waiting period of 5
days the developing callous and bone approximately 1 cm to
each side of the callous was harvested and cell cultures
established. Biochemical assays for total protein, alkaline
phosphatase activity and glycosamino-glycan content were
performed on spent media collected at each change and upon
the cells after their termination, in an attempt to more fully
characterize the osteoblast population. Since little is known
about bone forming cells isolated from this source it is impor-
tant to establish baseline data so as to be able to relate
reactions of these cells to altered environmental conditions.

ACKNOWLEDGEMENTS

I. Introduction

The process of bone specialization, vital for skeletal and mineral homeostatsis, is not well understood. It is thought that the precursor bone cells (osteoprogenitor cells) originate from mesenchyme, the embryonic connective tissue. The osteo-progenitor cells then differentiate into preosteoblasts and pre-osteoclasts which further differentiate into osteoblasts and osteoclasts. Osteoblasts are involved in bone formation, osteoclasts are involved in bone reabsorption. Although the development of the osteoblast has been studied extensively, the specialization of the osteoblast has received little attention.

Demineralization is known to result from hypogravity, hypokinesia and/or immobilization, therefore the USAF is particularly concerned with the role the osteoblast plays in the homeostatic mechanism vital for maintenance and continuous growth of bone. Current understanding of such cells is based primarily on histological evidence and few in vitro organ culture studies. The cellular competance of these cells to respond to local osteogenic stimuli has not yet been determined, thus it is important to establish baseline data about such osteogenic cells so as to be able corelate the reactions to altered environmental conditions possibly associated with demineralization.

I am a recently graduated student from Wright State University. I was interested in finding summer employment that offered interesting and valuable research experience. I believe my G.P.A. as well as my desire to work contributed to my assignment.

II. Objectives of the Research Effort

As the process of bone specialization is not well under-stood, it is a primary objective to establish baseline data about periosteal-derived osteogenic cells so as to be able to relate the reactions of this tissue to altered environmental conditions. The approach taken was to transfer in vivo fractured-induced activated osteoprogenitor cells to an in vitro environment for further study.

My assignment as graduate researcher was to help the principle investigator, Noel S. Nussbaum, Ph.D, realize several specific goals:

1. To establish the methodology for the isolation and characterization of osteoprogenitor cells from trauma-activated periosteum.
2. To determine the maximal growth response of cell populations derived at varying times after trauma.
3. To quantify the response of osteogenic cells to identified modulators.

Some personal goals included:

1. To gain valuable research experience.
2. To improve upon general laboratory techniques.
3. To learn more about the roles of osteoprogenitor cells both in bone formation and reabsorption through hands on experience and literary research.

III.

A closed, greenstick type of fracture is created in adult male white New Zealand rabbits. The fracture leads to a callous and it's the callous we harvest by the sequential enzyme digestion technique of Wong and Cohn (1979) as modified by Boonekamp et. al. (1984). Those cells within the callous are activated in vivo by the local fracture to divide and grow. An object is to add back those local factors in vitro to maintain the growth rate. So far we have seen some response to insulin.

As a part of establishing baseline data in order to characterize the osteogenic cells we have been performing some standard biochemical assays on the spent media after each change as well as the cells upon their termination. Assays include protein assays, (biorad) alkaline phosphatase and glycosaminoglycan.

Procedures:

Biorad Standard Assay

Reagents:

a) Biorad reagent: brilliant coomassie blue dye diluted 1:4 with dH_2O

b) Standards: dissolve 100mg fraction V Bovine Albumin
    per 10 mls PBS for a final concentration of 10 mg/ml.
    Refrigerate.

Method:

a) Standard curve: (prepared every time new standard
    solution is made). The standard solution (10 mg/ml) is
    diluted to final concentrations of 200, 400, 600, 800,
    and 1,000 ug/ml with dH_2O. A tube with 0 mg/ml
    (dH_2O) is prepared. Concentration vs. abs 595 is
    plotted.

b) Media samples are mixed by inverting several times and
    diluted tenfold (.1 ml media to .9 ml dH_2O). Cell
    samples are diluted 1:1 with dH_2O. All dilutions are
    vortexed.

c) .1 ml of each standard, water blank and samples are
    transferred to a prelabeled test tube. Duplicate
    tubes are run for each sample.

d) 5 mls of diluted dye reagent is added to each tube,
    tubes are vortexed and allowed to stand 10 min.

e) Average of 3 readings per tube (abs 595) for each
    standard(s), water blank and samples is determined,
    average absorbance of water blank is subtracted
    from each and concentration is determined from the
    standard curve. Concentration is multiplied by the
    dilution factor then converted to mg/ml and recorded.

Alcian Blue Assay (GAG)

Reagents:

a) 50 mM sodium acetate buffer containing 200 mM $MgCl_2$;
    Place 4.10 g sodium acetate, 40.66g $MgCl_2 \cdot 6H_2O$ and
    2.53 ml of 1.74 M acetic acid in a 1 liter volumetric
    flask. Add dH_2O to the mark and mix. Adjust PH to 5.8.

b) Alcian blue reagent:
    This reagent must be freshly prepared before use.
    Dissolve o.o5% (w/v) Alcian Blue 8GX (Polysciences,Inc..

Warrington, PA.) in the above buffer. Centrifuge
20,000 rpm for 20 minutes. Retain the supernatant
as the reagent.

c) Sodium dodecylsulphate solution (SDS solution):
Dissolve 2% (w/v) SDS in 50 mM sodium acetate buffer.
Adjust PH to 5.8.

d) Standards:
Dissolve 10 mg. chondroitin sulphate in 100 mls of
dH_2O. Refrigerate.

Method:

a) Standard Curve:
The standard solution (100 mg/L) is diluted to final
concentrations of 100, 80, 60, 40, 20, 10, and 5 mg/L.
A tube with 0 mg/L (dH_2O) is prepared.

b) .2 ml of each standard, water blank and sample is mixed
with 2 mls of fresh Alcian Blue reagent. Duplicate
tubes of each are prepared.

c) The solutions are placed in sorvall plastic centrifuge
tubes (18 mm x 10mm) and are equilibrated for 19 hours
(overnight) at room temperature.

d) After the incubation period, the tubes are centrifuged
at 20,000 rpm for 20 minutes.

e) The supernatant is discarded and the precipitate
washed with 5mls of 100% EtoH. The precipitate is
scraped from the sides of the tube with a metal spatula
if necessary.

f) The tubes are centrifuged at 20,000 rpm for 20 minutes.

g) The supernatant is discarded and the remaining complex
solubilized in 5 mls SDS solution. Again precipitate
is scraped from sides of the tube with a metal spatula
as needed.

h) ABS 620 is read (3 readings per tube). The spectro-
photometer is zeroed with the water blank. Standard
curve is plotted and concentrations of each sample is

determined. Whenever a standard curve is not plotted
one standard 40 mg/L is run to check validity of the
curve. Concentrations are converted to mg/ml and
recorded.
All results from the assays are entered into a SAS data file
for statistical analysis

IV. Goals and Objectives

My own personal goals have been achieved. I have improved
upon some general laboratory techniques, such as micropipeting,
aseptic technique, spectrophotometer analysis, microscopy,
and cell culturing. I have gained valuable experience in
learning some aspects of research, performing standard bio-
chemical assays and reading and understanding scientific
journals. I have also gained some insight into the process
of bone formation and reabsorption and what might affect this
process as well as some applications to malfunction such as
osteoporosis.

V. Recommendations:

By completion of this project the biochemical assays
will have been refined and the osteoprogenitor cells more fully
characterized. The next step is to add local growth factors,
hormones, and vitamins to culture media and monitor the effects
on the cells with the techniques developed in this project.
The object is to be able to stimulate the adult cells to divide
and grow.

VI. <u>References</u>

1. Cohn, D.V. and Wong, G.L. 1979. "Isolated Bone Cells." <u>Skeletal Research</u>, vol. I, ed. by: Simmons, D.J. and Kunin, A.S., Academic Press, pp. 3-20.

2. Boonekamp, P.M., Hekkelman, J.W., Hamilton, J.W, Cohn, D.V., and Jilka, R.I. 1984. "Effect of Culture on the Hormone Responsiveness of Bone Cells Isolated by an Improved Sequential Digestion Procedure." <u>Proc. Kon. Neder. Weten.</u> 87B: 371-381.

3. Ross, Michael and Reith, Edward. <u>Histology A Text and Atlas,</u> New York, Harper and Row, publishers, 1985.

1987 USAF-UES SUMMER FACULTY RESEARCH PROGRAM/
GRADUATE STUDENT SUMMER SUPPORT PROGRAM

Sponsored by the

AIR FORCE OFFICE OF SCIENTIFIC RESEARCH

Conducted by the

Universal Energy Systems, Inc.

FINAL REPORT

A TEST CHIP FOR EVALUATION OF MBE EPITAXIAL LAYERS
FOR NOVEL DEVICE APPLICATIONS

Prepared by: Kenneth P. Roenker, Ph.D./ Kevin P. Cahill

Academic Rank: Associate Professor/ Graduate Assistant

Department and   Electrical and Computer Engineering
University: University of Cincinnati

Research Location: Wright Aeronautical Laboratories, Avionics
                       Laboratory, Electronic Research Branch,
                       Device Research Group AFWAL/AADR

USAF Researcher: Dieter Langer, Chern Huang

Date: September 8, 1987

Contract No: F49620-85-C-0013

REFERENCE DR. ROENKER

SFRP FINAL REPORT NUMBER 116

1987 USAF-UES SUMMER FACULTY RESEARCH PROGRAM/
GRADUATE STUDENT SUMMER SUPPORT PROGRAM

Sponsored by the
AIR FORCE OFFICE OF SCIENTIFIC RESEARCH

Conducted by the
Universal Energy Systems, Inc.

FINAL REPORT

Prepared by :   David C. Carpenter, MS
Academic Rank :   Graduate Student
Department and   Nuclear Engineering Department
   University :   Texas A&M University
Research Location :   AFWL / AWYS
                           Kirtland AFB
                           Albuquerque, NM 87117-6008
USAF Researcher :   Dr. Michael Schuller

Date :   14 August 1987
Contract No :   F49620 85 C 0013

Preliminary Thermal Analysis of a Bimodal Nuclear Rocket Core

by

David C. Carpenter

ABSTRACT

The framework for a general purpose finite element analysis code
was developed to study the 2-D temperature distribution in a hot-channel
hexagonal fuel element in the core of a bimodal nuclear rocket. Prelim-
inary thermal-hydraulic analysis of the core pressure drops under heli-
um coolant conditions were also performed. Hydrogen coolant analysis
was not performed due to insufficient property data in a usable form.
Although the thermal gradients observed in the fuel element did not
seem to present a problem, a more detailed thermal stress analysis
was initiated. The stress analysis is not fully implemented in the code
at this time. Code development also progressed into 3-D temperature
distributions in anticipation of projected research.

Acknowledgements

MICROCOPY RESOLUTION TEST CHART

NATIONAL BUREAU OF STANDARDS-1963-A

I. INTRODUCTION

The economics of space travel requires that the specific impulse of a rocket engine be as high as possible while maintaining the mass ratio at earth escape as low as can be achieved. Solid core nuclear rockets with hydrogen as a propellant have demonstrated over two times the specific impulse of conventional chemical reaction rockets while reducing the mass ratio at earth escape from about 15 to about 3.2[1]. Similar to terrestrial gas-cooled reactors, the solid core reactor could also be used to generate electrical power for any specified payloads, hence the concept of the dual-mode or bimodal rocket system. The electrical production would be accomplished by circulating a second coolant through the reactor into a Brayton or Stirling cycle.

The Space Applications Division at the Air Force Weapons Laboratory (AFWL/AWYS), Kirtland AFB, New Mexico is charged with exploring the technologies required for space nuclear reactor systems. As such, AFWL is engaged primarily in the research and development of advanced concepts of space nuclear electrical power production. AFWL recently initiated preliminary design studies of a NERVA[2] derivative nuclear rocket. Whereas the NERVA was a single mode rocket engine, the research focused on a bimodal design using hydrogen as the propellant and helium as the working fluid in the thermodynamic cycle.

I was chosen to participate in this project due to my degrees in nuclear engineering. My research interests have dealt with the numerical analysis of nuclear reactor core designs, particularly in the area of fuel element thermal performance. Knowledge of finite element techniques aided in the study of the complicated geometry of the fuel elements being considered in the bimodal reactor.

II. OBJECTIVES OF THE RESEARCH EFFORT :

Analysis of nuclear reactor systems is a detailed and lengthy process involving several disciplines of study. Some of the areas of concern include heat transfer, thermodynamics, fluid dynamics, thermal energy conversion to electrical and/or mechanical power, radiation shielding, aerodynamics and neutron physics. Due to my background as a nuclear engineer, it was proposed that I determine the initial thermal characteristics of the reactor fuel elements. In addition, I was also charged with investigating some of the hydrodynamic analysis of the core including the mass flow rates and the fluid pressure drops. If time permitted, a static stress analysis of the fuel element was also to be calculated.

Design parameters for the reactor core such as dimensions, operating temperatures and core power were preliminary estimates based on previous research of gas-cooled reactors. All design parameters were to be left as input data to the computer programs to maximize the flexibility of the iterative design process. The hexagonal fuel elements were assumed to be blocks of a graphite matrix homogeneously imbedded with TRISO[3] fuel particles. Each fuel element had six hydrogen coolant channels and one helium coolant channel. The coolant holes were assumed to be coated with ZrC.

The finite element method was chosen as the analytical tool since it can better represent irregular shapes than finite difference techniques. Several goals were projected as code development criteria. These include using standard FORTRAN 77 for tranportability from machine to machine, computational efficiency on scalar machines, vectorization on parallel machines and flexiblity in the use of the code. One non-standard FORTRAN 77 statement is used to maximize the versatility of the code. The "include" statement allows the user to write subroutines specific to his needs so that he does not have to modify the source code. By using this statement, the code does not become fixed as to what problems it can solve or what materials it can analyze. It is believed that the "include" statement is in widespread use on many FORTRAN compilers so

that portability is not seriously hampered.

Although the original intent was to solve the heat conduction equation, it was decided to solve the general quasi-harmonic equation. This increases the potential use of the code beyond heat transfer. Besides other problems dealing with Poisson's equation, diffusion type problems can also be solved. In its current state, the program is limited to linear analysis of a problem (i.e., all properties are assumed constant and spatially and time independent). Several types of boundary conditions can be implemented - Dirichlet, Neumann (either as concentrated or distributed) and mixed or Robin's type. At this time, radiative cooling is not considered.

III. THERMAL-HYDRAULIC ANALYSIS :

The two parameters that were of primary interest in the initial phases of design were the fuel element temperature distributions and the helium coolant pressure drops across the core. Since the calculations were steady-state in nature, each area could be studied independently.

The core coolant pressure drop equation is derived assuming a steady, one-dimensional and constant mass flow rate. Since the reactor is designed to operate in a space environment, gravitational forces are negligible. From the conservation of momentum, the governing differential equation is

$$\dot{m}\frac{dv}{dz} + A\frac{dp}{dz} + \frac{1}{2}\rho v^2 f P_f = 0 \qquad \text{Eq. (1)}$$

where

$\dot{m}$ = mass flow rate

v = coolant velocity

A = coolant channel cross sectional area

ρ = coolant density

f = Fanning friction factor

P_f = Frictional (wetted) perimeter

p = coolant pressure

In gas-cooled reactors, the mass flow rate is used as a primary variable rather than coolant velocity. The two are related by

$$\dot{m} = \rho v A \qquad \text{Eq. (2)}$$

In addition, since a gas is involved, it is assumed that it behaves according to the ideal gas law. The equation of state is then

$$p = \rho R T \qquad \text{Eq. (3)}$$

Non-adiabatic flow occurs in the reactor core so that a conservation of energy equation must be employed.

$$T(z_2) = T(z_1) + \frac{1}{\dot{m} c_p} \int \bar{q}_w''(z) P_h \, dz \qquad \text{Eq. (4)}$$

A chopped cosine function was used to approximate the axial flux distribution while a J_0 Bessel function approximated the radial flux profile. The averaged wall heat flux is then determined by

$$\bar{q}_w''(z) = \frac{\int q_w''(r,z) \, r \, dr}{\int r \, dr} \qquad \text{Eq. (5)}$$

Substitution of equations 2 - 4 into equation 1 allow the pressure at point z_2 to be determined. The Fanning friction factor was taken from the Colebrook-White correlation[4].

$$\frac{1}{\sqrt{f}} = 3.48 - 4 \log_{10} \left\{ 2 \left[\frac{\epsilon}{d} \right] + \frac{9.35}{Re \sqrt{f}} \right\} \qquad \text{Eq. (6)}$$

where

ϵ = root-mean-square roughness height of the coolant channel

d = channel diameter

Re = Reynolds numbers

Since the roughness was not known, ϵ was set to zero.

The coolant channel mass flow rate was derived from equations governing flow among parallel coolant channels. To simplify calculations, the hexagonal cross sectional area of the core was converted to an equivalent circle due to the Bessel function radial flux approximation. Each

successive layer of fuel elements becomes an annular ring of equivalent area. Power distributions in each ring are then area averaged over the radial flux profile.

Due to the symmetry of the assumed cylindrical core, the channel mass flow rates in a given ring will be the same. The total pressure drop along the coolant channel in the i-th ring is[4]

$$\Delta p \simeq \frac{RT_i}{2p_i} \left(\frac{\dot{m}_i}{A} \right)^2 \kappa_i \qquad i = 1,2,\ldots,N \qquad \text{Eq. (7)}$$

where $\dot{m}_i$ is a representative channel mass flow rate in the i-th ring and κ_i is the overall loss factor due to friction and momentum changes (inlet, exit and other form losses are not considered). Since the total pressure drop along each channel must be the same and knowing that the total core mass flow rate is the sum of the individual channel flow rates, a system of N equations and N unknowns can be solved to give

$$\frac{\dot{m}_i}{\dot{M}} = \frac{\text{sqrt} \left(1/\kappa_i \right)}{\sum_j \text{sqrt} \left(1/\kappa_j \right)} \; ; \quad j = 1,2,\ldots,N \qquad \text{Eq. (8)}$$

The loss factor, κ_i, is weakly dependent on $\dot{m}_i$ so that an iterative process is required to obtain the desired solutions.

IV. FINITE ELEMENT ANALYSIS :

In its present state, the finite element program solves the quasi-harmonic second order partial differential equation as a 2-D or 3-D linear boundary value problem. The governing equation is of the form

$$-\{ \nabla \}^t \left([\alpha] \{ \nabla U(r) \} \right) + \beta U(r) = f \qquad \text{Eq. (9)}$$

The first step in the finite element method is to construct a trial solution for U which is approximated by a finite sum of known functions of the form

$$\tilde{U}(r;a) = \sum_j a_j \phi_j(r) \qquad \text{Eq. (10)}$$

10-8

where a_j are the unknown degrees of freedom and $\phi_j(\mathbf{r})$ are known trial functions.

The second step in the analysis is to apply an optimizing criterion to determine specific numerical values for the a_j. Traditionally there are two types of optimizing criteria used in finite element methods. They are the method of weighted residuals and the Ritz variational method. The Galerkin method of weighted residuals was chosen as the optimizing criterion due to its ease of use and to its applicability in a wider class of problems than the Ritz method. When they are both applicable, they produce identical solutions if the same trial solution is used.

If the approximation of equation 10 is substituted into equation 9, a nonzero function called the residual of the equation would exist and would be denoted as

$$R(\mathbf{r};a) \equiv -\{\nabla\}^t ([\alpha]\{\nabla \tilde{U}(\mathbf{r};a)\} + \beta\tilde{U}(\mathbf{r};a) - f \qquad \text{Eq. (11)}$$

The parameters a_j are determined by setting the integral (over the domain) of the weighted residual to zero.

$$\int \psi_i(\mathbf{r}) R(\mathbf{r};a) \, d\Omega = 0 \qquad \text{Eq. (12)}$$

In the Bubnov-Galerkin method, the weighting functions are the trial functions themselves, $\psi_i = \phi_i$.

The integral in equation 12 must then be integrated by parts using the chain rule. Application of the divergence theorem then gives the final form of the equation that will be solved numerically. In matrix notation, this would be

$$[K^e]\{a^e\} = \{F^e\} \qquad \text{Eq. (13)}$$

where the e superscript denotes that the equations apply on an elemental level. As an example, the 2-D anisotropic equation is shown in equation 14.

Parametric mapping of the dependent variables was used since it facilitates an accurate representation of curved domains. This is accomplished by using two sets of interpolating functions – one for the coordinate transformation which describes the geometry of the element and

$$\sum_{j}^{n} a_j \left\{ \iint \left[\alpha_{11} \frac{\partial \phi_i}{\partial x} \frac{\partial \phi_j}{\partial x} + \alpha_{12} \frac{\partial \phi_i}{\partial y} \frac{\partial \phi_j}{\partial x} + \alpha_{21} \frac{\partial \phi_i}{\partial x} \frac{\partial \phi_j}{\partial y} + \alpha_{22} \frac{\partial \phi_i}{\partial y} \frac{\partial \phi_j}{\partial y} \right. \right.$$

$$\left. \left. + \beta \, \phi_i \, \phi_j \right] d\Omega \right\} = \iint f \, \phi_j \, d\Omega + \oint q_n \, \phi_j \, ds \qquad \text{Eq. (14)}$$

the other for the interpolation of the dependent variable. The degree of interpolation for each set was assumed to be equal resulting in isoparametric elements. The disadvantage of this approach is that it is difficult to compute the elemental coefficient matrices directly in terms of the global coordinates. The difficulty is overcome by introducing an invertible Jacobian transformation between the curvilinear element domain Ω^e and a master element domain Ω. The master or parent element uses natural coordinates and is of simple geometric shape so that numerical integration is accomplished easily.

The 2-D parent element library consists of a 45^0 isosceles right triangle and a square. To increase the flexibility in the use of these elements, variable noding allows the user to change the interpolation from linear to full quadratic[5,6]. Cubic interpolation elements[7] are also in the library but the user is restricted to only these elements if they are chosen since the capability of interacting with the lower order elements does not exist at this time. The 3-D parent elements consist of a tetrahedral, a prism and a brick element[8]. These elements also vary from linear to quadratic interpolations. Higher order elements are not included. All of the parent elements used are based on the serendipity family of elements, mainly to alleviate the bookkeeping chores of tracking the central node used in the Lagrangian family of elements.

Integration of equation 14 is accomplished using Gause-Legendre quadrature. In the case of the triangle, a special set developed by Cowper[9] is used. The 3-D tetrahedral is not fully implemented due to difficulty in obtaining suitable quadrature points. Several choices are offered by A.H.Stroud[10]. Integration of the line integrals for the 2-D problems follows the development outlined in reference 11. The 3-D surface

integrals have not been developed yet so that the boundary conditions are limited to only Dirichlet or concentrated loads.

The 2-D heat conduction analysis was verified by checking several example problems in various textbooks. Further work is needed in the area of the concentrated loads and additional verification is required for Neumann or Robin's boundary conditions.

The actual design problem of generating a 2-D temperature profile in the fuel element was performed using the Dirichlet boundary conditions. This was mainly due to difficulties in obtaining representative fluid heat transfer coefficients. The volumetric heat source was based on the radially averaged flux at the core centerline. Symmetry was employed such that only 1/12 of the fuel assembly needed to be analyzed. Since the actual fuel composition was not known, several values of the thermal conductivity were used to bracket the temperature ranges. Three grid meshes of varying degrees of refinement were used to check the behavior of the problem. Three matrix solving routines were employed - Cholesky decomposition, L-D-L^t decomposition and Gause-Seidel/SOR iteration. The solutions obtained with these routines were in excellent agreement implying that the solution was correct for the given conditions.

V. RECOMMENDATIONS :

Several items need further refinement or implementation into the program. Such work will be performed on a continuous basis through unfunded research. Some of the items include completing the implementation of the 3-D quasi-harmonic analysis (flux type boundary conditions), completing the 2-D plane stress/plane strain analysis (much of which has already been coded) and adding post-processing analysis including gradient determination and plotting routines.

In addition, nonlinear and transient analysis will be added. This is required for the proposed transition phase of switching from hydrogen to helium coolants. The study is expected to be a 3-D transient problem coupling heat conduction, fluid dynamics and thermal stress analysis.

10-11

This will involve other solution techniques as well as adding the Navier-Stokes equations.

A modification to the overall solution algorithm is currently under-way. The mesh that was used to analyze the fuel element temperature distribution, five different parent elements were used. However, integration over these elements was carried out each time a new element was called. This resulted in the same information being repeated exces-sively. A significant amount of computer time can be saved if the solu-tion path centers around the number of parent element shapes rather than the number of mesh elements themselves.

A second modification is to implement a new parent element library routine to generate the 2-D elements. Based on the work of El-Zafrany and Cookson[12,13], the user will have the capability of mixing the order of interpolation within a given element up to high orders. This will cor-rect the existing problem of not having transition elements between the linear/quadratic and cubic elements that currently exist in the program. The purpose is to maximize the program flexibility which in turn should minimize the size of the mesh required to model the problem. This in turn would minimize computer time and cost.

Since the code is expected to be used for other various types of prob-lems, two other element libraries are planned - infinite elements[14] and those based on Hermite polynomials. The infinite parametric elements allow economic modelling of 'infinite domain' type problems. The hermitian elements preserve the continuity of not only the dependent var-iable but also its derivative. This becomes important in many diffusion type problems.

REFERENCES

1. Angelo, Joseph A., David Buden, Space Nuclear Power, Malabar, Florida, Orbit Book Company, Inc., 1985

2. Schroeder, R.W., "NERVA - Entering a New Phase", Astronautics and Aeronautics, May 1968, pg 42

3. Gulden, T.D et al,. "The Mechanical Design of TRISO Coated Particle Fuels for the Large HTGR", Nuclear Technology, 16, 100 (1972)

4. Melese, Gilbert and Robert Katz, Thermal and Flow Design of Helium-Cooled Reactors, La Grange Park, Illinois, American Nuclear Society, 1984

5. Bathe, Klaus-Jurgen, Finite Element Procedures in Engineering Analysis, Englewood Cliffs, New Jersey, Prentice-Hall, Inc., 1982

6. Cook, Robert D., Concepts and Applications of Finite Element Analysis, Second Edition, New York, New York, John Wiley & Sons, 1981

7. Reddy, J.N., An Introduction to the Finite Element Method, New York, New York, McGraw-Hill Book Company, 1984

8. Gartling, D.K., "Coyote II - A Finite Element Computer Program for Nonlinear Heat Conduction Problems, Part I - Theoretical Background", SAND86-1844, Sandia National Laboratory, Albuquerque, New Mexico, July 1987

9. Cowper, G.R., "Gaussian Quadrature Formulas for Triangles", Int J Num Meth Eng, 7, 1973, pp 405-408

10. Stroud, A.H., Approximate Calculation of Multiple Integrals, Englewood Cliffs, New Jersey, Prentice-Hall, Inc, 1971

11. Burnett, David S., Finite Element Analysis, Reading, Mass., Addison-Wesley Publishing Company, 1987

12. El-Zafrany, A and R.A. Cookson, "Derivation of Lagrangian and Hermitian Shape Functions for Quadrilateral Elements", Int J Num Meth Eng, 23, 1986, pp 1939-1958

13. El-Zafrany, A and R.A. Cookson, "Derivation of Lagrangian and Hermitian Shape Functions for Triangular Elements", Int J Num Meth Eng, **23**, 1986, pp 275-285

14. Beer, G. and J.L. Meek, " 'Infinite Domain' Elements", Int J Num Meth Eng, **17**, 1981, pp 43-52

1987 USAF-UES SUMMER FACULTY RESEARCH PROGRAM/

GRADUATE STUDENT SUMMER SUPPORT PROGRAM

Sponsored by the

AIR FORCE OFFICE OF SCIENTIFIC RESEARCH

Conducted by the

Universal Energy Systems, Inc.

Final Report

AIR FORCE OFFICER SELECTION REVISITED: ENTERTAINING

THE POSSIBILITIES FOR IMPROVEMENT

Prepared by: Victor H. Appel, Ph.D./ Andrew Carson

Academic Rank: Associate Professor / Graduate Student

Assisted by: Andrew D. Carson, M.A.

Academic Rank: Doctoral Student

Department and   Educational Psychology

   University   The University of Texas at Austin

Research Location: Air Force Human Resources Laboratory
                      Air Force Systems Command
                      Brooks AFB, Texas 78235-5601

USAF Researcher: Thomas W. Watson, Ph.D.

Date: September 20, 1987

Contract No: F49620-85-C-0013

REFERENCE DR. APPEL

SFRP FINAL REPORT NUMBER 4

1987 USAF-UES SUMMER FACULTY RESEARCH PROGRAM

GRADUATE STUDENT SUMMER SUPPORT PROGRAM

Sponsored by the

AIR FORCE OFFICE OF SCIENTIFIC RESEARCH

Conducted by the

Universal Energy Systems, Inc.

FINAL REPORT

CONSTRUCTION OF A PHASE CONJUGATE LASER RESONATOR USING

BRILLOUIN ENHANCED FOUR WAVE MIXING

Prepared by: Kyunam Choi

Academic Rank: Graduate Student

Department and   Department of Physics and Astronomy

  University: University of New Mexico

Research Location: USAFWL/ARBM
                        Kirtland AFB, NM 87117-6008

USAF Researcher: Dr. Chris Clayton

Date: July 30, 1987

Contract No: F49620-85-C-0013

CONSTRUCTION OF A PHASE CONJUGATE LASER RESONATOR USING

BRILLOUIN ENHANCED FOUR WAVE MIXING

by

Kyunam Choi

ABSTRACT

A study on the realization of a phase conjugate laser resonator
employing the Brillouin enhanced four wave mixing as its main
phase conjugation mechanism is discussed. The resonator output
beam can maintain monochromatic laser wavelengths with excellent
temporal and spatial beam profile while enjoying high phase-
conjugate fidelity. Details on experimental procedures together
with experimental results are reported.

ACKNOWLEDGEMENT

I would like to express my sincere gratitude to the Air Force
System Command and the Air Force Office of Scientific Research
for sponsoring the Graduate Student Summer Support Program
which made my research effort possible. Also I would like to
thank the Universal Energy Systems for administering such a
wonderful program.

The laboratory experience at the Air Force Weapons Laboratory
was so valuable to me that I cannot thank enough those who
helped me during the precious ten week period and after.
Especially, I would like to thank Dr. Chris Clayton and Capt.
Antonio Corvo for initiating my interest in GSSSP and supporting
me throughout the whole research period. My sincere gratitude
and respect extends to Dr. Jack McIver of the University of
New Mexico for leading me to the research topic and encouraging
me to overcome many technical difficulties with his kind advice.
I would like to thank Capt. Lee Schelonka and Dr. Mark Kramer for
their excellent advice and limitless help on experiments which
brought significant progress in my research effort. Mr. Dave
Martinez, Lt. Charles Wetterer and Miss Sally Sifuentes provided
me with warm support and a truly enjoyable working atmosphere. I
would like to thank Mr. Jim Carlisle and Mr. Y. S. Kuo of UNM for
many useful discussions and help.

I. INTRODUCTION

Optical phase conjugation (OPC) is a technique that utilizes the nonlinear properties of materials to do exact reversal on both the propagation direction and phase of each plane wave component in an arbitrary beam of light. The ability to do "time reversal" on aberrated beams gives us a lot of advantages over conventional optical beam manipulations.

There are two popular ways of achieving OPC; stimulated Brillouin scattering (SBS) and four-wave mixing (FWM). SBS is the self-reversal of the laser beam under a stimulated scattering process involving build up of a dynamic density grating in the medium due to the interaction of the pump and the stimulated scattering beam. The reflectivity of the SBS process is always less than one while the phase conjugate fidelity (PCF) remains high. SBS also requires simpler optical geometries compared to that of FWM which requires counter-propagating pump beams and a probe beam. FWM gives reflectivities greater than unity which makes FWM more useful than SBS in some applications.

Foremost among the applications of PC in lasers is the use of phase-conjugate mirrors (PCMs) in a laser resonator. There are several characteristics unique to phase-conjugate resonators (PCRs) as discussed by Auyeung et al. (1978). One of the key

12-4

features of PCR is the compensation of static and dynamic intra-
cavity polarization and phase aberrations due to gain medium
distortion and poor quality optical components. Other features
include excellent frequency and transverse mode stabilization and
automatic Q-switching by temporarily pumping the PCM. PCRs using
SBS require a threshold pump energy and their PC reflectivities
remain less than unity. Also, there is a progressive Brillouin
frequency downshift everytime SBS is taking place.

PCRs using FWM can give us more than unity reflectivity without
any frequency shift. The requirement for counter-propagating pump
beams is one disadvantage of FWM PC.

Brillouin Enhanced Four Wave Mixing (BEFWM) is a relatively new
PC technique in which any one of the two counter-propagating
pump beams and the probe beam is frequency shifted from the other
two beams by the Brillouin frequency of the FWM medium (Andreev,
1980; Bespalov,1979; Efimkov,1984). The PCR using BEFWM is quite
attractive since we can take advantages of both SBS and FWM PC
processes while removing their disadvantages by using the two
mechanisms complementarilly to each other (Damzen,1987).

My research interest during the last three years was mainly on
SBS and its applications on PCR. Studies on degenerate FWM were
also done. The research effort at AFWL demands the realization of

PCRs which emit diffraction-limited output beams from the conventional mirror end of the resonator with all the aberrations corrected by "time reversal" process. The construction and characterization of a PCR using BEFWM which is the most advanced nonlinear optical process leading to the realization of an ideal PCR has attracted interest among many scientists including those at AFWL.

II. OBJECTIVES OF THE RESEARCH EFFORT:

In the past, the study on BEFWM has been confined to the investigation of basic physics behind the phenomena. The application of BEFWM to PCR construction was first reported on January 1987 by Damzen and others. There is no doubt, however, that as the advantages of PCR using BEFWM becoming better understood, more and more applications will be developed.

My assignment as a participant in the 1987 Graduate Student Summmer Support Program (GSSSP) was to follow all the steps leading to the successful demonstration of PCRs using BEFWM and determine the possibilities of extending the technique beyond the limit of the current level of application.

The experimental investigation requires a pulsed, 1.06 μm single
longitudinal mode beam from a Nd:YAG laser at an energy level of
10 to 30 mJ per pulse energy. Since BEFWM requires a high quality
counter-propagating pump beam generated by SBS, we also had to
work on making an efficient and reliable SBS PC without any feed-
back into the pump laser system. The next stage of work involved
the generation of frequency downshifting and upshifting BEFWM i.e.
The frequency downshifting BEFWM has been known to generate 90%
reflectivity for very weak probe beams. Reflectivities and other
details were not known for frequency upshifting BEFWM. The final
goal was the demonstration of PCR making both frequency upshifting
and downshifting BEFWM processes take place in turn in a ring-like
PCR configuration as is in Fig.3. For frequency downshifting
BEFWM the p-polarized input pump beam is reflected by a moving
acoustic grating formed by the interference of s-polarized probe
beam and counter-propagating pump beam in the FWM medium. The
dynamic grating moves along the same direction with the input
pump beam so that the phase conjugated beam have the Brillouin
downshifted frequency from the pump laser frequency. For frequency
upshifting BEFWM the acoustic grating is moving toward the
counter-propagating pump beam. The alternating up and down shift-
ing of the frequency in the ring resonator makes the output
frequency of the laser beam remain the same at all times.

To make use of the pump beams more efficiently we designed a
double ring type BEFWM PCR which incorporates one unidirectional

ring type cavity on the pump side and another ring on the PCR side.
With the help of AFWL in both experimental instrumentation and
technical assistance I was able to follow all the steps leading to
the demonstration of BEFWM PCR. The steps are summarized as
follows:

(1) Acquisition and characterization of a Q-switched Nd-YAG laser
    with beam characteristics suitable for the experimental
    purposes.

(2) Generation of reliable SBS PC that will serve as a counter-
    pump beam.

(3) Demonstration and investigation on frequency up and down
    shifting BEFWM respectively including the effect of pump-
    probe ratio over efficiency.

(4) Realization of successive frequency up and down shifting
    process in the ring type oscillator.

(5) Establishment of long-lasting laser oscillation of BEFWM PCR
    with the addition of an amplifying unidirectional ring cavity
    on the pump part.

We were able to get results in steps (1),(2),(3) and part of (4).
Currently, we are working on the steps (4) and (5). Let's review
in detail each steps that has been accomplished until now.

III.   EXPERIMENTS AND RESULTS

a.   The laser beam should have a sufficiently long coherence
length to ensure efficient SBS and BEFWM generation. The laser
used in the experiment was dye Q-switched. The insertion of a
4% etalon in the oscillator cavity was sufficient to generate 100
percent single longitudinal mode oscillation. We measured the
spectral linewidth of the laser beam using a Fabry-Perot inter-
ferometer and found that the bandwidth is narrower than 0.1 cm^{-1}.
Fig. 1 is a schematic diagram of the oscillator-amplifier setup.
A 75cm-long oscillator with single longitudinal and transverse
mode laser output is followed by a double-pass two-rod amplifying
stage which generates 1.06μm laser beams of 100mJ maximum-output
energy per pulse with a 50nsec pulse duration at FWHM. The typi-
cal pump input energy to the PCR setup was between 10 and 50 mJ
per pulse. The beam diameter was 0.6cm. Fig.2(a) shows the
oscilloscope trace of the laser beam whose smooth temporal
profile indicates its single longitudinal mode oscillation

b.   The SBS efficiency attained was typically 60% with 70% being
the maximum. The SBS cell was a 10cm-long cylindrical container
made of Pyrex with a 2.3cm inner diameter. The SBS medium was
carbon-disulfide(CS_2). A focusing lens of 5cm focal length was
used. The SBS phase-conjugated beam enters the FWM cell as a
counter-propagating pump with its frequency Brillouin-downshifted

from the original laser frequency. The cube polarizer and quarter-wave plate combination works as an optical isolator which prevents the feedback of the SBS beam into the pump laser. The advantages of using SBS PC for generation of the counter-propagating pump was extremely large over the use of conventional mirrors since the retroreflected SBS PC beam retraced all the pump beam path automatically. Pulse compression took place in the SBS process and the 50nsec FWHM pump pulse was compressed to 40nsec. Fig.__(b) shows the SBS PC waveform.

c. The BEFWM took place in a CS_2 -filled cell of 13cm length and 2cm inner diameter. The cell was made of stainless steel and has uncoated Pyrex windows of 0.3cm thickness on both ends. The angle between the pump and probe beam in the FWM cell was about 1.6 degrees which was small enough to ensure phase matching in the BEFWM process. We performed experiments on frequency downshifting BEFWM only until we became familiar with that case. After that we moved into the frequency upshifting case. The maximum reflectivity of frequency downshifting BEFWM was about 21% with pump probe ratio of 35 to 1 while the reflectivity for frequency upshifting BEFWM was measured to be about 7%. To enhance the FWM efficiency we used a waveguide-like 40cm-long and 0.5cm-diameter copper tube filled with CS_2 as a FWM cell. But the expected enhancement did not take place. We are planning to use a copper tube with smaller bore diameter incorporated with a telescope

to match the beam diameter to the bore diameter. The schematic
diagram of the BEFWM PCR setup used in the experiment is shown
in Fig.3 with all the measured pump and probe energies listed on
it. Fig.2(c) and Fig.2(d) are the waveforms of the frequency
downshifted and upshifted BEFWM PC beam respectively. They show
appreciable pulse compression with a compression ratio of 2 to 1
from the original pump beam.

d. Without the use of any amplifying medium in the PCR ring
cavity we were able to demonstrate single round trip BEFWM PC
oscillation. A frequency downshifted BEFWM PC beam with an energy
1mJ per pulse was used as the probe beam for the frequency
upshifting process. This yielded a PC beam of about 0.07mJ per
pulse. Fig.2.(d) is the waveform of the frequency upshifting
BEFWM which was generated in the PCR ring cavity by using the
beam of Fig.2.(c) as the probe beam. If we insert an amplifying
medium with a gain of 3 or more in the PCR ring, we will be able
to see successive ring oscillations. Currently, we are building
an Nd:YAG amplifier with variable gains which will be used in
the PCR ring.

VI. RECOMMENDATIONS:

a. BEFWM scheme is far superior to any other FWM schemes since BEFWM uses the SBS PC beam as counter-propagating pump beam. This eliminates all the stringent mirror alignment problems we encounter in conventional FWM geometry.

b. We need to investigate the means of obtaining high efficiency FWM to get higher output energy from PCR using BEFWM. Current efficiency of around 20% should be enhanced by the use of waveguide-type FWM cell with suitable geometries.

c. While working on the project we arrived at the concept of using an unidirectional ring cavity for recycling the unused portion of the pump beam in the SBS process so that we can have multiple pump turn-on time. The PCR output beam will be a train of pulses if the amplification factor is sufficient. We believe that it will bring us the most rewarding advancement in BEFWM PCR study. Currently, we are building an amplifying stage that will be used in the unidirectional ring to amplify the recirculating pump laser beam. The schematic diagram in Fig.4. shows how the unidirectional ring works. Since the pump probe ratio for frequency downshifting BEFWM is fixed to one, the whole system treats the pump beam from the pump laser and the recycled beam equally.

REFERENCES

1. Andrev,N.F.,V.I.Bespalov,A.M.Kiselev,A.Z.Matreev,G.A.Pasmanik, and A.A.Shilov,JETP Lett.,Vol.32,1980,p.625.

2. Auyeung,J.,D.Fekete,D.M.Pepper,and A.Yariv,"A Theoretical and Experimental Investigation of the Modes of Optical Resonators with Phase-conjugate Mirrors",IEEE J. of Quantum Electronics, Vol.QE-15,No.10,October 1978,pp.1180-1188.

3. Bespalov,V.I.,A.A.Betin,G.A.Pasmanik,and A.A.Shilov,Sov. Tech. Phys. Lett.,Vol.5,1979,p.97.

4. Demzen,M.J.,M.H.R.Hutchinson,and W.A.Schroeder,"Single-frequency Phase-conjugate Laser Resonator Using Stimulated Brillouin Scattering",Optics Letters,Vol.12,No.1,January 1987,pp45-47.

5. Efimkov,V.F.,I.G.Zubarev,S.I.Mikhailov,M.G.Smirnov,and V.B. Sobolev,Sov.J.Quantum Electronics,Vol.14,1984,p.909.
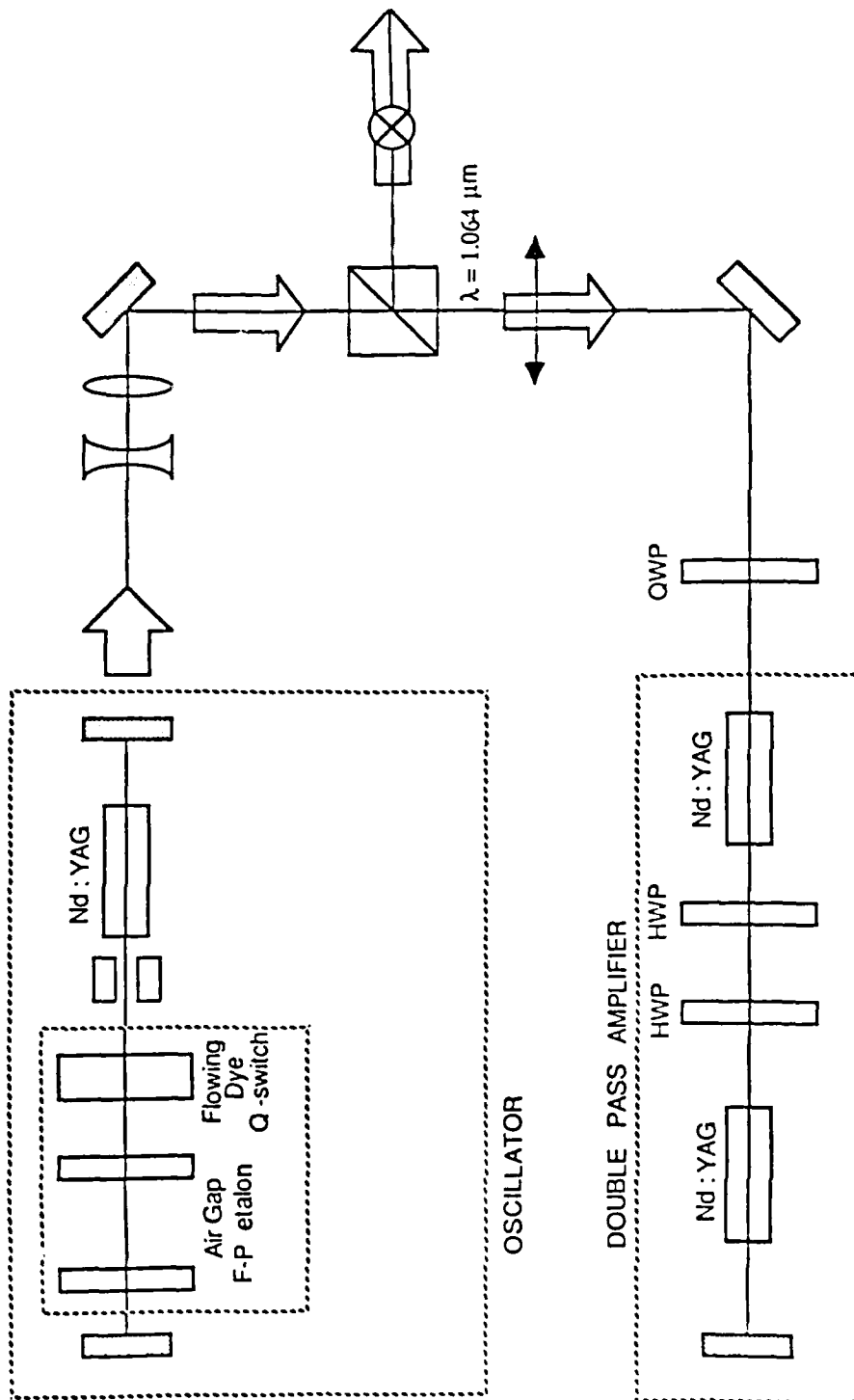
FIG. 1. THE PUMP LASER SETUP
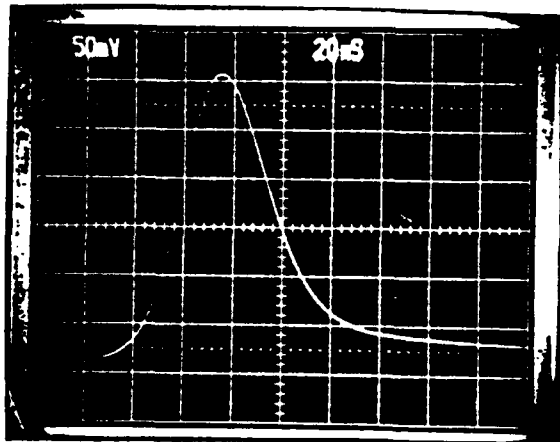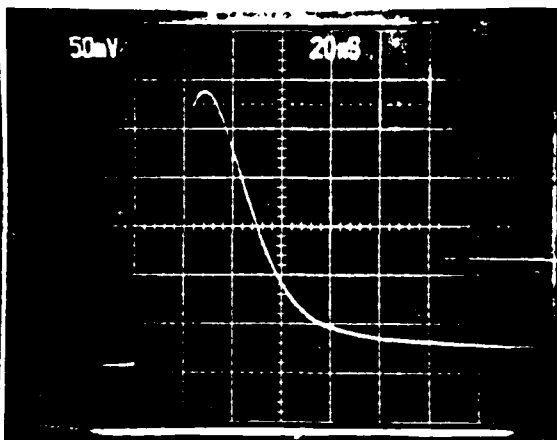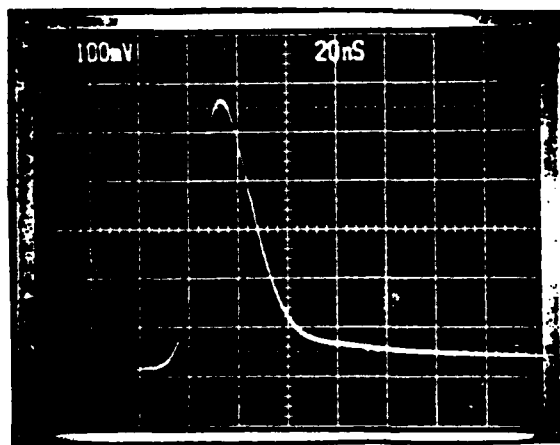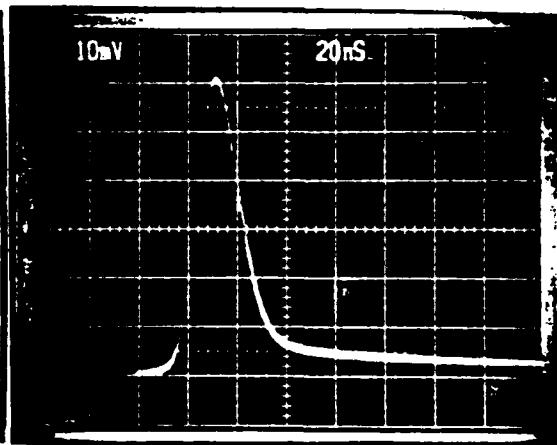
FIG.2. THE OSCILLOSCOPE TRACE OF (a) PUMP LASER BEAM, (b) SBS PC BEAM,
(c) FREQUENCY DOWNSHIFTING BEFWM AND (d) FREQUENCY UPSHIFTING
BEFWM
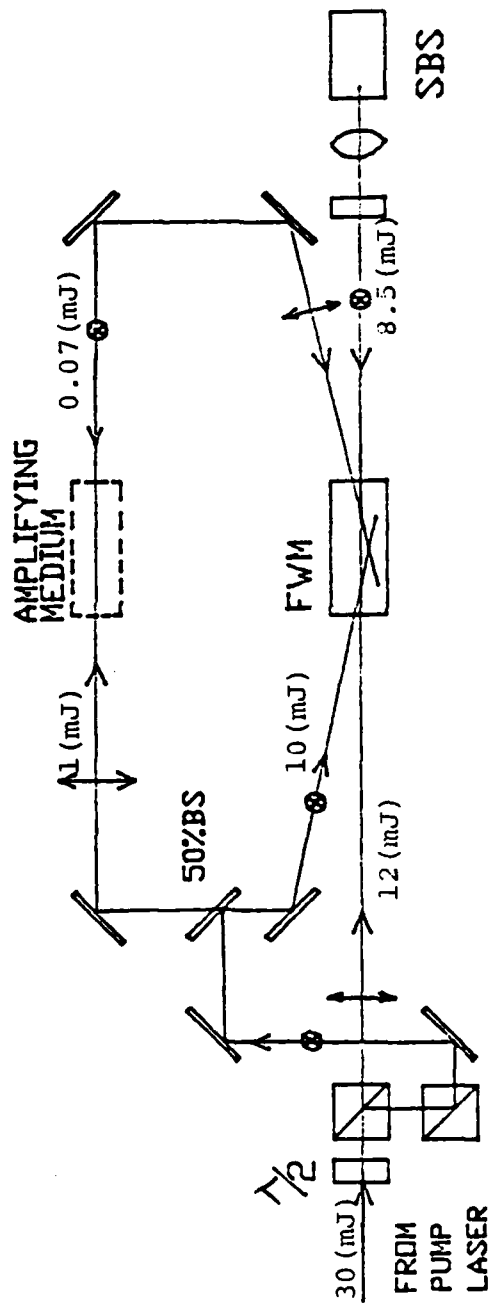
FIG.3. THE BEFWM PCR SETUP

12-16
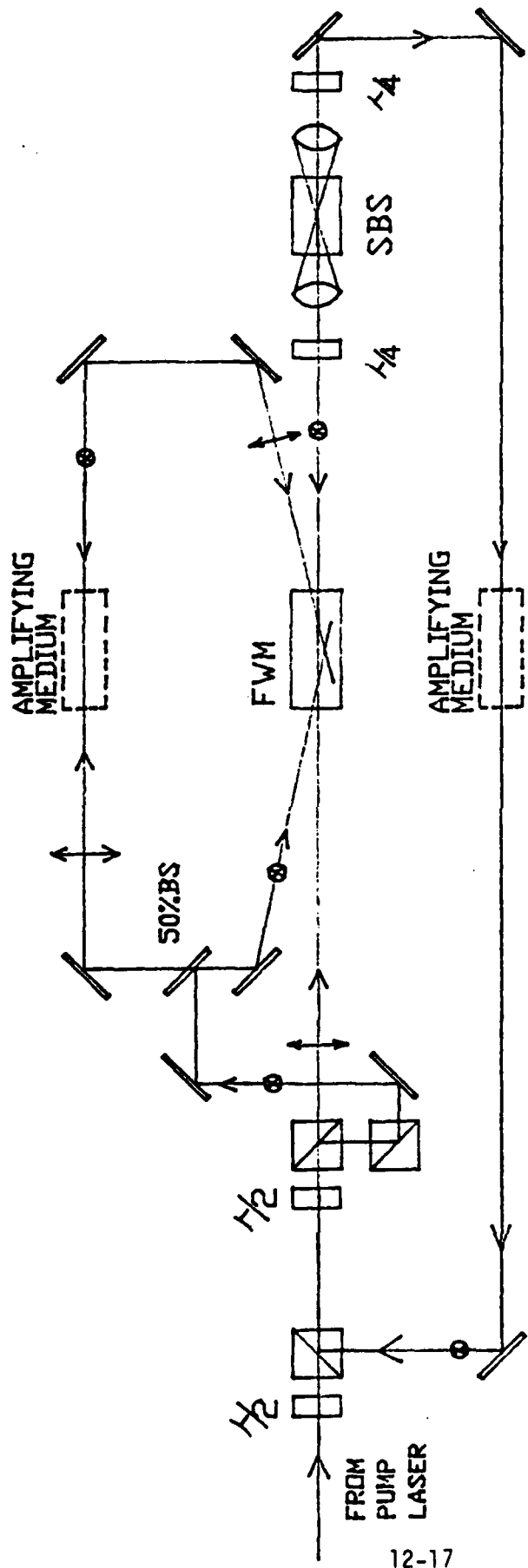
FIG.4. THE DOUBLE RING BEFWM PCR SETUP

12-17

1987 USAF-UES SUMMER FACULTY RESEARCH PROGRAM

GRADUATE STUDENT SUMMER SUPPORT PROGRAM

Sponsored by the

AIR FORCE OFFICE OF SCIENTIFIC RESEARCH

Conducted by the

Universal Energy Systems, Inc.

FINAL REPORT

Effect of Repeated Low Dose Soman On Acetylcholinesterase Activity

Prepared by: Mohammed A. Maleque, Ph.D.
                                  with Antionne Able and Otis Cosby, Jr.

Academic Rank: Associate Professor

Department: Pharmacology

University: Meharry Medical College
                                  Nashville, Tennessee

Participants: Antoinne C. Able
                                  Otis Cosby

Research Location: USAFSAM/RZB
                                    Brooks AFB
                                    San Antonio, TX 78235

USAF Researcher: Lt. Col. Stan L. Hartgraves

Date: 28 August 87

Contract No: F49620-85-C-0013

REFERENCE DR. MALEQUE

SFRP FINAL REPORT NUMBER 87

1987 USAF-UES SUMMER FACULTY RESEARCH PROGRAM/

GRADUATE STUDENT SUMMER SUPPORT PROGRAM

Sponsored by the

AIR FORCE OFFICE OF SCIENTIFIC RESEARCH

Conducted by the

Universal Energy system, Inc.

FINAL REPORT

TEN WEEKS OF LITERATURE SEARCHES AND COPYING

Prepared by:	Brant Davidson
Academic Rank:	Graduate Student
Department and	Mathematics
University:	University of Alabama at Birmingham
Research Location:	AFWAL/MLPO WRIGHT-PATTERSON AFB DAYTON, OHIO
USAF Researcher	Dr. Chu
Date:	August 19,1987
Contract No:	F49620-85-C-0013

TEN WEEKS OF LITERATURE SEARCHES AND COPYING

by

Brant Davidson

ABSTRACT

The first seven weeks of the project in Dayton were spent researching articles and books for Dr. Chu, the professor I was working for. Late in the ten week period that the project ran Dr. Chu presented me with 150 page computer program, originally written by H.L. Skriver of Risoe National Laboratory in Denmark, to copy in to a computer text file from which it could be compiled. The program is designed to calculate the band structure of certain types of superlattices. Unfortunately, it was impossible to run the program during the ten week period of my employment due to lack of time and the fact that the author forgot to specify the purpose of certain functions that are essential to the program. Dr Chu, the professor I am working for, expresses hope that he will be able to find a way to run the program running once he returns to Taledega.

ACKNOWLEDGMENTS

I would like to thank the United States Air Force Systems Command and the Air Force Office of Scientific Research for sponsorship of this research. I would also like to thank Universal Energy Systems for the opportunity to work at the Materials Laboratory and I deeply regret that the experience did not achieve the potential it had.

I would also like to state my deepest appretiation to Dr Pat Hememger, the leader of the MLPO inhouse research program, Steve Bucey, a graduate student at Kent State University, and Elizabeth Smela, a graduate student at the University of Pennsylvania. Their support, friendship, ideas, and help were invaluable during this experience.

I would also like to thank Laura Rea and Lt. Chris Phenicie for their help in finding a place for me to stay while I was in Dayton and in arranging some means of transportation to and from the base.

In addition, I wish to thank all the employees of MLPO who helped me in any way during my ten weeks with them. I may not remember every bit of help I received, but I am grateful for it nonetheless.

I. INTRODUCTION:

I am a graduate student in the field of mathematics. I am currently attending the University of Alabama at Birmingham while I try to attain my Master's degree. My interests lie in the areas of abstract theoretical mathematics, particularly set theory, topology, and differential geometry. In addition to my Bachelor's degree in mathematics I also have a Bachelor's degree in computer science. I have some limited practical experience working on computer programs to solve complicated mathematical problems.

About six months ago, Professor Chu of Taledega College had a friend of his at UAB distribute a memo asking graduates students with a mathematical background and experience with computers to apply for a high-paying summer job. Reading what few details were given in this memo, I doubted that I was really qualified for this job, but I did meet the basic requirements and I needed the money, so I applied.

Several weeks later, Dr Chu's friend called the four people on his list that met the unstated requirement of being american born and informed us that, if we still wanted the job, we must call Dr. Chu immediately. I happened to be in my office at the time, so I was able to call Dr. Chu right after his friend called me. I talked with Dr. Chu for a minute or so, and then he informed me that the application forms had to be in U.E.S.'s main office the next morning or he would be unable to bring a graduate student with him. I had a friend drive me the 50 miles to Taledega, I

filled out the forms, and sent them to U.E.S. by Federal Express, barely beating the time limit. Since I was being sponsored by a professor, I was automatically accepted.

In any event, this is how I came to work with Dr Chu, a man I never met before, at MLPO on the calculation of the band stucture of superlattices, a field that I knew nothing about.

II. OBJECTIVES OF THE RESEARCH EFFORT

When we met again at MLPO, Dr. Chu said that I would be responsible for creating and executing computer programs designed to calculate the band structure of superlattices and that, inorder to do this, I would have to do some mathematical modeling of the eigenvalue problem involved in these calculations. Without going into further detail on how I would do this, Dr. Chu kept me busy for the next few weeks doing literature researches, copying articles, and locating and checking out books for him from the technical library that was on the base.

Somewhere around the second or third week of the summer employment, Dr. Chu told me that he had heard of a computer program that would do the calculations we needed done and that, as soon as a copy of it arrived, all I had to do was type this program in. He gave me a few pages of the program and I went ahead and typed these into the computer.

On or about the fourth or fifth week of my ten week stay, Dr. Chu asked me to look into creating a computer program to diagonalize square matrices so that the eigenvalues and eigenvectors of such matrices could be found. I quickly located a program that someone else in the lab had written for diagonalizing real skew symmetric matrices. This is the most general form of matrices that has a known algorithm for how to diagonalize them. I explained this to Dr. Chu and he never mentioned the program to me

again nor did he request that I key it in.

While I was looking for a program to diagonalize square matrices, Dr. Chu requested that I evaluate the integral

$$\int_0^{r_{max}} r\,dr \int_0^{\infty} x^{1/2} \, Ai(x+1/r) \; dx \qquad (1)$$

when I was not doing literature researches or similar activity. I was informed that evaluation of this integral was unimportant and should only be done when no other work was available.

About three weeks before the end of ~~the end of~~ my stay in Dayton, the copy of the program that Dr. Chu had sent for arrived and I was promptly taken off literature searches and told to type the program into text files so that they could be compiled and run. I spent my last three weeks in Dayton typing in this one hundred and fifty page program.

III.

The computer program that Dr. Chu gave me actually consisted of five separate programs, each of which was developed by H.L. Skriver of the Risoe National Laboratory in Denmark. The programs were named STR, COR, LMTO, DDNS, and SCFC.

a.   STR purpose was to calculate canonical structure constants. The program is executed once for a given crystal structure. The input for STR is the translational vectors spanning the unit cell of the crystal and the basis vectors giving the positions of the

individual atoms in the cell. The output is a set of structure-constant matrices distributed on a suitable grid in an irreducible wedge of the Brillouin zone which is stored in a disk file.

b.   COR is used to calculate those extra structure constants which may be used for approximate treatment of the region between the sphere and the atomic polyhedron, and for the neglect of higher component. It is typically executed once for a given crystal structure. The input for COR is the basis vectors giving the positions of the atoms in the cell and the reciprocal-space vectors generated by STR. The ouput for COR is the correction-term structure constants used by LMTO to perform band calculations.

c.   LMTO is used to calculate band structure. It uses as input the structure-constant matrices generated by STR, the correction-term structure-constant matrices generated by COR — if it is to be used — and potential parameters as given at run time. LMTO's output is the eigenvalues evaluated at the k mesh established in STR.

d.   DDNS is designed to evaluate projected state densities and corresponding number of state functions by means of the tetrahedron technique. The input used is the eigenvalues generated by LMTO. The output of the calculated functions is stored on disk and may be retrieved later.

e.   SCFC is designed to solve the energy-band problem self-

consistently by means of the canonical scaling principle including hybridisation. SCFC treats only the outermost s, p, d, and f electrons while the charge density of the remaining electrons is kept fixed. The input fo SCFC is the projected state densities and number-of-states functions generated by DDNS. The ouput is the self-consistent potential parameters and the electronic pressure.

Each of these programs was typed into text files accessible thru the Prime System available at MLPO and compiled using the FORTRAN 77 compiler on that system. Unfortunatly, there were certain functions that the author did not give the code for, and so it was impossible to run the programs. Even if those functions had been specified, however, the program still could not have been run do to lack of time. Dr. Chu believes that he can get a friend of his at Auburn University to help him replace the unknown functions and run the program once he returns to Alabama.

IV.

The formula labeled (1) proved to be unusually difficult to integrate because of the complexity of evaluating the Airy function, $Ai(x)$, at arbitrary vaues of x, my lack of experience at solving partial differential equations, and also because of the small amount of time and emphasis that I was given to work on it. I eventually decided that the best way to proceed would be to approximate $Ai(x)$ as zero for some sufficiently high value of x, which is reasonable since $Ai(x)$ approaches zero rapidly, and then to apply backwards interpolation to get the other values I needed.

Once I had these values I could apply Swartz approximation twice to evaluate the integral. I was unable to do this because Dr. Chu gave me Skriver's program to type in with instructions to concentrate on that task first.

Since I was unable to run the program or evaluate the integral, I have no results to report. I am certain that a summuray of the library searches can be found in Dr. Chu's final report.

V. RECOMMENDATIONS

Since there are no results, any recommendation I could make would be unfounded. In fact, since I have no training in applied research physics and have virtually no knowledge of what I was suppossedly doing this summer, I would say that — if there were any results — any recommendation I could make should be ignored.

REFERENCES

Skriver, H.L., Comments and descriptions of the programs STR, COR, LMTO, DDNS, and SCFC from the book he wrote on them. Title is unknown, published sometime in 1983, pp 124-290.

1987 USAF-UES SUMMER FACULTY RESEARCH PROGRAM/

GRADUATE STUDENT SUMMER SUPPORT PROGRAM

Sponsored by the

AIR FORCE OFFICE OF SCIENTIFIC RESEARCH

Conducted by the

Universal Energy Systems, Inc.

FINAL REPORT

Ambiguity and Probabilistic Inference in a

Missile Warning Officer Task

Prepared by: Tamara J. Della-Rodolfa, B.S.

Academic Rank: Graduate Student

Department and   Department of Psychology

  University: Indiana University of Pennsylvania

Research Location: AAMRL/HE
                      Wright-Patterson AFB
                      Dayton OH 45433

USAF Researcher: John Forester

Date: 10 July 87

Contract No: F49620-85-C-0013

REFERENCE DR. ROBERTSON

SFRP FINAL REPORT NUMBER 115

1987 USAF-UES SUMMER FACULTY RESEARCH PROGRAM/

GRADUATE STUDENT SUMMER SUPPORT PROGRAM

Sponsored by the

AIR FORCE OFFICE OF SCIENTIFIC RESEARCH

Conducted by the

Universal Energy Systems, Inc.

FINAL REPORT

MODELING RATES OF HALOCARBON METABOLISM (VMAX)

USING QUANTITATIVE STRUCTURE-ACTIVITY RELATIONSHIPS (QSAR)

Prepared by:	Steve Dixon
Academic Rank:	Graduate Student
Department and University:	Chemistry Department Wright State University
Research Location:	AAMRL/THB Wright-Patterson AFB Dayton, OH 45433
USAF Researcher:	Dr. Melvin E. Andersen
Date:	20 Sept 87
Contract No:	F49620-85-C-0013

MODELING RATES OF HALOCARBON METABOLISM (VMAX)

USING QUANTITATIVE STRUCTURE-ACTIVITY RELATIONSHIPS (QSAR)

by

Steve Dixon

ABSTRACT

Vmax values were obtained in vivo with male rats for chlorinated
methanes, ethanes and ethenes by gas uptake methods. A QSAR study of Vmax
was carried out with electronic and steric chemical descriptors. Partial
atomic charges served as electronic parameters. Chlorine substitution
patterns were used to imply steric information. For 10 well-metabolized
chemicals, the best 2-term fit ($r^2=0.981$) involved the sum of all hydrogen
charges in the molecule and the difference between the numbers of chlorines
and hydrogens on the least substituted carbon. Two poorly metabolized
chemicals (CCl_4 and CH_3CCl_3) were added to the data set and a more quali-
tative approach taken. For methanes and ethanes, metabolism required a
chlorine and hydrogen on the same carbon; in methanes with two or more
chlorines, the effect of replacing a chlorine with a methyl group is
slight and predictable; for ethanes and ethenes, larger Vmax occur for
chemicals with two nonequivalent carbons. These structural features were
combined with a connectivity index and quantitated in a 3 parameter fit
($r^2=0.934$).

ACKNOWLEDGMENTS

I wish to thank the Air Force Systems Command and the Air Force Office of Scientific Research for sponsorship of the USAF-UES Graduate Student Summer Support Program.

Several individuals at the Armstrong Aerospace Medical Research Laboratory Toxic Hazards Division, Wright-Patterson Air Force Base were very helpful throughout the research period. My Effort Focal Point Dr. Melvin E. Andersen provided a clear direction for the research and was the source of many insightful discussions. I wish to thank Michael L. Gargas of the Biochemical Toxicology Branch for his guidance in a number of technical matters and for his help in familiarizing me with the operations of the Toxic Hazards Division. Finally, Jim Stokes of Northrop Services, Inc. should be recognized for his work in the installation and debugging of computer software I obtained.

I. INTRODUCTION:

Halogenated methanes, ethanes and ethenes are widespread environmental contaminants and a knowledge of the kinetics of their metabolism is essential to understanding their physiological effects. The parameter Vmax is the maximum metabolic rate of a chemical in saturable metabolism. Estimates of Vmax have been obtained in vivo using gas uptake studies (Gargas et al., 1986). The Biochemical Toxicology Branch of the Toxic Hazards Division at the Armstrong Aerospace Medical Research Laboratories, Wright-Patterson Air Force Base is interested in quantitatively modeling halocarbon Vmax values in terms of parameters derived from molecular modeling techniques applied to the structure of each chemical. Such a quantitative structure-activity relationships (QSAR) study could supply a means of estimating metabolic constants for halocarbons for which no kinetic data exist. Moreover, the process of deriving suitable modeling parameters from chemical structure should result in a deeper understanding of the chemistry involved in the metabolism of the halocarbons.

My research has been in the fields of molecular modeling and QSAR. I have had extensive experience in the use of various molecular orbital programs and I have developed a great deal of software to link the molecular modeling packages in use at Wright State University. In addition to a QSAR study of Vmax, the Biochemical Toxicology Branch was interested in obtaining a system of molecular modeling programs similar to those at Wright State University. My experience with these programs and in QSAR led to my appointment.

II. OBJECTIVES OF THE RESEARCH EFFORT:

Like all chemical processes, metabolism should be governed by a combination of electronic and steric factors. For oxidative metabolism (eg., the P-450 metabolism of halocarbons), it is reasonable to assume that positive centers on the substrate molecule are favorable sites for attack. Halogens pull electrons from nearby carbons and thus create positive centers. However, halogens are also bulky and may hinder a nucleophilic attack directed at the carbon to which they are bonded. One of the objectives, then, was to develop electronic and steric chemical descriptors which reflect the likelihood of nucleophilic attack at the positive centers in each halocarbon molecule. To simplify the problem, the data set was restricted to strongly metabolized chlorinated methanes, ethanes and ethenes. The appropriate chemical descriptors can be used as independent variables in a least-squares fit of the experimental Vmax values. The resulting multiple linear regression equation provides a means of estimating maximum metabolic rates for chlorocarbons outside the original set.

Later in the research project, a more qualitative approach was taken. Here, effort was directed at examining trends in simple chemical structure of the chlorocarbons and searching for any corresponding trends in Vmax. Of particular interest was the observation that tetrachloromethane and 1,1,1-trichloroethane are virtually non-metabolized. The objective was to find criteria for appreciable saturable metabolism of the chlorocarbons. Refining the criteria could lead to more quantitative information on Vmax.

III.

In developing electronic and steric parameters, the data set was
was limited to the 10 chemicals in Table 1. The Vmax values were deter-
mined previously from gas uptake studies and physiological modeling (Gargas
et al., 1986).

Electronic information was initially obtained through all valence
electron semiempirical molecular orbital calculations (Jaffe, 1969). First,
the molecular geometry of each chemical was optimized using the AM1 quantum
mechanical molecular model (Dewar et al., 1985). This involved a search
for the geometry giving the lowest total energy as prescribed by the AM1
Hamiltonian operator. The optimized structures were then used as input
for INDO/1 (Intermediate Neglect of Differential Overlap) molecular orbital
calculations (Pople et al., 1967; Ridley and Zerner, 1973). Electronic
chemical descriptors were derived from the partial atomic charges computed
by INDO/1.

Alternatively, subquantum mechanical PEOE (Iterative Partial Equali-
zation of Orbital Electronegativities; Gasteiger and Marsili, 1980)
calculations were carried out to obtain atomic charges. This method is
based on the principle that molecular charge distributions are the result
of charge transferred among atoms of differing electronegativities. The
algorithms of this program use experimental electronegativites and the
only geometry specifications required are atom connectivities.

The carbon charges computed from INDO/1 and PEOE are compared in
Table 2 for the 10 chlorocarbons. The two methods display similar trends,
but the INDO/1 charges are generally much larger in absolute value.

Table 3 is a sample of the types of electronic chemical descriptors derived from both INDO/1 and PEOE atomic charges. Although the carbon charges QC_1 and QC_{tot} are probably the most obvious and most easily justified chemical descriptors, it should be recognized that functions and combinations of these parameters and other charges in the molecule may be related to important factors in metabolism.

Chlorine substitution patterns were assumed to carry steric information. Table 4 is a list of some of the steric parameters which were tested in combination with the electronic parameters. The chemical descriptors in Table 4 are all derivable from the numbers of chlorines bonded to each carbon.

Since the data set was small, regression equations were restricted to 2-term fits. INDO/1 and PEOE electronic parameters were tested separately with each of the steric parameters. Statistical analyses were carried out using the SAS software package[1].

The INDO/1 charges when used in combination with the steric parameters did not yield any satisfactory 2-term fits. A moderately good fit was achieved, however, using the carbon charges QC_1 and QC_2 (see Table 3 for definitions):

$$Vmax = 24.0(\pm 6.0) + 199(\pm 32)QC_1 - 98.9(\pm 23.4)QC_2 \qquad (1)$$
$$n = 10 \qquad r^2 = 0.850 \qquad s = 9.01$$

Experimental and calculated Vmax values are compared in Table 5. The r^2 value 0.850 indicates that 85% of the variation in the experimental values is accounted for by Eq. 1. The root mean-square error s is rather large,

---

[1] SAS Institute, Inc., Box 8000, Cary NC 27511, U.S.A.

but as shown in Table 5, most of the predicted values are off by no more than 20%, which is an upper bound for the approximate experimental error range of 10-20%.

Eq. 1 indicates that Vmax increases as the calculated charge on the most positive carbon increases. This result is expected since a highly positive carbon is a favorable site for nucleophilic attack. The fact that QC_2 came in with a negative coefficient is less clear since QC_2 is defined as QC_1 in the case of methanes.

Of all the PEOE parameters tested, the best fit was achieved using the total hydrogen charge QH_{tot} in combination with the difference between the numbers of hydrogens and chlorines on the least substituted carbon:

$$Vmax = 130(\pm 4.5) - 623(\pm 34)QH_{tot} + 10.8(\pm 0.78)\cdot(nH_2 - nCl_2) \qquad (2)$$
$$n = 10 \qquad r^2 = 0.981 \qquad s = 3.21$$

This is an excellent fit and as shown in Table 6, the predicted values are well within 10% of the experimental values.

The coefficient of the steric term in Eq. 2 is positive. As the number of chlorines on the least substituted carbon increases, Vmax decreases. This can be explained in simple terms if enzymatic attack at the least substituted position is assumed to be the result of steric hindrance at the other carbon. As the less hindered position becomes more crowded with chlorines, an attack diverted to this carbon becomes less favorable.

The negative coefficient of QH_{tot} is difficult to explain. Perhaps the presence of many positive hydrogens tends to "distract" a nucleophile away from the carbon. Also, the positive character of carbon may be reduced if there are a sufficient number of hydrogens donating electron

density through the carbons to the polarizing chlorines.

IV.

Although Vmax values for tetrachloromethane and 1,1,1-trichloroethane were available, these chemicals were initially excluded from the data set because they were poorly metabolized. The electronic-steric models were all unsuccessful at fitting very low Vmax values. Moreover, some features of the regression equations had no clear physical significance. For these reasons, the data set was increased to 12 chemicals (Table 7) and a new approach was taken.

First, a criterion for metabolism was sought. This reduced to identifying a structural characteristic unique to both CCl_4 and CCl_3CH_3. The most obvious feature is that these two chemicals are the only saturated chlorocarbons in the data set which lack a chlorine and a hydrogen together on the same carbon. Although both molecules contain a highly positive carbon, these sites are obstructed by four bulky chlorines in the case of CCl_4 and three chlorines and a methyl group in CCl_3CH_3. The enzymatic attack may be directed to the methyl carbon in CCl_3CH_3. In this case, at least one C–H bond on carbon 2 would be broken in the metabolic process. MNDO (Modified Neglect of Diatomic Overlap; Dewar et al., 1977) bond order calculations carried out on CCl_3CH_3 and the well metabolized $CHCl_2CH_3$ indicate that a C–H bond is considerably stronger when the carbon is not bonded to a chlorine. These results are summarized in Fig. 1.

The apparent low reactivity of the methyl group in CCl_3CH_3 led to the observation that replacing a chlorine in a chlorinated methane with a

methyl group has a predictable effect on Vmax. Using this approach, the ethane series CH_2ClCH_3, $CHCl_2CH_3$, CCl_3CH_3 corresponds to the series CH_2Cl_2, $CHCl_3$, CCl_4 of methanes. From Table 7, the maximum metabolic rates for CH_2ClCH_3 and $CHCl_2CH_3$ are respectively 15 and 18 μmol/hr higher than the rates of the methane analogs. Thus, for the di- and trichloromethanes, methyl group substitutions are accompanied by comparable increases in Vmax, while CCl_4 and CCl_3CH_3 are essentially non-metabolized.

One final observation was that among the ethanes and ethenes, chemicals with unsymmetric chlorine substitution patterns tended to have higher maximum metabolic rates. This is perhaps due to the fact that an imbalance of chlorines on one end of the molecule creates a dipole moment along the C–C bond axis. This dipole may be related to the ease with which the molecule is drawn into a binding site on an enzyme and ultimately to the rate at which it is metabolized.

The ideas of this qualitative approach were summarized with two binary parameters. The first parameter C_{sub} was assigned a value of 1 if the molecule did not contain a carbon bonded to both a hydrogen and a chlorine; it was set equal to zero otherwise. A second parameter SYM_{Cl} was assigned a value of 1 for ethanes and ethenes with unequal numbers of chlorines on the two carbons and a value of zero otherwise. Because of the similarities between the series CH_2Cl_2, $CHCl_3$, CCl_4 and the series CH_2ClCH_3, $CHCl_2CH_3$, CCl_3CH_3, the values of SYM_{Cl} for the methanes were set equal to 1.

For the 12 chemicals in Table 7, a 2-term fit of Vmax was obtained:

$$Vmax = 31.2(\pm7.7) - 62.2(\pm10.7)C_{sub} + 32.3(\pm9.2)SYM_{Cl} \qquad (3)$$

$$n = 12 \quad r^2 = 0.809 \quad s = 13.3$$

To improve the fit, a graph theoretical molecular connectivity parameter was added. The Randic/Kier/Hall zeroth order valence connectivity index (Kier and Hall, 1983) provides electronic and structural information about a chemical. This index is defined as

$$^{\circ}\chi^{v} = \sum (\delta_i^v)^{-1/2}, \qquad (4)$$

where the sum is taken over all atoms and

$$\delta_i^v = \frac{Z_i^v - h_i}{Z_i - Z_i^v - 1} \qquad (5)$$

Here, Z_i is the total number of electrons on atom i, Z_i^v is the number of valence electrons on i and h_i is the number of hydrogens bonded to i. The best 3-term fit was

$$Vmax = 87.4(\pm15.2) - 82.3(\pm8.4)C_{sub} + 35.8(\pm5.8)SYM_{Cl}$$
$$- 197(\pm51)\cdot1/^{\circ}\chi^{v} \qquad (6)$$
$$n = 12 \quad r^2 = 0.934 \quad s = 8.32$$

The experimental and calculated metabolic rates are compared in Table 8. Most of the residuals are small and the low Vmax values are well fit.

V. RECOMMENDATIONS:

A natural extension of this work would be to include a number of fluorinated and brominated chemicals in the data set. Successful modeling of a more diverse data set would increase the predicting power of any regression equations obtained. The utility of the equations developed for the chlorinated hydrocarbons can be tested as soon as Vmax values are measured for some short-chained chlorocarbons outside the original set.

Another important step is to examine chemicals with longer carbon

chains. This again introduces greater diversity in the data set. Additional motivation for this step is the unexplained non-reactivity of tetrachloroethene. This chemical was not included in the present study but its Vmax has been determined to be zero. Some insight could be gained by measuring Vmax for chemicals obtained by replacing one or more of the chlorines in tetrachloroethene with methyl groups.

Finally, it may be worthwhile to explore the use of more advanced ab initio molecular orbital calculations in the search for chemical descriptors. Atomic charges, bond orders and electrostatic potentials may be of use.

Table 1. Data set for the Electronic-Steric Modeling Approach

Compound	$V_{max}/\mu mol \cdot hr^{-1}$ [a]
Dichloromethane	47.1
Trichloromethane	58.6
Chloroethene	40.0
1,1-Dichloroethene	77.4
cis-1,2-Dichloroethene	30.9
trans-1,2-Dichloroethene	30.9
Trichloroethene	83.7
Chloroethane	62.0
1,1-Dichloroethane	75.8
1,2-Dichloroethane	31.8

[a] V_{max} values were scaled to a 1.0 kg rat.

Table 2. Carbon Charges from INDO/1 and PEOE [a]

Compound	INDO/1		PEOE	
	Carbon 1	Carbon 2	Carbon 1	Carbon 2
CH_2Cl_2	0.207		0.0967	
$CHCl_3$	0.383		0.1800	
$CHClCH_2$	0.076	-0.083	-0.0024	-0.0872
CCl_2CH_2	0.268	-0.046	0.0996	-0.0677
cis-CHClCHCl	0.109	0.109	0.0165	0.0165
trans-CHClCHCl	0.107	0.107	0.0165	0.0165
CCl_2CHCl	0.297	0.138	0.1184	0.0359
CH_2ClCH_3	0.075	-0.088	0.0195	-0.0516
$CHCl_2CH_3$	0.254	-0.072	0.1046	-0.0347
CH_2ClCH_2Cl	0.088	0.088	0.0359	0.0359

[a] Carbon 1 refers to the most substituted carbon.

Table 3. Electronic Chemical Descriptors
Derived from INDO/1 and PEOE Atomic Charges

QC_1: The charge on the most positive carbon [a]

QC_2: The charge on the most negative carbon [a]

$$QC_1 - QC_2$$

$$QC_1^2$$

$$QC_2^2$$

$$(QC_1 - QC_2)^2$$

$$QC_1^2 + QC_2^2$$

$$QC_1^2 - QC_2^2$$

QC_{tot}: The sum of all carbon charges in the molecule

QH_1: The charge on the most positive hydrogen [b]

$$QH_1 - QC_1$$

QH_{tot}: The sum of all hydrogen charges in the molecule

QCl_{tot}: The sum of all chlorine charges in the molecule

---

[a] In the case of chlorinated methanes, the most positive
carbon is also the most negative carbon.

[b] The most positive hydrogen is bound to the most positive
carbon.

Table 4. Steric Parameters Tested

nCl_1: The number of chlorines on the most substituted carbon [a]

nCl_2: The number of chlorines on the least substituted carbon [a]

$$nCl_1 - nCl_2$$

nH_1: The number of hydrogens on the most substituted carbon

nH_2: The number of hydrogens on the least substituted carbon

$$nH_1 - nH_2$$
$$nH_1 - nCl_1$$
$$nH_2 - nCl_2$$

$nonH_1$: The number of non-hydrogen substituents on the most substituted carbon

$nonH_2$: The number of non-hydrogen substituents on the least substituted carbon

$$nonH_1 - nonH_2$$

[a] In the case of chlorinated methanes, the most substituted carbon is also the least substituted carbon.

Table 5. Parameters and Calculated Vmax Values from Eq. 1 [a]

Compound	QC_1	QC_2	Vmax (calc.)	Vmax (exp.)
CH_2Cl_2	0.207	0.207	44.8	47.1
$CHCl_3$	0.383	0.383	62.5	58.6
$CHClCH_2$	0.076	-0.083	47.4	40.0
CCl_2CH_2	0.268	-0.046	82.0	77.4
cis-CHClCHCl	0.109	0.109	35.0	30.9
trans-CHClCHCl	0.107	0.107	34.8	30.9
CCl_2CHCl	0.297	0.138	69.6	83.7
CH_2ClCH_3	0.075	-0.088	47.7	62.0
$CHCl_2CH_3$	0.254	-0.072	81.8	75.8
CH_2ClCH_2Cl	0.088	0.088	32.9	31.8

[a] QC_1 and QC_2 are from INDO/1.

Table 6. Parameters and Calculated Vmax Values from Eq. 2 [a]

Compound	QH_{tot}	nH_2-nCl_2	Vmax (calc.)	Vmax (exp.)
CH_2Cl_2	0.1342	0	46.3	47.1
$CHCl_3$	0.0821	-2	57.2	58.6
$CHClCH_2$	0.1844	2	36.7	40.0
CCl_2CH_2	0.1126	2	81.3	77.4
cis-$CHClCHCl$	0.1532	0	34.5	30.9
trans-$CHClCHCl$	0.1532	0	34.5	30.9
CCl_2CHCl	0.0783	0	81.2	83.7
CH_2ClCH_3	0.1590	3	63.2	62.0
$CHCl_2CH_3$	0.1415	3	74.1	75.8
CH_2ClCH_2Cl	0.1788	1	29.3	31.8

[a] QH_{tot} is from PEOE.

Table 7. Extended Data Set

Compound	$Vmax/\mu mol \cdot hr^{-1}$
Dichloromethane	47.1
Trichloromethane	58.6
Tetrachloromethane	2.6
Chloroethene	40.0
1,1-Dichloroethene	77.4
cis-1,2-Dichloroethene	30.9
trans-1,2-Dichloroethene	30.9
Trichloroethene	83.7
Chloroethane	62.0
1,1-Dichloroethane	75.8
1,2-Dichloroethane	31.8
1,1,1-Trichloroethane	0.0

(a)

Cl, Cl—C, H / 0.958, C—H, H, H

$V_{max} = 75.8 \, \mu mol/hr$

(b)

Cl, Cl—C, Cl / 0.973, C—H, H, H

$V_{max} = 0.0 \, \mu mol/hr$
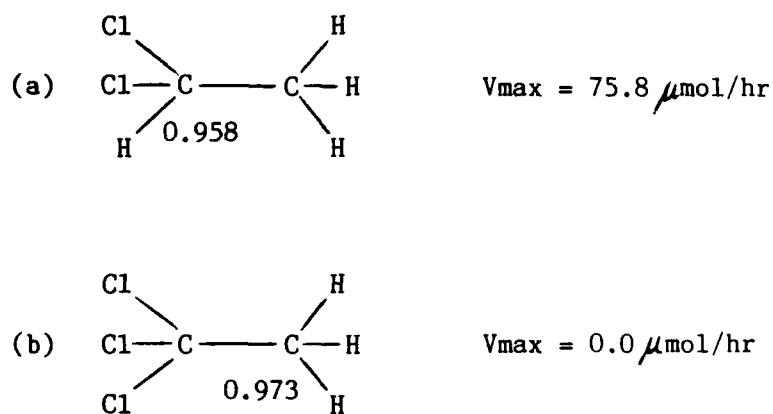
Figure 1. MNDO C–H bond orders for (a) 1,1–dichloroethane and (b) 1,1,1–trichloroethane.

Table 8. Parameters and Calculated Vmax Values from Eq. 6

Compound	C_{sub}	SYM_{Cl}	$1/^{\circ}\chi^{v}$	Vmax (calc.)	Vmax (exp.)
CH_2Cl_2	0	1	0.3361	57.1	47.1
$CHCl_3$	0	1	0.2513	73.8	58.6
CCl_4	1	1	0.1986	1.8	2.6
$CHClCH_2$	0	1	0.4135	41.9	40.0
CCl_2CH_2	0	1	0.2878	66.6	77.4
cis-CHClCHCl	0	0	0.2922	29.9	30.9
trans-CHClCHCl	0	0	0.2922	29.9	30.9
CCl_2CHCl	0	1	0.2233	79.3	83.7
CH_2ClCH_3	0	1	0.3520	54.0	62.0
$CHCl_2CH_3$	0	1	0.2601	72.0	75.8
CH_2ClCH_2Cl	0	0	0.2716	33.9	31.8
CCl_3CH_3	1	0	0.2040	0.8	0.0

REFERENCES

Dewar, M.J.S. and W. Thiel, J. Am. Chem. Soc., 1977, Vol. 99, p. 4899.

Dewar, M.J.S., E.G. Zoebisch, E.F. Healy and J.J.P. Stewart, "AM1: A New General Purpose Quantum Mechanical Molecular Model," J. Am. Chem. Soc., 1985, Vol. 107, pp. 3902-3909.

Gargas, M.L., M.E. Andersen and H.J. Clewell, III, "A Physiologically Based Simulation Approach for Determining Metabolic Constants from Gas Uptake Data," Toxicol. Appl. Pharmacol., 1986, Vol. 86, pp. 341-352.

J. Gasteiger and M. Marsili, Tetrahedron, 1980, Vol. 36, p. 2319.

Jaffe, H.H., "All-Valence-Electron Semiempirical Self-Consistent Field Calculations," Acc. Chem. Res., 1969, Vol. 2, pp. 136-143.

Pople, J.A., D.L. Beveridge and P.A. Dobosh, "Approximate Self-Consistent Molecular-Orbital Theory. V. Intermediate Neglect of Differential Overlap," J. Chem. Phys., 1967, Vol. 47, pp. 2026-2033.

Ridley, J. and M. Zerner, "An Intermediate Neglect of Differential Overlap Technique for Spectroscopy: Pyrrole and the Azines," Theoret. Chim. Acta, 1973, Vol. 32 p. 111.

1987 USAF-UES SUMMER FACULITY RESEARCH PROGRAM/

GRADUATE STUDENT SUMMER SUPPORT PROGRAM

Sponsored by the

AIR FORCE OFFICE OF SCIENTIFIC RESEARCH

Conducted by the

Universal Energy Systems, Inc.

FINAL REPORT

Directed Motion Doppler Shift Effects on

Nitric Oxide (0,0) Gamma Band Resonance Absorption

Prepared by:	James A. Drakes
Academic Rank:	Graduate Student
Department and University:	Physics Department
	University of Tennessee Space Institute
Research Location:	Arnold Engineering and Development Center
	Sverdrup Technology, Group EL3
	Arnold AFS
	Tullahoma, TN
USAF Researcher:	Dr. Wheeler K. McGregor
Date:	August 20, 1987
Contract No:	F49620-85-C-0013

Directed Motion Doppler Shift Effects on
Nitric Oxide (0,0) Gamma Band Resonance Absorption

by

James A. Drakes

Abstract

An investigation into the effects of flowfield-induced Doppler shifts was performed. The directed motion Doppler shift arises in expanding flowfields where the gas molecules are traveling with non-parallel trajectories. It was found that the shifting of the line center frequency of the absorption lines in the medium, caused by the gas expansion, lead to a marked increase in the transmittance of the medium. Our study examined a absorbing conical flow, using both a homogeneous and an annular NO number density profile. For the homogeneous model, the transmittance at the second band head, located at approximately 2262 Angstroms, was increased in the range of 5- to 17- percent upon the inclusion of flowfield Doppler shifts, depending on the exit velocity of the flow. The transmittance at the second band head of the annular flowfield showed an increase with the inclusion of the directed motion Doppler shift of from 8- to 22- percent, varying with the exit velocity.

Acknowledgements

I would like to thank the Air Force Systems Command and the Air Force Office of Scientific Research for their sponsorship of the Graduate Student Summer Support Program. I would also like to ackowledge the technical and clerical support of the EL3 group of Sverdrup Technology, Arnold Engineering and Development Center, Arnold AFS, TN.

In particular, I wish to thank Dr. Robert A. Reed and Dr. Wheeler K. McGregor for their guidance and motivation of this work. I am also greatly indebted to both Robert Hires and Martha Simmons for their capable assistance with the computer mainframe system and for their expenditure of time and energy on my behalf.

I. Introduction

The EL3 Technology Group of Sverdrup Technology, operating at Arnold Engineering and Development Center, Arnold Air Force Station is very concerned with the diagnostic testing and theoretical modeling of rocket motors. A proven experimental technique is to measure the amount of spectral transmission through the rocket plume and, based upon that measurement, calculate properties of the exhaust gases such as radial temperature, pressure, and number density profiles of various gas species. The theoretical problem is to predict the transmission spectra for a given set of flowfield conditions based upon the quantum mechanical model for the particular molecule of interest. The predicted transmission spectra for a source of NO (0,0) gamma band radiation when there exists small amounts of absorbing NO in the flowfield has already been successfully solved[1-3]. However, that solution considered only parallel flows. Nonparallel flows present an additional problem of radiation absorption and emission.

In a nonparallel flow, the absorbing gas molecules are moving towards and away from the radiation source along the line of sight, see Figure 1. Because of the motion, the radiation from the source is Doppler shifted as it appears to the absorbing molecules. Hence, the absorbing properties of the nonparallel flow differ from that of a parallel flow. The degree to which the radiation measurement is changed depends on the magnitude of the Doppler shift when compared to the width of the spectral lines contributing to the absorption.

17-4
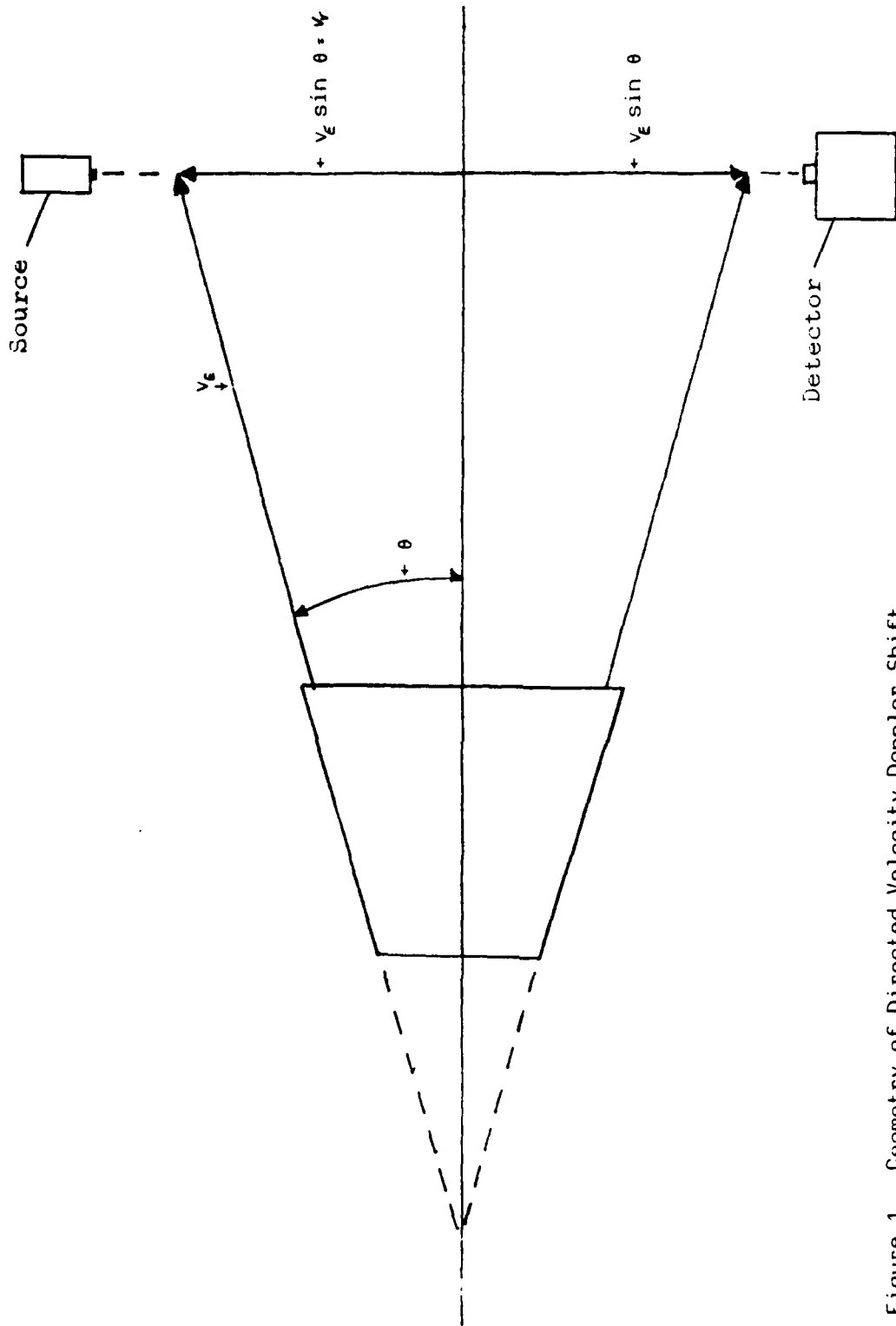
Figure 1. Geometry of Directed-Velocity Doppler Shift.

This report describes an effort to extend the parallel flow model of NO resonance line absorption to include nonparallel flows. Transmission spectra are predicted for both parallel and nonparallel flows to illustrate the error that can be introduced when nonparallel motion is neglected.

The author has recently completed his Master's program at the University of Tennessee Space Institute where the topic of his thesis was the effect of the directed motion Doppler shift on the calculation of band models of emission and absorption. That research was conducted at Arnold Engineering and Development Center, with the support of the EL3 group of Sverdrup Technology. The present work presents a similar problem, but will require a line-by-line calculation of the average transmission, as opposed to utilizing the band model method.

II. Objectives

The primary goal of this research was to determine the influence that the directed motion Doppler shift can have on low resolution spectroscopic measurements of the NO (0,0) gamma band. We wished to be able to estimate the consequences of slight distortions of spectral absorption lines upon the transmissive and absorptive behavior of the entire band. The degree of the spectral distortion caused by directed motion Doppler shifting is dependent upon the geometry of the flowfield. It is desired to provide upper and lower bounds to the anticipated discrepancies by evaluating this problem for best and worst cases.

A secondary goal of this summer work was to bring the

existing NO transmission computer program up to date. This code
will be very useful for predicting and interpreting future
resonance experiment results on not only NO but other molecules
as well.

III. NO Resonance Line Absorption

The application of resonance line absorption techniques to
the nitric oxide molecule has been previously examined[1-3]. In
that study, NO radiation from the (0,0) gamma band was produced
by a gas discharge lamp. The emitted beam passed through a
gaseous flowfield which contained trace amounts of NO. A
comparison of the measured transmitted energy to the incident
energy made it possible to predict the NO concentration in the
flowfield. The reverse problem, which was also addressed in the
earlier work[1-3], was to predict the transmission spectra when
given information about the NO concentration in the flow.

The transmission, T_j, of the jth source line, which has some
spectral distribution $I_{\nu_j}^0$, through an absorbing medium of length l
is given by[2],

$$ T_j = \int_0^{\infty} I_{\nu_j}^0 \, exp\left(- k_\nu \ell\right) d\nu \tag{1} $$

where ν is the frequency, and κ_ν is the frequency dependent
absorption coefficient of the absorbing molecule. If the
pressure is low in the gas discharge lamp, then the source line
intensity will have a Doppler, i.e. Gaussian, profile due to the
random motion Doppler shift caused by the thermal agitation of

the molecules. To avoid confusion, this will be refered to as the thermal Doppler profile and has the form [2].

$$I_{\nu_j}^o = I_{\nu_j^o}^o \exp\left\{-4\ln 2\left(\frac{\nu-\nu_j^o}{\gamma_3}\right)^2\right\} \qquad (2)$$

where $I_{\nu_j^o}^o$ is the line center intensity and γ_3 is the Doppler halfwidth at half maximum (HWHM).

The absorption line profile is described by the Voigt distribution since the pressure is non-neglible in the flowfield. The Voigt profile is a convolution of the thermal Doppler and collision broadening profiles. If we are considering absorption by only the spectral line in the medium which corresponds to the jth source line, then $k_\nu = k_{\nu_j}$, which is given by [2].

$$k_{\nu_j} = \frac{k_{\nu_j}^o \cdot a'}{\pi} \int_{-\infty}^{\infty} \frac{e^{-y^2}}{(a')^2 + (q_j - y)^2} dy \qquad (3)$$

where $a' = \sqrt{\ln 2} \; \gamma_L/\gamma_D$

$$q_j = 2\sqrt{\ln 2} \; \frac{y-\nu_j^o}{\gamma_3}$$

and $k_{\nu_j}^o$ is the line center absorption coeficient, with y as a dummy integration variable. The Lorentz HWHM is denoted by γ_L. The line center absorption coefficient is dependent upon the number density of absorbing molecules, N, and has the form [4].

$$k_{\nu_j}^o = \left(\frac{2e^2\sqrt{\pi(\ln 2)}}{m_e c^2}\right) \frac{Nf}{\gamma_D} \qquad (4)$$

where f is the band oscillator strength.

If more than one absorption line is to be considered, then the total absorption coefficient at a given spectral location is the sum of all the contributing absorption coefficients of nearby

lines which have a nonnegligible value at that frequency.

$$k_\nu = \sum_i k_{\nu_i} \qquad (5)$$

Putting this into Equation 1, the result is

$$T_j = I_{\nu_j^o}^o \int_0^\infty \exp\left\{-4\ln2\left(\frac{\nu-\nu_j^o}{\tau_b}\right)^2\right\} \exp\left\{-\ell\sum_i k_{\nu_i}\right\} d\nu \qquad (6)$$

where the sum is over all spectral lines that contribute to the absorption of the given source line. The total transmission in a particular spectral interval, $\Delta\nu$, is the sum of the transmission of the j source lines in the interval.

$$T_{\Delta\nu} = \sum_j I_{\nu_j^o}^o \int_0^\infty \exp\left\{-4\ln2\left(\frac{\nu-\nu_j^o}{\tau_j}\right)^2\right\} \exp\left\{-\ell\sum_i k_{\nu_i}\right\} d\nu \qquad (7)$$

The fractional transmission, or transmittance, in that interval is given by the ratio of incident to emergent energy.

$$t_{\Delta\nu} = \frac{\sum_j I_{\nu_j^o}^o \int_0^\infty \exp\left\{-4\ln2\left(\frac{\nu-\nu_j^o}{\tau_j}\right)^2\right\} \exp\left\{-\ell\sum_i k_{\nu_i}\right\} d\nu}{\sum_j I_{\nu_j^o}^o \int_0^\infty \exp\left\{-4\ln2\left(\frac{\nu-\nu_j^o}{\tau_b}\right)^2\right\} d\nu} \qquad (8)$$

where the sum over j is limited to only those source lines lying within the interval $\Delta\nu$.

IV. The Directed Motion Doppler Shift

The directed motion Doppler shift (DMDS) is a frequency shifting of the spectral position of the absorption lines in a medium due to motion of the medium along the observers line of sight. This phenomena was first studied by astrophysicists who were observing the rapidly expanding and contracting atmospheres of certain stars[5]. The effects of DMDS to high resolution

17-9

diagnostic flowfield measurements as well as the influence of DMDS to CO_2 band models for absorption in a conical flow[7] has also been examined.

In the particular case of rocket motors, a detector can be positioned to view the transmission of radiation from a source lamp through the rocket exhaust with its line of sight normally intercepting the exhaust axis of symmetry. When the gas exits the nozzle, the expansion of the gas causes molecules to move parallel and antiparallel to the line of sight of the detector, as is shown in Figure 1.

If the flow was not expanding, i.e. a parallel flow, the absorption lines of the gas in the plume would occur at the same spectral positions as the source lines, assuming that the same gas specie was present in both the source and the exhaust gas. However, when the gas is moving along the line of sight of the detector, as in a nonparallel flow, molecules which are moving toward the source will perceive the source radiation to be blue shifted, while those moving away from the source will perceive the source radiation to be red shifted. The amount of absorption by the nonparallel flow will be less than it would be by a parallel flow because the absorption lines do not coincide with the source lines.

Computationally, the DMDS is taken into account by replacing the line center frequency of the absorption line by its Doppler shifted frequency. The new line center is dependent upon the velocity with which the molecule is moving towards or away from the source, i.e. the radial velocity of the flow.

$$\nu_j^{\circ *} = \nu_j^{\circ} \left(1 \pm \frac{|\bar{v}_r|}{c} \right) \qquad (9)$$

where $c = 3.0 \times 10^8$ cm/sec. In the case of a conically expanding flow, $\bar{v}_r$ is merely the radial component of the exit velocity, $\bar{v}_e$, given by the sine of the angle from the axis of symmetry. To determine the absorption coefficient of the nonparallel flow, one merely inserts Equation 9 into Equation 3. Once this is done, the absorption coefficient will have a spatial dependence determined by the radial velocity distribution, thus comparisons with and without DMDS must involve the path integrated absorption coeffficient.

The influence which DMDS can have upon absorption in the flow can be judged qualitively by the ratio of the Doppler shift to the half width of the spectral lines. When this ratio is small, DMDS has very little significance. An example of this would be spectral lines ocurring when the pressure is at or near atmospheric. The spectral lines are so broad that a Doppler shift of magnitude typical of this study does not move the spectral line centers far enough to be noticed. However, as this ratio approaches unity, there will be a distinct difference in the appearance of the absorption line with and without DMDS. Hence, one requirement for observance of DMDS effects is low pressure. For comparison, the halfwidth of the spectral lines of interest to this study is approximately 0.091 cm^{-1}. The Doppler shift at the outer edges of the conical flow to be discussed is approximately 0.089 cm^{-1}.

V. Single Line Study

The study began with an examination of the DMDS on the transmittance of one source line through one absorption line. This case was described in Section III by limiting the sum in Equation 6 to the corresponding absorption line. The fractional transmission follows as the ratio given in Equation 8 with all the summations limited to only the one line of interest. This approach was advantageous as a first step because it eliminated considerable numerical complexity while yielding correct phenomenological results.

The computation of Equation 8 was performed using the P12(12.5) line of the NO (0,0) gamma band as the source and absorbing lines. The flowfield conditions assumed a conical flowfield with an exit velocity of 1.7×10^5 cm/sec and a maximum divergence of 20.4 degrees. The temperature of the flow was set at 994 K, while that of the discharge lamp was 950 K. The pressure of the flow was 10.34 Torr with the flow consisting of at least 99 percent N_2 and the remainder being NO.

Two different types of conical flowfields were considered to provide the upper and lower bounds of anticipated error. The first case considered a homogeneous flowfield in which the NO number density was constant along the optical path. This should give the lower error bound since it weights the interior of the flow with more molecules than would be present in an actual flow. The interior of the flow contributes the least to DMDS effects since the radial velocity is smallest in that region. The second case was an annular flowfield, in which all the absorbing molecules were concentrated in a very thin ring at the outer lip

17-12

of the flow. This region has the greatest radial velocities and should yield the largest DMDS effect. In reality, a gaseous flow will have a number density profile somewhere between these two extremes.

The results of both cases are shown in Figure 2. The absicsa is the log of the NO number density in cm^{-3}. The ordinate is the fractional transmission, Equation 8. The lowest two curves are the transmittance for the homogeneous flowfield with the upper one including DMDS. These curves show that for a given amount of NO, the transmittance is higher when DMDS is accounted for. This is due to the spectral shifting of the absorption line centers, making it easier for radiation to pass through the flow. Conversely, if a value of the transmittance was measured, a computation of the NO number density without DMDS would suggest a lower concentration than that suggested by the result with DMDS. For example, if t = 0.6, the DMDS computation will predict a 15 percent larger NO number density than the computation without DMDS.

The annular flowfield exhibits even greater sensitivity to the DMDS. The DMDS case again shows a higher transmittance for a given NO concentration. For a given transmittance, the computation without DMDS will again underestimate the NO number density. However, the magnitude of the discrepancy between the calculation with and without DMDS has increased. At t = 0.6, for example, the DMDS computation determines the number density to be 61 percent higher than the computation without DMDS.
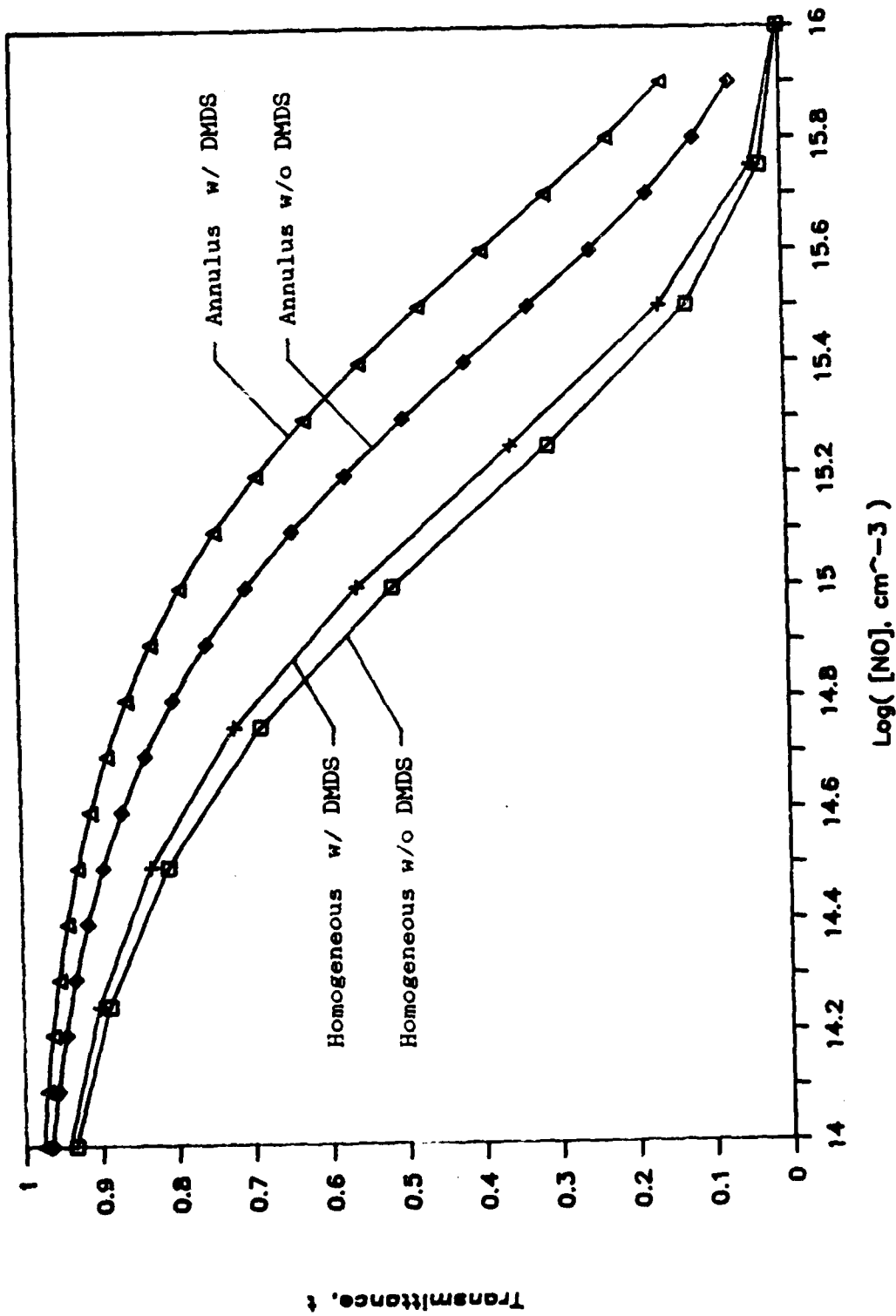
Figure 2. NO Single Line Transmittance

VI. Band Study

The work on the NO band spectra paralled that done for a single line, but with some exceptions. A transmittance calculation was done, Equation 8, but in this instance the transmittance was considered as a function of frequency as opposed to NO number density. The summations in Equation 8 were no longer restricted to just one source and absorption line, but were allowed to run over the entire set of spectral lines. The previous NO computer code was extremely revamped to accomodate path integration of every spectral line through homogeneous and inhomogeneous flowfields for cases with and without DMDS.

The procedure for the band study began with a homogeneous and proceeded to an annular conical flow comparison. The flowfield conditions were similiar to that of the single line study. An NO number density of 1.0×10^5 cm^{-3} was chosen from Figure 2 because that value was in a region whe e the discrepancy between the case with and without DMDS was fairly constant. The transmittance spectra was calculated for two different flow exit velocities.

The results for a conical flowfield with an exit velocity of 1.7×10^5 cm/sec are shown in Figure 3. The lower set of two curves is the homogeneous flow spectra, with the dotted curve representing the transmission spectrum calculated with DMDS. The upper set of two curves is the annular flow spectra, with the inner radius of the flow equal to 0.93 the outer radius. The dotted curve corresponds to the spectrum calculated with DMDS. The transmittance values printed on the graph correspond to that of the second band head (approximately 2262.2 Angstroms). In the

17-15
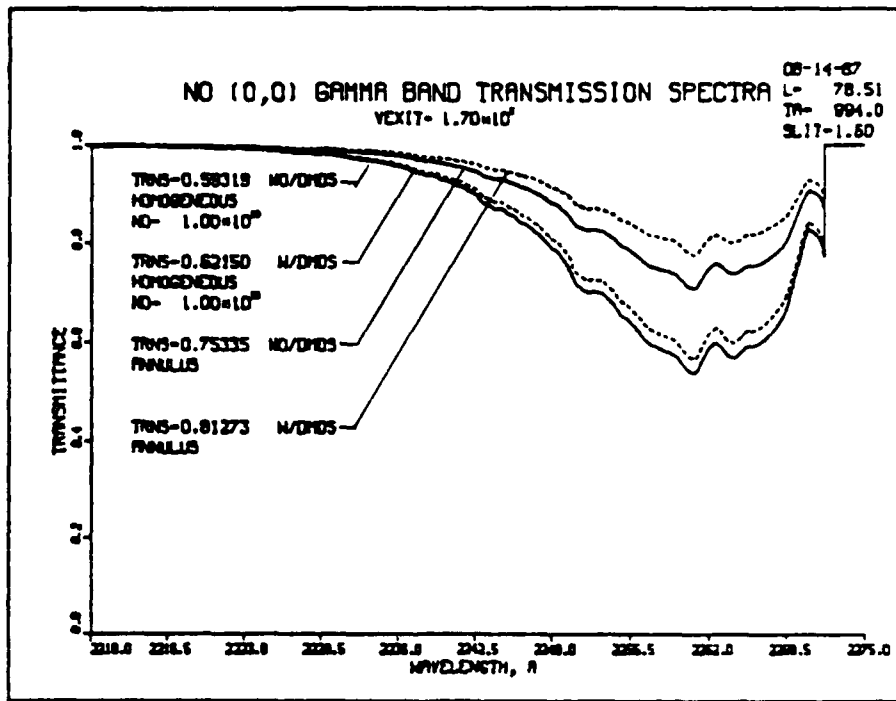
Figure 3. NO (0,0) Gamma Band Transmission Spectra, Conical Nozzle with Exit Velocity = 1.7 x10^5 cm/sec.
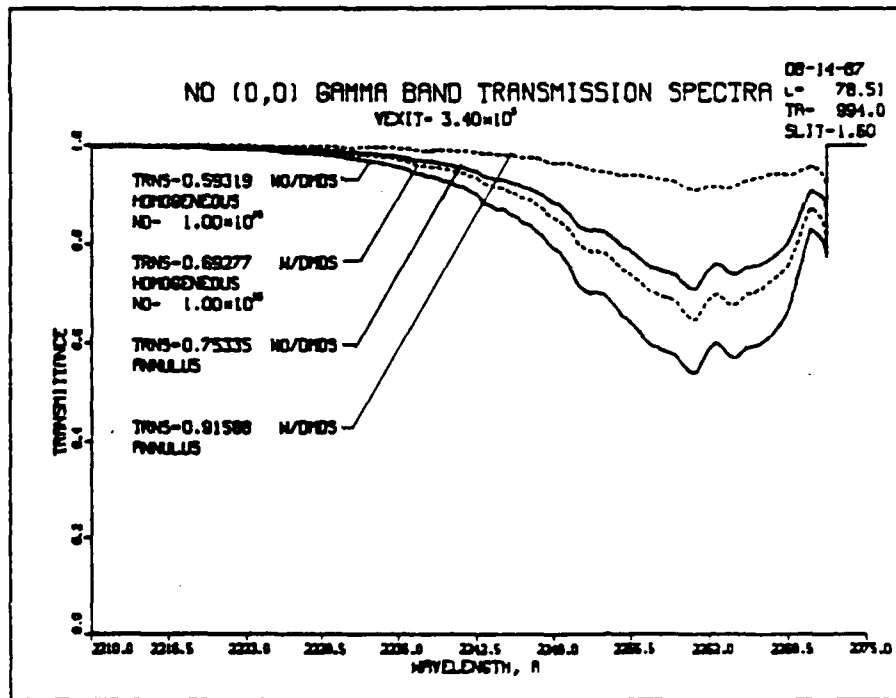
Figure 4. NO (0,0) Gamma Band Transmission Spectra, Conical Nozzle with Exit Velocity = 3.4 x10^5 cm/sec.

homogeneous flow, the transmittance of the DMDS case is 4.8 percent greater than that without DMDS. For the annular flow, the DMDS case has a transmittance at the second band head which is 7.9 percent greater. Thus, one would expect a predicted spectra based upon a very good knowledge of the number density profile of this particular flowfield to have a DMDS discrecranpcy in the range of 5 to 8 percent.

Figure 4 shows transmission spectra for a conical flowfield with an exit velocity of 3.4×10^5 cm/sec. The results are similar to that shown in Figure 3, but the DMDS discrepancy has greatly increased. At the second bandhead, the homogeneous flow transmittance with DMDS (dotted line) is 16.8 percent larger than the transmittance without DMDS (solid line). The difference in the transmittance between the cases with and without DMDS in the annular flowfield is over 21.5 percent.

Figures 3 and 4 demonstrate two things. First, the DMDS effect can have a noticeable effect on the predicted transmission spectra of the NO (0,0) gamma band. Since it is possible to see this effect on the prediced spectra, it is likely that a calculation of number density from a measured spectrum will also be affected by DMDS. The second point to be made is the dependence of DMDS upon the flowfield conditions. The large increase in the DMDS discrepancy between Figures 3 and 4, as well as that seen between the homogeneous and annular flows, displays that the effect is sensitive to the flowfield geometry and conditions.

VII. Recommendations

The next anaylsis which needs to be performed is the NO inversion technique with and without DMDS. In that computer program, a measured value of the transmittance at several radial lines of sight are used to determine the NO number density profile by the "onion-skin" method. This is of utmost importance since the results of the predicted spectra have shown that DMDS can be responsible for noticeable deviations. The next problem is to find out what effect will show up in the inversion.

References

1. Davis, M.G., W.K. McGregor, and J.D. Few. Journal of Quantitative Spectroscopy and Radiative Transfer (JQSRT). 16, 1109-1118 (1976).

2. Davis, M.G., W.K. McGregor, J.D. Few and H.N. Glassman. Transmission of Doppler Broadened Resonance Radiation Through Absorbing Media With Combined Doppler and Pressure Broadening (Nitric Oxide Gamma Bands as an Example). Arnold Engineering and Development Center. AEDC-TR-76-12. 1976.

3. Few, J.D., W.K. McGregor, and H.N. Glassman. Ultraviolet Spectral Absorption Measurements of Nitric Oxide Concentration in T-56 Combustor Exhaust. AIAA 14th Aerospaces Sciences Meeting. AIAA Paper No. 76-109. 1976.

4. McGregor, W.K., J.D. Few, D.R. Keefer, H.S. Lowry, and M.G. Davis. JQSRT. 23, 527-530 (1980).

5. Sobolev, V.V. Course in Theoretical Astrophysics. NASA, 1969.

6. Penner, S.S. and H.K. Chen. JQSRT, 13, 1315 (1973)

7. Drakes, J.A. Directed Motion Doppler Shift Effects on Infrared Band Models of Emission and Absorption in a Hypersonic Conical Flow. Master's Thesis, University of Tennessee, 1987.

1987 USAF-UES SUMMER FACULTY RESEARCH PROGRAM

GRADUATE STUDENT SUMMER SUPPORT PROGRAM

Sponsored by the

AIR FORCE OFFICE OF SCIENTIFIC RESEARCH

Conducted by the

Universal Energy Systems, Inc.

<u>FINAL</u> REPORT

Prepared by: Susan M. Dumbacher

Academic Rank: Graduate Student

Department and   Aerospace Engineering Department

 University: University of Cincinnati

Research Location: AFWAL/FIBRA

                      Wright Patterson AFB

                      Dayton, Ohio   45432

USAF Researcher: Dr. V. Venkayya

Date: 29 Sept 87

Contract No: F49620-85-C-0013

PRELIMINARY APPLICATIONS OF DECENTRALIZED ESTIMATION

TO LARGE FLEXIBLE SPACE STRUCTURES

by

Susan M. Dumbacher

ABSTRACT

The advent of space travel requires the examination of Large Flexible Space Structures (LFSS) as a means to achieve it. Much experimentation is being done in the field of control and estimation of parameters on these structures, since adequate testing cannot be done on earth to determine exactly the damping, frequencies and mode shapes of these structures. To vibrationally suppress a LFSS, or maintain it at a state of equilibrium, actuators and sensors are placed at various locations along the structure which are then used to damp out selected modes. To determine modal positions and velocities of a LFSS, decentralized estimation/control is examined here as an alternative to a fully centralized system.

ACKNOWLEDGEMENTS

I. INTRODUCTION

Large Flexible Space Structures (LFSS) include large antennas, solar sails, space stations, solar power satellites, and other structures which may one day be employed on space vehicles. The Draper II model in Figure 1 is an example of a space telescope . Typical characteristics of LFSS are low inherent damping, generally of the order of 1%, low and closely spaced structural frequencies, and an infinite number of modes required to completely describe the motion of the system. Usually, only a small number of these modes contribute significantly to the structure's dynamic response. Through model reduction, the significant modes of the system are retained. There are two main motives for model reduction. The first is the fact that an infinite number of modes cannot be represented in a Finite Element Model (FEM). The second is the impracticality of retaining a large number of modes in a computational application. As a result of this, the designer must choose some criterion to reduce the model. For efficient computation, a controller or estimator should be of even lower dimension than the reduced model.

The typical control objectives of a LFSS include pointing accuracy, such as that needed for large antennas or docking maneuvers, vibration suppression, which maintains a certain state of equilibrium in the structure, and shaping control. This paper deals only with vibration suppression. One assumption is made about the LFSS to be controlled: the sensors and actuators are collocated. This ensures positive realness of the controller(s), which has desirable stability properties, as outlined in [Ref 9].

II. OBJECTIVES

Vibration suppression of LFSS may be achieved through modal control, or the damping of selected modes. The use of centralized estimation to estimate modal variables at locations along the LFSS is often costly and time consuming. Decentralized estimation offers the advantage of a compact, distributed system but it is also less accurate. This will be elaborated upon shortly. A preliminary comparison study between the decentralized and centralized estimation is presented here, as well as the direction of future research. At present, it is assumed that information about the frequencies and mode shapes of the structure is known exactly. In the future, the effects of uncertainties in these parameters will be investigated.

III. DECENTRALIZATION

A decentralized controller has feedback to an actuator which depends only on the output from that collocated sensor, or from nearby sensors. A decentralized estimator's output depends only on information from the corresponding sensor or group of sensors. Each actuator/sensor pair, or group of pairs, uses only information contained within that subsystem.

The advantages of decentralization follow. Fewer synthesis or design problems exist, since information from each subsystem is self-contained. For example, if 100 sensor/actuator pairs existed, a centralized controller would need information fed over the entire structure. With decentralization, each subsystem is self-sufficient -- hence, information can be retained locally. Decentralized systems are simpler to implement on an onboard computer. Also, decentralization enforces the desired

architecture, namely collocated, decoupled actuators and sensors, to ensure positive realness of the controller(s). It is easier to design lower order sybsystems. Finally, each decentralized subsystem design problem, like a centralized system, is a standard multivariable problem. Thus, a designer can implement tools currently available.

One disadvantage of decentralization is a loss of accuracy, since all the information about the system is not processed optimally. Also, uncertainty exists as to whether a decentralized controller has the same desirable properties as an LQR centralized controller.

III. MODAL ANALYSIS

The basic equations of motion for a structure are

$$[M] \ddot{q} + [C] \dot{q} + [K] q = Q \qquad \text{(eq 1)}$$

where $[M]$, $[C]$ and $[K]$ are the mass, damping and stiffness matrices, and Q is the force vector acting upon the structure. Since LFSS generally have very low damping, the assumption of $[C] = [0]$ is valid. A small damping term will be added at a later time. The equations of motion in the form of (e 1) are coupled. To decouple these equations, implement the method of modal analysis as given in [Ref 1]. First, introduce the linear transformation

$$q(t) = [U] \underline{n}(t) \qquad \text{(eq 2)}$$

where $[U]$ is the modal matrix and $\underline{n}(t)$ is a generalized coordinate. (Eq 1) then becomes (assuming [C]=[0])

$$[M] [U] \ddot{\underline{n}} + [K] [U] \underline{n} = Q \qquad . \qquad \text{(eq 3)}$$

Premultiplying (eq 3) by $[U]^T$ and normalizing $[U]$ such that its amplitude is no longer arbitrary via

$$[U]^T [M] [U] = [I] \qquad \text{(eq 4a)}$$

$$[U]^T [K] [U] = [\sim \omega^2 \sim] \quad , \qquad \text{(eq 4b)}$$

where $[\sim \omega^2 \sim]$ is a diagonal matrix of the squares of the eigenvalues, and $[U]^T \underline{Q} = \underline{N}$, yields

$$\ddot{\underline{n}} + [\sim \omega^2 \sim] \underline{n} = \underline{N} \qquad \text{(eq 5a)}$$

or

$$\ddot{n}_r(t) + \omega_r^2 n_r(t) = N_r(t) \qquad \text{(eq 5b)}$$

for the rth mode. An example of normalizing $[U]$ will be given later.

For simplicity, a pinned-pinned beam structure will be presented as an example. The fourth order equation for a beam, as cited in [Ref 1], is

$$m \frac{\partial^2 y(x,t)}{\partial t^2} - EI \frac{\partial^4 y(x,t)}{\partial x^4} = f(x,t) \qquad \text{(eq 6)}$$

where EI is the stiffness, $y(x,t)$ is the displacement of the beam and $f(x,t)$ is the force distribution applied to the beam. Assuming that free vibration occurs, i.e. $f(x,t)=0$, and that $y(x,t)$ is separable in time and space as

$$y(x,t) = q(t) U(x) \qquad \text{(eq 7)}$$

then the solutions to (eq 6) obey

$$\ddot{q} + \omega^2 q = 0 \qquad \text{(eq 8)}$$

and

$$U^{(4)} + (m \omega^2 / EI) U = 0 \quad . \qquad \text{(eq 9)}$$

Solving this pinned-pinned beam problem for the natural frequencies, ω_n, and the mode shapes, U_n, in (eq 9) yields the values

$$\omega_n = (n\pi)^2 \sqrt{EI/(mL^4)} \quad , \quad n=1,2,\ldots,\infty \qquad \text{(eq10a)}$$

18-7

$$U_n(x) = A_n \sin(n\pi x/L) \quad . \qquad \text{(eq 10b)}$$

The mode shapes are arbitrary in amplitude, A_n. Normalizing such that

$$_0\!\int^L m\, U_n^2(x)\, dx = 1 \qquad \text{(eq 11)}$$

gives

$$U_n(x) = \sqrt{2/mL} \;\; \sin(n\pi x/L) \; . \qquad \text{(eq 13)}$$

The total displacement and velocity of the beam can then be represented as the sum of the mode shapes multiplied by the generalized coordinates:

$$y(x,t) = {}_n\!\sum_1 U_n(x)\eta_n(t) \qquad \text{(eq 14a)}$$

$$\dot{y}(x,t) = {}_n\!\sum_1 U_n(x)\dot{\eta}_n(t) \qquad \text{(eq 14b)}$$

IV. PROBLEM FORMULATION

The simple beam example used throughout this study is a pinned-pinned beam with an impulse force applied as shown in Figure 2. Let the state, $\underline{x}$, be defined as

$$\underline{x} = [\; \eta_1 \; \dot{\eta}_1 \; : \; \eta_2 \; \dot{\eta}_2 \; : \; \dots \; : \; \eta_n \; \dot{\eta}_n \;]^T \qquad \text{(eq 16a)}$$

where η_i and $\dot{\eta}_i$ are the ith modal position and velocity, respectively. The state space formulation then becomes

$$\dot{\underline{x}} = A\,\underline{x} + B\,\underline{u} \qquad \text{(eq 16b)}$$

$$\underline{y} = C\,\underline{x} \qquad \text{(eq 16c)}$$

$$A = \begin{bmatrix} A_1 & & \\ & A_2 & \quad 0 \\ & & \ddots \\ 0 & & \quad A_n \end{bmatrix} \quad , \quad A_i = \begin{bmatrix} 0 & 1 \\ -\omega_i^2 & -2\zeta_i\omega_i^2 \end{bmatrix} \quad ,$$

18-8

$$C = [0 \ C_1 : 0 \ C_2 : \ldots : 0 \ C_n] \ .$$

The matrix C takes the above form for a velocity sensor and, since actuators and sensors are collocated, $B = C^T$. The damping term ζ_i is included in the dynamics matrix A here to represent the slight damping inherent in the structure without destroying the decoupled form of the equations.

The basic estimator equation is given by

$$\dot{\hat{x}} = A \hat{x} + B \underline{u} + K_F (\underline{y} - C \hat{x}) \qquad \text{(eq 17)}$$

where $\hat{x}$ is the estimated state and K_F is the filter gain determined by the standard gain matrix and Riccati equations, as given in [Ref 14]. The results of the centralized estimation are shown, in conjuction with the actual motion and the preliminary decentralized results, in Figure 4. Note that the centralized estimate follows the actual motion closely.

For the decentralized case, the identical example of Figure 2 is used, but with two velocity sensors located as shown in Figure 3. As an arbitrary case, one sensor provides output for one estimator. A second sensor provides output for a second estimator. The first estimator models and estimates only the first mode of the system while the second estimator models and estimates only the second mode of the system. Hence, the result is two single-mode decentralized estimators. The ith estimator is given as

$$\dot{\hat{x}}_i = A_i \hat{x}_i + B_i \underline{u}_i + K_{F_i} (\underline{y}_i - C_i \hat{x}_i) \ . \qquad \text{(eq 18)}$$

Figures 4-5 show the oscillatory motion of the decentralized estimates about the actual motion. These oscillations render the results unacceptable. Examining the separated first and second mode estimates of the decentralized system, shown in Figure 6, it can clearly be seen that the

18-9

error between the decentralized estimate and the actual motion oscillates at undesirably high frequencies.

The error transfer functions for the decentralized estimates come from the relation

$$\dot{\underline{e}} = \dot{\underline{x}} - \dot{\hat{\underline{x}}} \qquad \text{(eq 19a)}$$

or

$$\dot{\underline{e}} = [\, A_{M_{CL}} \,] \, \underline{e} + [\, HA - A_{M_{CL}} H - K_F C \,] \, \underline{x} \qquad \text{(eq 19b)}$$

where H is a matrix of ones and zeros correcting dimensions between the actual state and the reduced-order estimated state and $A_{M_{CL}}$ is the closed-loop estimator dynamics matrix. The Bode magnitude plots of the oscillatory decentralized error, shown in Figures 7-8, indicate higher frequencies in the first and second mode filters. By varying the gains in (eq 19b), the frequency response of the filters may be shaped as shown in Figures 7-8. Figure 9 shows the separated first and second estimated modes of motion with shaped filters. It can be seen that much of the high frequency error has now been removed. The total actual motion of the system and decentralized estimation results with the first mode filter shaped are shown in Figure 10. Much improvement over Figure 4 is observed. The results for the total actual motion of the system and decentralized estimation with both filters shaped are given in Figure 11. A generalized method to select filter gains for shaping out unwanted frequencies is desired. This method is as yet undeveloped, but would be based upon trends observed by varying the gains in (eq 19b).

V. RECOMMENDATIONS

18-10

In conclusion, decentralized estimation results are acceptable for the simple beam example presented. In the future, various sensor locations and applied force patterns, as well as estimation using nearby sensor(s), will be evaluated. For comparison purposes, a performance scalar value must be determined. Mean Square Error parameters are not applicable here, due to the difference in order between centralized and decentralized systems. After combinations of parameters are evaluated for the simple beam problem, a 10-bar truss model will be treated by the scheme. At this point, it is likely that typical problems associated with LFSS will be encountered, such as closely spaced frequencies and the need for considerable model reduction. Finally, an LQR controller will be added to evaluate the stability using the centralized and decentralized filters. At this time, a more thorough comparison between the two types of estimation procedures can be made.
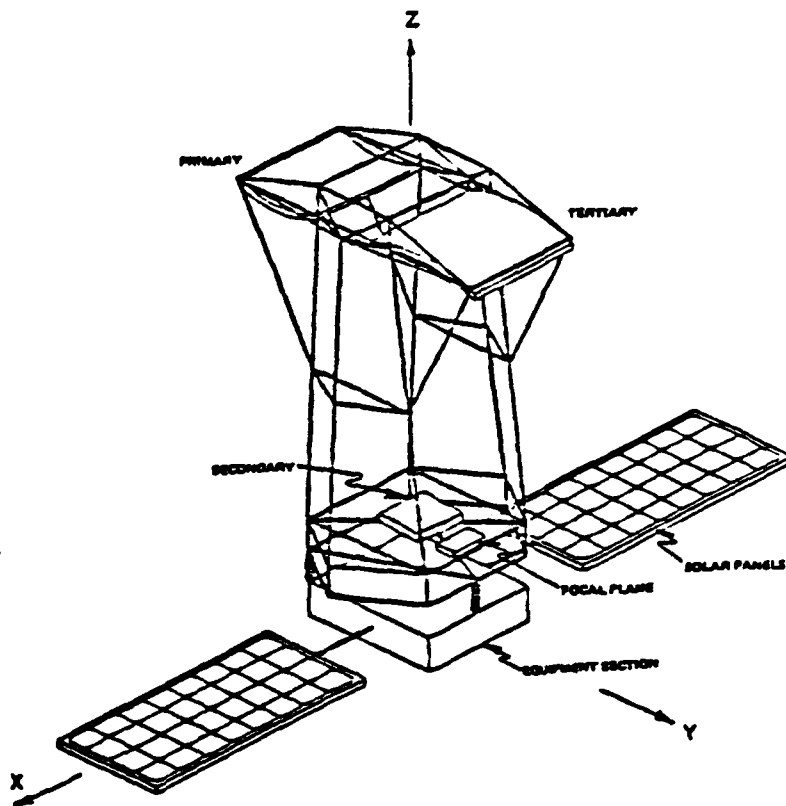
FIGURE 1: The DRAPER II Space Telescope Structure
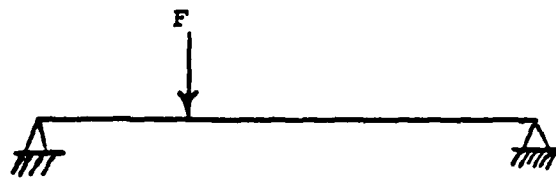
FIGURE 2: Pinned-Pinned beam with impulse force applied as shown.
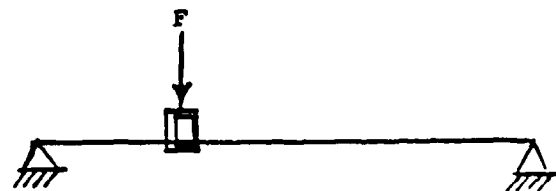
FIGURE 3: Pinned-pinned beam with impulse force applied and 2 sensors located as shown.
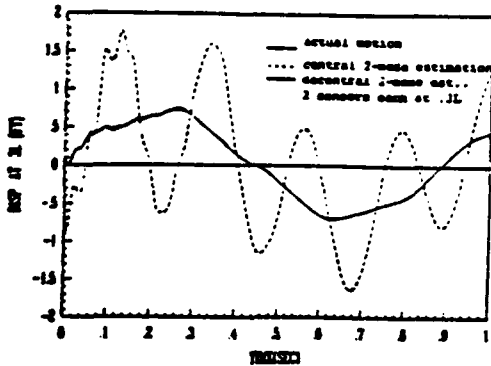
FIGURE 4a: DISP. AT 2L CENTRAL AND DECENTRAL ESTIMATION
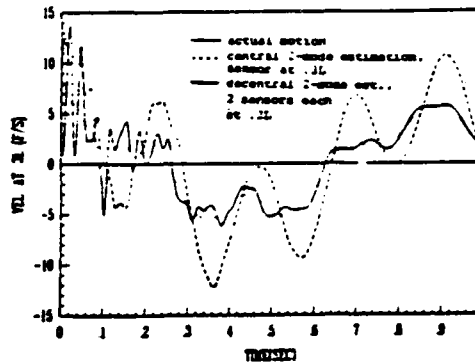
FIGURE 4b: VEL AT 2L CENTRAL AND DECENTRAL ESTIMATION
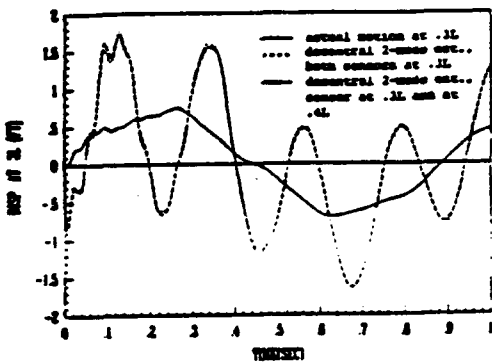
FIGURE 5a: DISP. AT 2L DECENTRAL ESTIMATION SENSORS AT 2L,4L
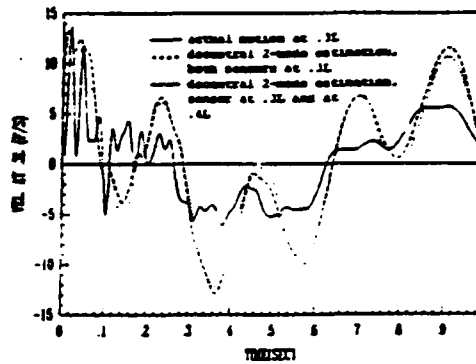
FIGURE 5b: VEL AT 2L DECENTRAL ESTIMATION SENSORS AT 2L AND 2L,4L

ACTUAL AND DEC. EST. MOTION AT 2L

FIGURE 6a: Kalman gains for both filters by LQG equality

ACTUAL AND DEC. EST. MOTION AT 2L

FIGURE 6b: Kalman gains for both filters by LQG equality

18-13
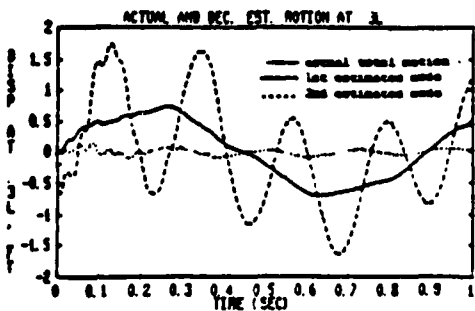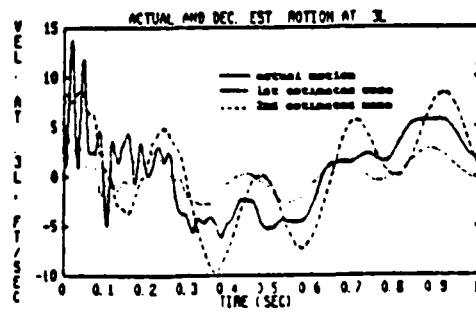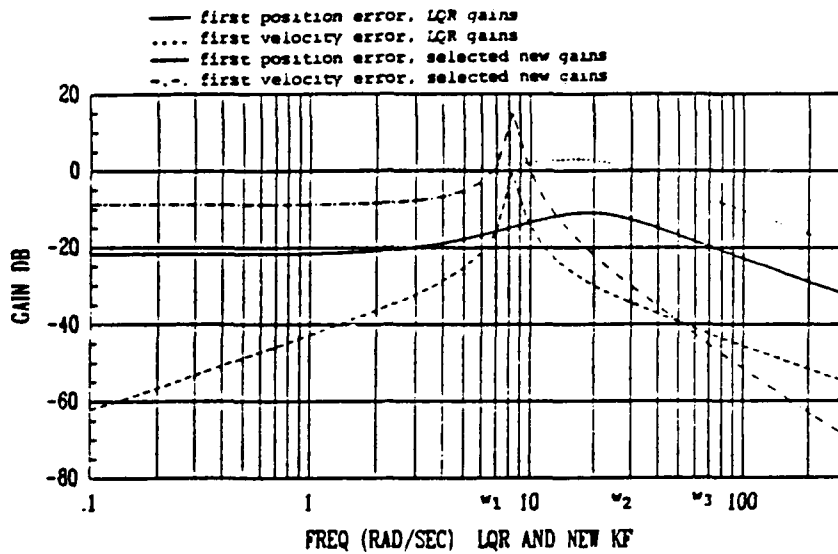
FIGURE 7: 1ST STATE ERROR TF DUE TO 2ND MODE VELOCITY
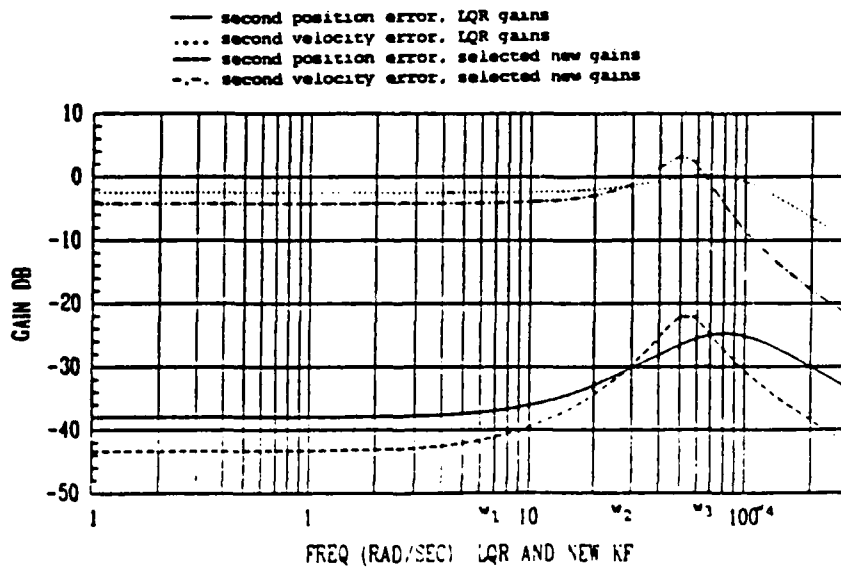
FIGURE 8: 2ND STATE ERROR TF DUE TO 1ST MODEVELOCITY

18-14

MICROCOPY RESOLUTION TEST CHART

NATIONAL BUREAU OF STANDARDS-1963-A

FIGURE 9a

FIGURE 9b

FIGURE 10a

FIGURE 10b

FIGURE 11b

FIGURE 11a

18-15
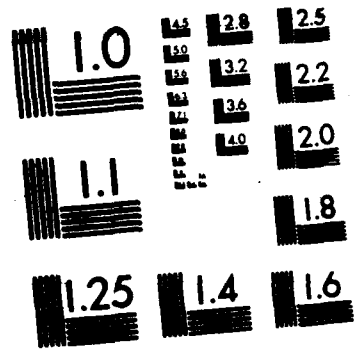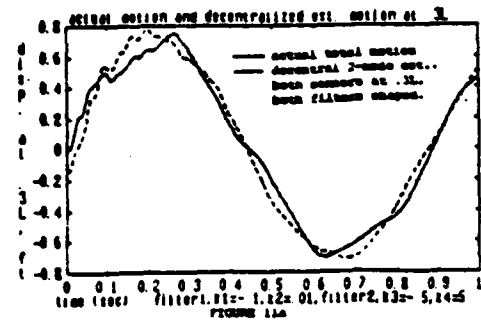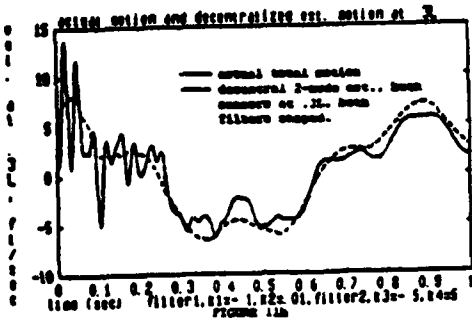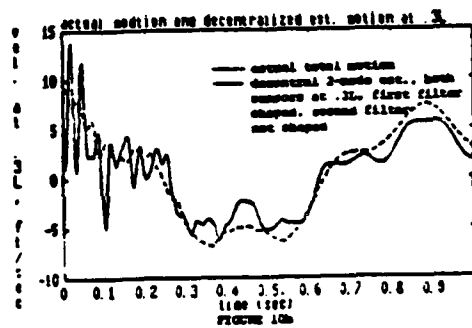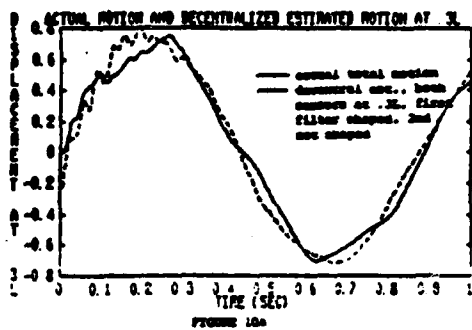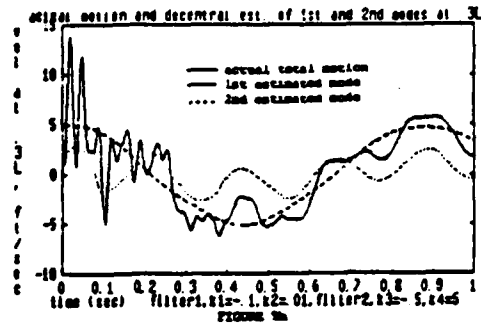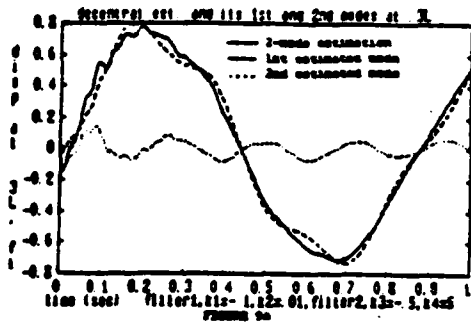
REFERENCES

[1]   Meirovitch, L., <u>Analytical</u> <u>Methods</u> <u>in</u> <u>Vibrations</u>, The Macmillan
      Company, New York, 1967.

[2]   Hughes, P.C., "Space Structure Vibration Modes: How Many Exist? Which
      Ones are Important?", IEEE Control Systems Magazine, February, 1987.

[3]   Silverberg,L., "Uniform Damping Control of Spacecraft", Journal of
      Guidance, Vol.9, No.2, March-April 1986, pp. 221-7.

[4]   Uskokovic, Z. and J. Medanic, "Sequential Design of Decentralized
      Low-Order Dynamic Regulators", Proceedings of 24th Conference
      on Decision and Control, Ft. Lauderdale, FL, December, 1985, pp.837-42.

[5]   Looze, D.P., M. Athans and J.S. Eterno, "Decentralized Control of
      Sequentially Assembled Large Space Structures", Proceedings of 24th
      Conference on Decision and Control, Ft. Lauderdale, FL, December, 1985,
      pp. 1844-51.

[6]   Miller, D.F., V.B. Venkayya and V.A. Tischler, "Integration of
      Structures and Controls -- Some Computational Issues", Proceedings of
      24th Conference on Decision and Control, Ft. Lauderdale, FL, December,
      1985, pp. 924-31.

[7]   McClamroch, N.H., "Vibration Control of Flexible Structures Using
      Member Dampers", Proceedings of 24th Conference on Decision and
      Control, Ft. Lauderdale, FL, December, 1985, pp. 936-9.

[8]   Williams, J.P. and R.C. Montgomery, "Failure Detection and
      Accommodation in Structural Dynamics Systems Using Analytic
      Redundancy", Proceedings of 24th Conference on Decision and Control,
      Ft. Lauderdale, FL, December, 1985, pp. 906-10.

[9]   Joshi, S.M., "Robustness Properties of Collocated Controllers for
      Flexible Spacecraft", Journal of Guidance, Vol.9, No.1, Jan.-Feb.,
      1986, pp. 85-91.

[10] Yam, Y., T.L. Johnson and J.H. Lang, "Flexible System Model Reduction
      and Control System Design Based Upon Actuator and Sensor Influence
      Functions", IEEE Transactions on Automatic Control, Vol. AC-32, No. 7,
      July, 1987, pp. 573-82.

[11] Young, J.W., "A Structural Dynamics Approach to the Simulation of
      Spacecraft Control/Structure Interaction", Proceedings of the Workshop
      on Identification and Control of Flexible Space Structures , JPL
      Publication 85-29, 1985, pp. 39-60.

[12] Santiago, J.M., W.J. Lange, Jr. and M. Jamshidi, "An overview of Latest
      Model Reduction and Control Methods of Large Flexible Space Structures"
      Proceedings of the Workshop on Identification and Control of Flexible
      Space Structures , JPL Publication 85-29, 1985, pp. 381-95.

[13] Fanson, J.L., J.C. chen and T.K. Caughey, "Stiffness Control of Large
      Space Structures", Proceedings of the Workshop on Identification and
      Control of Flexible Space Structures , JPL Publication 85-29, 1985,
      pp. 351-64.

[14] Kwakernaak, H. and R. Sivan, <u>Linear</u> <u>Optimal</u> <u>Control</u> <u>Systems</u>, John Wiley
      and Sons, Inc., New York, 1972.

1987 USAF-UES SUMMER FACULTY RESEARCH PROGRAM

GRADUATE STUDENT SUMMER SUPPORT PROGRAM

Sponsored by the

AIR FORCE OFFICE OF SCIENTIFIC RESEARCH

Conducted by the

Universal Energy Systems, Inc.

FINAL REPORT

DISPOSAL OF CHEMOTHERAPEUTIC WASTES

Prepared by:	Robert E. Masingale, Sr., Ph.D.
	and Donna N. Edwards, graduate
	assistant
Academic Rank:	Professor of Chemistry
Department and	Division of Science and Mathematics
University	Jarvis Christian College
Research Location:	USAFOEHL/ECQ
	Brooks AFB TX 78235-5501
USAF Researcher:	Elliot K. Ng, Maj, USAF, BSC
Date:	4 August 1987
Contract No:	F49620-85-C0013

REFERENCE DR. MASINGALE

SFRP FINAL REPORT NUMBER 88

1987 USAF-UES SUMMER FACULTY RESEARCH PROGRAM/

GRADUATE STUDENT SUMMER SUPPORT PROGRAM

Sponsored by the

AIR FORCE OFFICE OF SCIENTIFIC RESEARCH

Conducted by the

Universal Energy Systems, Inc.

FINAL REPORT

Validity of Heat Index as Indicator of Level of Heat Storage for

Personnel Wearing Protective Clothing in Hot Environments

Prepared by: K. Suzanne Enlow

Academic Rank: Graduate Student

Department: Department of Health Education

University: University of Alabama

Research Location: School of Aerospace Medicine, Chemical

                      Defense Branch, Brooks AFB

USAF Researchers: S.H. Constable Ph.D.; S.A. Nunneley, M.D.

Date: July, 1987

Contract No.:   F 49620-85-C-0013

Validity of Heat Index as Indicator of Level of Heat Storage for

Personnél Wearing Protective Clothing in Hot Environments

by

K. Suzanne Enlow

ABSTRACT

The use of protective clothing such as the Chemical Defense

Ensemble (CDE) in moderate to hot environments substantially reduces

work capacity due to heat stress. The purpose of this research was to

determine the validity of a heat stress index in predicting the level

of heat storage when used during work/rest cycles with intermittent

microenvironmental cooling...

ACKNOWLEDGEMENTS

I.   Introduction:

I have an undergraduate degree from the University of Alabama in Community Health Care/Education which included a natural science/mathematics core. My interest in the applied sciences and my work with rural Alabama health projects led me to enter the Master of Art program in Health Promotion at the University of Alabama. Discussions in exercise physiology classes of Dr. Phil Bishop's investigation of the impact of the CDE on work capacity at S.A.M. in 1986 sparked my interests and prompted me to apply for a similar research fellowship.

II.   Objectives of the Research Effort:

The purpose of this research was to evaluate the effectiveness of a heat stress index used during work-rest cycles coupled with microenvironmental cooling during rest in predicting levels of heat storage for personnel engaged in physical labor while wearing the CDE.

II. Overall Approach:

Work by humans in the presence or threat of a physical, chemical or radiation hazard requires the use of protective clothing. The protective clothing varies from that of the American football player to the Chemical Defense Ensemble (CDE) of the U.S. Armed Forces. Commonly, this clothing impairs the normal physiological cooling mechanisms of the body. In warm to hot environments, this compromise of the cooling ability may result in internal heat storage to the extent that work capacity is significantly reduced relative to work in the same environment without the clothing (Joy & Goldman, 1968; Pandolf & Goldman, 1978; Yates, et al, 1980; Webber, et al, 1981; Frye & Flick, 1983; Carpenter & Flick, 1984). In some circumstances, the thermal burden of this protective clothing may be an inconvenience. In emergency rescue, firefighting, military operations, and other situations, the consequent heat storage may be a serious threat to both health and mission success (Joy & Goldman, 1968).

One solution to the heat storage problem of personnel wearing protective clothing in hot environments would be to combine intermittent rest breaks with microenvironmental cooling during rest periods only. Such an approach reduces the requirement for cooling system portability, is more practical than macroenvironmental cooling and would increase the total work output for a given time period by shortening the cooling (rest) time.

Skin temperature, internal or core temperature, and heart rate

are physiological variables which predict human responses to the environment (Gagge & Gonzalez, 1980). Various sensory scales have been used to predict thermal comfort (Houghton & Yaglou, 1923; Winslow et al, 1937; Williams & Shitzer, 1974). A number of varying combinations of these physiological variables and sensory scales have been developed into heat stress indices or predictors (Fanger, 1973; HHS, 1973). Shitzer and colleagues (1978), using macroenvironmental temperature changes and exercise, demonstrated changes in thermal comfort without accompanying changes in internal and skin temperatures. Others such as Gagge (1938), Hardy (1953) and Fanger (1973) have demonstrated skin temperature to be related to thermal comfort without macroenvironmental cooling or heating. However, previous studies have not investigated the problems of heat storage and prediction of its level with subjects wearing protective clothing, such as the Chemical Defense Ensemble, and a personal cooling vest.

Subjects. Subjects for these experiments were six Air Force and two civilian volunteers. Subjects varied in age , fitness, size, and state of heat acclimation and included two females and six males. Subject characteristics are given in Table 1. Because this study was limited to volunteers, this sample may have a higher aerobic fitness level than would be representative of the Air Force.

Methods. All testing was conducted in accordance with S.A.M. ACHE Protocol 86-9. Maximal oxygen uptake was determined using standard gas bag collection methods. Additionally, the metabolic cost

Table 1:   Summary of Subject Characteristics

Subject	Age (yrs)	Ht (cm)	Wt (kg)	vo2max (l/min)	vo2max (ml/min kg)	maxHR
1	21	168.9	60.82	2.99	49.09	194
2	38	176.2	80.43	4.57	55.03	175
3	45	154.6	52.22	1.90	37.30	158
4	42	173.5	78.67	4.59	58.84	192
5	31	182.2	74.14	4.10	55.32	188
6	38	170.0	79.41	3.10	39.09	180
7	25	175.8	64.55	3.55	54.77	191
8	39	185.0	85.43	4.34	57.81	190

of walking on the treadmill dressed only in shorts and tee shirt was also measured. All subjects who did not have previous experience with the protective clothing (PC) were given a practice trial which allowed them to familiarize themselves with the clothing and treadmill walking. Subjects then performed one of the following tests in an environmental chamber at mean dry, wet and globe temperatures of 38/24/44 or 28/23/34 degrees Centigrade, respectively:

1) Treadmill walking at 3 mph and either 3% or 6% grades, depending upon level of fitness, while wearing the PC. Subjects walked until they achieved a rectal temperature of 39.0 C. This test is referred to as "NO REST."

2) The same treadmill exercise except subjects walked 30 minutes at 38.0 C (45 minutes at 28.0 C) followed by 30 minutes (15 minutes at 28.0 C) of rest. Work VO2 with the PC was normally measured during this trial. This test is designated "NO COOL."

3) The same treadmill exercise while wearing the PC except a personal cooling system in which liquid was the cooling medium was used during rest. This test is designated "LIQUID."

4) The same treadmill exercise while wearing the PC except a personal cooling system in which air was the coolong medium was used during rest. This test is designated "AIR."

5) The same treadmill exercise except the subject wore only military fatigue pants and shirt. This test is designated "NO PC."

The PC which was worn consisted of a complete chemical defense

ensemble (CDE) outfit including M1/protective mask and hood. Military
fatigue shirt and trousers were worn under the PC. For safety
reasons, athletic shoes were worn instead of protective rubber
overboots. One of the personal cooling systems consisted of a
snug-fitting ILC Dover liquid cooling vest covering approximately .5
square meters of the upper torso. The vest contained approximately 48
meters of tygon tubing with quick detach, self-sealing connectors.
Coolant was supplied to the vest by an electrically powered cooling
system with an output of one liter per minute of coolant at 10 to 15
degrees C. Coolant was 95% water with 5% propylene glycol. The other
personal cooling system consisted of a mesh vest which received air
from an inlet hose and distributed it to the chest and back. Air was
supplied to the vest from a specially designed air cooling system
which produced air at 10 degrees C. Outlet air was directed through a
flow meter and heater and then into the vest and mask. The heater was
used to control the air temperature at the vest. Air was supplied to
the vest and then disbursed throughout the upper part of the garment
and essentially exhausted to the atmosphere.

Skin temperatures, rectal temperatures, and heart rates were
monitored continuously and recorded every 30 seconds on a PDP-11
computer utilizing a custom system developed by John Garza (OAO
Corp.). Chest and thigh skin temperatures were measured with YSI 700
thermistors. Rectal temperature was measured from a probe located 10
cm beyond the sphincter. At 38.0 degrees C, rating of perceived

exertion (Borg, 1962; see Figure 1) and rating of thermal comfort (Williams & Shitzer, 1974; see Figure 2) were measured at 10 and 30 minutes of work and at the same intervals during rest. At 28.0 degrees C, the ratings were measured at 15, 30 and 45 minutes of work and at 7.5 and 15 minutes of rest.

IV. Results and Discussion:

Correlations between thermal comfort index (COM) and the physiological variables core or internal temperature (TRE), chest skin temperature (TCH), thigh skin temperature (TTH), heart rate (HR), and relative perceived exertion (RPE) are given for each subject and the group in Table 2. All statistics were calculated with STATS Plus, a statistical package for the Apple IIe. Thermal comfort was not a good indicator of core temperature as $-0.09 > R < +0.48$ for individuals and $R = +0.31$ for the group. Also, COM was not a good indicator of TTH ($-0.11 > R < +0.55$ for individuals and $R = +0.28$ for the group) even though the thigh muscles were doing the majority of the work. However, COM was a good indicator of TCH ($R = +0.80$), HR ($R = +0.70$), and RPE ($R = +0.73$) for the group. Correlations for the individuals varied, but were high for the majority ($+0.48 > R < +0.92$ for TCH, $+0.54 > R < +0.91$ for HR, and $+0.67 > R < +0.97$ for RPE). Regression equations for the prediction of TCH, HR, and RPE from COM are given in Table 3. The very low correlations between COM and TRE and between COM and TTH agree with results from earlier studies in which

PERCEIVED EXERTION SCALE

6

7 VERY,VERY LIGHT

8

9 VERY LIGHT

10

11 FAIRLY LIGHT

12

13 SOMEWHAT HARD

14

15 HARD

16

17 VERY HARD

18

19 VERY, VERY HARD

20

FIGURE 1

THERMAL SENSATIONS

0.0 UNBEARABLY COLD
0.5
1.0 VERY COLD
1.5
2.0 COLD
2.5
3.0 COOL
3.5
4.0 COMFORTABLE
4.5
5.0 WARM
5.5
6.0 HOT
6.5
7.0 VERY HOT
7.5
8.0 UNBEARABLY HOT

FIGURE 2

Table 2: Correlations Between Comfort Index and Physiological Variables.

Subject	TRE	TCH	TTH	HR	RPE
1	0.32	0.88	0.41	0.87	0.93
2	-0.03	0.82	0.17	0.90	0.97
3	0.48	0.48	0.35	0.91	0.69
4	-0.09	0.78	0.11	0.54	0.73
5	0.48	0.92	0.44	0.85	0.84
6	0.30	0.80	-0.11	0.56	0.67
7	0.27	0.86	0.25	0.70	0.75
8	0.37	0.92	0.55	0.91	0.80
ALL	0.31	0.80	0.28	0.70	0.73

Table 3: Regression Equations for Prediction of TCH, HR, and RPE from Thermal Comfort.

Variable	Slope	Intercept	R^2
TCH	0.389	-8.57	0.633
HR	0.032	1.27	0.489
RPE	0.144	3.74	0.530

macroenvironmental heating and cooling were used (Shitzer et al, 1978). However, the high correlations for the remaining variables contradict these earlier studies but support steady-state temperature studies (Gagge, 1938; Hardy, 1953; Fanger, 1973). The relationship between thermal comfort and chest skin temperature, heart rate, and relative perceived exertion could be explained due to the fact that thermal sensation is linked primarily to skin temperature which in this case was cooled by a personal cooling vest. In addition, HR and RPE decreased during the cooling cycles as the subject was at rest at this time.

V. Recommendations:

The above results demonstrate COM to be a good predictor of TCH, HR, and RPE when correlations and simple linear regressions are used. It would be useful to calculate multiple regressions using the same variables in order to determine if the combined varibles provide an even better predictor of level of heat storage.

VI. Author's Note:

Portions of this paper, particularly background material and experimental methods, were supplied by my supervising professor, Dr. Phillip A. Bishop.

REFERENCES

Borg, G., *Physical Performance and Perceived Exertion* , Lund, Sweden: Gleerup, 1962.

Carpenter, A.J. and C.A. Flick, "Report on Liquid Cooling Development," *Technical Memo 2/290404* , 4 May 1984, VNC, School of Aerospace Medicine, Brooks Air Force Base, TX.

Fanger, P.O., *Thermal Comfort* , New York: McGraw-Hill, 1973.

Frye, A.J. and C.A. Flick, "Report on Chamber Evaluation of Groundcrew Liquid Cooling System," *Technical Memo 2/20009 & 2/290404* , 1983, VNC, SAM, Brooks AFB, TX.

Gagge, A.P., C.E.A. Winslow, & L.P. Herrington, "The Influence of Clothing on Physiological Reactions of the Human Body to Varying Environmental Temperatures," *American Journal of Physiology* , 1938, 124, pp. 30-50.

Gagge, A.P. and R.R. Gonzalez, "Rational Indices of Heat Stress and Strain in Warm Environments," *Satellite of 28. Int. Congress of Physiological Sci.* , Pecs, Hungary: Pergamon Press, 1980, 32, pp. 553-7.

Hardy, J.D., "Control of Heat Loss and Heat Production in Physiologic Temperature Regulation," The Harvey Lecturers , 1953, 49, pp. 242-70.

Health and Human Services, The Industrial Environment-its Evaluation and Control , Washington, D.C.: U.S. Government Printing Office, 1973.

Houghten, F.C. and C.P. Yaglou, "Determining Lines of Equal Comfort," ASHVE Trans. , 1923, 28, pp. 361-84.

Joy, R.J.T. and R. Goldman, "A Method of Relating Physiology and Military Performance: a study of some effects of vapor barrier clothing in a hot climate," Military Medicine , 1968, pp. 458-70.

Pandolf and R.F. Goldman, "Convergence of Skin and Rectal Temperatures as a Criterion for Heat Tolerance," Aviat. Space and Environ. Med. , 1978, 49, pp. 1095-1101.

Shitzer, A., E.B. Rasmussen and P.O. Fanger, "Human Responses During Recovery from Heat Stress with Relation to Comfort," Ergonomics , 1978, 21 (1), pp. 21-34.

Webber, B., L. Montgomery, L. Miller and B. Williams, "A Comparison of Three Liquid-Ventilation Garments during Treadmill Exercise," Aviat.

Space and Environ. Med. , 1981, 52, pp. 400-415.

Williams, B.A. and A. Shitzer, "Modular Liquid-Cooled Helmet Liner for
Thermal Comfort," Aerospace Medicine , 1974, 45, pp. 1030-36.

Winslow, C.E.A., L.P. Herrington and A.P. Gagge, "Relations Between
Atmospheric Conditions, Physiological Reactions and Sensations of
Pleasantness," Amer. J. Hyg. , 1937, 26, pp. 103-115.

Yates, R.E., C.R. Replogle and J.H. Veghte, "Thermal and Acceleration
Effects on Aircrew Members in Chemical Defense Wear," AMRL-Technical
Report 79-71 , 1980, pp. 1-36.

1987 USAF-UES SUMMER FACULTY RESEARCH PROGRAM

GRADUATE STUDENT SUMMER SUPPORT PROGRAM

Sponsored by the

AIR FORCE OFFICE OF SCIENTIFIC RESEARCH

Conducted by the

Universal Energy Systems, Inc.

<u>FINAL</u> <u>REPORT</u>

INVESTIGATION INTO THE APPLICABILITY

OF

FRACTURE MECHANICS TECHNIQUES

TO

AIRCRAFT WHEEL LIFE STUDIES

Prepared by: Thomas J. Enneking

Academic Rank: Graduate Student

Department and   Civil Engineering

University: University of Notre Dame

Research Location: AFWAL/FIEMA
                      Wright Patterson AFB, Ohio   45433

USAF Researcher: D. H. Treanor, 1Lt. USAF

Date: August 7, 1987

Contract No.:   F49620-85-C-0013

Investigation into the Applicability of Fracture Mechanics
Techniques to Aircraft Wheel Life Studies

by

Thomas J. Enneking

ABSTRACT

In response to a specified logistic need, an in-house
program was initiated in late 1986 to investigate test and
analytical methods for wheel life estimation and
verification. In conjunction with this program, an
additional ten week study was initiated June 1, 1987 to
explore analytical techniques for fatigue analysis and
experimental methods to verify these analytical techniques.
In particular, the applicability and feasibility of applying
fracture mechanics concepts to aircraft wheel assemblies was
assessed. A detailed literature review was performed to
identify current research activity involving aircraft wheels
and fatigue studies. This was expanded to include finite
element techniques and stochastic methods as applied to
wheel life and reliability estimates. Based on the results
of this study, and previous studies, a combined analytical
and experimental methodology was proposed for the estimation
and verification of aircraft wheel service life. This
proposed multi-task approach contains several alternatives
within the individual tasks. The optimum alternatives,
i.e., those with the highest probability of success and an
acceptable cost (effort), will be the object of further
studies.

Acknowledgements

I wish to thank the Air Force Systems Command and the Air Force Office of Scientific Research for sponsorship of this student support program. Universal Energy Systems should also be mentioned for their assistance in the administrative aspects of this program.

This ten week summer experience was very beneficial to me in several different ways. All personnel from the Flight Dynamics Lab which I encountered during this period should be thanked for their assistance. Dr. Arnold Mayer, Assistant for Research and Technology Vehicle Equipment Division, Mr. Aivars Petersons, Mechanical Branch Chief, and Mr. Paul Ulrich, Mechanical Subsystems Group Leader, provided me with continual support and encouragement throughout the program. Lt. Dave Treanor's daily concern and interest in my work served as a source of stimulation and everyone in the Mechanical Subsystems Group provided a truly enjoyable working environment. Thank you all.

I. INTRODUCTION

My present research interests are in fracture mechanics and the utilization of stochastic techniques for life estimation in structures. Additionally, during previous employment as a structural consultant, I was involved in the determination of stress states and dynamic characteristics for a variety of mechanical components. Thus, this ten week assignment in the Vehicle Equipment Division of the Flight Dynamics Lab provided an excellent opportunity to utilize my previous experience and expertise while increasing my capabilities and experience in other areas.

In response to a specified logistic need, an in-house program under the direction of Lt. David Treanor was initiated in late 1986 to investigate test and analytical methods for wheel life prediction. Its initial specific objective is to develop a methodology for determining representative loading spectra for military aircraft and experimental qualifications for verification of wheel life. In conjunction with this program, an additional ten week study was initiated June 1, 1987 to explore analytical techniques for fatigue analysis and experimental methods to verify these analytical techniques. In particular, the applicability and feasibility of applying fracture mechanics concepts to aircraft wheel assemblies was to be assessed.

Ground to tire loads are transmitted through the flange to the wheel giving rise to concentrated bending and tensile stress states. When the wheel is rotating, these cyclic

stresses are superimposed on the mean stress due to tire inflation and any residual stresses present. The critical stress area of the wheel is often the bead seat radius of the flange at the tire/wheel interface.

Fatigue is a major problem in many structural components and although wheels are often considered "deadweight" by many aircraft designers, an FAA study (10) showed that more than 30% of the over 5000 operational failures reported from 1970-1975 were due to wheel problems. This does not include wheels which were removed from service ahead of their expected service life due to cracks found during routine tire changes and inspections. In addition to high impact landing loads and significant lateral loads due to low speed turns and drift, aircraft wheels may be required to roll over 100,000 miles over the design life of the aircraft, depending on the type, during routine taxiing, often in a highly corrosive environment.

A detailed literature review was performed and a combined analytical and experimental methodology was proposed to better understand wheel behavior and estimate life. Recommendations for future experimental and analytical tasks were presented.

II. OBJECTIVES AND APPROACH

The original proposed goals and objectives for this ten week study were to:

1) Assess the feasibility of applying fracture mechanics techniques to aircraft wheels to more accurately predict crack initiation, propagation, and fracture.

2) Define the input requirements and analysis tools required to utilize fracture mechanics techniques as a design tool.

3) Develop experimental methods to verify analytical results.

The initial approach was multi-phased including a problem identification phase and a study of deterministic fatigue topics: material properties, non-destructive test or inspection methods, fracture mechanics concepts, and finite element modeling. Experimental techniques were also studied.

Based on preliminary results documented in the Five Week Progress Report (34), which is available from the author, the objectives were broadened in scope but condensed into the following single objective:

- Develop a combined analytical and experimental methodology for estimating and verifying the service life of an aircraft wheel.

In order to accomplish this objective, a more detailed literature review was required along with a better under-standing of present techniques utilized by the vendors in

aircraft wheel design and load determination. The proposed

methodology is discussed in detail in the next section.

Final conclusions and recommendations are summarized in

Section IV. The reference list is actually in two parts.

References numbered 1 - 30 are included in the Five Week

Progress Report (34) while references numbered 31 - 40 are

listed in Section V of this report.

III. PROPOSED METHODOLOGY

The "military aircraft wheel life problem" has been

present in the aircraft industry for more than 25 years.

Thus the following methodology, shown schematically in

Figure 1, is an involved research plan whose ultimate goal

is a better understanding of wheel behavior so that ideally,

at its conclusion, a verifiable approach will be available

to estimate a wheel service life with confidence. Five

major tasks were identified. A variety of options within

each task are possible. The detailed literature review and

load determination tasks are currently ongoing. Each task

is discussed in detail in the following subsections.

III.A. Detailed Literature Review

Before initiating a program of this scope, it is

necessary to identify and understand as much previously

published information concerning the problem, both academic

and industrial, as possible. Thus a major portion of this

ten week assignment was spent in this task. Several topics

were identified as key topics and specifically addressed in

21-7
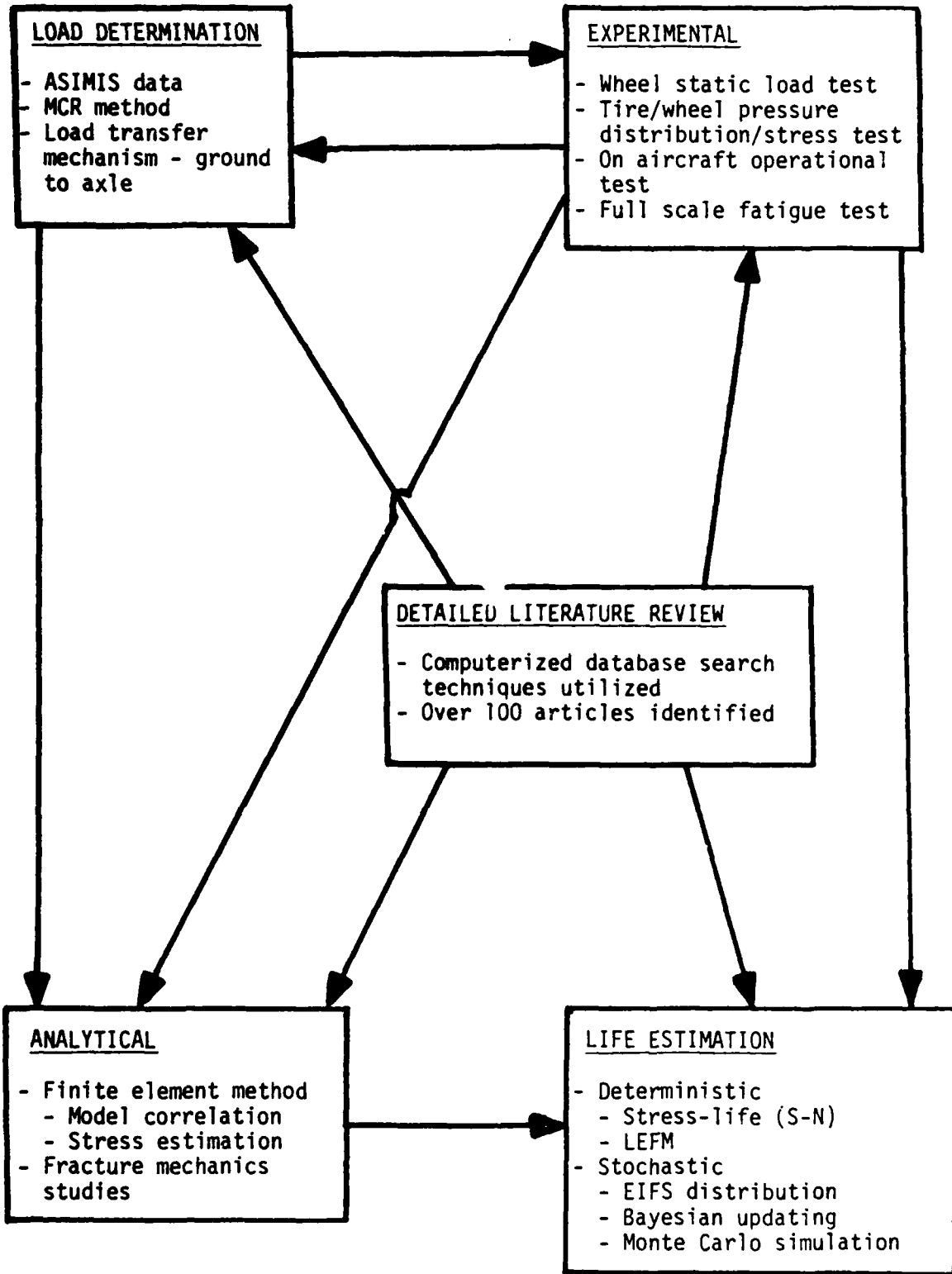
Figure 1 - Proposed Methodology for Wheel Life Study

the detailed literature review. These are shown in Table 1.
Over 100 articles were identified using both traditional and
computerized literature database search techniques.
Over half of these have been reviewed in detail. Table 1
indexes the contents of forty of these articles with respect
to the key topics. References numbered 1- 30 are included in
the Five Week Progress Report (34). The remaining reference
numbers are from the list in Section V of this report.
Additional references have been provided to the Mechanical
Subsystems Branch. This study should be continued and
Table 1 continually updated to form a complete information
database for wheel studies.

III.B. Load Determination

Load determination methods have been investigated
during an in-house effort under the direction of Lt. Dave
Treanor (29). The proposed MCR (multi-channel recorder)
method involves obtaining flight data from the ASIMIS (Air-
craft Structural Integrity Management Information System)
program and using this data with rigid body mechanics
techniques to determine ground loads. A more detailed
understanding of these ground load equations and data reduc-
tion techniques (cycle counting) utilized in the MCR method
(39) is required in this task of the proposed wheel life
program. This method could be used for both aircraft cur-
rently in service and proposed aircraft whose mission envi-
ronment is similar to an aircraft currently in service.

Table 1 - Detailed Literature Review

Reference No.	Wheels and/or Landing Gear	Fracture Mechanics	Other Fatigue Study Methods	Finite Element Method	Wheel Load Determination	Material Properties	Experimental Methods	Stochastic Methods	Environmental Effects	Non-Destructive Inspection
1	X		X		X		X		X	
2		X		X			X			
3		X	X	X		X	X		X	X
4	X	X	X		X	X	X		X	
5						X				
6		X		X			X			
7	X		X			X				
8	X				X					
9		X								
10	X	X	X		X	X	X		X	X
11			X		X	X	X		X	
12		X								
13		X			X					
14		X					X			
15		X					X			
16	X		X		X		X			
17		X		X						
18	X		X		X		X			
19		X	X					X		
20		X	X					X		
21	X		X		X		X			
22		X		X	X	X	X			X
23	X		X	X	X		X			
24	X		X	X						
25		X	X				X		X	X
26	X		X				X			
27		X	X						X	
28	X				X		X			
29	X		X	X	X		X			
30	X	X						X		
31		X						X		
32	X				X		X			
33		X								
34	X	X	X	X	X	X	X		X	X
35	X	X			X	X			X	
36	X	X			X		X			
37		X	X	X				X		
38		X	X							
39	X		X		X		X			
40		X						X		

Several other issues also remain unresolved in this task:

- What is the load transfer mechanism from the ground to the axle? How does the pressure distribution between the wheel and tire change with changes in loading?

- Is the cycle counting technique used in the MCR method acceptable for a fracture mechanics based fatigue life study? Does the wheel rotation increase the number of cycles? Are load sequences properly identified?

- Are accelerations at the center of gravity of the aircraft amplified, attenuated, or unchanged by the structural characteristics of the airframe and landing gear between the aircraft center of gravity and the axle during typical wheel loading maneuvers?

Experimental data is required to resolve these issues.

III.C. Analytical Studies

A basic understanding of the three dimensional behavior of an aircraft wheel is required to accurately estimate its life. Previous wheel studies have utilized large three dimensional models, however correlation with test data has, for the most part, been unsuccessful. This could be attributed to at least two factors: 1) the load mechanism was not properly understood and/or modeled, 2) the structural characteristics of the wheel were modeled inaccurately. An analytical study is proposed to determine the type of model required to accurately estimate wheel behavior. The finite element method will be used. Several

finite element codes (SAPIV, COSMIC NASTRAN, I-DEAS) are presently being investigated for use in this study. Modeling will increase in complexity from a two dimensional plane strain model through axisymmetric to three dimensional shell and solid models. Fourier series approximations for non-axisymmetric loads on an axisymmetric model will be investigated. Experimental data will be required to verify model behavior. This will be discussed in the following section. However, it should be noted here that the loading to be used in this correlation phase is not the actual loading but a more easily quantified loading initially on the wheel only.

After developing the model required for correlation, stress intensity factors will be determined and crack propagation studies performed using the loads determined in the previous load determination task. Other analytical studies could also be performed. System models of tire/wheel systems or complete landing gear systems could be developed. Finite element models of test coupons could be used in elastic-plastic studies in conjunction with coupon testing to estimate crack initiation due to corrosion. These studies have not been developed in detail at this time.

III.D. Experimental Verification

Several tests have been identified which either verify assumptions made in the load determination and analytical

model correlation tasks and/or provide information required for model fatigue studies.

Model Correlation

- A "Wheel-Only" static load test is required to verify the modeling of the stiffness of the three dimensional wheel structure.

- A tire/wheel pressure distribution test is required to identify the load transfer mechanism (pressure distribution) between the tire and wheel. Differing horizontal and vertical loads should be input into the tire/wheel system. Strains should be measured at key locations in the wheel concurrently with the pressure measurement. Then the measured pressure distribution could be applied to the wheel model, which has been correlated to the static load test data, and stresses determined and compared with the measured stresses to verify its response to tire transmitted loads.

Load Verification

- An on-aircraft operational test is required to completely verify the load method (MCR method). This would quantify the difference, if any, between aircraft center of gravity accelerations and wheel accelerations. In addition, the effects of wheel rotation on cycle counting and load sequencing would be identified.

- A modal test of the aircraft landing gear system could be conducted to verify the relationship between the accelerations if an on-aircraft operational test is not feasible, however, the latter is prefered.

- Wheels which have failed in service should be examined and maintenance records should be used to document and quantify the "wheel life problem".

Fatigue Studies

- "Wheel-Only" full scale fatigue tests, in a controlled environment with controlled loads, could be performed to verify which life estimation technique (S-N or fracture mechanics based) most closely estimates actual life.

- Fatigue testing of coupons in a corrosive environment subject to controlled loads could be performed to verify results from elastic-plastic finite element studies.

III.E. Life Estimation

Several methods are available for estimating wheel life. Traditionally wheel vendors have utilized the stress-cycle (S-N) method for fatigue life estimation. This method has a long history of use and has been shown to work well for long life components subjected to constant amplitude loading. However, it is completely empirical in nature and provides no physical insight into the fatigue mechanism or degree of damage.

Linear elastic fracture mechanics (LEFM) principles have been used for approximately twenty years in research environments to estimate crack propagation life based on a known or assumed initial crack size. This approach is based on standard elasticity theory assumptions, small displacements and linear constitutive law, and a negligible plastic zone at the crack tip. If crack initiation is of primary importance however, elastic-plastic analyses must be performed. Total estimated life is then the summation of crack initiation life and crack propagation life.

Stochastic methods could also be used in life estimation techniques. Research is currently ongoing in the areas of stochastic modeling of fatigue crack growth (32,37). In the absence of deterministic values for initial flaw sizes, an equivalent initial flaw size (EIFS) distribution could be estimated probabilistically from some later measured flaw size. Life could then be estimated using this EIFS distribution. Reliability studies using probabilistic techniques could be performed to determine the optimum inspection intervals and stochastic based estimates for life. This is also an on-going research area for other structural components (40). Bayesian updating techniques could be utilized to continually revise original life estimates based on the information from available, or if possible more detailed, maintenance records.

IV. CONCLUSIONS AND RECOMMENDATIONS

The following conclusions were developed from the results of the ten week study:

1. The "wheel life problem" is not something recently discovered or easily solved. Reports more than 25 years old document situations similar to todays.

2. The traditional S-N method for fatigue life evaluation is still the primary design method of wheel vendors.

3. Corrosion is a significant contributor to crack initiation in wheels. Corrosion in combination with fatigue is a complex research topic which is not yet fully understood.

4. Non-destructive test (NDT) or inspection (NDI) techniques are highly dependent on operator capability and have a poor history of reproducibility. Presently available techniques cannot be used to directly identify initial flaws for fracture mechanics studies but could be utilized with stochastic methods to estimate equivalent initial flaw sizes (EIFS).

5. Based on previous wheel studies, the major detrimental loading mechanism is lateral load due to low speed turns and drift. However, underinflated tires increase load transmission to the wheels and constant high flightline temperature and brake temperatures on the main landing gear wheels have an adverse effect on wheel material properties and crack growth rates.

6.   Finite element techniques have been utilized in wheel studies to determine stresses for use in S-N life prediction, however, correlation with test results have been, for the most part, unsuccessful.

7.   Wheel fatigue life is spent in initiating and propagating a crack to failure. Previous wheel studies are inconclusive as to whether a majority of the wheel life is spent in the initiation or propagation phases.

8.   Accuracy of the life prediction method (stress-life, strain-life, fracture mechanics or other) may not control the accuracy of the prediction. Output result (life) at the very best can only be as good as the input data (e.g. initial flaw sizes, load spectra, stress distribution).   Thus a basic understanding of the three dimensional behavior of the wheel is required.

9.   Stress-life, strain-life, and linear elastic fracture mechanics provide increasing levels of understanding into the mechanism of fatigue, howeve,r no one method is best for all situations.

10. Current analytical techniques, finite element modeling and analysis, fracture mechanics, and stochastic life prediction methods must be combined with experimental methods and load determination techniques in a total integrated approach to wheel studies to take full advantage of all available technology in the development of an optimum wheel.

Based on these conclusions, the following recommendations were developed. They are divided into analytical (A_) and experimental (E_) tasks.

Experimental

E1. Perform a tire/wheel pressure distribution test using several vertical and horizontal loads. Simultaneously calculate the wheel stress state and the pressure distribution at the tire/wheel interface.

E2. Perform a "Wheel-Only" static load test to determine stress and deflection at various points for use in a finite element model correlation study.

E3. Perform an on-aircraft operational test to verify the load determination technique (MCR method).

E4. Perform full scale "Wheel-Only" fatigue tests with controlled loading in a controlled environment.

E5. Utilize maintenance records and examine wheels which failed in service to document and quantify the "wheel life problem".

Analytical

A1. Develop an analytical loading methodology utilizing the pressure distribution data from (E1) for an axisymmetric finite element model.

A2. Construct finite element models of the wheel of increasing complexity until good correlation with data from (E1) and (E2) above is achieved at critical locations.

A3. Using the correlated finite element model of the wheel and the loads from (E4) above analytically calculate stresses and predict life (S-N approach).

A4. Perform a fracture mechanics based life estimation study using the correlated finite element model of the wheel and the controlled loads from (E4) above to calculate stress intensity factors and crack propagation rates. Non-linear elastic-plastic studies for crack initiation could also be performed.

A5. Using the correlated finite element model of the wheel and "actual" loads from the load determination task, analytically calculate stresses and estimate life using the best approach, (A3) or (A4) above.

A6. Utilize probabilistic and statistical techniques in a reliability study of the wheel to determine optimum inspection intervals and a stochastic based estimation of life.

V. REFERENCES

31. Battelle Columbus Division, The Probabilistic Fracture Mechanics Program Technical Highlights, Advanced Materials Department, Mechanical Section, June 1986.

32. Bender, J.R., Angel, R.W., Gard, F.H. and Prentice, E.P., "Flight Vehicle Wheel Testing Methods", Technical Documentary Report No. WADD TR60-885, January 1962.

33. Bloom J.M. and Hechmer J.L., "Limits of Linear Elastic Fracture Mechanics", _Journal of Pressure Vessel Technology_, Vol. 106, May 1984, pp. 196-200.

34. Enneking, T.J., "Investigation into the Applicability of Fracture Mechanics Techniques to Aircraft Wheel Life Analysis - Five Week Progress Report", performed for AFWAL/FIEMA, July 1987.

35. Mitchell, M.R., "Fundamentals of Modern Fatigue Analysis for Design", _Fatigue and Microstructure_, ASM, 1979.

36. Nagar, A., "Fatigue Crack Growth in Aircraft Main Landing Gear Wheels", submitted for publication in _Fracture Mechanics Nineteenth Symposium ASTM_, April 1987.

37. Ortiz, K., _On the Stochastic Modeling of Fatigue Crack Growth_, Ph.D. Dissertation, Stanford University, Stanford, California, 1984.

38. Osgood, Carl C., "Fracture Mechanics Comes of Age", _Machine Design_, February 12 and March 12, 1987.

39. Rodriguez, A., _F/FB-111 Service Life Monitoring Summary Report, Vol III, FB111A Technical Analysis_, December 1983, General Dynamics, Fort Worth Division.

40. Yang, J.N. and Trapp, W.J., "Reliability Analysis of Aircraft Structures Under Random Loading and Periodic Inspection", _AIAA Journal_, Vol 12, No 12, 1975, pp. 494-496.

1987 USAF-UES SUMMER RESEARCH PROGRAM
SUMMER FACULTY RESEARCH PROGRAM
GRADUATE STUDENT SUMMER SUPPORT PROGRAM

Sponsored by the

AIR FORCE OFFICE OF SCIENTIFIC RESEARCH

Conducted by the

Universal Energy Systems, Inc.

FINAL REPORT

CONSTRUCTION AND PRELIMINARY VALIDATION
OF AN EQUAL OPPORTUNITY CLIMATE ASSESSMENT INSTRUMENT

Prepared by:	Dan Landis, Ph.D Gloria Fisher, M.Ed., M.S.
Academic Rank:	Professor (Landis) Graduate Student (Fisher)
Department and	Psychology Department
University:	University of Mississippi
Research Location:	DEOMI Patrick Air Force Base, FL
USAF Researcher:	Lt Col Mickey Dansby
Date:	21 Aug 87
Contract No:	F49620-85-C-0013

REFERENCE DR. LANDIS

SFRP FINAL REPORT NUMBER 84

1987 USAF-UES SUMMER FACULTY RESEARCH PROGRAM/

GRADUATE STUDENT SUMMER SUPPORT PROGRAM

Sponsored by the

AIR FORCE OFFICE OF SCIENTIFIC RESEARCH

Conducted by

UNIVERSAL ENERGY SYSTEMS, INC.

FINAL REPORT

An Analysis of the Mutagenicity of Beryllium

Compounds Using the Ames Test

Prepared By:	Ms. Inge Ford-Belgrave
Academic Rank:	Graduate Student
Department and University:	Biology Department Texas Southern University
Research Location:	USAF/OEHL Brooks Air Force Base
USAF Researcher:	Dr. Bruce Poitrast
Date:	13 September 1987
Contract No.:	F49620-85-C-0013

An Analysis of the Mutagenicity of Beryllium Compounds using the Ames

Test

by Inge B. Ford

I. Abstract

Unprotected exposure to beryllium and its alloys has been associated
with an array of clinical disorders, including alterations in mole-
cular genomes in both animals and humans. Beryllium will be induced
with several strains of _Salmonella_ _typhimurium_ (each strain is
specific for a type of mutagen) and cytosol fractions of mammalian
cells in order to determine its mutagenic capacity. The intent of
this analysis is:

(1) to determine whether beryllium and/or its alloys are indeed muta-
    genic;

(2) to determine the degree of mutagenicity of beryllium alloys;

(3) to determine if beryllium metabolites have mutagenic properties
    utilizing the Ames test;

(4) to analyze microscopically if tissues, other than those known
    today, are affected by the metal; and

(5) to determine to what extent the metal affects the tissue within
    mammalian systems.

Acknowledgements

An Analysis of the Mutagenicity of Beryllium Compounds Using the Ames

Test

Introduction/Background

The industrial revolution has created many unique forms of technology

combining both ingenium creativity and natural elements. Metals, for

example, have been the source of countless applications in industry.

One such metal, beryllium, has because of its increased utilization and

notable toxicity in the workplace, caused considerable concern among

industrial hygiene engineers and physicians involved with the prevention

and treatment of occupational disease respectively (24).

Beryllium is a gray metal which qualitatively has both lightweight and

high tensile strength properties. Beryllium and all of its related

compounds are to some degree soluble in water and/or in dilute acids

and alkalis (22). The primary source of beryllium, beryl ore, is found

in large localized deposits, namely in Brazil, USSR, USA, and various

parts of Africa. For reasons of abundance, diversity and cost effective-

ness the exploitation and implications of beryllium are found in areas

such as 1) aerospace explorationin the fabrication of lightweight

metallic components for spacecrafts and fuel propulsion systems;

2) nuclear reactor components and rocket nozzles; and 3) electrical and

metallurgical programs (21, 22).

Although the utilization of beryllium and its alloys has increased in-

dustrially tenfold during the part forty or so years, a complete under-

standing regarding the toxicity of this metal remains still an enigma.
The chief hazardous substances of this metal, as designated by the
Environmental Protection Agency (EPA), include the hydroxide, oxide
and nitrate forms.   Beryllium dust or fumes are considered the premier
hazardous waste constituents; whereby, human exposure usually results
from inhalation of the toxin, specifically in occupations such as
beryllium alloy makers or fabricators, beryllium ore miners, phosphor
manufacturers, missile technicians, and electrical equipment workers
(22).

When referring to animal systems, health authorities agree that the
toxic effect of beryllium due to inhalation, as opposed to ingestion,
is obviously more dangerous.   Current data reveals that beryllium and
associated compounds are not readily absorbed through intact skin or
the gastrointestinal tract (11, 19, 21).

The effects and symptoms of exposure to beryllium are categorized as
either local (acute) or systemic (chronic).   For example, exposure to
soluble beryllium salts may manifest itself as one or more acute con-
ditions that when detected soon enough, be reversible when exposure is
ceased and with timely treatment (22).   Some acute conditions include
dermatitis, acute pneumonitis, conjunctivitis, and chronic pulmonary
granulomatosis (berylliosis).   With the exception of berylliosis, the
onset of the aforementioned may be delayed two weeks from the initial
time of exposure.   Granulomatus lesions usually result from contact
with beryllium metal or soluble salts in areas of abraded skin.   These

lesions are hard and have a central non-healing area. In most cases, the lesions must be surgically excised (21, 24).

Systemic or chronic beryllium disorders invariably include pulmonary manifestations. Inhalation of soluble beryllium compounds may cause nasopharyngitis; whereby, mucous membranes become edematous and ulcerated. The speed and severity in which the symptoms appear is directly related to the type and intensity of exposure to the substance. Some of the classic symptoms of chronic beryllium disease include respiratory infection, fatigue, non-productive cough, substernal pain, shortness of breath, and some weight loss. In many cases these symptoms are not detected until an illness or surgery occur (22, 24). Chronic beryllium disease, including chronic granulomatosis, are slow developing disorders and usually have a high mortality rate.

Studies of beryllium have revealed that the substance has the capacity to inhibit many enzymes, specifically alkaline phosphatase. Tepper (1961) implied that beryllium interferes with the "fidelity" of DNA replication, In Vivo, forming protein complexes such that a "cell mediated immune response" is provoked in mammals (eg. guinea pigs and man) (15, 24).

In animal studies, absorbed beryllium characteristically leaves higher deposits in bone as compared to lower levels observed in other tissues. In rabbits, conditions such as osteosarcoma and pulmonary adenocarcinoma have been noted. These tumors are histologically similar to those

found in humans and have been known to readily metastasize (11, 21). Other studies using rats (intravenously injected) showed that they were susceptible to beryllium carcinogenesis, but the extent of malignancy is not well documented.

Beryllium has been named suspect, by health authorities, as a carcinogen in humans. There is no conclusive evidence, as such, to support this. However, recent studies indicate that there is an increased risk of lung cancer in beryllium exposed workers (21). Yet, a correlation has been made between mutagenicity and carcinogenicity of toxins in micro-organisms and mammalian systems (10).

For this study, beryllium will be used in conjunction with strains of Salmonella typhimurium andcytosol fractions of mammalian cells in order to determine its mutagenic capcacity. Why is this necessary? One reason is because of the increased utilization of beryllium in the workplace, and potentially elevated risks it poses to the unprotected worker. Secondly, there exists a greater hazard of atmospheric beryllium fallout to the populace, i.e. from more frequent rocket testing and/or the burning of coal containing beryllium. Thirdly, the method for testing the mutagenicity of beryllium is both rapid and accurate. Many agents may be considered mutagenic but not carcinogenic, further sensitivity assays may reveal that most carcinogens are also mutagens. The Ames test is a bacterial assay that is sensitive for the detection of toxic mutagens/carcinogens. This test system allows for mass screening of various compouns economically, simply, and with

great sensitivity (1, 6, 17).

The significance of this project with respect to USAF research stems mainly from the ongoing analysis of rocket fuel which is used in aeronautic testing. The Occupational and Environmental Health Lab at Brooks Air Force Base is a Branch that is greatly interested, in general, in the toxicological effects of metals on biological systems; however, interest in the effects of specific metals, such as beryllium is significant because of its increased utilization in the preparation of propulsion fuel and fabrication of technically advanced aeronautic equipment.

II. Objectives of the Research Effort:

An array of metal ions and metal mutagens have been indicated as inhibitors in the fidelity of DNA synthesis and may alter the processing of RNA molecules. The Ames Test, a mutagenicity assay, is a cost effective method for the determination and existence of mutagens in corporating metals, microsomal components, and varied tester strains of Salmonella typhimurium. The purpose of this project is to examine the effects of beryllium and its metabolic alloys in rats to determine if beryllium metabolites have mutagenic properties utilizing the Ames test, and to determine the degree of mutagenicity of beryllium alloys.

This investigation, it was decided, required additional time so that materials and conducive requirements be established for performing

in vitro assays for the mutagenic properties of beryllium.

III. In order to test for the mutagenicity of beryllium and its
compounds, revised methods of the salmonella mutagenicity test will be
employed. Different strains of Salmonella typhimurium, each sensitive
to different mutagenic aberrations, i.e. frameshift or base-pair
substitution mutations are used so that the presence fo mutagens may
be demonstrated.

A. Growing Bacteria

   Strains of S. typhimurium (TA 97, Ta 98, TA 100, TA 1535) are
   utilized so that sensitivity for general mutagenesis may be tested.
   The strains are cultuted in nutrient broth Oxoid nutrient broth
   No. 2) to a density of 1 - 2 X 10^9 cells per ml Cultures are
   innoculated from master plates and incubated at 37° in a gyrorotary
   incubator and shaken at 210 rpm to insure proper aeration. The
   growth period for the bacterium should not exceed 16 hrs as pre-
   scribed in the procedure by Ames. The density of the cultures can
   be determined by turbidity measurements at 650nm (6, 17). All
   bacterial tester strains require histidine for growth, therefore,
   it is advisory to confirm the viability of all strain genotypes.
   Methods for checking the viability of strains require sterile
   solutions, glasswares and broth.

   1. The histidine requirement for growth on selective agar is en-
      sured by adding the nutrients to a minimal glucose agar before
      preparation of test plates containing 0.1 ml of 0.1M L-histidine
      and 0.1 ml of 0.5 mM biotin. The solutions must be spread

evenly such that they are thoroughly absorbed by the agar. Biotin is required by all the standard test strains of UVRB (ultraviolet revertant) gene deletion group. The control plates will contain biotin but no histidine. However, testing for biotin growth is not mandatory because its dependency is relatively small, and is satisfied by the trace amounts found in the nutrient broth.

2. Strains having deep rough character should be tested for crystal violet sensitivity. This test is facilitated by a sterile filter paper disc containing crystal violet which is placed on the surface of teh seeded plate with cultures of the test strains. A clear zone of inhibition around the disc with a diameter of 14mm after 12 h at $37^{o}C$ indicates the presence of a rfa mutation particularly in TA 97 and TA 98.

3. The R-factor strains, TA 98 and Ta 100 should be routinely tested for the presence of the ampicillin resistance factor. This is done by spreading a small amount of an ampicillin solution across the surface of the agar. After incubation 12- 24 h. at $37^{o}C$, strains which do not contain the R-factor will show a zone of growth inhibition around the ampicillin streak, whereas R factor containing strains will not.

The test is of special interest because the plasmid associated with the bacteria may become lost. Complete or partial loss may be prevented by growing overnight culture in oxoid broth, to which 25 mg/ml ampicillin is added. Cells that retain the R factor can be determined by diluting an overnight culture

10^6 times with sterile phosphate buffered saline (0.02 M

phosphate, 0.15M NaCl, pH 7.4) and plated 0.1ml in triplicate

on nutrient agar without ampicillin at 37^OC. The result should

yield almost the same number of colonies on plates with and

without ampicillin indicating that all the bacterial cells

carry the R-factor plasmid.

IV. Detecting Mutants

By utilizing the Ames test, general mutagenesis screening can be done

rapidly and cost effectively. The histidine operon on the gene is

where notable mutations occur in Salmonella strains. Tester strains

TA 97 and TA 98 are effective in detecting frameshift mutations where-

as TA 100 and TA 1535 will detect base-pair substitution mutations.

The latter are considerably more sensitive for the detection of

mutagens because they have a lower response rate to mutations (4, 5, 7

8, 11).

The mutants are detected by the number of revertant colonies that may

arise during the 48 h incubation period. The number of revertants

corrletate with the histidine concentration and the final number of auto-

trophs (background bacteria) scored.

Spontaneous revertants are expressed as the number of colonies per plate

and are clearly visible in a uniform bacterial lawn. The number of

spontaneous revertants is not dependent on the number of bacterial

cells initially plated (eg. 10^5 - 10^8). Consequently, the number of

autotrophs should be constant if the histidine concentration is con-
stant. However, variability may still be encountered for this reason,
it is recommended that a minimum of three (3) spontaneous mutation
control plates be included for reach assay. Historical valves of
revertants/plate (-59): TA 98 (30-50), TA 100 (120-200); and with S_9
valves will be considerably different. Deviations that are obviously
outside the accepted range indicate the genetic characteristics of the
strain being tested on the growth medium should be checked.

An abnormal increase in the number of spontaneous revertants may indi-
cate contamination, therefore, reisolation from the master copy (ini-
tial sample) may be necessary. Overall the mutagenicity test results
are essentially reported as the number of revertants per ug of the
test compound which is taken from the linear portionof the dose-response
curve.

V. Isolating Microsomal Components

In order to screen for the general mutagenesis of varied compounds,
liver homogenates (S_9 microsomal fractions) are obtained from rats.
By using the S_9 fraction, one is able to detect a variety of chemical
mutagens. Microsomes are used because they provide insight regarding
mammalian metabolism _in vitro_. Notably, a wide variety of carcino-
gens can be detected as mutagens.

The method for preparation of the S_9 microsomal fraction closely
follows the techniques of researchers Maron (#17), Kier (#14), Czygan

(#9) and Fennell (#12). The fractions will be isolated from rats induced with an injection of phenobarbital based on the technique of Fennell (#12). All steps of the procedure are carried out at 0-4° using cold, sterile solutions and glassware. This measure is employed so as to diminish enzyme activity loss. The S_9 mix can be stored as desired, noting that less than one half of the sample should be stored and that all storage be verified by plating 0.1 ml of teh sample on agar containing histidine and biotin.

VI. Preparing Plates with Microsome

This phase of the procedure is called the "plate incorporation test". A mixture of the bacterial strain, the test compound, and the S_9 fraction is poured onto a minimal glucose agar plate. Both positive and negative controls are run simultaneously with each assay. The positive control contains standard diagnostic mutagens for each strain. The negative control contains bacteria, S_9 mix, and solvent (meaning no test chemical). Histidine and biotin are added to the top agar. About 2 ml of top agar is plated into 13 X 100 mm capped culture tubes maintained at 45° in a heating block. From fresh overnight cultures 0.1ml of the tester strain, less than 0.1 ml of the test chemical (concentrations ranging between 0.1 - 1 uM of Be compounds), and 0.5 ml of S_9 are mixed and poured onto the top agar. The samples are incubated at 37° for 48 h and revertant colonies are observed and counted (5, 6, 17).

Thin lawn backgrounds in comparison to lawn background on the negative

control plate indicates bacterial toxicity. It is worthy of note, that colonies should not be scored and are essentially bacterium that have survived from the presence of histidine in the top agar. Subsequently, they are part ofthe spontaneous revertants which occur in each tester strain.

VII. Urine Assay

This test is of particular importance in the detectionof mutagenic metabolites which may have been converted in the liver and excreted as glucuronides or oxides of the ingested compound. The feasibility of such a test lies in the fact that it is simple, inexpensive and ex-tremely sensitive for maximum recovery of mutagenic agents. The technique developed by Ames will be employed for the detection of mutagens in urine of rats. The addition of commercial B-glucuronides will readily demonstrate mutagenic activity. The experiment will be conducted for a duration of 24 weeks. Holtzan male rats will be housed in metabolic cages and fed Purina laboratory Chow and distilled water, ad libitum. After one week intervals, rats will be housed in separate cages for urine collection. Urine will be collected in darkened, ice-chilled flasks containing a drop of chloroform. Twenty-four hour samples will be colelcted, centrifuged, then frozen at $-15^{o}C$ for 1 - 2 days until assayed. Before use, urine will be sterilized by Millipore filtration. The criterion for mutagenicity closely relates to linear findings of the dose-response curve.

Notably, limitations may arise when metabolites are present in low

concentration and histidine in range of 0.7 - 1.3 umole/ml. To compensate for this limitation, an adsorptive process with XAD-2 resin, a styrene divinylbenzene copolymer, is used which allows for the concentration of relatively nonpolar mutagenic components.

VIII. Recommendations

A. A culmination of quantitative data regarding the mutagenicity of beryllium compounds via the Ames test is in process. A preliminary time table regarding the experimental protocol are as follows:

1) Sept. - Dec. 1987 all tester strains of Salmonella typhimurium (TA 97, TA 98, TA 100, TA 1535) will be developed and measured for viability and the detection of mutants using one or more of the specified techniques mentioned in sections III and IV.

2) Jan. - March 1988 the screening for mutagenesis of beryllium compounds by incorporating S_9 microsomal fractions from rat liver homogenates and the utilization of the plate incorporation test of the metal; and the collection and assay of urine samples from rats exposed to beryllium, such that mutagenic metabolites due to liver conversion are detected.

3) April - June 1988 a continual analysis of the effects of beryllium compounds using varied concentrations (ie. as seen in the plate incorporation test) of the metal; and the collection and assay of urine samples from rats exposed of beryllium, such that mutagenic metabolites, as a result of liver conversion are detected.

The overall results should indicate to what degree beryllium compounds are mutagenic, the effects of beryllium in/on specific tissues, and to provide a linear correlation(denoted for detecting mutagenesis in urine) as seen on a dose-response curve.

B. The ongoing concern among researchers involved in the analysis of metals delves into both the occupational and environmental arenas. The occupational implications of beryllium mutagenesis encompasses the short and long term effects of the metal on workers who are exposed and not properly protected. On the other hand, environmental concerns include the toxicological effects of beryllium on systems in greater proportions; an exemplary incident nay be exposure of beryllium to the general populace via the burn-off of coal (beryl ore). The atmospheric concentrations of the metal may vary from region to region, but the quantitative effect(s) may be numerous.

Further studies of the carcinogenic and mutagenic affects of beryllium may include methods for identifying particular mutants. Various methods may include electrophoretic assays, light absorption (ie. spectrophotometric assays, and enzymatic assays for inducing muta-genic activation.

1987 USAF-UES Summer Faculty Research Program/

Graduate Student Summer Support Program

Sponsored by the

Air Force Office of Scientific Research

Conducted by the

Universal Energy Systems, Inc.

FINAL REPORT

The Effects of High Noise Levels on the Acoustic-Phonetic

Structure of Speech: A Preliminary Investigation

Prepared by: Beverley A. Gable

Academic Rank: Graduate Student

Department and   Department of Psychology

University: Ohio University

Research Location: Biological Acoustics Branch,

                    Biodynamics and Bioengineering

                    Division, Aerospace Medical

                    Research Laboratory

USAF Research: Dr. Thomas Moore

                    Dr. Zinny Bond

                    Kate Young

Date: September 17, 1987

Contract No.:   F49620-85-C-0013

The Effects of High Noise Levels on the Acoustic-Phonetic Structure of Speech: A Preliminary Investigation

by

B.A. Gable

ABSTRACT

The purpose of this study was to provide some preliminary data concerning the acoustic-phonetic structure of speech produced under high noise levels. Acoustical measurements were made of a set of sentences spoken by four subjects in two conditions: the 95dB noise condition and the no-noise condition. Sentences produced under 95dB noise were different from sentences produced under ambient noise in both durational and spectral characteristics.

ACKNOWLEDGMENTS

I would like to thank the Air Force Systems Command and the Air Force Office of Scientific Research for sponsorship of this research. Universal Energy Systems must be mentioned for their help to me in all administative and directional aspects of this program.

I appreciate the assistance of all the people at AMRL/BBA who made my summer pleasant and profitable. I particularly want to thank Dr. Thomas Moore, Dr. Zinny Bond, and Dr. Charles Nixon for giving me the opportunity and guidance to work on this research. Kate Young was invaluable to the completion of this research and a pleasure to work with. The help of Sgt Mike Jacobs was also invaluable in overcomming many technical roadblocks. The assistence of Barbara Rabold and the concern of Maj Mark Stevenson was greatly appreciated.

Finally, I would like to thank Mark Schirtzinger for his support and encouragement throughout the summer.

I. INTRODUCTION:

The acoustical structure of normal speech has been the
focus of many investigations. Bond (1985) defined
normal speech as, "speech produced with minimal
distraction or disturbance of the speaker." A good
understanding of normal speech has been formed, yet
ordinary discourse usually involves speech that is
effected by circumstances such as high noise levels,
distraction, and physical exertion of the speaker.
Therefore, there is a need for investigating speech
produced in adverse circumstances. There are only a
few such investigations.

A study by Dreher and O'Neill (1957) examined speech
produced under high levels of white noise. A pannel
of listeners were presented spondee words and
sentences produced by speakers who were exposed to
high noise levels. The signal to noise ratio was 4
dB. The results showed that speech produced under
noise was more intelligible than speech produced in
quiet. There was no difference between speech
produced at different noise levels 70 to 100 dB SPL.
Dreher and O'Neil reported that the intensity and
duration of speech were greater under noise than in
quiet.

Results by Ladefoged (cited in Bond, 1985) were not consistent with the results by Dreher and O'Neil (1957). Speech was produced by speakers under levels of noise which were high enough to mask the auditory feedback by bone conduction. The exact level of masking noise was not reported, but Bond (1985) estimated that it was approximately 120 dB SPL. The results showed that the length and quality of vowels were affected. Furthermore, results showed a shift to a lower quality of voice and pitch pattern. Ladefoged did not test the intelligibility of the speech, but he did mention that the speech appeared intelligible yet disorganized.

Pisoni et al., (1985) investigated the acoustical changes in speech under noise (80 to 100 dB SPL). Results showed that as noise increased, there was an increase in intensity, fundamental frequency, word duration, and variability of F0. Furthermore, at higher frequencies, there was an increase in the relative distribution of energy in the speech spectrum. Vowel formants shifted towards more centralized positions; F1 rose while F2 and F3 dropped.

Bond (1985) reviewed these three studies and concluded:

It would seem, therefore, that the presence of masking noise at some levels causes speakers to change their speech towards more intelligible but that masking beyond these levels cause speech to become disorganized and undoubtedly less intelligible. It is also possible of course, that the differences between the results represent the effects of noise on different speakers.

Bond also concluded that data was scarce regarding how adverse conditions cause changes in the acoustical structure of speech and subsequently affect intelligibility. Thus, there is a need for further research.

Bond, Moore, and Gable (1986) investigated the effects of noise and the use of an oxygen mask on the production of isolated words. A comparison between speech produced in the 95dB noise condition and in the no-noise condition indicated that the formants became more centralized in noise, and that fundamental frequency, total energy, word duration, and vowel duration all increased in the presence of noise. There were two exceptions. First, word duration for Subject one decreased in the presence of noise.

Second, the results on vowel duration for subject one were mixed; some words showed increased vowel duration in noise while others showed decreased vowel duration.

The next question to be addressed is whether speech is affected differently when the units of production are different, such as words, sentences, or longer texts. The present study addressed this question. The present study investigated the acoustical changes in sentences produced under high levels of noise, as well as, the variability of speaker reactions to high levels of noise.

II.   OBJECTIVES:

This investigation examined speech samples of four speakers produced in different noise environments. This was done to obtain the effects of listening to noise on the acoustic-phonetic structure of speech. Such data provide information about human speech production under adverse conditions. Therefore, the data are relevant to an understanding of speech production in general. The data may also be relevant to testing automatic speech recognition systems.

24-7

III. METHOD:

The speakers were four male volunteers. Each speaker participated in two speaking conditions. Before the actual experiment, the speakers were familiarized with the materials to be recorded. After each recording, the speakers were debriefed

Materials. The recordings were made using a TEAC Tascam 44 4-channel tape reccrd . Speakers wore a headset (H-157) with boom micro ne (M-167).

Two different speaking condition ecorded for the four speakers: no noise a. k noise. Each speaker recorded two repec ch of the 20 sentences. Thus, 40 tokens . ad in each of two different noise conditions; tota. of 80 tokens.

Measurements: The measurements were made in a similar manner to those made by Bond, Moore, and Anderson (1986). Both repetitions of all 20 sentences were digitized at 16 KHz using a 6.4 KHz anti-aliasing filter and 16 bit resolution. All tokens were stored on disk. The tokens were recorded and analyzed using the computer programs SPIRE (Speech Interactive

Research Environment) and SEARCH (Structured
Environment for Assimilating Acoustic Regularities of
Speech) on a Symbolics 3670 computer (Kassel, 1986;
Shipman). The boundaries for each segment were
located on the display of the wide-band spectrogram
and waveform. The segmentation was done in the manner
described by Peterson and Lehiste (1960).
Segmentation was difficult at times for three reasons.
First, the boundaries were occasionally indistinct.
Second, the recording quality was occasionally
obscure. Third, there was an occasional presence of
noise. The sentences were transcribed in order to be
analyzed using SEARCH.

IV.   RESULTS:

a. Average Total Energy. Measurements of the average
total energy of the vocalic sections of each word were
made for each speaker. Across words, all four
speakers showed an increase in total energy in the
noise conditions compared to the no-noise condition.

b. Pitch Frequency at Midpoint. Measurements were
made on the vocalic partions of each word for each
speaker. All four speakers showed an increase in
pitch frequency in noise.

c. Vowel Duration. Subject three showed no difference in vowel duration. Subject one showed slightly shorter vowel durations in noise than in quiet. Subjects two and four showed slightly longer vowel durations in the noise condition than in the no-noise condition.

d. Duration of Stop Closure for Voiceless Stops. All four subjects showed a slightly longer stop closure for voiceless stops in noise.

e. Duration of Stop Closure for Voiced Stops. Subjects one, two, and four showed no difference with a slight tendency toward shorter stop closures for voiced stops in noise. Subject three showed a shorter stop closures for voiced stops in noise.

f. Formants. For each subject. the first, second, and third formants were measured across words for each vowel. Of the three formants, the first formant showed the largest difference between the noise and the no-noise conditions. The first formant showed the greatest increase in frequency in the noise condition. Furthermore, tense vowels showed more of a difference than did lax vowels.

First Formant. F1 was measured for all vowels. Subject one showed an increase in F1 in noise except for the vowel /ʌ/, which showed no difference between the noise and the no-noise condition.

Subject two showed an increase in F1 in the noise condition.

Subject three showed an increase in F1 for the following vowels: /i/, /ɛ/, /ae/, /a/, /ɝ/, /ɚ/, /c/, and /o/. Subject three showed a decrease in F1 for the following vowels: /I/, /e/, /u/, /ʊ/, /ə/, and /ʌ/.

Subject four showed an increase in F1 in the noise condition.

Second Formant. The four subjects showed different patterns for F2. Subject one showed a decrease for all vowels in noise except the vowels /o/, /ə/, and /c/. The vowel /o/ showed no difference between the noise and the no-noise conditions. The vowels /ə/ and /c/, showed an increase in noise.

Subject two showed an increase in F2 in noise for the

following vowels: /i/, /o/, /a/, /ə/, /ʌ/, and /c/.
Subject two showed a decrease in F2 in noise for the
following vowels: /I/, /e/, /ae/, /u/, /ʊ/, /ɜ/, and
/ɝ/. Subject two showed no difference between the
noise and the no-noise conditions for the vowel /ɛ/.

Subject three showed an increase in F2 in noise for
all vowels except the vowels /o/, /a/, and /c/, which
showed a deacrease in F2 in noise.

Subject four showed an increase in F2 in noise for all
vowels except /I/ and /ɝ/. The vowel /I/ showed a
decrease in F2 in noise and /ɝ/ showed no difference
between the noise and the no-noise conditions.

Third Formant. The four subjects showed different
patterns for F3. Subject one showed an decrease in F3
in noise for all vowels except /I/, which showed an
increase in F3 in noise.

Subject two showed a decrease in F3 in noise for all
vowels except /o/, /a/, and /c/, which showed an
increase in F3 in noise.

Subject three showed an increase in F3 in noise for
the following vowels: /e/, /ɛ/, /o/, and /c/.

Subject three showed a decrease in F3 in noise for the following vowels: /i/, /I/, /ae/, /u/, /ʊ/, /a/, /ə/, /ɜ/, /ʌ/, and /ɚ/.

Subject four showed an increase in F3 in noise for the following vowels: /e/, /ɛ/, /ae/, /ʊ/, and /ə/. Subject four showed a decrease in F3 in noise for the following vowels: /I/, /o/, /a/, /ɜ/, /ʌ/, /ɚ/, and /c/. Subject four showed no difference between the noise and the no-noise conditions for the vowels /i/ and /u/.

g. <u>Aspiration after all voiceless stops</u>. For all four subjects, total energy and frication frequency increased in the noise condition and duration decreased.

h. <u>Fricatives</u>. The duration, total energy, and frication frequency across all fricatives for each subject was measured. All four subjects showed an increase in frication frequency and total energy for fricatives in noise. Subject one and two showed a slight decrease in duration while subjects three and four showed a slight increase in duration for fricatives in noise.

24-13

i. **Word Initial /l/**. In noise, the first formant increased for all subjects except subject four who showed a decrease in the first formant. The second formant decreased for all subjects except subject three who showed an increase in the second formant in noise.

j. **Word Initial /r/**. The first formant increased for all subjects except subject four who showed a decrease in the first formant in noise. The second formant increased in noise for subjects one and four, but decreased for subjects two and three. The third formant decreased for all subjects except subject four who showed an increase in noise.

k. **Word Initial /y/**. The first formant increased for all subjects in the noise condition. The second formant increased slightly for subjects two and four, but decreased for subjects one and three. The third formant increased slightly for subject two and four, but decreased for subject three and remained the same for subject one.

l. **Word Initial /w/**. In the noise condition, the first formant increased for all subjects. The second formant decreased for subjects one and four, but

increased for subjects two and three. The third
formant decreased for subjects two and four, increased
for subject three and remained unchange for subject
one.

m. Nasals. Duration decreased in the noise condition
for subjects one, two, and three, but increased
slightly for subject four.

n. Flap. Duration increased slightly in the noise
condition for subjects one and three, but decreased
for subjects two and four.

V.   CONCLUSIONS:

The present results on sentences produced under high
levels of noise are somewhat consistent with the
results on isolated words. Fundamental frequency and
total energy increased in the presence of noise, and
for some vowels the formants became more centralized.
However, word duration was not fully analyzed, some
vowels did not become more centralized in the noise
condition, and vowel duration showed mixed results.
Consistent with the results on isolated words, vowel
duration increased slightly in noise for subjects two
and four. Subject one showed a decrease in vowel

duration in noise and subject three showed no
difference between the 95dB noise and no-noise
conditions.

The present results are based on only four speakers.
Therefore, caution should be excersized when making
generalizations. The results indicated that the
changes in the acoustic-phonetic structure of speech
produced under high levels of noise are relatively
systematic. The present results are similar to those
by Pisoni (1985), when speaking in noise, speakers
modify both the prosodic and segmental acoustic-
phonetic properties of their speech. To maintain
intelligibility of speech in noise, speakers change
the pattern of formants frequencies and the amount of
total energy in fricatives, aspirations after
voiceless stops, and vowels.

VI.   RECOMMENDATIONS:

The recommendations made after studing speech under
high acceleration (Bond, Moore, & Anderson, 1986).
apply to the present research on noise. The changes
in speech should be taken into account when attempts
are made to introduce automatic speech recognition
technology into the flight environment. For example,

the recognizer trained under quiet conditions may perform poorly when used under high noise conditions As Bond, Moore and Anderson suggested, research defining the systematic changes in the acoustic-phonetic structure of speech may lead to the developement of compensatory algorithms for automatic speech recognition technology in the cockpit.

Further research concerning the effects of noise on speech should address an additional question outlined by Bond (1985): What are the effects of noise on the inteligibility of speech? Additional research should also address other adverse speaking circumstances, such as high cognitive load. Systematic changes of speech under high cognitive load may be found and need to be taken into account by automatic speech recognition technology.

VII. APPENDIX A:

Sentences to be used for analysis.

a. CID list E.
1. You can catch the bus across the street.
2. Call her on the phone and tell her the news.
3. I'll catch up with you later.

4. I'll think it over.

5. I don't want to go to the movies tonight.

6. If your tooth hurts that much you ought to
   see a dentist.

7. Put that cookie back in the box!

8. Stop fooling around.

9. Time's up.

10. How do you spell your name?

b. CID list J

11. Breakfast is ready.

12. I don't know what's wrong with the car,
    but it won't start.

13. It sure takes a sharp knife to cut this meat.

14. I haven't read a newspaper since we bought a
    television set.

15. Weeds are spoiling the yard.

16. Call me a little later!

17. Do you have change for a five-dollar bill?

18. How are you?

19. I'd like some ice cream with my pie.

20. I don't think I'll have any dessert.

REFERENCES

Bond, Z. S. Speech Produced Under Adverse Circumstances: Acoustic Structure and Intelligibility, A Proposal, Unpublished manuscript, 1985.

Bond, Z. S., Moore, T.J. and Anderson, T.R. The effects of High Sustained Acceleration on the Acoustic Phonetic Structure of Speech: A Preliminary Investigation, Aerospace Medical Research Laboratory Technical Report, 1986, AAMRL-TR-86-011.

Bond, Z.S., Moore, T.J., and Gable, B.A. Unpublished manuscript, 1986.

Dreher, J. and O'Neill, J. Effects of Ambient Noise on Speaker Inteeligibility for Words and Phrases, Journal of the Acoustical Society of America, 1957, 29, 1320-1323.

Kassel, R. H. A User's Guide to SPIRE, Massachusetts Documentation, Speech Communication Group, Research Laboratory of Electronics, Massachusetts Institute of Technology, 1986.

Peterson, G. E. and Lehiste, I. Duration of Syllable Nuclei in English, Journal of the Acoustical Society of America, 1960, 32, 693-703.

Pisoni, D. B., Bernacki, R. H., Nusbaum, H. C., and Yuchtman, M. Acoustic-Phonetic Correlates of Speech Produced in Noise, ICASSP-IEEE International Conference on Acoustics, Speech, and Signal Processing, 1985 1581-1584.

Shipman, D. W. Development of Speech Research Software on the MIT Lisp Machine, Massachusetts Documentation, Massachusetts Institute of Technology, Cambridge, MA.

1987 USAF–UES SUMMER FACULTY RESEARCH PROGRAM/

GRADUATE STUDENT SUMMER SUPPORT PROGRAM

Sponsored by the

AIR FORCE OFFICE OF SCIENTIFIC RESEARCH

Conducted by the

Universal Energy Systems, Inc.

<u>FINAL REPORT</u>

<u>THE EFFECT OF ATTENTIONAL FOCUS LEVEL ON TASK PERFORMANCE</u>

<u>UTILIZING INFORMATION FROM DIFFERENT STIMULUS STRUCTURE</u>

<u>LEVELS</u>

Prepared by:	Deborah A. Gagnon
Academic Rank:	Doctoral Candidate
Department and	Psychology Department
University:	State University of New York at Buffalo
Research Location:	AAMRL/HEA Wright–Patterson AFB Dayton, Ohio 45433-6573
USAF Researcher:	Michael Venturino
Date:	15 Sept 1987
Contract No:	F49620-85-C-0013

The Effect of Attentional Focus Level on Task Performance Utilizing Information From Different Stimulus Structure Levels

by

Deborah A. Gagnon

ABSTRACT

An experiment is described that will allow for the analysis of performance on an object and scene two-alternative forced choice task under different stimulus structure attention focuses. Seventeen subjects participated in a pilot study at the State University of New York at Buffalo. Suggestions for a data analysis are made.

Acknowledgements

I would like to thank the Air Force Office of
Scientific Research for sponsorship of the Graduate Student
Summer Support Program which made this worthwhile
educational experience possible and Universal Energy Systems
for their commendable job in administrating the program.

I cannot express enough my thanks to Dr. Michael
Venturino of AAMRL/HEA for both professional and personal
guidance, encouragement, and wisdom. His influence will
surely be with me for a long time to come. Thanks also to
Dr. Tom Furness for his understanding in allowing me to
pursue this research in a unique manner. Dr. Irving
Biederman, now at the University of Minnesota in
Minneapolis, was most supportive throughout this endeavor
and his expertise in the problem area was an invaluable
resource. It is not an overstatement to say that the
research could not have been accomplished without his help.
Finally, I would like to thank my colleagues and Dr. James
Sawusch of the Psychology Department at the State University
of New York at Buffalo, for their comments and help in this
effort.

I. INTRODUCTION:

One of the tasks required of the combat flight pilot is
to monitor his environment for specific information while
also attending to and maintaining a perception of the
overall mission, aircraft and environment situations. An
evaluation of the human information processor's ability to
extract specific information from the scene when not
attending to it and conversely, his ability to attain scene
knowledge at those times that attention is focused on a
specific item is of particular interest in the design of
virtual cockpit displays. Such displays super-impose
information that is typically found in conventional cockpit
panels as well as target information directly on the pilot's
helmet mask as the information is needed in the flight or
combat situation. To extract the information, the pilot
must switch the locus of his attention from the overall
scene to the information displayed on the mask interface and
thus to more "specific" information.

The development of an interfaced cockpit environment is
one of the primary efforts of the Human Engineering Division
of the Armstrong Aerospace Medical Research Laboratory
located at Wright-Patterson Air Force Base in Dayton, Ohio.
The design of the mask interface necessitates consideration
of general information processing abilities and is the
impetus behind this research. The information garnered from
this study is expected to reflect the general limitations of

25-4

the human information processor and therefore generalize to
the pilot population.

My research interest as a Ph.D. student in experimental
psychology has been in the area of object recognition and
scene perception. In particular, I have been involved in
research that seeks to determine the variables necessary to
achieve perception of objects and scenes. The theoretical
construct I have been working under is that of a
componentially-based description of both objects and scenes.
The experimental studies involve manipulating certain
aspects of the component constituents (e.g. symmetry,
contour deletion, component deletion, etc.) to determine
their effect on speeded recognition tasks. A componential
description is one in which objects are represented as
arrangements of simple convex volumes (cylinders, bricks,
cones, wedges, etc.) While my research background is not
directly concerned with the problem of interest to
AAMRL/HEA, my knowledge of scene research and the
experimental paradigm I have employed proved to be highly
applicable in this new domain.

II. OBJECTIVES OF THE RESEARCH EFFORT:

The visual environment of the pilot can be thought of
as a complex stimulus configuration from which the pilot
perceives, processes, and extracts information. This visual
environment can be described at several different structural

levels of information. Previous research into stimulus
structure employed compound letters as the experimental
stimuli. These can be described as large letters composed of
smaller ones (see Figure 1). For such stimuli at least two
different levels of stimulus structure can be described: the
local level (comprised of the smaller letters that
constitute the larger element) and the global level (the
larger element). Compound letters have a certain advantage
to them for experimental purposes in that the various levels
can be arbitrarily and independently manipulated, that is,
there is no relation between the letters used at the local
level and the letter used at the global level. The
disadvantage to these stimuli is that they are artificial in
nature. Their applicability to real-world situations is
thus suspect.

Compound letter stimuli lie in contrast to naturalistic
scenes in which structural redundancies (correlations
between one level and another) in large part determine the
perception of the constituent entities. The constituent
entities in a scene are simply the objects that compose the
scene and can be considered analogous to the local level of
compound letter stimuli. The global element could be the
scene itself. (I would like to mention here that I believe
local and global assignments to be relative distinctions.
i.e. a description of a scene could range from the very
local description of vertices and edges to a very global
description that would include meta-scene information.

25-6

Thus, an object description would be global relative to a
vertice-and-edge description.) Any attempt at manipulating
the local level of a scene structure destroys the overall
configuration. For example, the strategy I have employed in
my scene research at the State University of New York at
Buffalo has been to depict scenes as consisting of component
"clusters". Clusters are formed by extrapolating the
largest volume (component) from each of the objects in the
scene. The combination of the components in their unique
relations to one another elicits the activation of a scene
schema (viz. world knowledge about such scenes is activated)
and allows for scene recognition. Recognition is possible
because of the structural redundancies of scenes and
probably underlies our ability to quickly attain a schema
for novel scenes. If the normal structure of scenes is
broken, scene recognition is unattainable or at least
impaired. This can be demonstrated by comparing the
"jumbled" version of one of my component scenes in Figure 2
to the "coherent" version. The advantage of using real-
world scene stimuli lies in the fact that they are
"natural". Thus, any findings from their use will reflect a
process that human beings naturally engage in and will
afford greater ecological validity to a real-life design
problem.

My objective at AAMRL/HEA is to look at how performance
on a task that requires access to one level of the stimulus
structure is affected by an attentional focus on another

level. Another objective is to maximize the
generalizability of the findings so that they will be of
some value in the design of virtual man-machine interfaces.
It is clear that there is a real trade-off in terms of
advantages and disadvantages in using the two sorts of
stimuli I described above but it is also clear that
naturalistic scene stimuli were needed in order to meet the
second objective. The question I would like to be able to
answer then could be formulated as follows: given a focus on
one structural level of a scene stimulus (either at the
local [object] level or global [scene] level), how does one
perform on a task that utilizes information from the other
level in comparison to performance on the task when
attentional focus is at same-level?

Finally, it was decided that it might be interesting to
assess the effect of a spatial cue on the solicitation of
local information. Specifically, we wondered about the
temporal location of the cue in respect to the scene
stimulus presentation. This objective necessitated the
addition of another dimension to the experimental design,
that of pre- versus post-cue.

III. METHODS

    A. DESIGN

The paradigm I constructed to study the above question is in the spirit of the compound letter research done by Kinchla, Solis-Macias, and Hoffman (1983) but it is also borrowed in part from scene research conducted by Biederman (1972, 1974). The subject was shown a scene tachistoscopically in which an object was cued. The subject was then given either two scene names or two object names for a two-alternative forced choice task. The subject was to choose the name that described the scene if two scene names were given or choose the object that was cued if two object names were given. The critical manipulation was in the relative probability that the subject would receive scene name choices and object name choices.

Subjects were read instructions before the experiment began in which they were explicitly told that 80% of the two-alternative forced choices would be of either scene or object names and 20% would be of the other. If there was an 80% probability for scene choices, the subject would be considered to be in a global attention focus. Alternatively, if there were an 80% probability for object choices, the subject would be in the local attention focus. After completing one block of stimuli in this condition, the subjects were read instructions for the second half of the experiment in which they were told that the probabilities were now switched so that whatever task level enjoyed the 80% choice advantage in the first half was now the 20% task type. This had the effect of switching the focus of

attention from local to global level (or vice versa) between the two blocks. Subjects were given 15 practice trials before each block of stimuli to familiarize them to the change in probability.

All subjects saw 128 color, real-world scene slides in the experimental condition. These were divided into two blocks of 64 slides each. Two slides at the beginning of each block and two slides at the end of each block were considered buffers and were included to eliminate any start-of-block and end-of-block anticipatory effects; these eight stimuli were not included in the data analysis.

B. PROCEDURE

The subject would initiate a trial by a key-press on the terminal keyboard. One half second after the key-press, a slide with right angles at each corner was shown for 500 msec. The purpose of the slide was to frame the portion of the screen where the scene would appear and thereby ensure that the subject would not miss the quick presentation of the scene (exposure duration was below threshold for an eye movement.) Depending on which cue condition the subject was in, a cue would appear either simultaneously with the frame or immediately following the scene stimulus; in either case the cue was shown for 500 msec. If the cue preceded the scene, the subject was in the pre-cue condition; otherwise, he was in a post-cue condition. Regardless, following

either the frame alone or the frame-plus-cue, a scene slide

was presented. The exposure duration for the scene slide

varied depending on whether the two-alternative forced

choice was to be object choices (duration = 150 msec) or

scene choices (duration = 100 msec.) Local task trials were

shown for an extra 50 msec. because a 100 msec. duration was

judged to be too short to elicit adequate performance

measures. If the intent of this research was to simply

compare performance on a local task versus a global task

then this would not be allowable, but the intent was to

compare performance on the same task under different

focuses. Giving a greater exposure duration to the local

task then does not affect the comparisons we wished to make.

Rather, it simply assured that there would be above chance

performance on the local task so that an analysis could be

made.

As soon as the scene went off, a pattern of random

color patches (the mask) was flashed for 500 msec. If the

subject was in the post-cue condition, the cue was super-

imposed over the mask (salience of the cue was judged to be

as good as in the pre-cue condition when the intensity of

the mask was lowered relative to the cue). Immediately

following this sequence of slides, the two-alternative

forced choice was presented to the subject on the projector

screen. One scene or object label was typed on the left of

the screen and the other on the right. The subjects were

instructed to make their decision as quickly and as

accurately as they could. The choices were shown for 3 sec. by which time the subject had to have indicated his choice by pressing a left microswitch if he thought the left choice was correct or a right microswitch if he thought the right choice was correct. The correct response was randomized and balanced between right and left. An analysis will be made to determine if there is any evidence of a response bias for the left response as a result of a left to right reading pattern. Finally, a trial ended with the presentation of feedback that provided the subject with the correct response and his reaction time.

A questionnaire was given to some subjects following the experiment. The purpose of the questionnaire was to assess how well the two scene choices for each scene described the scene. The subject reviewed each of the 120 experimental scenes over again and rated the two scene labels from each scene for their "goodness" as descriptors for the scene on a scale from 1 to 5 (1 = low rating, 5 = high rating). Subjects were instructed not to rate the labels according to whether the scene corresponded to the label description but rather, how much the scene looked like what the label described. As an example, one of the scenes was of a library check-out counter. The scene alternatives in the experiment were library check-out counter and hospital admissions desk. A subject might have rated both labels highly: it would obviously look like a library check-out counter since that's what it was but it also highly

resembled a hospital admissions desk. The ratings will be correlated with performance measures (viz. RT and errors) to determine if there is a component attributable to the ease with which the subject could reject the alternative label.

C. SUBJECTS

The experiment was conducted at the State University of New York at Buffalo in August, 1987. Seventeen subjects were run for pilot data; ten of these completed the questionnaire as well. Most of the subjects were obtained from the introductory psychology subject pool and participated as part of the course requirement. The remaining subjects were graduate student volunteers. All subjects were required to be native english speakers and to have normal or corrected-to-normal vision. The focus order, block order, forward and reverse presentation, cue condition, and the particular set of trials that were going to be "critical" (i.e. belong to the 20% task under each focus) were balanced across subjects.

D. APPARATUS AND STIMULI

The scene stimuli were created in July, 1987 by the experimenter in Buffalo, NY. An Olympus 35-mm camera was used to take color scene slides with a 100 or 400 ASA speed Ektachrome film. Scenes were carefully composed so as to

contain at least one object that was not undergoing a large
amount of camouflage, not too eccentric from the central
fixation point, and subtending an optimum visual angle that
made it neither too salient nor too inconspicuous (all these
were subjective judgments on the part of the experimenter as
she was taking the picture and will be analyzed in the final
data analysis.) This object warranted such extensive
consideration because it would serve as the target object in
the scene. Scenes were also photographed with a
consideration towards the ease with which they could be
labeled. Both scenes and target objects required
consideration of alternative scene and object labels before
they would be selected; i.e. a scene that was similar yet
distinctive from the one being photographed and an object
that could conceivably appear in the same scene and was of
approximately the same size, function, and location in the
scene needed to exist if not in the scene being photographed
then at least potentially so. If a good alternative label
was not available then the scene would be useless in an
experiment that involved making a two-alternative forced
choice. A wide variety of scenes were photographed (e.g.
kitchen, public pool, waterfront, sand quarry, car
dashboard, etc.)

The experiment was conducted in a darkened experimental
room. Five Kodak Carousel projectors fitted with Gerbrands
Electronic Tachistoscopic shutters were used (one each for
the frame, cues, scenes, mask, and two-alternative forced

choice slides). An SWTP 6809 microcomputer was programmed to handle the balancing requirements, the timed portion that regulated when the shutters were to open and close, a relay board that controlled the advancing of specific projectors after each trial, the on-screen program that the subject interacted with in the experiment, the storage of reaction time and error data, and the presentation of feedback information. The subject-to-screen distance was 8.5 feet and the projected slides had an approximate visual angle of 11°.

Subjects pressed one of two microswitches with the index or middle finger of their preferred hand to indicate their response on each trial. The microswitch pressed served as the input to the microcomputer and was the source of reaction time and accuracy data.

IV. RESULTS

The final analyses for the pilot data have not been completed as of this writing. Ten weeks proved to be much too short a time period in which to construct a research project of this magnitude from start to finish. A brief overview of the important aspects of the analyses that we would like to make are described below.

At the outset of designing this experiment, a prediction was made as to what the general findings would be (this is shown graphically in Figure 3). The behavior that

we expected to find is an interaction between attentional focus type (viz., whether focus is at the same- or different-level than the task) and task level. The particular shape the interaction takes (and its shape as drawn in Figure 3) can only be speculated upon at this point. Interactions such as this are difficult to interpret and it is not always clear what conclusions can be drawn from them (Loftus, 1978). Biederman (1979) has suggested a method for such situations in which the interaction is difficult to interpret that we intend to follow in analyzing the data.

The critical analysis will be a between subjects comparison of performance measures (RT and errors) for a specific stimulus when attentional focus and task were at different stimulus structure levels (a critical trial) to the same stimulus when attentional focus and task were at the same level (a non-critical trial) for another subject. A within-subjects test will generate means comparisons for critical trial performance versus non-critical trial performance within a task. This analysis will serve as a measure for determining whether our probability manipulation had the hoped-for effect of focusing attention at the local or global level.

Additional analyses will determine the effect balancing variables, visual angle of the eccentricity, target camouflage, length bias for left- versus right-label
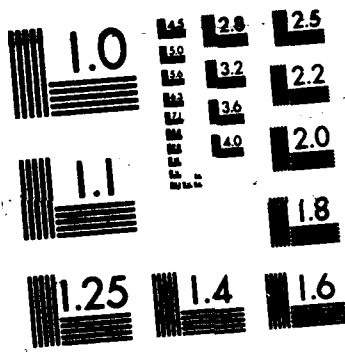
scenes (to determine whether they should be kept for the actual experiment), and cue condition (pre- expected to do better than post-cue).

V. RECOMMENDATIONS:

The research I have just described can contribute to the research enterprise that AAMRL/HEA is currently conducting. Just as importantly, it can make a contribution to at least three areas of basic research: local and global stimulus structure research, local versus peripheral attention research, and scene perception research. This project has value because it seeks to describe a basic human information processing ability rather than simply addressing a specific design question. In other words, it asks a theoretical question whose answer will have value beyond the immediate design application.

The data for the pilot study should be analyzed and used as a guide for experimental design improvements. Data collection will then ensue at the University of Minnesota in Minneapolis during the month of January, 1988. Eighty subjects are anticipated to be run in the completed design.

REFERENCES

Biederman, I., Perceiving Real-World Scenes. Science. 1972, Vol. 177, pp.77-80.

Biederman, I., Rabinowitz, J.C., Glass, A.L., Stacy, E.W. Jr., On the Information Extracted From a Glance at a Scene. Journal of Experimental Psychology. 1974, Vol. 103, pp. 597-600.

Biederman, I. & Tsao, Y.C., On Processing Chinese Ideographs and English Words: Some Implications from Stroop-Test Results. Cognitive Psychology. 1979, Vol. 11, pp.125-132.

Biederman, I., Human Information Processing of Real-World Scenes. Final Report: U.S. Army Research Institute Grant No.: MDA903-79-G. 1982.

Kinchla, R.A., Solis-Macias, V., & Hoffman, J., Attending to Different Levels of Structure in a Visual Image. Perception & Psychophysics. 1983, Vol. 33, pp. 1-10.

Loftus, G.R., On Interpretation of Interactions. Memory & Cognition. 1978, Vol. 6, pp. 312-319.

Pomerantz, J.R., Global and Local Precedence: Selective Attention in Form and Motion Perception. Journal of Experimental Psychology: General. 1983, Vol. 112, pp. 516-540.

Ward, L., Determinants of Attention to Local and Global Features of Visual Forms. Journal of Experimental Psychology: Human Perception and Performance. 1982, Vol. 8, pp. 562-581.

```
SSSSSSSSS
SSSSSSSSS
SSS
SSS
SSSSSSS
SSSSSSS
SSS
SSS
SSS
SSS
```

1. AN EXAMPLE OF A COMPOUND LETTER STIMULUS.
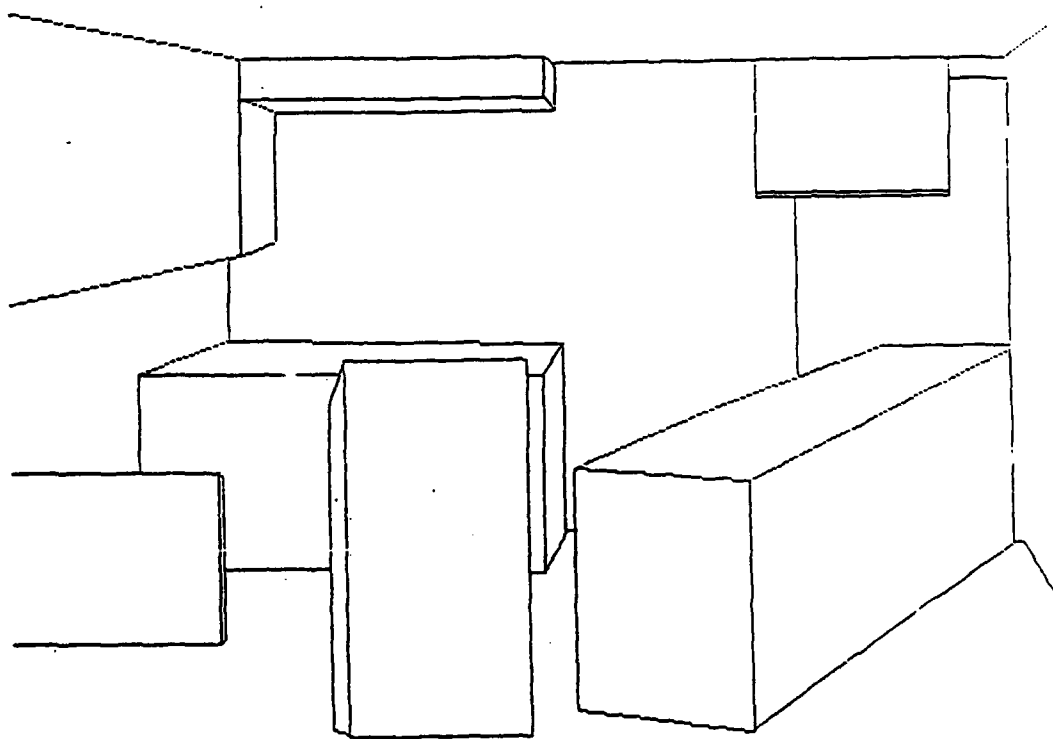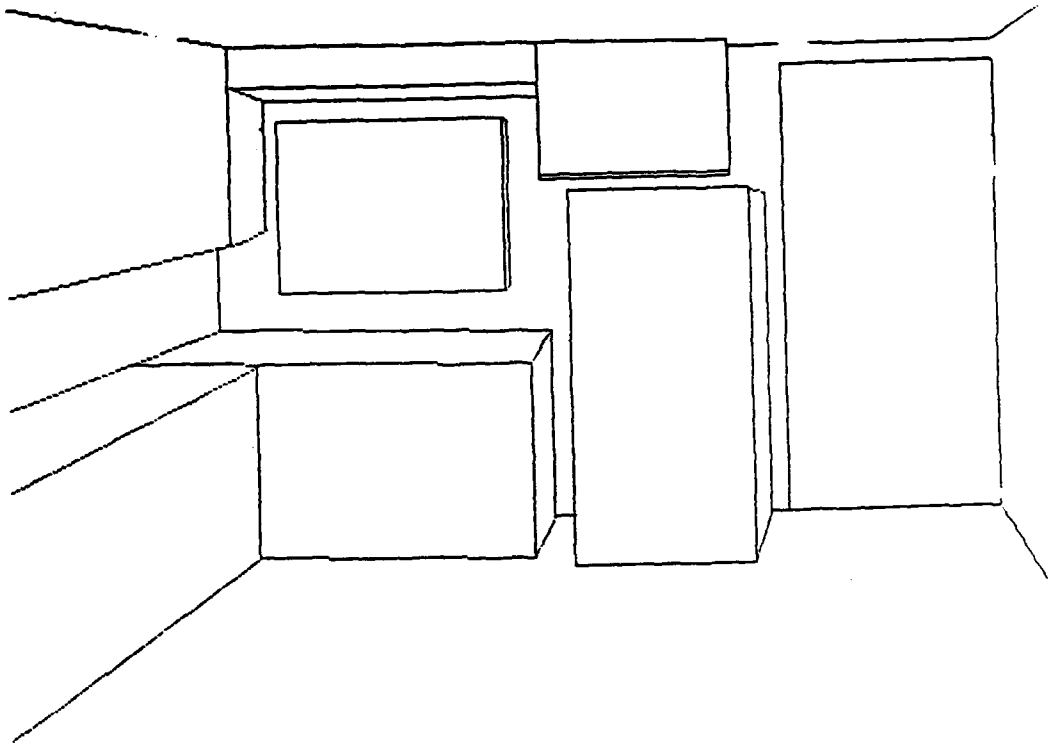
2. COHERENT VS. JUMBLED VERSIONS OF A COMPONENTIAL SCENE.

PERFORMANCE
(RT OR % ERRORS)

GLOBAL TASK
(SCENE CHOICES)

LOCAL TASK
(OBJECT CHOICES)

FOCAL
(FOCUS AND TASK AT
SAME LEVEL)

PERIPHERAL
(FOCUS AND TASK AT
DIFFERENT LEVEL)
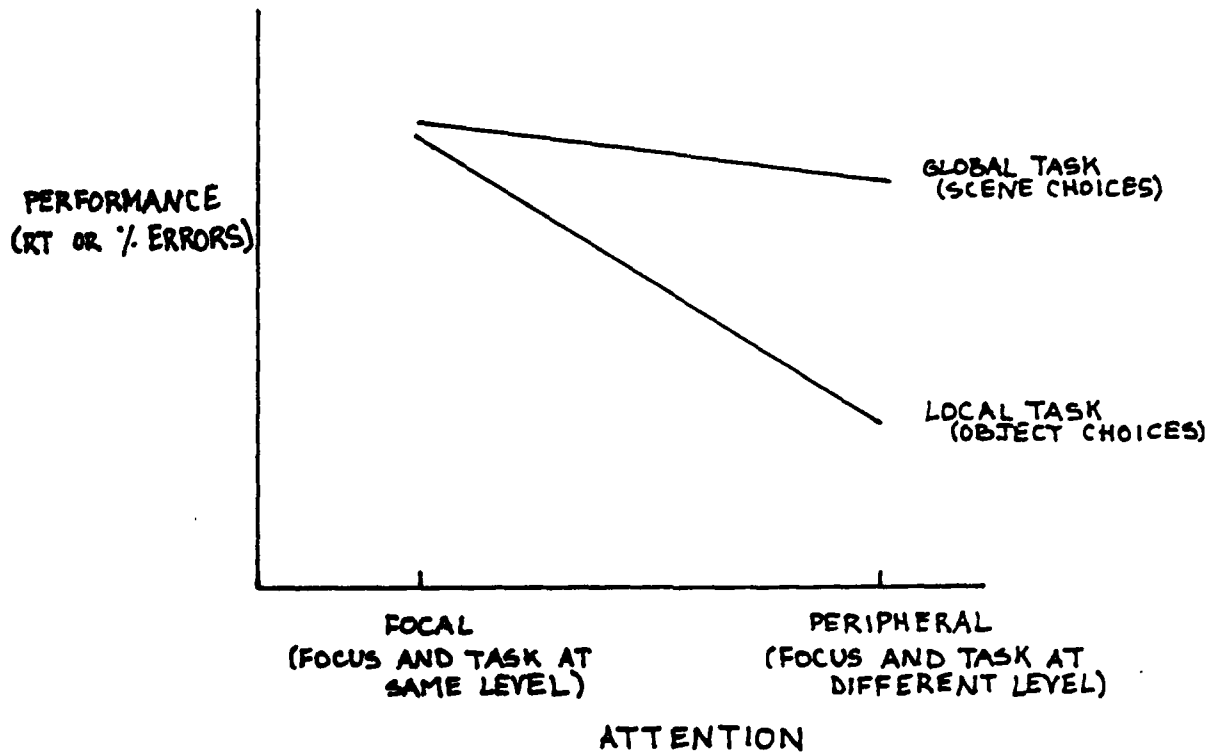
ATTENTION

3. THE PREDICTED INTERACTION BETWEEN ATTENTION TYPE AND TASK TYPE.

1987 USAF-UES SUMMER FACULTY RESEARCH PROGRAM\

GRADUATE STUDENT SUMMER SUPPORT PROGRAM

Sponsored by the

AIR FORCE OFFICE OF SCIENTIFIC RESEARCH

Conducted by the

Universal Energy Systems, Inc.

FINAL REPORT

PROVIDING ON-LINE GUIDANCE TO COMPUTER USERS

Prepared by:	Edward M. Gellenbeck
Academic Rank:	Doctoral Candidate
Department and	Department of Computer Science
University:	Oregon State University
Research Location:	USAF School of Aerospace Medicine
	Brooks AFB, Texas and
	Southwest Research Institute
	San Antonio, Texas
USAF Researcher:	Dr. Bryce Hartman
Date:	September 4, 1987
Contract No:	F49620-85-C-0013

PROVIDING ON-LINE GUIDANCE TO COMPUTER USERS

by

Edward M. Gellenbeck

ABSTRACT

The conceptual design for an on-line guidance interface is presented. The design is based on research in user-oriented interface design and artificial intelligence. The on-line guidance interface offers help to users in goal-oriented, context-sensitive terms. It is accessed through a window on a multi-tasking computer system. The guidance interface is examined as an interface to information retrieval services. The paper concludes with a list of references in the area of user-oriented interface design.

ACKNOWLEDGMENTS

I. INTRODUCTION

Dr. Bryce Hartman of the USAF School of Aerospace
Medicine in San Antonio, Texas is deeply interested in
developing computer-based training facilities for fighter
pilots. Together with the Human Performance Engineering
Department at Southwest Research Institute (SwRI), he has
been developing such a training facility in San Antonio.
One of the most important components to this training
facility is a human-computer interface that is able is
establish a relationship with the trainee that is
intentional in a compelling way, as well as being
interactive and adaptive. This computer-based training
facility is referred to as the Intentional Tutor.

Dr. Richard Schori of Oregon State University spent the
summer of 1986 as a USAF-UES Summer Faculty Researcher
working with Dr. Hartman on the Intentional Tutor project.
Subsequently, Dr. Schori was awarded an USAF-UES Mini Grant
to continue his research at Oregon State University. I was
recruited by Dr. Schori to assist in his research efforts in
the area of microcomputer-based information presentation and
retrieval.

As a PhD. student in Computer Science at Oregon State
University, I am able to contribute to this research based
on my strong background in system level programming which I
gained through formal education (M.S. in computer science
from California State University, Chico 1986) and
professional work (system programmer, IBM 1984). Since my
doctoral concentration at Oregon State University is
artificial intelligence, my research efforts are oriented
towards applying artificial intelligence techniques to this
application area.

Both Dr. Schori and myself were selected for the 1987
USAF-UES Summer Fellow Program to continue our research
efforts relevant to the Intentional Tutor project at the
School of Aerospace Medicine, Brooks Air Force Base, Texas.

II. OBJECTIVES OF THE RESEARCH EFFORT

Literature Review

One of my summer objectives was to conduct a literature review in the area of user-oriented human-computer interface design. The increase in computing power and software sophistication has brought about an interest in user-oriented interface design. Interface design deals with a wide spectrum of concerns ranging from user physiology and psychology to computer hardware and software. Traditionally, ergonomics and human factors research have been the two disciplines most closely aligned with interface design.

A number of researchers are currently active in applying the cognitive sciences to the design and construction of user-oriented human-computer interfaces. The emphasis of user-oriented interface design is toward understanding the goals, tasks, knowledge and cognitive limits of computer users rather than specific hardware and/or software technology.

The library at Southwest Research Institute has served as my source for reference material on user-oriented interface design. This paper concludes with a list of the literature reviewed. An examination was made of the current research questions outstanding in the area of human-computer interfacing and how artificial intelligence techniques might contribute to these research efforts. Section III, subsection "Advantages of the Expert Advisor" describes five areas where AI techniques may be used to improve human-computer interfaces.

Applications to Information Retrieval

Another objective of my summer research was to explore the application of user-oriented human-computer interface design to computer-assisted information retrieval. Dr. Hartman and Glenn Humphress of SwRI have labeled a component of the Intentional Tutor as Big Gulp. Big Gulp refers to the ability of the tutee, during the Intentional Tutor training session, to network with a myriad of information sources available through a diverse set of application programs.

The focus of this report presents an original conceptual design I have developed for a Big Gulp interface dubbed the Expert Advisor. It is based on current expert system technology and has applications across a variety of disciplines. The Expert Advisor interface is discussed in Section III of this report and its application to Big Gulp is covered in section IV.

III. EXPERT ADVISOR

Introduction

This section presents a conceptual design for an user-oriented interface referred to as the Expert Advisor. The Expert Advisor's function is to help the user map his or her goals to tasks which are performed on a computer system. Norman (1986) refers to the gap between goals and tasks as the gulf of execution. Specifically, the Expert Advisor aids the user in goal formulation, planning the computer task sequence, and executing the tasks. The Expert Advisor has not been implemented.

The Expert Advisor takes the user's goals to be the central, top-level units that mediate interaction. It

provides support for real world goals, which may take days or even months to perform and require the integration of a variety of application programs. This differs from traditional interfaces which take the application programs to be the structural units of the interface and offer no support to users in planning and managing their activities (Cypher 86).

The major input to the design of the Expert Advisor interface comes from an analysis of the environment in which the computer system is used. Environment, in this context, refers to a group of computer users in an organization who share a common set of goals, tasks and domain knowledge. Example environments include an accounting department of a large corporation or the airplane mechanics in the USAF. Individuals in the environment are expected to vary in their computer expertise from novices to experts. An expert, both in the application domain and the computer system, will serve as the knowledge source for a expert system designed to perform the mapping from user goals to computer tasks.

Expert Advisor Objectives

The objectives of the Expert Advisor are to:

1. provide computer users with guidance in accomplishing their goals better and/or faster,
2. provide guidance to users in goal-oriented and context-sensitive terms rather than generic command-oriented terms,
3. allow users to pick up computer expertise through interaction with the system rather than through formal study or courses,
4. keep the costs of obtaining the guidance low and predictable, and
5. keep the locus of control with the user.

These objectives follow from the results of a study of the
goals and guidance-seeking behavior of computer users
conducted by Lang, Auld, and Lang (1981). The user's mental
model of the Expert Advisor is to be that of an interactive
expert who is aware of the user's goals and information that
will be needed by the user to satisfy these goals.

Architecture

An expert system will serve as the architectural unit
for the Expert Advisor. It will be accessed through a
window on a multitasking computer system and run
concurrently with the application programs. At any time the
user may switch between the Expert Advisor and the
application programs.

The environment will have a hierarchy of knowledge
bases associated with it which codify the goal and task
mappings. A top-level knowledge base will map task-oriented
goals to one or more application programs. Each application
program will have it's own knowledge base also consisting of
goal and task mappings. These knowledge bases are developed
by a knowledge engineer, an expert system shell and an
expert from the environment. An inference engine accesses
all the knowledge bases within the hierarchical structure.

Example Session

As an example, suppose the environment consists of
upper-division students in the English department of a
college accessing a UNIX based mini-computer. These users
share common goals such as writing term papers, compiling
research notes, and sending electronic mail to classmates.
Figure 1 illustrates some of the possible knowledge bases
and their hierarchy in this environment.

Figure 2 illustrates a typical computer session in this
environment using the Expert Advisor as the interface. The

user's goal in this case is to write a paper. He would
enter the goal in natural language in the Expert Advisor's
window and the inference engine would attempt to match the
user's goal to a goal in the environment's top-level
knowledge base (Fig. 2a). Failing an exact match, a list of
near matches is presented.to the user (Fig. 2b). The user
will select the appropriate goal and the corresponding task
sequence will be displayed which represents a plan of action
to the user for satisfying the goal (Fig. 2c). In this
case, writing a paper has three tasks, each with a
corresponding knowledge base which can provide further
guidance.

If the user selects the first task and requests HOW
from the pop-up menu the Expert Advisor will present a list
of editor options to the user (Fig. 2d). The user may then
select an editor and request DO from the pop-up menu. The
Expert Advisor will automatically start up the editor in a
window on the display eliminating the need for the user to
learn all the start-up procedures associated with each
application program. The user can move lower in the
knowledge base hierarchy and seek guidance in the use of the
editor by selecting this task and requesting HOW or by
entering a new goal using natural language. Now entering
the text becomes the subgoal and a plan can be displayed
which executes it.

Browsing of the goal statements in the knowledge base
is permitted. A reconnoiter mode is available to the user
which permits experimentation while saving the current
status of the data and program. The expert system inference
engine can answer how and why questions in a context-
sensitive manner by looking up or down in the knowledge
base.
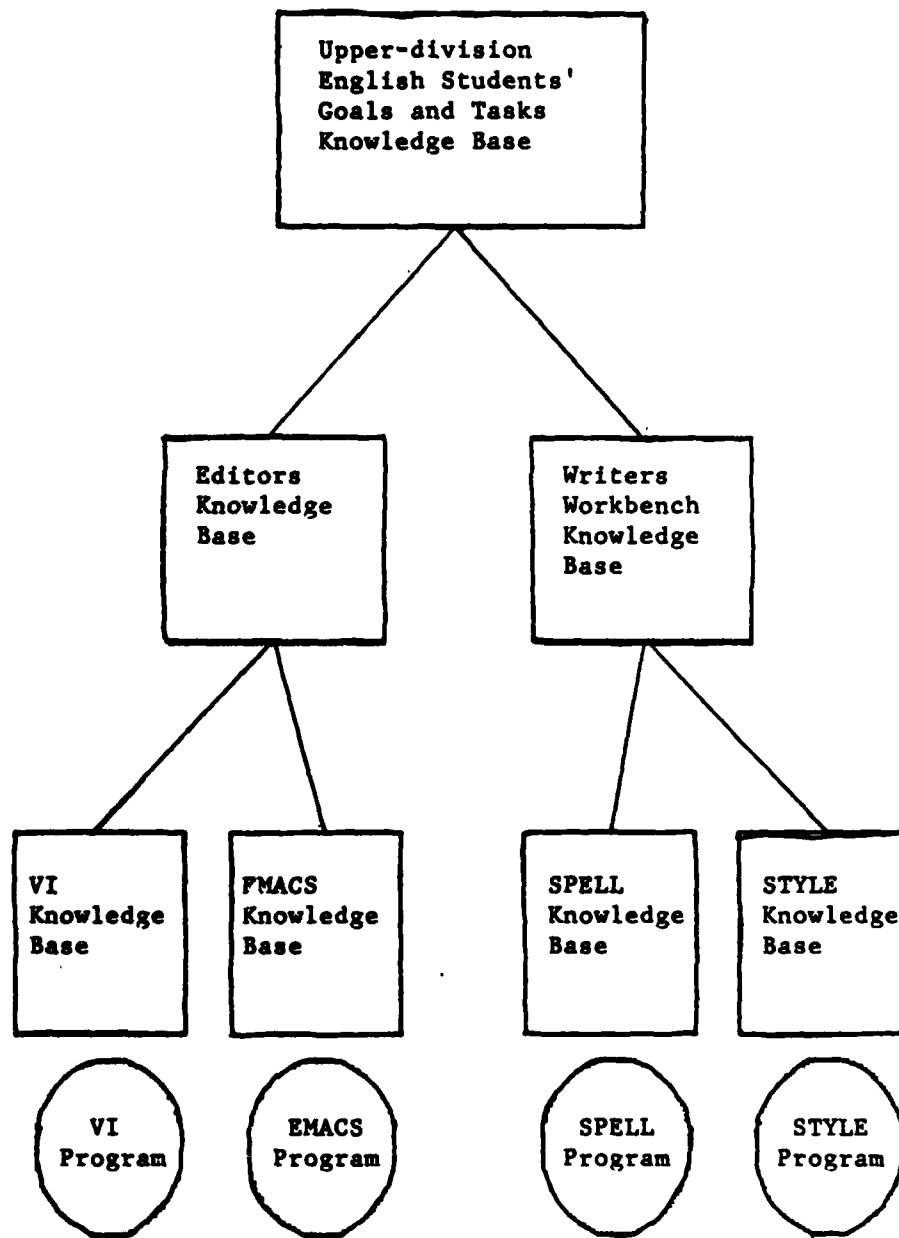
Figure 1. A subset of the knowledge base hierarchy accessed by the Expert Advisor for upper-division college students in the English department.

```
GOAL: write a paper


                      new goal
                      do
                      undo
                      how
                      why
                      browse
                      reconnoiter
```

```
GOAL: write a paper

Write an informal paper
Write a research report
Write a formal paper
Write an Eng 305 report
Write a His
Write a Phil   new goal
Write a thes   do
               undo
               how
               why
               browse
               reconnoiter
```

a.   b.

```
GOAL: write an informal paper

Use an editor to enter the text
Use writers workbench to
   proofread your paper
Use a formatter to print your
   paper
                      new goal
                      do
                      undo
                      how
                      why
                      browse
                      reconnoiter
```

```
GOAL: write an informal paper

GOAL: use an editor to enter
      the text

Use VI as the editor
        or
Use EMACS as the editor

                      new goal
                      do
                      undo
                      how
                      why
                      browse
                      reconnoiter
```

c.   d.

Figure 2. A sample session with the Expert Advisor. In (a) the user has entered the goal of writing a paper. In (b) the user selects from a list of closely matching goals. In (c) the user is requesting help on how to use an editor. In (d) the user has selected EMACS and requests the Expert Advisor start it up in a window on the display.

Advantages of the Expert Advisor

Miller and Neches (1987) suggest five areas where AI
techniques may be applied to improving interfaces. The
Expert Advisor contributes in each of these areas.

1. Explain the Task Domain and Application to the User

The first area, helping the user understand the task
domain and application is accomplished by the Expert
Advisor. The knowledge bases accessed by the Expert Advisor
encode knowledge about the domain which can be used to map
users goals to a plan of action. Tasks unfamiliar to the
user can be interpreted as subgoals and explained as more
basic tasks in the action sequence. In addition, the
browsing facility provides the user with a list, in task-
oriented terms, of the ways in which the computer system may
be used to accomplish his goals better or faster.

2. Explain the Interface to the User

Second, the Expert Advisor helps the user understand
the interface and the ways of interacting with it by the
consistent use of natural language and point and click
technology. User goals are entered in natural language and
a list of closely matching goals presented back to the user.
This helps the user in clarifying their goals by presenting
a range of likely refinements. Point and click technology
allows users to easily control the actions of the Expert
Advisor. The knowledge base hierarchy provides a structure
to the goal and task mappings. Reconnoiter mode makes it
easy for the user to test hypotheses about how the system
performs.

3. Reduce the Cognitive Demands of the User

Third, the Expert Advisor will provide support for the
cognitive demands of the users by supporting the planning
and managing of tasks. The task sequence appearing in the
Expert Advisor's window will act as an extension to user's
memory, minimizing the amount of time users must keep the
plan in their own memory. Opportunistic and higher priority
activities can be interleaved with the current user goal;
the Expert Advisor provides reorienting information upon
resumption of the current user's goal.

4. Explain the User to the System

Miller and Neches suggest that AI may be applied to
helping the computer system understand the user. User
differences may be classified along two dimensions: user
system knowledge and user domain and task structure (Moran
81). The Expert Advisor's compiled knowledge base is geared
toward a user in a particular environment. It is more
specialized in domain knowledge, user goals, and task
structure than traditional interfaces. The user's ability
to move within the hierarchy of goals, subgoals and tasks
satisfies the guidance needs of novice as well as
experienced users.

5. Support the Interface Design process

Fifth, the Expert Advisor provides a consistent
interface to application programs. This is particularly
helpful to novices who don't even know how to begin. Each
application program will have its own knowledge base which
is accessed through the Expert Advisor inference engine. A
knowledge engineer and a expert system shell will maintain
consistency even if different experts are used during the
evolution of the environment. Additional knowledge

structures can be added incrementally as new goals and tasks
are identified. Additional knowledge bases can be added as
new application programs are added to the system.

IV. BIG GULP INTERFACE

The Expert Advisor conceptual design is now examined as
an interface applicable to on-line information retrieval.
The rise in the number of on-line information services can
be overwhelming to casual users. Not only are users
required to map their goals and needs to the appropriate
information service, users must also develop expertise in
the mechanics of a variety of information retrieval
programs.

Many information systems in use today use a human
intermediary to help users clarify their initial goals,
terminology and search strategies (Ingwersen 86). The fact
that human intermediary experts exist suggest the
possibility and utility of an Expert Advisor interface.

User-driven Model for Information Systems

Traditionally, information retrieval systems have been
technology-driven and content-driven. Taylor (1986)
proposes a third approach: the user-driven model. He argues
that a major input to system design and operation should be
derived from an analysis of the information use environment.
The results of this analysis will provide the mapping
between user goals and tasks and the type of organized
information that exists in the system.

The conceptual design of the Expert Advisor is based on
a user-driven model. The Expert Advisor can be viewed as a
stepping stone to a user-driven information system. It
provides a user-driven interface to the today's technology
and content-driven information retrieval systems.

Co-operative Expert System

Information retrieval is an ill-structured task. The process of satisfying the information needs of an individual is not well understood and appears to be highly context-sensitive and individualistic.

In general, expert systems have attempted to provide a concrete, communicable solution to well-structured problems. Coombs (1984) has looked at building co-operative expert systems which focus on enriching a user's understanding of a problem areas and the development of the user's skills at handling the problem. He implemented an expert system which helps users decide what questions to ask and ways to look for answers.

The Expert Advisor interface applied to information retrieval should be designed to encourage guided discovery learning. This can be done by minimizing the costs of obtaining guidance as well as by suggesting new sources of information to the user.

Multiple Information Sources

The number of information sources available on-line is increasing daily. The Expert Advisor can aid the user in identifying which of the available information sources may be relevant to the user's goal through a systematic search through the knowledge bases for ways of satisfying the user's goals.

Multiple Application Programs

Over the last twenty years, a number of information retrieval programs have been implemented which perform a common set of operations. At present, there are over 300 different document retrieval services to which individuals can subscribe (Forsyth 86). Each of these programs uses

variations in command languages to activate these operations. Treu (1982) has worked at developing an intelligent computer interface which makes it appear to the user that the application programs are interfaced through a standard interface language.

The Expert Advisor can be designed to accomplish this standardization of terminology. Procedures can be written which perform the translation from the standard operations to the application command language.

V. Recommendations

The conceptual design of the Expert Advisor should be evaluated and revised if necessary. Assuming a positive evaluation, a suitable environment should be identified and a detailed design of the Expert Advisor undertaken.

LITERATURE REVIEWED

Bates, M. and J. Vittal. "Tools for the Development of Systems for Human Factors Experiments: An Example for the SSA." IEEE Transactions on Systems, Man and Cybernetics 12 (1982): 133-148.

Black, J. B., Kay D. S., and E. M. Soloway. "Goal and Plan Knowledge Representations: From Stories to Text Editors and Programs." In Interfacing Thought: Cognitive Aspects of Human-Computer Interaction ed. John M. Carroll, Cambridge, MA: MIT Press, 1987.

Card, S. K., Moran, T. P., and A. Newell. The Psychology of Human-Computer Interaction. Hillsdale, NJ: Lawrence Erlbaum Associates, 1983.

Carroll, J. M. and J. C. Thomas. "Metaphor and the Cognitive Representation of Computing Systems." IEEE Transactions on Systems, Man and Cybernetics 12 (1982): 107-116.

Carroll, J. M., ed. Interfacing Thought: Cognitive Aspects of Human-Computer Interaction. Cambridge, MA: MIT Press, 1987.

Coombs, M. and J. Alty. "Expert Systems: an Alternative Paradigm." In International Journal of Man-Machine Studies 20 (1984): 21-43.

Cullingford, R. E., Krueger, M. W., Selfridge, M. and M. A. Bienkowski. "Automated Explanations as a Component of a Computer-aided Design System." IEEE Transactions on Systems, Man and Cybernetics 12 (1982): 168-181.

Cypher, A. "The Structure of User's Activities." In User Centered System Design, eds. Norman, D. A. and S. W. Draper, Hillsdale, NJ: Lawrence Erlbaum Assoc., 1986.

Davies, R., ed. Intelligent Information Systems. NY: John Wiley and Sons, 1986.

Dzida, W., Herda, S., and W. D. Itzfeldt. "User-perceived quality of Interactive Systems." IEEE Transactions on Software Engineering 4 (1978): 270-296.

Forsyth, R. and R. Rada. Machine Learning: Applications in Expert Systems and Information Retrieval. New York: John Wiley and Sons, 1986.

Genter, D. and A. Stevens, eds. Mental Models. Hillsdale, NJ: Erlbaum, 1983.

Hammond, N. and P. Barnard. "Dialogue Design: Characteristics of User Knowledge." In Fundamentals of Human-computer Interaction, ed. Andrew Monk, London: Academic Press, 1985.

Haplin, S. M. "A Proposal for an Intelligent Interface in Man-machine Systems." Proc. 23rd IEEE Conference Decision and Control (1984): 592-595.

Ingwersen, P. "Cognitive Analysis and the Role of the Intermediary in Information Retrieval." In Intelligent Information Systems, ed. R. Davies, NY: John Wiley and Sons, 1986.

Jackson, P. and P. Lefrere. "On the Application of Rule-based Techniques to the Design of Advice-giving Systems." International Journal of Man-Machine Studies 20 (1984): 63-86.

Jagodzinski, A. P. "A Theoretical Basis for the Representation of On-line Computer Systems to Naive Users." International Journal of Man-Machine Studies 18 (1983): 215-252.

Lang, K., Auld, R. and T. Lang. "The Goals and Methods of Computer Users." International Journal of Man-Machine Studies 17 (1982): 375-399.

Malone, T. W. "Computer Support for Organizations: Towards an Organizational Science." In Interfacing Thought: Cognitive Aspects of Human-Computer Interaction, ed. John M. Carroll, Cambridge, MA: MIT Press, 1987.

Marcus, R. S. "User assistance in Bibliographic Retrieval Networks through a Computer Intermediary." IEEE Transactions on Systems, Man and Cybernetics 12 (1982): 116-133.

Miller, J. R. and R. Neches. Intelligent Interfaces.
Conference Tutorial Program, Sixth National Conference on
Artificial Intelligence, July 1987.

Miyata, Y. and D. A. Norman. "Psychological Issues in
Support of Multiple Activities." In User Centered System
Design, eds. Norman, D. A. and S. W. Draper, Hillsdale, NJ:
Lawrence Erlbaum Assoc., 1986.

Monk, A. ed. Fundamentals of Human-computer Interaction.
London: Academic Press, 1985.

Moran, T. P. "An Applied Psychology of the User." ACM
Computer Surveys 13 (1981): 1-11.

Nickerson, R. S. "Why Interactive Computer Systems Are
Sometimes Not Used by People Who Might Benefit From Them."
International Journal of Man-Machine Studies 15 (1981): 469-
483.

Niwa, K. "A Knowledge-based Human-computer Cooperative
System for Ill-structured Management Domains." IEEE
Transactions on Systems, Man and Cybernetics 16 (1986): 335-
342.

Noah, W. W. and S. M. Halpin. "Adaptive User Interfaces for
Planning and Decision Aids in C3I Systems." IEEE
Transactions on Systems, Man, and Cybernetics 16 (1986):
909-918.

Norman, D. A. "Cognitive Engineering." In User Centered
System Design, eds. Norman, D. A. and S. W. Draper,
Hillsdate, NJ: Lawrence Erlbaum Assoc, 1986.

Norman, D. A. and S. W. Draper, eds. User Centered System
Design. Hillsdale, NJ: Lawrence Erlbaum, 1986.

O'Malley, C. E. "Helping Users Help Themselves." In User
Centered System Design, eds. Norman, D. A. and S. W. Draper,
Hillsdale, NJ: Lawrence Erlbaum Assoc., 1986.

Partridge, S. K. "So What Is Task Orientation, Anyway?" IEEE
Transactions on Professional Communications 29 (1986): 26-
32.

Price, L. A. "Thumb: An Interactive Tool for Accessing and Maintaining Text." <u>IEEE Transactions on Systems, Man and Cybernetics</u> 12 (1982): 151-161.

Rich, E. "Users are Individuals: Individualizing Users Models." <u>International Journal of Man-Machine Studies</u> 18 (March 83): 199-214.

Ridgway, L. S. "Read My Mind: What Users Want From Online Infoarmation." <u>IEEE Transactions on Professional Communication</u> 30 (1987): 87-90.

Rouse, W. B. and N. M. Morris. "Understanding and Enhancing User Acceptance of Computer Technology." <u>IEEE Transactions on Systems, Man, and Cybernetics</u> 16 (1986): 965-973.

Sacerdoti, E. D. "Planning in a hierarchy of Abstraction Spaces." <u>Artificial Intelligence</u> 5 (1974): 115-135.

Shneiderman, B. <u>Designing the User Interface: Strategies for Effective Human-Computer Interaction</u>. Reading, MA: Addison-Wesley, 1986.

Sondheimer N. K. and N. Relles. "Human Factors and User Assistance in Interactive Computing Systems: An Introduction." <u>IEEE Transactions on Systems, Man and Cybernetics</u> 12 (1982): 102-107.

Taylor, R. S. <u>Value-added Processes in Information Systems</u>. Norwood, NJ: Ablex Publishing Co., 1986.

Thesen, A. and D. Beringer. "Goodness-of-fit in the User-computer Interface: A Hierarchical Control Framework Related to Friendliness." <u>IEEE Transactions on Systems, Man and Cybernetics</u> 16 (1986): 151-162.

Thomas, J. C. and J. M. Carroll. "Human Factors in Communication." <u>IBM Systems Journal</u> 20 (1981): 237-263.

Treu, S. "Uniformity in user-computer interaction languages: a compromise solution." <u>International Journal of Man-Machine Studies</u> 16 (1982): 183-210.

1987 USAF-UES Summer Faculty Research Program/
Graduate Student Summer Support Program

Sponsored by the
Air Force Office Of Scientific Research
Conducted by the
Universal Energy Systems, Inc.

Final Report

Mode Extraction from an Electromagnetic
Slow Wave System

Prepared by: James A. Gerald
Academic Rank: Graduate Student
Department and   Electrical and Computer Engineering
University: New Mexico State University
Research Location: AFWL/AWPB
                      Kirtland AFB
                      Albuquerque, NM 87117
USAF Researcher: 2Lt Eugene Lednum
Date: August 6, 1987
Contract No: F49620-85-C-0013

Mode Extraction from an Electromagnetic Slow Wave System

by

James A. Gerald

Abstract

Expressions for the electromagnetic fields in a coaxial waveguide with a corrugated outer conductor were obtained. In this analysis, the depth, width, and period of the corrugations remained variable along with the radius of the inner conductor and the overall radius of the structure. Also, for the purpose of analysis, the structure has been divided into two regions, I and II. Region I is the portion of the waveguide contained within the inner radius b of the corrugated outer conductor, and Region II is the portion of the waveguide contained within the corrugations or slots. To meet the boundary conditions, several functions have been used to approximate the z-directed component of the electric field at the radius b. A comparison of how well the fields match at the radius b for each approximation has been made. The phase velocity in the slow wave structure was of particular interest, and methods for obtaining it have been presented.

Acknowledgments

I. Introduction:

In May of 1987, I received my Bachelor of Science degree in Electrical Engineering from the University of Mississippi. My studies there included an emphasis in electromagnetics and mathematics. I also had the pleasure of working as a research assistant under both Dr. Charles E. Smith and Dr. Darko Kajfez while pursuing my degree.

Dr. Wheless and I met for the first time at the University of Mississippi where he was working on his Ph.D. in electrical engineering. I took my first electromagnetic fields course under him while he was there, and as part of my work, I spent several hours becoming familiar with the automated measurements system he had been using as part of his studies.

Earlier this year Dr. Wheless asked me if I would consider applying for a summer appointment under UES. This was the first I had heard of the program's existance, but as a result, he and I have been working together all summer. During this time I have had a very rewarding experience at Kirtland Air Force Base.

Over the past few years, the Beam Physics Branch of the Air Force Weapons Laboratory at Kirtland AFB has posed many unanswered questions regarding the behavior of electromagnetic waves in various slow wave structures. Also of interest to them have been possible methods for extracting energy from these structures in a circular waveguide TE11 mode. The corrugated, coaxial waveguide, a slow wave structure that the branch uses fairly often, provided both Dr. Wheless and myself with a problem to study during our ten week appointment.

II. Objectives of the Research Effort:

At this time, the corrugated, coaxial slow wave structures being used by the Beam Physics Branch have been operating in a TM mode similar to TM01 in a standard coaxial cable; however, extracting the energy from the slow wave structure has not yet been accomplished in an efficient manner. Aside from being able to extract the energy from the structure more efficiently, the Air Force would also like to convert this TM mode to a TE11 mode in a standard circular waveguide for transmission. Determining an efficient method of mode extraction from the slow wave system was thus established as our research goal.

In order to accomplish this goal, Dr. Wheless and I divided the problem into three separate steps. First, we needed to determine certain properties of electromagnetic waves in a corrugated, coaxial, slow wave structure. These properties include the field expressions, the wave impedance for forward travelling waves, and the phase velocity. Dr. Albert W. Biggs has performed a similar analysis [1]; however, he approximated the cylindrical structure with a planar structure. The cylindrical geometry has been analized by R. G. Hutter, but with fixed relationships between w_g, w_t, and d [2].

The second step involves extracting the energy from the slow wave structure by obtaining a good impedance match between it and a standard coaxial structure. Using several short matching sections, one could gradually progress from a slow wave to a fast wave structure and at the same time reduce reflection as much as possible.

The third step, the mode conversion, we saved for last since methods exist for converting the TM01 mode to TE11 using radial extraction. We set as our eventual goal, however, to convert the mode on axis without placing aperatures in the side of the waveguide.

Over the course of the summer, the first two steps have been brought as far as our ten week stay would allow, and although both require further study and development, the results have provided insight into the direction that needs to be taken for mode extraction. Also, in order to do justice to a discussion of each, we have divided the task of writing our final reports into two distinct areas, one to be covered by each of us. The work on determining the field expressions and other properties in a corrugated, coaxial waveguide appears in my final report. Likewise, the work on impedance matching and conversion from a slow to a fast wave structure appears in the report written by Dr. Wheless [3].

III. The Slow Wave Structure and Coordinate System:

Several terms should be introduced with regard to the corrugated, coaxial waveguide as shown in Figure 1. Slot or gap depth represents the depth d of the corrugations. Slot or gap width represents the width w_g of the corrugations. The width w_t of the metal tooth separating corrugations is called the tooth width, and the period of the corrugations w is called a cell width, where $w = w_g + w_t$. A cell begins at the leading edge of a gap and ends at the trailing edge of a tooth.

The two regions of interest are defined by the following:

Region I: $a \leq \rho \leq b$

Region II: $b \leq \rho \leq r$.

Each region will be treated separately, with the field expressions being matched at $\rho = b$.

IV. Transverse Components in Cylindrical Coordinates:

In cylindrical coordinates, first determining E_z and H_z and then determining the ρ and ϕ components from them is usually more convenient. To do this, the following spatial relationships are needed:

$$E_\rho = \frac{1}{(k^2 - \beta_m^2)}\left[\frac{\partial^2}{\partial\rho\partial z}E_z - j\omega\mu\,\frac{1}{\rho}\,\frac{\partial}{\partial\rho}H_z \right] \tag{1}$$

$$E_\phi = \frac{1}{(k^2 - \beta_m^2)}\left[\frac{1}{\rho}\,\frac{\partial^2}{\partial\phi\partial z}E_z + j\omega\mu\,\frac{\partial}{\partial\rho}H_z \right] \tag{2}$$

$$H_\rho = \frac{1}{(k^2 - \beta_m^2)}\left[j\omega\epsilon\,\frac{1}{\rho}\,\frac{\partial}{\partial\phi}E_z + \frac{\partial^2}{\partial\rho\partial z}H_z \right] \tag{3}$$

$$H_\phi = \frac{1}{(k^2 - \beta_m^2)}\left[-j\omega\epsilon\,\frac{\partial}{\partial\rho}E_z + \frac{1}{\rho}\,\frac{\partial^2}{\partial\phi\partial z}H_z \right] \tag{4}$$

These equations hold for both travelling and standing waves and were derived by applying $(\nabla_z\times)$ to the transverse components of Maxwell's curl equations as suggested by Om P. Gandhi [4] without the assumption that $\frac{\partial}{\partial z}E_z = -\gamma_m E_z$.

V. Region I:

A. Wave Equation:

Since the devices in use at the Beam Physics Branch operate in a TM mode, the z-component of the magnetic field must be

$$H_z^I = 0. \tag{5}$$

Assuming the time-harmonic case and leaving out the factor $e^{j\omega t}$ in all equations leads to the wave equation for E_z^I

$$\nabla^2 E_z^I + k^2 E_z^I = 0. \tag{6}$$

Where

$$E_z^I = R(\rho)\phi(\phi)X(z), \qquad (7)$$

equation (6) separates into the following three independant differential equations:

$$\rho^2\frac{\partial^2}{\partial\rho^2}R + \rho\frac{\partial}{\partial\rho}R + (k_m^2\rho^2 - n^2)R = 0. \qquad (8)$$

$$\frac{\partial^2}{\partial\phi^2}\phi + n^2\phi = 0. \qquad (9)$$

$$\frac{\partial^2}{\partial z^2}X + (k^2 - k_m^2)X = 0. \qquad (10)$$

The solutions to these equations are

$$R(\rho) = \begin{cases} A_1 J_n(k_m\rho) + A_2 N_n(k_m\rho), & k_m^2 > 0 \qquad (11) \\ \\ A_1 I_n(\tau_m\rho) + A_2 K_n(\tau_m\rho), & k_m^2 = -\tau_m^2 < 0 \qquad (12) \end{cases}$$

$$\phi(\phi) = B_1\cos(n\phi) + B_2\sin(n\phi). \qquad (13)$$

$$X(z) = C_1 e^{-\tau_m z} + C_2 e^{+\tau_m z}, \quad \tau_m^2 = k_m^2 - k^2. \qquad (14)$$

Taking τ_m to be

$$\tau_m = j\beta_m, \qquad (15)$$

$$k_m^2 = k^2 - \beta_m^2, \qquad (16)$$

$$\tau_m^2 = \beta_m^2 - k^2, \qquad (17)$$

$$\text{and} \quad k^2 = \omega^2\mu\epsilon. \qquad (18)$$

Note that since phase velocity is given by

$$\frac{v_p}{c} = \frac{k}{\beta_o}, \qquad (19)$$

slow waves occur when

$$\beta_o^2 > k^2. \qquad (20)$$

B. <u>Boundary Conditions</u>:

Taking into account the rotational symmetry of the measured fields in the slow wave systems used by the Beam Physics Branch, the index n in equations (11) through (13) must be

$$n = 0. \qquad (21)$$

27-8

This reduces equation (13) to a constant and results in $R(\rho)$ being a linear combination of Bessel functions of order zero.

Due to the inner conductor, E_z^I must be zero at $\rho = a$. Thus $R(a)$ is given by

$$R(a) = 0 = \begin{cases} A_1 J_0(k_m a) + A_2 N_0(k_m a), & k_m^2 > 0 \qquad (22) \\ \\ A_1 I_0(\tau_m a) + A_2 K_0(\tau_m a), & k_m^2 = -\tau_m^2 < 0 \quad (23) \end{cases}$$

Choosing A_1 and A_2 to be

$$A_1 = N_0(k_m a) \qquad (24)$$

$$\text{and} \quad A_2 = -J_0(k_m a), \qquad (25)$$

for $k_m^2 > 0$, and

$$A_1 = K_0(\tau_m a) \qquad (26)$$

$$\text{and} \quad A_2 = -I_0(\tau_m a) \qquad (27)$$

for $k_m^2 = -\tau_m^2 < 0$, and substituting these into equations (11) and (12),

$$R(\rho) = \begin{cases} N_0(k_m a) J_0(k_m \rho) - J_0(k_m a) N_0(k_m \rho), & k_m^2 > 0 \quad (28) \\ \\ K_0(\tau_m a) I_0(\tau_m \rho) - I_0(\tau_m a) K_0(\tau_m \rho), & k_m^2 < 0. \quad (29) \end{cases}$$

Also for the purposes of this analysis, only forward travelling waves have been considered. The lack of any boundary to cause relfections along the z-axis in Region I thus reduces equation (14) to

$$X(z) = C_1 e^{-j\beta_m z}. \qquad (30)$$

Substituting these results into equation (7) yields

$$E_z^I = A_m^I \, B_m^I(\rho) \, e^{-j\beta_m z}, \qquad (31)$$

where A_m^I is a constant and

$$B_m^I(\rho) = R(\rho). \qquad (32)$$

In Region I, only one other boundary condition may be applied. At $\rho = b$, E_z^I must be zero on the teeth, but

may have some non-zero value across the gaps. The
periodic nature of the slow wave structure allows a
functional representation for E_z^I to be constructed from
the complex Fourier series as done by Ramo, Whinnery,
and Van Duzer [5], where

$$E_z^I(\rho=b) = e^{-j\beta_o z} \sum_{-\infty}^{\infty} c_m e^{-j2\pi mz/w}. \qquad (33)$$

E_z^I as given by equation (31) may also be expanded in an
infinite series, so that

$$E_z^I = \sum_{-\infty}^{\infty} A_m^I B_m^I(\rho) \, e^{-j\beta_m z} . \qquad (34)$$

A comparison of these two expressions at $\rho = b$, leads to
the following:

$$\beta_m = \beta_o + 2\pi m/w, \qquad (35)$$

$$\text{and} \quad A_m^I = \frac{c_m}{B_m^I(b)} . \qquad (36)$$

C. **Transverse Components**:

The transverse components are obtained from
equations (1) through (4). Since $H_z^I = 0$ and

$$\frac{\partial}{\partial \phi} E_z^I = 0, \qquad (37)$$

$$E_\phi^I = 0, \qquad (38)$$

$$\text{and } H_\rho^I = 0. \qquad (39)$$

The other two components are

$$E_\rho^I = \sum_{-\infty}^{\infty} -jA_m^I \frac{\beta_m}{k_m^2} \left[\frac{\partial}{\partial \rho} B_m^I(\rho) \right] e^{-j\beta_m z}, \qquad (40)$$

$$\text{and } H_\phi^I = \sum_{-\infty}^{\infty} -jA_m^I \frac{\omega \epsilon}{k_m^2} \left[\frac{\partial}{\partial \rho} B_m^I(\rho) \right] e^{-j\beta_m z}, \qquad (41)$$

where, for $k_m^2 > 0$

$$\frac{\partial}{\partial \rho} B_m^I(\rho) = -k_m [N_o(k_m a) J_1(k_m \rho) - J_o(k_m a) N_1(k_m \rho)]. \qquad (42)$$

and for $k_m^2 = -\tau_m^2 < 0$,

$$\frac{\partial}{\partial \rho} B_m^I(\rho) = \tau_m [K_o(\tau_m a) I_1(\tau_m \rho) + I_o(\tau_m a) K_1(\tau_m \rho)]. \qquad (43)$$

Note that for some terms of the series, k_m^2 may be greater than zero while for others it is less.

The wave impedance, Z_{TM}, of interest for the matching sections is defined by the forward travelling terms of these transverse components. Based on them,

$$Z_{TM} = \frac{\sum_n^\infty -jA_m^I \frac{\beta_m}{k_m^2} \left[\frac{\partial}{\partial\rho}B_m^I(\rho)\right] e^{-j\beta_m z}}{\sum_n^\infty -jA_m^I \frac{\omega\epsilon}{k_m^2} \left[\frac{\partial}{\partial\rho}B_m^I(\rho)\right] e^{-j\beta_m z}} , \quad (44)$$

where n satisfies

$$\beta_n \geq 0 \quad (45)$$

$$\text{and} \quad \beta_{n-1} < 0. \quad (46)$$

VI. Region II:

A. Boundary Conditions:

As in Region I, equations (5) through (21) hold for Region II as well. Thus for Region II we may start by applying the boundary condition that E_z^{II} must be zero at $\rho = r$. This leads to

$$R(\rho) = \begin{cases} N_0(k_m r)J_0(k_m\rho) - J_0(k_m r)N_0(k_m\rho), & k_m^2 > 0 \quad (47) \\ \\ K_0(\tau_m r)I_0(\tau_m\rho) - I_0(\tau_m r)K_0(\tau_m\rho), & k_m^2 < 0 \quad (48) \end{cases}$$

as in Region I.

Due to the presence of the teeth in Region II, C_2 in equation (14) does not equal zero. Therefore E_z^{II} is given by

$$E_z^{II} = A_m^{II} B_m^{II}(\rho) \left[e^{-j\beta_m z} + \Gamma_m e^{+j\beta_m z}\right] \quad (49)$$

where A_m^{II} is a constant and

$$B_m^{II}(\rho) = R(\rho) \quad (50)$$

as given in equations (47) and (48).

27-11

Also due to the teeth, E_ρ^{II} must be zero at $\pm\frac{1}{2}$ w_g.
From equation (1), the z-dependance of E_ρ^{II} may be
written

$$X_\rho(z) = e^{-j\beta_m z} - \Gamma_m e^{+j\beta_m z}. \qquad (51)$$

At $z = \frac{1}{2}$ w_g, this becomes

$$e^{-j\beta_m w_g/2} - \Gamma_m e^{+j\beta_m w_g/2} = 0, \qquad (52)$$

which separates into the following two equations:

$$\cos(\beta_m w_g/2) = \Gamma_m \cos(\beta_m w_g/2) \qquad (53)$$

$$\text{and} \quad \sin(\beta_m w_g/2) = -\Gamma_m \sin(\beta_m w_g/2). \qquad (54)$$

Choosing

$$\Gamma_m = 1 \qquad (55)$$

satisfies equation (53) and yields

$$\frac{\beta_m w_g}{2} = m\pi \qquad (56)$$

from equation (54). Thus

$$\beta_m = \frac{2\pi m}{w_g}, \qquad (57)$$

and equation (51) becomes

$$X_\rho(z) = 2j\sin(\beta_m z) \qquad (58)$$

$$\text{or} \quad X_\rho(z) = 2j\sin(2\pi mz/w_g). \qquad (59)$$

Equation (49) may now be written

$$E_z^{II} = A_m^{II} B_m^{II}(\rho) \cos(2\pi mz/w_g), \qquad (60)$$

with the factor of two being incorporated into the
leading constant A_m^{II}.

Applying the boundary condition at $\rho = b$, E_z^{II} is
expanded in terms of a standard Fourier series, where

$$E_z^{II}(\rho=b) = \sum_0^\infty a_m \cos(2\pi m/w_g) + \sum_1^\infty b_m \sin(2\pi m/w_g). \qquad (61)$$

On expanding (60) in a similar manner and comparing the
two expressions,

$$E_z^{II} = \sum_0^\infty A_m^{II} B_m^{II}(\rho) \cos(2\pi mz/w_g), \qquad (62)$$

$$b_m = 0, \qquad (63)$$

$$\text{and} \quad A_m^{II} = \frac{a_m}{B_m^{II}(b)} . \qquad (64)$$

B. Transverse Components:

Using equations (1) through (4) and noting that equation (37) holds for Region II as well,

$$E_\phi = 0, \tag{65}$$

$$\text{and} \quad H_\rho = 0. \tag{66}$$

The other two components are

$$E_\rho^{II} = \sum_1^\infty -A_m^{II} \frac{2\pi m}{w_g k_m^2} \left[\frac{\partial}{\partial \rho} B_m^{II}(\rho) \right] \sin(2\pi mz/w_g), \tag{67}$$

$$\text{and} \quad H_\phi^{II} = \sum_0^\infty -j A_m^{II} \frac{\omega \epsilon}{k_m^2} \left[\frac{\partial}{\partial \rho} B_m^{II}(\rho) \right] \cos(2\pi mz/w_g), \tag{68}$$

where for $k_m^2 > 0$

$$\frac{\partial}{\partial \rho} B_m^{II}(\rho) = -k_m [N_0(k_m r) J_1(k_m \rho) - J_0(k_m r) N_1(k_m \rho)]. \tag{69}$$

and for $k_m^2 = -\tau_m^2 < 0$

$$\frac{\partial}{\partial \rho} B_m^{II}(\rho) = \tau_m [K_0(\tau_m r) I_1(\tau_m \rho) + I_0(\tau_m r) K_1(\tau_m \rho)]. \tag{70}$$

Note that, as in Region I, for some terms of the series, k_m^2 may be greater than zero while for others it is less. Also note that for $m = 0$, k_m^2 is always

$$k_0^2 = k^2. \tag{71}$$

VII. Fourier Expansions for E_z at $\rho = b$:

A. Constant Across the Gap:

In Region I, the Fourier coefficients for equation (33) are given by

$$c_m = \frac{1}{w} \int_{-w/2}^{w/2} E_z^I(\rho=b) e^{j\beta_m z} dz. \tag{72}$$

In this case,

$$E_z^I(\rho=b) = \begin{cases} E_g, & \text{in the gaps} \\ \\ 0, & \text{on the teeth,} \end{cases} \tag{73}$$

27-13

as suggested by A. H. W. Beck [6]. Equation (72) then becomes

$$c_m = \frac{1}{w} \int_{-w_g/2}^{w_g/2} E_g e^{j\beta_m z} dz .$$ (74)

Therefore,

$$c_m = \frac{2}{w\beta_m} E_g \sin(\beta_m w_g/2).$$ (75)

In Region II, the Fourier coefficients for equation (61) are

$$a_o = E_g,$$ (76)

and $a_m = b_m = 0, \ m > 0.$ (77)

B. Triangular Pulse Across the Gaps:

Using the triangular pulse suggested by the numerical results of Ray Lemke and M. C. Clark [7], the coefficients for Region I are given by equation (72), where

$$E_z^I(\rho=b) = \begin{cases} E_g\left[1 + \dfrac{2z}{w_g} \right], & -w_g/2 \le z \le 0 \\[2mm] E_g\left[1 - \dfrac{2z}{w_g} \right], & 0 \le z \le w_g/2 \\[2mm] 0, & \text{on the teeth.} \end{cases}$$ (78)

Thus

$$c_m = \frac{1}{w} \int_{-w_g/2}^{0} E_g\left[1 + \frac{2z}{w_g} \right] e^{j\beta_m z} dz + \frac{1}{w} \int_{0}^{w_g/2} E_g\left[1 - \frac{2z}{w_g} \right] e^{j\beta_m z} dz$$ (79)

resulting in

$$c_m = \frac{4}{w_g w \beta_m^2} E_g \ [1 - \cos(\beta_m w_g/2)].$$ (80)

In Region II,

$$a_o = \frac{2}{w_g} \int_{0}^{w_g/2} E_z^{II}(\rho=b) dz,$$ (81)

and $a_m = \frac{4}{w_g} \int_{0}^{w_g/2} E_z^{II}(\rho=b) \cos(2\pi m z/w_g) dz.$ (82)

Substituting from equation (78),

$$a_o = \frac{2}{w_g} \int_0^{w_g/2} E_g \left[1 - \frac{2z}{w_g} \right] dz, \tag{83}$$

$$\text{and} \quad a_m = \frac{4}{w_g} \int_0^{w_g/2} E_g \left[1 - \frac{2z}{w_g} \right] \cos(2\pi mz/w_g) dz. \tag{84}$$

From these,

$$a_o = E_g/2 \tag{85}$$

$$\text{and} \quad a_m = \frac{8}{\beta_m^2 w_g^2} E_g [1 - \cos(\beta_m w_g/2)], \quad m > 0. \tag{86}$$

C. $\underline{E_g[1 - (2z/w_g)^2]^{1/2} \text{ Across the Gap:}}$

Taking $E_z^I(\rho = b)$ to be

$$E_z^I(\rho = b) = \begin{cases} E_g[1 - (2z/w_g)^2]^{1/2}, & \text{in the gaps} \\ \\ 0, & \text{on the teeth,} \end{cases} \tag{87}$$

results in the integral

$$c_m = \frac{1}{w} \int_{-w_g/2}^{w_g/2} E_g [1 - (2z/w_g)^2]^{1/2} e^{j\beta_m z} dz \tag{88}$$

From Gradshteyn and Ryzhik [8],

$$J_\nu(x) = \frac{\left[\frac{x}{2} \right]^\nu}{\Gamma(\nu + 1/2)\Gamma(1/2)} \int_{-1}^1 (1 - t^2)^{\nu - 1/2} e^{jxt} dt. \tag{89}$$

Applying this to equation (88) yields

$$c_m = \frac{\pi E_g}{\beta_m w} J_1(\beta_m w_g/2). \tag{90}$$

In Region II,

$$a_o = \frac{2}{w_g} \int_0^{w_g/2} E_g [1 - (2z/w_g)^2]^{1/2} dz, \tag{91}$$

$$\text{and} \quad a_m = \frac{4}{w_g} \int_0^{w_g/2} E_g [1 - (2z/w_g)^2]^{1/2} \cos(2\pi mz/w_g) dz. \tag{92}$$

Again from Gradshteyn and Ryzhik [8],

$$J_\nu(x) = \frac{\left[\frac{x}{2}\right]^\nu}{\Gamma(\nu+1/2)\,\Gamma(1/2)} \int_{-1}^{1} (1-t^2)^{\nu-1/2} \cos(xt)\,dt. \qquad (93)$$

and

$$\int (a+cx^2)^{1/2}\,dx = \frac{1}{2}x(a+cx^2)^{1/2} + \frac{a}{2\sqrt{-c}}\arcsin(x\sqrt{-c/a}) \qquad (94)$$

Applying these results in

$$a_o = \frac{\pi}{8}E_g, \qquad (95)$$

$$\text{and} \quad a_m = \frac{2\pi}{\beta_m w_g}E_g\,J_1(\pi m). \qquad (96)$$

D. Comparison of Approximations:

At the mouth of each slot, the impedance given by

$$Z_{in} = \frac{E_z^I}{H_\phi^I} \qquad (97)$$

must also be

$$Z_{in} = \frac{E_z^{II}}{H_\phi^{II}}. \qquad (98)$$

Figure 2 is a comparison of these two expression for the
Fourier coefficients given by part A of this section.
Likewise, Figure 3 compares those from part B and
Figure 4 those from part C. In each case, $w_g = 0.7$ cm,
$w_t = 0.7$ cm, $d = 1.8$ cm, $a = 6.5$ cm, $b = 8.2$ cm, and
$\beta_o = 224.4$ rad/m at a frequency of 3.5 GHz.

VIII. Phase Velocity:

By using the procedure of section VII, E_z^I and E_z^{II}
are forced to match at $\rho = b$. This procedure, however,
does not force H_ϕ^I and H_ϕ^{II} to match. These would match

perfectly only if the exact behavior of $E_z(\rho=b)$ were known and a correct value for β_o was obtained.

An approximate β_o, and thus phase velocity, may be obtained using one of two methods. First, β_o may be varied until the best match between H_ϕ^I and H_ϕ^{II} is obtained. As an alternative, β_o may be varied until Z_{in} from equation (97) matches Z_{in} from equation (98) closely.

Using the second method described above and the geometry for Figures 2 through 4, a β_o of 224.4 rad/m was obtained for a frequency of 3.5 GHz with only the zero order term from each series being used. This indicates a relative phase velocity of

$$\frac{v_p}{c} = 0.33 \ . \tag{99}$$

Experimentally,
$$\frac{v_p}{c} = 0.34 \tag{100}$$

for $\beta_o = 224.4$ rad/m, suggesting a frequency of 3.6 GHz.

IX. Recommendations:

As can be seen from Figure 2 through 4, a perfect match for $E_z(\rho=b)$ has not yet been obtained. Also, as slot width and depth vary, the accuracy of the approximations may vary. To obtain a perfect match, a numerical solution for $E_z(\rho=b)$ becomes necessary. Such a solution would also incorporate the change in character of E_z with changes in dimensions. From the numercal solution, the Fourier coefficients for $E_z(\rho=b)$ may then be obtained.

Other possible extensions of the work presented
here include the following:

a) a numerical solution for non-periodic structures
   of this type which would allow an analysis of a
   matching section,

b) a program based on numerical techniques for
   designing matching sections,

c) a study of periodic structures of this type for
   which one variation occurs over several teeth.
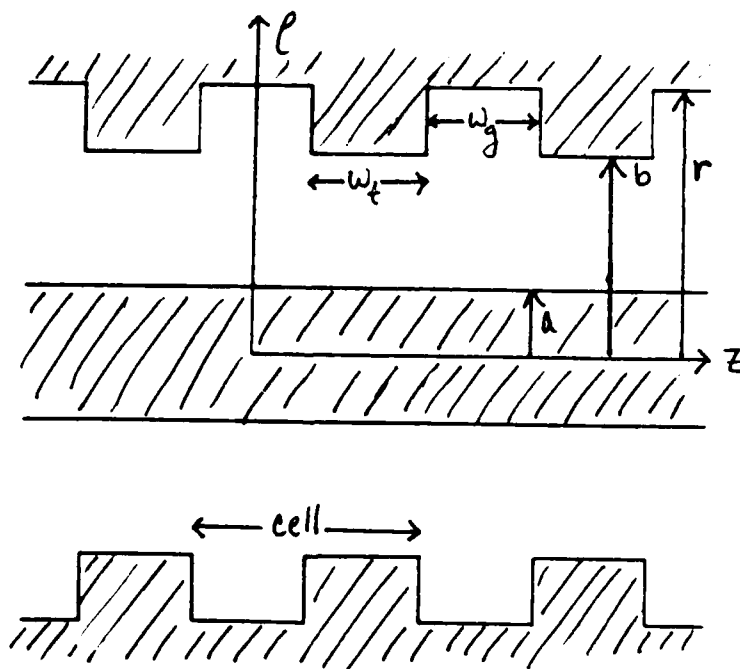
Figure 1: Geometry
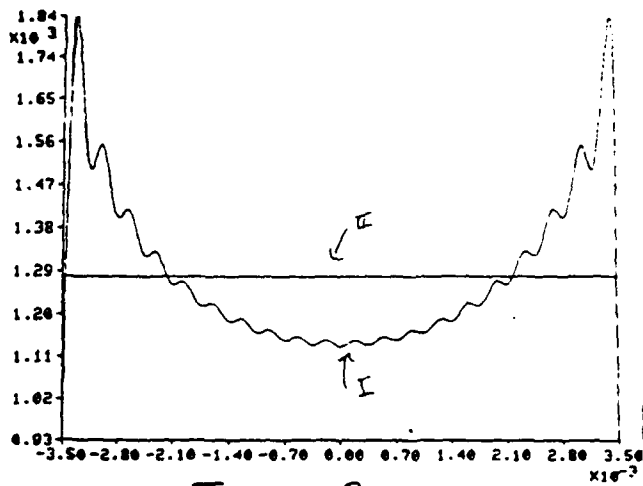
Figure 2
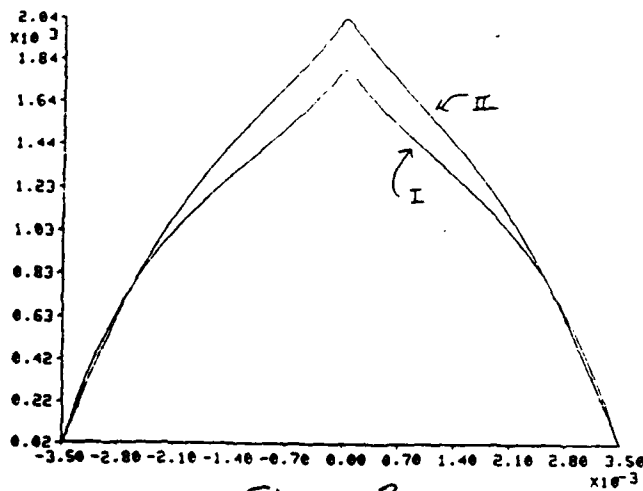
Figure 3
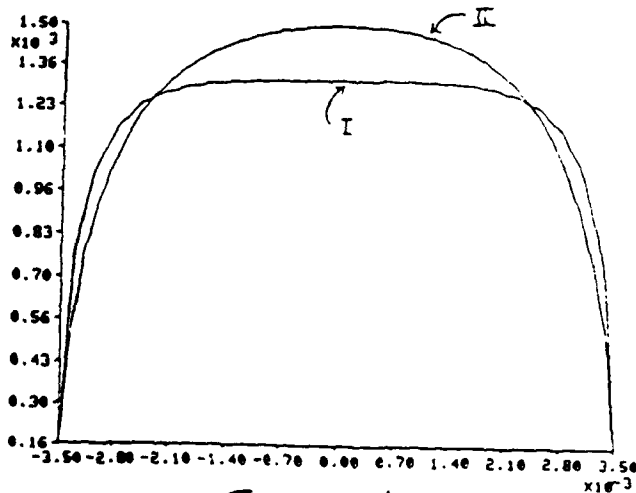
Figure 4

References

1. Biggs, Albert W., _Final Report: Corrugated Waveguides for Slow Waves_. 1986 USAF-UES Summer Faculty Research Program.

2. Hutter, Rudolf G. E., _Beam and Wave Electronics in Microwave Tubes_, pp. 106-108, Princeton, N.J., D. Van Nostrand Company, Inc., 1960.

3. Wheless, W. Perry, Jr., _Final Report: Mode Extraction from an Electromagnetic Slow Wave System_. 1987 USAF-UES Summer Faculty Research Program.

4. Gandhi, Om P., _Microwave Engineering and Applications_, pp. 14-16, New York, NY, Pergamon Press, 1981.

5. Ramo, Simon, John R. Whinnery, and Theodore Van Duzer, _Fields and Waves in Communication Electronics_, pp. 477-481, New York, NY. John Wiley and Sons, 1984.

6. Beck, A. H. W., _Space-Charge Waves_, pp. 57-61, New York, NY, Pergamon Press, 1958.

7. Lemke, R. W., and M. C. Clark, "Theory and Simulation of High Power Microwave Generation in a Magnetically Insulated Transmission Line Oscillator"

8.. Gradshteyn, I. S., and I. M. Ryzhik, _Table of Integrals, Series, and Products_, p. 86 and p. 953, New York, NY, Academic Press, 1980.

1987 USAF-UES SUMMER FACULTY RESEARCH PROGRAM/

GRADUATE STUDENT SUMMER SUPPORT PROGRAM

Sponsored by the

AIR FORCE OFFICE OF SCIENTIFIC RESEARCH

Conducted by the

UNIVERSAL ENERGY SYSTEMS, INC.

FINAL REPORT

Mesopic Visual Performance With and Without Glare

in

Contact Lense Wearers

Prepared by:	Maurice B. Gilbert
Academic Rank:	Medical Student
Department and University:	School of Medicine and Graduate Studies Meharry Medical College
Research Location	USAFSAM/NGOP Brooks Air Force Base San Antonio, TX 78235-5000
USAF Researcher:	Lt. Col. Robert E. Miller,II
DATE:	September 21, 1987
Contract Number:	F49620-85-C-0013

Mesopic Visual Performance With and Without Glare in

Contact Lense Wearers

By

Maurice B. Gilbert

ABSTRACT

Mesopic vision testing of human subjects was performed in order to examine the effects of glare on visual function. Pilot age individuals were checked and each was tested with both contact lenses and spectacles. They were examined with the aid of a nyktometer. An apparatus which tests the subject under simulated mesopic (twilight) vision conditions both with and without a glare light source. Both contacts and spectacles correct for visual acuity, yet which of the two is better for twilight visual performance. The study will generate needed data for comparison. This will allow the vision lab a chance to make recommendations concerning twilight visual needs.

Acknowledgements

I wish to thank the Air Force Systems Command and the Air Force Office of Scientific Research for sponsorship of this research. I would like to thank the Universal Energy Systems Program for allowing me the opportunity to expand my knowledge and capabilities in their worthwhile program.

This being my second exposure with the Ophtholmology Branch at USAFSAM, will allow me the opportunity to become a better researcher and clinician. Lt. Col. Robert E. Miller II, was always willing to extend his knowledge to myself, not just for the project, but for the sake of learning. Technical support by TSSGT Jay J. Placette was most appreciated. He had a knowledge for the instruments utilized, which I used in the screening of subjects. My thanks and appreciation to AIC Trevor Abbott and Mrs. Francis Williams, whom without their assistance, a majority of items would not have been accomplished.

I. INTRODUCTION:

Mesopic Vision is the visual illumination between cone photopic system and rod scotopic system. This visual spectrum occurs under natural conditions between the daylight and evening hours and may be referred to as twilight vision. The transition which occurs between these ranges result in a shift in the sensitivity of the human retina toward shorter wavelength of light. This transitional area of vision has also been termed partial dark adaptation.

The Ophthalomology Branch of the USAF School of Aerospace Medicine at Brooks Air Force Base, is concerned with the effects of glare on mesopic visual performance. Visual acuity in the mesopic range is examined utilizing subjects who have been prescribed both spectecles and contact lenses. A comparision of the two is made to measure human mesopic vision and evaluate the effectiveness of contact lenses. Currently, large numbers of pilots are required to utilize spectacles, because their acuity is not 20/20. Yet, there may be in instances when the utilization of spectacles is not the optimal choice. Contact lenses may offer a viable alternative for USAF aircrew.

Having previously worked with the Ophthalmology Branch during the Summer of 1986, I became familiar with the objectives and the function of the branch. Having a background in biology and biomedical research has given support to my ability in experimental design.

Also, with my training in basic medical science would allow me the ability to apply human function to the research effort. These factors would allow me to be objective in helping to design and investigate a research protocol for mesopic visual performance.

II. OBJECTIVES OF THE RESEARCH EFFORT

At present, there have been few scientific investigation concerning mesopic vision. Assessment of visual function is usually performed in the photopic and/or scotopic range. A comparison spectacles and contact lenses at the mesopic level is done to examine visual target acuity with and without a glare source in pilot age observers. An examination of scientific literature revealed few comparisons and contrast review concerning contact and optical lenses at mesopic visual illumination. This comparison would have to be investigated by our lab in an effort to which visual optic would function better.

Contact lenses offer and advantage over spectacles, because they reduce blockage of peripheral vision in the pilot. Testing contacts in military field conditions as well as visual target acuity testing will help determine the better visual optical aid for various conditions. As a participant in the 1987 Graduate Student Summer Support Program, I was assigned to examine twenty (20) pilot age observers in the mesopic range. Each subject would be a wearer of both contact and spectacle lenses. It was determined that

the protocol required the utilization of the nyktometer. This instrument
is designed to test visual acuity in this range.

III. MATERIALS AND METHODS

Participants in the experiment were required to sign and have witnessed
a human subject voluntary consent form. Each was informed of his/her rights,
possible benefits or hazards and entitlement to medical care or compensation
in the event of injury. A participant could withdraw at anytime, without
consequences.

After an initial briefing, a review of the subjects general medical
history was illicited. Questions were asked concerning their general health,
current medications, infections or other conditions, which may alter the
experimental outcome. Visual acuity was examined with the Smellen Chart.
Participants would have a minimum acuity of 20/20.

Grading of lense deposits was accomplished with the use of a slit-lamp.
The scale was as follows:

Grade 1: Film and deposits detected by micro-
          scope.
Grade 2: Film and deposits dectectable under
          certain conditions.

Grade 3: Film and deposits visible under normal room lightning conditions without special equipment on a dry lense, but which are not visible while the lense is wet.

Grade 4: Film and deposits detectable under normal room lightning conditions with or without any special equipment while the lense is wet or dry.

Testing was for a two (2) consecutive day period. Each subject was assigned a random number which determined whether the subject was to be tested with contacts or spectacles on their first day, with the second day used for the other. Subjects were examined monocularly varing OD or OS by random assignment. After evaluation and a three minute pre-dark adapt, each was tested with the Rodenstock nyktometer.

RESULTS:

Testing was completed on seven (7) subjects. A pool which consisted of five (5) females and two (2) males with an age range between 24 and 42. All except one (1) were non-smokers. None had any stated medical conditions

which would adversely effect the outcome of the test. All had a minimum visual acuity of 20/20 corrected. Each subject was tested for maximum target acuity with the nyktometer. If the subject was able to visualize all target positions on the primary disc (501), then they were examined with the secondary disc (502). When the subject was no longer able to identify the corrected position, testing was stopped. The following chart shows the number of positive identification for each target position.

HIGHEST TARGET ACUITY FOR NYKTOMETER

	CONTACT LENSES				SPECTACLES			
POSITION	DISC 501		DISC 502		DISC 501		DISC 502	
	OD	OS	OD	OS	OD	OS	OD	OS
WITHOUT GLARE 1	—	—	—	—	—	—	—	—
2	2	1	—	—	1	—	—	—
3	2	—	1	—	—	2	1	—
4	1	2	1	2	1	2	1	—
5	—	1	—	—	1	—	—	1
6	2	3	—	—	2	2	—	—
WITH GLARE 7	—	—	—	—	1	—	—	—
8	—	3	—	—	—	1	—	—
9	3	1	—	—	2	1	—	—
10	—	—	—	—	—	1	—	—
11	—	—	—	—	—	—	—	—
12	—	—	—	—	—	—	—	—

*Note: ___ Means No Response

DISCUSSION

Experimental protocol design and a sequence of unfortunate delays result-
ed in an inability to complete testing on twenty (20) subjects. Of the
seven (7) participants who completed the study, five of them were females.
This has biased the study as completed to date. In an effort to collect
data within the allotted time, I accepted eligible subjects without regard
to sexual bias. Within the study, I questioned the effect of medical health
on the subjects ability to visualize the target. Specific questions may
assist in screening those individuals with a physiological limit related
to an organic basis. Common systemic conditions associated with increased
light thresholds follow, vitamin A deficiency, chronic alcoholism,
malnutrition syndromes, myotonic dystrophy and others. Therefore, questions
about general health may assist in screening medically correctible deficit
in mesopic visual functions.

RECOMMENDATIONS:

A. Utilization of the nyktometer is an efficient method of testing
    mesopic visual performance. The data generated by the study,
    demonstrated a higher level of positive identification with the
    usage of contact lenses. However, before a true comparision of
    contacts and spectacles may be done. Further subjects data should
    be generated in order to make a qualified recommendation.

B. A sample population should be established which simulates the current and/or projected number of pilots. This would help in correlation, and making a valid prediction of the advantage of contacts versus spectacles.

REFERENCES

Brown, J.L., Critical Duration for Resolution of Acuity Targets. VISION RES. 1976, Vol. 16, pp. 309-315.

Hartmann C., Investigations of Mesopic Vision and Sensitivity to Glare By Means of the New Nyktometer. Klin Monutshl Augenheilkd. 198, Vol 176 (5), pp. 859-63.

Ikeda Mitsva, Mesopic Luminous-Efficiency Functions. J. Opt. Soc. Am. Vol 71, pp. 280.

Sagawa Ken., Spectral Luminous Efficiency Functions in the Mesopic Range. J. Opt. Soc. Am. A. Vol 3, pp. 71-75.

Yaguchi Hiroira., Mesopic Luminous Efficiency Functions For Various Adapting Levels. J. Opt Soc. Am. Vol 1, pp. 120-123.

1987 USAF-UES SUMMER FACULTY RESEARCH PROGRAM/

GRADUATE STUDENT SUMMER SUPPORT PROGRAM

Sponsored by the

AIR FORCE OFFICE OF SCIENTIFIC RESEARCH

Conducted by the

Universal Energy Systems, Inc.

FINAL REPORT

GROUND RUN-UP AFTERBURNER DETECTION

AND NOISE SUPPRESSION

Prepared by:	Jeffrey J. Girard
Academic Rank:	Ph.D. Graduate Student
Department and	Mechanical and Materials Engineering
University:	Washington State University, Pullman, WA
Research Location:	HQ AFESC/RDCS/RDCF
	Tyndall, AFB
	Panama City, FL 32404
USAF Researcher:	Lt. B. Bowen, and Cpt. T. Moorehouse
Date:	21 Aug 87
Contract No:	F49620-85-C-0013

GROUND RUN-UP AFTERBURNER DETECTION

AND NOISE SUPPRESSION

by

Jeffrey J. Girard

ABSTRACT

Two projects were completed, both related to aircraft static engine run-up noise. A purchase description was written for an acoustic detection system to determine whether an aircraft in a shelter has engaged afterburners. A test plan was written for a test to supply information required for evaluation of noise suppression techniques employed in hush houses for ground run-up.

Acknowledgements

I wish to thank the Air Force Systems Command and the Air Force
Office of Scientific Research for sponsorship of the research.
Universal Energy Systems must be mentioned for their concern and
help to me in all administrative and directional aspects of this
program.

My experience was rewarding and enriching because of many
different influences. Maj. Larry Bramlitt as effort focal point
overcame several obstacles in the administrative end at the base.
The guidance of Joseph Walker and Stan Strickland was
appreciated. The help of P. J. Gavankar, Cpt. Tom Moorehouse, and
Lt. Brit Bowen was invaluable. Dr. P. G. Vaidya provided a great
deal of advise toward the accomplishment of this work. I would,
also, like to thank Jack Hayes.

I. INTRODUCTION:

Noise is produced during the static testing of aircraft engines. This noise may be monitored in order to determine when the aircraft afterburners are engaged. Also, if run-up is conducted for routine maintenance at air bases, the impact of this noise upon the surrounding community must be minimized.

My research interests have been in the area of acoustics, primarily as it affects the stability of fluid flows. In previous summer work I participated in an investigation of acoustic levitation. This involved the manipulation of bubbles in a molten glass. I have been a student of Dr. P. G. Vaidya, for four years at Washington State University. I was brought to Tyndall as an assistant to Dr. Vaidya.

II. OBJECTIVES OF THE RESEARCH EFFORT:

Aircraft engine run-up may be conducted in Hush Houses or Hardened Aircraft Shelters (HAS). HAS are designed for protection of maintenance operations from attack. Hush Houses protect the surrounding community from the high levels of noise due to engine static tests. The Fire Protection System (FPS) in the shelters is designed to extinguish fires which are due to ignition of a large pool of fuel inside of the shelters. The flame which burns in jet exhaust when a jet is in afterburner mode may be interpreted as a fuel fire. One objective of my work was to devise an acoustic

method to determine when an aircraft in a shelter has engaged
afterburners. The other objective was to develop a test plan to
obtain information to be used in evaluation of improvements to
Hush House design.

III.

a. For both projects, the data compiled by Lee (1978), was
invaluable. This test report showed noise levels as a function of
angle, frequency, distance, for various aircraft at various power
settings with and without Hush House. For an aircraft,
afterburner setting is 5 to 10 dB louder than at full power.

The acoustic detection of afterburner would be quite simple if the
loudest jet at full power was quieter than the quietest jet in
afterburner mode. However, the F-111 is louder at full power than
the F-5 in afterburner. A simple threshold loudness level would
not suffice.

I decided to use rise time as the main criterion. The rise in
noise level during afterburner ignition is quite steep. Also, All
afterburner noise will be above a known high level. The detection
system will monitor the noise at a set frequency. If the level
rises fast enough to be afterburner ignition, and if the level is
high enough to be from afterburners then the detection system will
check to see if the new high level of noise is sustained. It is
expected that it will take three seconds of afterburner flame for

the FPS to alarm. So if the noise is detected to be afterburners
and if the noise is sustained, then a signal will be sent to the
FPS.

The noise suppression project required two reports. In one, the
current design was evaluated based upon existing liturature and
data. A report by Witten, et al (1987), described many pertinent
details. Also, suggestions for improvement were made in my
report. It was evident from acoustic data that the existing
design was sufficient for frequencies above 100 Hz. Lower
frequency levels were not effectively suppressed. This type of
noise affects body organs and buildings.

My suggested improvements were aimed at the low frequency content
of the noise. More mass should be added to the house walls. A
barrier may be placed to channel the escaping noise upward.
Active suppression may be applied at the air inlets and exhaust
opening.

The test plan was developed to obtain data required for evaluation
of these improvements. The noise which escapes the Hush House is
fairly uniformly distributed around the house. The noise will be
sampled at 250 ft. in 10 degree increments from front to back. In
addition, at 25 ft. and 2500 ft. the noise will be sampled only at
the 90 degree position. This is a total of 21 positions. This
data will be processed to show sound pressure spectra and
A-weighted spectra. The A-weighted levels show primarily the

effect of the noise upon human ears. Noise attenuates

logarithmically over distance. The three 90 degree positions

should show this sufficiently.

b. The reports supplied for each of the projects are currently

under review.

IV. RECOMMENDATIONS:

Tests will be required for the detection system. The rise time

due to afterburner ignition must be defined as well as expected

noise levels. Developmental tests will be needed for fine tuning.

The effects of low frequency noise upon humans and structures

should be more fully determined.

REFERENCES

Lee, R.A., Community Noise Exposure Resulting from Aircraft
Operations. AFAMRL AMD AFSC WPAFB, Ohio, AMRL-TR-73-110, Feb.
1978.

Witten, A., et al, Analysis of Impacts of Hush House Operations.
USAFLC, WPAFB, Ohio, Apr. 1987.

1987 USAF-UES SUMMER FACULTY RESEARCH PROGRAM/

GRADUATE STUDENT SUMMER SUPPORT PROGRAM

Sponsored by the

AIR FORCE OFFICE OF SCIENTIFIC RESEARCH

Conducted by the

Universal Energy Systems, Inc.

FINAL REPORT

ALTERATIONS OF SEGMENTAL VOLUME DURING

ORTHOSTATIC STRESS IN NONHUMAN PRIMATES

Prepared by:	Beverly Elaine Girten
Academic Rank:	Graduate Research Associate
Department and University:	Exercise Physiology/Physiological Chemistry, The Ohio State University
Research Location:	Armstrong Aerospace Medical Research Laboratory, BBD, Wright-Patterson Air Force Base, Dayton, Ohio
USAF Researcher:	Clarence M. Oloff
Date:	September 30, 1987
Contract No.:	F49620-85-C-0013

ALTERATIONS OF SEGMENTAL VOLUME DURING

ORTHOSTATIC STRESS IN NONHUMAN PRIMATES

by

Beverly Elaine Girten

ABSTRACT

The overall goal of this project was to investigate the effect of
exposure to short-term simulated weightlessness on the volume changes
that occur in young adult nonhuman primates. A series of experiments
involving head-up and head-down tilt protocols were conducted to test
the feasibility of using impedance plethysmographic equipment and
procedures to define segmental volume changes in Rhesus monkeys. The
specific objectives involved monitoring the calf, thigh, pelvic, ab-
dominal and thoracic volumes prior to, during, and following exposure
to short-term orthostatic and antiorthostatic stress. Initial work on
this project involved preliminary testing of the data recording sys-
tem. Four adult male Rhesus monkeys were tested during this phase,
and impedance plethysmography was utilized to determine segmental
volume changes. Ten animals were tested during the primary experi-
ment. The data obtained indicated that fluid exchange between the
peripheral and the more central body segments was taking place during
all angles of head-up or head-down, and the redistribution seems to be
graded and a function of the angle of tilt. These results suggest
that the peripheral arterial/venous system is able to compensate for
mild stresses produced by low angles of head-up and head-down tilt;
however, it is not able to maintain this compensation during or
following the higher angles of tilt.

ACKNOWLEDGEMENTS

I. INTRODUCTION

I am a doctoral student and Graduate Research Associate at The Ohio State University, and am working in the areas of exercise physiology and physiological chemistry. Most of my studies have centered on bioenergetics, sub-cellular enzyme studies, and cardiovascular function of a variety of organisms, including man.

This year's summer research program at the Armstrong Aerospace Medical Research Laboratory provided an opportunity to merge my interest in cardiovascular and aerospace physiology through participation in a collaborative project involving impedance plethysmography and orthostatic tolerance. This merger of interest and the overall experience gained through involvement in this project has provided me with a better understanding of fluid dynamics during orthostatic stress and has helped establish a basis for future investigation in this area.

The relationship of this investigation to weightlessness is based upon the concept that exposure to weightlessness physiologically unloads portions of an organism by greatly reducing the hydrostatic pressures normally produced by the Earth's gravitational forces. The fairly rapid headward shift of blood and other fluids that occurs in the early stages of space flight has been termed the cephalic fluid shift (CFS). Recently, some investigators have suggested that the CFS may be responsible, in part, for the

cardiovascular deconditioning and space motion sickness that
is brought about by the microgravity environment (6).
Specific changes that appear to be a direct result of the
CFS that could lead to the chronic effects above include
distension of central and cerebral veins, heart chambers and
the respiratory vascular bed. Major functional responses
that could result from these changes include alteration of
cardiac activity by increasing cardiac output and stroke
volume (1, 2), influence of reflex mechanisms that change
peripheral resistance and venous compliance (5), and changes
in the pattern of salt and water excretion that could lead
to hypovolemia and increased hematocrit (3, 4, 8). Another
factor which could influence cardiovascular deconditioning
and result from fluid distribution changes is alteration of
gas exchange in the lungs resulting from distension of the
pulmonary vascular bed that compresses the air-filled parts
of the lung (7).

In order to develop effective countermeasures that could
be used to prevent some of these consequences of exposure to
zero gravity, it is necessary to have a better understanding
of the fluid/volume changes that take place in the body
during weightlessness. A number of researchers have used
head-down bed rest to simulate effects of zero gravity
during ground-based cardiovascular investigations, while
others have used head-down and head-up tilt protocols. This

study used head-down tilt to induce orthostatic stress and head-up tilt to induce an anti-orthostatic stress.

II. OBJECTIVES OF THE RESEARCH EFFORT

The overall goal of this project was to investigate the effect of exposure to simulated weightlessness on the volume changes that occur in young adult nonhuman primates. A series of experiments involving head-up and head-down tilt protocols were conducted to test the feasibility of using impedance plethysmographic equipment and procedures to define segmental volume changes in Rhesus monkeys. The specific objectives were to monitor calf, thigh, pelvic, abdominal and thoracic volumes prior to, during, and following exposure to short-term orthostatic and anti-orthostatic stress.

These objectives have been accomplished and the methods and information resulting from these accomplishments are presented in the next two sections of this report. By meeting these objectives, the summer research effort has provided valuable information with regard to segmental hemo-dynamic response to simulated weightlessness.

III. METHODS AND PROCEDURES

The initial work on this project involved preliminary testing of the data recording system that was used to determine the segmental volume changes in nonhuman primates dur-ing orthostatic stress. Four adult male Rhesus (Macca

mulata) monkeys were utilized during the first phase of the preliminary test. Each animal was instrumented to obtain blood volume measurements in their calf, thigh, pelvic, abdominal and thoracic body segments by impedance plethysmography. Head-up (HUT) and head-down (HDT) tilt table tests were used to induce progressive orthostatic stress over a period of 35 minutes. The following position/time sequence was used for each of the HUT tests.

Position (deg./angle)	Elapsed Time (minutes)	Time in Position (minutes)
Flat	5	5
+5	10	5
Flat	15	5
+10	20	5
Flat	25	5
+20	30	5
Flat	35	5

The HDT test sequence used the same protocol except angles of -5 degrees, -10 degrees, and -20 degrees were used. During these and subsequent tests, the animals were placed on their backs and then rotated slightly to the right. The animals were anesthetized with an intramuscular injection of ketamine prior to instrumentation, and an intravenous infusion of ketamine was used throughout each test.

The preliminary test helped to identify procedural alterations needed for the primary experiment utilizing 10 Rhesus. Specific changes included: (1) monitoring vital signs and room temperature before, during, and after each

test; (2) a 30-minute stabilization period after administration of the anesthetic; and (3) use of an automated data acquisition system that allowed data to be collected more frequently.

Repeated measure analysis of variance tests were made to compare head-up and head-down tests for each body segment. A rejection criterion of $P < 0.05$ was used in these statistical tests; the Tukey's post hoc test was used in cases where significant differences were found.

IV. RESULTS AND CONCLUSIONS

Figures 1-18 illustrate the data obtained during the HUT and HDT tests and summarize the results of the statistical analysis of these tests. Figures 1-6 illustrate the HDT tests while Figures 7-12 illustrate the results obtained during the HUT sequence. These figures show the mean resistances calculated every 15 seconds for the calf, thigh, pelvic, abdominal, thoracic, and forearm segments respectively. The open squares in Figures 1-6 present the mean base resistances, across the ten animals, as functions of elapsed time (minutes) for each body segment. The solid line in these figures shows the digital filtered and smoothed trace that was obtained from the mean response data for each segment. Both the mean values and the corresponding filtered traces were obtained from the individual test sequence data after they were normalized to the resistance

Figure 1

HEAD DOWN TILT FLUID REDISTRIBUTION

CALF IMPEDANCE VS. TIME

□ CAZ MEANS — CAZ SMOOTH

● Significantly different (P <0.05) from F1(1) point
■ Significantly different (P <0.05) from end of previous flat period
▲ Significantly different (P <0.05) from end of previous tilt period
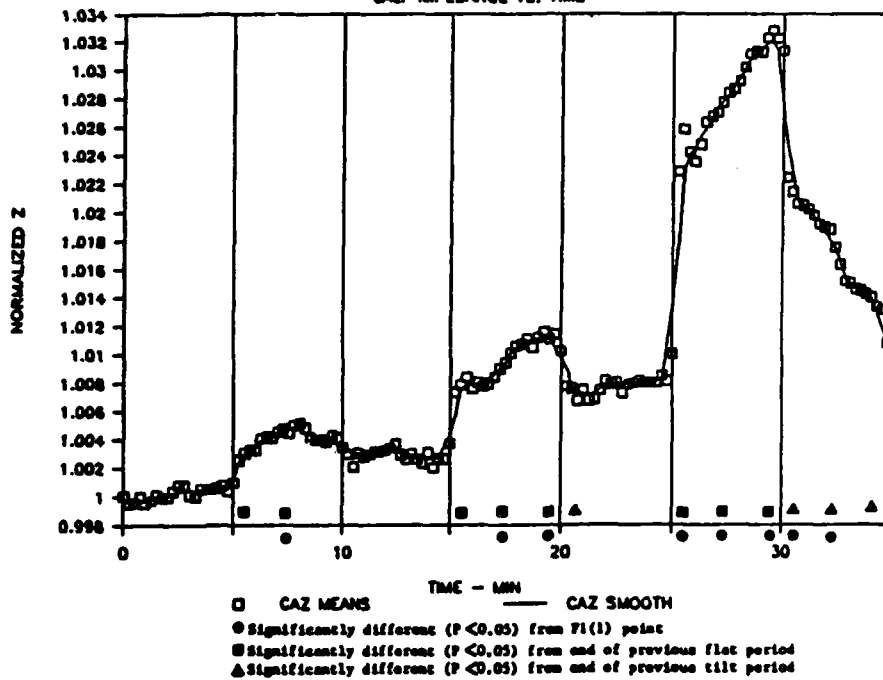
Figure 2

HEAD DOWN TILT FLUID REDISTRIBUTION

THI IMPEDANCE VS. TIME

□ THI MEANS — THI SMOOTH
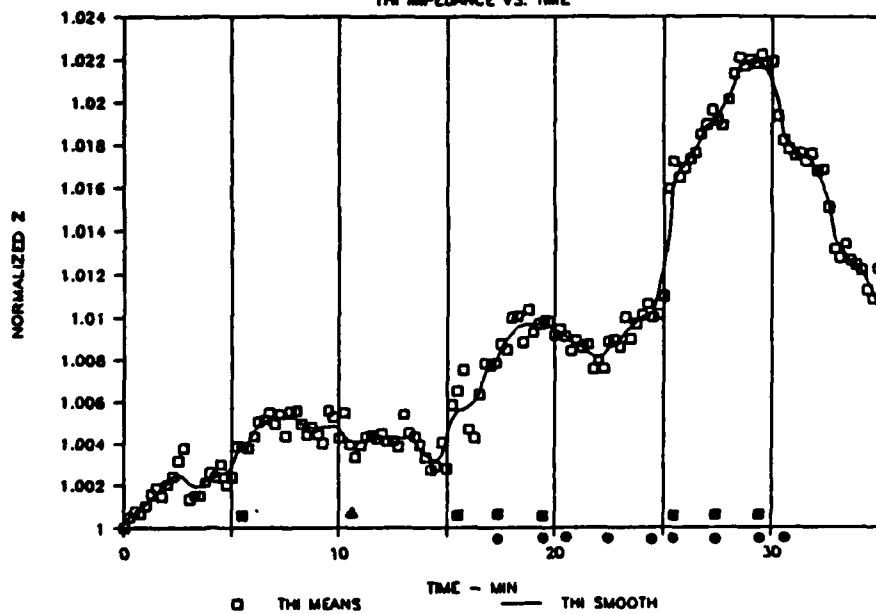
Figure 3

HEAD DOWN TILT FLUID REDISTRIBUTION

PELVIC IMPEDANCE VS. TIME

☐   PELZ MEANS   ——— PELZ SMOOTH
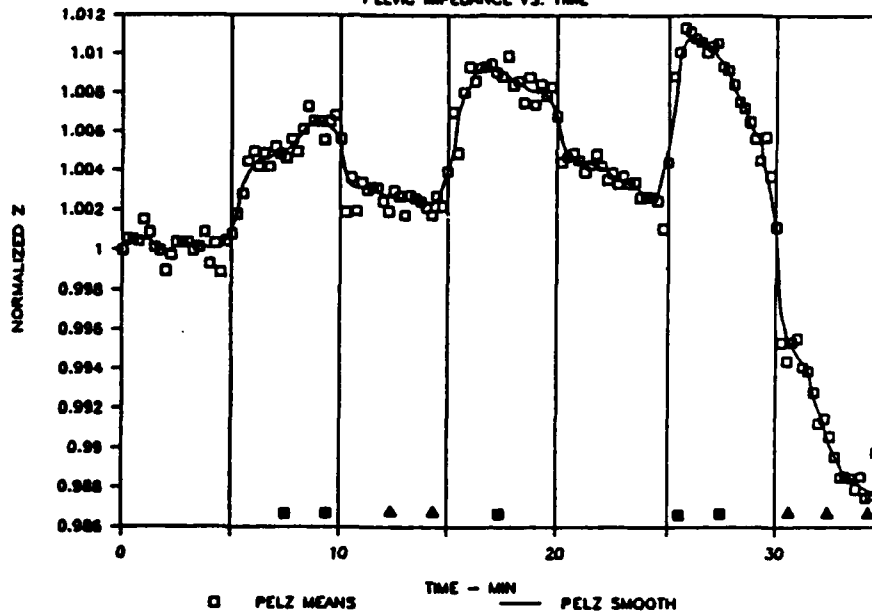
Figure 4

HEAD DOWN TILT FLUID REDISTRIBUTION

ABDOMINAL IMPEDANCE VS. TIME

☐   ABZ MEANS   ——— ABZ SMOOTH
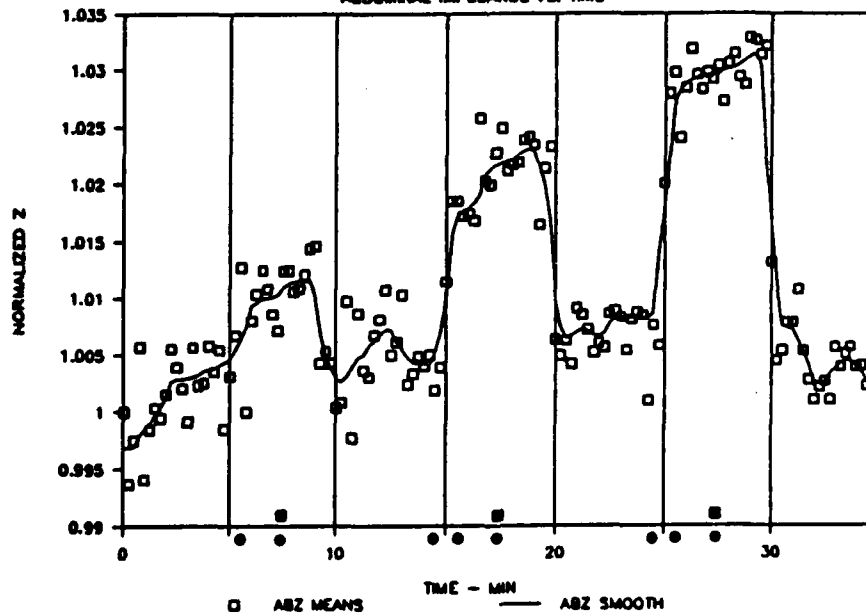
Figure 5

HEAD DOWN TILT FLUID REDISTRIBUTION

THORACIC IMPEDANCE VS. TIME

□   THOZ MEANS   ——   THORZ SMOOTH
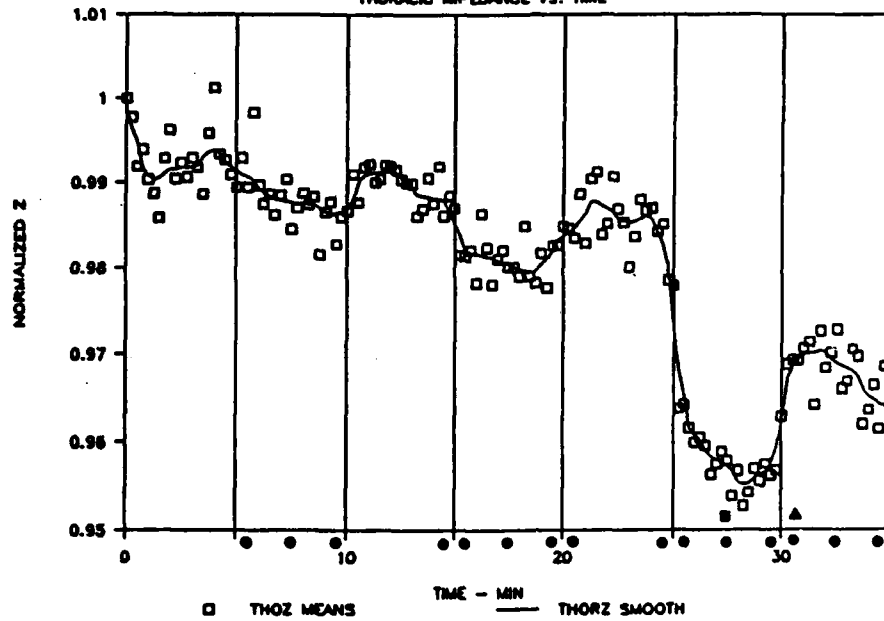
Figure 6

HEAD DOWN TILT FLUID REDISTRIBUTION

ARM IMPEDANCE VS. TIME

□   ARMZ MEANS   ——   ARMZ SMOOTH
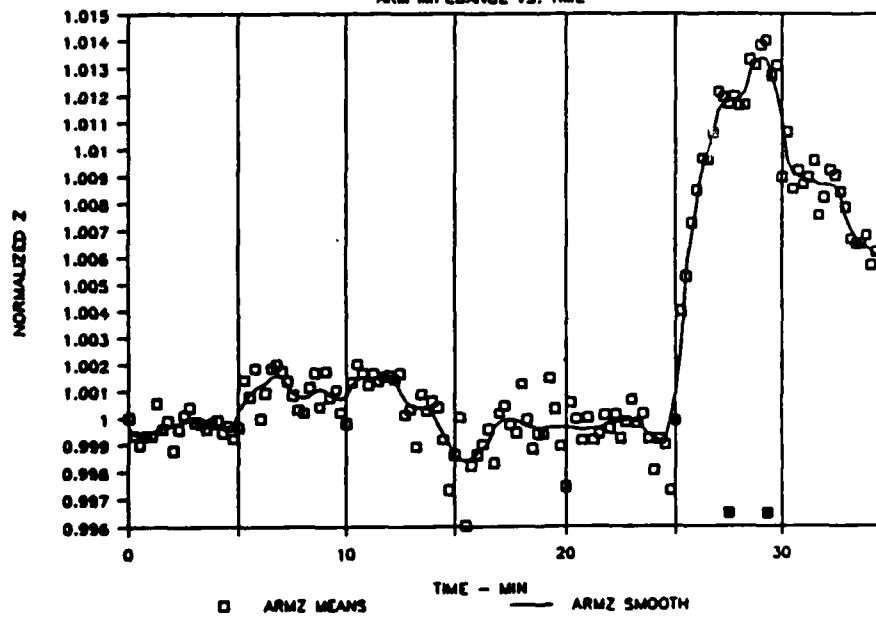
Figure 7

HEAD UP TILT FLUID REDISTRIBUTION
CALF IMPEDANCE VS. TIME
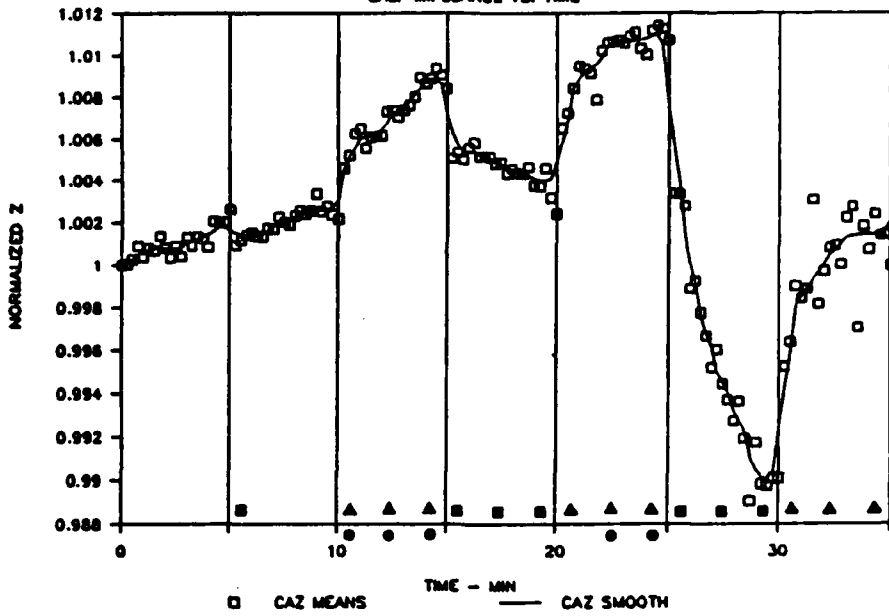
Figure 8

HEAD UP TILT FLUID REDISTRIBUTION
THI IMPEDANCE VS. TIME
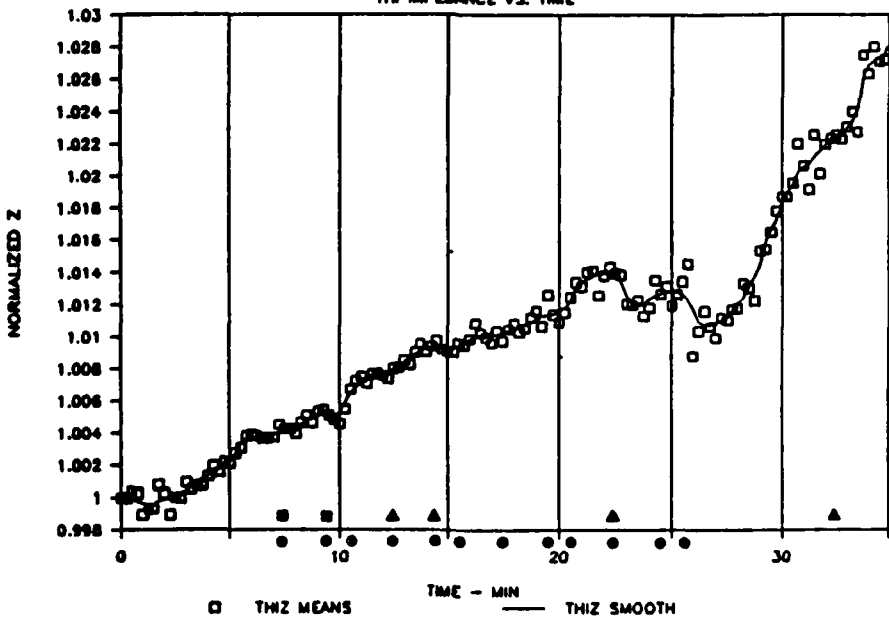
Figure 9
HEAD UP TILT FLUID REDISTRIBUTION
PELVIC IMPEDANCE VS. TIME
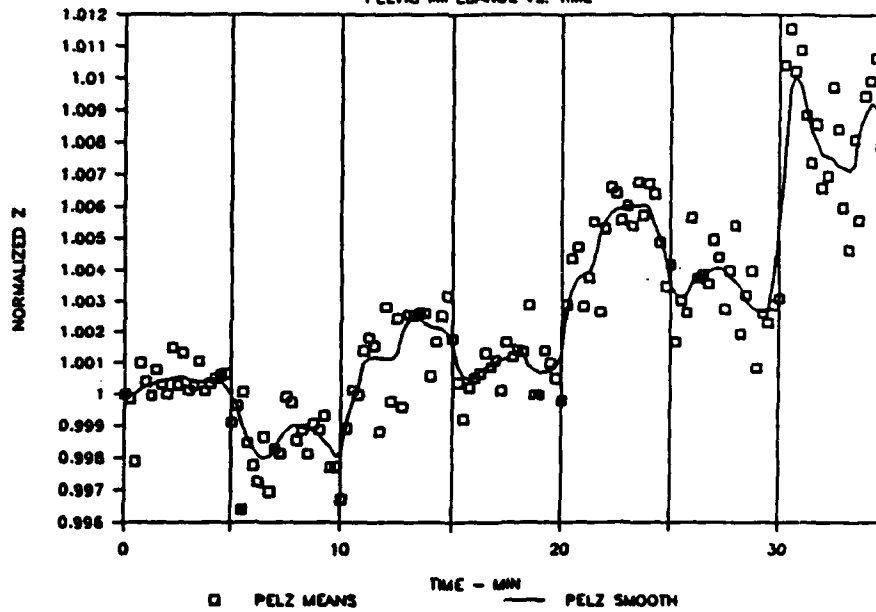
Figure 10
HEAD UP TILT FLUID REDISTRIBUTION
ABDOMINAL IMPEDANCE VS. TIME
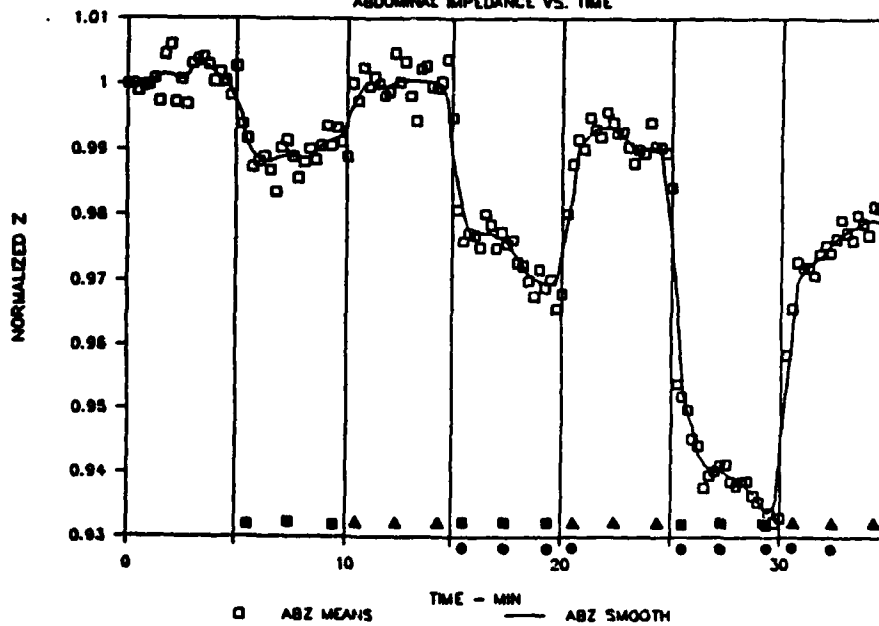
Figure 11

HEAD UP TILT FLUID REDISTRIBUTION

THORACIC IMPEDANCE VS. TIME

□ THOZ MEANS   TIME — MIN   —— THOZ SMOOTH
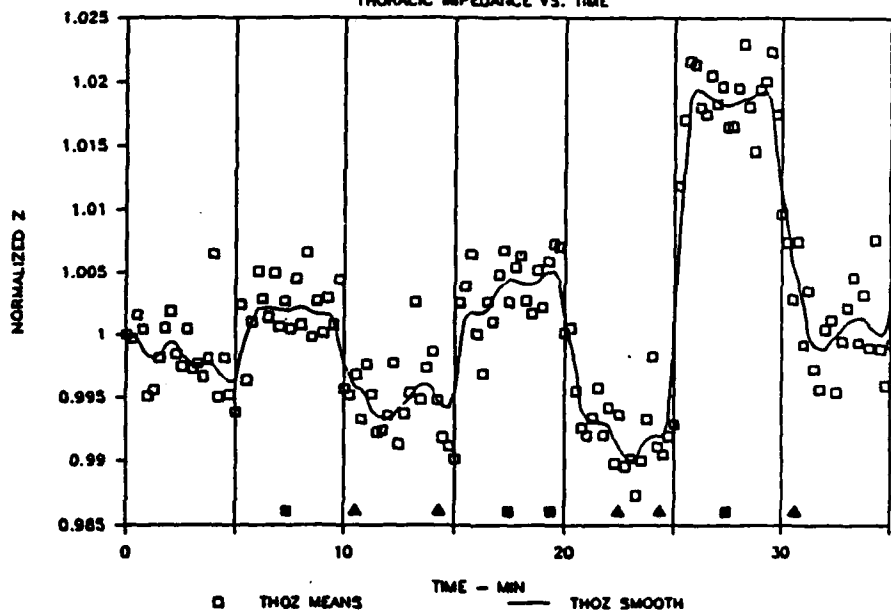
Figure 12

HEAD UP TILT FLUID REDISTRIBUTION

ARM IMPEDANCE VS. TIME

□ ARMZ MEANS   TIME — MIN   —— ARMZ SMOOTH
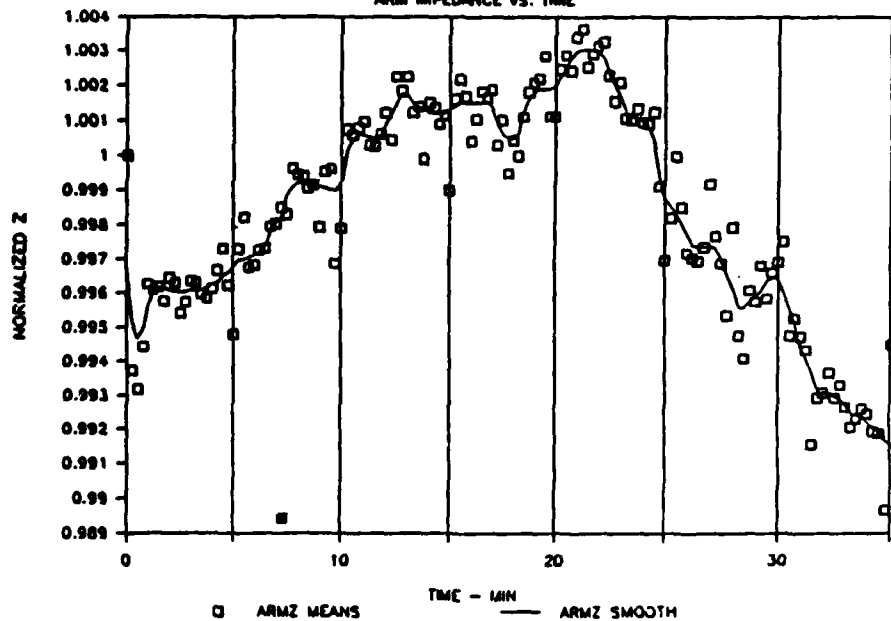
values at 0 elapsed time. An increase in sequential (norm-alized) impedance indicates a corresponding decrease in segmental volume.

Figures 13-18 give the mean resistance values for each body segment measured during both the HUT (open squares) and HDT (pluses) tests. These figures are presented to illus-trate the differential fluid redistribution effects of the head-up versus the head-down stress periods.

These data indicate a slight fluid redistribution in the arms and legs that continues throughout the first 15 to 20 minutes of the 35-minute test period as evidenced by the resistance baseline increases found in the calf, thigh, and arm segments. This fluid seems to have transferred to the central body segments as evidenced by the slight decrease in the abdominal and thoracic baseline resistances during the same time period. Very little fluid redistribution was found in the peripheral segments of the body during the 5 and 10 degree HUT and HDT periods as compared to the larger resistance changes that took place during the 20 degree tilt. Fluid exchange between the more central body segments was found to take place during all three angles of HUT or HDT. This redistribution seems to be graded and a function of the angle of tilt. The volume changes produced in the various body segments during the 5 and 10 degree tests were

Figure 13

HUT AND HDT FLUID REDISTRIBUTION

CALF SEGMENT

□ HEAD UP   + HEAD DOWN

▲ Significant (P <0.05) difference between HUT and HDT
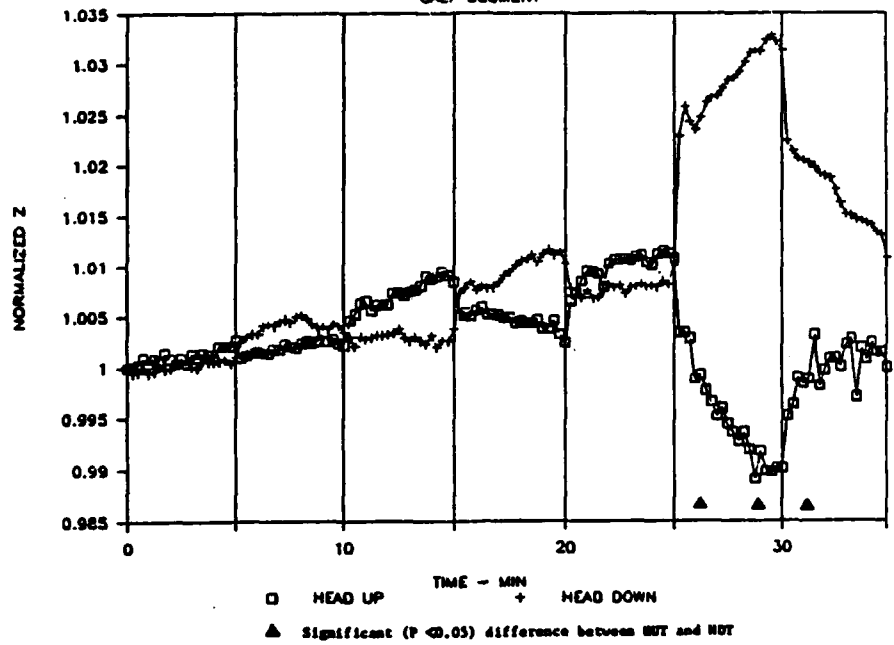
Figure 14

HUT AND HDT FLUID REDISTRIBUTION

THIGH SEGMENT

□ HEAD UP   + HEAD DOWN
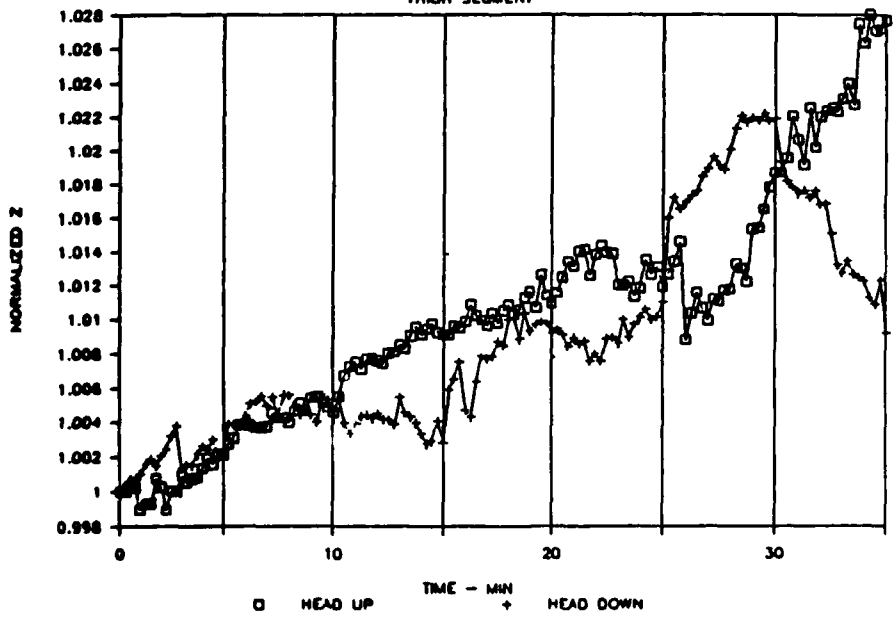
Figure 15

HUT AND HDT FLUID REDISTRIBUTION
PELVIC SEGMENT
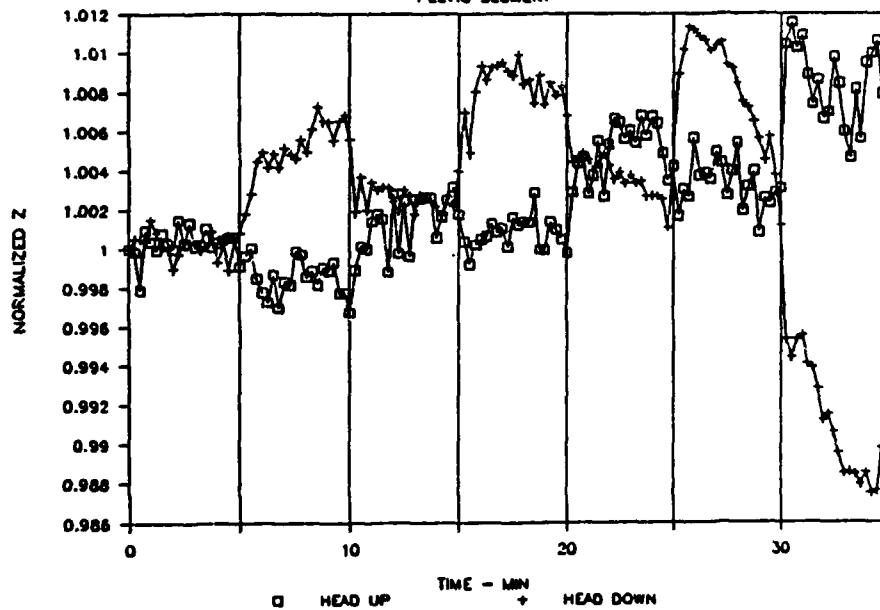
Figure 16

HUT AND HDT FLUID REDISTRIBUTION
ABDOMINAL SEGMENT

30-17
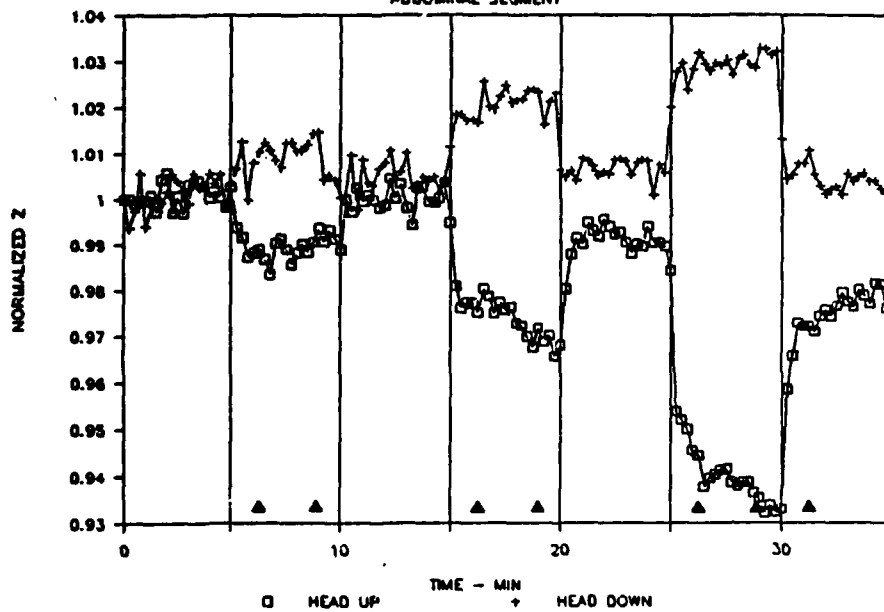
Figure 17

HUT AND HDT FLUID REDISTRIBUTION

THORACIC SEGMENT
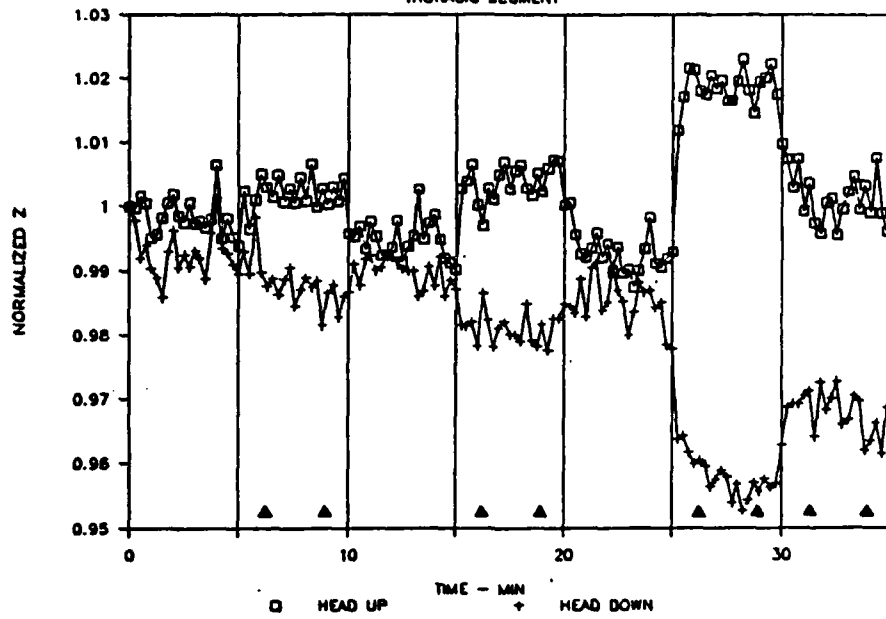
Figure 18

HUT AND HDT FLUID REDISTRIBUTION

ARM SEGMENT

30-18
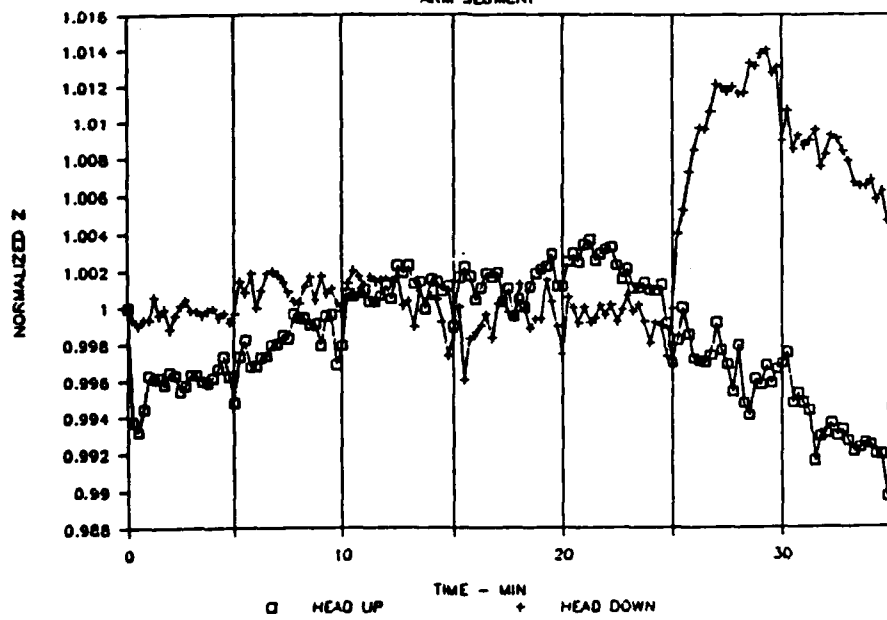
generally reversed during the subsequent flat periods. This change was not found during the 20 degree tilt tests.

V. RECOMMENDATIONS

These experiments suggest that the peripheral arterial/venous system is able to compensate for the mild stresses produced by the lower angles of HUT and HDT, but this system did not appear able to maintain this compensation during or following the higher angles of tilt. The concept of fluid volume compensation has been incorporated into many past human orthostatic tests, such as lower body negative pressure tests made at low negative pressures prior to higher exposures during the Skylab experiments. Procedures developed during this summer's experiments may provide a method for comparing the compensatory mechanisms used by various primates during orthostatic stress.

Follow-on research should investigate longer time periods of orthostatic stress in a variety of primates. Investigations of this type could be done in conjunction with short and long term hypokinesis studies to provide details concerning mechanisms of actions involved in changes in weightless environments and possibly to help in the formulation of effective countermeasures.

REFERENCES

1. Blomqvist, C.G., "Cardiovascular Adaptation to Weight-lessness," S.A.E. Technical Paper Series No. 820830, presented at the Twelfth Intersociety Conference on Environmental Systems, San Diego, 19-21 July 1982.

2. Hoffler, C.W. and R.L. Johnson, "Apollo Flight Crew Cardiovascular Evaluation," Biomedical Results of Apollo (eds. R.L. Johnson, L.F. Dietlein, and C.A. Berry), NASA, Washington, D.C., pp. 227-264, 1975.

3. Johnson, P.C., "Fluid Volume Changes Induced by Space Flight," Acta Astronautica, 6:32-37, 1979.

4. Leach, C.S. and W.C. Alexander, "Endocrine, Electrolyte and Fluid Volume Changes Associated with Apollo Mis-sions," Biomedical Results of Apollo (ed. R.L. Johnson, L.F. Dietlein, and C.A. Berry), NASA, Washington, D.C., pp. 163-184, 1975.

5. Levy, M.N. and J.M. Talbot, "Cardiovascular Deconditioning of Space Flight," The Physiologist, 26:5:297-303, 1983.

6. Matsnev, E.I., et al., "Space Motion Sickness: Phenomenology, Countermeasures and Mechanisms," Aviat., Space, Environ. Med., 54:4:312-317, 1983.

7. Michels, D.B. and J.B. West, "Distribution of Pulmonary Ventilation and Perfusion During Short Periods of Weightlessness," J. Appl. Physics, 45:987-998, 1978.

8. Pace, N., "Weightlessness: A Matter of Gravity," N. Engl. J. Med., 297:32-37, 1977.

1987 USAF-UES SUMMER FACULTY RESEARCH PROGRAM/

GRADUATE STUDENT SUMMER SUPPORT PROGRAM

Sponsored by the

AIR FORCE OF SCIENTIFIC RESEARCH

Conducted by the

Universal Energy Systems, Inc.

FINAL REPORT

Designing Simulator Tasks to Study the

High Speed, Low Altitude Environment

Prepared by:	Laura Giusti
Academic Rank:	Graduate Student
Department and	Department of Psychology
University:	San Diego State University
Research Location:	Armstrong Aerospace Medical Research Laboratory
	Human Engineering Division
	Wright-Patterson Air Force Base, Ohio 45433-6573
USAF Researcher:	Dr Rik Warren
Date:	August 5, 1987
Contract No.:	F49620-85-C-0013

Designing Simulator Tasks to Study the

High Speed, Low Altitude Environment

by

Laura Giusti

ABSTRACT

An experiment was designed as an instrument to measure the
effectiveness of proposed experimental training regimes and display
designs. A computer simulation of a terrain-following, terrain-avoidance
task was used to determine the subjects' capabilities in the high-speed,
low altitude flying environment. Subjects controlled only the pitch and
altitude of their aircraft and were instructed to successfully maneuver
over and between twenty equidistant buildings. Preliminary results
suggest that the task will be an effective measure for evaluating training
regimes and display designs.

Acknowledgments

I would like to thank the Air Force Systems Command, the Air Force Office of Scientific Research, and the Armstrong Aerospace Medical Research Laboratory for providing me the opportunity of participating in this research. I also wish to thank my supervisor, Dr Rik Warren for his assistance and enthusiasm during this ten-week program.

I consider my summer research to have been an invaluable experience I will appreciate for many years, thanks to the support and encouragement of too many to include here. However, I would like to express my special gratitude to Ligia Ramirez, Kim Reardon, Jeff Wood, and especially to Celia Oliver for her seemingly endless source of knowledge, support and faith in my abilities.

I. INTRODUCTION

Accurate perception and performance during low altitude flight are vital skills which need to be thoroughly researched in order to increase effectiveness and safety.

In the Human Engineering Division of the Armstrong Aerospace Medical Research Laboratory (AAMRL) at Wright-Patterson Air Force Base, the Perception and Control of Low-Altitude Flight (PACLAF) program uses flight simulators to study perception and performance during low altitude flight. In a series of ongoing experiments, the PACLAF program is identifying relevant visual information used by pilots, and taking various measures of performance during low-altitude flight simulation tasks. Within this series of experiments, research designs are being developed to incorporate the collection of physiological data during low-altitude flight tasks.

My undergraduate work in physiological psychology at Miami University consisted primarily of recording and analyzing electrophysiological data from animals. In these studies, depth electrodes were surgically implanted in specific brain regions and soldered to a connector for subsequent data collection. Slow-wave brain activity (EEG) and high-frequency brain activity (unit activity) were recorded during simple learning tasks. Standard electrophysiological techniques were used for off-line data analyses. Specifically, fast Fourier transform procedures and zero-crossing analysis were applied to the EEG data while peristimulus time histograms and standard scores were produced to characterize the unit activity data.

One of my objectives in research has been to use these standard electrophysiological techniques in human EEG recordings. Further, I have wanted to expand my research knowledge to more applied issues.

Because of my lack of experience with flight simulators, however, it was necessary to introduce me to the field with an existing study. Ultimately, from my physiological research experience at Miami and my recent exposure and participation in the current simulator study, I was able to assist in the research and design of the proposed physiological study.

II. OBJECTIVES OF RESEARCH

Flight simulation research was designed to investigate the human-machine interaction which determines the effectiveness and safety of a given task. The PACLAF program specifically designs simulator tasks for studying human performance in the high-risk environment of low-altitude, high-speed flight.

When operating in the low-altitude environment, terrain clearance is the dominant task to which all others become secondary (Miller, 1984). Therefore, the critical tasks within the environment which demand the full attention and capability of the pilot are the terrain-following, terrain-avoidance maneuvers.

The current study in the PACLAF program involves a task in which the subjects were instructed to fly over and between twenty buildings (the Building Jump task). This task is consistent with terrain-following terrain-avoidance maneuvers and is instrumental as a tool to investigate performance skills during high-speed, low-altitude flight.

After my general introduction to flight simulation, and the current series of studies in the PACLAF program, my objectives were as follows:

1.   To participate in the ongoing Building Jump experiment designed to create a tool with which to measure proposed experimental training regimes and display designs.

2.   To aid in the collection and storage of data from the experiment.

3.   To perform statistical analyses on the data, and

4.   To begin design of a similar study incorporating physiological measures.

III. THE BUILDING JUMP EXPERIMENT

A.   INTRODUCTION

The Building Jump experiment, along with other experiments in the PACLAF program, was designed to investigate the most effective manner in which to study high-speed, low-altitude flight on computer simulators.   In order to be effective, the simulated task must require active control by the observer (Warren & McMillan, 1984) and identify the task parameters which will influence the degree of task difficulty.

1.   Active Control. Traditional passive control, or passive psychophysics, does not permit the observer to respond to the display in a manner which will affect it. Active psychophysics, in contrast, requires observer control to change the dynamics of the display. Active control can be accomplished by the use of a force-stick for pitch and altitude control, a throttle for thrust control, or rudder pedals for roll control. Observer

input on these controls will cause a change in the display and thus require constant monitoring and updating of input by the observer.

2. Task Parameters. The quality of performance can also be affected by the level of difficulty of the task parameters. Variations in displays, and therefore variations in cues presented to the observer, have dramatic effects upon flight performance. The task parameters which influence the degree of difficulty of the task, such as number and kind of visual cues and their relationship within the moving simulation, must be identified to determine their effect on performance.

By identifying and understanding the task parameter's influence on performance, and including some kind of observer control, the simulation becomes a sensitive measure of the difficulties inherent in high-speed, low-altitude maneuvers, and an effective tool for future studies.

Following these guidelines, the PACLAF program created the Building Jump task which was designed specifically as a measuring device to determine the effectiveness of proposed experimental training regimes and display designs. By the observer's control of pitch and altitude over and between the twenty buildings and the use of a simplistic, unobtrusive display, the Building Jump appears to be an effective, sensitive tool as a baseline of performance. Although the task has a high face validity, it is still necessary, however, to experimentally refine and evaluate the usefulness of the proposed Building Jump task.

B. APPARATUS AND DISPLAYS

The "Building Jump" simulation of F-16 dynamics was generated by a PDP-11 computer and displayed by ann IRIS 3020 graphics computer which projected the moving display onto a 2.4 meter by 1.8 meter rear-projection screen in the Visual Bay. The display consisted of a straight, black, perspective view of a roadway extending from the bottom of the display to the end of the green grass and the beginning of the blue sky and twenty equidistant, light-grey, block buildings in the center of the roadway. The perspective algorithm produced nonlinear changes in display such that for a 50-ft. wide roadway, a 10-ft. drop in altitude (from 20 to 10 ft.) produced a 35' increase in roadway angle, whereas a 10-ft. drop in altitude (from 220 ft. to 210 ft.) produced only a 2' increase in roadway angle. Therefore, dramatic changes occurred in the display at exceptionally low altitudes and produced a "ground rush" experience that contributed to increased control difficulty.

C. SUBJECTS

Ten paid subjects (7 women and 3 men) of average or corrected vision participated. None were pilots.

D. PROCEDURES

The subjects viewed the display from an aircraft seat 1.2 meters from the center of the screen. They manipulated their aircraft's pitch and altitude by a force stick connected to the right side of the seat, and were instructed to direct their aircraft above and between each building. As

the aircraft approached each building, at the controlled 100 mph, the subject would direct his aircraft above the top of the building, pass over it, then descend to a designated 50-ft. altitude. When the craft descended below the 50-ft. mark, the approaching building would turn dark grey, indicating the fulfillment of the low-altitude requirement and signaling his freedom to ascend to the top of the next building. The building would return to its original grey color when the craft was once again above the 50-ft. threshold. A successful completion of the task required that the subjects avoid crashing into the ground or the buildings, and that he descend below a 50-ft. threshold between each building. If the subject completed the task without a mistake, a score of 100 would be displayed on the screen along with an error count of 0. If, however, a subject made one or more of the three types of errors, the number of errors made would appear on the display along with the score calculated as the percentage of the trial completed prior to the first error.

E. EXPERIMENTAL DESIGN

There were five conditions which varied by the distance between each successive building. Although within each trial or condition the distances between buildings were constant, between each trial the distances varied from 700 to 1500-ft. in five increments of 200 ft. each.

After a practice flight to introduce the subject to the dynamics of the F-16 simulator, the subjects flew the five randomly-ordered conditions, rested for ten minutes outside the Visual Bay, then returned for the second randomly-ordered set of the same five conditions. Thus,

each subject, after four days of trails, was exposed to each condition eight times, in eight randomly-ordered pairings for a total of forty trials.

F.   DATA COLLECTION, STORAGE AND ANALYSIS

Data was collected on the IRIS and PDP-11 computers and reviewed in the two following forms:

1)   A graphic depiction of the time-history flight path was created by the IRIS illustrating the line of buildings and the subject's flight path above and between each building. These graphic paths were then transformed into data points by plotting their wave length (Tau) and amplitude (delta) coordinates.

2)   The PDP recorded the overall mean altitude and standard deviation for each trial.

The data was stored temporarily on RK05 disks, then transferred to RK07 disks for long term storage, and finally onto separate tapes for each subject's individual trials.

To determine the baseline of performance for the Building Jump experiment, the Delta-Tau coordinates are averaged across each condition and all subjects. The means for each condition determine the expected performance and become the tool which which to measure the effectiveness of the proposed training regime or display design.

F.   RECOMMENDATIONS FOR THE BUILDING JUMP TASK

In continuation of the Building Jump experiment, I would
recommend shorter inter-building distances in order to create a more
difficult, and for some, an impossible task. At present, subjects are able
to complete all tasks with few or no mistakes, therefore, their data
demonstrates very little variability other than the graphically depicted
flight path.

IV. GENERAL RECOMMENDATIONS

For future studies of the PACLAF program, I would recommend taking
standard physiological measures from subjects during experiments in which
workload variations were being tested. Taking physiological measurements,
such as heart rate, eyeblinking rate, and EEG will give the experimenter
another measurement of workload difficulty and, therefore, increase
predictability of performance.

REFERENCES

Miller, Capt M.M. "Low Altitude Training: How Low Can You Go?" Proceedings
   of the Image III Conference, Phoenix, Arizona, 1984.

Warren, R., and Riccio, G.E. "Visual Cue Dominance Hierarchies:
   Implications for Simulator Design," SAE Special Publication SP-634,
   Flight Simulation/Simulators, 1985.

Warren, R. and McMillan, G.R. "Event Perception Needs an Active Psycho-
   physics: An Altitude Control Example," Proceedings of the
   Image III Conference, Phoenix, Arizona. 1984.
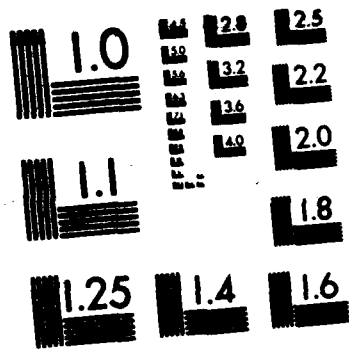
MICROCOPY RESOLUTION TEST CHART

NATIONAL BUREAU OF STANDARDS-1963 A

1987 UASF-UES SUMMER FACULTY RESEARCH PROGRAM/

GRADUATE STUDENT SUMMER SUPPORRT PROGRAM

Sponsored by the

AIR OFFICE OF SCIENTIFIC RESRARCH

Conducted by the

Universal Energy Systems, Inc.

FINAL REPORT

A COMPARATIVE STUDY OF THE THORACO-LUMBÁR TRANSITION VERTEBRAE IN

MACACA mulatta AND PAPIO anubis.

Prepared by: Nadia C. Greenidge

Academic Rank: Graduate Student/ Research Assistant

Department and   New York University, Dept. of Anthropology;
 University: New York University Hospital for Joint
                    Diseases, Dept. of Bioengineering

Research Location: Armstrong   Aerospace   Medical   Research
                    Laboratory, Biomechanics Effects Branch
                    Wright-Patterson AFB, Ohio

USAF Researcher: Dr. Leon Kazarian

Date: 3 Sept 87

Contract No: F49620-85-C-0013

A COMPARATIVE STUDY OF THE THORACO-LUMBAR TRANSITION VERTEBRAE IN MACACA mulatta AND PAPIO anubis.

by

Nadia C. Greenidge

ABSTRACT

The morphological characteristics of the thoraco-lumbar transition vertebrae of Macaca mulatta and Papio anubis were surveyed with the aid of a computer assisted digitizer. Linear and angular measurements of five representatives from each species were compared for both intra- and interspecies variations and differences. In addition to comparing the thoraco-lumbar vertebrae to each other they were also compared to representative thoracic and lumbar units in an effort to clearly define the amount of variation between the different vertebral levels. The rhesus monkey and the baboon exhibit a fracture locus, in respect to ejection impact injury, that is similar to that found in man. The continued use of these animals as models for human impact injury requires a close and detailed database on their specific morphologies and variations.

ACKNOWLEDGEMENTS

I wish to thank the Air Force Systems Command and the Air Force Office of Scientific Research for sponsorship of this research. Universal Energy Systems must be mentioned for their concern and help to me in the administrative aspects of this program.

I wish to most sincerely thank all of the staff and technicians at Technical Photo especially, Bobby Lucas and Jim Keller. I also extend my thanks to AAMRL-BBD staff members Ed Eveland, Suzanne Smith, Clarence Oloff and Marvin Sauder. Dr. Leon Kazarian I must give my extreme praise for allowing me to return to his laboratory for a second Summer and for his most valuable encouragement and knowledge throughout this entire project.

INTRODUCTION: Emergency egress from high performance air craft often results in severe trauma to the vertebral column. Vertebral fractures, dislocations and back pain associated with many successful (nonfatal) ejections often require lengthy recovery periods and pilot removal from flight status (2).

The Biodynamics Effects Branch of the Armstrong Aerospace Medical Research Laboratory, Wright-Patterson Air Force Base is particularly concerned with the pathological and design problems associated with air crew ejections. Special attention has been given to the development and validation of nonhuman primate models, especially Macaca mulatta and Papio anubis, for use in experimental investigations of air crew injuries (1,4,6,7). An intensive comparative osteometric study of the vertebral levels most commonly affected in ejection exposure would provide useful database information for the continued evaluation, experimentation, and modeling of impact related air crew injuries.

My research interests have been in the areas of basic and clinical orthopaedic research. Many of my previous studies have encompassed such broad topics as the biomechanical factors which influence low-back pain in industrial workers and the use of electrical stimulation as an alternative to exercise in the rehabilitation of chronic back pain and post surgery patients. My diverse background in physical anthropology, comparative anatomy, biomechanics, and my current research in comparative primate morphology and three-dimensional kinematics of the spine

AAMRL-BBD to investigate the morphology of the thoraco-lumbar transition vertebrae in the rhesus and baboon.

OBJECTIVES OF RESEARCH EFFORT: The highest incidence of vertebral fractures , resulting from acceleration/impact forces, occurs in the thoraco-lumbar transistion area of the vertebral column (5,6,8). Even with the use of nonhuman primates as models for ejection seat and crash injuries the locus of vertebral injury remains relatively unchanged (4,6). This fact appears to indicate that there is a 'primate' pattern for vertebral response to seated impact forces. The literature contains several references addressing both comparative (mainly humans versus apes and injury dynamics) and human (for surgical applications) vertebral formulas indicating variations of the total number of vertebrae at various cord levels and the level of the thoraco-lumbar transition, and the over-all gross and anthropometric vertebral morphology (10,11,12,14). A detailed comparative description of the thoraco-lumbar transition vertebrae in Old World monkeys has not been clearly presented. This study will both qualitatively and quantitatively compare the thoraco-lumbar transition vertebrae in two species of Old World monkey in an effort to better understand the anatomical features which influence the 'primate' injury pattern to vertical impact.

METHODS: A general morphological description of a representative thoracic and lumbar vertebrae was initially performed and the corresponding features were grossly compared to

the thoraco-lumbar transition vertebrae. Linear and angular measurements were performed on 5 rhesus (3 vertebrae each, n=15) and 5 baboons (n=15) (refer to appendix 1 and 2). The primary vertebrae of investigation was the thoraco-lumbar transition vertebrae, defined via the orientation of the posterior facets. Twenty-five independent linear (or distance) measurements were taken to obtain a three-dimensional quantitative description of the vertebrae. These measurements provide the information necessary to investigate both the intra- and interspecies variations related to size, specifically allometric (scaling factor) variation and sexual dimorphism (which is not traditionally analyzed in terms of allometric scaling factors). This investigation also includes an estimation of the biomechanical/kinematic characteristics of the thoraco-lumbar transition and associated vertebrae. Eight independent angular measurements (4 x-axis, 4 y-axis) were taken on both the superior and inferior articular facets of each of the aforementioned thoraco-lumbar transition vertebrae. These data will be used to address the thoraco-lumbar transition vertebrae kinematics in terms of potential motion and in reference to impact injury production. The extent or range-of-motion of vertebral motion segments can be estimated from ligamentous/osseous specimens but this investigation will be limited to addressing the characteristic type of vertebral motion in the transition vertebrae and not its specific quantitative range. However, a comparative study of the three-dimensional kinematic characteristics of the thoraco-lumbar vertebrae in primates is essential to our continued understanding and

32-6

evaluation of ejection seat injuries and experimentation. The type of motion characteristic in the human thoracic (rotation) and lumbar (flexion-extension) vertebrae have been well documented in respect to descriptive morphology and quantitative angular measurements (involving the mean values for human measurement norms but often not specifically addressing intraspecific variations) (4,12). Kazarian et al.(4,5,6,7) have described the gross anatomy, injury kinematics and pathologies of both human and nonhuman primate ejections , but a detailed comparative survey of the normal skeletal morphology and intraspecies variation of the thoraco-lumbar transision vertebrae in the primates most commonly used as experimental models has not been described in detail. In an effort to provide more specific intraspecific information on the thoracicization and lumbarization of the superior and inferior (respectively) articular facets of the thoraco-lumbar transition vertebrae, in these primates, four additional angular measurements were taken (2 x-axis, 2 y-axis). The representative thoracic (T8) and lumbar (L2) vertebrae's superior and inferior facet angles (respectively) were measured and later compared to their counterparts on the thoraco-lumbar transition vertebrae.

RESULTS/GROSS ANATOMICAL DESCRIPTION: The vertebral column in all mammals serves as the attachment site for the muscles which support the trunk and as protection for the spinal cord. In quadrupedal primates the vertebral column is commonly loaded in the two following orientations: 1) locomotor quadrupedal loading where the vertebrae is suspended horizontally between the head

and pelvis like a beam which supports the internal organs and ribs that hang underneath like a sack, and 2) postural loading which primarily consists of vertical upright postures associated with feeding behaviors in which the vertebrae are axially loaded much as they are in humans except lacking the lardotic curvature.

The thoraco-lumbar transition vertebrae of the rhesus and baboon are reported in the literature (4,6) as being located in the T_9 to T_{10} vertebral levels. This trend held true for all of the rhesus observed and for the smaller, presummably female, baboon specimens. The larger male baboons displayed a thoraco-lumbar transition area in the T_{12} level. Sexual dimorphism is well documented in all species of baboons, but an attempt to determine whether size factors or differential postural behaviors influence the level of the thoraco-lumbar transition vertebrae would require observations of a significantly larger sample size and precise locomotor versus postural data on both an intra- and interspecies level.

The typical thoracic vertebrae are intermediate in size between the cervical and lumbar vertebrae with a basic morphology quite similar to that described for humans in Grey's Anatomy (there are major differences between the vertebral skeletal morphology of human and non-human primates but this is beyond the scope of this report which contains only comparative information between the rhesus and baboon). In a gross observation of these vertebrae they appear to be very similar in the two species of non-human primates. The major superficial differences are in the appearance of the vertebral centrum and the spinous processes.

The vertebral centrum of the rhesus monkey is much less robust with a greater superior-inferior than anterior-posterior length, as is common in baboons. The spinous processes in both species are long and slender but with a more caudal angulation in the rhesus.

The most striking difference between the lumbar vertebrae of the rhesus and the baboon is the length of the lumbar accessory process (human lumbar vertebrae do not have this process). The accessory process in the rhesus is quite robust and extends well below the inferior border of the inferior articular facet. Approximately one-third of the overall length of the accessory process in the rhesus is below the inferior facet. In the baboon while the process appears to also be quite robust (overall diameter) the length is much reduced to approximately two-thirds of the length of the inferior articular facet. The lumbar accessory porcesses preform several importent functions: 1) increase the strength characteristics of the vertebral units, 2) interlocking mechanism between adjacent vertebrea which prevents rotation and decreases the chance of angular displacement 3) increases the stability of the vertebrea and decreases the probability of injury at that level, 4) added surface area during acceleration, and 5) assures uniform loading of the vertebral centrum (Kazarian, personal communication).

The transition vertebrae for both species approach the lumbar in size and form. The superior articular processes appear thoracic-like in their morphology. They are flat with a nearly vertical orientation (acute angle relative to the plane of the x-axis), directed backwards and slightly inwards (relative to

the plane of the y-axis) and upward. The inferior articular processes approximate a lumbar -like morphology being convex and turned outward. The inferior thoraco-lumbnar transition vertebrae does not possess an accessory process in either species.

RESULTS/ LINEAR MEASUREMENTS: Statistical analysis was performed on the 25 linear measurements the Videoplan Student's T-Test package. Both intraspecies (variation between the means of measurements within the same species investigating differences related to the orientation or the side from which the measurements were taken) and interspecies differences were investigated (P=.05).

Intraspecies pooled data: in this analysis all of the variables for each orientation were pooled together or considered as a single data set. The orientation comparisons were performed on the pooled data sets of measurenments from opposing sides/orientations of the same plane. No significant differences between the subjects within the rhesus group was observed. The baboon specimens also showed no significant differences in relation to orientation comparisons except in the lengths of the transverse processes. The analysis of the linear data pooled according to measurement orientation exhibited no overall significant differences within like species in either the rhesus or the baboon specimens.

Interspecies pooled data: in this analysis the same orientation pooling of data was performed as in the previous presentation The interspecific measurement comparisons investigated the differences of the same measurement between the two different species. All of the values (means) tested showed a significant difference between rhesus and baboons in respect to size related measurements.

Interspecies individual measurements: in an effort to rule out the possibility of a masking effect over-shadowing measurement variation (or the lack there of) in the individual measurements, which comprise the pooled data sets, the individual variables were compared between species. The individually analyzed linear measurements agreed with the pooled analysis in showing statistically significant differences in all of the compared measurements between the two species.

Basis statistics (means and S.D.): the Student's T-Tests showed the variation between the means of the same measurements taken in directly opposing orientation within the same species exhibited no major statistically significant differences, and the same measurements compared in different species were significantly different. The basic statistics tests showed very little variance within the rhesus measurements, conversely the baboons showed a high level of variation for the majority of linear .pa measurements taken. This variability was directly evident by consistantly high standard deviations which at times approached 50% of the mean value.

RESULTS/ANGULAR MEASUREMENTS: Two different types of analyses were performed on the angular measurements (using the aforementioned Student's T-Test statistical package). First, the x-axis and y-axis transition vertebrae were compared for intraspecies side differences and then an interspecies analysis was performed for each axis. Secondly, intraspecies comparisons were done between the superior and inferior articular facet angular measurements and their counterparts on the representative thoracic and lumbar vertebrae.

Thoraco-lumbar transition vertebrae: the superior articular facets of the rhesus show a statistically significant difference between the left and right side angular measurements. In the baboon the superior thoracic-like articular facets exhibit no significant difference. The superior interspecies comparisons show a significant difference between the left x-axis and the right y-axis measurements. The inferior lumbar-like elements appear to be much less variable in their joint axis orientation presenting only a significant difference between the intraspecies baboon left versus right y-axis measurements. This difference in variation might be significant in that the superior ,or thoracic-like, vertebral facets allow for rotational motions in the spine which are a significant component in the production of complex multi-axis ejection seat injuries (3,5,6,9). However, flexion-extension is suggested to be the major contributory motion involved in emergency egress fractures (3,4,5,6,9) and the relative kinematic stability, which is afforded to the

representative lumbar units of these species, is compromised due to the lack of the accessory processes in the transition vertebrae .

Transition versus representative thoracic and lumbar vertebrae: in the rhesus both the pooled and individual superior y-axis comparisons showed a significant difference between the representative thoracic superior articular facet angles and the superior transition facet angles. The pooled and individual superior y-axis comparisons in the baboon exhibit no significant differences between these measurements. Simularly, the superior x-axis values show no significant differences for either the pooled or individual measurements for either species.

The inferior, lumbar-like, y-axis measurements in the rhesus show no significant difference in the pooled or lumbar versus transition vertebrae. There is a significant difference between the rhesus right lumbar versus transition vertebrae. The baboons have a significant difference in the pooled analysis and the left y-axis lumbar versus inferior transition vertebrae. The pooled inferior x-axis measurements show a significant difference between both species. The rhesus show significant differance between all inferior x-axis measures of the representative lumbar versus the inferior transition vertebrae. The baboons only show significant difference in non-pooled x-axis values in the lumbar versus transition measures on the left side.

CONCLUSION: The intraspecies linear analysis indicated that variation in linear measurements (dimensional) within the rhesus

were negligable. The baboon, however, while they do exhibit size related variation it is not apparently related to orientation (or the side from which the measurement was taken) but appears to be purely allometric or sexually dimorphic in nature.

The intersepcific variations are quite significant for all of the linear measurement comparisons. The differences observed between the two species also appear to be allometric as all of the mean values for data obtained from the baboon are significantly greater (larger) than comparable measures from the rhesus. This size factor in the baboon in association with the significant level of observable sexual dimorphism can prove quite important when considering which animal to use as a model for injury research. Serious attention must be paid to interspecies allometric variations and to sexual dimorphism when comparing the two nonhuman primate species to each other or to humans.

I do not attribute much significance to the specific side of facet angle variations but the fact that the transition vertebral elements are statistically significantly different from their representative counterparts may warrent further investigation. The rhesus transition thoracic- and lumbar-like elements are not consistantly morphologically similar to their representative counterparts. In the baboons the thoracic-like facet angulations appear to be directly analagous to their thoracic representatives, however the lumbar elements follow the same type of pattern found in the rhesus except with less overall variation. A morphological grade in facet angulation appears to be present in the rhesus from the most superior (cranial)

thoracic vertebrae down thru the most inferior (caudal) lumbar vertebrae. The rhesus exhibits the most overall variation in both the thoracic- and lumbar-like elements while the baboon's variation in vertebral levels appear to be more morphologically distinct rather than exhibiting a gradual change from one level to the next. The works of Whitney (13) and Med (8) suggest that the type of asymmetry observed in the rhesus specimens is similar to that found in humans. The change from a classical thoracic to a classical lumbar type of articulation, both in humans and the rhesus, is often a gradual process extending over several vertebrae, rather than a precise and complete change in passing from one vertebral pattern to the next, as appears to be the case in baboons. The morphology of the articular facets determines the kinematic characteristics of the vertebrae (8,10). The vertebral kinematics of both species, in terms of patterns of motion, should be exactly what would be expected for their particular 'type' of vertebrae and vertebral level. A detailed comparative kinematic analysis which would include correlations between three-dimensional morphological measurements and the precise angles, orientations and translations of spinal motion has not been done. It would therefore be impractical to speculate as to which species is a better morpho-kinematic model

of the rhesus monkey appear to more closely approximate those of humans.

RECOMMENDATIONS: this study had a great deal of potential but, unfortunately, time and availability of skeletanized and ligamentous specimens did not permit a complete investigation. First, the skeletal morphology section of this study needs to be supplemented by a greater number of sample specimens to include normal humans. Completely skeletanized materials can be readily obtained from Natural History Museums which would cut out specimen preparation time and provide habitat and vital statistics on all of the specimens. Secondly, a complete comparative three-dimensional kinematic analysis, between the two primate species and humans, should be performed in order to properly address the role of specific linear and angular measures to spinal mechanics and to provide a proper kinematic database for use in modeling ejection seat injuries. My laboratory at New York University has readily available a three-dimensional kinematic analysis device, which I am currently using for part of my thesis research, and an advanced image analysis device for two-dimensional direct-object digitizing. Once I return to New York University I intend to write a Mini-grant proposal, under the advise of Dr. Kazarian, in an effort to implement the aforementioned recommendations.

LINEAR   MEASUREMENTS   TAKEN   OF   THE   THORACO-LUMBAR   TRANSITION

VERTEBRAE:

Superior:
1) length and width of the spinal canal
2) length and width of the superior vertebral body
3) intertransverse length
4) intertransverse facet length
5) sup. length from lamina to .facet cord bisector
6) sup. length from lamina to ant. margin of centrum
7) left and right pedicle width

Inferior:
1) length and width of the vertebral body
2) intratransverse facet length
3) inf. length from lamina to facet cord bisector
4) inf. length from lamina to ant. margin of centrum

Anterior:
1) ant. vertebral body height
2) medial vertebral body width

Left:
1) length from transverse process to ant. margin of centrum
2) intertransverse sup/inf facet distance
3) posterior vertebral body height
4) total length of the vertebrae, including the spinous process

Right:
1) length from transverse process to ant. margin of centrum
2) intertransverse sup/inf facet distance

Posterior:
1) left and right transverse process length

APPENDIX 2

A. ANGULAR MEASUREMENTS FROM TRANSITION VERTEBRAE:

X-Axis Measurements:
1) superior and inferior left
2) superior and inferior right

Y-Axis Measurements:
1) superior and inferior left
2) superior and inferior right

B. ANGULAR MEASUREMENTS FROM REP. THORACIC AND LUMBAR VERTEBRAE:

Thoracic Y-Axis:
1) superior left and right

Thoracic X-Axis:
1) superior left and right

Lumbar Y-Axis:
1) inferior left and right

Lumbar X-Axis:
1) inferior left and right

REFERENCES

1) The AAMRL Mission. Wright-Patterson AFB, Ohio

2) Chubb RH, Detrick HR, Shannon RH: Compression fractures of the spine during USAF ejections. Aerosp. Med. 36(10): 968-972, 1965.

3) Hearon BF, Thomas HA, Raddin JH: Mechanisms of vertebral fracture in the F/FB-111 ejection experience. Avait. Space & Environ. Med. 53(5): 440-448, 1982.

4) Kazarian LE: The primate as a model for crash injury. AMRL-TR-75-101, 1975.

5) Kazarian LE, Beers K, Hernandez J: Spinal injuries in the F/FB-111 crew escape system. Avait. Space & Environ. Med. 50(9): 948-957, 1979.

6) Kazarian LE, Boyd DD, Von Gierke HE: The dynamic biomechanical nature of spinal fractures and articular facet derangement. AMRL-TR-71-17, 1971.

7) Kazarian LE, Von Gierke HE: The validation of biodynamic models. AMRL-TR-78-105, 1978.

8) Med M: Articulations of the thoracic vertebrae and their variability. Folia Morph. 10(2): 212-215, 1972.

9) Mohr GC, Brinkley JW, Kazarian LE, Millard WW: Variations of spinal alignment in egress systems and their effect. Aerosp. Med. 40(9): 983-988, 1969.

10) Schultz AH, Straus WI: The numbers of vertebrae in primates. Proceedings of the American Philosophical Society. 89(4): 601-626, 1945.

11) Todd TW: Numerical significance in the thoraco-lumbar vertebrae of the mammalia. Anat. Rec. 24: 261-286, 1922.

12) White AA, Panjabi MM: Clinical Biomechanics of the Spine. J.B. Lippincott Co.: Philadelphia, 1978.

13) Whitney C: Asymmetry of vertebral articular processes and facets. AJPA. 9(4): 451-155, 1926.

14) Wigh RE: The thoracolumbar and lumbosacral transitional joints. Spine. 5(3): 215-222, 1980.

1987 USAF-UES SUMMER FACULTY RESEARCH PROGRAM/

GRADUATE STUDENT SUMMER RESEARCH PROGRAM

Sponsored by the

AIR FORCE OFFICE OF SCIENTIFIC RESEARCH

Conducted by the

Universal Energy Systems, Inc.

FINAL REPORT

Six Degree of Freedom Simulation

Computer Program for Aeroelastic

Free-Flight Projectiles

Prepared by:	Thomas Harkins
Acaademic Rank:	Master's Student
Department and	Mechanical Engineering Department
University:	Louisiana State University
Research Location:	AFATL/FXA
	Eglin AFB, Florida 32542
USAF Researcher:	Mr. Gerald L. Winchenbach
Date:	September 30, 1987
Contract No.:	F49620-85-C-0013

Six Degree of Freedom Simulation

Computer Program for Aeroelastic

Free-Flight Projectiles

by

Thomas Harkins

ABSTRACT

The objective of this research effort was to determine
how much influence aeroelastic effects had on determining the
aerodynamic coefficients of a free-flight projectile. These
coefficients were determined from parameter estimation
techniques based on rigid body motion. A general six degree of
freedom simulation program was developed in FORTRAN code. The
program was then modified by adding elastic inertia terms. The
flight simulator was run with the rigid body aerodynamic
coefficients, but the model itself was allowed to "flex"
during its flight. Preliminary results showed that the body's
flexing had no effect on the trajectory.

ACKNOWLEDGEMENTS

I. INTRODUCTION

Experimental methods are used to test the performance of a prototype or a scaled model. At the Aeroballistic Research Facility, located on Eglin AFB, testing of high fineness ratio penetrators has been performed. The free-flight ballistic range is instrumented with timers and two-plane (vertical and horizontal) shodowgraph stations that can measure the angular orientation and translational position of the ballistic model. The shadowgraph stations are located every fifteen feet of the 750 foot range. The data are reduced using a parameter estimation technique developed by Hathaway and Whyte (Ref. 1) which is a modified form of the Chapman and Kirk technique. This estimation technique compares trajectory data with analytical predictions and calculates the aerodynamic coefficients as a result. In free-flight aerodynamic data analysis, the reduction is not successful until the motion data can be reproduced using the calculated coefficients to a probable error equivalent of the experimental data.

This requirement dictates that the analytical model be an accurate representation of the physical behavior of the actual model. However, a measurable amount of aeroelastic flexing has been observed from the shadowgraphs of the high fineness ratio penetrators. This flexing raises certain doubts about the validity of using the current rigid body motion as the analytical model.

11. OBJECTIVES

The objectives of the summer research program are:

1. Find a technique for analyzing aeroelastic free flight projectiles.

2. Study the effects of the flexibility of an aerodynamic body, in particular, a high finess ratio penetrator.

III. FLEXIBILITY ANALYSIS

The equations of motion are influenced by the elastic deformation of the body. These equations are derived by taking into account the change in the center of mass and moments of inertia. The rigid body equations of motion are modified by adding "elastic inertia" terms. The elastic inertia terms are determined analytically by describing the dynamics of an arbitrarily deformed mass element (Ref. 2).

Since the aerodynamic coefficients are not known before the model is tested, the loads on the model are indeterminate, and a forced vibration analysis of the penetrator cannot be performed. It is necessary to find a function of deformation with respect to time so that the elastic inertia terms can be calculated as the simulation program is integrated numerically.

The body is assumed to vibrate at its natural frequency. This frequency is calculated using the NASTRAN finite element computer program. The deformation of the body is then defined

as
$$\xi = A*sin(wt)*F(x,y,z)$$
where A is the amplitude determined from experimental data, w is the natural frequency, and F(x,y,z) is the mode shape.

It should be noted that for the case being considered, bending deformations are taken into account and the torsional axial deformations are neglected. Considering the stiffness of the projectile in bending compared with that in torsion or tension, the assumption is reasonable.

The dynamics of the elastic penetrator can now be determined by numerically solving the equations of motion of the elastic body, where the elastic inertia coefficients have been determined a priori with a free-free vibration analysis of the fundamental mode shape. The details of the dynamic simulation are described in the next section.

IV. MODEL SIMULATION

The simulation program uses the fourth-order, Runge-Kutta integration algorithm. A program listing is given in Appendix A. Physical characteristics of the model, as well as the aerodynamic coefficients (determined from experimental data using the parameter estimation technique) are read into the program from an input file. The initial position, time, and velocities are also read into the program. The program takes the "earth-fixed" initial data and transforms them into "body-fixed" values. The output of the program is in both body-fixed and earth-fixed coordinates. However, all

33-6

integration is done in the body-fixed coordinate system.

Subroutine EOM6 is called each time the derivatives of the variables being integrated need to be calculated. The variables and their derivatives are stored in a matrix called FF(2,12). This allows for easy manipulation of all twelve of the variables. It should be noted that the deformation term, which determines the value of the elastic inertia terms, is located in EOM6.

The graphics routine at the end of the program uses PLOT 10 software developed for the Tektronics computer system.

V. RESULTS

With the program mentioned, all that is necessary to run a rigid body simulation is to set the elastic inertia terms to zero. This sets the base line for comparison of the elastic cases. The model simulated has a length over diameter ratio of 35, with an initial Mach Number of 5.

Using the same initial velocity, the elastic cases simulated had an amplitude of 0.02 and 0.12 inches. This corresponded to 0.5 and 3.0 degrees, respectively. Figure 1 shows the characteristics of the trajectory for the elastic case of 0.12 inches of amplitude. The comparison of the elastic simulation with the rigid body simulation showed no meaningful difference in the trajectory.

As a result, no definite conclusions can be drawn from these simulation tests. Further work must done in order to determine whether the simplifications have made the simulation too limited. Time limitations precluded a thorough

analysis of the problem.

VI. RECOMMENDATIONS

The initial phase of the research into the elastic effects on free flight ballistics has been completed. A six degree of freedom simulation program for single-plane elastic bending has been developed and run successfully. The problem at hand has clearly been defined. The following items remain to be done:

1. Additional fineness ratios and flexibility amplitudes should be simulated using the QUICK6 program.

2. Using the elastic body equations of motion, a general theory should be derived which establishes the boundary (both in flight conditions and body characteristics) between which rigid body aerodynamics are acceptable or not.

3. An aerodynamic forcing function should be determined from the rigid body equations of motion. This function would be driven by the body's flexibility effects.

33-8

REFERENCES

1   Hathaway, W. and R. White, Aeroballistic Range Data
Analysis For Nonsymmetric Configurations, <u>AFATL-TR-76-109</u>,
    September, 1976.

2   Courter, R. W., <u>The Effect of Model Flexibility on the
    Accuracy of Aerodynamic Coefficients Determined from Free-
    Flight Ballistic Tests</u>, AFATL/FXA, July, 1987.
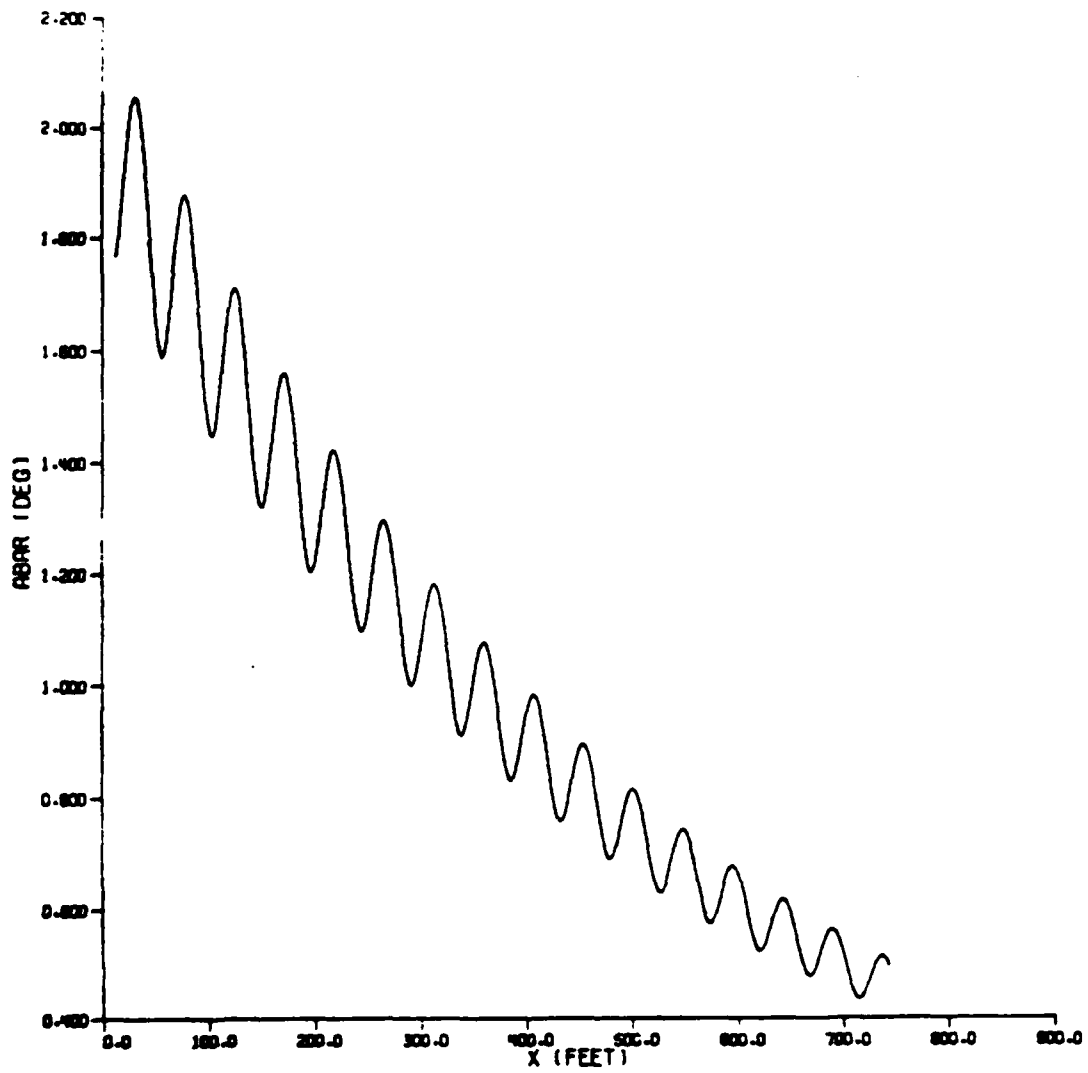
FIG. 1: ALPHA BAR VS. DOWN RANGE POSITION

APPENDIX A

```
      PROGRAM QUICK
      COMMON AREA,D,AIXX,AIYY,AIZZ,OMEGA,AMP,AKX,AKY,AKZ
      COMMON AKXDOT,AKYDOT,AKZDOT,RHO,TEMP,CDFF,VT,VET,ABAR,ALPHA,BETA
      COMMON FMASS,GRAV,EPS2,QA,DO2V,SASN,T
      COMMON CLD,CLP,CLPHI,CMO,CMA,CMA3,CMQ,CMQ2,CMPB,CMPHIA,CNPHIA
      COMMON CNO,CNB,CNB3,CNR,CNR2,CNPA,CXO,CXA2,CXB2,CXM,CYO
      COMMON CYB,CYB3,CYPA,CNNPHA,CYPHIA,CZO,CZA,CZA3,CZPB,PHIPN,REFM
      COMMON IOUT
      COMMON FF(3,12)
      COMMON /SPLT/YA,XA,ZA,PHIA,THETA,PSIA,ABARA
      DIMENSION AK(4,12)
      REAL XA(700),YA(700),ZA(700),XDA(700),YDA(700),ZDA(700)
      REAL UBA(700),VBA(700),WBA(700),PBA(700),QBA(700),RBA(700)
      REAL THETA(700),PSIA(700),PHIA(700),ABARA(700),ALPHAA(700)
      REAL BETAA(700),VTA(700),VETA(700),TA(700)
      EQUIVALENCE(X,FF(1,1)),(Y,FF(1,2)),(Z,FF(1,3))
      EQUIVALENCE(UB,FF(1,4)),(VB,FF(1,5)),(WB,FF(1,6))
      EQUIVALENCE(PB,FF(1,7)),(QB,FF(1,8)),(RB,FF(1,9))
      EQUIVALENCE(THET,FF(1,10)),(PSI,FF(1,11)),(PHI,FF(1,12))
      EQUIVALENCE(XD,FF(2,1)),(YD,FF(2,2)),(ZD,FF(2,3))
      EQUIVALENCE(UBDOT,FF(2,4)),(VBDOT,FF(2,5)),(WBDOT,FF(2,6))
      EQUIVALENCE(PBDOT,FF(2,7)),(QBDOT,FF(2,8)),(RBDOT,FF(2,9))
      EQUIVALENCE(THETD,FF(2,10)),(PSID,FF(2,11)),(PHID,FF(2,12))
      OPEN(UNIT=5,FILE='HILDI1')
      OPEN(UNIT=6,FILE='HILDO1')
      REWIND(UNIT=5)
      REWIND(UNIT=6)
C    ***********************************************************
C            THIS PROGRAM IS A SIX DEGREE OF FREEDOM
C            TRAJECTORY SIMULATOR. THE INTEGRATION
C            ALGORITHM USED IS THE RUNGE-KUTTA FOURTH
C            ORDER ROUTINE. THE STATE VARIABLES AND
C            THEIR DERIVITIVES ARE SET EQUIVALENT IN
C            THE FF MATRIX.
C    ***********************************************************
      IR=5
      IW=6
      DO 3010 J=1,12
      DO 3020 I=1,3
 3020 FF(I,J)=0.0
      DO 3010 I=1,4
 3010 AK(I,J)=0.0
      DO 700 I=1,700
      TA(I)=0.0
      XA(I)=0.0
      YA(I)=0.0
      ZA(I)=0.0
      XDA(I)=0.0
      YDA(I)=0.0
      ZDA(I)=0.0
      UBA(I)=0.0
      VBA(I)=0.0
      WBA(I)=0.0
      THETA(I)=0.0
      PSIA(I)=0.0
      PHIA(I)=0.0
      PBA(I)=0.0
      QBA(I)=0.0
      RBA(I)=0.0
      VETA(I)=0.0
      VTA(I)=0.0
      ABARA(I)=0.0
      ALPHAA(I)=0.0
      BETAA(I)=0.0
 700  CONTINUE
C    ***********************************************************
C    ***********************************************************
      READ(IR,1000)SHOT,DI,WGT,CG,CDFF,SPAN,RHO,TEMP
      READ(IR,1010)THET,THETD,PSI,PSID,PHI,PHID
      READ(IR,1020)X,Y,Z,XD,YD,ZD
      READ(IR,1030)T,DLT1,XMAX,TMAX
      READ(IR,1040)AMP,AIXX,AIYY,AIZZ,OMEGA,AKX,AKY,AKZ,AKXDOT,AKYDOT,
     +            AKZDOT
      READ(IR,1050)CLD,CLP,CLPHI,CMO,CMA,CMA3,CMQ,CMQ2,CMPB,CMPHIA,
     +            CNPHIA,CNO,CNB,CNB3,CNR,CNR2,CNPA,CXO,CXA2,CXB2,
     +            CXM,CYO,CYB,CYB3,CYPA,CNNPHA,CYPHIA,CZO,CZA,CZA3,
     +            CZPB,PHIPN,REFM
C    ***********************************************************
C    ***********************************************************
 1000 FORMAT(5X,F10.4)
 1010 FORMAT(6X,F9.2)
 1020 FORMAT(3X,F8.3)
 1030 FORMAT(5X,F6.2)
 1040 FORMAT(7X,F10.4)
 1050 FORMAT(7X,F10.4)
C    ***********************************************************
C    *****  SET UP THE COUNTERS AND INITIAL VALUES  *****
C    ***********************************************************
```

33-12

```fortran
      KOUNT=0
      IOUT=1
      NCNT=0
      NPR=2
      TOUT=0.0
      GRAV=32.17405
      CINER=1/13558159.2
      DEGRAD=3.1415927/180.
      RADDEG=1.0/DEGRAD
      D=DI/12.
      AREA=3.1415927*D*D/4.
      AIXX=AIXX*CINER
      AIYY=AIYY*CINER
      AIZZ=AIZZ*CINER
      THET=THET*DEGRAD
      PSI=PSI*DEGRAD
      PHI=PHI*DEGRAD
      FMASS=WGT/GRAV
      CT=COS(THET)
      CS=COS(PSI)
      CP=COS(PHI)
      ST=SIN(THET)
      SS=SIN(PSI)
      SP=SIN(PHI)
      UB=XD*CT*CS+YD*CT*SS-ZD*ST
      VB=XD*(ST*SP*CS-CP*SS)+YD*(ST*SP*SS+CP*CS)+ZD*CT*SP
      WB=XD*(ST*CP*CS+SP*SS)+YD*(ST*CP*SS-SP*CS)+ZD*CT*CP
      VT=SQRT(UB*UB+VB*VB+WB*WB)
      PB=PHID-PSID*ST
      QB=THETD*CP+PSID*CT*SP
      RB=PSID*CT*CP-THETD*SP
C********** INTEGRATION CODE BEGINS ********************
      NV=12
      GO TO 50
   30 T=T+DLTT/2.
      IOUT=2
      NCNT=NCNT+1
      DO 40 J=1,NV
   40 FF(3,J)=FF(1,J)
      DO 160 I=1,4
      IF(I-1)300,58,50
   50 CONTINUE
      IF(IOUT-3)56,210,210
   56 CALL EOM6
   58 IF(IOUT-1)300,30,60
   60 CONTINUE
      DO 90 J=1,NV
   90 AK(I,J)=FF(2,J)
      IF(I-3)100,110,140
  100 F=1.0
      GO TO 120
  110 F=2.0
      T=T+DLTT/2.0
  120 DO 130 J=1,NV
  130 FF(1,J)=FF(3,J)+AK(I,J)*F*(DLTT/2.0)
      GO TO 160
  140 DO 150 J=1,NV
  150 FF(1,J)=FF(3,J)+DLTT*(AK(1,J)+2.0*(AK(2,J)+AK(3,J))+AK(4,J))/6.0
  160 CONTINUE
      IF(NCNT-NPR)165,210,210
  165 IF(T-TMAX+.00001)170,190,190
  170 IF(X-XMAX)180,190,190
  180 IOUT=1
      GO TO 50
  190 IOUT=3
      GO TO 50
  210 NCNT=0
C***************************************************
C     THE NEXT SEGMENT OF THE PROGRAM
C     IS FOR CONVERTING THE COMPUTED
C     DATA TO AN ACCEPTABLE FORMAT.
C     THE OUTPUT IS ALSO STORED IN
C     ARRAYS SO THAT IT CAN BE PLOTTED.....
C***************************************************
      THETDG=THET*RADDEG
      PSIDG=PSI*RADDEG
      PHIDG=PHI*RADDEG
      BUGGER=999.9
      IF(BUGGER.EQ.999.9)GO TO 399
      GO TO 403
  399 IF(PHIDG.LT.0.0)GO TO 400
      GO TO 401
  400 PHIDG=PHIDG+360
      GO TO 399
  401 IF(PHIDG.GT.360.)GO TO 402
      GO TO 403
  402 PHIDG=PHIDG-360.
      GO TO 401
```

```
  403 CONTINUE
      VET=SQRT(XD*XD+YD*YD+ZD*ZD)
      ABAR=ATAN(SQRT(WB*WB+VB*VB)/UB)*RADDEG
      ALPHA=ATAN(WB/UB)*RADDEG
      BETA=ATAN(VB/UB)*RADDEG
      IF(KOUNT-700)280,260,260
  260 WRITE(IW,270)
  270 FORMAT(1X,'EXCEEDED MEMORY')
      GO TO 300
  280 CONTINUE
      KOUNT=KOUNT+1
      TA(KOUNT)=T
      XA(KOUNT)=X
      YA(KOUNT)=Y
      ZA(KOUNT)=Z
      XDA(KOUNT)=XD
      YDA(KOUNT)=YD
      ZDA(KOUNT)=ZD
      VETA(KOUNT)=VET
      UBA(KOUNT)=UB
      VBA(KOUNT)=VB
      WBA(KOUNT)=WB
      VTA(KOUNT)=VT
      THETA(KOUNT)=THETDG
      PSIA(KOUNT)=PSIDG
      PHIA(KOUNT)=PHIDG
      PBA(KOUNT)=PB
      QBA(KOUNT)=QB
      RBA(KOUNT)=RB
      ABARA(KOUNT)=ABAR
      ALPHAA(KOUNT)=ALPHA
      BETAA(KOUNT)=BETA
      MOW=KOUNT
      IF(IOUT-3)290,300,290
  290 IOUT=1
      GO TO 50
C*********************************************************************
  300 CONTINUE
      WRITE(IW,9999)
      WRITE(IW,9000)
      DO 8600 L=1,MOW
      WRITE(IW,9100)TA(L),XA(L),YA(L),ZA(L),ABARA(L),
     +      ALPHAA(L),BETAA(L)
 8600 CONTINUE
C
      WRITE(IW,9999)
      WRITE(IW,9200)
      DO 8700 L=1,MOW
      WRITE(IW,9300)TA(L),THETA(L),PSIA(L),PHIA(L),PBA(L),QBA(L),RBA(L)
 8700 CONTINUE
C
      WRITE(IW,9999)
      WRITE(IW,9400)
      DO 8800 L=1,MOW
      WRITE(IW,9500)TA(L),XDA(L),YDA(L),ZDA(L),VETA(L)
 8800 CONTINUE
C
      WRITE(IW,9999)
      WRITE(IW,9600)
      DO 6900 L=1,MOW
      WRITE(IW,9700)TA(L),UBA(L),VBA(L),WBA(L),VTA(L)
 8900 CONTINUE
C
C
 9000 FORMAT(1X,'T(SEC)',3X,'X(FEET)',3X,'Y(FEET)',3X,'Z(FEET)',1X,
     +      'ABAR(DEG)',1X,'ALPHA(DEG)',1X,'BETA(DEG)')
 9100 FORMAT(1X,F7.4,6(1X,F9.3))
 9200 FORMAT(1X,'T(SEC)',3X,'THET(DEG)',2X,'PSI(DEG)',2X,'PHI(DEG)',
     +      2X,'P(RAD/SEC)',2X,'Q(RAD/SEC)',2X,'R(RAD/SEC)')
 9300 FORMAT(1X,F7.4,6(2X,F9.3))
 9400 FORMAT(1X,'T(SEC)',4X,'VX(FT/SEC)',3X,'VY(FT/SEC)',3X,'VZ(FT/SEC)'
     +      3X,'VET(FT/SEC)')
 9500 FORMAT(1X,F7.4,4(3X,F10.4))
 9600 FORMAT(1X,'T(SEC)',4X,'UB(FT/SEC)',3X,'VB(FT/SEC)',3X,
     +      'WB(FT/SEC)',3X,'VT(FT/SEC)')
 9700 FORMAT(1X,F7.4,4(3X,F10.4))
 9999 FORMAT(1X,///)
      CALL PLOT
      END
C **********************************************************************
C     SUBROUTINE EOM6 CALCULATES THE DERIVITIVES OF
C     THE STATE VARIABLES TO BE USED IN THE RUNGE-
C     KUTTA ROUTINE  IT SHOULD BE NOTED THAT THE
C     FORCE AND MOMENT EQUATIONS ARE USED TO CALCULATE
C     UBDOT,VBDOT,WBDOT,PBDOT,QBDOT AND RBDOT ONLY
C     XD,YD,ZD,THETD,PSID,AND PHID ARE CALCULATED FROM
C     THE TRANSFORMS OF THE EQUATIONS MENTIONED ABOVE
C **********************************************************************
```

33-14

```fortran
      SUBROUTINE EOM6
      COMMON AREA,D,AIXX,AIYY,AIZZ,OMEGA,AMP,AKX,AKY,AKZ
      COMMON AKXDOT,AKYDOT,AKZDOT,RHO,TEMP,CDFF,VT,VET,ABAR,ALPHA,BETA
      COMMON FMASS,GRAV,EPS2,QA,DO2V,SASN,t
      COMMON CLD,CLP,CLPHI,CMO,CMA,CMA3,CMQ,CMQ2,CMPB,CMPHIA,CNPHIA
      COMMON CNO,CNB,CNB3,CNR,CNR2,CNPA,CXO,CXA2,CXB2,CXM,CYO
      COMMON CYB,CYB3,CYPA,CNNPHA,CYPHIA,CZO,CZA,CZA3,CZPB,PHIPN,REFM
      COMMON IOUt
      COMMON FF(3,12)
      EQUIVALENCE(X,FF(1,1)),(Y,FF(1,2)),(Z,FF(1,3))
      EQUIVALENCE(UB,FF(1,4)),(VB,FF(1,5)),(WB,FF(1,6))
      EQUIVALENCE(PB,FF(1,7)),(QB,FF(1,8)),(RB,FF(1,9))
      EQUIVALENCE(THET,FF(1,10)),(PSI,FF(1,11)),(PHI,FF(1,12))
      EQUIVALENCE(XD,FF(2,1)),(YD,FF(2,2)),(ZD,FF(2,3))
      EQUIVALENCE(UBDOT,FF(2,4)),(VBDOT,FF(2,5)),(WBDOT,FF(2,6))
      EQUIVALENCE(PBDOT,FF(2,7)),(QBDOT,FF(2,8)),(RBDOT,FF(2,9))
      EQUIVALENCE(THETD,FF(2,10)),(PSID,FF(2,11)),(PHID,FF(2,12))
      ALZZ=0.0002977*OMEGA*AMP*AMP*SIN(2*OMEGA*T)
      EIZZ=0.000595*AMP*AMP*(SIN(OMEGA*T)**2.)
      CT=COS(THET)
      CS=COS(PSI)
      CP=COS(PHI)
      ST=SIN(THET)
      SS=SIN(PSI)
      SP=SIN(PHI)
      TT=TAN(THET)
      XD=UB*CT*CS+VB*(ST*SP*CS-CP*SS)+WB*(ST*CP*CS+SP*SS)
      YD=UB*CT*SS+VB*(ST*SP*SS+CP*CS)+WB*(ST*CP*SS-SP*CS)
      ZD=-UB*ST+VB*CT*SP+WB*CT*CP
      THETD=QB*CP-RB*SP
      PSID=QB*SP*(1/CT)+RB*CT*CP
      PHID=PB+QB*TT*SP+RB*TT*CP
      VT=SQRT(UB*UB+VB*VB+WB*WB)
      EPS2=(VB*VB+WB*WB)/(VT*VT)
      QA=AREA*RHO*VT*VT/2.0
      DO2V=D/(VT*2.0)
      SASN=EPS2*SIN(PHIPN)/VT
      FMACH=VT/(49.025*SQRT(TEMP))
      AL=QA*D*(CLD+CLP*PB*DO2V+CLPHI*EPS2*SIN(PHIPN))
      AM=QA*D*(CMO+CMA*(WB/VT)**3.)+CMA3*((WB/VT)**3.)+CMQ*QB*DO2V+
     +CMQ2*QB*DO2V*((WB/VT)**2.)+CMPB*PB*DO2V*VB/VT+CMPHIA*SASN*WB+
     +CNPHIA*SASN*VB)
      AN=QA*D*(CNO+CNB*(VB/VT)+CNB3*((VB/VT)**3.)+CNR*RB*DO2V+
     +CNR2*RB*DO2V*((VB/VT)**2.)+CNPA*PB*DO2V*WB/VT-CMPHIA*
     +SASN*VB+CNPHIA*SASN*WB)
      FX=QA*(CXO+CXA2*((WB/VT)**2.)+CXB2*((VB/VT)**2.)+CXM*(FMACH-
     +REFM))
      FY=QA*(CYO+CYB*(VB/VT)+CYB3*((VB/VT)**3.)+CYPA*PB*
     +DO2V*(WB/VT)-CNNPHA*SASN*VB+CYPHIA*SASN*WB)
      FZ=QA*(CZO+CZA*(WB/VT)+CZA3*((WB/VT)**3.)+CZPB*PB*DO2V*(VB/VT)-
     +CNNPHA*SASN*WB-CYPHIA*SASN*VB)
      FXG=FMASS*GRAV*ST
      FYG=FMASS*GRAV*CT*SP
      FZG=FMASS*GRAV*CT*CP
      PBDOT=(AL+QB*RB*(AIYY-AIZZ+EIZZ))/AIXX
      QBDOT=(AM-PB*RB*(AIXX-AIZZ)-2.0*QB*ALZZ)/AIYY
      RBDOT=(AN+PB*QB*(AIXX-AIYY))/AIZZ
      UBDOT=(-FX+FXG)/FMASS+(RB*VB-QB*WB)
      VBDOT=(FY-FYG)/FMASS+(PB*WB-RB*UB)
      WBDOT=(FZ-FZG)/FMASS+(QB*UB-PB*VB)
      RETURN
      END
      SUBROUTINE PLOT
C     PLOT SUBROUTINE WRITTEN BY GREGG ABATE
C     ROUTINES IN THIS PROGRAM WERE TAKEN FROM EXISTING PLOT ROUTINES
      COMMON /SPLT/Y,X,Z,PHI,THETA,PSI,ALP
      DIMENSION Y(700),X(700),Z(700),THETA(700),PHI(700),PSI(700),
     1ALP(700)
5     CALL MENU(IPL)
      CALL ERASE
      CALL ANMODE
      GO TO (10,20,30,40,50,60,70,80),IPL
10    CALL XYPLOT(X,Y,IPL)
      GO TO 5
20    CALL XYPLOT(X,Z,IPL)
      GO TO 5
30    CALL XYPLOT(X,PHI,IPL)
      GO TO 5
40    CALL XYPLOT(X,THETA,IPL)
      GO TO 5
50    CALL XYPLOT(X,PSI,IPL)
      GO TO 5
60    CALL XYPLOT(X,ALP,IPL)
      GO TO 5
70    CALL THPSI(THETA,PSI,IPL)
      GO TO 5
80    RETURN
      END
```

33-15

```fortran
      SUBROUTINE MENU(I)
      CALL CONNEC(L="TAPE8")
      CALL CONNEC(L="TAPE9")
      CALL TCSLIB
      CALL TYPBPS(IB)
      IBAUD=IB/10
      CALL INITT(IBAUD)
      CALL BINITT
      CALL MOVABS(0,780)
      CALL DRWABS(1023,780)
      CALL DRWABS(1023,0)
      CALL DRWABS(0,0)
      CALL DRWABS(0,780)
      CALL ANMODE
      WRITE(8,19)
19    FORMAT(//////,T60,'PLOT MENU',//,T50,
     1'1     X VS. Y',/,T50,
     1'2     X VS. Z',/,T50,
     1'3     X VS. PHI',/,T50,
     1'4     X VS. THETA',/,T50,
     1'5     X VS. PSI',/,T50,
     1'6     X VS. ALAPHA BAR',/,T50,
     1'7     THETA VS. PSI',/,T50,
     1'8     RETURN TO MAIN PROGRAM',//,T50,'ENTER # OF CHOICE?',//,T50,'
     1->')
5     READ(9,18)I
18    FORMAT(I2)
      IF(I.GE.1.AND.I.LE.8)RETURN
      WRITE(8,17)
17    FORMAT(T45,'TRY ENTERING A VALID NUMBER THIS TIME!')
      GO TO 5
      END
      SUBROUTINE THPSI(THETA,PSI,IPL)
      DIMENSION THETA(700),PSI(700),LAB(3),IPSI(10),ITHE(11)
      DATA IPSI/80,83,73,32,40,100,101,103,41,32/
      DATA ITHE/84,72,69,84,65,32,40,100,101,103,41/
C
C     CREATE SQUARE SCREEN
C
C     CALL TCSLIB
C     CALL TYPBPS(IB)
C     IBAUD=IB/10
C     CALL INITT(IBAUD)
C     CALL BINITT
      CALL TWINDO(150,750,100,700)
C
C     MIN &  MAX VALUE DETERMINATION
C
      AMIN=99999.
      AMAX=-99999.
      CALL MNMX(THETA,AMIN,AMAX)
      CALL MNMX(PSI,AMIN,AMAX)
      IF(ABS(AMIN).GT.AMAX)AMAX=ABS(AMIN)
      AMIN=-AMAX
C
C     ROUND OFF   MAX  & MIN VALUES
C
100   MIN=AMIN/5.-1
      AMIN=5*MIN
      AMAX=-AMIN
C
C     SET UP DATA WINDOW
C
      CALL DWINDO(AMIN,AMAX,AMIN,AMAX)
C
C     DRAW AXES
C
      ITIC=(AMAX-AMIN)/5+1
      CALL MOVEA(AMIN,0.)
      CALL DRAWA(AMAX,0.)
      CALL MOVEA(0.,AMAX)
      CALL DRAWA(0.0,AMIN)
      X=AMIN
      DO 200 I=1,ITIC,2
      CALL MOVEA(X,0.5)
      CALL DRAWA(X,-0.5)
      X=X+10.
200   CONTINUE
      Y=AMIN
      DO 220 I=1,ITIC,2
      CALL MOVEA(-0.5,Y)
      CALL DRAWA(0.5,Y)
      Y=Y+10.
220   CONTINUE
C
C     DRAW A BOX AROUND THE PLOT
C
      CALL MOVABS(100,50)
```

```fortran
      CALL DRWABS(800,50)
      CALL DRWABS(800,750)
      CALL DRWABS(100,750)
      CALL DRWABS(100,50)
C
C     PLOT POINTS
C
      NCOM=700
      CALL MOVEA(-PSI(1),-THETA(1))
      DO 280 I=2,NCOM
      CALL DRAWA(-PSI(I),-THETA(I))
  280 CONTINUE
C
C     LABEL AXES
C
      X=AMIN
      JXLAB=AMAX
      DO 240  I=1,ITIC,2
      ENCODE(3,1,LAB)JXLAB
    1 FORMAT(I3)
      CALL   MOVEA(X,0.5)
      CALL   DRAWA(X,-0.5)
      CALL MOVREL(-10,-5)
      CALL BLABEL(0,3,LAB)
      X=X+10.
      JXLAB=JXLAB-10
  240 CONTINUE
      CALL MOVABS(120,350)
      CALL HLABEL(10,IPSI)
      CALL MOVABS(420,75)
      CALL HLABEL(11,ITHE)
      Y=AMIN
      JYLAB=AMAX
      DO 260 I=1,ITIC,2
      ENCODE(3,1,LAB)JYLAB
      CALL MOVEA(0.5,Y)
      CALL   DRAWA(-0.5,Y)
      CALL MOVREL(-30,0)
      CALL BLABEL(0,3,LAB)
      Y=Y+10.
      JYLAB=JYLAB-10
  260 CONTINUE
      CALL MOVABS(0,780)
      CALL BELL
      CALL TINPUT(KEY)
      CALL ERASE
      CALL ANMODE
      RETURN
      END
      SUBROUTINE BLABEL(ITYPE,N,IADE)
      DIMENSION  IADE(50)
      IF(ITYPE.EQ.1)GO TO 100
      CALL AOUTST(N,IADE)
      GO TO 999
  100 DO 120 I=1,N
      ICHR=IADE(I)
      CALL  ANCHO(ICHR)
      CALL  LINEF
      CALL BAKSP
  120 CONTINUE
  999 RETURN
      END
      SUBROUTINE XYPLOT(XDATA,YDATA,IPL)
      DIMENSION XDATA(700),YDATA(700),XDAT(501),YDAT(501)
     1,IXLAB(15),IYLAB(15,6)
     1,ITIT(20),ISUB(20),XTITLE(5)
     1,IYLABP(15)
      DATA IXLAB/88,32,68,105,115,116,97,110,99,101,32,40,102,116,41/
      DATA IYLAB/89,32,68,105,115,116,97,110,99,101,32,40,102,116,41,
     190,32,68,105,115,116,97,110,99,101,32,40,102,116,41,
     180,72,73,32,40,100,101,103,41,6*32,
     184,72,69,84,65,32,40,100,101,103,41,4*32,
     180,83,73,32,40,100,101,103,41,6*32,
     165,76,80,72,65,32,66,65,82,32,40,100,101,103,41/
      DATA ITIT/84,73,84,76,69,32,49,13*32/
      DATA ISUB/84,73,84,76,69,32,50,13*32/
      DO 20  I=1,15
   20 IYLABP(I)=IYLAB(I,IPL)
      XDAT(1)=700
      YDAT(1)=700
      DO 10 I=1,700
      XDAT(I+1)=XDATA(I)
   10 YDAT(I+1)=YDATA(I)
      CALL LINE(0)
      CALL SYMBL(0)
      CALL SIZES(0)
      CALL CHECK(XDAT,YDAT)
      CALL DSPLAY(XDAT,YDAT)
```

```
      CALL MOVABS(500,050)
      CALL HLABEL(15,IXLAB)
      CALL MOVABS(0,500)
      CALL HLABEL(15,IYLABP)
      CALL MOVABS(500,730)
      CALL HLABEL(20,ITIT)
      CALL MOVABS(450,730)
      CALL HLABEL(20,ISUB)
C     CALL CHRSIZ(2)
C     CALL MOVABS(400,025)
C     CALL AOUTST(50,XTITLE)
C     CALL MOVABS(050,780)
      CALL BELL
      CALL TINPUT(KEY)
      CALL MOVABS(0,780)
      CALL ERASE
      CALL ANMODE
      RETURN
      END
```

33-18

1987 USAF-UES Summer Faculty Research Program

Graduate Student Summer Support Program

Sponsored by the

Air Force Office of Scientific Research

Conducted by the

Universal Energy Systems, Inc.

<u>FINAL REPORT</u>

<u>Sustained Delivery of Volatile Chemicals By Means of Ceramics</u>

Prepared by: **P.K. Bajpai, Ph.D and Deborah E. Hollenbach**

Academic Rank: Professor and M.S. Graduate Student

Department and   Biology Department

University: University of Dayton

Research Location: AAMRL/TH

                        Wright Patterson AFB

                        Dayton, OH 45433

USAF Researcher: **Dr. M.E. Andersen**

Date: September 30, 1987

Contract No.:   F49620-85-C-0013

REFERENCE DR. BAJPAI

SFRP FINAL REPORT NUMBER 7

1987 USAF-UES SUMMER FACULTY RESEARCH PROGRAM/

GRADUATE STUDENT SUMMER SUPPORT PROGRAM

Sponsored by the

AIR FORCE OFFICE OF SCIENTIFIC RESEARCH

Conducted by the

Universal Energy Systems, Inc.

FINAL REPORT

THE EFFECTS OF HYPERBARIC OXYGEN AND ANTIOXIDANT
DEFICIENCIES ON RAT RETINAL ULTRASTRUCTURE

Prepared by:	Ms. Adrienne L. Hollis
Academic Rank:	Graduate Student
Department and University:	Department of Biomedical Sciences, Meharry Medical College
Research Location:	Armed Forces Institute of Pathology, Division of Aerospace Research
USAF Researcher:	Col Richard Henderson, M.D., Chief, Division of Aerospace Research, Armed Forces Institute of Pathology, Washington, D.C. 20306-6000
Date:	September 28, 1987
Contract No:	F49620-85-C-0013

The Effects of Hyperbaric Oxygen and Antioxidant
Nutrients on Rat Retinal Ultrastructure

by

Adrienne L. Hollis

ABSTRACT

In previous studies, we have shown that the electro-
physiological response of the rat retina is rapidly
diminished in animals fed diets deficient in both vitamin E
and selenium for 6 weeks and treated with hyperbaric oxygen
(HBO). Animals deficient in vitamin E alone also show
diminished electroretinograms but only after prolonged
hyperbaric oxygen treatment. Through quantitative
histopathological studies, damage to the retinal pigment
epithelial layer as well as the outer nuclear layer has been
observed in animals fed a diet for 15 weeks that was
deficient in vitamin E only. The alterations in retinal
tissues observed by electrophysiology and quantitative
histopathology should correlate with ultrastructural
studies. In this study, we have prepared retinal tissue
samples for electronmicroscopy studies and have obtained
electron micrographs for future cytopathological analyses.
The cytopathological parameters to be studied include outer
segment disk membrane deterioration, lipofuscin content of
the RPE, phagosome number in the RPE, separations betweeen
tips of photoreceptors and apical surface of RPE, and
migration of photoreceptor cells into the inner retina.

ACKNOWLEDGEMENTS

Preliminary analysis of our data indicate that after 6 weeks, rats fed the diet deficient in both vitamin E and selenium have an increased number of mitochondria in their retinal pigment epithelium. This increase was, however, independent of HBO treatment. We could not, however, detect any alterations in the number of phagosomes or inclusion bodies in the RPE after 6 weeks. This conclusion correlates with the results obtained in our light microscopy studies of these rats. Electrophysiological studies, however, show that functional damage is occuring in the deficient animals after 6 weeks of diet. This suggests that the initial retinal damage may not be detectable by morphological analyses. The damage could be occuring at the molecular level, e.g. causing alterations in the permeability of the membrane to certain ions. Alternatively, we may be able to detect damage in the retina when we measure other parameters. The electron micrographs for the 15 week experiment will be analyzed in the near future.

I. INTRODUCTION

Hyperbaric oxygen (HBO) therapy is utilized to increase tissue oxygenation. HBO involves the use of barometric pressures greater than one atmosphere. Hyperbaric oxygen has been shown to be effective in the treatment of many clinical disorders such as gas gangrene, air embolism, carbon monoxide poisoning, and decompression sickness. HBO has also been used to enhance wound healing and in the treatment of multiple sclerosis and sickle cell anemia.

With the increasing use of hyperbaric oxygen therapy, questions concerning the possibility of adverse effects have necessarily been raised. The deleterious effects of hyperoxia on the central nervous system have been studied and Dickens (1) has shown that respiration of rat brain tissue is irreversibly poisioned by the exposure of the isolated tissues to high oxygen pressure and that even at 1 atmosphere of oxygen there is a slow poisioning of the tissue. Damage to brain tissue was found to positively correlate with an increase in pressure.

Oxygen participates in a large number of biochemical reactions, some of which generate oxygen-containing free radicals. Oxy-radicals can be produced as a result of the univalent reduction of oxygen instead of oxygen reduction by two-electron transfer through the cytochrome system. Free

radicals result in cellular damage by abstracting a hydrogen
atom from a polyunsaturated fatty acid (PUFA) in a
biomembrane to start the degenerative process identified as
lipid peroxidation.

The production of free radicals is known to be inhibited by
a number of protective cellular mechanisms present in all
oxygen metabolizing organisms. These mechanisms include the
action of free radical scavengers such as alpha-tocopherol
(vitamin E) and enzymatic processes such as those of
selenium-dependent glutathione peroxidase. Vitamin E
preferentially partitions into membranes and functions by
quenching lipophilic free radical species. Taylor (2) has
shown that vitamin E deficient rats are more sensitive to
the toxic effects of oxygen at elevated pressure than rats
maintained on a diet supplemented with vitamin E. Lung
damage was more pronounced after exposure to high oxygen
pressures in the rats not given vitamin E, and these vitamin
E deficient rats also demonstrated in vivo hemolysis. In
vitro lipid peroxidation, measured by malondialdehyde
production is related to vitamin E status. Takeuchi et al.
(3) have shown that diets deficient in vitamin E result in a
greater extent of lipid peroxidation in rat serum and
supplementation with vitamin E reverses this effect.
Selenium-dependent glutathione peroxidase functions in the
cell as part of a defense mechanism against oxygen-induced
damage (4). This enzyme reduces toxic hydrogen peroxide to
its corresponding alcohol or to water. Dietary deficiency

of selenium has been associated with liver necrosis, and also appears to result in immunosuppression in experimental animals (5). Rats deficient in vitamin E and/or selenium have been shown to have increased in vivo lipid peroxidation. Humans deficient in vitamin E and/or selenium may also be susceptible to hyperbaric oxygen toxicity.

Retinal lipids have a high content of polyunsaturated fatty acids and are therefore particularily vulnerable to the toxic effects of free radicals (6). The retina also consumes a large quantity of oxygen and contains photosensitizing agents (e.g. retinal) capable of inducing free radical production (7). It has been suggested by Henderson et al. (8) that in the presence of hyperbaric oxygen, there would be an increase in the amount of retinal damage. A deficiency in vitamin E and selenium leads to lowered levels of retinal vitamin E and glutathione peroxidase, respectively.

My research interests have been in the area of application of electroretinographic and quantitative histopathological techniques to study retinal damage in rats deficient in vitamin E and/or selenium and treated with hyperbaric oxygen. Because both of these techniques have shown that retinal damage has occured in the rats, we felt that it was important to examine the rat retina for ultrastructural damage. By the use of the electron microscope, the area of the retina that is damaged may be assessed.

35-7

II.   OBJECTIVES OF THE RESEARCH EFFORT:

The research conducted in this 10 week session focused on
the ultrastructural alterations observed in the retinas of
rats deficient or supplemented with vitamin E and/or
selenium and either treated or not treated with hyperbaric
oxygen. A factorial experimental design was used in which
rats were fed four different test diets: 1) a basal diet
deficient in both vitamin E and selenium (the B diet); 2) a
basal diet supplemented with vitamin E (the B+E diet); 3) a
basal diet supplemented with selenium (the B+Se diet) and;
4) the basal diet supplemented with both vitamin E and
selenium (the B+E+Se diet). In each of these dietary groups
half of the rats were treated with hyperbaric oxygen (HBO)
and half were maintained as nonhyperbaric controls (nonHBO).
Hyperbaric oxygen treatment was provided at 3.0 ATA for 1.5
hr/day for 5 days per week to mimic the conditions used in
long term hyperbaric oxygen therapy in humans. After 6
weeks on the diets, all of the animals fed the B diet and
some of the animals fed the B+E+Se diet, both treated and
not treated with HBO were sacrificed for study. The animals
in the remaining dietary-treatment groups were sacrificed
after 17 weeks on the dietary regimins. Specimens of rat
retinal tissues which were embedded in Epon were used for
cytopathological analysis. The significant damage that we
had observed by quantitative histopathological techniques
occured in the central region. For this reason, we decided

35-8

to concentrate on the central region in our ultrastructural studies.

Using the electron microscope, micrographs of the central region of the retina were obtained. These electron micrographs will later be analyzed and quantitated at Meharry Medical College. The following parameters in the central retinal region will be measured:

a) deterioration of the outer segment disk membranes, particularly at the distal end of the photoreceptor cells.

b) fraction of the RPE volume occupied by lipofusion (electron dense bodies).

c) number of phagosomes per unit cross-sectional area of RPE.

d) separations between tips of photoreceptors and apical surface of RPE.

e) migration of photoreceptor cells into the inner retina.

f) accumulation of extracellular debris between the outer segment tips and the RPE.

The following table details the retinal samples used in the study.

TABLE 1 - Retinal Samples

	diet	HBO/nonHBO	number	time on diet
a)	B	HBO	6	6 wks
b)	B	nonHBO	8	6 wks
c)	B+E	HBO	4	17 wks
d)	B+E	nonHBO	4	17 wks
e)	B+Se	HBO	4	17 wks
f)	B+Se	nonHBO	4	17 wks
g)	B+E+Se	HBO	4	17 wks
	B+E+Se	HBO	4	6 wks
h)	B+E+Se	nonHBO	3	17 wks
	B+E+Se	nonHBO	4	6 wks

Total number of rats   45

Originally, we planned to use one eye from each animal, giving a total of 45 blocks. However, 90 blocks (both eyes of each animal) were studied. Each block was trimmed and sections cut from the central retinal region. Each tissue section was stained with uranyl acetate and lead citrate and examined using a Zeiss 109 Electron Microscope. My training

objectives included learning how to use the elecron miscrope
and learning how to process tissues for electron microscopy
and to develope and print the negatives for the micrographs.
Negatives were printed at a final magnification of 12,600.
Each electron micrograph will be quantitatively analyzed (at
Meharry Medical College) using the Zeiss Interactive Digital
Analysis System (ZIDAS). Analysis of variance (ANOVA) will
be performed on all the parametic variables. If ANOVA
indicates a significant difference between the means (at $p <$
0.05) then Duncan's multiple range tests will be used to
compare the individual means for each diet-treatment group.
These stastistical analyses will be performed by W.L. Stone
and Adrienne Hollis.

III. RESULTS

Using a Zeiss Interactive Digital Analysis System (ZIDAS),
preliminary analyses were done on the animals that had been
sacrificed after 6 weeks on their various diets. Table 2
shows the dietary-treatment groups as well as the parameters
measured and the values that were obtained.

TABLE 2- Parameters Measured on Groups on Diet for 6 Weeks

Number Present in Retinal Pigment Epithelial Layer*

Group	Inclusion Bodies	Phagosomes	Mitochondria
B+Se+E noHBO (n=2)	76.97± 4.43	19.60±3.97	119.84±30.1
B+Se+E HBO (n=2)	65.31±18.1	23.17±0.82	133.29±40.1
B noHBO (n=6)	54.42± 6.64	40.44±9.27	179.85±10.5
B + HBO (n=6)	78.85± 7.98	30.11±4.84	169.97±13.3

*These measurements are reported as ±SEM per 100um length of
the central RPE.

ANOVA showed that there were no significant differences in
the number of inclusion bodies or in the number of
phagosomes in any of the dietary-treatment groups. ANOVA
did indicate that diet was significant ($p < 0.030$) in the
number of mitochondria present in the RPE. Duncans Multiple
Range Analysis, showed that no real significance was
observed between the individual means of the
dietary-treatment groups. These preliminary results show
that no major ultrastructrual damage is observed, by
measuring these particular parameters, after 6 weeks of
diet. These results agree with the quantitative
histopathological studies done at this same time point.
Those studies failed to show any major alterations in the

retinal tissues. Katz et al. (9) found an increase in the RPE cell height from rats fed a diet deficient in vitamin E and selenium for 24-25 weeks. Ultrastructural studies showed that the increase in RPE cell height was due to a large accumulation of undigested photoreceptor outer segments (9). We expect to see ultrastructural damage in the animals on the dietary regimens for 17 weeks. The analysis of this data is currently underway.

Figures 1 through 4 are electron micrographs showing the RPE layer in each of the 4 dietary-treatment groups.

IV. RECOMMENDATIONS

Follow-up research will consist of measuring the number of inclusion bodies, phagosomes and mitochondria in the animals on the 17 week dietary regimen. If there are no differences between the B+Se+E groups at 6 and 17 weeks on diet, we may be able to combine the data. This would increase the number of animals in each group and decrease the SEM. The nuclei height as well as the accumulation of extracellular debris between the outer segment tips and the RPE will be measured. Any deterioration of the outer segment disk membranes, particularly at the distal end of the photoreceptor cells will also be noted. In addition, the migration of photoreceptor cells into the inner retina will be examined, and comparisions of the size of the inclusion bodies and phagosomes will be performed.

Figure 1. This is an electron micrograph of the retinal pigment epithelial layer of an animal fed a diet supplemented with both vitamin E and selenium, for 6 weeks. The animal received no hyperbaric oxygen therapy.

Ib- Inclusion body

Mi- Mitochondria

Nu- Nucleus

Ph- Phagosome

Figure 2. This is an electron micrograph of the retinal pigment epithelial layer of an animal fed a diet supplemented with vitamin E and selenium, for 6 weeks. The animal also received hyperbaric oxygen therapy for 4 weeks.

Ib- Inclusion body
Mi- Mitochondria
Nu- Nucleus
Ph- Phagosome

Figure 3. This electron micrograph shows the retinal pigment epithelial layer of an animal fed a diet for 6 weeks, that was deficient in both vitamin and selenium. The animal received no hyperbaric oxygen therapy.

Ib– Inclusion body

Mi– Mitochondria

Nu– Nucleus

Ph– Phagosome

Figure 4. This is an electron micrograph of the retinal pigment epithelial layer of an animal fed a diet deficient in both vitamin E and selenium, for 6 weeks. The animal also received hyperbaric oxygen therapy for 4 weeks.

Ib- Inclusion body

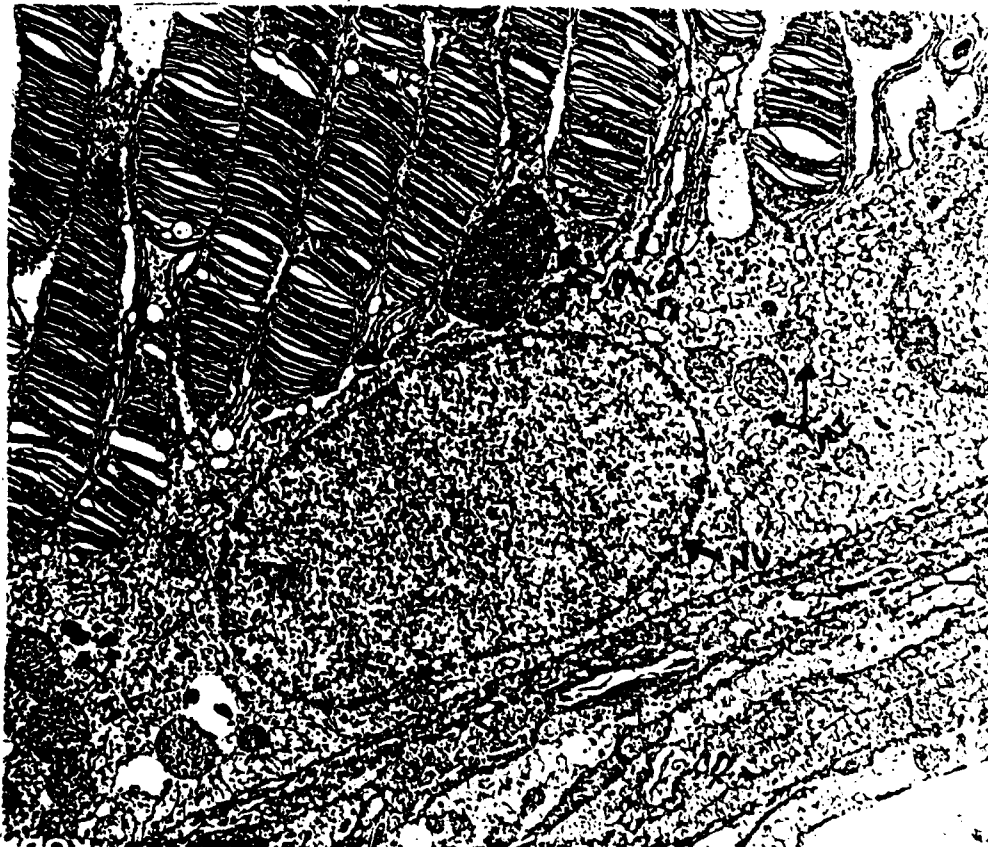Mi- Mitochondria

Nu- Nucleus

Ph- Phagosome

REFERENCES

1. Dickens, F., " The Toxic Effects of Oxygen on Brain
    Metabolism and on Tissue Enzymes. I. Brain
    Metabolism"Biochem J. 40: 145-171, 1946.

2. Taylor, D.W. "The Effects of Vitamin E and of
    Methylene Blue on the Manifestation of Oxygen
    Poisioning in the Rat". J. Physiol., London
    131: 200-206, 1956.

3. Takeuchi, N., Matsumya, K., Takahashi, Y., Higashino,
    K., Tanaka, F., and Katayama, Y., "Thiobarbituric
    Acid Reactive Substances (TBARS) and Lipid Metabolism
    in Alpha-tocopherol Deficient Rats". Experimental
    Gerontology.12: 63-68, 1977.

4. Combs Jr., G.F. and Combs, S.B. The Role of Selenium
    in Nutrition. Academic Press, 1986.

5. Spallhotz, J.E., "Anti-inflammatory Immunologic and
    Carcinostatic Attributes of Selenium in Experimental
    Animals". Adv. Exp. Med. Biol. 135, 43-62.

6. Farnsworth, C.C., Stone, W.L., and Dratz, E.A.,
    "Effects of vitamin E and Selenium Deficiency
    on the Fatty Acid Composition of Rat Retinal
    Tissue". Biochem. Biophys. Acta, 552,
    281-293, 1978.

7. Stone, W.L., Katz, M.L., Lurie, M., Marmor, M.F. and Dratz, E.A. "Effects of Dietary vitamin E and Selenium on Light Damage to the Rat Retina". Photochem. Photobiol., 29, 725-730, 1979.

8. Henderson, R.A., Demoss, D., Howard, G. and Stone, W.L. "Hyperbaric Oxygen Toxicity to the Retina in Antioxidant Deficient Rats". Federation Proceedings, 1985.

9. Katz, M.L., Parker, K.R., Handelman, G.J., Bramel, T.L. and Dratz, E.A. "Effects of Antioxidant Nutrient Deficiency on the Retina and Retinal Pigment Epithelium of Albino Rats: a Light and Electron Microscopic Study". Exp. Eye Res., 34, 339-369.

1987 USAF-UES SUMMER FACULTY RESEARCH PROGRAM/

GRADUATE STUDENT SUMMER SUPPORT PROGRAM

Sponsored by the

AIR FORCE OFFICE OF SCIENTIFIC RESEARCH

Conducted by the

Universal Energy Systems, Inc.

FINAL REPORT

A Comparative Study of Differing Vortex Structures

Arising in Unsteady Separated Flows

Prepared by:	Stephen A. Huyer
Academic Rank:	Graduate Student, Masters
Department and	Aerospace Engineering Sciences
University:	University of Colorado
Research Location:	Frank J. Seiler Research Laboratories
	USAF Academy
	Colorado Springs, CO
USAF Researcher:	Dr. Michael C. Robinson
Date:	16 September 1987
Contract No:	F49620-85-C-0013

A Comparative Study of Differing Vortex Structures

Arising in Unsteady Separated Flows

by

Stephen A. Huyer

ABSTRACT

The vortex structures arising in two separate unsteady separated
flow cases were examined in detail. The flowfields resulting from the
deployment of a periodically deforming leading edge (PDLE) and an
oscillating flat plate were studied and compared. The PDLE produced two
separate vortex structures during each cycle. It was found through flow
visualization and hot-wire anemometry that these two structures exhibited
different behavior. The primary vortex was characterized by low,
constant velocities within the vortex, increasing threefold to 120%
freestream values in a space of 3 mm. The second vortex exhibited a more
even vortex rotation rate. The vortex structures produced by an
oscillating flat plate were also examined. It was found that a reduced
frequency of 3 yielded a more cohesive vortex compared to that produced
by a reduced frequency of 1. The structures produced by PDLE deployment
were also considerably weaker than those produced by an oscillating flat
plate.

ACKOWLEDGEMENTS

I wish to thank those at Frank J. Seiler Research Laboratories and the Air Force Office of Scientific Research for sponsorship of this research. Also, thanks to Universal Energy Systems for the opportunity to demonstrate my ability in the area of unsteady separated flows.

I would especially like to thank Chris Kedzie for his help in updating the software needed in acquiring the pressure data and Capt. Eric Stephen for familiarizing me with the assorted equipment. Of course, the assistance of Dr. Michael Robinson and Professor Marvin Luttges was invaluable. I have learned more about unsteady flows and experimentation in general than I have in all my college fluid classes combined.

I.) INTRODUCTION

Currently, there is numerous research underway concerned with understanding the vortex development process associated with unsteady separated flows. When applied to airfoils, these flows are characterized by highly transient lift, drag, and moment coefficients. When the vortex is initiated and present over the upper surface of an airfoil, relatively high lift coefficients are observed (as great as four to five times steady state counterparts). As the vortex is shed off the trailing edge, a highly negative moment coefficient results. By understanding and controlling these flows, it may be possible to exploit them and create a new generation of super maneuverable aircraft.

Frank J. Seiler Research Laboratories, located at the United States Air Force Academy, are particularly suited for research concerning low speed aerodynamics. The facilities were particularly suited for acquiring both flow visualization data and hot-wire anemometry data. Through a series of data reduction software programs, it was possible to construct some interesting and enlightening graphs. These graphs yielded vortex velocity profiles along with corresponding variance levels. For discussion purposes, the variance was taken as a rough correlate to vorticity distribution. This is valid since a vortex is a transitory flow structure exhibiting both laminar and turbulent characteristics. The variance levels, which are characteristic to turbulent flow studies, may be indicative of the vorticity present in the structure. Additionally, a Fast Fourier Transform analysis was performed providing spectral data for each of the flow cases. My research interests are mainly concerned with the understanding of unsteady separated flows. I have been a research assistant at the University of Colorado for one year. In that time, I have authored one paper which was presented at the

AIAA 19 th Fluid Dynamics, Plasma Dynamics and Lasers Conference and have co-authored one ocher paper which was presented at the same conference.

II.) OBJECTIVES OF RESEARCH EFFORT

For many years, numerous researchers have investigated the flows produced by unsteady, forced separation of the boundary layer. Examples include pitching or oscillating airfoils, periodic deployment of control surfaces or ramps, surface air pulse injection, periodically deforming airfoil surfaces, accelerating flows, among others. Although the unsteady motion histories may differ from case to case, they possess at least one common characteristic: the accumulation of vorticity which in turn produces vortex structures under certain test conditions. While each example may generate vortex structures, it is obvious that the development and character of each individual vortex structure must be different. A comparative study concerning the development of these individual vortex structures will doubtlessly be helpful in understanding the development of these flows and the mechanisms of vorticity from which they are produced. To that end, the vortex structures produced by a periodically deforming leading edge (PDLE) and an oscillating flat plate will be compared and contrasted. Additionally, a set of experimental measurement techniques will be used to quantitatively define the vortex structure. While none of the measurement techniques is necessarily novel in their approach, it is hoped that most researchers will gain helpful insight to at least some of the approaches set forth.

III. METHODS

An NACA 0015 full span airfoil model with 15.24 cm chord length was
modified by adding a movable fence-type spoiler at the 12.5% c position.
In order to simulate the PDLE, a thin latex membrane was attached to the
upper surface of the spoiler, wrapped around the leading edge, then
attached to the bottom of the airfoil. A 24 volt D.C. motor mounted on
the airfoil endplate drove the PDLE up and down sinusoidally from a
position flush with the airfoil surface to an effective maximum thickness
of 19.17% c. When fully deployed, the PDLE created a backward step 6.35
mm in height. A freestream velocity of 3.05 m/sec was used resulting in
a Reynolds number of 25,000. A reduced frequency of 2.0 based on airfoil
chord length was studied with the airfoil angle of attack set at 15°.

An flat plate with a 15.24 cm chord length was oscillated about the
25% c axis using a scotch yoke mechanism. The mean angle of attack was
set at 15° with oscillation amplitude of 10°. A 24 volt D.C. motor drove
the airfoil up and down sinusoidally at different frequencies
corresponding to reduced frequency values (K) of 1 and 3. The
corresponding freestream velocity was set at 3.05 m/sec for K = 1 and
1.502 for K = 3.

This paper will be outlined as follows. For each experimental case,
(1) a brief theoretical discussion will be provided followed by (2) a
summary and discussion of the experimental results. Afterward, a
comparative analysis will be conducted.

IV PERIODICALLY DEFORMING LEADING EDGE

(1) During PDLE deployment, a multiple vortex environment will result
under certain test conditions. For the range of test variables used by
Huyer and Luttges , Two main vortex structures were formed. The primary

36-6

vortex forms as a result of both vorticity production due to the accelerating motion of the PDLE and accumulating vorticity in the region immediately downstream of the PDLE. This vortex formed at approximately maximum PDLE deployment. Under static conditions, vorticity in the boundary layer has a tendency to move upstream due to decreasing velocities in the boundary layer which produce increasing pressures. The vorticity, however, will propagate downstream through the boundary layer and shed into the airfoil wake due to the energy supplied by the free potential flow. Inserting the PDLE into the the flow creates a rearward step which forces the boundary layer to separate. This forced separation creates an adverse pressure gradient allowing vorticity to accumulate at specific spatial locations above the airfoil surface. The vorticity accumulated in the region immediately downstream of the PDLE interacts with vorticity coming off the resulting in the formation of the primary vortex.

The second vortex results due to vorticity production over the surface of the PDLE as it is being retracted. This vorticity accumulates in a region immediately downstream of the PDLE. It is possible that this accumulation is forced by the pressure gradients created by the primary vortex.

(2) Hot-wire data provided velocity profiles with corresponding variance levels for PDLE deployment at two chord locations (20.83% c and 50% c). A test case of K = 2 and 15° was examined. Fig. 1 shows the flow visualization photo along with corresponding velocity profiles and variance levels at both maximum and minimum PDLE deployment. At these points in the cycle, it was possible to determine the character of the primary and second vortex. In the first photo, the arrow located at 20.83% c corresponds to the primary vortex with the other arrow pointed
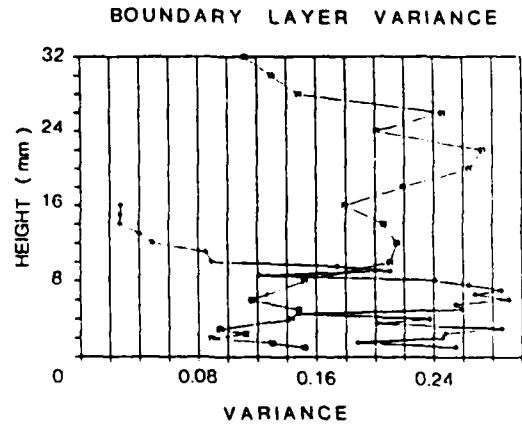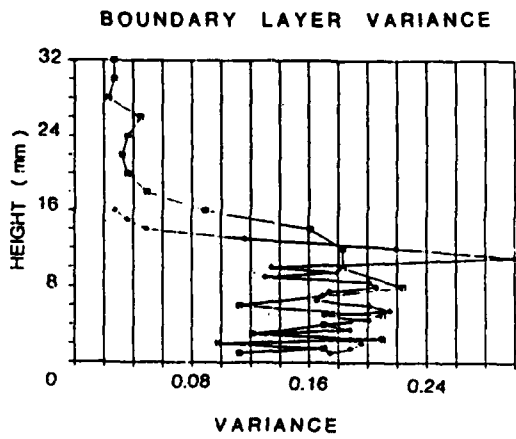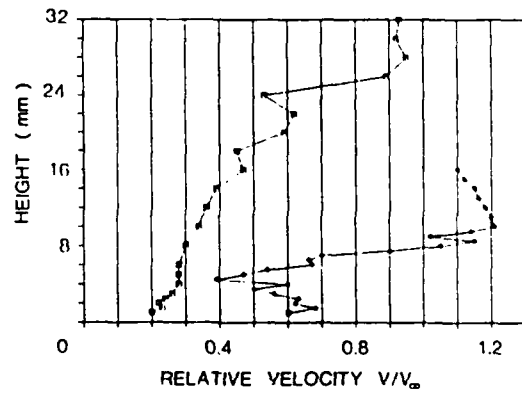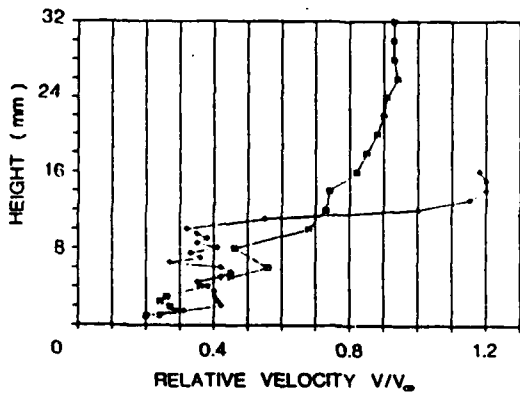
Fig. 1) Flow visualization photo along with corresponding velocity profiles and variance levels for a periodically deforming leading edge (PDLE). V inf = 3.05 m/sec, K = 2.0, 15° angle of attack. The arrows correspond to chord locations of 20.83% c and 50% c. ◆———◆ :20.83% c, ◻———◻ : 50% c.

at the second vortex. In the second photo the reverse is true.

C = 20.83% c

In the first photo, the presence of a vortex structure can clearly be seen from the flow visualization photo and corresponding velocity profile. The velocities in the region between 1-10 mm are relatively constant at 40% freestream. Within a distance of 3 mm, these velocities increase threefold to 120% freestream. The variance plots demonstrate this phenomenon as well. The variance remains relatively constant in the region between 1-10 mm at 19%. At 11 mm there appears a sharp in crease in variance. These factors indicate the strength of the vortex and associated vorticity are along the outer fringes of the vortex.

Although not shown, the velocities and variance plots demonstrate definite spatial shifts in vorticity as the vortex convects downstream. As the cycle increases 12.5%, the variance appears to be concentrated in the region between 8-12 mm with a decrease in the region between 1-8 mm to 14% freestream. as the cycle progresses, the variance in the lower region decreases further averaging 10%. Prior to the development of the second vortex, the variance levels demonstrate a downward shift in concentration focused at 6 mm.

The second photo shows the second vortex centered at 20.83% c. The velocity profile indicates that this vortex is different in character compared to the primary vortex. The second vortex appears to exhibit a more even rotation rate with velocities at the outer edge of the vortex reaching 122% freestream values. The variance levels are more evenly distributed in the region between 1-8 mm implying a more even distribution of vorticity throughout the vortex. As the cycle progresses, there are again spatial shifts in variance corresponding to

36-9

the convection of the second vortex and accumulation of vorticity into the primary vortex.

C = 50% c

Measurements taken at midchord show the velocities and variance levels associated with a developed vortex. Rather than provide a detailed analysis as was performed at 20.83% c, a summary of the differences in both velocities and variance levels will be given followed by a brief discussion.

Both the velocities and variance levels are distributed over a larger region (approximately twofold). Additionally, the velocities are significantly less with maximum vortex velocities approaching 95% freestream values. This indicates that the vortex grows and becomes more diffuse as it convects downstream. The vorticity is also more evenly distributed throughout the vortex and appears to be less on average when compared to the vortex at 20.83% c. This indicates the vortex accumulates little if any additional vorticity as it convects downstream.

A Fourier spectrum analysis was performed for the hot-wire signals at 20.83% c and midchord and are shown in Fig. 2. Relative amplitude is plotted as a function of height for the primary and secondary frequencies. The frequency of 13.7 Hz is approximately the same as the forcing function frequency. Notice in the region between 0-4 mm the 26.4 Hz frequency dominates whereas in the rest of the region, the primary frequency dominates. It appears that in this area proximal to the airfoil surface, reverse flows may occur. These reverse flows are an indication of vorticity accumulation in the region behind the PDLE. Also, the shape of the curves are more bell shaped. The peak value at 9

FREQUENCY AMPLITUDE vs. HEIGHT

PDLE, 20.83% c

RELATIVE AMPLITUDE

HEIGHT (mm)

□   13.7 Hz   +   26.4 Hz

FREQUENCY AMPLITUDE vs. HEIGHT

PDLE, 50% c

RELATIVE AMPLITUDE

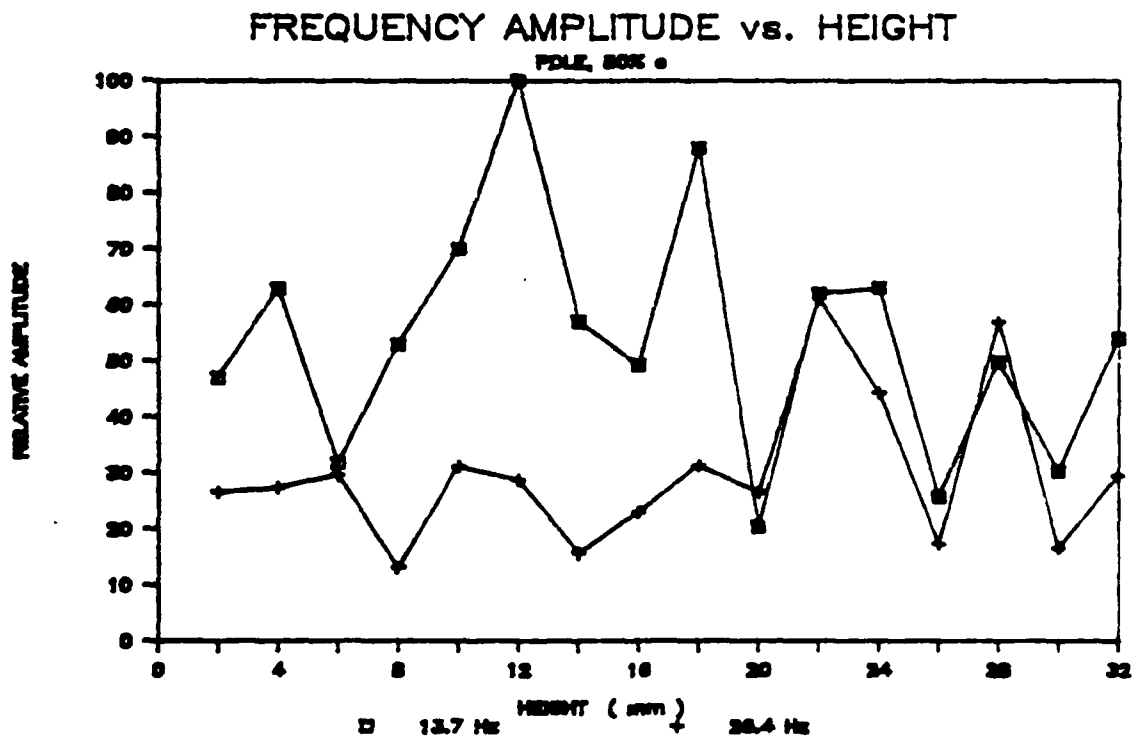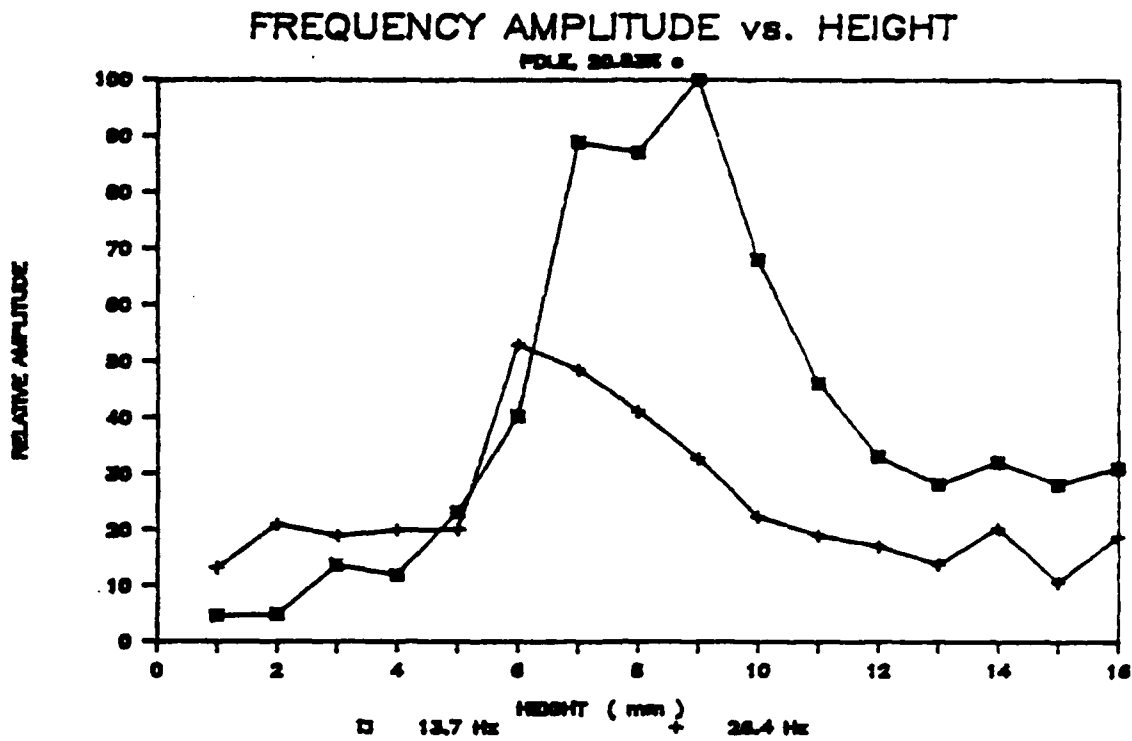HEIGHT (mm)

□   13.7 Hz   +   26.4 Hz

Fig. 2) Relative frequency amplitude as a function of height for a PDLE
for the primary (13.7 Hz) and secondary (26.4 Hz) frequencies.   The
overall absolute maximum amplitude for all frequencies and heights is
defined as 100%.   The top figure corresponds to a chord location of 20.83%
c and the lower figure corresponds to a chord location of 50% c.

mm may represent the approximate center of the flow disturbances created
by PDLE deployment.

At midchord, the shapes of the curves are much different. Lost is
the bell curve shape and a more random distribution is observed. Also,
in the region near the airfoil surface, the primary frequency dominates.
From 20-32 mm, the primary and secondary frequencies appear very close in
magnitude. All this information suggests a more turbulent flow regime.

V OSCILLATING FLAT PLATE

(1) Robinson et al. and Luttges et al. have provided much documentation
concerning the unsteady flows produced by oscillating flat plates and
airfoils. It was found that any change in the input test parameters
altered the flow fields significantly. The structures produced were
found to be repeatable, however. In general, the flow field was
characterized by the initiation and growth of a leading edge vortex
structure, interaction between the vortex and the upper surface of the
airfoil, and the development of a trailing edge vortex. these flow
patterns result as long as the static stall angle was exceeded at some
point during the cycle. The production of vorticity results during the
up-stroke of the oscillation cycle. As the airfoil increases in angle,
larger velocity gradients are created producing vorticity. As the static
stall angle is exceeded, the boundary layer begins to separate resulting
in adverse pressure gradients. This allows vorticity to be accumulated,
generally in the region near the leading edge. The angle at which the
leading edge vortex is initiated is dependent upon the input parameters
such as reduced frequency and oscillation amplitude. As the leading edge
vortex convects downstream, it may accumulate additional vorticity as
long as the airfoil is pitched upward. As the vortex convects

downstream, vortex-surface, vortex-vortex, and other interactions result in increased diffusion of the vortex structure. A trailing edge vortex resulting from accumulated vorticity from the lower surface of the airfoil ensues creating a separated region near the trailing edge of the airfoil.

(2) Experimental studies were conducted for an oscillating flat plate using reduced frequency values of 1 and 3. In both cases, the mean angle was set at 15° with an oscillation amplitude of 10°. Fig. 3 shows the initial vortex for reduced frequency values of 1 and 3 respectively along with velocity profiles and corresponding variance levels. Although there is definite phase dependence concerning the angle at which the vortex forms, in both cases, there appeared definite spatial shifts in the variance levels as the vortex was first initiated, then convected downstream. In general, as long as the boundary layer remained attached to the flat plate, there was little sign of variance. As the vortex is initiated and the front of the vortex is measured by the hot-wire probe, there are low levels of variance in the region below the vortex and above the vortex. The variance is concentrated in the vortex itself. As the vortex convects downstream, the spatial shifts in variance help define the distribution of vorticity throughout. While this measurement technique does not give a defined magnitude of vorticity, the distribution may be found and the magnitude may be computed using other methods that will be discussed later.

As can be seen in Fig. 3, the vortex structures formed for $K = 1$ and 3 are markedly different. For $K = 1$, the vortex is centered at 25% c when the flat plate is approximately at maximum angle of attack. The
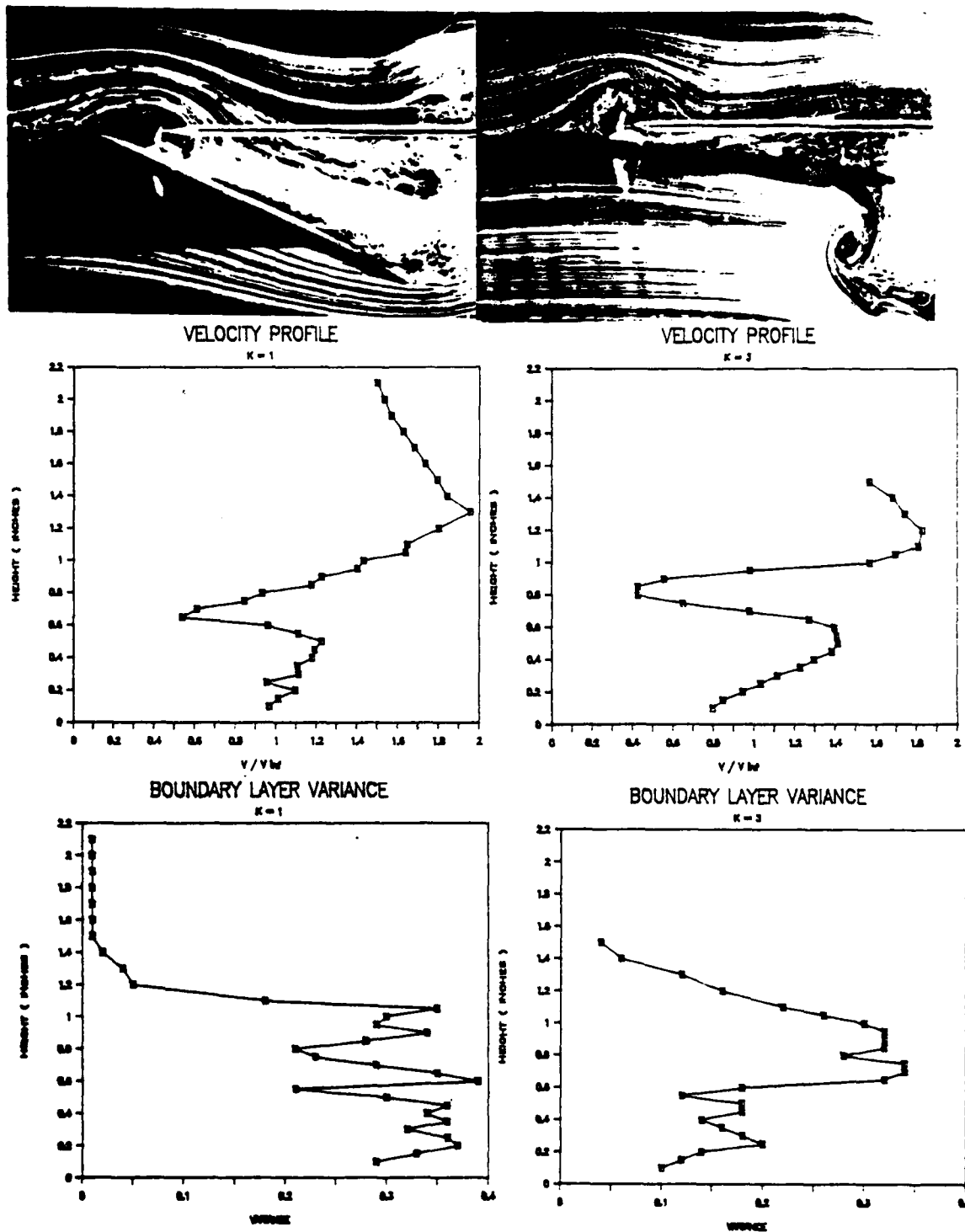
36-13

Fig. 3) Flow visualization photos along with corresponding velocity profiles and variance levels for an oscillating flat plate. 15° mean angle with oscillation amplitude of 10°. The figure on the left corresponds to V inf = 3.05 m/sec and K = 1, the second figure corresponds to V inf = 1.502 m/sec and K = 3.

36-14

velocity profile shows peak velocities approaching 200% freestream values at 1.3" above the airfoil surface and the vortex appears to be centered at 0.6". The profile indicates an approximate constant rotation rate throughout the vortex although the profile is not "smooth." The variance levels average approximately 35% freestream values in the region between 0.1"-1.0" dropping off rapidly as one ventures outside the vortex. As inferred by the variance plots, it appears that the vorticity is distributed approximately evenly throughout the vortex.

In contrast, the vortex formed for K = 3 appears to be centered at 25% c when the flat plate is at approximately 10°. The velocity profile shows peak velocities reaching 180% freestream values. The shape of the velocity profile, however, is much smoother by comparison and demonstrates a more even rotation rate. The center of the vortex is situated at 0.8". The size of this vortex, however, appears to be smaller by comparison. The variance levels indicate a different distribution of vorticity. The vorticity appears to be concentrated at the center of the vortex as opposed to being evenly distributed throughout the vortex. This is quite different from the dynamic stall vortex formed at K = 1.

A Fourier spectrum analysis was also performed. Fig. 4 shows amplitude as a function of height for the primary and secondary frequencies for K = 1 and 3. Again the primary frequency is the forcing function frequency with the secondary frequency being the second harmonic of the primary frequency. The absolute maximum value is defined as 100% and for both cases, this absolute maximum occurs at the primary frequency. The chord location is 25% c.

In general, the primary frequency dominates throughout the boundary layer for K = 1. The exception to this, however, is between 0.9" and

FREQUENCY AMPLITUDE vs. HEIGHT
FLAT PLATE, K = 1.0

□ 7.8 Hz   HEIGHT (inches)   + 13.7 Hz

FREQUENCY AMPLITUDE vs. HEIGHT
FLAT PLATE, K = 3.0
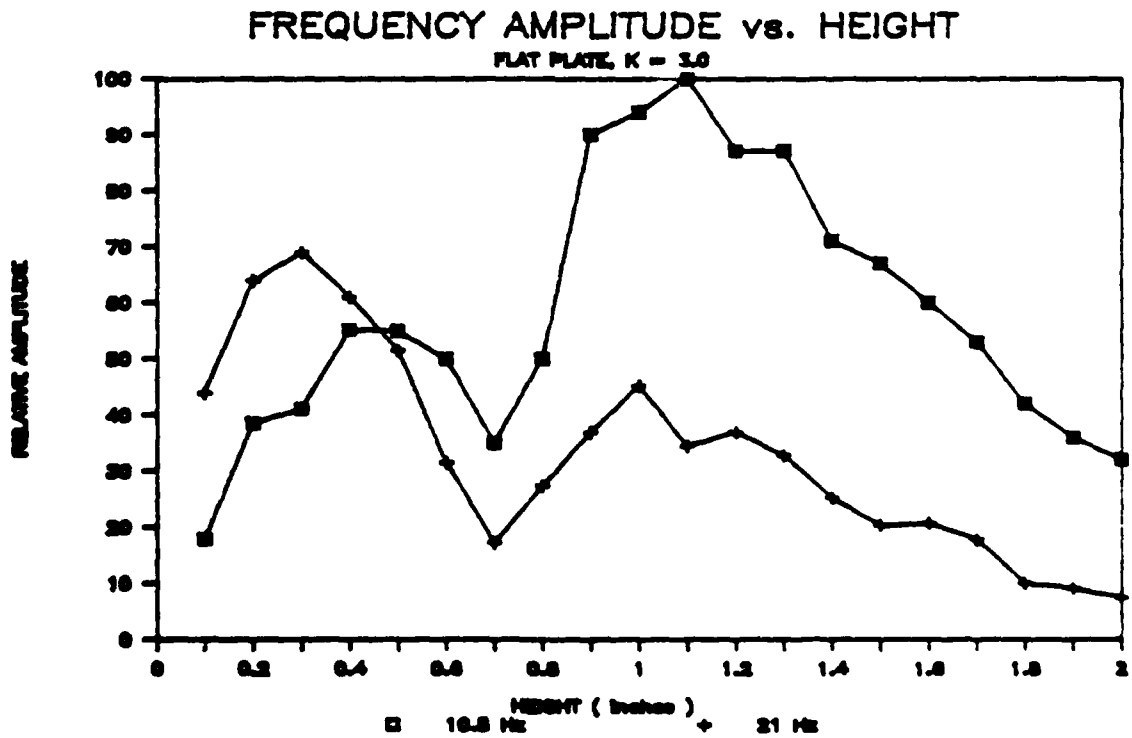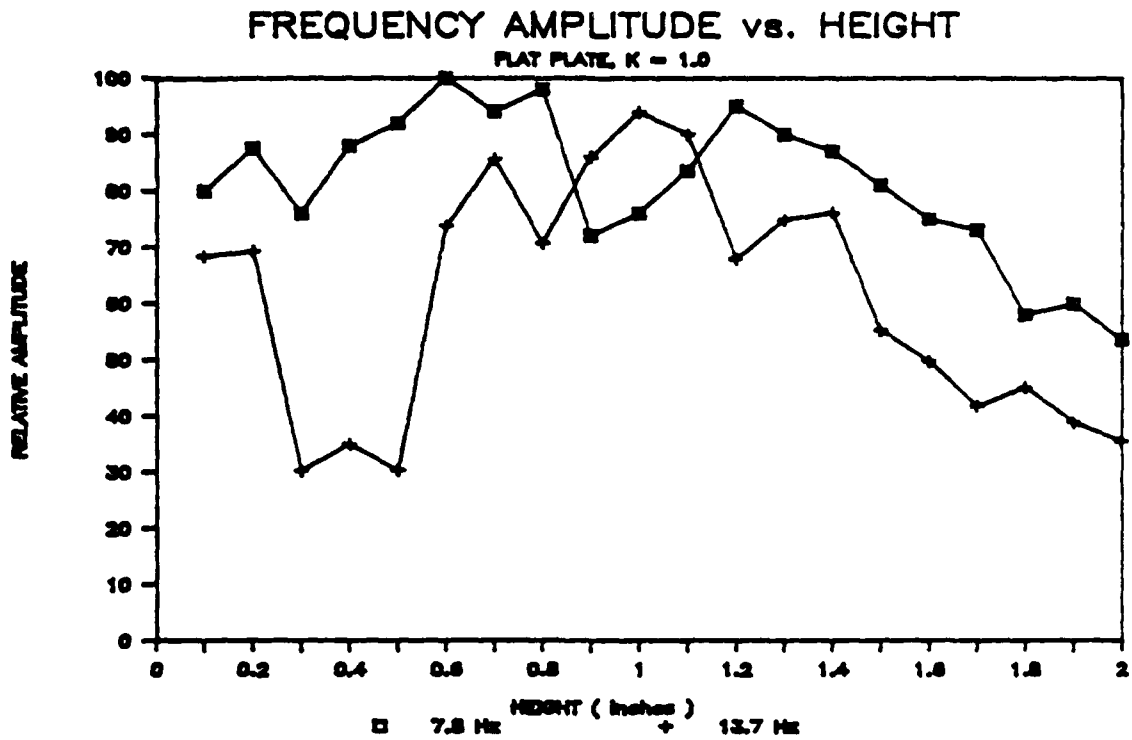
□ 10.5 Hz   HEIGHT (inches)   + 21 Hz

Fig. 4) Same as Fig. 2 except for oscillating flat plate. The top figure refers to a K value of 1 with frequencies of 7.8 Hz and 13.7 Hz, the bottom figure refers to a K value of 3 with frequencies of 10.5 Hz and 21 Hz.

1.1" above the surface of the airfoil where the secondary frequency dominates. Also, the primary frequency does not exhibit a bell curve type of shape but the secondary frequency vaguely resembles one.

The plots for K = 3 are much different, however. In the region between 0.1" and 0.5", the secondary frequency noticeably dominates. This may indicate the presence of reverse flows close to the surface of the flat plate. Additionally, the primary frequency does resemble a bell curve shape. These two factors suggest a more cohesive, less turbulent vortex for the test case of K = 3.

VI DISCUSSION AND CONCLUSIONS

Flow visualization and hot-wire measurements demonstrated significant differences in flow field behavior not only between the flow structures formed due to PDLE deployment and an oscillating flat plate but between the different input parameters for each case. Two main vortex structures were formed during PDLE deployment. The velocities of the primary vortex exhibited step function type of behavior whereas the second vortex demonstrated a more uniform rotation rate. This was shown by both the velocity profiles and variance levels.

Similarly, the dynamic stall vortex associated with the test parameter, K, were different for the two cases studied. The two vortex structures were initiated and developed at different points in the cycle. The velocities associated with K = 1 showed rather disjointed velocity changes as opposed to smooth velocity changes for K = 3. Additionally, the variance levels demonstrated different vorticity distributions for the two vortices.

The vortex structures that formed due to PDLE deployment and the

oscillating flat plate are also different. The vortex structures associated with PDLE deployment are much less energetic by comparison. They are much smaller structures and they transition to turbulence more rapidly. This seems to indicate that less vorticity is produced and/or accumulated into a defined vortex structure.

VII RECOMMENDATIONS

The research over the summer was primarily engaged with quantitatively describing the flow structures arising in unsteady separated flows. A comparative analysis was then made to demonstrate the effectiveness of the measurement techniques used. While I quantitatively described the vorticity distribution using variance levels and showed that a frequency spectrum analysis could be used to determine the cohesiveness of a vortex structure, there was no technique used to actually predict the magnitude of vorticity present in the flow. If this is known, a complete picture may be provided.

There is, however, a way to estimate the magnitude of vorticity in the boundary layer. Previous studies have used pressure transducers mounted on the surface of the airfoil to compute the pressure distribution about the airfoil. If this is known, the lift may readily be computed. Once the lift is known, the circulation about the airfoil may be computed directly. Finally, there is an integral relation relating the circulation to the vorticity vector. Hence, the magnitude of vorticity may readily be computed providing a complete picture to quantitatively describe the resulting unsteady flow fields.

36-18

REFERENCES

Huyer, S.A., Luttges, M.W., "Unsteady Separated Flows Driven by Periodic Leading Edge Deformation," AIAA 19th Fluid Dynamics, Plasma Dynamics and Lasers Conference, Honolulu, HA, Paper No. 87-1234, June 8-10, 1987.

Luttges, M.W., Robinson, M.C., Kennedy, D.A., "Control of Unsteady Separated Flow Structures on Airfoils," AIAA Shear Flow Control Conference, Boulder, CO, Paper No. 85-0531, March, 1985.

Robinson, M.C., Luttges, M.W., "Unsteady Separated Flow: Forced and Common Vorticity About Oscillating Airfoils," Workshop on Unsteady Separated Flows, United States Air Force Academy, August 10-11, 1983.

Reynolds, W.C., Carr, L.W., "Review of Unsteady, Driven, Separated Flows," AIAA Shear Flow Conference, Boulder, CO, Paper No. 85-0556, March 1985.

Reynolds, A.J., Turbulent Flows in Engineering, London, U.K., John Wiley and Sons, 1974.

Taylor, C., Morgan, K., Brebbia, C.A., Numerical Methods in Laminar and Turbulent Flow, New York, NY, John Wiley and Sons, 1978.

1987 USAF-UES SUMMER FACULTY RESEARCH PROGRAM/

GRADUATE STUDENT SUMMER SUPPORT PROGRAM

Sponsored by the

AIR FORCE OFFICE OF SCIENTIFIC RESEARCH

Conducted by the

Universal Energy Systems, Inc.

FINAL REPORT

Perturbed Functional Iteration Applied to the

Navier-Stokes Equations

Prepared by:	David L. James
Academic Rank:	Graduate Student / Assistant
Department and	Mathematics Department
University:	Eastern Illinois University
Research Location:	Arnold Engineering Development Center Arnold AFS, TN 37389
USAF Researcher:	Dr. G. Kyle Cooper
Date:	13 Aug 87
Contract No:	F49620-85-C-0013

Perturbed Functional Iteration Applied to the

Navier-Stokes Equations

by

David L. James

ABSTRACT

The Navier-Stokes partial differential equations were written as a set of averaged finite difference equations. Of the methods available, Perturbed Functional Iteration was chosen to solve the Navier-Stokes equations. The Perturbed Functional Iteration scheme (PFIS) was applied to both a two dimensional problem, both implicitly and explicitly; and a three dimensional problem, explicitly. PFIS quickly gave accurate results in the test cases.

Acknowledgements

I would like to thank the Air Force Systems Command and the Air Force
Office of Scientific Research for sponsorship of this research. I would
also like to thank Universal Energy Systems for the support given to me
for this project.

I was able to accomplish a great deal because of the help afforded me at
AEDC. Dr. Kyle Cooper helped me to find the mistakes in my typing and
Mike Stokes helped me to get on and use the Apollo minicomputer effectively.
The CFD group at Sverdrup was great; they made my stay very enjoyable.
Lastly, I would like to thank Dr. Suhrit Dey for his encouragement and
guidance in my endeavor.

I.   INTRODUCTION:

An accurate, fast, and stable numerical method is being sought to solve
the Navier-Stokes equations as they relate to fluid dynamics; specifically,
computational fluid dynamics. The Perturbed Functional Iteration scheme
(PFIS) is such a method.

The Air Force, by its very nature, and its subcontractors at Arnold
Engineering Development Center, are interested in computational fluid
dynamics and accurate mathematical models. Finding a method which would
prove to be fast, accurate, stable, and easy to implement would add
greatly to the realm of computational fluid dynamics.

My research interests lie in the area of developing or modifying computer
methods that are fast, as well as accurate and stable. If this can be
accomplished, there will be a method that yields an accurate answer and
takes considerably less time. PFIS is such a scheme, and vectorized PFIS
executes at a high speed.

II.   OBJECTIVES OF THE RESEARCH EFFORT:

Perturbed Functional Iteration has been shown to be super-quadratic in
convergence (Dey). Dr. Cooper of Sverdrup Technologies and Dr. Dey of
Eastern Illinois University had been working to apply Perturbed Functional
Iteration to the Navier-Stokes equations. The initial objectives were
to apply PFIS to the two dimensional model of the Navier-Stokes equations,
with both implicit and explicit codes.

My assignment as a participant in the 1987 Graduate Student Summer Support Program was to take the two dimensional code and attempt to increase the speed from the code using structured programming techniques. I was also to attempt to get a three dimensional version of the code up and running using PFIS. These objectives have been accomplished.

III.

Perturbed Functional Iteration was invented by Dr. Suhrit Dey in 1976. It is a modification of Picard's Method. Picard's Method tells us that if we have an "answer" to an equation, we can find a better answer by putting the answer we already have back into the equation. At the kth step

$$x \qquad \qquad \qquad \qquad 1$$

where $g(x)$ is a function of x having no x^1 terms in it. PFIS was based on the idea that this was too slow and it could diverge in certain cases. PFIS adds a perturbation to get to the answer much quicker. At the kth step of PFIS

$$x^{k+1} = g(x^k) + \omega^k \qquad \qquad 2$$

ω is the perturbation added to $g(x)$ and $g(x)$ is as above. The stopping condition is for the perturbation to be "sufficiently small," which is dependent on the problem being solved. To find ω we must evaluate g at our "answer," evaluate g again at the answer we just obtained, evaluate the derivative of g at our obtained answer, then perform the calculation

$$\omega \qquad \qquad \qquad \qquad 3$$

To get our next "answer" calculate

$$\alpha' - \beta'' + \gamma''$$

as before. This method was applied to the velocity equations of Navier-Stokes. In the two dimensional case the equations are:

$$\frac{\partial u}{\partial t} + u\frac{\partial u}{\partial x} + v\frac{\partial u}{\partial y} = \cdots$$

and,

$$\frac{\partial v}{\partial t} + u\frac{\partial v}{\partial x} + v\frac{\partial v}{\partial y} = \cdots$$

as a test case. The solutions are:

$$u = \frac{\cdots}{\cdots}$$

$$v = \frac{1 + x + y^2}{1 + t}$$
8.

The solution is dependent upon where the point is in the plane. In the three dimensional case, the equations are:

$$\frac{\partial u}{\partial t} + u\frac{\partial u}{\partial x} + v\frac{\partial u}{\partial y} + w\frac{\partial u}{\partial z} = \cdots$$

$$\frac{\partial v}{\partial t} + u\frac{\partial v}{\partial x} + v\frac{\partial v}{\partial y} + w\frac{\partial v}{\partial z} = \cdots$$

$$\frac{\partial w}{\partial t} + u\frac{\partial w}{\partial x} + \cdots$$

The solutions are:

The two dimensional codes were run on the Cray, a CDC 7600 mainframe, and an Apollo DN580 minicomputer. The three dimensional code was run on the Cray and the Apollo. The codes all gave the same results within machine accuracy. A list of times is given in the table below:

	2D Explicit	2D Implicit	3D Explicit
Cray	2.4919	2.1889	2.9967
CDC 7600	635.867	537.19H	807.912
Apollo DN580	698.696	578.217	803.144

Table 1: CPU execution times for PFIS.
(10 X 10 Cases)
NOTE: All times are in seconds.

Using a percentage comparison for speed for the same code on different machines, the Cray was two orders of magnitude faster for all codes. In comparison of the 2D implicit and 2D explicit codes, the percentage increase of implicit over explicit was from approximately ten to twenty percent. In terms of coding and execution times combined, the explicit code is more easily coded, so that the increased execution time is negligible.

IV. RECOMMENDATIONS:

Vectorized PFIS is a relatively simple method to use with a relatively high order of accuracy. The worst percentage error that was calculated for the model used was approximately 8% with an average percentage error of approximately 2%. The method does require that a derivative be taken,

but, in contrast to Newton's Method, no Jacobian must be calculated and inverted. This is an excellent reason for implementing the method. The three dimensional explicit code was running very well, but an implicit code has not as yet been written. I would recommend that such a code be written to compare with the explicit code.

Also, different test cases should be run so that PFIS can be compared to other methods (i.e. Newton's Method) now used to solve the Navier-Stokes Equations. I believe this would be an excellent way to show how good PFIS really is.

REFERENCES

Dey, S.K., Numerical Solution of a System of Nonlinear Equations by Perturbations, Demonstratio Mathematica 9, 1976, pp. 691-705.

Dey, S.K., Numerical Analysis class notes, Spring Semester, 1987.

Dey, S.K., PFIS Vectorized for the Three Dimensional Problem, 1987.

1987 USAF-UES SUMMER FACULTY RESEARCH PROGRAM/

GRADUATE STUDENT SUMMER SUPPORT PROGRAM

Sponsored by the

AIR FORCE OFFICE OF SCIENTIFIC RESEARCH

Conducted by the

Universal Energy Systems, Inc.

<u>FINAL REPORT</u>

<u>AN OPTICAL SENSOR SYSTEM FOR MONITORING STRUCTURAL DYNAMICS</u>

<u>WITH APPLICATIONS TO SYSTEM IDENTIFICATION</u>

Prepared by: George Henry James III

Academic Rank: Ph.D. Student

Department and   Aerospace Engineering Department

  University: Texas A&M University

Research Location: Air Force Astronautics Laboratory
                    Edwards AFB, CA 93523-5000

USAF Researcher: Dr. Alok Das

Date: 28 Aug 87

Contract No: F49620-85-C-0013

AN OPTICAL SENSOR SYSTEM FOR MONITORING STRUCTURAL DYNAMICS

WITH APPLICATIONS TO SYSTEM IDENTIFICATION

by

George Henry James III

ABSTRACT

A unique optical sensor system using video cameras, digital processing, and photogrammetric triangulation has been shown to be feasible for use in monitoring structural dynamics. The system can determine natural frequencies, mode shapes, and displacement time histories. The major advantages of the system were the possibility of non-contact measurement, ease of marker application, simple operation and upkeep, the ability to cover a large area, and exellent large amplitude and low frequency response. The major disadvantages of the system were low spatial resolution and long processing times.

Using the ERA algorithm, the first five natural frequencies of the 5 ft. by 5 ft. aluminum grid test structure were calculated in a high coverage mode, in a high resolution mode, and in a 2D mode. The first three mode shapes were calculated using ERA with the high coverage data. Recommendations for improvements in the system, future research, and possible uses are provided.

ACKOWLEDGMENTS

I wish to thank the Air Force Systems Command the Air Force Office of Scientific Research, and the Air Force Astronautics Laboratory for the sponsorship of this work. Universal Energy Systems is to be commended for their administration of the program.

The support and direction of Dr. Alok Das was greatly appreciated. The work would not have been successful without the help of Lt. Waid Schlaegel, Lt. Tim Strange, Lt. John Ward, and Angel Cruz. Dr. Gurbux Alag a UES-SFRP fellow also provided much enlightenment. I also wish to thank Dr. John Junkins of Texas A&M University for providing the optical sensor system and the necessary training for its operation, Dr. Jer-Nan Juang of NASA-Langley Research center for providing the ERA algorithm, and Motion Analysis Corporation for providing a 60 Hz. video camera.

Introduction

Large flexible structures envisioned for space based operation will rely heavily on analytical modelling. The size, cost, and operating environment of these structures will prohibit extensive full scale testing until final deployment. Also, the control systems of large space structures will interact strongly with the dynamics of the structure and will necessarily be based on an analytical model which accounts for the structural dynamics. Additionally, these analytical structural models will not be able to account for every effect such as flawed structural members, joint damping, material inconsistencies, or material degradation. Structural identification methods will be used to upgrade an analytical model to match the known experimental response of a structure or a representative sub-structure [1].

The Interdisiplinary Space Technology Branch of the Air Force Astronautics Laboratory is interested in developing structural identification methods for use with large space structures. Possible applications of these structures include large deployable radar antennas or directed energy weapon platforms. These applications will also require precise shape control of the surface and need an accurate structural model.

My Ph.D. level research currently focuses on three

aspects of structural identification. The first aspect is data acquisition. I am currently developing a non-contact optical method for monitoring structural dynamics. Secondly, I am working with the Eigensystem Realization Algorithm (ERA) [2-8] to extract modal frequencies and mode shapes from structural dynamics data. And finally I am analyzing the structural identification method of Creamer and Junkins [9,10].

Objectives of the Research Effort

The initial portion of my work with the 1987 Graduate Student Summer Support Program was to be experimental in nature. A non-contact video based system [11] provided by Dr. John Junkins of Texas A&M University was to be used to monitor the results of several inputs to a test structure. These inputs include impulse loading, single frequency resonance, and quasi-random excitation. Techniques for marker application to the structure, synchronization with accelerometers, and stereo measurements of 3D motion [12,13,14] were to be developed in this phase of the work.

The next phase of my work was to extract the necessary dynamical information from the test data [15-18]. This dynamical information included natural frequencies, mode shapes, and frequency response functions. Software tools such as MATRIX$_x$ marketed by Integrated Systems Incorporated

and the ERA algorithm developed by Dr. Jer-Nan Juang of
NASA-Langley research center were to be used in this phase
of the work.

The final phase of my work was to use the structural
identification method of Creamer and Junkins to upgrade an
appropriate analytical model of structure. This section of
the work would have exercised the method with real experi-
mental data. Limitations of the method, possible improve-
ments in the method, and experience with the method's use
would have been the end results of this phase of the work.

The most important factor which limited the completion
of all of these goals was the large amount of data
generated with each test and the time necessary to analyze
the data. A smaller, more realistic set of objectives was
decided on. First, impulsive loadings only were to be studied.
This greatly simplified the data analysis and eased time
matching requirements between the optical sensor system and
the AFAL data acquisition system. Second, a demonstration
of the feasibility of the optical system for structural
dynamics and system identification was sought. Third, the
major limitations of the system, possible improvements in
the system, and the major sources of error in the system
were to be detailed to guide further work. And finally,
the ERA algorithm was to be used to identify natural
frequencies and mode shapes. This was to develop

experience in using this package. No attempt was made to perform structural identification except to tailor the data taken and analyzed for use with the method in the immediate future.

HARDWARE CONSIDERATIONS

The test article used in this work was a 5' by 5' grid made of aluminum slats 2" wide and 1/8" thick. The slats were connected at 20 joints as seen in Figure 1. The joints were riveted in 4 places and a 10/32 inch bolt and nut was tightened in the center of each joint. These bolts held accelerometers and optical markers as well as provided extra joint stiffness. Endevco model 7751-500 accelero- meters were placed at locations 1,3,5,7,9,13,16,17,19,20. Circular markers for the optical sensing system were placed at every joint. These markers were 3" in diameter and made of Scotchlite reflective sheeting number 3290. A Kistler type 9722A500 impact hammer was used to excite the structure and monitor the load input. A Bruel & Kjaer type 4810 mini-shaker and a Kistler model 9712A5 force transducer were available to excite the structure, however these were not used in the work reported here. All the electronics for accelerometer and and load cell condition- ing and filtration were built by AFAL personnel. An Integrated Systems Incorporated MAX_100 handled 16 channels of data acquisition as well as provided control for the

Figure 1. AFAL Structural Identification Test Article
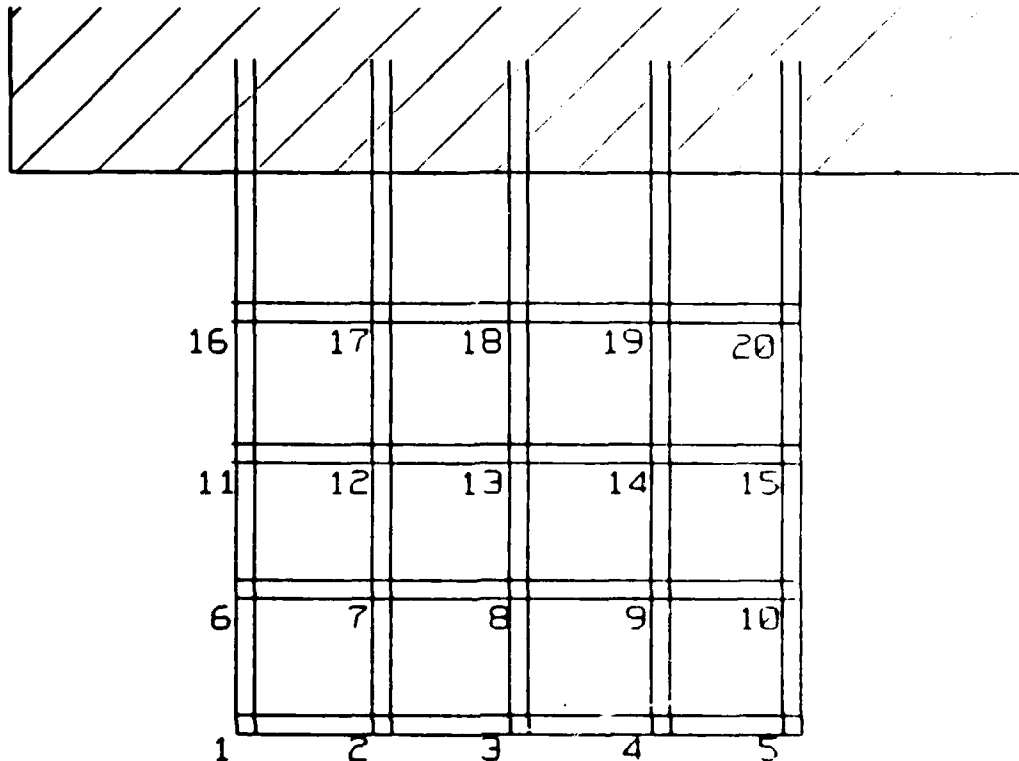
shaker.

The optical sensor system was produced by Motion Analysis Corporation and consisted of a Sun 2/120 computer, a Motion Analysis VP110 video processor, a Panasonic AG-6300 video recorder, and an RCA TC2811 60 hz video camera. A second camera and recorder were also required to allow stereo measurements since the displacements of interest were out of the plane of the structure. Floodlights were used to illuminate the markers on the structure. A reference frame was built to enclose the grid structure which allowed reference targets to be placed for calibra-

tion of the video cameras via resection.

The two cameras were set u to view grid from two different angles such that the _ e markers were visible by both cameras. The motion is then simultaneously recorded by both cameras which are synchronized by the VP110. The VP110 is then used to digitize the video recordings one at a time and transfer the data to the Sun computer. The video processor digitizes only those pixels which cross a grey scale threshold as set by the user. This allows the outlines of markers which are either lighter or darker than the surrounding scene to be digitized. The wall behind the test article and the reference frame were painted black to allow the reflective markers to stand out as lighter than the background. The surface finish of the structure did interfere with the intensity contrast requirements. Tissue paper was used to cover the problem areas of the structure.

SOFTWARE CONSIDERATIONS

Motion Analysis ExpertVision software was used to process the digitized data on the Sun computer. The centroid of each digitized marker outline is calculated for each frame of video data. These centroids are then linked in time by a nearest neighbor algorithm to produce the path of each marker though time. At this point the paths are two dimensional and in the coordinants of the individual camera

imaging arrays.

A series of programs have been written by this
researcher to calculate the paths of each marker centroid
in 3D space given the two paths in the individual camera
space. This process is called triangulation. Two sets of
equations are available for making this conversion. The
colinearity equations [13] are nonlinear and require an
iterative solution. However, the colinearity coefficients
have physical interpretations such as camera position,
camera orientation, focal length, and priciple point
offsets. Alternatively, the Direct Linear Transform (DLT)
[12] equations produce a set of equations which can be
solved with a linear least squares algorithm. The DLT
coefficients do not have physically realizable interpreta-
tions. The two methods were found to give comparable
results and the DLT solution was used in this work for
simplicity.

A seperate but closely related problem is the
resection of camera parameters or calculation of the
coefficients mentioned in the previous paragraph. A
separate set of programs was written to perform this
function for both the colinearity equations and the DLT
equations. A set of stationary noncoplaner points of
known 3D coordinants are filmed from both cameras and
proper coefficients are calculated for each came.
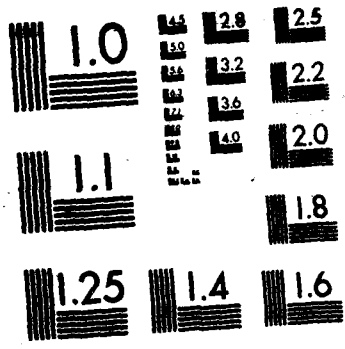
MICROCOPY RESOLUTION TEST CHART
NATIONAL BUREAU OF STANDARDS-1963-A

individually. The DLT formulation again produces a linear least squares problem and the colinearity formulation a nonlinear formulation. Twelve known point on the wall behind the structure and the reference structure were used in this work.

The accelerometer time histories and the optically calculated displacement time histories for the out of plane displacements were uploaded to the AFAL VAX computer. $MATRIX_x$ was used to detrend, normalize, and plot the data. The data was normalized by dividing the Fourier transform of the time histories by the load input provided by the impact hammer and taking the inverse transform. The ERA algorithm was used to calculate the natural frequencies and mode shapes using the VAX as a host computer.

RESULTS

Figures 2-5 show the non-normalized, non-detrended time histories. These time histories are all for point one on the structure due to an impulse at point four on the structure. The data are all displacement out of the plane of the test article. Figure 2 is the data from a high coverage test or a test where all 20 points on the structure were monitored. The long period of time before the impulse provides information on the basic accuracy of the system. The measured value of the undisplaced position is 11.8125 inches.

Displacement Time Histories

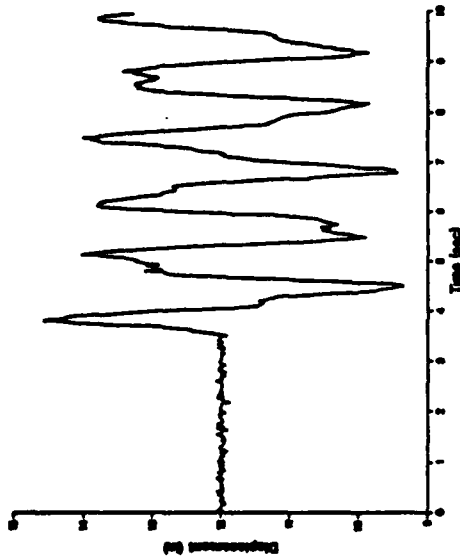Figure 2: Test 61 - High Coverage Test
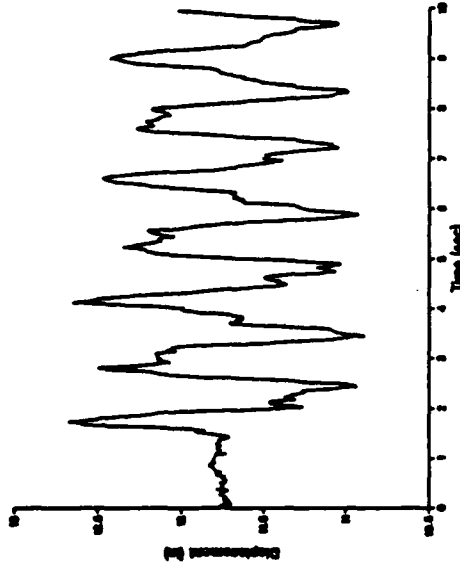
Figure 3: Test 171 - High Resolution Test
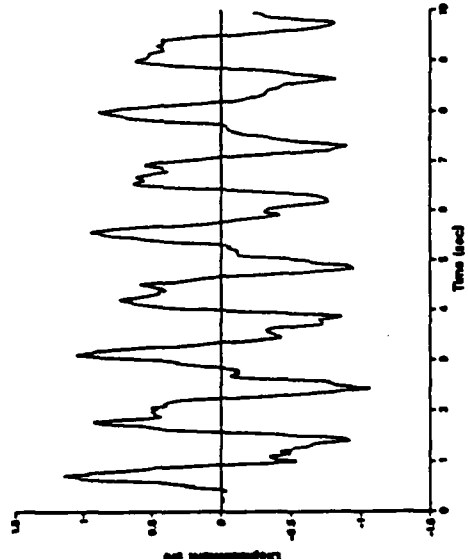
Figure 4: Test 91 - 2-D Test

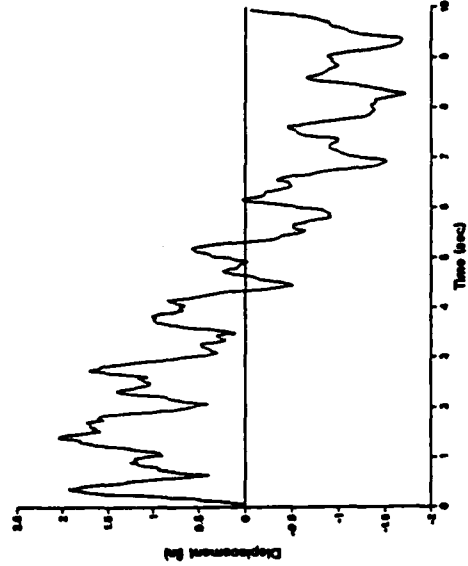Figure 5: Test 91 - Integrated Accelerometer Data

Figure 3 provides data from a high resolution test in which only locations 1,2,6,and 7 were monitored. This allowed higher spatial resolution to be utilized in the 3D calculations. Figure 4 provides data from a 2D test in which a marker was placed on the side of the structure at point 1. This eliminated the need for triangulation as all the point 1 motion was planar and gave some indication as to the effect of the 3D calculations on the final answers. Figure 5 shows a 60 Hz. accelerometer output integrated twice. This allows a comparison of the optical data with the standard accelerometer data. A drift can be seen in the data, however the magnitudes are in good agreement with the optical data.

Figures 6-9 provide the corresponding Fourier transforms for the time histories of Figures 2-5. The effect of the spatial resolution limitation can be clearly seen. The high coverage test can only pick out the the three lowest modes which have the largest displacements. The high resolution test can be seen to pick out the first five frequencies. The 2D test can pick out eight peaks. The accelerometer data produces several higher frequencies. Two frequencies were reported by ERA around .1 Hz. in the accelerometer data. These correspond to the drift seen in the time history. Another mode was reported at 1 Hz. and may possibly be due to aliasing. These Fourier transforms

Displacement Fast Fourier Transforms

Figure 6: Test 91 - High Coverage Test
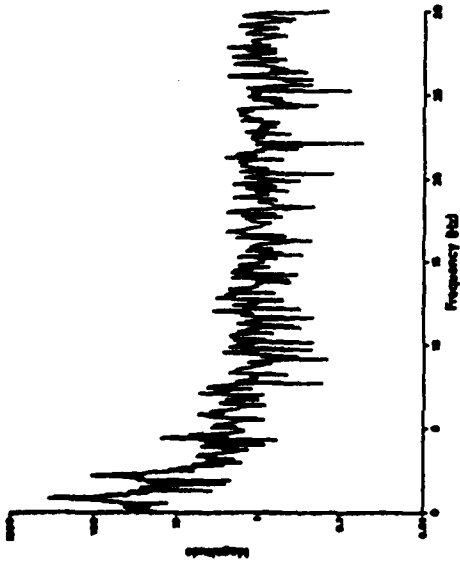
Figure 7: Test 171 - High Resolution Test
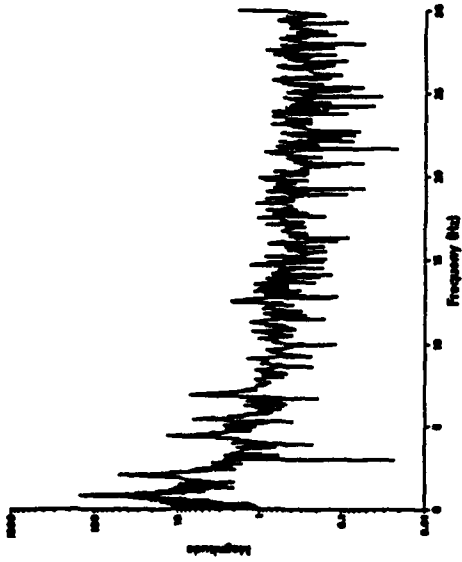
Figure 8: Test 91 - 2-D Test
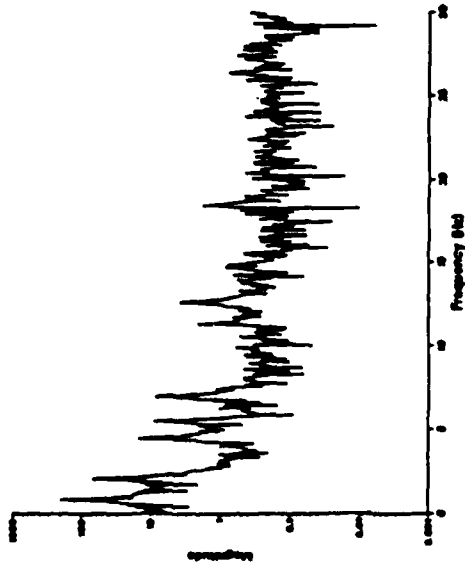
Figure 9: Test 91 - Integrated Accelerometer Data
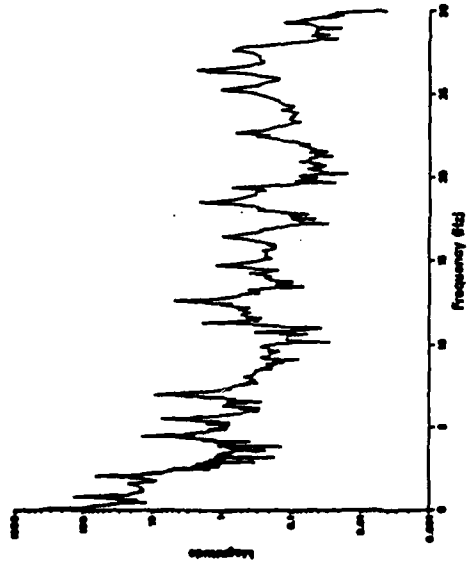
were found to be very useful in setting the ERA parameters
which deal with the number of retained singular values or
the order of the system. Larger singular values tend to
correspond to higher amplitude frequencies. Table 1
provides the actual frequencies determined for each test as
well as the values from an AFAL Nastran code.

TEST	1st	2nd	3rd	4th	5th
Test61	.826	2.178	4.337	---	---
Test171	.825	2.069	4.435	5.434	6.927
Test91	.826	2.081	4.456	5.499	6.956
Accel.	.827	2.074	4.466	5.500	6.960
Nastran	.831	2.216	4.799	5.856	7.522

Table 1. Natural Frequencies of the AFAL Test Article

The high coverage test data was used in conjunction
with ERA to calculate mode shapes. The resulting shapes
qualitatively agree with the observed and the analytical
mode shapes. No attempt was made to pursue this farther in
this work.

RECOMMENDATION

The first recommendation is that a detailed study of
the spatial resolution of the system should be performed.
An extensometer calibrator or similar device which can move
a marker in a series of repeatable and quantifiable
displacements could be used to experimentally carry this
out.

The use of flat markers provided some distortion of the shape since the markers are not viewed normal to the surface. The use of spherically shaped markers is recommended especially for calibration markers. Hemispherical markers might also be used for the structure itself. This might allow the calculation of more accurate marker centroids. It is also recommended that the accelerometers be moved to the back of the structure or enclosed in hemispherical markers as the centroid calculations were affected by the accelerometers.

For the test configuration used for this work, it may be advantageous to use dark markers on a light background. The structure surface could then remain uncovered and unpainted. It is also recommended that a stand alone frame be used for calibration. This would allow calibration dimensions and angles to be measured accurately especially if thin members and spherical targets are used. such a fixture could also be used to control the background intensity.

No electronic means of handeling aliasing are available with this system and 200 Hz. cameras are recommended to lessen the effect of this problem. High speed cameras would also be needed for frequencies above 10-15 Hz. Performing simultaneous triangulation and resection would also be a useful capability. This would

allow recalibration of the cameras at each step and lessen the accuracy with which the calibration points must be measured. An appropriate method for weighting of the variables must be developed. Faster processing times would be helpful especially with high speed cameras and simultaneous resection and triangulation.

The optical sensing system has application in calculating mode shapes experimentally. The system should be tried with resonate excitation of each mode individually. This should produce displacements of the higher modes which are large enough to be measured by this system. This would also require time matching and time synchronization with the accelerometers and load cell. The use of proximity sensors at joints 16-20 would also be helpful because of the small displacements.

REFERENCES

1.   A.S.C.E., "Identification of Large Space Structures on Orbit," AFRPL TR-86-054, September 1986.

2.   Juang, Jer-Nan, and Pappa, Richard S., "An Eigensystem Realization Algorithm (ERA) for Modal Parameter Identification and Model Reduction," Journal of Guidance, Control, and Dynamics, Vol. 8, No. 5, September-October 1985, pp.620-627.

3.   Juang, Jer-Nan, "Mathematical Correlation of Modal Parameter Identification Methods via System Realization

Theory," NASA TM-87720, April 1986.

4. Juang, Jer-Nan and Pappa, Richard S., "Effects of Noise on ERA-Identified Modal Parameters," presented at AAS/AIAA Astrodynamics Specialist Conference, Vail, Colorado, AAS 85-422, August 1985.

5. Pappa, Richard S. and Juang, Jer-Nan, "Galieo Spacecraft Modal Identification using an Eigensystem Realization Algorithm," Journal of the Astronautical Sciences, Vol. 33, No.1, January-March 1985, pp.15-33.

6. Juang, Jer-Nan, and Suzuki, Hideto, "An Eigensystem Realization Algorithm in Frequency Domain for Modal Parameter Identification," proposed abstract for AIAA Guidance, Navigation, and Control Conference, Williamsburg, Virginia, August 1986.

7. Longman, Richard W., and Juang, Jer-Nan, "A Recursive Form of the Eigensystem Realization Algorithm for System Identification," presented at the AIAA/AAS Astrodynamics Conference, Williamsburg, Virginia, August 1986.

8. Ho, Bin-Lin, On Effective Construction of Realizations from Input-Output Descriptions, Ph.D. Dissertation, Electrical Engineering Department, Stanford University, 1966.

9. Creamer, Nelson G., Identification of Linear Structural Models, Ph.D. Dissertation, Engineering Science and Mechanics Department, Virginia Polytechnic Institute

and State University, 1987.

10. Creamer, Nelson G. and Junkins, John L., "An Identification Method for Flexible Structures," presented at AIAA 28th Structures, Structural Dynamics, and Materials Conference, Monterey, California, April, 1987.

11. Walton, James S., "The Accuracy and Precision of a Video-based Motion Analysis System, "Proceedings of the 30th International Technical Symposium on Optical and Optoelectric Applied Science and Engineering, Vol. 693: "High-Speed Photography, Videography, and Photonics IV," San Diego, California, August 1986.

12. Walton, James S., Close-Range Cine-Photogrammetry: A Generalized Technique for Quantifying Gross Human Motion, Ph.D. Dissertation, Physical Education Department, Pennsylvania State University, May 1981.

13. Brown, Duane C., "Application of Close-Range Photogrammetry to Measurements of Structures in Orbit," Vol. 1, Geodetic Services Incorporated Technical Report GSI 80-012, September 1980.

14. Brumfield, M.L., Pappa, R.S., Miller, J.B., and Adams, R.R., "Langley Research Center Photogrammetric Measurements of Solar Array Dynamics: Preliminary Results," Proceedings of the Large Space Antenna Systems Technology Conference, Hampton, Virginia, December 1984, NASA Conference Publication 2368, part2, pp. 517-546.

15. Ewins, D. J., Modal Testing: Theory and Practice, Research Studies Press Ltd., Letchworth, Hertfordshire, England, 1984.

16. Chen, Jay-Chung, "Evaluation of Spacecraft Modal Test Methods," presented at AIAA Dynamics Specialist Conference, Palm Springs, California, May 1984.

17. Weaver, H. Joseph, Application of Discrete and Continuous Fourier Analysis, John Wiley & Sons Publishers, New York, New York, 1983.

18. "Modal Analysis Basic Theory and Measurement Techniques", an intensive course by University of Cincinatti, Department of Mechanical and Industrial Engineering, Cincinnati, Ohio, presented at AFWL/ARBH, Kirtland AFB, NM, May 4-6, 1987.

19. Paz, Mario, Structural Dynamics, Theory and Computation, Van Nostrand Reinhold Company, New York, New York, 1985.

1987 USAF-UES SUMMER FACULTY RESEARCH PROGRAM

GRADUATE STUDENT SUMMER SUPPORT PROGRAM

Sponsored by the

AIR FORCE OFFICE OF SCIENTIFIC RESEARCH

Conducted by the

Universal Energy Systems, Inc.

FINAL REPORT

Prepared by:	Stephen R. Jenei, B.Sc.
Academic Rank:	Graduate Student
Department and	Department of Biology
University	University of Dayton
Research Location:	AAMRL/THT
	Wright-Patterson AFB Dayton, OH
USAF Researcher:	David R. Mattie, Ph.D.
Date:	30 September 1987
Contract No.:	63020104

Delivery of Inhibin by ALCAP Drug Delivery Capsules

by

Stephen R. Jenei

ABSTRACT

Inhibin, a protein that blocks the secretion of follicle-stimulating hormone (FSH) has only recently begun to be accepted as a true hormone. By suppressing FSH secretion, inhibin may prevent gamete production by Sertoli cells in males. Inhibin was delivered in vivo in a sustained manner via alumino-calcium-phosphorus (ALCAP) oxide ceramic drug delivery capsules in albino male rats. Rats were sacrificed after one, two, three, and four weeks of implantation for histological studies of pituitary glands and reproductive organs using both light and transmission electron microscopy, and studies on sperm morphology by scanning electron microscopy. Plasma levels of LH, FSH, and testosterone were measured by radioimmunoassay, Results of this study will provide early information on the long-term effects of sustained levels of inhibin in male reproduction including regulation of FSH.

Acknowledgements

graduate advisor, Praphulla K. Bajpai, Ph.D., for his help and support in
my graduate thesis work

I. INTRODUCTION:

Recently, a protein has been isolated and characterized which blocks the secretion of follicle-stimulating hormone (FSH). This protein, inhibin, has been postulated for years and is now accepted as a true hormone. By blocking FSH secretion, inhibin may prevent gamete production by both testes and ovaries. Unlike other substances with similar properties, this hormone appears to work only on FSH-producing cells of the pituitary gland without disturbing the action of other hormones such as luteinizing hormone (LH).

FSH plays a major role in follicular growth and maturation in the female and in initiation and maintenance of spermatogenesis in the male. In the female, FSH induces ovarian follicle maturation and acts in the development of granulosa cell responsiveness to other hormones. Granulosa cells are stimulated by FSH to secrete estrogens, progestins, and non-steroid substances. These are responsible for folliculogenesis and oocyte maturation. In the male, the Sertoli cells of the testis are the major target of FSH which are responsible for spermatogenesis, steroidogenesis, and synthesis of protein hormones and cybernin (Sheth, 1986).

Many hormone-based fertility regulating substances, including those previously tested on males, can produce adverse side effects that prevent their use among the general public. This study was designed to study the delivery of inhibin (which has been isolated from porcine follicular fluid donated by Dr. Salvator Raiti of NIDCH) by means of a ceramic drug delivery devise that has been developed at the University of Dayton.

II. OBJECTIVES OF THE RESEARCH EFFORT:

Drugs and hormones have traditionally been administered orally or by injection. These result in a pulsatile pattern of drug availability and activity within the body. Often the peak levels of the drug or hormone far exceed the necessary therapeutic requirements. Upon ingestion several drugs are broken down along the digestive tract thereby greatly reducing or eliminating the intended effect of the drug.

To alleviate the problems associated with the oral and injection routes of drug administration, attempts are being made to design drug delivery systems which can release drugs or hormones in a sustained manner in amounts which are effective but non-toxic over a prolonged period of time. Several materials including silicone rubber and organic polymers, and devices such as miniature external pumps and fluid pressure driven internal pumps have served as useful drug delivery systems. However, each of these have certain inherent disadvantages.

Aluminum-calcium-phosphorus oxide (ALCAP) ceramics were developed and used successfully to substitute traumatized bone. The inherent resorbability and porosity of these ceramics led to attempts of using ALCAP ceramic reservoirs as drug delivery systems. The ALCAP ceramic capsules, which have been tested to be biocompatible, biodegradable, and non-toxic, are capable of delivering a wide variety of substances including proteins in a sustained fashion for long periods of time.

The biocompatibility and lack of toxicity of ALCAP ceramics has been established by in vitro and in vivo systems. Mutagenicity and cytotoxicity tests of ALCAP ceramics were conducted by Mattie et al. (1984). The Ames/Salmonella test was used to assess the mutagenic potential of ALCAP ceramics. Plate incorporation tests were conducted

with 1, 3, and 10 mg of powdered ALCAP ceramic per plate. ALCAP ceramics were non-mutagenic at the above dose levels of ceramic powder. Clonal cytotoxicity assay conducted by incubating ALCAP ceramic powder with Detroit 985 cells showed that ALCAP ceramics did not inhibit the growth of these cells. It was concluded that ALCAP ceramics are non-toxicity and non-mutagenic biomaterials.

Mattie, Latendresse, and Bajpai (1985) examined the biocompatibility and toxicity of ALCAP ceramics by means of the hemolysis test using human plasma and the short term muscle implant test in rabbits. They concluded that ALCAP ceramics were biocompatible and non-toxic.

McFall and Bajpai (1984) implanted ALCAP ceramics subcutaneously in rats and reported that aluminum, calcium, and inorganic phosphorus released from the ceramics was excreted in the urine after passing through the surrounding tissue, plasma, and kidneys. They also reported that aluminum, calcium, and inorganic phosphorus resorbed from ALCAP ceramics did not accumulate in the brain, bone, heart, liver, and spleen of the implanted rats. Calcium and inorganic phosphorus released from the ceramic did not initiate soft tissue calcification in any of the tissue examined.

My assignment as a participant in the 1987 Graduate Student Summer Support Program was to study the long-term effects of inhibin on the male rat when delivered by the ceramic capsules in a sustained manner. This was comprised of a long-term study of inhibin delivered in vivo using intact animals. The study lasted four four weeks and included histological studies of reproductive organs using both light and electron microscope, estimation of plasma levels of LH, FSH, and testosterone by radioimmunoassay, and studies on sperm maturation and morphology. The

data obtained in this study will provide information on the long-term effects of sustained levels of inhibin in male reproduction including regulation of FSH as well as information on the delivery of proteins from the ceramic capsules.

III MATERIALS AND METHODS

The crude porcine follicular fluid (pFF) used in this experiment was donated by Dr. Salvatore Raiti of the National Hormone and Pituitary Program of the NICHD. The crude pFF was first desalted by chromatography on a Sephadex G-25 Course gel exclusion column with a bed volume of 500 ml. The pFF was centrifuged to remove cell and tissue debris and then applied to the column with a sample volume of 120 ml and the elution was collected in 10 ml fractions. The protein concentration of the column elution was followed by measuring the absorbance (A_{280}) of each fraction. The pFF proteins were then collected by pooling the void volume fractions and lypholizing. The pFF protein powder was then stored at -20 $^{\circ}$C.

The pFF protein was further purified using affinity gel chromatography. Four grams of lypholized pFF protein was resuspended in 75 ml of Buffer A (Appendix A) at pH 7.5. The protein was applied at 4 $^{\circ}$C to Procion Red A dye-ligand affinity gel (Sigma Chemical Co., St. Louis, MO) column (4 x 25 cm) with a bed volume of 200 ml. After loading the protein, 700 ml of Buffer A was run through the gel at a flow rate of 2.5 ml/min. to wash off the non-binding proteins. The protein was then eluted by changing the buffer to Buffer B (Appendix A). The protein concentration was determined by measuring the absorbance (A_{280}) of the fractions collected. The tightly bound proteins were eluted using a 6 M urea buffer. The fractions eluted by Buffer B were pooled and the proteins collected by precipitation with a 2:1 addition of 100% ethanol at -20 $^{\circ}$C and

centrifugation at 10,000 x g. The protein pellet was dried and stored at -20 °C until use.

The alumino-calcium-phosphorus ALCAP ceramic capsules were fabricated from a 50:34:16 mixture of aluminum oxide, calcium oxide, and phosphorus pentoxide (Fisher Scientific Co., Fairlawn, NJ) which have been calcined at 1350 °C for 12 hours. The calcining causes the thermal mixing of the atoms of the powders and establishes a crystalline lattice structure to the composite. The calcined ALCAP material was ground in a roller ball mill and sieved through a stainless steel mesh (Tyler Sieve Stack) to achieve a uniform size of 38 microns or less. The ground ALCAP powder was mixed with 0.25% (w/w) polyvinyl alcohol (PVA) which acts as a binder and die lubricant in the fabrication process. A 5/16" die set for pressing cylindrical forms was filled with 1.0025 g of the ALCAP/PVA mixture and pressed in a hydraulic press at 7000 lbs. of load. The compacted ALCAP powder cylindric forms were then sintered at 1500 °C for 36 hours. The sintering process allows the fusion of ceramic particles to yield a final hard form ceramic capsule. After sintering, the capsules were weighed and the densities calculated. The sintered capsules were then impregnated with 1:50 (w/v) solution of DL-polylactic acid (Lot Δ PLA021, New Jersey Medical School, Newark, NJ) in chloroform in vacuo for 1 hour and then air dried at room temperature. The polymer impregnation of the capsules decreases the average pore size of the capsules.

For this investigation, 72 Fischer F344 white, male rats were divided into four sets of 18 each for the time periods of 1, 2, 3, and 4 weeks. Each weeks set was further divided into three groups consisting of intact controls, sham operated controls, and experimentals. All of the experimental animals were implanted interperitoneally with two ALCAP

capsules containing 40 mg of partially purified porcine follicular fluid inhibin (from Procion Red A column). Each group was sacrificed at the end of the respective time period.

The animals were sacrificed by halothane overdose and gravity perfusion with saline and fixative. For each animal, the lower abdomen was opened to expose the inferior vena cava and 5 ml of blood was taken using a 21g needle and 10 ml syringe. The blood was allowed to stand at room temperature for 1/2 hour then centrifuge at 10,000 x g for 10 min. Serum was collected and stored at -20°C until radioimmunoassays could be performed.

The left testis and vas deferens was then exposed and an incision made in vas deferens to allow collection of 5 µl spermatozoa with a micropipette and placed into 3 ml of Tyrode's solution at 37°C to liquify. A smear of the sperm was prepared on a glass slide and air dried before staining with Geimsa stain and attaching a coverslip. The sperm were then centrifuged at 500 x g and resuspended in 25% gluteraldehyde/phosphate buffer.

The descending aorta was then exposed below the ileolumbar artery branch and a suture placed around artery with forceps. The artery wall was cut with a razor blade and a canula inserted and tied off. Hemostats were then placed on the artery above left kidney and beneath the canula. The reproductive system was then gravity perfused (100 mmHg) with rinse solution (Appendix B) for 1 min. Then with Fixative I (Appendix C) for 2 min. and finally with Fixative II (Appendix C) for 3-1/2 min.

The testes, epididymus, prostate, and seminal vesicles were removed and stored in Fixative II for 2 hrs. The pituitary glands were removed and stored in 10% neutral buffered formalin. For light microscopy study, the

testes, epididymus, prostate and seminal vesicles were weighed, cut transversely, and then dehydrated and paraffin infiltrated in a Tissue Tek III - Vacuum Infiltration Processor (Appendix D). The paraffin infiltrated tissues were then embedded in paraffin blocks. The paraffin blocks were then cut in a microtome in 5 micron sections for mounting on slides and staining. All sections were stained with eosin B and hematoxylin stains (Appendix E) and coverslips attached with synthetic resin.

The testes and pituitary glands were cut into 1 mm^3 sections and processed for TEM according to Standard Operating Procedures numbered 250, 251, and 252 in the Ultrastructural Research Laboratory of AAMRL/THT.

IV. CONCLUSIONS

To date, much of this investigation is still in progress and hence no results are available as of yet. However, this study will be completed over the next few months as part of this investigators Master's Degree thesis at the University of Dayton, Dayton, Oh. Completion of radioimmunoassays of serum hormone levels and ultrastructural studies of the testes should provide valuable information in this study.

REFERENCES

Mattie, D.R., J.R. Latendresse, and P.K. Bajpai. 1985. Biocompatibility of ALCAP Ceramics with Erythrocytes and Muscle. IRCS Med. Sci. 13:420-421.

McFall, F. and P.K. Bajpai. 1984. Fate of Resorbable Alumino-Calcium-Phosphorus Oxide (ALCAP) Ceramic Implants in Rats. Transactions for the Society of Biomaterials. 7:354.

Sheth, A.R., and N.J. Arbatti. 1985. Inhibin: An Updated Review. Indian J. Exp. Biology. 23:475-494.

APPENDIX A

Matrix Red A Gel Affinity Chromatography

I. To make 1 liter of Buffer A obtain:

       0.05 M Tris base

       0.05 M Tris HCl

       0.15 M KCl

       0.002 M EDTA

       H_2O to 1 liter

Adjust pH to 7.25 with HCl or NaOH.

II. To make 1 liter of Buffer B obtain:

       0.05 M Tris base

       0.05 M Tris HCl

       1.20 M KCl

       1.00 M Urea

       0.002 M EDTA

       H_2O to 1 liter

Adjust pH to 7.25 with HCl or NaOH.

APPENDIX B

Preparation of Vascular Perfusion Rinse Solution

To prepare 1 liter of Rinse Solution:

NaCl	9 g
Heparin	0.25 g
Procaine-HCl	5 g
Deionized H_2O up to	1 L

Adjust pH to 7.35 using HCl or NaOH and pass solution through 3.0 µ filter. The Rinse Solution is made up fresh just before use and is not stored.

Preparation of Sorensen's phosphate (0.2 M)

Solution A:

monobasic sodium phosphate	27.80 g
(NaH_2PO_4)	
distilled water	1000 ml

Solution B:

dibasic sodium phosphate	53.65 g
($Na_2HPO_4.7H_2O$)	
distilled water	1000 ml

For diluted 0.1 M phosphate (pH 7.2) add 28.0 ml of Solution A and 72.0 ml of Solution B with 100 ml of distilled water.

APPENDIX C

Preparation of Vascular Perfusion Fixatives

A. To prepare 1 liter of Fixative I (1.5%) combine:

0.2 M NaH_2PO_4	45 ml
0.2 M Na_2HPO_4	405 ml
25% formalin	60 ml
25% gluteraldehyde	60 ml
distilled H_2O	up to 1 L

Adjust the pH to 7.35 using HCl or NaOH. Pass through 3.0 μ filter.

B. To prepare 1 liter of Fixative II (3.0%) combine:

0.2 M NaH_2PO_4	45 ml
0.2 M Na_2HPO_4	405 ml
25% formalin	120 ml
25% gluteraldehyde	120 ml
polyvinylpyrrolidone (PVP, M.W. 40 KD)	25 g
picric acid	0.5 g
distilled H_2O	up to 1 L

Adjust the pH to 7.35 using HCl or NaOH. Pass through 3.0 μ filter.

Note: Gluteraldehyde is very unstable and polymerizes. These solutions must be kept at 4 °C.

APPENDIX D

Tissue Processing Schedule

I. Dehydration and paraffin infiltration using a Tissue-Tek III V.I.P. Vacuum Infiltration Processor (Lab-Tek Products, Div. of Miles Laboratories, Inc., Naperville, IN).

    A.   10% Neutral Buffered Formalin

    B.   10% Neutral Buffered Formalin

    C.   80% Ethanol

    D.   95% Ethanol

    E.   95% Ethanol

    F.   100% Ethanol

    G.   100% Ethanol

    H.   50% Ethanol/50% Histoclear

    I.   100% Histoclear

    J   100% Histoclear

    K.   Paraffin

    L.   Paraffin

II. Embedding was completed using a paraffin dispenser.

III. Embedded tissues were sectioned at a thickness of 4 microns using an American Optics Rotery Microtome. Cut sections were put onto microscope slides using purified pigskin gelatin dissolved in a 45 $^\circ$C water bath. Tissue sections were affixed to slides by heating in a 60 $^\circ$C oven until paraffin melts (10-15 min.) then allowed to cool.

APPENDIX E

Standard Hematoxylin and Eosin Y Staining Procedure

Station	Time (min.)	Solution	Comments
1	5.0	100% xylene	Paraffin removal
2	5.0	100% xylene	
3	1.0	100% ethyl alcohol	Hydration
4	1.0	100% ethyl alcohol	
5	1.0	95% ethyl alcohol	
6	1.0	95% ethyl alcohol	
7	1.0	80% ethyl alcohol	
8	1.0	Distilled water	Wash
9	7.0	Erlich's Hematoxylin	Stain
10	2.0	Distilled water	Wash
11	0.4	3% ammonia water	
12	1.0	Distilled water	Wash
13	1.0	80% ethyl alcohol	
14	5.0	Eosin Y	Stain
15	0.3	95% ethyl alcohol	Dehydration
16	0.3	95% ethyl alcohol	
17	0.3	100% ethyl alcohol	
18	0.5	100% ethyl alcohol	
19	0.5	100% ethyl alcohol:xylene (50:50)	
20	1.0	100% xylene	
21	1.0	100% xylene	

Slides are left in xylene until ready to coverslip. The slides are cleaned of any residual debris and a coverslip added using a synthetic resin mounting agent. The slides are then left to dry (2-3 days).

MR. KENNETH JENKS

FINAL REPORT NUMBER 40

NO REPORT SUBMITTED

1987 USAF-UES SUMMER FACULTY RESEARCH PROGRAM/

GRADUATE STUDENT SUMMER SUPPORT PROGRAM

Sponsored by the

AIR FORCE OFFICE OF SCIENTIFIC RESEARCH

Conducted by the

Universal Energy Systems, Inc.

FINAL REPORT

A System to Investigate Synthesized Voice

Feedback in Man-Machine Interfaces

Prepared by: Michele E. Johnson

Academic Rank: Graduate Student

Department and   School of Electrical Engineering

University: Cornell University

Research Location: Rome Air Development Center/IRAA

USAF Researcher: Captain David B. Stockton

Date: August 25,1987

Contract No: F49620-85-C-0013

A System to Investigate Synthesized Voice

Feedback in Man-Machine Dialog

by

Michele E. Johnson

Abstract

The Rome Air Development Center (RADC), Intelligence Analysis Branch, is sponsoring an in-house research effort to study and develop advanced man-machine interfaces. At present, most interfaces consist of a keyboard and a display terminal, and feedback to a user is visual. Verbal dialog is an alternative interface that has the potential to reduce the human operator's visual load, and to take advantage of the verbal communication skills that almost every human being possesses. This paper describes the elements of a system that RADC will use to investigate verbal feedback to a human operator, more specifically to examine the interactions between synthesized message characteristics and the performance of tasks requiring comprehension of audio information. Also included is information which will be of use to those continuing this work at RADC.

41-2

ACKNOWLEDGEMENTS

I. Introduction:

I received a BSEE degree from Cornell University in May. 1984, and am presently at Cornell working towards a M.Eng. degree with a specialization in signal processing. My task at RADC was to develop a system to investigate synthesized verbal feedback to a human operator. The method of investigation will be to evaluate a subject's performance of a secondary task with his/her audio channel heavily loaded. Loading of the audio channel is accomplished by the primary task of transcription of audio information, and the secondary task consists of execution of a sequence of keystrokes as instructed by synthesized voice messages. Preparation for the task involved reviewing literature on human perception of speech as well as familiarizing myself with RADC's Audio Signal Management System.

II. Research Objectives:

The following research objectives were determined at the start of the project:

A. Develop a computer program to interactively control the speech synthesizer and collect data on the subject's performance and responses.

B. Define the primary and secondary tasks.

C. Run experiments and evaluate results.

The experiment control program has been written and is

operational. Secondary tasks have been defined. The creation of primary tasks and the actual experimentation will be continued by Capt. Stockton.

III. The System and the Experiment:

The main hardware elements of the system and their functions are as follows:

A. Audio Signal Management System - mixing and manipulation of the primary audio signal, transcription

B. host computer (Texas Instruments Professional Computer) - creation and execution of experiments, performance data collection and processing

C. DECtalk speech synthesizer - synthesis of messages

D. Tektronix Computer Display Terminal - keyboard for subject's responses (displays may be added in the future)

The subject's primary task is to transcribe audio information using the ASMS facilities. The ASMS is a workstation that allows a listener to manipulate an audio signal in order to extract more information. The ASMS can, for example, repeat a specific segment over and over again(loop), change the rate of speech without changing the pitch, and remove silences. This primary task loads the

subject's audio channel. In addition to transcription, the subject will be required to respond to synthesized messages requiring the execution of specific sequences of keystrokes on the Tektronix keyboard. The speed and accuracy of the subject's responses are recorded by the experiment control program (CONTROL) and will form the basis for evaluation of secondary task performance. The transcription will be compared to a correct transcription of the audio passage as evaluation of primary task performance. This will involve the ASMS software and will be handled by Digicomp Research Corp. More information on the ASMS may be found in "Audio Signal Management System Final Technical Report", Digicomp Research Corp. and "Audio Signal Management Exploratory Development Model User Manual", HRB Singer.

Most of the message variables such as speech rate, pitch and emphasis can be controlled by controlling the synthesizer's voice and by controlling the pitch and duration of the phonemes that make up the message. Timing of the message, or its placement within the primary audio stream to the subject, will be controlled by the user interactively with the host computer. The volume of primary and secondary audio streams heard in each ear will be controlled by the mixer settings. The set of varibles that can be controlled will permit a large number of different experiments to be performed.

III. The DECtalk Speech Synthesizer:

The Speech Processing Laboratory at RADC includes a DECtalk DTC01 manufactured by Digital Equipment Corp. and running software version 2.0. This speech synthesizer is used to create the synthesized voice messages for the experiment. Although the DECtalk is described as a text-to-speech converter, it can speak other types of raw data in addition to text. DECtalk can speak text that contains stress and syntax symbols to improve emphasis, phrasing and intonation. Many symbols of this type such as commas, periods, question marks, and exclamation points are familiar to us all. DECtalk can also speak phoneme strings, and the duration and target pitch of each phoneme can be specified. For the experiment described here, the phoneme editor (PEDIT) of the DECtalk Interface System is used to manipulate phoneme pitch and duration to create phoneme strings which are spoken by DECtalk during the experiment.

Another feature of DECtalk is programmed control of voice characteristics. Twenty-nine parameters such as sex, speech rate, breathiness, head size and synthesizer gains may be specified by the user. A new voice may be designed, saved, and invoked to speak any utterance. The voice editor (VEDIT) is used to create a file of voice parameter values which can be accessed by CONTROL to change DECtalk's voice.

DECtalk has the ability to keep the host computer informed of the status of speech. Since DECtalk has a 5 second buffer, and a 6 ms synthesizer delay, a program can not assume that speech begins as text is printed to DECtalk and ends as text is exhausted. In cases such as this, a special type of DECtalk command, an escape sequence, is useful. A marker, or index, can be inserted into text or phoneme strings at any point via an escape sequence. Another escape sequence called index reply instructs DECtalk to respond with a specific string as speech passes the marked point. In this way the program can accurately determine the start and stop times of speech.

For the purposes of this experiment, the DECtalk is under program control, but an offline or setup mode is also available. From setup mode the DECtalk can be configured to echo the text or phoneme strings it receives to a terminal, log error messages to a terminal, or change the characteristics of the communication line connecting DECtalk to the host. DECtalk must be operated at 9600 baud for this experiment, and defaults to 1200 baud at power up. An HP2645A terminal has been connected and can be used to issue DECtalk setup commands. To change the baudrate, press the "transmit break" key on the HP2645A and type the following:

        SETUP> SET HOST SPEED 9600 <RET>

        SETUP> EXIT <RET>

More information on the setup mode commands can be found in chapter 3 of the DECtalk Owner's Manual. This manual also

41-8

contains information on text strings, stress and syntax symbols and voice modification. The DECtalk Programmer Reference Manual contains the information on escape sequence commands.

IV. CONTROL:

CONTROL.BAS is the experiment control program, a listing of which is included as Appendix A. The purpose of the program is to enable a user to speak a large number of utterances more easily (i.e. more easily than by using PEDIT, CEDIT, or DECRDWR) and with more control over the time of speech. In addition, CONTROL allows the user to change voices easily during the course of an experiment session. Each session proceeds as follows:

A. The user chooses to either run an experiment, quit, or view the results of a previous experiment.

B. If running an experiment, the user is prompted for the experiment name. The items in the experiment, i.e. utterances and voices, are displayed.

C. The user can change the Tektronix timeout here if desired. The timeout is the length of time the subject is given to respond at the Tektronix keyboard. Timing starts at the start of printing to DECtalk. The program defaults to a 5 second timeout at the start of each session, i.e. each time the program is run. Note that

41-9

since more than one experiment may be run in a
single session, changing the timeout installs
that value for all the proceeding experiments
unless the timeout is changed again.

D. The user chooses either user or computer
control. Under user control, the items may be
executed in any order and items may be repeated.
Under computer control the items are executed in
the order in which listed in the experiment.
The only advantage to computer control is the
automatic loading of voices which saves a single
keystroke per voice.

E. Assuming the experiment is under user control,
the program nexts prompts the user for the
number of the next item to be loaded. The item
is loaded and, if a .VOC (voice) file, DECtalk's
voice is changed. If the next item is a .UTT
(utterance) file , the phoneme string is read
into an array. At this point the program waits
for user input before speaking. If the speak
command is received the phoneme string is sent
to the DECtalk, and the utterance is spoken. In
this way, the user can control the time of
speech since the phoneme string is prepared but
not sent to DECtalk until prompted by the user.
By increasing DECtalk's baudrate to 9600, and
using this store-and-then-speak scheme, the
delay from user command to speech was reduced to
less than one second. This delay is short

enough for the user to accurately place the
synthesized messges in the primary audio stream
to the subject.

F.   Items are executed until none remain (under
computer control) or until the user quits.   The
user is then given the option to save the
results in a .RES file. The first line of a
.RES file displays the timeout value. The rest
of the lines display 5 columns of response
information: item name, time of start of speech,
time of end of speech, time of subject's first
response, and the subject's response. An "*"
after the time of response, and "*****" in the
response column indicate that timeout was
reached with no response from the subject.

G.   The user is again prompted to run quit or view.
This cycle continues until the user quits.

CONTROL is able to process .UTT and .VOC files.   A .UTT
file can be created by FEDIT and consists of a list of
phoneme numbers, pitches and durations.   The file is headed
with the number of phonemes listed and the beginning pitch.
As the phonemes are read in by CONTROL, the phoneme numbers
are   converted   to   2-character   symbols   which   DECtalk
understands.   A .VOC file can be created by VEDIT and
consists of a list of voice parameter numbers and values.
The parameter numbers are converted to symbols as the new
voice is sent to DECtalk.   The other data structures are
arrays to hold the experiment items and results and are

41-11

self-explanatory or commented in the program listing.

The DECtalk Interface System i.e. CEDIT, PEDIT, and VEDIT, is written in Basic and implemented on the Texas Instruments Professional Computer running MS-DOS version 2.11A and Basic version 1.10. For the sake of consistency and compatibility, and to take advantage of the ease with which conversations, utterances and voices can be created by the editors it was decided to implement CONTROL in Basic on the TI as well. This decision led to the project's major problem, that of determining the subject's response time. Timing precision of at least one-tenth of a second is needed for measuring human response speeds. The TI's system clock does provide this degree of precision, but Basic ver. 1.10 functions do not. The next few paragraphs summarize the alternatives that were explored.

From the standpoint of speed and simplicity, the most attractive possibility was calling an assembly language subroutine from Basic. In fact, a subroutine has been written (TIMING.EXE) and functions properly if invoked from MS-DOS. The subroutine can be loaded into a Basic program and called, but incorrect parameter passing causes system crashes. Another problem faced here was the extremely inadequate TI assembly language documentation.

.

We also attempted to run a more advanced version of Basic on the TI with its PC Emulate program. The PC emulator may be called by typing BAS with the advanced Basic disk in

drive A. Unfortunately, PC Emulate documentation is essentially non-existent, and it appears that communication files cannot be accessed except through the ROM system routines.

A promising possibility is to run an advanced version of Basic on the Compaq Deskpro 286 (Xenix operating system). Hard disk file storage and access questions must be resolved.

Another promising possibility is to rewrite CONTROL in C and run it on the Compaq. This fits in well with Capt. Stockton's plan to move the dialog work to the more powerful and flexible Compaq, which also houses the ITT recognizer software. It will still be necessary to access MS-DOS files from Xenix since CONTROL uses files created by the editors, and these are large programs which will not be rewritten.

An attempt was made to port the ASMS time signal over to the experiment host computer. B. Swetman began work on this task, but due to time constraints was unable to eliminate a memory pool usage problem.

Basic version 3.0 for the TI is due to arrive at RADC by the end of the summer. This version includes timer functions with the precision that is needed.

V. Synthesized Messages:

A set of 12 utterances has been developed that can be used as a basis set for the creation of new utterances. The 12 final versions are listed in PRESS.CNV. New utterances may be created from these by replacing words and making minor modifications. The utterances are instructions to the subject such as "Press the red key once." and these are the synthesized messages or the secondary task instructions. A short list of guidelines for utterance creation is included here. Many of these helpful hints were originated by Capt. Stockton.

1. The Visi-Pitch (Kay Elemetrics model 6087) is a very useful tool. The Visi-Pitch will display the frequencies of voiced segments of speech spoken into its microphone. In many, but not all, cases, a very good message can be created by reproducing with the PEDIT the pitch track seen on the Visi-Pitch. In this context a "good" utterance is one that emphasizes the desired information. For example, in "Press the red key once." it may be desirable to emphasize "red" or "once".

2. Speaking along with DECtalk is helpful in establishing a good rate of speech and a natural rhythm.

3. Taping your own speech, and then comparing it with DECtalk's is helpful, but be alert for the effects of context. That is, a word or phrase spoken in isolation will often sound different when spoken as an

41-14

element of a list.

4. Unvoiced segments such as b, d, p, and t are not sustained, and should be of minimum duration to avoid choppy speech. However, if a short pause is desired to separate words with a tendency to slur together, and the first word ends in an unvoiced phoneme, increasing its duration will give the desired result. This is often useful as the minimum phoneme duration, and thus the minimum silence phoneme duration is 50 ms, and pauses of this length are quite disruptive.

5. Emphasis is created by differences of pitch, and sounds with small or gradual changes in pitch are heard as phrases. A pitch change across an unvoiced phoneme will be heard as a step in pitch.

6. For imperative utterances such as those used in this experiment, a pitch track that begins high and steps down with each word and ends with a sharp drop in pitch is often a good place to start.

7. During the course of informal testing of the mixing of the primary audio and the synthesized speech, it was noted that the content of the first word of an utterance was lost, and that it served instead as an announcement to the listener that a secondary message was being broadcast. It would be interesting, and perhaps necessary, to investigate the effect of a non-informative, warning tone preceeding an message.

VI. Recommendations:

Although the experiment described here involves verbal feedback rather than full verbal dialog, at some point a system with speech recognition capabilities will be needed to further explore the verbal man-machine interface. For this reason, CONTROL should be implemented on the Compaq which also serves as host to the ITT speech recognizer.

It is generally agreed that familiarity or training with synthetic speech results in greater intelligibility. Thus, any experimenters working with this system must ensure that all subjects are trained to understand DECtalk speech. It is not necessary to create new utterances for training purposes. DECtalk's default speech can be considered the worst case and used without modification to train subjects.

REFERENCES

1. Pisoni, D.B., H.C. Nusbaum. and B.G. Greene. "Perception of Synthetic Speech Generated by Rule," Proceedings of the IEEE, November 1985, pp. 1665-1676.

2. Stockton, D.B., and E.J. Cupples, "Goal Directed Man-Machine Dialog for Audio Information Processing," Rome Air Development Center, Griffiss AFB, Rome, NY.

1987 USAF-UES SUMMER FACULTY RESEARCH PROGRAM

GRADUATE STUDENT SUMMER SUPPORT PROGRAM

Sponsored by the

AIR FORCE OFFICE OF SCIENTIFIC RESEARCH

Conducted by the

Universal Energy Systems, Inc.

FINAL REPORT

A STUDY OF SMALL, SHALLOW EARTHQUAKES AND QUARRY BLASTS IN HEALY, ALASKA

Prepared by: Scharine Kirchoff

Academic Rank: Graduate Student (Ph. D program)

Department and   Geology and Geophysics

   University.   University of Alaska - Fairbanks
                         Geophysical Institute

Research Location: AFGL/LWH
                         Hanscom AFB
                         Hanscom AFB, Ma. 01731

USAF Researcher: Dr. John J. Cipar

Date: August 19, 1987

Contract No: F49620-85-C-0013

A Study of Small, Shallow Earthquakes and Quarry Blasts in

Healy, Alaska

by

Scharine Kirchoff

ABSTRACT

In an effort to improve the capability to discriminate between

seismic events, several small, shallow earthquakes and quarry blasts

located in Healy, Alaska were selected for this study. Seismic signal

characteristics between the two sources' signals were discerned. An

analysis of the earthquake seismogram spectra reveal more high frequency

components than those of the quarry blasts. Further analysis of two

distinct waveform-wavetrain envelopes in the seismograms support the

high frequency content of the earthquakes. Using a theoretical

modelling technique, synthetic seismograms were subsequently created

to analyze how the signals depend on source and propagation

differences. Recommendations to improve the fit of the individual

phases in the seismograms were also made.

Acknowledgements

I would like to thank the Air Force Systems Command and the Air Force Office of Scientific Research for sponsorship of this research and the Graduate Student Summer Support Program. In addition, Universal Energy Systems was extremely helpful with all of my questions and did an excellent job in managing this program.

I. INTRODUCTION:

One of the problems associated with monitoring a nuclear test ban
treaty is that, in some instances, nuclear explosions have produced
seismic waveforms and wavetrains that closely resemble those generated
by earthquakes. Seismic techniques are the primary short term means
for discriminating between explosive and earthquake generated sources.
Since commercial quarry blasts offer a convenient and economical
explosive energy source for seismic recordings, they are studied here
in conjunction with earthquake recordings to attempt to solve the
enigma between explosion and earthquake discrimination.

The Solid Earth Geophysics Branch of the Earth Sciences Division of
the Air Force Geophysics Laboratory at Hanscom Air Force Base is
particularly interested in the acquisition and interpretation of
seismic data from explosions and earthquakes. For example, their
most recent field project in which I was an active participant, the
Eastern Massachusetts Quarry Blast Experiment (EMQBE), encompassed
the recording of ground motion resulting from three quarry blasts in
Littleton, Massachusetts. Quarry blast data can provide valuable
information about regional geology, velocity variations and discon-
tinuities of the earth's crust and upper mantle including information
about how seismic waves propagate through the earth.

My research interests and education have been in the area of explosion
seismology and geology. My masters degree thesis encompassed a study

of the 1985 Defense Nuclear Agency Minor Scale surface explosion, a
4.8 kiloton chemical explosion in the White Sands Missile Range.
Refraction data, recorded by the Solid Earth Geophysics Branch, was
combined with synthetic seismogram modelling in order to constrain a
crustal model of the Southern Rio Grande Rift and to elucidate the
structure and physical properties of the earth's crust beneath the
Tularosa Basin in New Mexico. My research interests and educational
background are complementary to the mission of the Solid Earth
Geophysics Branch's focus on discriminating between nuclear explosions
and earthquakes, event location, and yield estimates. In addition,
my interests and background contributed to my assignment to the Solid
Earth Geophysics Branch of the Earth Sciences Division.

II. OBJECTIVES OF THE RESEARCH EFFORT:

Presently, there are limited publications which probe into seismic
discrimination between explosions and earthquakes that are located in
the same event area. Due to the abundance of earthquakes in Alaska
and the increased blasting activity of the Usibelli Coal Mine in Healy,
Alaska from the increased demand for coal in the Pacific-rim countries,
a unique seismic data set was recorded. The earthquakes and quarry
blasts were recorded at the seismographic station MCK which is operated
by the University of Alaska - Fairbanks Geophysical Institute Seismological
Laboratory. Figure 1 shows the location of station MCK, the data
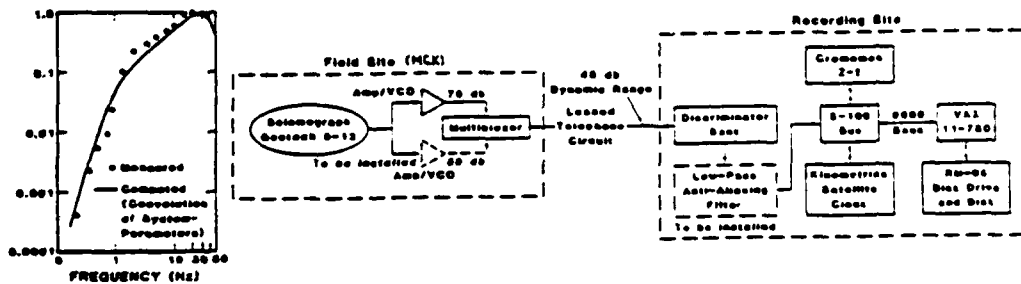recording site at the University of Alaska, and the Usibelli Coal Mine
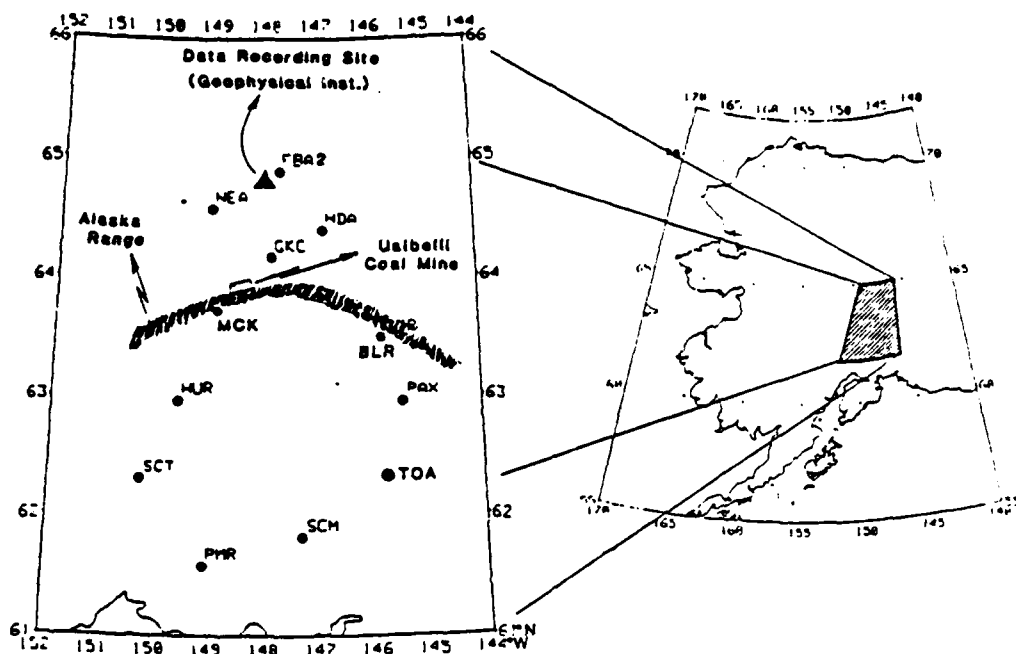
Figure 1. Location of the seismic station MCK,
the data recording site at the University of Alaska
and the location of the Usibelli Coal Mine (above).
Configuration of data telemetry and recording of
local seismic data (below).

(located approximately 10 km from the receiver site) in the Alaska
Range. In addition to the uniqueness of the data set, the geology and
structure of the earth's crust beneath Healy is additionally interesting.
The Alaska Range is a structurally complex melange which overlies a
sharp bend in the Wadati-Benioff zone. A recent compilation of all
earthquakes that occurred between 1970-85 (Biswas, Lahr and Page, 1966)
shows the "Mount Denali Cluster" of earthquakes in interior Alaska where
the sharp bend of the Wadati-Benioff zone occurs near the 100 kilometer
depth contour. Thus, the uniqueness of the available earthquake and
quarry blast data and the interesting structure of the Healy area are
reasons in which I pursued this project for the GSSSP program and for
my Ph.D dissertation. My primary goals as a participant in the 1987
Graduate Student Summer Support Program (GSSSP) was to establish that
differences between my selected quarry blast seismograms and small,
shallow earthquakes exist and, in addition, to model the selected
records and subsequently explain their differences. The computer
programs utilized in my research were entitled Seismic Analysis Code
(SAC) and ASREXP. SAC was provided by Lawrence Livermore National
Laboratories and was utilized for the computations and plotting of
amplitude spectrums and for filtering seismograms. ASREXP was supplied
by Dr. John J. Cipar, my USAF research colleague and seismologist at
the Solid Earth Geophysics Branch.

III.

a. The first step in my researching the differences between quarry
blast and earthquake seismograms was to carefully observe visual
differences between the signals. Figures 2 and 3 show some of the
selected quarry blast records (approximately 10,000 lb. blasts) and
small, shallow earthquakes. Small, shallow earthquakes (<4 magnitude,
2-4 km hypocentral depth) were selected, versus larger, deeper earth-
quakes, because of the assumed similarities of their ray propagation
paths compared to the surface quarry blasts. Figure 1 additionally
includes a configuration of data telemetry and recording of local
seismic data at station MCK. Note the instrument response at the left
with a peak response at 25 Hz. The data at station MCK was obtained
at 100 samples per second and reveal a good signal-to-noise ratio.
Figure 2, the quarry blast seismograms, when compared to Figure 3, the
earthquake seismograms, are longer period and reveal first motion
arrivals that are compressional (station MCK has reversed polarity).
Theoretically, first motion arrivals on explosion seismograms should
be compressional since the radiation pattern is azimuthally symmetric.
However, earthquake double couple fault motions produce alternating
quadrants of dilatation and compression, therefore these seismograms
agree with current theory.

Additional observable differences involve the apparent high frequency
content of the earthquake seismograms. Amplitude spectra, not shown,
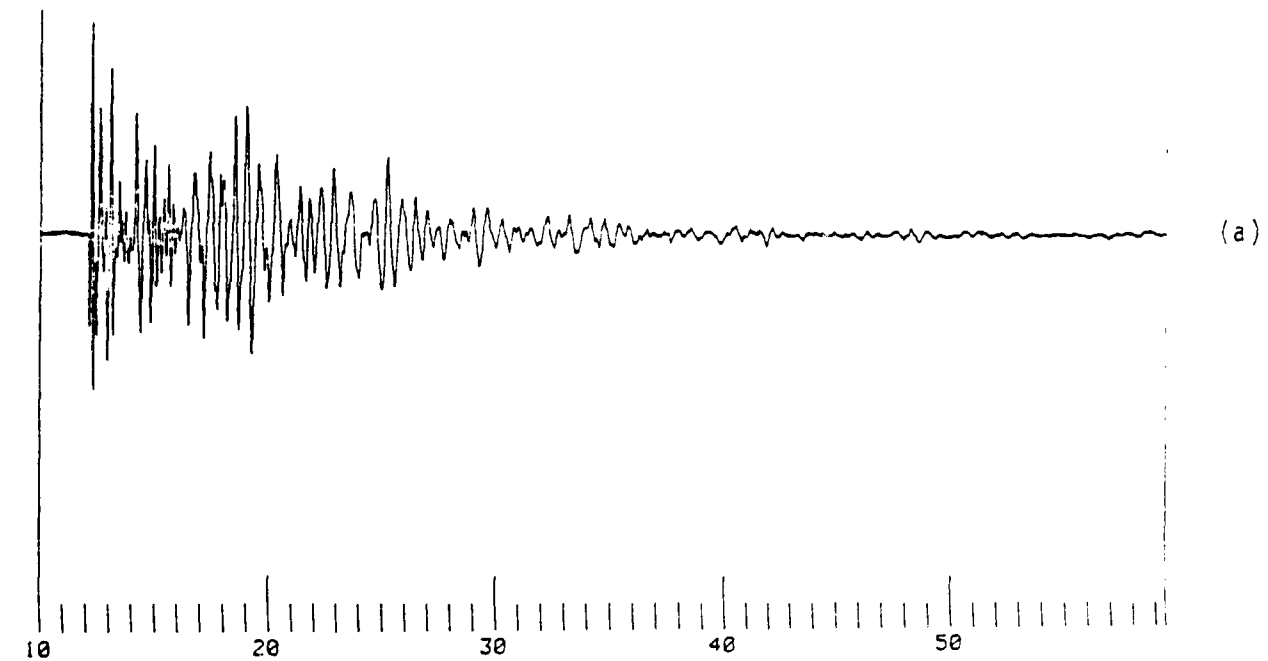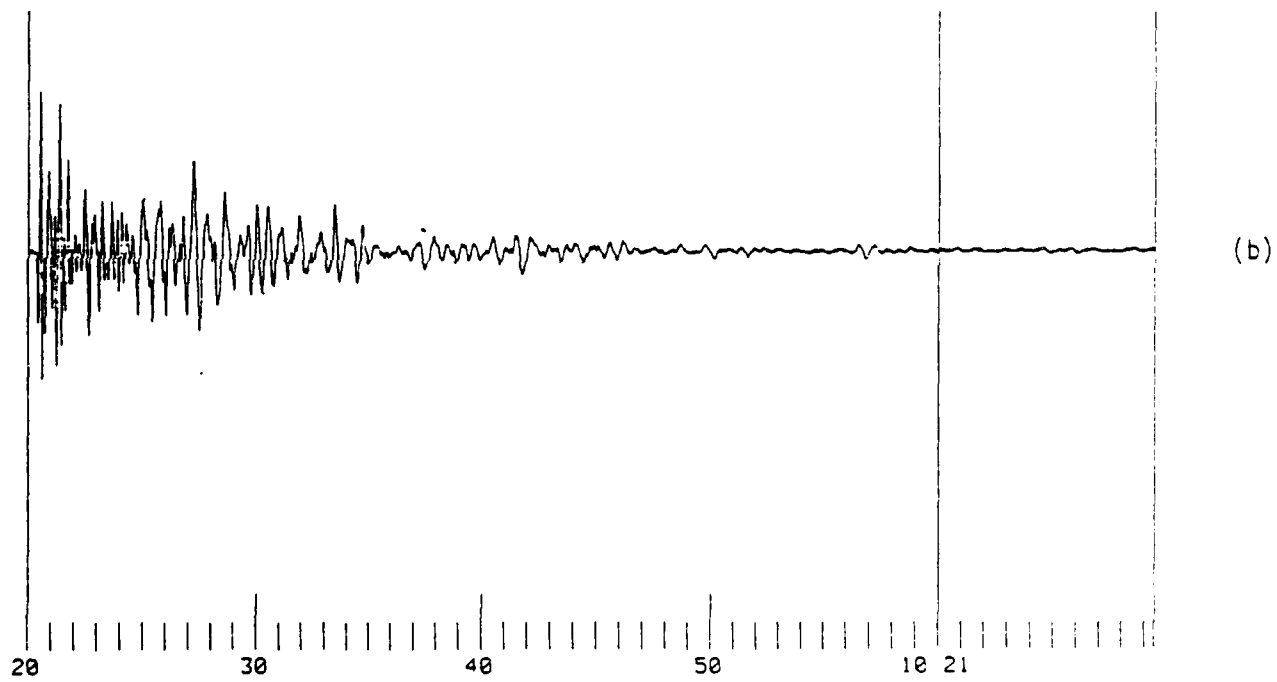
Figure 2. Two of the selected quarry blast records from approximately 10,000 lb. blasts at the Usibelli Coal Mine.
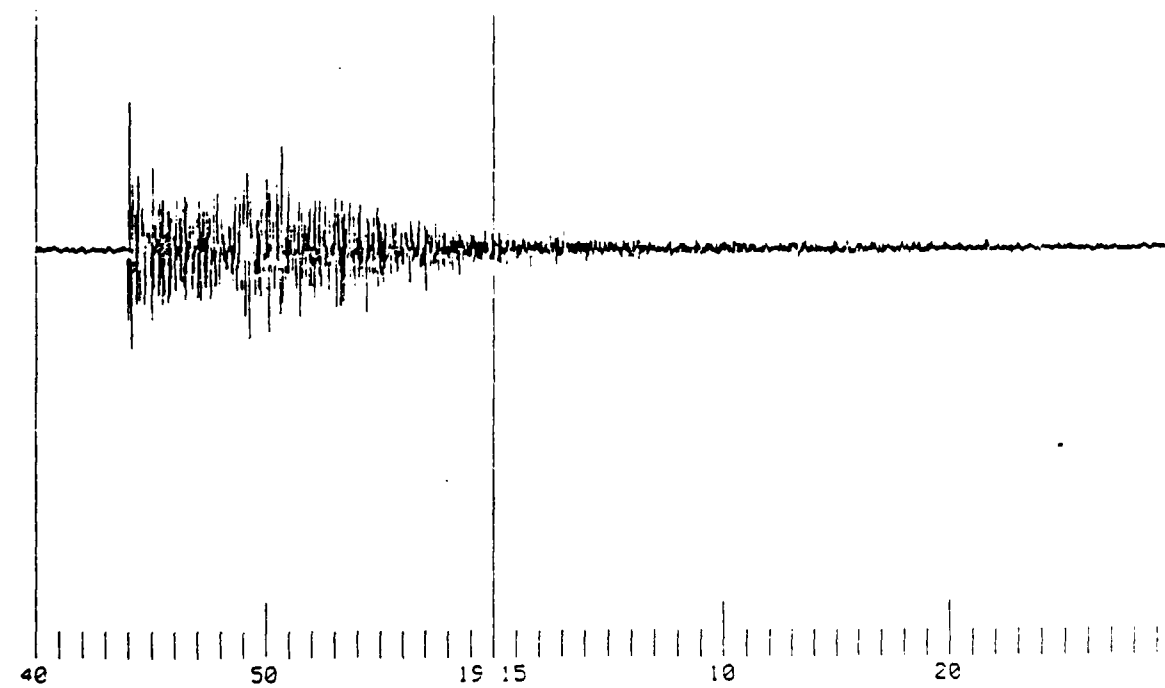
1985   DAY 254   TIME 19 14   STATION MCK
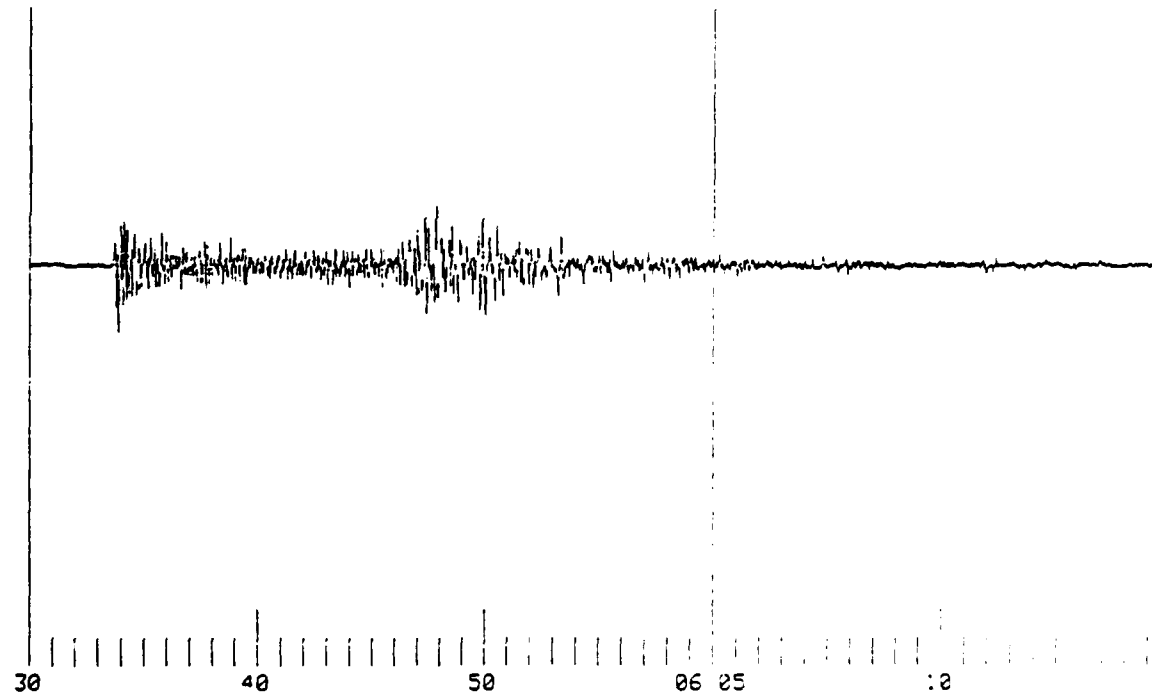
1985   DAY 278   TIME 06 04   STATION MCK

Figure 3. Two of the selected small, shallow
earthquakes (<4 magnitude, 2-4 km hypocentral
depth).

of the earthquakes and quarry blasts, selected from those previously discussed, support the observable differences in their frequency content. The quarry blast amplitude spectra show a rapid amplitude decay and lower frequency content compared to the small, shallow earthquake amplitude spectra.

Another difference between the selected earthquake and quarry blast seismograms involve the existence of two distinct waveform-wavetrain packets or envelopes in the seismograms. In order to better examine the envelopes, let's designate the early arrival envelope of the quarry blast seismograms (Figure 2) the P envelope whereas the second distinct envelope will be the Rg envelope. The earthquake records' (Figure 3) early arrival envelope will also be designated as a P envelope, however the later arriving envelope will be labeled the S envelope. Using a four pole band-pass butterworth filter, the selected seismograms were filtered at center frequencies of 0.5, 0.75, 1.0, 1.5, 2.0, 4.0, 6.0, 10.0, 12.0, 14.0 and 16.0. Subsequently, the maximum peak-to-peak amplitude of the two envelopes in each seismogram were plotted versus center frequency. Note Figure 4 where additional differences between the two sources are apparent. There exist two distinctly different groups of curves -- those curves represented by the small, shallow earthquakes versus the curves represented by the quarry blasts. The first arrival P envelope of the earthquake versus the quarry blast reveal the following:

Figure 4. The relationship between amplitude and center frequency of earthquakes and blasts selected for this study.

1. the earthquake frequency signature encompass a larger bandwidth than those of the blasts.

2. after peaking at a maximum amplitude, the earthquake amplitudes oscillate slowly as they decay and thus do not decrease linearly.

3. the earthquake arrivals gradually rise to a peak amplitude whereas the quarry blast curves rapidly peak and rapidly decay.

The second arrival curves, the S envelope in the earthquakes and the Rg envelope in the quarry blast seismograms, reveal the following:

1. the earthquake curves reach a maximum amplitude exponentially.

2. the quarry blast curves reach a maximum amplitude in a characteristic parabolic manner, and again they encompass a smaller frequency bandwidth.

b. Thus, the procedures followed in step a, the observational discrimination between the quarry blast and small, shallow earthquake seismograms, strongly suggest that their signals are distinctly different. The first motion arrivals and the differences in the two sources' frequency content validate their observed differences.

IV.

a. The next approach taken in this effort involved the synthetic waveform modelling of the selected vertical component seismograms. The theoretical ground motion, or impulse response of the earth, was generated by a solution of the integral representation of a

disturbance which has traversed through an earth model in some specified mode of propagation. This is computed using the Cagniard-de-Hoop method to solve the inhomogeneous wave equation and by applying the method of generalized reflection and transmission coefficients for a multilayered model. During this process, the effects of instrumentation and source time function are kept constant while the attenuation properties of each layer are ignored to reduce the complexity. A discussion of the algorithms may be found in Helmberger (1968, 1974) and Helmberger and Harkrider (1977).

The compressional reflected and refracted waves which were used in generating the synthetic seismograms are described by listing the layer numbers of the crust in which they have traversed. The travel paths of head waves are not necessary in ray files because ASREXP computes the head wave response for incident waves that reach the critical angle. In addition, in an effort to generate synthetic seismograms at the MCK station, a variation of a crustal model published by Hanson, Berg and Gedney (1968) was used (Figure 5b).

b. The synthetic waveform modelling effort produced the following results:

1. Although a crustal model of the Healy area was utilized, it did not produce synthetic seismograms that fit all of the phases of the observed records. For example, Figure 5a, a synthetic seismogram model of Figure 2a, a quarry blast record, shows similar waveform

42-14
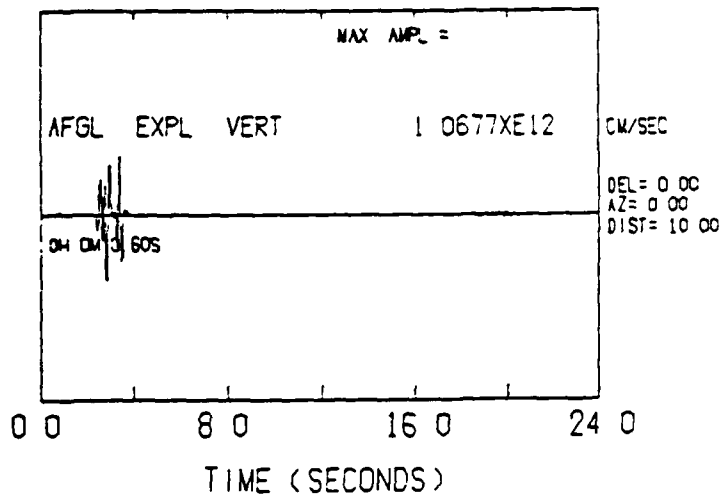
Figure 5a. Synthetic seismogram model of a quarry blast (Figure 2a).
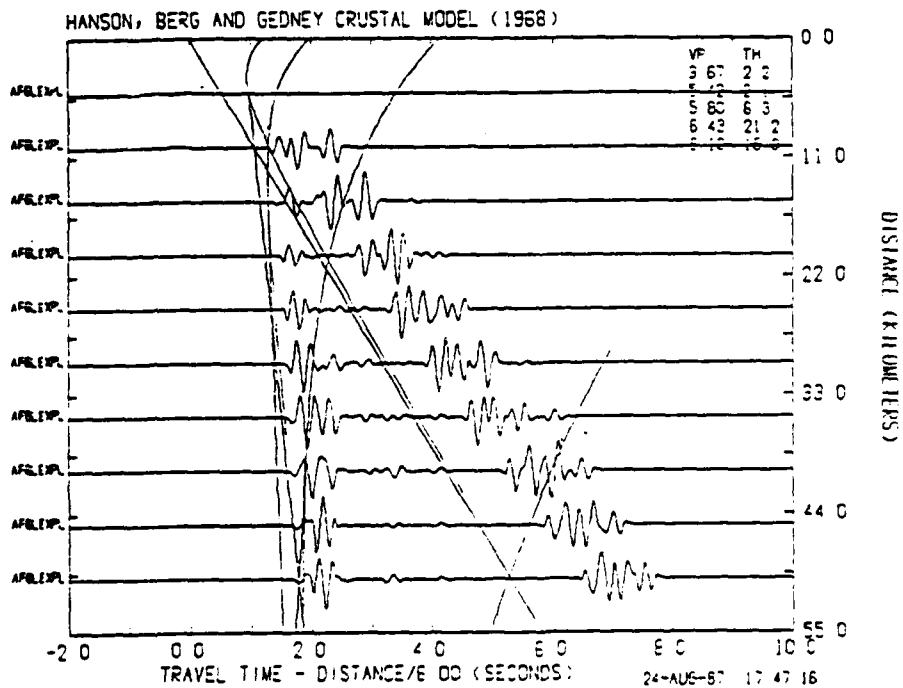
Figure 5b. Synthetic record section of a quarry blast (Figure 2a).

characteristics and good timing, however the last large amplitude

arrival does not reveal an accurate amplitude determination.

2. In order to better examine the phase development of the selected

data, synthetic vertical component record sections were generated.

Figure 5b, a synthetic record section of Figure 2a, a quarry

blast record, shows the travel times for a range of 0-55 km

source-to-receiver distances. Note that when the travel times

of the various reflected and refracted arrivals are compared to

the arrivals on the observed quarry blast record, they additionally

do not provide an appropriate fit.

V. RECOMMENDATIONS

Since the arrival time and shape of seismic phases provide us with

information regarding the structure and physical properties of the

earth's crust, the following recommendations are suggested for

improving the fit of waveform phases:

1. One explanation for the inaccurate fit previously discussed

involves the possibility of gradational layering below some or

all of the crustal discontinuities. Note that the earlier phases

of Figure 5a closely approximate the observed quarry blast in

Figure 2a, however the later phases do not. This suggests that

the upper crustal discontinuity is, indeed, a sharp boundary,

whereas the lower crustal discontinuities may be gradational.

The earth model used in generating the synthetic seismograms

is characterized by sharp discontinuities within the earth's crust, therefore any further attempt at modelling the selected records should include an investigation of the effects of gradational layering.

2. An additional recommendation involves the limitations of the ray file utilized. The ray file used in the synthetic waveform modelling contains only three rays representative of P to S conversions. Helmberger and Morris (1970) found, in their investigation of a marine refraction profile, prominent second arrivals at short distances representative of transformed shear waves. According to White and Stephen (1980), wave conversion occurs most efficiently where the seismic wave encounters a large velocity contrast over a distance of less than half a wavelength. The Healy area, for example, is ideal for compressional to shear wave (or vice versa) conversion due to the sharp interface between the upper alluvial sediments and schist and the lower granitic rocks. Thus, the ray file should be expanded to include additional converted rays and multiple bounces in the upper crust.

3. The third recommendation involves the effects of time-delayed blasting (ripple fire blasting method). In the previously generated synthetics, a single explosive source was used for modelling the quarry blasts, however many (Frantti, 1963, Willis, 1963, Pilant and Knopoff, 1964) have shown that time-delayed blasting produces changes in the seismic signal spectra. Therefore, future attempts

42-17

at modelling should include multiple sources with time-delays

representative of the method used at the Usibelli Coal Mine.

In order to complete the synthetic waveform modelling and subsequently

discern differences in the synthetically generated phases and the

observed signals (and to predict differences associated with the various

sources), a proposal will be submitted to the AFOSR Mini Grant Program.

REFERENCES

Biswas, N. N., J. C. Lahr, and R. A. Page, Some results on the seismicity of Alaska, EOS, 67, 1236, 1986.

Frantti, G. E., Spectral energy density for quarry explosions, Bulletin of the Seismological Society of America, 53, 989-996, 1963.

Hanson, K., E. Berg, and L. Gedney, A seismic refraction profile and crustal structure in central interior Alaska, Bulletin of the Seismological Society of America, 58, 1657-1665, 1968.

Helmberger, D. V., The crust-mantle transition in the Bering Sea, Geological Society of America Bulletin, 58, 179-214, 1968.

Helmberger, D. V., Generalized ray theory for shear dislocations, Bulletin of the Seismological Society of America, 64, 45-64, 1974.

Helmberger, D. V. and D. G. Harkrider, Modeling earthquakes with generalized ray theory, in Modern Problems in Elastic Wave Propagation, edited by J. Miklowitz and J. D. Achenbach, 499-518, John Wiley and Sons, New York, New York, 1977.

Helmberger, D. V. and G. B. Morris, A travel time and amplitude interpretation of a marine refraction profile: transformed shear waves, Bulletin of the Seismological Society of America, 60, 593-600, 1970.

Pilant, W. L. and L. Knopoff, Observations of multiple seismic events, Bulletin of the Seismological Society of America, 54, 19-39, 1964.

White, R. S. and R. A. Stephen, Compressional to shear wave conversion in oceanic crust, Royal Astronomical Society Geophysical Journal, 63, 547-565, 1980.

Willis, D. E., A note on the effect of ripple firing on the spectra of quarry shots, Bulletin of the Seismological Society of America, 53, 79-85, 1963.

1987 USAF-UES SUMMER FACULTY RESEARCH PROGRAM/

GRADUATE STUDENT SUMMER SUPPORT PROGRAM

Sponsored by the

AIR FORCE OFFICE OF SCIENTIFIC RESEARCH

Conducted by the

Universal Energy Systems, Inc.

FINAL REPORT

A STUDY OF SERVICE DEMAND DISTRIBUTION AND TASK ORGANIZATION

FOR THE ANALYSIS OF ENVIRONMENTAL SAMPLES AND ASSOCIATED

SUPPORT SERVICES AT THE USAF OCCUPATIONAL AND ENVIRONMENTAL

HEALTH LABORATORY - BROOKS AFB, SAN ANTONIO, TEXAS

Prepared by:	Don E. Deal, Ph.D. and Gary Lake
Academic Rank:	Assistant Professor
Department and	Industrial Engineering
University:	University of Houston
Research Location:	USAF/OEHL
	Brooks AFB
	San Antonio, Texas 78235
USAF Researcher:	Mr. Frank Marcie
Date:	30 August 1987
Contract No:	F49620-85-C-0013

REFERENCE DR. DEAL

SFRP FINAL REPORT NUMBER 35

1987 USAF-UES SUMMER FACULTY RESEARCH PROGRAM/

GRADUATE STUDENT SUMMER SUPPORT PROGRAM

Sponsored by the

AIR FORCE OFFICE OF SCIENTIFIC RESEARCH

Conducted by the

Universal Energy Systems, Inc.

<u>FINAL REPORT</u>

<u>WAVE PROPAGATION IN LAYERED STRUCTURES</u>

Prepared by: David W. Landis

Academic Rank: Graduate Student

Department and   Department of Civil Engineering

  University: Auburn University

Research Location: HQ AFESC/RDCS
                          Tyndall AFB
                          Panama City, Florida

USAF Researcher: John R. Hayes

Date: September 1987

Contract No.:   F49620-85-C-0013

Wave Propagation in Layered Structures

by

David W. Landis

ABSTRACT

Protective military shelters are typically constructed
of massive, monolithic, reinforced concrete slabs. This is
considered necessary in order to protect personnel and vital
equipment inside the shelter from the spall caused by the
high-intensity blast waves caused by conventional weaponry.
Recent studies show that layered structures may be an
alternative to the massive monolithic construction.

The objective of this study is to show that the
implementation of layered structures can significantly
reduce or eliminate the incidence of interior spalling of
the concrete walls. The layered structures considered in
this study are concrete-sand-concrete and concrete-
polystyrene-concrete models.

This study presents the results of a numerical study to
evaluate the effectiveness of layered structures in reducing
the transmission of high-intensity blast waves. The results
show that layered structures can be very effective in the
reduction in stress wave transmission.

ACKNOWLEDGEMENTS

I. INTRODUCTION

Protective military shelters are designed to house
personnel, vital functions, or equipment of value. As a
result, the structures are usually massive, consisting
primarily of reinforced concrete and soil as the main
building materials. Damage to these protective shelters
resulting from conventional (non-nuclear) weapons occurs as
a result of one or more of the following effects:
penetration, fragmentation, and blast. Penetration is a
consideration only in the case of a direct hit, and
fragmentation in cases of direct hits or near misses [1,2].

Conventional protective shelters are typically
constructed of massive monolithic concrete walls. This is
considered necessary to protect the personnel and equipment
inside from the interior spalling of the concrete walls.
Recent studies [1,3,4] have indicated that the use of
layered structures may provide an alternative to the massive
monolithic concrete walls currently in use.

II. OBJECTIVES OF THE RESEARCH EFFORT

Conventional protective shelters are typically
constructed of thick concrete walls. When these monolithic
walls are loaded with a high-pressure blast wave, the
interior face of the wall often spalls, causing injury to
equipment and occupants in the shelter. Previous approaches
to prevent spalling include the use of thicker walls, steel
spall plates on the interior wall face, and soil berms at
the wall exterior. The results of this research effort will
show that the implementation of layered structures can
significantly reduce or eliminate the incidence of interior
spalling of the concrete walls. The layered structures
considered in this study are shown in Figure 1.
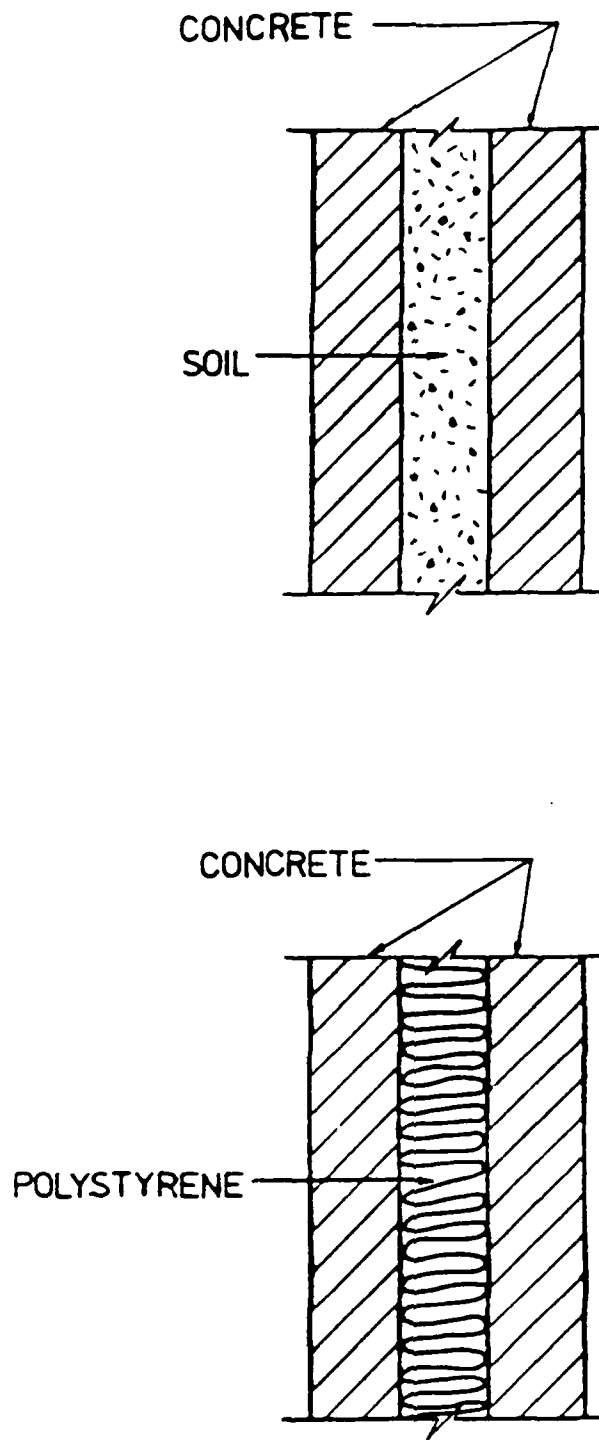
Figure 1. Layered structures considered in this study.

III. THEORETICAL OVERVIEW

Spalling is the fracturing caused when a high-intensity stress wave reflects from a free surface. In the case of a blast wave encountering a monolithic concrete wall (see Figure 2a), the compressive longitudinal wave contacts the exterior surface of the wall and propagates through the wall until it reaches a material boundary. In this case, the material boudary is the free surface at the interior face of the wall. When the compression wave reaches this free surface, it is reflected at full stress level as a tension wave. It is this reflected tensile wave which causes the concrete to spall at the interior face of the wall. The spalled fragments of concrete are then thrown away from the face of the wall at very high velocities, often causing severe injury to the personnel or equipment inside.

In the case of a layered structure (see Figure 2b), the compression wave propagates through the exterior layer until it encounters the boundary between the exterior layer of concrete and the absorption layer (sand or polystyrene in this case). At this material boundary, a portion of the compression wave is transmitted to the absorption layer and the remaining stress wave is reflected back through the exterior layer. The magnitude of the stress wave transmitted is determined by the relative impedances of the two materials. The absorption layer absorbs any spalled fragments from the exterior layer. The transmitted compression wave propagates through the absorption layer until

SOLID
CONCRETE

REFLECTED TENSILE
WAVE

SPALLING AT
INTERIOR FACE
OF WALL

COMPRESSIVE
LONGITUDINAL WAVE

P_o

DYNAMIC
BLAST
LOADING

a) MONOLITHIC WALL

CONCRETE

ABSORPTION LAYER

CONCRETE

REFLECTED TENSILE WAVE AT MATERIAL
BOUNDARIES

LITTLE OR
NO SPALLING

P_o

COMPRESSIVE LONGITUDINAL WAVE

b) LAYERED WALL
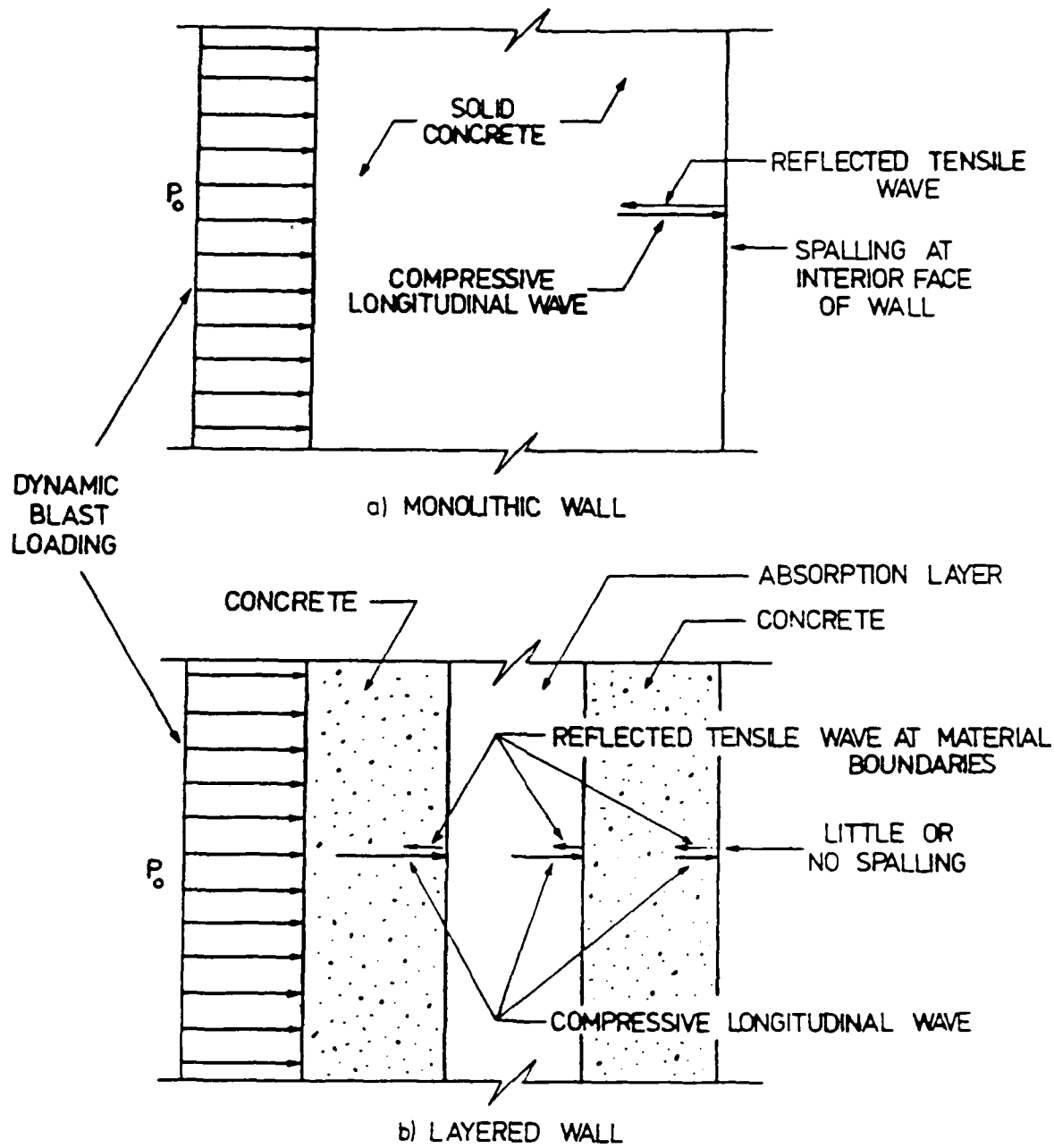
Figure 2. Layered structure theory.

the boundary between the absorption layer and the interior

layer is encountered. A portion of the compression is

transmitted to the interior layer of concrete and the

remaining stress wave is reflected back through the

absorption layer. The magnitude of the stress wave

transmitted is determined by the relative impedances of the

absorption layer and the interior layer of concrete. If the

compression wave has been sufficiently reduced, then the

interior wall will not spall.

IV. DESCRIPTION OF STUDY

A Finite Element Method (FEM) analysis implementing the
ADINA computer programs was conducted on a simple model of a
layered structure. Six FEM models were utilized. Each
model consisted of three layers: an 8" exterior layer of
concrete, an absorption layer of varying size and material
(see Table 1), and an 8" interior layer of concrete (see
Figure 3). The material properties are shown in Table 2.
For the simplicity of this analysis, the materials were
assumed to exhibit linear behavior only.

The FEM models consisted of 9-noded, two-dimensional
finite elements. The number of elements used in the model
was increased until reasonably smooth stress curves were
obtained. The element size used in the final analysis is
0.16" square.

A rectangular pressure wave was selected so that the
results could be interpreted with greater ease. The
duration of the pulse was selected in a manner such that the
stress wave reflections would not interfere in the analysis.
A duration of 50 E-6 seconds was determined to be adequate
for the analysis. See Figure 4 for the load time history.

The dynamic analysis was executed on the CDC Cyber 730
at HQ AFESC, Tyndall AFB, FL, using the ADINA computer
programs [5]. The Newmark method of implicit time
integration was used with a consistent mass formulation.
The Newmark method is unconditionally stable, therefore time
step considerations were based entirely upon wave velocity

DYNAMIC LOAD

8" CONCRETE
50 ELEMENTS

8" or 4"
CONCRETE, SAND, or POLYSTRENE
50 or 25 ELEMENTS

8" CONCRETE
50 ELEMENTS
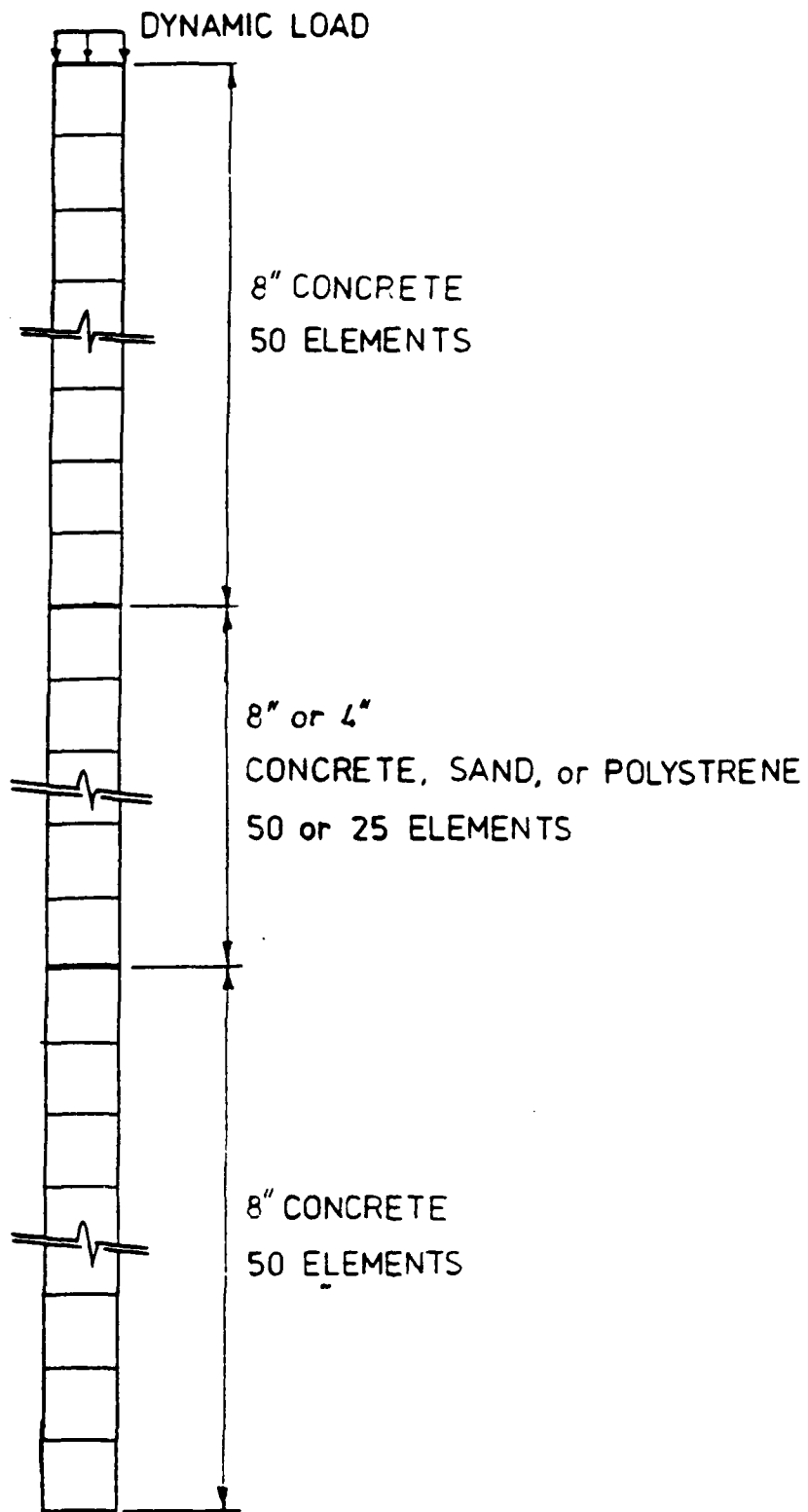
Figure 3.   Finite element model used in the wave propagation
analysis.
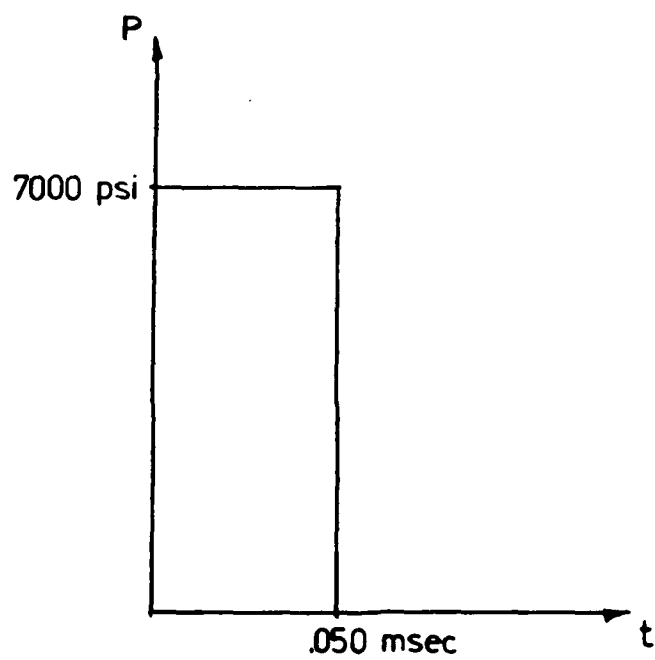
Figure 4. Dynamic load used in the wave propagation analysis.

and the location of element integration points. The time step must be less than or equal to the time required for the wave to travel from one integration point to the next. The time step used in this analysis is 0.6175 E-6 seconds.

Table 1. Absorption layer size and material.

Model	Absorption Layer
IA	8" concrete
IB	4" concrete
IIA	8" sand
IIB	4" sand
IIIA	8" polystyrene
IIIB	4" polystyrene

Table 2. Material properties.

Material Parameter	Concrete	Sand	Polystyrene
Unit Weight (pcf)	145	110	5.744
Mass Density (lb-sec /in)	217.164 E-6	164.75 E-6	8.604 E-6
Young's Modulus (psi)	3,640,000	100,000	2,100
Poisson's Ratio	0.18	0.25	0.15

V. RESULTS OF ANALYSIS

A time history for a point in the solid concrete model is shown in Figure 5. This time history shows both the incident compression wave and the reflected tension wave. As expected, the reflected tension wave is the same magnitude as the incident compression wave. This time history is very similar to results obtained from Split-Hopkinson Pressure Bar studies [6] (see Figure 6).

A time history for a point in the absorption layer of the concrete-sand-concrete model (model IIA) is shown in Figure 7. The magnitude of the transmitted compression wave is less than that of the incident compression wave. The second and third waves in the figure are a result of reflections propagating in the exterior layer of concrete.

A time history for a point in the polystyrene of model IIIB is shown in Figure 8. The magnitude of the transmitted compression wave is much less than that of the incident compression wave. As in the concrete-sand-concrete model, the second and third waves in the figure are a result of reflections propagating in the exterior layer of concrete.

A time history for a point in the interior concrete wall of the concrete-polystyrene-concrete model (model IIIA) is shown in Figure 9. Note that the magnitude of the transmitted compression wave is much less than that of the applied pulse.
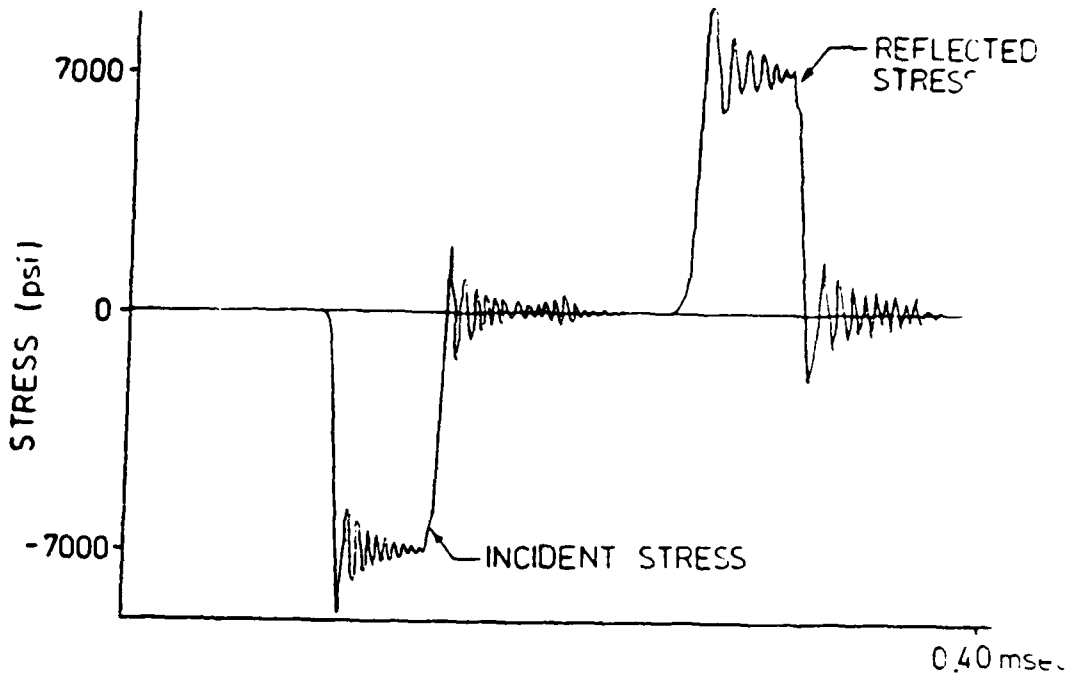
Figure 5.   Typical stress time history for a point in the
            solid concrete model.
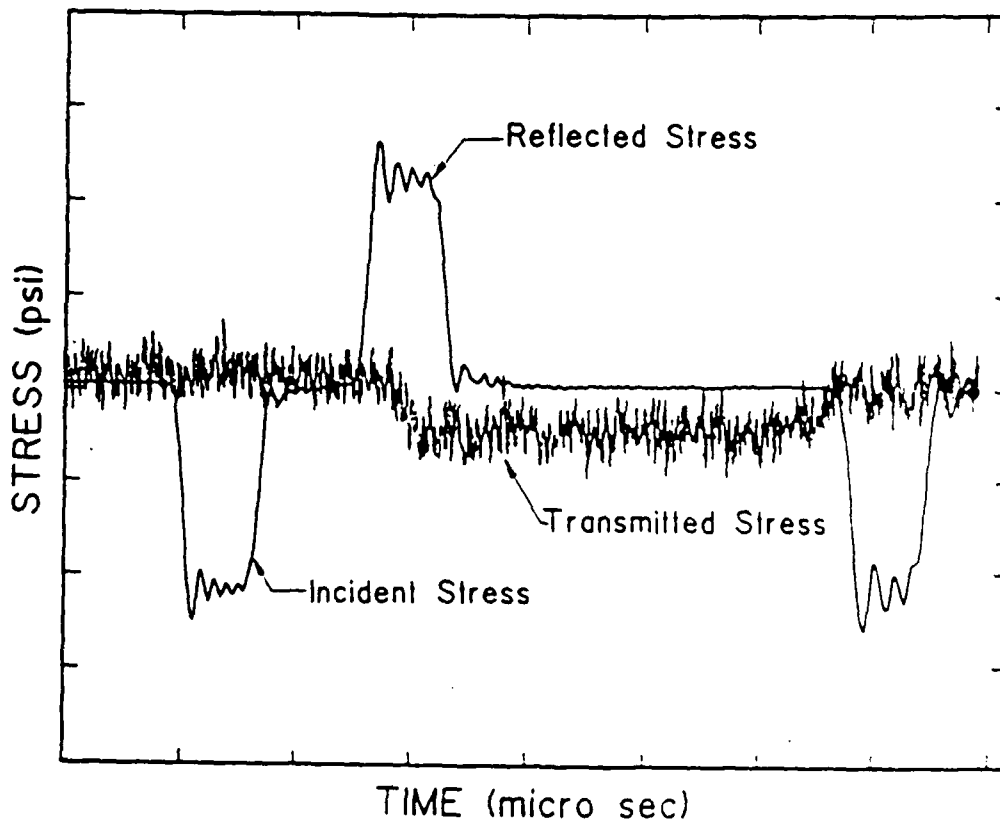
Figure 6.   Typical Split-Hopkinson Pressure Bar stress
            trace.
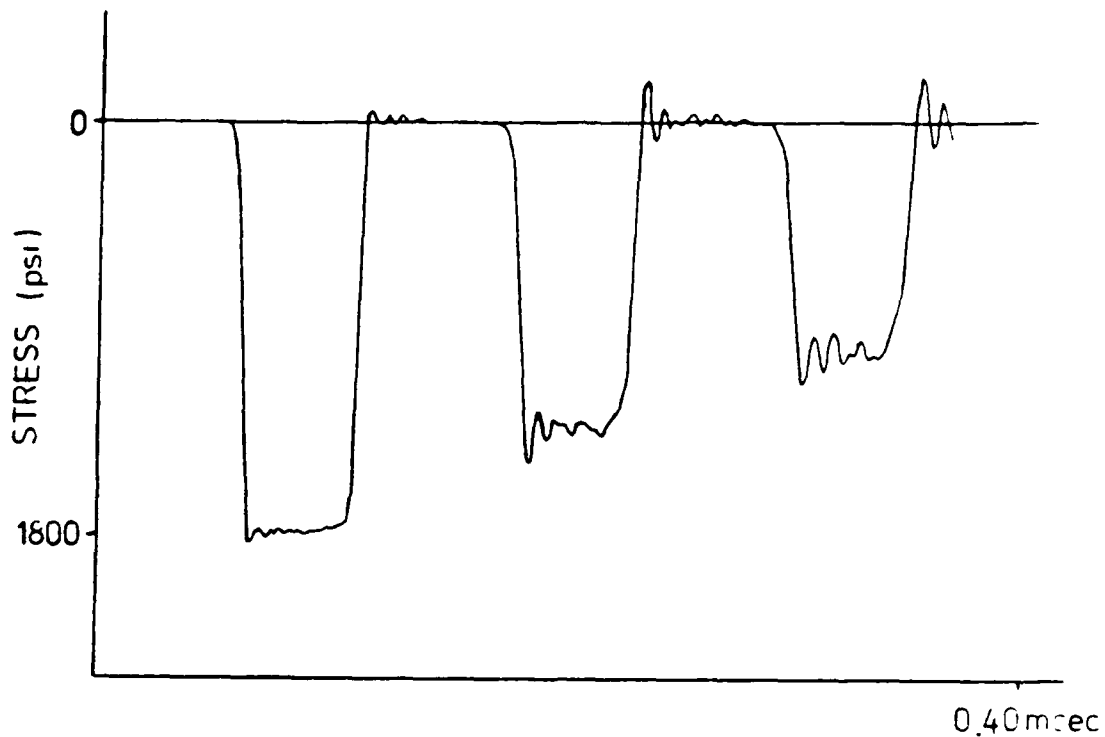
Figure 7. Stress time history for a point in the sand layer
in the concrete-sand-concrete model.
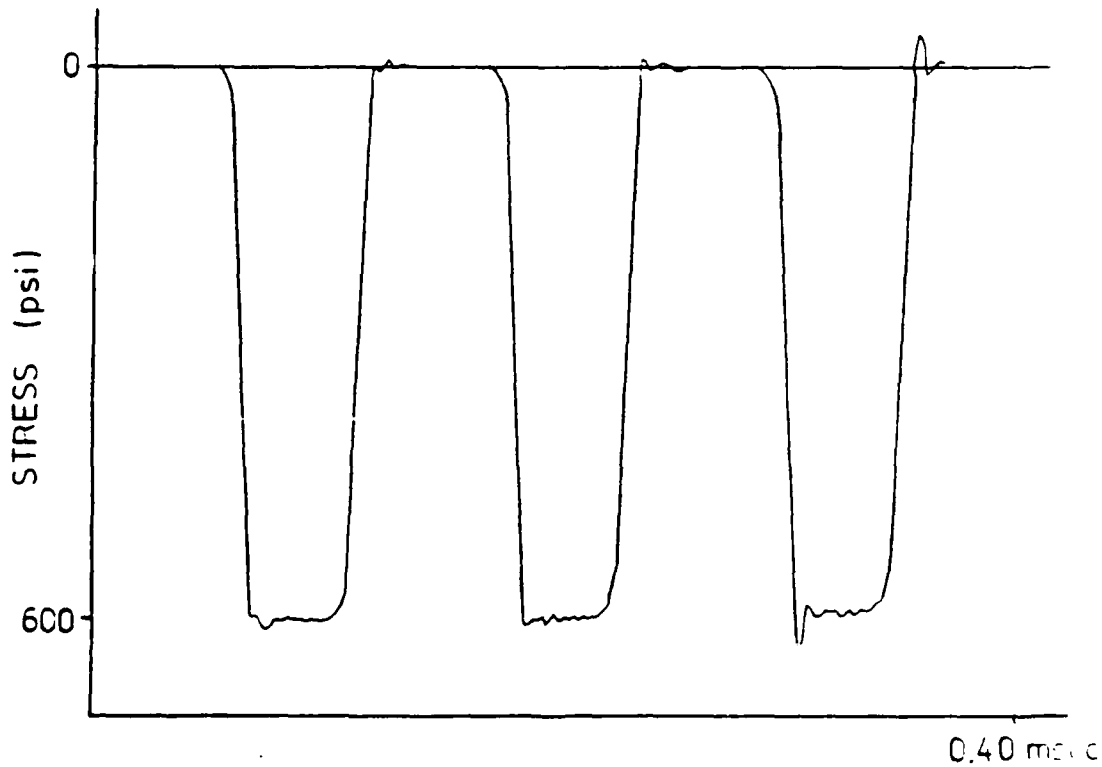
Figure 8. Stress time history for a point in the polystyrene
in the concrete-polystyrene-concrete model.

44-16
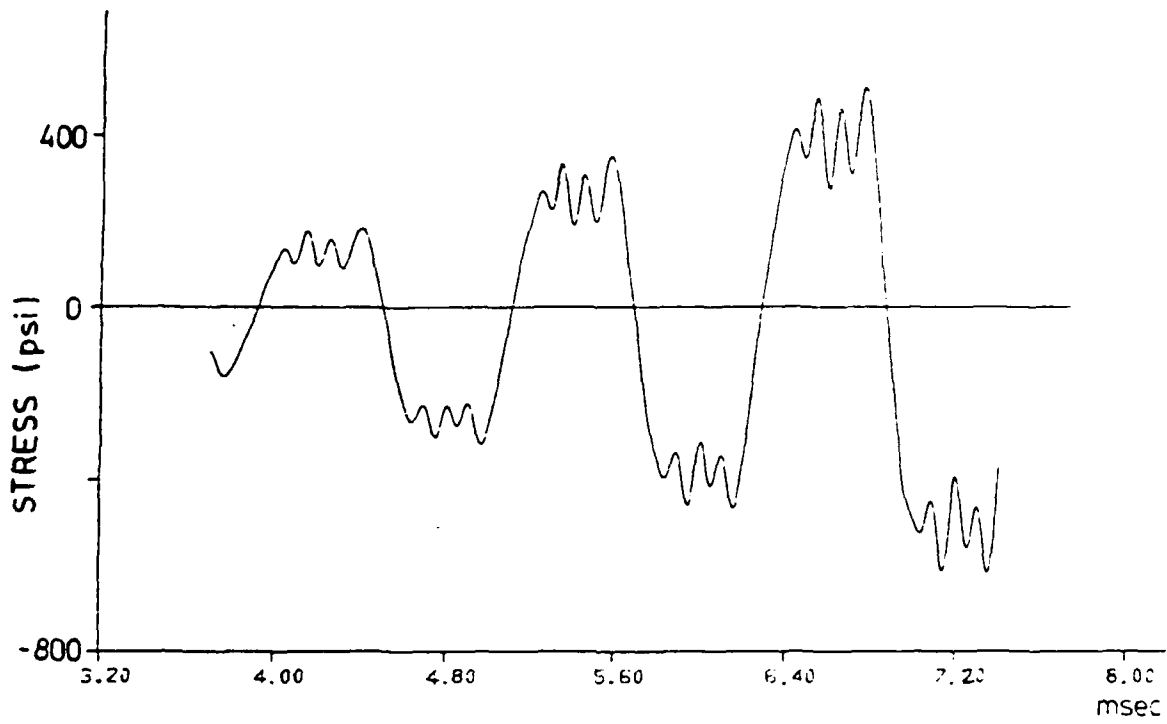
Figure 9.   Stress time history for a point in the interior
            concrete wall in the concrete-polystyrene-concrete
            model.

Transmission ratios (magnitude of stress at interior face of interior wall / magnitude of applied pulse) are shown in Table 3. The concrete-sand-concrete models were effective at reducing the transmitted stresses, with a transmission ratio of 0.64 to 0.71 (or a reduction in stress of about 29 to 36 percent). The concrete-polystyrene-concrete models reduced the stress a significant amount, with transmission ratios of 0.04 to 0.08 (or a reduction in stress of about 92 to 96 percent).

Table 3. Summary of transmission ratios.

Model	Transmission ratio
IA	1.0
IB	1.0
IIA	0.71
IIB	0.64
IIIA	0.04
IIIB	0.08

VI. RECOMMENDATIONS

Current protective shelters utilize massive monolithic concrete walls, steel spall plates, or large earth berms in an attempt to control spalling caused by high-intensity blast waves. This study shows that layered systems are a viable alternative in controlling interior spalling. The results of this study are very promising but are by no means conclusive.

It is recommended that a more comprehensive study be conducted. Further numerical studies should take into account nonlinear behavior of the materials. This may show an even greater reduction in transmitted stresses. Further studies should also investigate the effect of varying the thicknesses of the exterior layer, the absorption layer, and the interior layer.

The polystyrene proved to be the best material for the attentuation of stress waves in this study. Further studies should investigate the effect of other types of foams on the transmission of stress waves. Foams with even lower impedances may even further reduce the transmitted stresses.

The stress waves obtained in this study compared very well to those obtained in the Split-Hopkinson Pressure Bar tests. It is further recommended that additional experimental studies with the Split-Hopkinson Pressure Bar be conducted to verify the results of the numerical studies.

REFERENCES

1. Tedesco, J.W., Hayes, J.R., and Landis, D.W., "Dynamic Response of Layered Structures Subject to Blast Effects of Non-Nuclear Weaponry", _Journal of Computers and Structures_, Vol. 26, No. 1/2, pp. 79-86, 1987.

2. _Fundamentals of Protective Design for Conventional Weapons_, Department of the Army, Waterways Experiment Station, Corps of Engineers, Vicksburg, MS, 1984.

3. Eytan, R., Design of Layered Structures Against Conventional Weapons. Proceedings of the Second Symposium on the Interaction of Nonnuclear Munitions with Structures, Panama City Beach, FL, 15-18 April, pp. 68-73, 1985.

4. Balags, P. and Vretblad, B., Model Tests on Composite Slabs of Light Gauge Metal and Concrete Subjected to Blast Loading. Proceedings of the Second Symposium on the Interaction of Nonnuclear Munitions with Structures, Panama City Beach, FL, 15-18 April, pp. 68-73, 1985.

5. _ADINA - A Finite Element Computer Program for Automatic Dynamic Incremental Nonlinear Analysis_, Report AE 84-1, ADINA Engineering, Inc., Watertown, MA, 1983.

6. Tedesco, J.W., _Pressure Waves in Foam and Foam-Sand Samples_, Final Report, submitted to AFOSR, Washington, D.C., September 1985

1987 USAF-UES SUMMER FACULTY RESEARCH PROGRAM

GRADUTE STUDENT SUMMER SUPPORT PROGRAM

Sponsored by the

AIR FORCE OFFICE OF SCIENTIFIC RESEARCH

Conducted by the

Universal Energy Systems, Inc.

<u>FINAL REPORT</u>

<u>INSTALLATION OF THE ADINA FEM COMPUTER PROGRAMS</u>

Prepared by:	Sharon K. Landis, E.I.T.
Academic Rank:	Master's Degree Candidate
Department and University:	Computer Science and Engineering Auburn University
Research location:	HQ AFESC Tyndall AFB, FL 32403
USAF Researcher:	John R. Hayes, Senior Scientist
Date:	September 1987
Contract No.:	F49620-85-C-0013

INSTALLATION OF THE ADINA FEM COMPUTER PROGRAMS

by

Sharon K. Landis

ABSTRACT

The ADINA computer program package consists of four separate computer programs to be used in conjunction with one another: ADINA-IN, ADINA, ADINAT, and ADINA-PLOT. The ADINA programs are for the static and dynamic, linear and nonlinear finite element analysis of solids, structures, and fluid-structure systems.

Due to the large size of the ADINA programs, ADINA-IN, ADINA, ADINAT and ADINA-PLOT must be broken into smaller modules to minimize the amount of central memory occupied by the ADINA programs. If the ADINA programs occupy less central memory, then a larger finite element problem can be solved. Also, a user-friendly interface was developed to aid the users at HQ AFESC/RDC in executing any of the ADINA programs.

ACKNOWLEDGEMENTS

I wish to thank the Air Force Systems Command and the Air Force Office of Scientific Research for sponsorship of this research. Universal Energy Systems must be mentioned for their concern and help to me in all administrative and directional aspects of this program.

My experience was rewarding and enriching because of many different influences. John R. Hayes provided resources and support. Major Larry Bramlitt graciously solved many of my seemingly endless problems. Dr. Joseph Tedesco provided direction as well as introducing me to the UES GSSSP program. The help of Ken Williams was invaluable in overcoming many technical roadblocks on the CDC Cyber 730 computer.

I. INTRODUCTION

The finite element method is one of many attempts by scientists to reduce the complexity of some real-life problems to manageable proportions in order to analyze them. The ultimate goal of the different numerical procedures developed over the years is to find the solution to a complicated problem by solving a simpler one that closely represents the actual problem.

The finite element method is an example of simplifying a complicated problem by replacing the model with a series of smaller geometric shapes that closely approximate the original structure.

The Civil Engineering section of the Research and Developement Division of the Air Force Engineering and Services Center is interested in beginning in-house structural analysis. The ADINA program package consists of four separate computer programs to be used in conjunction with one another: ADINA-IN , ADINA, ADINAT, and ADINA-PLOT. The ADINA programs provide finite element analysis of linear and nonlinear, static and dynamic analysis of solids, structures, and fluid-structure systems.

My research interest has been in the area of Software Engineering and Software Testing. As a cooperative education student, my main duties were testing and evaluation of hardware/software computer systems. In addition, as a graduate research assistant, I worked on the design of a communications network for the Stategic Defense Initiative.

II. OBJECTIVES OF THE RESEARCH EFFORT

My main objective was to install the ADINA programs on HQ
AFESC's Control Data Corporation Cyber 730 computer, and to write
a service manual detailing the steps required to install the ADINA
programs. My secondary objective was to create a user-friendly
interface to the ADINA programs by guiding a user through a series
of menus. Finally, my third objective was to evaluate HQ
AFESC/RDC's current hardware and software in order to suggest any
improvements.

III. ADINA DESCRIPTIONS

A. ADINA-IN

ADINA-IN is a preprocessor for the ADINA and ADINAT
programs. ADINA-IN reads an unformatted data file containing
commands and creates a formatted datafile to be used by ADINA
or ADINAT. The ADINA-IN commands are easy to use and need
not be in any particular order. ADINA-IN is used to generate
the model, control the model parameters, determine the
analysis type and parameters, and control the output from
ADINA and ADINAT. ADINA-IN is also used to display the model
and model parameters; it is used to plot any view of the
model and to print out requested model and program
parameters. ADINA-IN includes a bandwidth minimizer which
provides for the most efficient program execution for any
particular problem.

B.   ADINA

ADINA (Automatic Dynamic Incremental Nonlinear Analysis) is the main module of the ADINA system. ADINA is a finite element computer program for the static and dynamic displacement and stress analysis of solids, structures, and fluid-structure systems. ADINA can be used for linear or nonlinear analyses. Input for ADINA can be accomplished manually or through the use of ADINA-IN. Creating a datafile for ADINA manually is a very tedious process, therefore the use of ADINA-IN is highly recommended.

c.   ADINAT

ADINAT (Automatic Dynamic Incremental Nonlinear Analysis of Temperatures) is a compatible hear transfer analysis program to the stress analysis program ADINA. ADINAT can be used for general linear and nonlinear steady-state and transient hear transfer analysis. ADINAT may also be used to solve other field problems, such as seepage and electric conduction.

D.   ADINA-PLOT

ADINA-PLOT is a post-processor for the ADINA and ADINAT programs. ADINA-PLOT uses a datafile created by ADINA and an unformatted command file created by the user to plot and list the results of the analysis. Deformed and undeformed meshes, mode shapes, time histories, variations of user-defined quantities, vector plots of principal stresses or strains, and response spectrums can be plotted or listed using ADINA-PLOT. Plotting of one variable as a function of

45-6

another variable can also be accomplished. These operations can be performed on the entire model or on selected areas of the model.

IV. INSTALLATION PROCEDURES

ADINA R&D Inc. delivered two magnetic tapes to HQ AFESC: Tape I contains the four Fortran source programs for ADINA-IN, ADINA, ADINAT, and ADINA-PLOT (tape format: 9 track, 1600 bpi, ASCII code, fixed block, record length 80, blocksize 5120, and unlabeled). Tape II contains files with simple verification problems and printer files that contain the results of the verification problems (tape format: 9 track, 1600 bpi, ASCII code, fixed block, record length 132, blocksize 5016, and unlabeled). A considerable amount of time was spent attempting to load the magnetic tapes on the Cyber 730.

Since the default values in some of the ADINA Fortran source codes did not agree with AFESC's equipment, some modifications to the ADINA Fortran source programs were necessary. These modifications enabled the ADINA programs to execute as efficiently as possible on AFESC's equipment.

The ADINA-IN, ADINA, ADINAT, and ADINA-PLOT programs comply with Fortran 77 programming standards and were compiled using the Fortran 5 compiler (FTN5) on the Cyber 730. A procedure file was created to compile the ADINA programs, using the correct defaults, simplifying the steps required to compile the ADINA programs. Figure 1 shows an example menu that will display on the user's terminal screen when the user requests to compile the ADINA programs.

Due to the large size of the ADINA programs, ADINA-IN, ADINA, ADINAT, and ADINA-PLOT must be broken into smaller modules to minimize the amount of central memory occupied by the program at

```
*  **********   CREATING ADINA LOAD MODULES  **********

1.  CREATE ADINA-IN LOAD MODULE.
2.  CREATE ADINA LOAD MODULE.
3.  CREATE ADINAT LOAD MODULE.
4.  CREATE ADINA-PLOT LOAD MODULE.
5.  CREATE ADINA-IN, ADINA, ADINAT, AND ADINA-PLOT LOAD MODULES

            Select from the list above and press NEXT:___
────────────────────────────────── 5 ──────────────────────────────────

THIS PROCEDURE WILL CREATE EXECUTABLE LOAD MODULES FOR
ADINA-IN, ADINA, ADINAT AND ADINA-PLOT.   THE USER
SHOULD FIRST VERIFY THAT THE EXECUTABLE LOAD MODULES EXIST
IN THE APPLICATIONS LIBRARY WITH THE "CATLIST,UN=APPLLIB"
COMMAND.   IF "ADINAIN", "ADINA", "ADINAT" AND "ADINAP"
ARE NOT LISTED IN THE DIRECT ACCESS FILES, THE USER SHOULD VERIFY
THAT THE UPDATED SOURCE FILES "ADNI", "ADN", "ADNT" AND "ADNP"
EXIST IN THE USER'S DIRECTORY AS WELL AS THE SEGMENTATION
DIRECTIVES "AISEGM", "ADSEGM", "ATSEGM", AND "APSEGM" BEFORE
EXECUTING THIS PROCEDURE.
```

F5 | HELP | F6 | QUIT |

Figure 1.

any given time. Larger problems can be processed if the amount of core memory used by the program is reduced. This is accomplished by segmenting the program. Segmentation works by breaking up or segmenting, a source program into groups of subroutines called segments. Much work was done trying to optimally segment the ADINA programs.

V. INTERFACE TO ADINA

Obtaining a solution to a problem involves these basic steps: the awareness of the problem; the diagnosis of the problem; the research and approach for treating the causes; the application of the solutions; the verification that the problem is solved; and the decision about future actions to prevent the problem from returning [4]. These were the criteria used in creating a menu-driven user-friendly interface to the ADINA programs.

The use of batch files will permit the ADINA programs to run in background mode, thus allowing the user continued access to the Cyber while any of the ADINA programs are executing. A procedure file was created to help the user's at AFESC to execute the ADINA programs. Figure 2 displays an example menu that would appear on the user's terminal when using this procedure file.

By using the Universal Plotting Software System (UNIPLOT), output plot files from ADINA-IN and ADINA-PLOT can be easily displayed on a graphics terminal, line printer, or a pen plotter. ADINA-IN and ADINA-PLOT accomplish this by creating a neutral plot library file that contains generic plotting commands. Using a post processor (UNIPOST), these generic plotting commands can be modified to run on the specific device requested by the user. Procedure files allowed the AFESC users to plot to either a

ADINA PROCEDURE FILE

ADINA DATA FILE: _____
ADINA PORTHOL FILE: _____

Specify values and press NEXT when ready
―――――――――――――――――ADINA――――――――――――――――――

THIS PROCEDURE WILL EXECUTE ADINA (AUTOMATIC DYNAMIC INCREMENTAL
NONLINEAR ANALYSIS) FINITE ELEMENT METHOD COMPUTER PROGRAM.
ADINA IS A FINITE ELEMENT COMPUTER PROGRAM FOR THE STATIC AND
DYNAMIC DISPLACEMENT AND STRESS ANALYSIS OF SOLIDS, STRUCTURES,
AND FLUID-STRUCTURE SYSTEMS. ADINA CAN BE USED FOR LINEAR OR
NONLINEAR ANALYSES. PLEASE CONSULT THE ADINA USER'S MANUAL
FOR FURTHER DETAILS. OUTPUT WILL BE AUTOMATICALLY ROUTED
TO THE LINE PRINTER.

F5 | HELP | F6 | QUIT |

Figure 2.
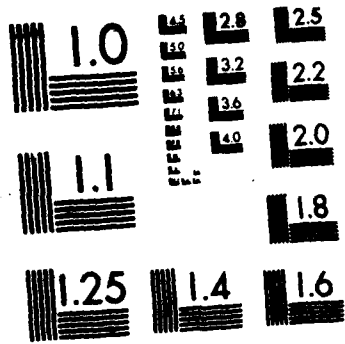
MICROCOPY RESOLUTION TEST CHART
NATIONAL BUREAU OF STANDARDS-1963-A

CALCOMP 907 plotter, a Tektronics compatible terminal screen, or a dot-matrix printer. In addition to the procedure file, a manual was created describing the procedure files and how to use the procedure files.

VI. EVALUATION OF HARDWARE/SOFTWARE

Since I spent more time than expected on installing the ADINA programs and creating the procedure files to interface with the ADINA programs, I was unable to adequately evaluate HQ AFESC/RDC's equipment. My initial evaluation determined that the engineers need access to more IBM AT (or compatible) microcomputers. I also reccommend communications links to both the Cyber 730 and the Wang minicomputer to better utilize the personnel's time.

VII. RECOMMENDATIONS

HQ AFESC's Cyber 730 proved to be extremely fast and accurate, but the small central memory severely limited the size of finite element analysis problem that could be solved. Only small problems (< 3500 degrees of freedom) could be analyzed.

The following are three possible solutions to solve the problem of the AFESC;s Cyber 730 small central memory for executing ADINA jobs:

1. Keep the current Cyber 730 (256 K words central memory) and upgrade the central memory to the maximum capacity of one Meg (1024 K words or four times the current central memory)

```
COSTS:
Model 7040-200 memory expansion ($600,000)
Hardware maintenance for memory ($2000/month)
Air conditioning upgrade ($35,000)
Power supply upgrade
Computer room reconfiguration
```

2.   Acquire Eglin AFB's Cyber 845 with two Meg of central memory. This option is not very definite since it depends on if Eglin AFB acquires a new Cyber.

COSTS:

Air conditioning upgrade ($50,000)
Software maintenance ($5000/month)
Computer room reconfiguration

The Cyber 845 has a maximum central memory capacity of 16 Meg, but this would require the following additional costs:

Model 18112-1 memory expansion ($45,000)
Hardware maintenance of memory ($260/month)
NOS/VE operating system software ($100,000 initial licensing
                        fees)
Disk drives ($54,000/drive)
Hardware maintenance of drives ($300/drive/month)
Disk drive controller ($25,000)

3.   Purchase computer time from another computer, preferably another Cyber since AFESC's Cyber 730 has proven itself extremely fast and accurate executing ADINA jobs.   Three possible Cyber remote sites to consider are:

    a.   FSU's Cyber 205
    b.   Eglin AFB's Cyber 845
    c.   Control Data Corporations's Cyber Net

It is also possible to purchase computer time from a supercomputer (Cray-XMP), but this would require a licensing change from ADINA R&D Inc.

REFERENCES

1. Brooks, Frederick P. Jr.,"No Silver Bullet: Essence and
    Accidents of Software Engineering", COMPUTER, Vol. 20,
    No. 4, April 1987, pp. 10 - 19.

2. Deitel, Harvey M., An Introduction to Operating Systems,
    Reading, Massachusetts, Addison-Wesley, 1984.

3. Madnick, Stuart E. and Donovan, John J., Operating Systems,
    New York, McGraw-Hill, 1974.

4. Shooman, Martin L., Software Engineering: Design,
    Reliability, and Management, New York, McGraw-Hill, 1983

1986 USAF-UES SUMMER FACULTY RESEARCH PROGRAM/

GRADUATE STUDENT SUMMER SUPPORT PROGRAM

SPONSORED BY THE

AIR FORCE OFFICE OF SCIENTIFIC RESEARCH

CONDUCTED BY THE

UNIVERSAL ENERGY SYSTEMS, INC.

FINAL REPORT

EXPERIMENTAL STUDY OF ISOTHERMAL FLOWS

IN A DUMP COMBUSTOR

Prepared by:	Craig A. Langenfeld
Academic Rank:	Graduate Student
Department and University:	Mechanical Engineering The Ohio State University
USAF Researcher:	Dr A. S. Nejad
Date:	September 25, 1987
Contract No:	F49620-85-C-0013

EXPERIMENTAL STUDY OF ISOTHERMAL FLOWS

IN A DUMP COMBUSTOR

BY

Craig A. Langenfeld

The Ohio State University

Department of Mechanical Engineering

206 W. 18th Street

Columbus, OH 43210

ABSTRACT

Isothermal flows in a dump combustor were studied for configurations of no swirl and of weak swirl, S = 0.3. Detailed mean flow and turbulence measurements in the axial and radial directions were obtained using a two-component coincident LDV system. Mean axial and radial velocity, axial and radial turbulence intensities and Reynolds stress profiles are plotted. The relativity of the data to previous work in the same model but for the axial and tangential directions is discussed. For the no swirl case, the flow does not become fully developed flow even at 24 step heights downstream. Turbulence intensities and Reynolds stresses peak at a shear layer generated by recirculating flow for locations before reattachment and decay out further downstream. For both no swirl and weak swirl, the Reynolds stress in the axial-radial plane was greater than for the axial-tangential plane for the shear layer region between the main flow and the recirculating flow.

ACKNOWLEDGMENTS

I. INTRODUCTION

I am currently a graduate student at the Ohio State University working for a Master of Science degree in Mechanical Engineering. It was through my advisor, Dr M. Samimy, of the Mechanical Engineering Department that I became involved with swirling flows in a dump combustor. In the summer of 1986, I participated in the USAF-UES Graduate Student Support Program in coordination with Dr Samimy's appointment to the Summer Faculty Research Program. I was also involved in follow up research in swirling flows. Having this experience contributed to my assignment to the Air Force Wright Aeronautical Laboratories.

II. OBJECTIVES OF THE RESEARCH EFFORT

The work discussed here is one phase of a larger study. The overall objective of the study is two fold. The first aspect is to explore isothermal swirling flows and to aid in understanding the physical processes. The second is to establish a bench mark set of experimental data for turbulence model development and assessment.

The work of Samimy et al (1) under this study did succeed in meeting these objectives in many ways. They were able to obtain detailed mean and turbulence data, including 2nd and 3rd order moments of turbulence fluctuations, with

good accuracy using a two-component LDV system. Their work, however, involved only measurements in the axial and tangential directions. The specific goal of this effort was to complement this previous work by exploring the radial direction by resolving the axial and radial directions with the two-componet LDV system. The radial data is helpful in understanding swirling flow and is important to establishing a bench mark set of data.

III. EXPERIMENTAL FACILITIES AND TECHNIQUES

The experimental model used in this effort is the same as that used and documented by Samimy et al (1). The only modification was in the optical access window on the combustor. An annular ring with an access window was fit in the pipe that enabled the window hole to be repositioned. This enabled the LDV probe volume to traverse the combustor model vertically to resolve the axial and radial directions.

The swirl generator used in this experiment was a constant angle axial flow type swirler with a swirl number of 0.3. Swirl number is defined as:

$$S = \int_{R_h}^{R_i} UW r^2 dr \bigg/ \left(R_i \int_{R_H}^{R_i} U^2 r\, dr \right) \qquad (1)$$

where U and W are the axial and tangential velocities, and R_h

and R_i are the hub and outer ring radii. The swirler had 12 curved inlet guide vanes and was located 50 mm upstream of the dump plane.

The TSI, Inc. frequency counter based two-component coincident LDV system, the LDV settings, the number of samples, and the method of seeding the flow were the same as that used by Samimy et al (1) in order to more accurately complement their work.

IV. EXPERIMENTAL RESULTS

Mean Flow Results

A total of 13 axial locations were investigated for the case of no swirl. The first location was 0.38 step heights from the dump plane and the last was 24 step heights downstream. No measurements closer than 0.38 step heights from the dump plane were possible since the swirler housing would block the laser beams of the LDV system. For the case of weak swirl, S = 0.3, the same 13 locations were desired but limitations forced only the first three locations to be investigated at this time.

Figure 1(a) shows selective axial profiles for the case of no swirl. As was expected and required for this data to complement the work by Samimy et al (1), the profiles agree

46-6

very closely to the axial profiles obtained when the axial-tangential plane was investigated (1). As was pointed out by Samimy et al, the slow decay of the core flow and the recirculation in the base region are typical of axisymmetric (2) and two-dimensional (3) backstep flows. Reattachment occurred approximately 8 step heights from the dump plane, agreeing closely with the previous work (1).

The axial profiles obtained for S = 0.3 shown in Figure 1(b) also agree with those of Samimy et al (1). There is a strong deceleration at the vortex core but vortex breakdown does not occur (1).

Figure 2(a) shows the mean radial velocity measurements for the no swirl configuration. For the positively marked radial locations, a positive radial velocity indicates flow is in a radially outward direction and negative velocity is in the inward direction, and vice versa for the negatively marked radial locations. The radial velocities are very small relative to the axial velocity of the incoming flow, as indicated by the scale. This also explains the difference in the smoothness of the radial to axial velocity profiles. Figure 2(a) shows relatively no radial velocity component for the central flow but radial velocities for the area of recirculating flow immediately after the dump plane. Further downstream, as the recirculation zone becomes smaller and the main flow expands, there is seen a velocity component in the

radially outward direction. This non-parallel flow is still seen at the last location investigated 24 step heights downstream.

The radial velocities for the locations studied for S = 0.3 are shown in Figure 2(b). For the central core (1) of the vortex, the radial velocities are in the radially inward direction for these locations immediately downstream of the swirler. Outside the central core the flow has a radially outward component until reaching the shear layer generated by the main flow and recirculation flow. In the recirculating area of the radial velocities are similar to those for the case of no swirl.

Turbulence Results

Figure 3(a) and (b) show the axial turbulence intensities obtained for the S = 0.0 and S = 0.3 cases, respectively. The profiles agree closely with Samimy et al (1), showing local peak values of turbulence intensities in the shear layer between the main flow and recirculating flow and also in the shear layer at the edge of the vortex for the case with swirl.

Figure 4 shows the radial turbulence intensities for both no swirl and weak swirl configurations. For the no swirl case, the radial turbulence intensities have local peaks and

slow development in the streamwise direction similar to the axial and tangential (1) intensities, with magnitudes similar to the tangential intensities. For the few swirl profiles, the radial turbulence intensities profiles are similar to those for the axial direction with local peaks at the edge of the vortex core and at the shear layer between the main and recirculating flows.

The Reynolds shear stress profiles for the axial-radial plane are shown in Figure 5(a) for S = 0.0 and Figure 5(b) for S = 0.3. For the no swirl case, the profiles for locations immediately downstream have sharp peaks at the shear layer, with peaks broadening and increasing in magnitude for profiles further downstream but before reattachment. After reattachment the Reynolds stress decays out symmetrically about the axis. The shear stress uv in the axial-radial plane is much greater than the shear stress uw in the axial-tangential plane for S = 0.0. In Figure 5(b) the Reynolds stresses peak at the edge of the vortex core and at the shear layer generated by the recirculating flow. The Reynolds stresses in the axial-radial plane are significantly smaller than that for the axial-tangential plane (1) at the edge of the vortex core but are slightly greater at the shear layer caused by the recirculation.

V.   CONCLUSIONS AND RECOMMENDATIONS

Detailed mean flow and turbulence data in a dump combustor configuration with and without swirl was obtained using a two-component coincident LDV system. The data showed strong turbulence intensities for the region between core flow and recirculating flow and showed very slow development for the case of no swirl. The data complemented previous work by Samimy et al (1) in providing a good data base for computational code development. Investigating further locations downstream for the case of S = 0.3 and investigating locations for S = 0.5 would also provide a better understanding and improve the data base for computer codes. Other efforts could explore the flows using different profile swirl generators such as free or forced vortex generators, flows at higher Reynolds numbers, or flows involving combustion.

REFERENCES

1. Samimy, M., Nejad, A.S., Langenfeld, C.A., Craig, R.R., and Vanka, S.P., "Isothermal Swirling Flow In A Dump Combustor," AIAA Paper No. 87-1352.

2. Lilley, D.G., "Swirling Flows in Typical Combustor Geometries," AIAA Paper No. 85-0184, 1985.

3. Smyth, R., "Turbulent Flow Over A Phase Symmetric Sudden Expansion," Journal of Fluids Engineering, Vol 101, 1979, pp. 348-353.
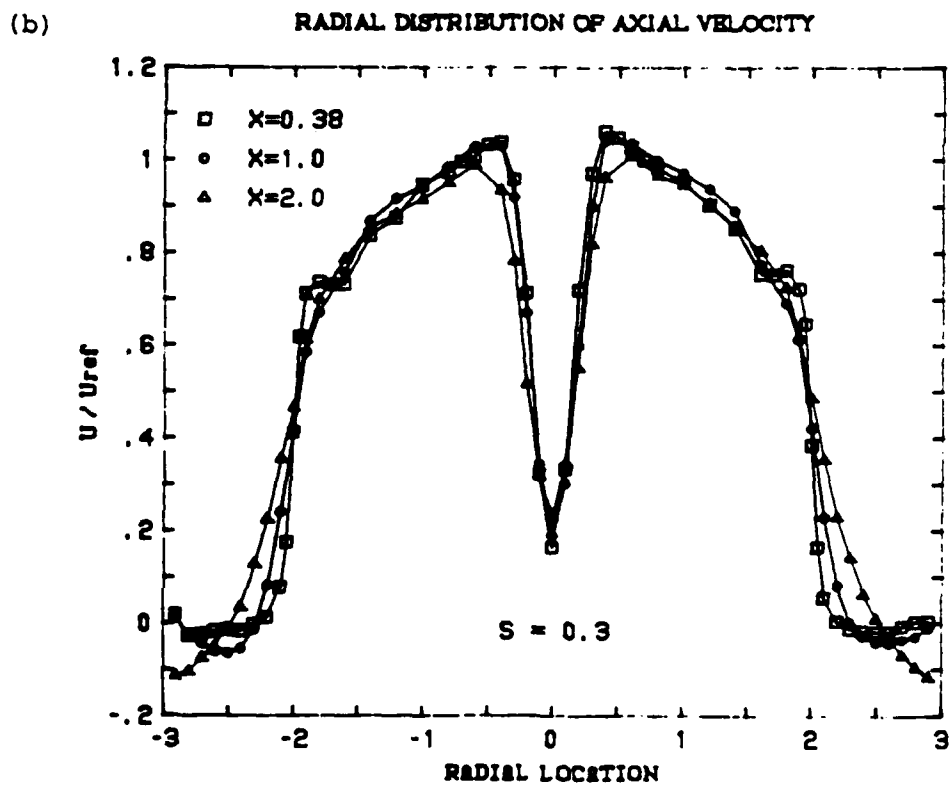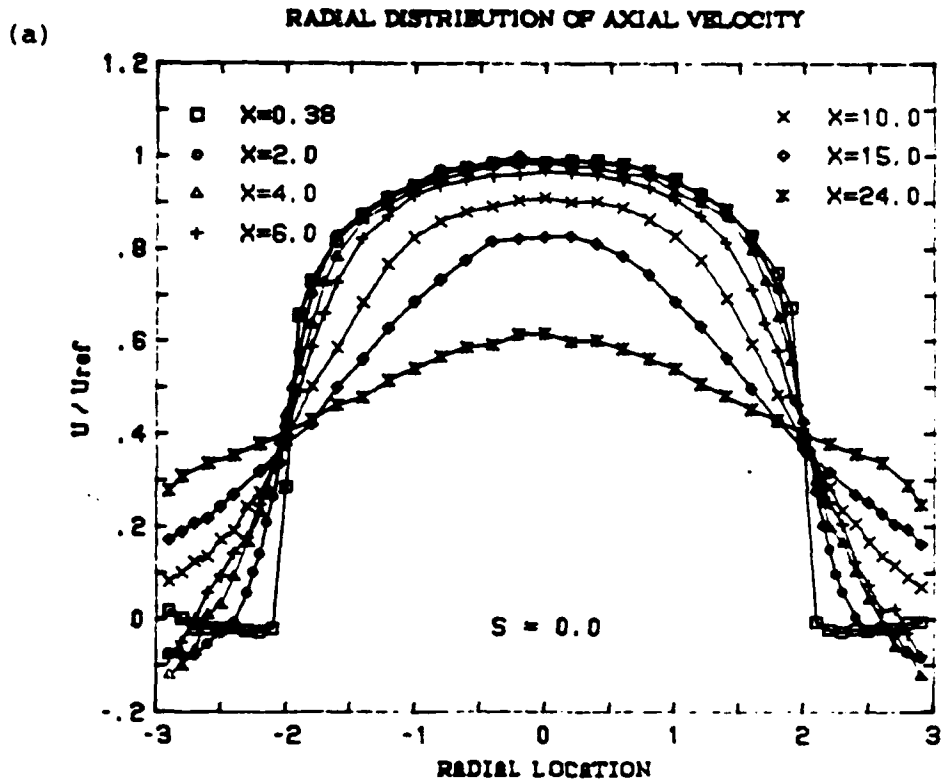
FIGURE 1   Axial Mean Velocities for S = 0.0 And S = 0.3

(b)

RADIAL DISTRIBUTION OF RADIAL VELOCITY

$$S = 0.0$$

(b)

RADIAL DISTRIBUTION OF RADIAL VELOCITY

$$S = 0.3$$
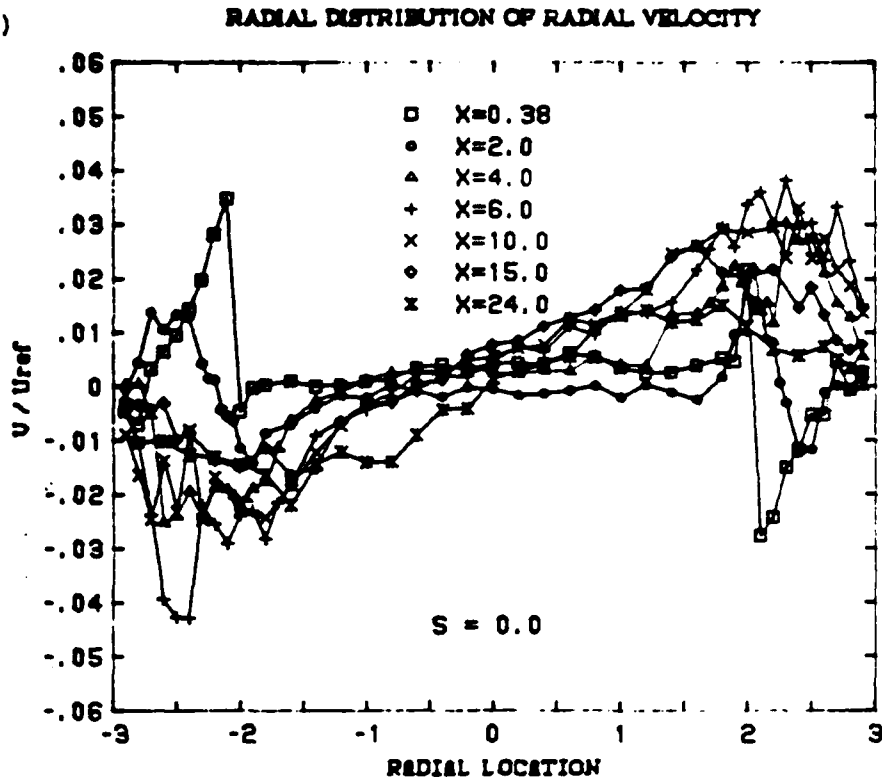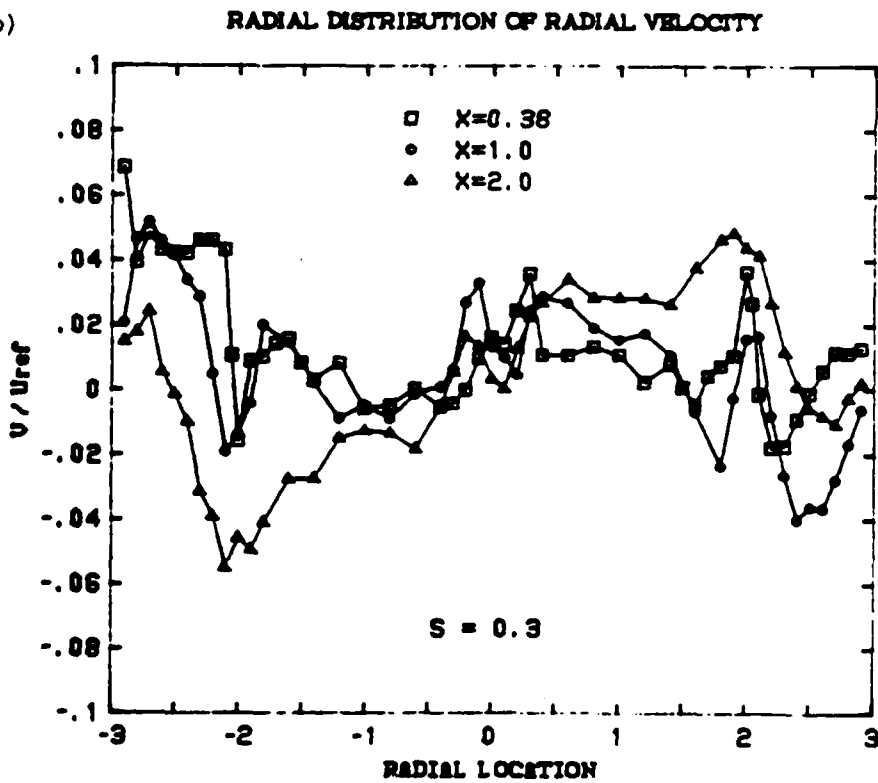
FIGURE 2 Radial Mean Velocities For $S = 0.0$ And $S = 0.3$

(a)

RADIAL DISTRIBUTION OF AXIAL TURBULENCE

(b)

RADIAL DISTRIBUTION OF AXIAL TURBULENCE
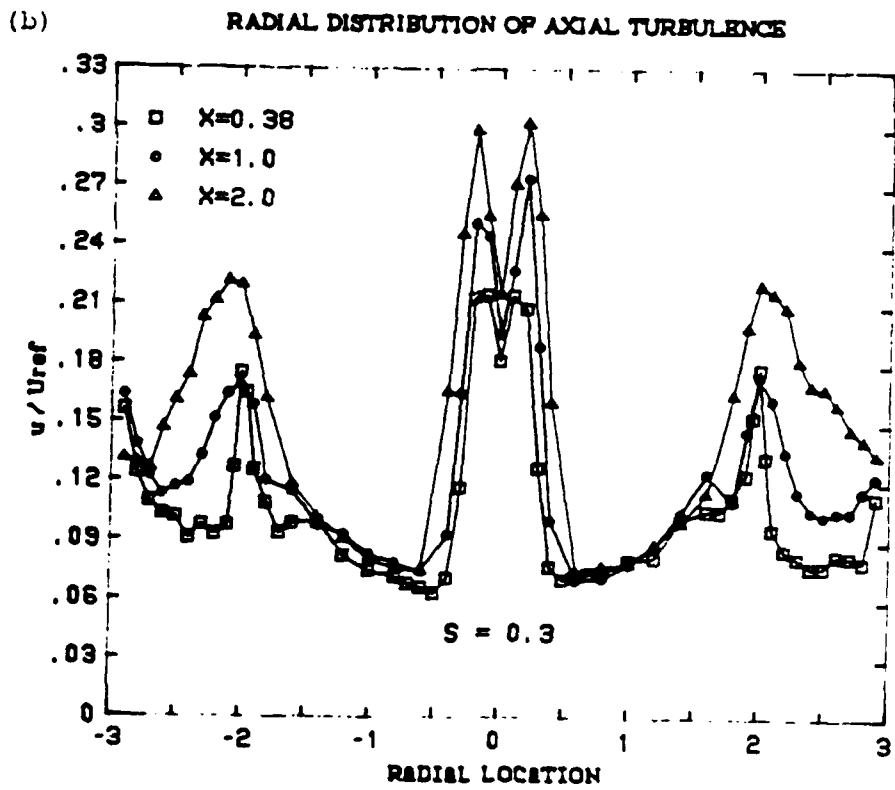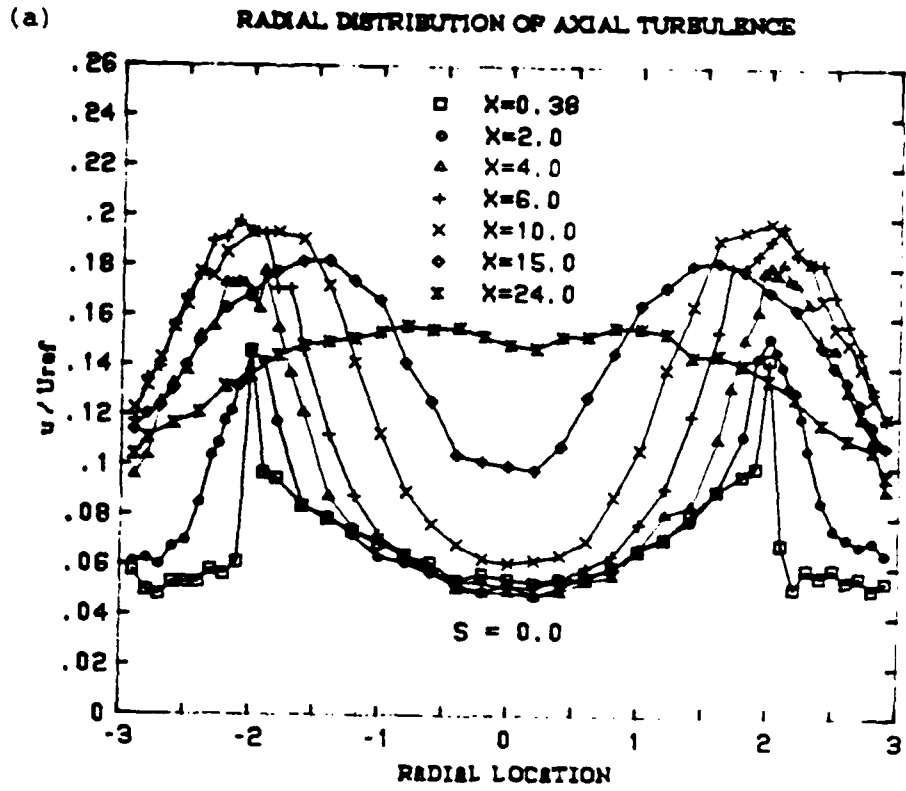
FIGURE 3 Axial Turbulence Intensities for S = 0.0 And S = 0.3
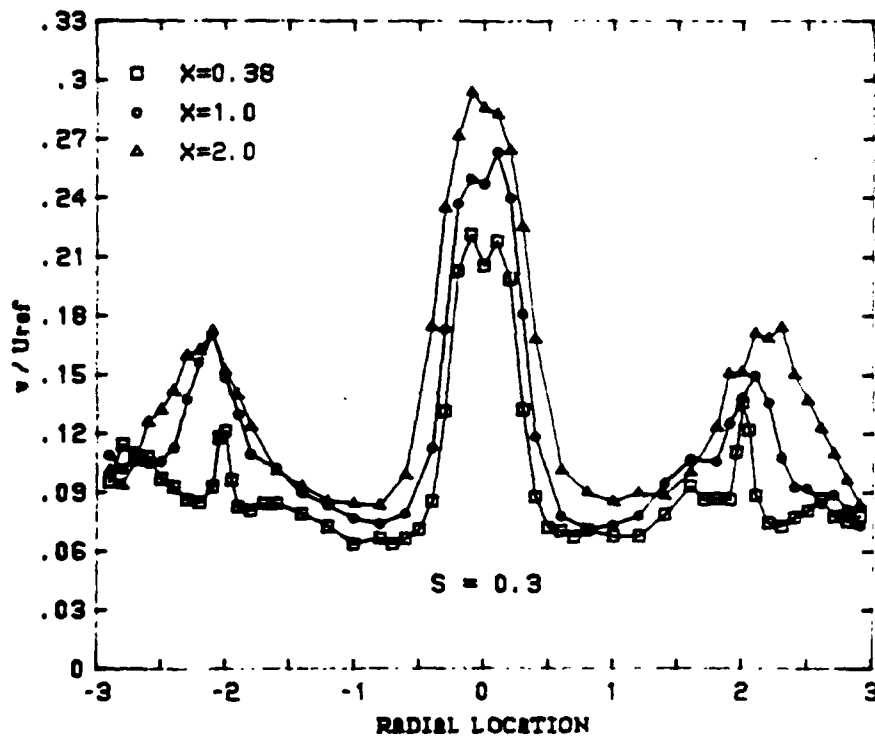
FIGURE 4   Radial Turbulence Intensities For S = 0.0 And S = 0.3

46-15

(a)

RADIAL DISTRIBUTION OF REYNOLDS STRESS

(b)

RADIAL DISTRIBUTION OF REYNOLDS STRESS
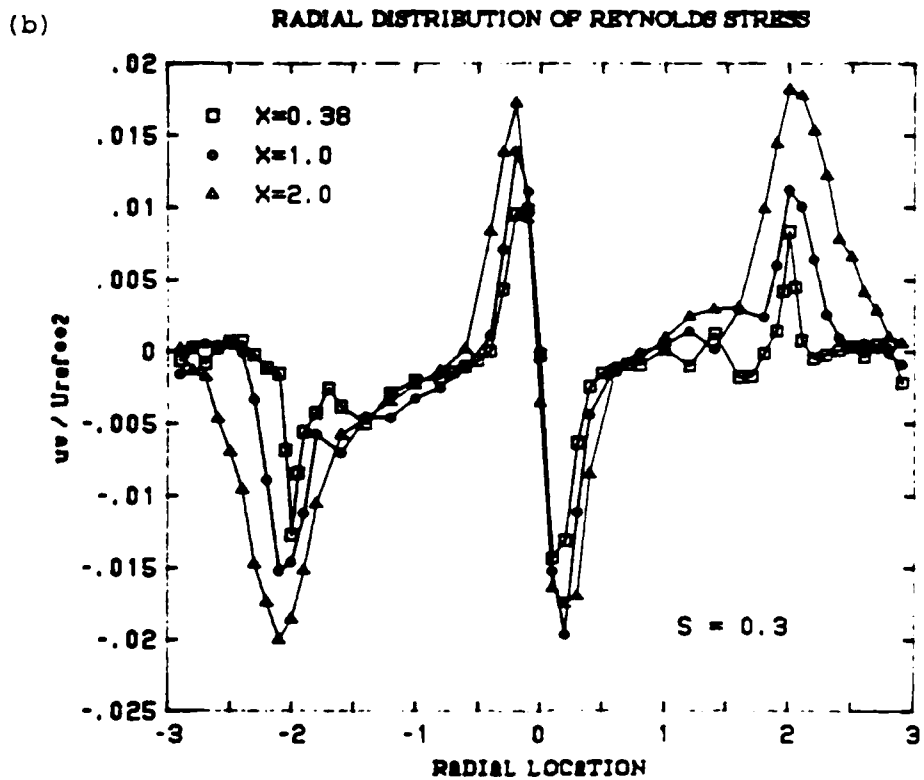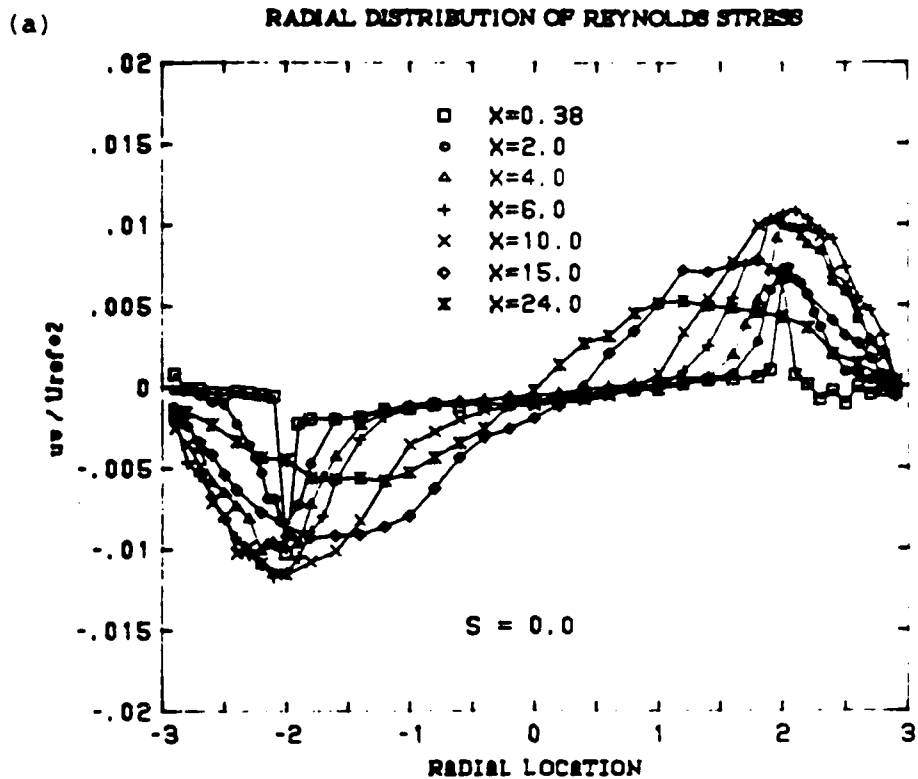
FICURE 5 Reynolds Stress For Axial-Radial
Plane For S = 0.0 And S = 0.3

1987 USAF-UES SUMMER FACULTY RESEARCH PROGRAM/
GRADUATE STUDENT SUMMER SUPPORT PROGRAM

Sponsored by the
AIR FORCE OFFICE OF SCIENTIFIC RESEARCH
Conducted by the
Universal Energy Systems, Inc.
<u>FINAL REPORT</u>

<u>A COMPUTER SIMULATION OF A PLASMA ARMATURE RAILGUN</u>

Prepared by: Christopher B. Leger
Academic Rank: graduate student
Department: Mechanical Engineering Department
University: Louisiana State University
Research Location: AFATL/SAS, Eglin AFB, FL.
USAF Researcher   Kenneth Cobb
Date: September 25, 1987
Contract No: F49620-85-C-0013

A COMPUTER SIMULATION OF A PLASMA ARMATURE RAILGUN

by

CHRISTOPHER B. LEGER

ABSTRACT

A computer simulation for a plasma armature railgun was developed for use on a Zenith 248 micro computer. The purpose of the simulation is to predict gun performance both for design purposes and to estimate the results of specific shot conditions. The simulation models projectile velocity, power supply currents, armature mass, and armature length. These parameters are modeled using equations expressing their time rates of change and then using numerical integration. The acceleration includes terms for ablation and viscous drag effects, and the ablation is made velocity dependent. This gives good agreement with experimental results.

I. INTRODUCTION:

The electromagnetic railgun is a device that uses intense magnetic fields and electric currents to accelerate projectiles. Velocities of several kilometers per second give the projectile great kinetic energy with which to destroy a target. This makes the railgun an attractive possibility for use in antitank applications and anti-satellite or anti-ballistic missile applications in space.

The Air Force is doing development work on various railgun concepts at Eglin AFB. The major areas needing improvement are increasing maximum projectile velocity, improving multiple-shot capability, reducing self-inflicted internal damage, increasing overall efficiency, and decreasing overall size and weight. This development includes the building and testing of new designs. Due to the many parameters involved, the performance of a new gun can only be roughly estimated with simple calculations. Therefore, a more complete model would be of great use in the design process to provide expected peak currents, voltages, velocities, etc. This would allow the designer to be more accurate in sizing components, helping to eliminate expensive failures or gross overdesign.

II. OBJECTIVES:

At the beginning of the project it was clear that there was a need for a convenient, realistic computer model to predict railgun performance at Eglin. The group that I worked with, AFATL/SAS, was doing development work on plasma armature railguns. They were trying different rail and bore configurations, new power supply circuitry, longer barrel lengths, and various projectile masses. There was an existing rail gun computer simulation program written by Ken Cobb in Fortran for use on the Vax computer system. The simulation modeled the old power supply circuitry well, but the equations for the armature/projectile acceleration did not include such real effects as ablation or friction.

Initially my project goals were to adapt the existing railgun simulation for use on the Zenith 248 micro computer. Next, I was to improve the plasma armature model by including friction effects, ablation mass addition, and conductivity changes in the equations. Finally I was to put these equations in the program and make it suitable for use in design work.

Shortly after beginning the work, the development team announced plans to build a new high velocity gun using a different power supply circuitry. Since the old railgun simulation could not model this new power supply configuration, it would be useless for predicting the new gun's performance. It was decided to write two simulation programs, one using the old power supply circuitry and the other using the new circuitry. Since the second program had to be developed almost entirely from scratch, the total amount of work was almost doubled. Therefore, modeling the plasma armature with a variable resistance was dropped because it would be the most complicated parameter to model, when in actual tests this resistance appears to be relatively constant.

III. APPROACH:

In order to familiarize myself with railguns, their simulation, and other work that had been done, I spent a few weeks reviewing literature on the subject. Next, I had to work with the Zenith 248 and modify the existing simulation program to work on the micro computer. In conjunction with Dr. Courter and Mr. Cobb, the set of equations to model the plasma armature was developed.

The new program using the new power supply then had to be written. I made it as much like the older simulation as possible by using similar logic and the same variable names. The equations for the newer power supply then had to be developed and put in a soluble form. Finally, the new plasma armature equations were installed in both programs.

In addition to developing the two simulation programs, a graphics program was written to be used in conjunction with Graftalk graphics software. With the addition of a batch file, the program package was complete. The batch file runs either simulation program, then runs the graphics routine to produce graphs of the desired parameters.

IV. THEORY:

The electromagnetic railgun achieves acceleration through the interaction of magnetic fields and electric currents. A simplified sketch of a railgun is shown in figure 1. Current enters on one rail, passes through the armature, then exits on the other rail. The acceleration of the projectile is the result of the Lorentz force, $F = B x I$, acting on the current carrying armature. This force is perpindicular to the armature current, and magnetic field, thus it tends to push the projectile down the rails.

In order to achieve the necessary high velocities, very large currents are required. The armature in a plasma armature gun is produced by the vaporization and ionization of a metal foil as it shorts across the rails when it first enters the breech. Best results are obtained when the projectile and foil backing enter the breech at a reasonably high velocity.

Ideally, such a system could accelerate a projectile to almost unlimited velocities if provided with a high enough current. However, real effects such as friction and wall ablation tend to limit performance. Friction occurs to some extent between the projectile and rails, and there is also friction between the armature and rails. At high enough velocities the projectile is only in contact with the rails intermittently, so its friction loss is difficult to characterize.
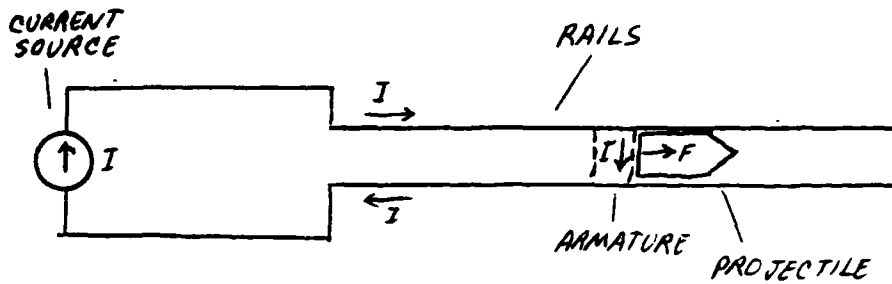
FIGURE 1: SIMPLIFIED RAILGUN DIAGRAM
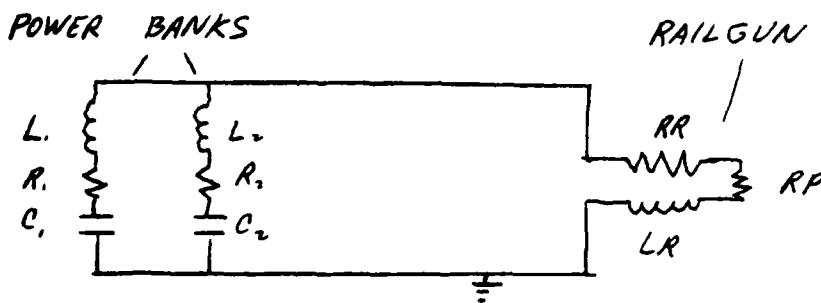
FIGURE 2: CAPACITOR BANK POWER SUPPLY
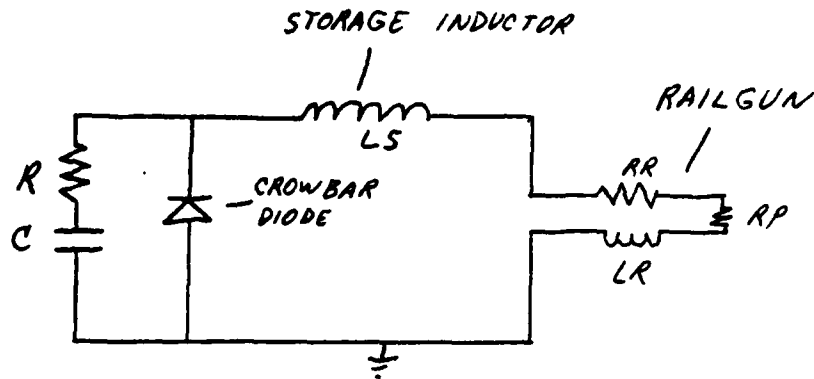
FIGURE 3: CROWBAR POWER SUPPLY

The real effect which tends to cause the most trouble is ablation from the rails and insulators. Ablation from the rails causes degradation of their surfaces thus limiting their use to only a few shots. Performance is lost as the ablated material is incorporated into the plasma. This mass must be accelerated to the armature speed, so it uses up a significant portion of the power delivered by the Lorentz force.

The power supply to drive a railgun must be capable of providing very high currents for short periods of time, usually a few milliseconds. Ideally, a constant current is desired to provide roughly constant acceleration and prevent system damaging peak currents. Since heat is generated in all resistive elements proportional to the square of the current, this loss is minimized with a constant current.

Several methods exist to produce these currents, including homopolar generators, capacitor banks, and battery banks. The capacitor bank power supply is the type that I modeled. The original power supply was a bank of large capacitors and inductors in parallel. The new Crowbar power supply is similar except that it uses diodes to isolate (crowbar out) the capacitors from the circuit. The original power supply is shown in figure 2, and the Crowbar power supply is shown in figure 3.

With the old power supply, the capacitors are first charged up, then the switch is thrown. The resulting current pulse is shaped by the inductors in the circuit. The diodes are present only to prevent reverse charging of the capacitors. Increasing the size of the inductors tends to give a more constnat power pulse, but it greatly increases the time necessary to reach maximum current. The best acceleration with this power supply is produced by a rounded current peak early in the shot. The current then decays rapidly. The capacitors initially contain all the energy. The inductors then store energy until the current reaches a peak. The inductors then resist

the change in current by releasing energy. Since the capacitors are still in the circuit, their rate of discharge is decreased and the current falls off rapidly.

The crowbar power supply circuit produces a current which can be nearly constant. A bank of capacitors discharge in the circuit. Most of the energy is stored by the storage inductor until the current reaches a peak. At that point, the inductor would try to dump energy back into the capacitor. Diodes then turn on to provide an alternate path for the current to bypass the capacitor. The current then decays much more slowly. The switching is analogous to a spring/mass system in which the mass is released from the spring when it reaches its highest velocity.

V. CROWBAR POWER SUPPLY EQUATIONS

The crowbar program uses two sets of equations to calculate the total current in the gun. One set models the system before the diodes turn on and the other models it after the diodes crowbar the capacitors out of the circuit. Before crowbar occurs, the following equations apply:

$$RID = CI \tag{1}$$
$$DCIDT = (EC-(R+RB+RC+RR+RP+LI*VEL)RID)/(LB+LS+LC+L+LI*XX) \tag{2}$$
$$DVDT = -CI/C \tag{3}$$
$$EC = EC+DVDT*DT \tag{4}$$
$$CI = CI+DCIDT*DT \tag{5}$$

Before the diode turns on, the total current (1) is equal to the current through the capacitor. The time derivative of the capacitor current (2) is a function of capacitor voltage minus circuit voltage drops divided by circuit inductances. The time derivative of the capacitor voltage (3) is simply the negative of the current divided by the capacitance. Equations (4) and (5) are the single steps of integration for the capacitor voltage and current.

The voltage across the diode must then be checked to determine if the diode will begin conducting.

$$ED = EC-(R+RB)*CI-LB*DCIDT \qquad (6)$$

Equation (6) expresses the voltage across the diode as the capacitor voltage minus the voltage drops across the resistances and inductances associated with the capacitor. Whenever ED becomes equal to the diode conduction voltage, it is locked in at that value. Then the electrical circuit becomes branched, and the crowbar has occurred.

After the crowbar has taken place, the new circuit equations are:

$$RID = RID+DRIDDT*DT \qquad (7)$$
$$DRIDDT = (VD-RID(RC+RP+RR+LI*VEL))/(LS+LC+LI*XX) \qquad (8)$$
$$DCIDT = (EC-CI(R+RB)-VD)/LB \qquad (9)$$
$$DVDT = -CI/C \qquad (10)$$
$$CI = CI+DCIDT*DT \qquad (11)$$
$$EC = EC+DVDT*DT \qquad (12)$$

In equation (7), the total current is no longer equal to the capacitor current. Instead, it must be determined and integrated separately. Equation (8) expresses this current change in terms of the voltage drops divided by the inductances for the circuit loop containing the railgun. Equation (9) is similar except it is written for the circuit loop containing the capacitor. Equation (10) is the same expression as before to get the time derivative of the capacitor voltage. Equations (11) and (12) integrate the capacitor current and voltage. Although the total current, RID, is now completely independent of CI and EC, they are still calculated to see how they behave.

VI. PROJECTILE AND ARMATURE EQUATIONS:

After the driving current has been calculated it is used as one of
the inputs to the set of equations modeling the projectile and armature.
These equations are arranged in a specific order to facilitate the
numerical integration of several parameters. The equations are:

$$DMDT = ABLAT(1-(PHI*AREA*VEL)/(RID^2*RP*ARCL))(RID*VMUZ$$
$$-BETA*AREA) \tag{13}$$

$$ACEL = (\tfrac{1}{2}*LSKIN*RID^2-DMDT*VEL-\tfrac{1}{2}*RHO*CFRICT*AREA*VEL^2)/TM \tag{14}$$

$$DLDT = CLENGTH(DMDT/RID^{1.5}-3*MPLAS*DRIDDT/2*RID^{2.5}) \tag{15}$$

$$XX = XX+VEL*DT \tag{16}$$

$$VEL = VEL+ACEL*DT \tag{17}$$

$$MPLAS = MPLAS+DMDT*DT \tag{18}$$

$$ARCL = ARCL+DLDT*DT \tag{19}$$

$$RHO = MPLAS/(ARCL*BORE^2) \tag{20}$$

First, the mass ablation is calculated. Equation (13) is a modification
of Parker's ablation model. Parker uses an equation like the following:

$$DMDT = ABLAT*RP*RID^2 \tag{21}$$

Equation (13) has two additional constants, PHI and BETA, but reduces
to Parker's equation if these are set equal to zero. PHI reduces the
ablation by an amount proportional to the inverse of the heat flux on
the walls around the armature. For low heat fluxes, PHI causes the
total ablation to be greatly reduced. The reduction of ablation due
to the PHI term can also be considered in terms of the time for the
material surface to go from ambient to vaporized conditions. Clearly
this is heat flux dependent. This also allows the ablation to be made
time dependent, as the total ablation energy is the duration of the
heat flux minus the PHI time lag all multiplied by the heat flux after
BETA has been subtracted. BETA reduces the heat flux going into
ablation by a constant amount to account for conduction of heat away
from the surface, regardless of whether vaporization is occuring.

The acceleration of the projectile and armature is calculated next.
Equation (14) clearly has terms expressing the Lorentz force, a friction
drag force, and an ablation drag force. The acceleration is then the
net force divided by the total mass being accelerated.

The rate of change of the length of the armature is calculated by
equation (15). This expression is an extension of the scaling las
given by Powell and Batteh. They expressed the armature length as
a function of current and bore size as:

$$\text{ARCL} = C*\text{MPLAS}*\text{RID}^{-16/11}*\text{BORE}^{5/11} \tag{22}$$

An attempt to use this expression gave poor results as it predicted
very long arc lengths at the beginning of a shot when the current was
still very low. Clearly this could not actually happen, so the arc
length must not always be at its equilibrium length. Instead, a
differential approach is taken. Equation (15) is the time derivative
of Powell and Batteh's scaling law. The armature length can then be
determined by numerical integration. This technique allows a non-
equilibrium length to exist early in the shot.

Equations (16) through (19) are the single steps of integration for
the position, velocity, plasma mass, and arc length, respectively.
In each case, the parameter is updated to its value for the next time
step. Equation (20) also updates the density of the armature for the
next time step. It is necessary to put the integrations after the
equations for the time rates of change to use only values for the
present time step. This avoids the use of two sets of variables,
one for the present time step and one for the next or updated time step.

VII. RECOMMENDATIONS:

The computer models developed during this project appear to be
reasonably accurate and useful. Their major disadvantages are the
use of several empirical coefficients and the incomplete modeling of
the plasma armature. Although the models have been developed, the
appropriate empirical coefficients must still be determined by trying
to model the experimental results of actual shots. Once this is done
the model should be a powerful tool for use in designing new railguns
or predicting the results of test shots.

From a scientific perspective, this model is far from complete. In
particular, the model of the plasma armature is just a rough approxima-
tion. A model which could predict and include such parameters as
temperature, pressure, current distribution, electrical resistance,
and species present in the plasma would be extremely useful if it
could be incorporated into this simulation. This may be difficult
as the number and difficulty of the equations involved is sure to
increase, and the simulation may no longer be short enough to run on
the micro computer. Such a model adapted to a more powerful computer
system would then be a useful goal.

Acknowledgements

References

Parker, J. V., et. al., "Performance Loss Due to Wall Ablation in Plasma Armature Railguns," AIAA 18th Fluid Dynamics and Plasmadynamics And Lasers Conference, Cincinatti, Ohio, July 1985. AIAA-85-1575

Powell, J. D., and J. H. Batteh, "Plasma dynamics of an arc-driven, electromagnetic, projectile accelerator," J. Appl. Phys., April 1981, pp. 2712-2730.
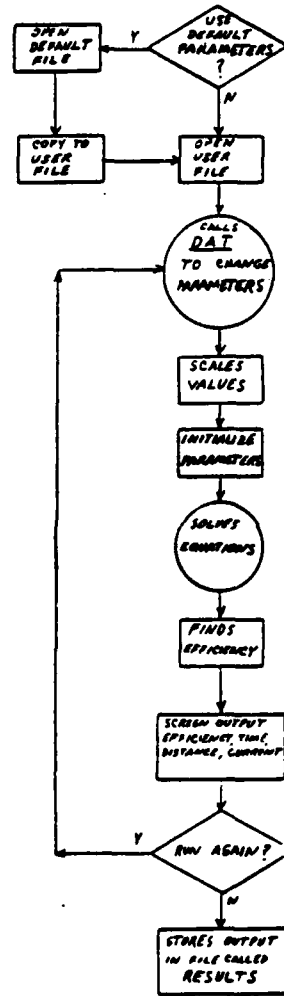
CROWBAR

DAT
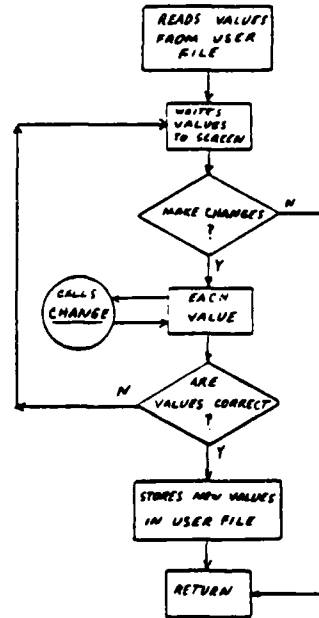
CHANGE

EQUATION SOLUTION

FROM MAIN
T = 0

INCREMENT
T = T + DT

RAIL RESISTANCE
RR = f(VD, VEL, XX, T, COEFAR)

RID = CI
DCIDT = f(EC,R,RB,RC,RR,RP,LI, VEL,RD,LI,LS,LC,I,LI,XI)
DVDT = f(CI, C)

RID = RID + DRIDDT + DT
DRIDDT = f(VD, RID, RC, RP, RR, LI, VEL, LS, LC, XI)

P = f(EC, CI)
ENG, TENG = f(P, DT)

EC = EC + DVDT + DT
CI = CI - DNVDDT + DT

EC:VD   N
Y

EC = VD
CI = 0
DVDT = 0

STORES   CI, EC

AREA = f(BORE, ARCL)

DCIDT = f(EC, R, RB, CI, VQLB)
DVDT = f(CI, C)
CI = CI + DCIDT + DT
EC = EC + DVDT + DT

DMDT = f(ABLAT, ARCL, VEL, PHI, AREA, RID, RP, VMUZ, BETA)
DMDT ≥ 0
ACEL = f(LSKIN, RID, DMDT, VEL, RHO, CFRKT, AREA, TM)
DLDT = f(OLENGTH, DMDT, RID, MPLAS, DRIDDT)
DLDT ≥ 0
XX = XX + VEL + DT
VEL = VEL + ACEL + DT
MPLAS = MPLAS + DMDT + DT
ARCL = ARCL + DLDT + DT
RHO = f(MPLAS, ARCL, BORE)

STORES   RR, VEL, XX, RID, MPLAS, ARCL, ACEL, T, VMACCH

TKEP = f(PM, VEL)
EMKE = f(TKEP, INMKE)

ED = f(EC, R, RB, CI, LB, DCIDT)   ED = VD

END OF BARREL
XX ≥ BLI   Y
N

ENELEFT = f(C, EC)
TENECAP = f(TETCAP, ENELEFT)
FINMKE = f(PM, VEL)
EFF = f(FINMKE, INMKE, TENECAP)

SCREEN OUTPUT XX, MPLAS, ARCL, EFF, T, VEL, VMACCH, RID, EC, ACEL

TO MAIN

47-15

```
       REAL A,A1,A2,ABAR,ACEL,BLX,C,CI,COEFRR,
      $DCIDT,DIDEN,DINUM,DP,DRIDDT,DRRDT,DT,DVDT,
      $EC,EFF,EMKE,ENELEF,ENG,FINKE,INIKE,LI,LSKIN,P,PM,R,
      $RI,RID,RIDO,L,RP,RR,TRR,STCAP,T,TEC,TENECA,TENG,
      $TKEP,TKIN,TMSEC,TSTCAP,TTCI,TTRID,TVEL,TX,VO,VBREECH,
      $VEL,VMUZ,XX,ABLAT,RHO,CFRICT,BORE,ARCL,AREA,DMDT,TM,MPLAS,
      $VD,RC,LS,LC,ED,LB,RB,PHI,BETA,CLENGTH,DLDT,RPFLG,RPCONST
       INTEGER 1,II,IPL,IPLT,IPRT,IT,IX,J,K,N,NB
       CHARACTER W*1,Y*1,Z*1,B*1
       DIMENSION TEC(200),TVEL(200),TX(200),VBREECH(200),
      $TTRID(200),TMSEC(200),TTCI(200),TRR(200),
      $TMPLAS(200),TARCL(200),TACEL(200)
       Y='Y'
       Z='N'
C**** WRITE(*,*)'**********************************************'
C**** WRITE(*,*)'THIS PROGRAM MODELS AN ELECTROMAGNETIC RAIL GUN'
C**** WRITE(*,*)'POWERED BY A SINGLE POWER SUPPLY.  THE INPUT'
C**** WRITE(*,*)'VALUES FOR THE POWER SUPPLY ARE THE EQUIVALENT'
C**** WRITE(*,*)'CAPACITANCE, RESISTANCE, AND INDUCTANCE FOR ALL'
·C**** WRITE(*,*)'THE PARALLEL BANKS.  THE EQUATIONS ARE NOT SET'
C**** WRITE(*,*)'UP TO USE COMBINATIONS OF BANKS THAT ARE NOT'
C**** WRITE(*,*)'IDENTICAL AND PARALLEL.'
C**** WRITE(*,*)'AT THE BEGINNING OF THE PROGRAM, THE USER IS SHOWN'
C**** WRITE(*,*)'ALL THE PRESENT VALUES FOR THE VARIOUS PARAMETERS'
C**** WRITE(*,*)'AND IS PROMPTED TO CHANGE ANY VALUES HE WANTS.'
C**** WRITE(*,*)'DURING EACH RUN, THE EQUATIONS UPDATE VALUES FOR'
C**** WRITE(*,*)'POSITION, VELOCITY, CURRENT, ETC.  THESE VALUES'
C**** WRITE(*,*)'ARE PRINTED ON THE SCREEN.  AT THE COMPLETION'
C**** WRITE(*,*)'OF EACH RUN THE USER IS GIVEN THE OPTION OF GOING'
C**** WRITE(*,*)'BACK TO THE BEGINNING AND CHANGING ANY PARAMETERS.'
C**** WRITE(*,*)'IF THE USER IS SATISFIED WITH THE RESULTS, HE MAY'
C**** WRITE(*,*)'EXIT THIS PROGRAM AND GO INTO THE PLOT ROUTINE.'
C**** WRITE(*,*)'THIS PROGRAM DRAWS DATA FROM THE DEFAULT FILE'
C**** WRITE(*,*)'"DATCROD" AND SAVES IT IN THE USER FILE "DATCROU".'
C**** WRITE(*,*)'AT THE END OF THE PROGRAM, DETAILED RESULTS ARE'
C**** WRITE(*,*)'STORED IN THE FILE "RESULTS" WHICH THE PLOTTING'
C**** WRITE(*,*)'ROUTINE "GRAPH" USES TO MAKE PLOTS.'
C**** WRITE(*,*)'**********************************************'
       WRITE(*,*)'**********************'
       WRITE(*,*)'PROGRAM CROWBAR'
       WRITE(*,*)'**********************'
       WRITE(*,10)
10     FORMAT('0','USE CTRL-S KEYS AS A TOGGLE TO STOP SCROLLING'/1X,
      $'USE CTRL-PRTSC KEYS AS A TOGGLE TO PRINT ALL'/1X,
      $'THAT APPEARS ON THE SCREEN.')
       WRITE(*,62)
62     FORMAT(' ','IF YOU WANT A PRINTOUT OF THE INPUT DATA, USE'/
      $1X,'THE CTRL-PRTSC TOGGLE NOW.  PRESS IT AGAIN'/1X,
      $'WHEN ALL PRINTOUTS ARE FINISHED.')
C
C**** READS DATA FROM DEFAULT FILE 'DATCROD' AND STORES IT
C**** IN USER FILE 'DATCROU' IF YOU ANSWER YES
C
12     WRITE(*,14)
14     FORMAT('0','DO YOU WANT TO USE THE DEFAULT PARAMETERS  Y,N?'\)
       READ(*,'(A1)')W
       IF (W.EQ.Y) THEN
       OPEN(8,FILE='DATCROD',STATUS='OLD')
       OPEN(7,FILE='DATCROU',STATUS='NEW')
       READ(8,20)L,C,R,EC
       WRITE(7,20)L,C,R,EC
       READ(8,20)PM,VO,LI,RI,BLX,VMUZ,LSKIN,RP,RPCONST,COEFRR,DT
       READ(8,20)ABLAT,RHO,CFRICT,BORE,ARCL,MPLAS
       READ(8,20)VD,RC,LS,LC,LB,RB,PHI,BETA,CLENGTH
       WRITE(7,20)PM,VO,LI,RI,BLX,VMUZ,LSKIN,RP,RPCONST,COEFRR,DT
       WRITE(7,20)ABLAT,RHO,CFRICT,BORE,ARCL,MPLAS
       WRITE(7,20)VD,RC,LS,LC,LB,RB,PHI,BETA,CLENGTH
       CLOSE(8)
       CLOSE(7)
       ENDIF
C      WRITE(*,61)RP,RPCONST,COEFRR,MPLAS
 61    FORMAT(G12.4)
C
```

```
C**** CALLS SUBROUTINE 'DAT' TO CHANGE ANY PARAMETERS
C
17      CALL DAT
        OPEN(7,FILE='DATCROU',STATUS='OLD')
        READ(7,20)L,C,R,EC
        READ(7,20)PM,VO,LI,RI,BLX,VMUZ,LSKIN,RP,RPCONST,COEFRR,DT
        READ(7,20)ABLAT,RHO,CFRICT,BORE,ARCL,MPLAS
        READ(7,20)VD,RC,LS,LC,LB,RB,PHI,BETA,CLENGTH
18      FORMAT(I12)
20      FORMAT(G12.4)
        CLOSE(7)
C
C**** MULTIPLY VALUES BY SCALING FACTOR "A" TO GET CORRECT UNITS
C
        A=1.E-6
        L=L*A .
        R=R*A
        LI=LI*A
        RI=RI*A
        RP=RP*A
        LSKIN=LSKIN*A
        DT=DT*A
        ABLAT=ABLAT*A/1000.
        RC=RC*A
        LS=LS*A
        LC=LC*A
        LB=LB*A
        RB=RB*A
        RPFLG=RP
C
C**** INITIALIZATION OF EQUATION PARAMETERS
C
        WRITE(*,566)
566     FORMAT('0','CALCULATIONS ARE NOW BEING MADE'/1X,'HIT '
       $'CTRL-PRTSC TO GET A HARD COPY OF THE RESULTS')
76      T=0
C**** DIODE VOLTAGE IS NEGATIVE IN THE EQUATIONS
        VD=-VD
C**** IPL IS A PRINTOUT FLAG
        IPL=1
C**** IPRT DETERMINES THE FREQUENCY OF OUTPUTS IN MICROSECONDS
        IPRT=10.0*BLX/(DT/A)
C**** INITIAL ACCELERATED MASS OF PROJECTILE AND PLASMA
        TM=PM+MPLAS
C**** INITIAL VOLTAGE ON CAPACITOR
998     VEL=VO
C**** INITIAL KINETIC ENERGY IMPARTED BY PRE-ACCELERATOR
        INIKE=.5*TM*VEL**2.
C**** INITIAL POSITION OF THE PROJECTILE DOWN THE BARREL
        XX=0.
C**** TOTAL STORAGE CAPACITY OF BRANCH CAPACITORS (JOULES)
        TSTCAP=0.0
C**** DRIVING CURRENT THROUGH PROJECTILE AND COPPER RAILS
        RID=0.0
C**** TIME DERIVATIVE OF DRIVING CURRENT
        DRIDOT=0.0
C**** TOTAL ENERGY DELIVERED BY CAPACITORS WITH TIME
        TENG=0.0
C**** INITIALIZE RAIL RESISTANCE (RR)
        RR=0.0
C**** INITIALIZE CAPACITOR LOOP CURRENT
90      CI=0.0
C**** INITIALIZE ENERGY USED
        ENG=0.0
C**** INITIALIZE POWER USED
        P=0.0
C**** INITIALIZE ENERGY STORED IN CAPACITOR
        TSTCAP=.5*C*EC*EC
C**** INITIALIZE DIODE ACTUAL VOLTAGE ED AS CAPACITOR VOLTAGE
        ED=EC
C**** INITIALIZE MASS ABLATION RATE
        DMDT=0.0
```

```
C**** TIME DEPENDENT KVL EQUATIONS
C**** THERE ARE TWO SETS OF EQUATIONS, ONE THAT IS USED BEFORE THE
C**** CROWBAR IS ACTIVATED AND ONE USED AFTERWARD
C
C
C
120    DO 500 IT=1,100000
       T=T+DT
C**** ARRAY INCREMENT TO STORE CALCULATED VALUES
       IPLT=IT/IPRT
       IF(MOD(IT,IPRT).GT.0)THEN
       IPL=1
       ELSE
       IPL=0
       ENDIF
C
C**** CALCULATES RAIL RESISTANCE
C
       DRRDT=(COEFRR*VEL)/((T-DT/2)**.5)
       RR=(COEFRR)*(8.*XX)/(3.*SQRT(T))
       ABAR=(VEL-V0)/T
       IF(ABAR.GT.0.)GO TO 122
       RR=0.
       GO TO 124
122    CONTINUE
       A1=SQRT((V0**2./ABAR**2.)+(2.*XX/ABAR))
       A2=SQRT(V0**2./ABAR**2.)
       RR=COEFRR*ABAR*(2.*(2.*A1+A2)*SQRT(A1-A2))/3.
124    IF(COEFRR.LT.1.E-10)RR=RI*XX
C
C
       IF(RID.LT.0.0.AND.RP.LT.1.0) VMUZ=-VMUZ
C
C**** IF CROWBAR HAS NOT YET TURNED ON
       IF(ED.GT.VD)THEN
       RID=CI
       IF(RPFLG.LE.1.0E-6)THEN
       IF(MPLAS.LT.1.0E-6)MPLAS=1.E-4
       RP=RPCONST/MPLAS**.66667
       VMUZ=RP*RID
       ENDIF
       IF(RPFLG.GT.1.E-6.AND.RPFLG.LE.10.E-6)THEN
       RIDO=RID
       IF(RIDO.LT.5.)RIDO=5.
       IF(VMUZ.LT.5.)VMUZ=5.
       RP=VMUZ/RIDO
       ENDIF
       IF(RPFLG.GT.10.0E-6)VMUZ=RP*RID
       DIDEN=LB+LS+LC+L+LI*XX
       DINUM=EC-(R+RB+RC+RR+RP+LI*VEL)*RID
       DRIDDT=DINUM/DIDEN
       DCIDT=DRIDDT
       DVDT=-CI/C
       ENDIF
C
C
C**** INSTANTANEOUS POWER DELIVERED BY BRANCH CAPACITORS
602    P=EC*CI
C**** INCREMENTAL CHANGE IN ENERGY FOR EACH CAPACITOR
       DP=P*DT
C**** INSTANTANEOUS ENERGY GIVEN UP BY CAPACITORS
       ENG=ENG+DP
       TENG=TENG+DP
C
C
C**** IF CROWBAR HAS TURNED ON
       IF(ED.LE.VD)THEN
       RID=RID+DRIDDT*DT
       IF(RPFLG.LE.1.0E-6)THEN
       IF(MPLAS.LT.1.0E-6)MPLAS=1.E-4
       RP=RPCONST/MPLAS**.66667
       VMUZ=RP*RID
       ENDIF
```

```
         IF(RPFLG.GT.1.E-6.AND.RPFLG.LE.10.E-6)THEN
         RIDO=RID
         IF(RIDO.LT.5.)RIDO=5.
         IF(VMUZ.LT.5.)VMUZ=5.
         RP=VMUZ/RIDO
         ENDIF
         IF(RPFLG.GT.10.0E-6)VMUZ=RP*RID
         DRIDDT=(VD-RID*(RC+RP+RR+LI*VEL))/(LS+LC+LI*XX)
         IF(EC.LT.-2.9)THEN
         EC=-3.
         CI=0.
         DVDT=0.
         GOTO 289
         ENDIF
         DCIDT=(EC-(R+RB)*CI-VD)/LB
         DVDT=-CI/C
         CI=CI+DCIDT*DT
         EC=EC+DVDT*DT
         ENDIF
C
C
C**** IF CROWBAR HAS NOT YET TURNED ON
         IF(ED.GT.VD)THEN
         EC=EC+DVDT*DT
         CI=CI+DRIDDT*DT
         ENDIF
C
C
C**** STORES CAPACITOR CURRENT AND VOLTAGE IN ARRAY
289      IF(IT.LT.IPRT)GO TO 411
         IF(IPL.EQ.1) GO TO 411
290      TTCI(IPLT)=CI
         TEC(IPLT)=EC
C
C
C
C
411      AREA=BORE*ARCL*4
C**** RIDO IS USED FOR RID IN DENOMINATORS TO PREVENT DIVIDE BY ZERO
         RIDO=RID
         IF(RIDO.EQ.0.0) RIDO=1.0
C
         IF(RID.LT.0.0)THEN
         WRITE(*,*)'CURRENT WENT NEGATIVE, EQUATIONS ARE UNDEFINED'
         GOTO 549
         ENDIF
C
         DMDT=ABLAT*((ARCL/VEL-PHI*AREA/(RIDO**2*RP))*(VEL/ARCL)*
        *(RID*VMUZ/AREA)-BETA)*AREA
         IF(DMDT.LT.0.0)DMDT=0.0
         ACEL=(LSKIN*RID**2/2-DMDT*VEL-RHO*CFRICT*AREA*VEL**2/2)/TM
         DLDT=CLENGTH*(DMDT/RIDO**1.5-1.5*MPLAS*DRIDDT/RIDO**2.5)
         IF(DLDT.LT.0.0)DLDT=0.0
         XX=XX+VEL*DT
         VEL=VEL+ACEL*DT
         MPLAS=MPLAS+DMDT*DT
         ARCL=ARCL+DT*DLDT
         RHO=MPLAS/(ARCL*BORE**2)
         TM=PM+MPLAS
C
C**** STORES VALUES IN ARRAYS FOR OUTPUT LATER
C
         IF(IPL.EQ.1) GO TO 3000
         TRR(IPLT)=RR*1.E6
         TVEL(IPLT)=VEL
         TX(IPLT)=XX
         TTRID(IPLT)=RID+DRIDDT*DT
         TMPLAS(IPLT)=MPLAS
         TARCL(IPLT)=ARCL
         TACEL(IPLT)=ACEL
         TMSEC(IPLT)=T*1000.
         IF(RP.GT.1.)VMUZ=RP*RID
         VBREECH(IPLT)=LI*RID*VEL+LI*XX*DRIDDT+RI*XX*RID+VMUZ
C
```

```
C
3000  TKEP=0.5*PM*VEL**2
C****  KINETIC ENERGY OF PROJECTILE GAINED FROM EM FORCES
       EMKE=TKEP-INIKE
C
C
C
C****  DORMANT OUTPUTS FOR DEBUGGING PROGRAM
C      WRITE(*,*)'TIME   XX    MPLAS   DMDT    RID    VMUZ  RP'
C      WRITE(*,999)T,XX,MPLAS,DMDT,RID,VMUZ,RP
999    FORMAT('0',G9.4,2X,F8.3,2X,G11.4,2X,G9.4,2X,G12.4,2X,F6.0,
      $2X,G12.4)
C
C
C****  IF CROWBAR IS NOT YET ACTIVATED, SOLVES ACTUAL DIODE VOLTAGE
C****  IF CROWBAR IS ACTIVATED, LOCKS IT IN WITH "ED=VD"
       IF(ED.GT.VD)THEN
       ED=EC-(R+RB)*CI-LB*DCIDT
       ELSE
       ED=VD
       ENDIF
C
C
C****  EXITS LOOP WHEN PROJECTILE EXITS BARREL
       IF(XX.GE.BLX) GO TO 590
500    CONTINUE
C
C
590    CONTINUE
C****  CALCULATE SYSTEM ENERGY TRANSFER EFFICIENCY
       ENELEFT=0.5*C*EC**2
       TENECAP=TSTCAP-ENELEFT
       FINKE=.5*PM*VEL**2.
       TKIN=FINKE-INIKE
       EFF=TKIN/TENECAP
       EFF=EFF*100.
C
C
C****  GIVES SOME OUTPUT ON SCREEN
       WRITE(*,593)EFF
593    FORMAT('0','TOTAL SYSTEM EFFICIENCY IS ',F6.2,' %.'/)
       WRITE(*,425)
425    FORMAT(1X,'TIME',2X,'DISTANCE',1X,'VELOCITY',2X,'DRIVING',
      $5X,'RAIL',7X,'BRANCH CURRENTS'/7X,'TRAVELLED',10X,'CURRENT',
      $3X,'RESISTANCE',/2X,'(MSEC)',2X,'(M)',4X,'(M/S)',4X,'(AMPS)',
      $4X,'(MICRO OHMS)',7X,'(AMPS)'/)
       DO 556 J=1,IPLT,1
       WRITE(*,460)TMSEC(J),TX(J),TVEL(J),TTRID(J),TRR(J),TTCI(J)
460    FORMAT(1X,F5.3,2X,F5.3,2X,F7.2,2X,F10.2,2X,F8.2,3X,F9.1)
556    CONTINUE
       WRITE(*,565)
565    FORMAT('0','DO YOU WANT TO CHANGE ANY PARAMETERS Y,N?'\)
       READ(*,'(A1)')W
       IF(W.EQ.Y)GOTO 17
C
C
C****  CREATES A RESULTS FILE OF ALL THE OUTPUT DATA
C
558    OPEN(8,FILE='RESULTS',STATUS='NEW')
       DO 557 I=1,IPLT
       WRITE(8,461)TMSEC(I),TVEL(I),VBREECH(I),TTRID(I),TEC(I),
      $TACEL(I),TX(I),TMPLAS(I),TARCL(I)
461    FORMAT(1X,F6.3,1X,F7.1,1X,F6.0,1X,F8.0,1X,F6.0,1X,G10.4,1X,
      $F6.3,1X,F6.5,1X,F5.3)
557    CONTINUE
       CLOSE(8)
C
C****  WRITES "RESULTS" TO THE SCREEN
C
       WRITE(*,462)
462    FORMAT('0',2X,'TIME',4X,'VEL',3X,'BREECH',3X,'RID',6X,'EC',
      $7X,'ACEL',6X,'XX',3X,'MPLAS',2X,'ARCL')
```

```fortran
      WRITE(*,463)
463   FORMAT(' ',3X,'(MS)',2X,'(M/S)',2X,'(VOLTS)',1X,'(AMPS)',2X,
     $'(VOLTS)',2X,'(M/S**2)',4X,'(M)',3X,'(KG)',3X,'(M)')
      DO 559 I=1,IPLT
      WRITE(*,461)TMSEC(I),TVEL(I),VBREECH(I),TTRID(I),TEC(I),
     $TACEL(I),TX(I),TMPLAS(I),TARCL(I)
559   CONTINUE
C
C
549   STOP
      END
C
C
C
      SUBROUTINE DAT
C**** THIS SUBROUTINE DISPLAYS THE INPUT DATA AND ALLOWS CHANGES
C
      REAL L,C,R,EC,PM,VO,LI,RI,BLX,VMUZ,LSKIN,RP,COEFRR,DT,NB
      REAL ABLAT,RHO,CFRICT,BORE,ARCL,MPLAS,PHI,BETA,CLENGTH
      REAL VD,RC,LS,LC,LB,RB,RPCONST
      INTEGER N,I
      CHARACTER B*1,W*1,A*45
      W='N'
C
C**** READS IN DATA FROM USER FILE
      OPEN(7,FILE='DATCROU')
9     FORMAT(I12)
      READ(7,11)L,C,R,EC
11    FORMAT(G12.4)
      READ(7,13)PM,VO,LI,RI,BLX,VMUZ,LSKIN,RP,RPCONST,COEFRR,DT
      READ(7,13)ABLAT,RHO,CFRICT,BORE,ARCL,MPLAS
      READ(7,13)VD,RC,LS,LC,LB,RB,PHI,BETA,CLENGTH
13    FORMAT(G12.4)
C
C**** WRITES INPUT DATA ON SCREEN
C
8     WRITE(*,4)L
4     FORMAT('0',1X,'POWER BANK INDUCTANCE, (MICRO-H)',20X,'L=',
     $G12.4)
      WRITE(*,5)C
5     FORMAT(' ',1X,'POWER BANK CAPACITANCE, (FARADS)',T55,'C=',
     $G12.4)
      WRITE(*,6)R
6     FORMAT(' ',1X,'POWER BANK RESISTANCE, (MICRO-OHMS)',T55,
     $'R=',G12.4)
      WRITE(*,7)EC
7     FORMAT(' ',1X,'INITIAL CAPACITOR VOLTAGE, (VOLTS)',T55,'EC=',
     $G12.4)
      WRITE(*,43)VD
43    FORMAT(' ',1X,'DIODE CONDUCTION BIAS, (VOLTS)',T55,'VD=',
     $G12.4)
      WRITE(*,44)RC
44    FORMAT(' ',1X,'POWER CABLE RESISTANCE, (MICRO-OHMS)',T55,
     $'RC=',G12.4)
      WRITE(*,45)LS
45    FORMAT(' ',1X,'STORAGE INDUCTANCE, (MICRO-H)',T55,'LS=',G12.4)
      WRITE(*,46)LC
46    FORMAT(' ',1X,'POWER CABLE INDUCTANCE, (MICRO-H)',T55,'LC=',
     $G12.4)
      WRITE(*,48)LB
48    FORMAT(' ',1X,'BUS INDUCTANCE, (MICRO-H)',T55,'LB=',G12.4)
      WRITE(*,49)RB
49    FORMAT(' ',1X,'BUS RESISTANCE, (MICRO-OHMS)',T55,'RB=',G12.4)
      WRITE(*,17)PM
17    FORMAT(' ',1X,'PROJECTILE MASS, (KG)',T55,'PM=',G12.4)
      WRITE(*,15)VO
15    FORMAT(' ',1X,'INITIAL PROJECTILE VELOCITY, (M/S)',T55,'VO=',
     $G12.4)
      WRITE(*,19)LI
19    FORMAT(' ',1X,'RAIL INDUCTANCE/UNIT LENGTH, (MICRO-H/M)'
     $,T55,'LI=',G12.4)
      WRITE(*,16)RI
16    FORMAT(' ',1X,'LINEAR RAIL RESISTANCE/UNIT LENGTH, '
```

```
               »'(MICRO-OHM/M)',T55,'RI=',G12.4)
               WRITE(*,21)BLX
21             FORMAT(' ',1X,'BARREL LENGTH, (M)',T55,'BLX=',G12.4)
               WRITE(*,22)VMUZ
22             FORMAT(' ',1X,'MUZZLE VOLTAGE, (V)',T55,'VMUZ=',G12.4)
               WRITE(*,23)LSKIN
23             FORMAT(' ',1X,'LINEAR INDUCTANCE OF RAILS, (MICRO-H/M) DUE'
               $' TO'/5X,'SMALLER SKIN DEPTH JUST BEHIND THE PROJECTILE'/
               $5X,'(F=0.5*LSKIN*I**2)',T55,'LSKIN=',G12.4)
               WRITE(*,3)
3              FORMAT('0',1X,'TO CONTINUE HIT RETURN')
               READ(*,'(A1)')B
               WRITE(*,24)RP
24             FORMAT(' ',1X,'PLASMA RESISTANCE, (MICRO-OHMS)',
               $/5X,'NORMALLY ORDER OF 500.    IF COMPUTATION OF  '/
               $5X,'RP(MPLAS) IS DESIRED, USE RP<1'/
               $5X,'IF CONSTANT VMUZ DESIRED USE 1.<RP<10. ',
               $T55,'RP=',G12.4)
               WRITE(*,60)RPCONST
60             FORMAT(' ',1X,'PLASMA RESISTANCE CONSTANT',
               $/5X,'PR=RPCONST/MPLAS**.667'/
               $5X,'PR=700 MICRO OHMS FOR PUG 1'/
               $5X,'WHERE FOR EARLY PLASMA ,MPLAS TAKEN=.0002 KG'/
               $5X,'RPCONST PROPORTIONAL TO W*F(M0,Z)*(W/H)**.333'/
               $5X,'WHERE F(M0,Z)=(M0*Z/(1+Z))**.667'/
               $5X,'FOR 1 CM PUG 1 RPCONST=2.393E-6',
               $T55,'RPCONST=',G12.4)
               WRITE(*,25)COEFRR
25             FORMAT(' ',1X,'COEFFICIENT FOR RAIL MATERIAL FROM'/
               $5X,'  DRRDT=2*(RESISTIVITY*PERMEABILITY/PI)**5/H'/
               $5X,'FOR COPPER THE VALUE IS 2.155E-5'/
               $5X,'IF IT IS DESIRED TO USE LI, PUT COEFRR=0',
               $T55,'COEFRR=',G12.4)
               WRITE(*,27)ABLAT
27             FORMAT(' ',1X,'ABLATION COEFFICIENT FOR RAILS, '
               -$'(GRAMS/MJOULE)',T55,'ABLAT=',G12.4)
               WRITE(*,28)RHO
28             FORMAT(' ',1X,'DENSITY OF PLASMA, (KG/M**3)',T55,'RHO=',G12.4)
               WRITE(*,29)CFRICT
29             FORMAT(' ',1X,'FRICTION COEFFICIENT FOR PLASMA AGAINST WALL',
               $T55,'CFRICT=',G12.4)
               WRITE(*,30)BORE
30             FORMAT(' ',1X,'BORE WIDTH, (METERS)',T55,'BORE=',G12.4)
               WRITE(*,31)ARCL
31             FORMAT(' ',1X,'INITIAL ARMATURE LENGTH, (METERS)',T55,
               $'ARCL=',G12.4)
               WRITE(*,32)MPLAS
32             FORMAT(' ',1X,'INITIAL PLASMA MASS, (KG)',T55,'MPLAS=',G12.4)
               WRITE(*,33)PHI
33             FORMAT(' ',1X,'ABLATION PARAMETER PHI (VELOCITY DEPENDENT)',
               $T55,'PHI=',G12.4)
               WRITE(*,34)BETA
34             FORMAT(' ',1X,'ABLATION PARAMETER BETA (CONSTANT HEAT SINK)',
               $T55,'BETA=',G12.4)
               WRITE(*,35)CLENGTH
35             FORMAT(' ',1X,'LENGTH EQUATION COEFFICIENT (ORDER OF E+10)',
               $T55,'CLENGTH=',G12.4)
               $G12.4)
               CLOSE(7)
C
C
               WRITE(*,*)'DO YOU WANT TO CHANGE ANY VALUES Y,N?'
               READ(*,'(A1)')B
               IF(B.EQ.W)GOTO 401
C
C**** MAKES CHANGES USING SUBROUTINE "CHANGE"
C
               A='THE BANK INDUCTANCE IS, (MICRO-H)'
               CALL CHANGE(A,L)
               A='THE BANK CAPACITANCE IS, (FARADS)'
               CALL CHANGE(A,C)
               A='THE BANK RESISTANCE IS, (MICRO-OHMS)'
```

```
        CALL CHANGE(A,R)
        A='INITIAL CAPACITOR VOLTAGE IS, (VOLTS)'
        CALL CHANGE(A,EC)
        A='DIODE CONDUCTION BIAS IS, (VOLTS)'
        CALL CHANGE(A,VD)
        A='POWER CABLE RESISTANCE IS, (MICRO-OHMS)'
        CALL CHANGE(A,RC)
        A='STORAGE INDUCTANCE IS, (MICRO-H)'
        CALL CHANGE(A,LS)
        A='POWER CABLE INDUCTANCE IS, (MICRO-H)'
        CALL CHANGE(A,LC)
        A='BUS INDUCTANCE IS, (MICRO-H)'
        CALL CHANGE(A,LB)
        A='BUS RESISTANCE IS, (MICRO-OHMS)'
        CALL CHANGE(A,RB)
        A='PROJECTILE MASS IS, (KG)'
        CALL CHANGE(A,PM)
        A='INITIAL PROJECTILE VELOCITY IS, (M/S)'
        CALL CHANGE(A,VO)
        A='RAIL INDUCTANCE IS, (MICRO-H/M)'
        CALL CHANGE(A,LI)
        A='RAIL RESISTANCE IS, (MICRO-OHMS/M)'
        CALL CHANGE(A,RI)
        A='BARREL LENGTH IS, (M)'
        CALL CHANGE(A,BLX)
        A='MUZZLE VOLTAGE IS, (VOLTS)'
        CALL CHANGE(A,VMUZ)
        A='RAIL SKIN INDUCTANCE IS, (MICRO-H/M)'
        CALL CHANGE(A,LSKIN)
        A='PLASMA RESISTANCE IS, (MICRO-OHMS)'
        CALL CHANGE(A,RP)
        A='PLASMA RESISTANCE CONSTANT,(1 CM BORE 2.393E-6)'
        CALL CHANGE(A,RPCONST)
        A='RAIL COEFRR IS, (COPPER=2.155E-5)'
        CALL CHANGE(A,COEFRR)
        A='ABLATION COEFFICIENT ABLAT IS, (KG/MJOULE)'
        CALL CHANGE(A,ABLAT)
        A='PLASMA DENSITY RHO IS, (KG/M**3)'
        CALL CHANGE(A,RHO)
        A='FRICTION COEFFICIENT IS, (ORDER .002)'
        CALL CHANGE(A,CFRICT)
        A='GUN BORE DIMENSION IS, (M)'
        CALL CHANGE(A,BORE)
        A='INITIAL ARC LENGTH IS, (M)'
        CALL CHANGE(A,ARCL)
        A='INITIAL PLASMA MASS IS, (KG)'
        CALL CHANGE(A,MPLAS)
        A='ABLATION TERM PHI IS, (VELOCITY DEPENDENT)'
        CALL CHANGE(A,PHI)
        A='ABLATION TERM BETA IS, (CONSTANT HEAT SINK)'
        CALL CHANGE(A,BETA)
        A='LENGTH COEFFICIENT IS, (ORDER OF E+10)'
        CALL CHANGE(A,CLENGTH)
        A='INTEGRATION TIME INCREMENT IS, (MICRO-S)'
        CALL CHANGE(A,DT)
C
C
400     WRITE(*,50)
50      FORMAT('0','ARE ALL THESE VALUES CORRECT Y,N?'\)
        READ(*,'(A1)')B
        IF(B.EQ.W) GOTO 8
C
C
C****   REPLACES NEW VALUES IN USER DATA FILE "DATCROU"
        OPEN(7,FILE='DATCROU')
        WRITE(7,11)L,C,R,EC
        WRITE(7,11)PM,VO,LI,RI,BLX,VMUZ,LSKIN,RP,RPCONST,COEFRR,DT
        WRITE(7,11)ABLAT,RHO,CFRICT,BORE,ARCL,MPLAS
        WRITE(7,11)VD,RC,LS,LC,LB,RB,PHI,BETA,CLENGTH
        CLOSE(7)
401     RETURN
        END
C
```

```
C
C
      SUBROUTINE CHANGE(A,V)
C
C**** VARIABLE "V" IS THE CHANGING VALUE
C**** CHARACTER ARRAY "A" IS THE VARIABLE DESCRIPTION
C
      REAL V
      CHARACTER A*45,B*1,Y*1
      Y='Y'
      WRITE(*,10)A,V
10    FORMAT('0',A45,G12.4)
      WRITE(*,15)
15    FORMAT('0','DO YOU WANT TO CHANGE THIS VALUE Y,N?'\)
      READ(*,'(A1)')B
      IF(B.EQ.Y)THEN
      WRITE(*,20)
20    FORMAT(' ','ENTER THE NEW VALUE')
      READ(*,*)V
      ENDIF
      RETURN
      END
```

1987 USAF-UES SUMMER FACULTY RESEARCH PROGRAM/

GRADUATE STUDENT SUMMER SUPPORT PROGRAM

Sponsored by the

AIR FORCE OFFICE OF SCIENTIFIC RESEARCH

Conducted by the

Universal Energy Systems, Inc.

<u>FINAL REPORT</u>

<u>INVESTIGATION OF LASER DIODE COUPLING USING NONLINEAR OPTICS</u>

Prepared by:	Bruce W. Liby
Academic Rank:	Summer Fellow
Department and	Department of Physics and Astronomy
University:	University of New Mexico
Research Location:	Air Force Weapons Lab/ARBM Kirtland AFB, NM 87117-6008
USAF Researcher:	Lt. Scott Holswade
Date:	1 September 1987
Contract No:	F49620-85-C--0013

INVESTIGATION OF LASER COUPLING USING NONLINEAR OPTICS

by

Bruce W. Liby

Abstract

A discussion of the original goals is contained, as well as how
they were changed and why. The pertinent operating characteristics
of the laser diodes to be used are described, and recommendations
for follow on experiments are presented.

Acknowledgements

I. Introduction:

The coupling of laser diodes has been an area of extensive research for several years. Both novel and traditional techniques have been employed in these efforts. Diode lasers are attractive sources of near infrared coherent radiation. They are easy to manufacture, inexpensive, compact, and extremely efficient. The major liability of these devices is the small output powers they produce. Thus the interest in coupling them.

One method recently done by Yariv and co-workers was to couple the diodes via an optically nonlinear crystal. At AFWL, the Quantum Optics Branch (ARBM) is heavily involved in nonlinear processes, such as four-wave mixing and Stimulated Brilloun Scattering. They also have several projects concerning the coupling of lasers. Consequently, an experiment like this is of interest for both reasons of basic research and for potential applications.

My background suits me well for this effort. I am experienced in nonlinear optics, particularly three-wave mixing and second harmonic generation.

II. Objectives of the research effort

To date only two experiments have been done to couple lasers using nonlinear optics. One of these was with diodes and I was to duplicate

48-4

this experiment and improve upon it if possible. However, as the summer went on it was clear that this goal was not achievable within the ten week period. This was due to the long time it has taken to procure equipment and set up the lab. As of the writing, these tasks have still not been completed.

Consequently, the objectives were changed. The goals were reduced to characterizing the diode lasers, familiarizing myself with their use, researching the literature and designing the experiment. This was to provide a background for the original project and extensions of that work. I am to begin a student coop position here at the lab after the summer program is through. So the effect of all this is to simply delay the original goals.

III.

The first task was to characterize the diode lasers. The most important parameter is coherence length. We decided that we need to have a coherence length at least equal to the optical path between the two lasers we wish to couple. This means at least 10 cm. of coherence.

The diode lasers used were HITACHI HPL 1400 models. The power supply was a Spectra SDL 800 model. Both lasers were put into a Michelson interferometer and the interference fringes were viewed with a pyroelectric detector.

Both lasers always had over 60cm of coherence lenth when operating at 60mA. However, this length would vary from day to day. At times over 200 cm were observed - the limit of our measuring device. Turning up the current seemed to increase the coherence length. This isn't suprising as the linewidth should become narrower with increasing power output. During a breakdown of the air conditioning in the lab, we couldn't get the beams to interfere. The room temperature was 86°. By blowing cool air over the laser we could again achieve 60cm of coherence, easily enough for our experiment.

The lasers were also tested for power vs current. They were found to agree exactly with the manufactures specifications. We were unable to determine the wavelength of the lasers due to lack of necessary equipment.

We also decided to try to see the effect of feedback on the system. This work is still in progress. The first attempt consisted of inserting a glass slide between the laser and interferometer. This slide was adjusted until frequency reflections fed back into the diode. This should destroy the coherence and indeed the interferences fringes disappeared. The glass slide had to be entirely removed to regain them. This diode soon ceased to function so it is unclear whether coherence collapse actually took place. The reason for the failure of the diode is not yet known for sure, but it is probably due either to a high operating current or to the feedback that took place above.

It was also learned that the operating current seriously affects the working lifetime of the lasers. At threshold their lifetime is about 10,000 hours. At 20% above it drops to 1,000 hrs. and at double it drops to less than 10 hours. In the future we will operate at about 20% over threshold.

IV. Recommendations

As I shall continue working at the lab as a coop student, I intend to undertake the following:

a. I will continue to attempt to measures the effects of feedback on coherence. In addition to the method I described, I will try to feed the back lasing back into the diode and observe the effect.

b. When the lab is finally set up, I will attempt to achieve my original goal and repeat the experiment of the first reference. I will attempt to use uncoated diodes. If that doesn't work, I'll go to coated ones. Also, I will directly interfere the two lasers when they are coupled.

c. Upon successful completion of this, I will try to couple in more diodes.

d. I will try different nonlinear materials if available.

REFERENCES

Cronin-Gocomb, M., Yariv, A. and Ury, I., "Coherent Coupling of Diode Lasers by Phase Conjugation", Appl.Phys. Lett.,48 (1986), pp. 1240-1242.

Fienberg, J., and Bacher, G.D., "Phase-Locking Lasers with Phase Conjgation:, Appl. Phys. Lett., 48 (1986), pp. 570-572.

Scrifes, D.R., Streifer W, and Burnham, R.D., "Experimental and analytic studies of coupled multiple stripe diode lasers", IEEE J. of Quant. Electron., QE-15 (1979), pp. 917-921.

Streifer, W., Burnham, R.D., Paogi, T. L., and Scrifes, D.R., "Phased array diode lasers", Laser Focus, June (1984), pp. 100-109.

Vahala, K., Harer, C., and Yarn, A., "Observation of relaxation Resonance effectrs in the field Spectrum of Semiconductor lasers", Appl. Phys. Lett., 42 (1983), pp. 211-213.

1987 USAF-UES SUMMER FACULTY RESEARCH PROGRAM

GRADUATE STUDENT SUMMER SUPPORT PROGRAM

Sponsored by the

AIR FORCE OFFICE OF SCIENTIFIC RESEARCH

Conducted by the

Universal Energy Systems, Inc.

FINAL REPORT

Isolation of Osteogenic Cells From

The Trauma-Activated Periosteum

Prepared by:	A. Jeannine Lincoln
Academic Rank:	Graduate Student
Department and	Physiology and Biophysics
University:	Wright State University
Research Location:	Biodynamics Effects Branch,
	Armstrong Aerospace Medical Research
	Laboratory, Wright-Patterson Air
	Force Base, Dayton, OH. 45433
USAF Researcher:	Noel S. Nussbaum, Ph.D.
Date:	September 14, 1987
Contract No.:	F49620-85-C-0013

Isolation of Osteogenic Cells From

The Trauma-Activated Periosteum

by

A. Jeannine Lincoln

ABSTRACT

Adult male New Zealand white rabbits had greenstick-type
closed fractures of the ribs induced in them under anaesthetic.
The healing process was allowed to begin and progress. The
fractured ribs were removed from the rabbit after five days from
the time of fracture. Osteoblast-like cells were harvested and
cultured from the bone and soft callous of the fracture sites.
In an attempt to characterize the osteoprogenitor cells, biochem-
ical assays were performed every 2-3 days on the media changes
collected from each cell culture. These assays determined the
total protein concentration, alkaline phosphatase activity, and
glycosamino glycan content. The data obtained from these assays
was used to characterize the osteoblast cells obtained from the
trauma-activated periosteum since little is known about bone
development from non-embryonic sources.

ACKNOWLEDGEMENTS

I would like to thank the Air Force Office of Scientific
Research and also the Air Force Systems Command for sponsoring
this research. In addition, I would like to thank Dr. Leon
Kazarian, Chief, Biodynamic Effects Branch, Armstrong Aerospace
Medical Research Laboratory, USAF, for his efforts with this
project. Finally, I particularly wish to thank Noel S. Nussbaum,
Ph.D. for his inclusion of me in this project and for the support
and guidance he gave throughout.

I.   Introduction

The mechanism of bone cell specialization, which is vital for skeletal homeostasis, has had little experimental attention. Osteogenic cells are believed to be contributed by both the periosteum and endosteum of the remaining bone following trauma to the bone.   Embryonically, it is thought that osteoprogenitor cells (precursor cells) originate from mesenchyme, or embryonic connective tissue.   The osteoprogenitor cells then differentiate into preosteoblasts and preosteoclasts.   The cellular stimuli causing this differentiation in adult tissue may also result from the release of various chemical substances associated with the inflammatory response, the release of lysosomes from macrophages, and/or chemotactic agents which are responsible for the coordination of these processes.   Osteoclasts are involved in bone reabsorption; osteoblasts are necessary for bone formation.

The Air Force is interested in determining the role osteoblasts play in maintaining homeostasis of bone formation, particularly its role in preventing demineralization of bone.   Immobilization, hypogravity, and/or hypokinesia are characterized by demineralization of the bone.   Demineralization is a significant problem and thus the USAF is concerned with preventing this process.   Osteoblasts have received little experimental attention.   The few studies undertaken have involved some in vitro organ cultures but were mainly only histolobical studies.   This lack of information

requires the accumulation of baseline data about osteogenic cells.
This data could then be .compared. to similar data obtained by
altering environmental conditions. This comparison would determine
the possible association of demineralization to varied environmental
conditions.

I recently graduated from Olivet College with a biochemistry
major. As I am entering graduate school this Fall, I attempted
to find summer employment that would be helpful to me at graduate
school. I also wanted a more extensive research experience than
what I have had in the past. I believe that the program enabled
me to gain some valuable research techniques and also acquainted
me with an area of research with which I was unfamiliar.

II. Objectives of the Research Effort

The lack of information about bone specialization requires
the accumulation of baseline data about osteoblast cells. This
is necessary in order to relate normal functioning of these cells
to varied environmental conditions.

The procedure used to acquire this baseline data involved
removing trauma-induced activated osteoprogenitor cells from the
in vivo environment to an in vitro environment. The goals of the
research project in which I was involved were established by Noel
S. Nussbaum, Ph.D., the principle investigator. They included the
following:

1.) To establish a methodology for the isolation and chara-
cterization of osteoprogenitor cells from the trauma-activated

mature periosteum.

2.) To determine maximal growth responses of osteogenic cells at various times following trauma.

3.) To observe the response of osteogenic cells to certain modulators and to quantify. this response.

II.   Methods and Materials

Adult male New Zealand white rabbits had greenstick-type closed fractures of the ribs induced under anaesthetic. The healing process was allowed to begin and progress. The fractured ribs were removed from the rabbit after five days from the time of fracture. Osteoblast cells were harvested and cultured from the bone and healing soft callous of the fracture site according to the method of Wong and Cohn (1979) and that modified by Boonekamp, et al. (1984). A variety of local factors were added to the cells in vitro to determine a combination which would aid the cells in achieving maximal growth.

In an attempt to characterize the osteoprogenitor cells, biochemical assays were performed every 2-3 days on media changes collected from each cell culture. The assays were designed to determine the total protein concentration, alkaline phosphatase activity and the glycosamino glycan content. My assigned responsibility was to conduct the alkaline phosphatase assay.

Alkaline Phosphatase Assay:

Reagents:

a.) Buffered substrate: 550 micromoles per vial of sodium

thymolphthalein monophosphate substrate in diethanolamine buffer (pH 10.2).

b.) Color Developer: 0.1 mol/l sodium carbonate and 0.1 mol/l sodium hydroxide.

c.) Thymolphthalein Standard: (100 U/l) 1.0 millimol/l thymolphthalein in 70 % 1-propanol.

Procedure:

1.) Standard Curve: (A new curve was plotted each time a new bottle of thymolphthalein standard was used.) Five test tubes containing 50 microliters each of the 100 U/l standard were diluted to concentrations of 50 U/l, 25 U/l, 12.5 U/l, and 0 U/l (50 microliters dH_2O) were prepared and labeled. One of the five tubes contained 50 microliters of the pure standard (100 U/L). Absorbance was read at 590 nm from the spectrophotometer and ABS. versus concentration was plotted.

2.) Procedure for samples: Test tubes were prelabeled for each sample, duplicates being made for each. 50 microliters of each sample were placed in the appropriate test tubes. A water blank sample was also prepared containing 50 microliters of dH_2O. The buffered substrate was prewarmed to 37 $^\circ$C for about 5 minutes in a solid block temperature control unit. At timed intervals, 0.5 mls. of the warmed buffered substrate were added to each sample, the mixtures vortexed, and the test tubes placed in the temperature control unit to incubate at 37 $^\circ$C for exactly 10 minutes. Substrate was added to successive tubes at thirty

second intervals in accordance with an established time sequence. After the incubation period, the test tubes were removed from the heating unit and 2.5 mls. of the color developer was immediately added to the sample to quench the reaction. Each tube was vortexed again. A serum blank was also prepared by labeling a test tube and adding the buffered substrate to the empty tube. After the incubation period, the addition of the color developer, and vortexing, 50 microliters of a media sample was added to the tube. If a standard curve was not plotted, one standard (50 U/L) was run to check the validity of the established curve. Absorbance at 590 nm wavelength was read from the spectrophotometer. The spectrophotometer was zeroed with dH_2O. Three readings were made per tube. An average of the three was made and the value for the serum blank was subtracted from the average determined for each sample. This corrected average of absorbance for each sample was then used to determine concentration of alkaline phosphatase in U/L from the standard curve. The results were then entered into a SAS data base for statistical analysis.

IV. Recommendations

This project resulted in the characterization of the osteo-progenitor cells and determined some of the conditions which make cell growth in vitro more viable. The assays (protein, alkaline phosphatase, and glycosamino glycan) were also refined in an attempt to achieve better results. A possible area of future

study might involve the addition of such things as growth factors, hormones, and/ or vitamins to the culture media in an attempt to enhance the cells' growth and division. The possible application of the in vitro results to cells in vivo would ideally enhance the capabilities of osteoblast functions following trauma or as a means of preventing demineralization due to immobilization, hypogravity, and/ or hypokinesia.

V. References

1. Cohn, D.V. and Wong, G.I. 1979. "Isolated Bone Cells."
    Skeletal Research, vol. I, ed. by: Simmons, D.J. and
    Kunin, A.S., Academic Press, pp. 3-20.

2. Boonekamp, P.M., Hekkelman, J.W., Hamilton, J.W., Cohn,
    D.V., and Jilka, R.I. 1984. "Effect of Culture on the
    Hormone Responsiveness of Bone Cells Isolated by an
    Improved Sequential Digestion Procedure." Proc. Kon.
    Neder. Weten. 87B: 371-381.

3. Selkurt, Ewald E. Physiology, Boston, Little, Brown and
    Company, publishers, 1984.

1987 USAF-UES SUMMER FACULTY RESEARCH PROGRAM/

GRADUATE STUDENT SUMMER SUPPORT PROGRAM

Sponsored by the

AIR FORCE OFFICE OF SCIENTIFIC RESEARCH

Conducted by the

UNIVERSAL ENERGY SYSTEMS, INC.

FINAL REPORT

THE EFFECTS OF CATARACT SURGERY

ON PUPILLARY RESPONSE

Prepared by:	Yolanda A. Malone
Academic Rank:	Medical Student II, SMPII
Department and University:	School of Medicine Meharry Medical College
Research Location:	Ophthalmology Department USAF School of Aerospace Medicine Brooks Air Force Base, TX 78235-5000
USAF Researcher:	Captain Daniel R. Peters
Date:	September 22, 1987
Contract No.:	F49620-85-C-00132

The Effects of Cataract Surgery
on Pupillary Response

by

Yolanda A. Malone

ABSTRACT

Patients responses after monocular cataract surgery were video taped via the use of a pupilpgrapher. The pupilographeer allowed filming of both eyes simultaneously. The pupils were then analyzed through the use of video editing equipment, at intervals of .125 seconds. The data was plotted as a function of time with respect to pupil size. Standard deviation for the right versus the left eye, surgically operated versus the unoperated eye and time were calculated. Maximum and minimum ranges were also examined. At completion there appeared to be no difference in response rate nor the degree of response in relation to the operated versus the unoperated eye in cataract patients.

ACKNOWLEDEGEMENT

I would like to express my appreciation to the Air Force Systems Command and the Office of Scientific Research Department of Ophthalmology for sponsorship of this research effort. Many thanks to Universal Energy Systems for their guidance and administrative assistance. This has been a very rewarding and enriching summer thanks to the guidance, counsel and encouragement of Captain Daniel Robert Peters. The time and energy that he expended to make sure that the research was a success was invaluable. The concern of Lt. Col. Green served as a source of stimulation. The resourcefulness of A1C Lisa Robinson and the knowledge she provided was very helpful. Many thanks to all at Brooks Air Force Base in the Department of Ophthalmology that added to the different aspects of this research experience.

I. INTRODUCTION AND STATEMENT OF OBJECTIVES

The eye is a visual apparatus whose anterior portion is composed
of lens, cornea, iris, ciliary muscles, and vitreous humor, and the
light sensitive retina. The compound optical system of the eye consist
of the lens and cornea. Together, they function to alter the direction
of light rays so that they focus on the retina. Each of these
components go through stages of development during which defects
can occur. Defects in the development of the cornea may result in
leukoma, whereas opacification in the development of the lens may
occur during the growth of the fetal, infant or adult nucleus
resulting in cataracts.

The pupillary response to light should always be brisk even
if a mature cataract is present. Therefore, a mature cataract will
never be the sole source of an afferent pupillary defect (Marcus
Gunn). Afferent pupillary defects are usually the result of macular
degeneration, retinal detachment, or optic nerve disease. In such
a situation, the pupil of the diseased eye will either have a demi-
nished or absent direct reaction to light, but will have an abnormal
consensual constriction when the other eye is stimulated. Pupill-
oconstrictor response of the iris occurs as a result of light stim-
ulation of the retina. Impulses are carried by the optic nerve to
the optic chiasm, where pupillary fibers decussate. From the optic
chiasm pupillary impulses travel to the optic tract then to the
brachium of the superior colliculus, and on to the pretectal region
where synapses occurs on the pretectal nucleus. Here axons of the

pretectal nucleus extends to the Edinger Westphal nucleus of the occulomotor nerve (parasympathetic), and on to the ciliary ganglion where they synapse. New fibers then proceed, via the long and short ciliary nerves to the sphincter muscles of the iris where they result in pupillary constriction.

The lens is surrounded by a capsule and is suspended from the ciliary body of the zonules. Anteriorly there is a layer of epithelial cells between the capsule and the cortex of the lens. The more centrally located fibers make up the nucleus. Changes in color, opacities and vacuoles in the nucleus and opacities in the lens cortex indicate the beginning of cataracts. These lens defects are the leading cause of visual impairment among adults in the U.S. Cataracts occur most frequently with aging, and in this instance are referred to as senile or degenerative cataracts. The condition results from hardening of the transparent protein fibers that make up the lens. Other causes of cataracts include heredity, metabolic disorders, developmental defects, intrauterine infection, trauma, certain drugs and toxic agents, and eye disease such as glaucoma and iritis.

Cataract extraction is the most frequent ophthalmic surgical procedure performed world wide today. Over five hundered thousand cataract surgeries are performed in the U.S. alone each year. Although, surgical techniques do vary, the basic goal is to remove the opacificed lens or capsule. The techniques have been highly refined and perfected with most of the complications very well described in the literature. One aspect of this surgery, however, which has not been adequately addressed is the effect, if any, the

procedure itself may have on pupillary function. Aside from the unavoidable physical manipulation of the pupil during cataract surgery, a number of other factors may affect long-term function in an operated eye. Such factors may include:

1. use of pre and post operative topical eye pads

2. use of anterior or posterior intraocular lens

3. placement of peripheral iridectomy

4. use of intra-operative, intraocular agents (Helon)

5. prolonged retinal light exposure.

In light of this apparent void of information, we set out to examine pupillary function in eyes after cataract extraction using the un-operated eye as the control. Prior research interests, for me, have involved areas ranging from "The Effects of Ortho-Palladated Compunds on Cancer" (at Alabama A&M University) to Fourier Tansform Infrared Spectroscopy (at City College of New York). My assignment to the Ophthalmology Department and more specifically to this pupillary response study was a result of not one but several of my previous research experiences.

II. MATERIALS AND METHODS

The patient pool was obtained from the Ophthalmology Department of Wilford Hall USAF Medical Center at Brooks Air Force Base. Surgery was performed by both staff ophthalmologists and residents under staff supervision. Patients were screend for H/O afferent pupillary defects (Marcus Gunn) presence of Cataracts of fellow eye,

iris atrophy, segmentalpalsy, aniscoria, uveitis, glaucoma and trauma. Subsequently, the patient's eyes were simultaneously filmed via the use of a pupilographer. A total of ten responses to light were performed and recorded. The tape was then reviewed through the use of video editing equipment and pupil size was measured at .125 second intervals. Standard deviations of the pupillary dilation were calculated for the ten trials at each time interval and curves based on pupillary dilation versus time were generated for comparison.

III. RESULTS

Maximum dilation of the unoperated eyes for these nine subjects ranged from 7.0mm to 4.2mm (2.8mm) with a mean of 5.2mm. Maximum dilation for the operated eyes ranged from 6.9mm to 4.2mm (2.7mm) with a mean of 5.1mm. Maximum pupillary constriction of unoperated eyes ranged from 4.9mm to 2.8mm (2.1mm) with a mean of 3.4mm. Maximum pupillary constriction of operated eyes ranging from 5.0 to 2.8 (2.2mm) with a mean of 3.5mm. Actual pupillary constriction varied from a maximum of 2.1mm to a minimum of 1.4mm in unoperated eyes and from a maximum of 2.2mm to a minimum of 1.1 in operated eyes. See Table 1.

In five patients, pupillary diameter of the unoperated eyes were larger than the operated eyes throughout constriction. (See graphs 1-5.) In the other four patients, the operated eyes were larger than the unoperated throughout constriction. (See graphs 6-9.)

Data was analyzed using the Paired t-test and were significant

at the .06 level of probability.

Time from onset of light stimulation to maximum pupillary con-
striction ranged from 750msec - 1.0sec with a mean of .888 sec Time
to maximum constriction was identical between the operated and un-
operated eye reached maximum constriction approximately 0.125msec
before the unoperated eye.

IV. DISCUSSION

This study was carried out in order to evaluate the effect of
cataract surgery, if any, on pupillary function post-operatively.
Patients were screened for evidence of significant pupillary or ocular
trauma and were eliminated from the study if these were found by
the examiner. Close comparison of pupillary reaction in these nine
patients revealed remarkably equal total pupillary excursions in
the operated eye compared with the unoperated eyes. Pupillary response
time to maximum constriction was identical in all cases except one,
and this difference may have resulted from inherent limitations of
the editing and measuring techniques. In this study, pupillary
measurements were extrapolated from a television monitor with pupillary
diameters being the measured variable. Ideally, computer assisted
analysis would provide more accurate and reliable pupillary
measurements. Such a method is currently being worked out, and when
operational, will eliminate this type of possible error. This study
provides the first objective data, that in a group of carefully
selected patients, the effect of cataract surgery and intraoperative
manipulations on the normal pupillary light response is negligable.

It provides further support for safety and value of this extremely common intraocular surgery.

IV. RECOMMENDATIONS

1. Continuation of the study of cataract surgery and its effect on pupillary function in an effort to establish other factors that might interfere with pupillary function.

2. Development of a more precise method of measuring pupillary size.

3. Compare the effect of intracapsular cataract surgery to extra-capsular cataract surgery in relation to pupillary function.

4. Compare the degenerative, congenital and traumatic cataract to each other in terms of pupillary function.
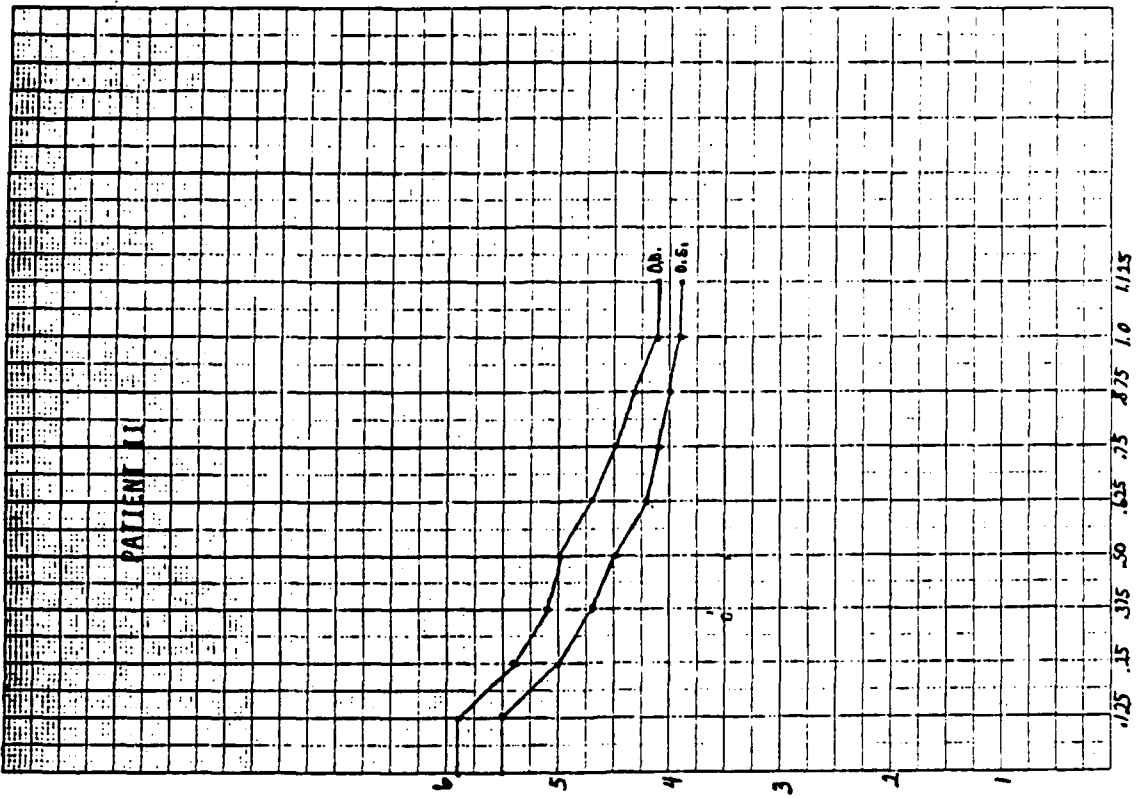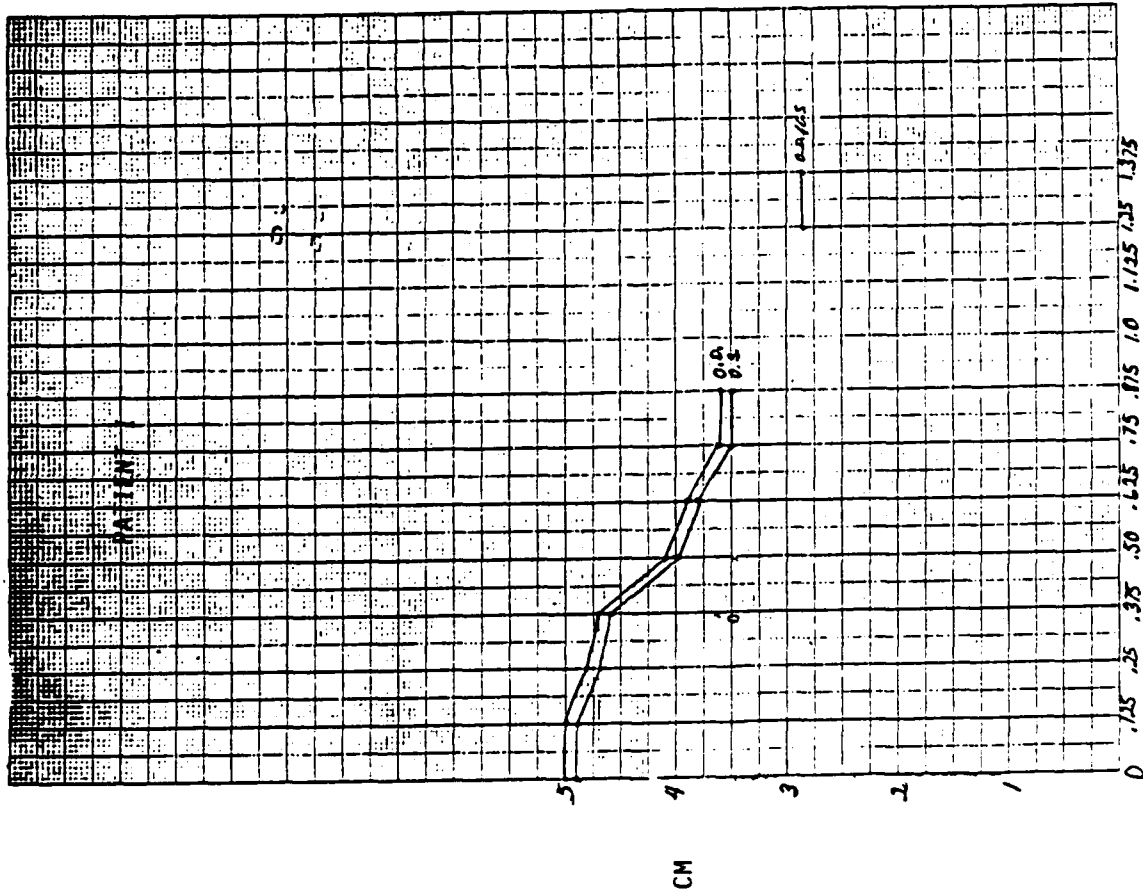
TABLE I
COMPILED DATA AND DERIVED VARIABLES

SUBJECT	UNOP-PRE	UNOP-POST	OP-PRE	OP-POST	UNOP-DIFF	OP-DIFF	UNOP-OP
1	4.5	3.1	4.4	3.0	1.4	1.4	-0.0
2	4.9	2.8	5.0	2.8	2.1	2.2	-0.1
3	5.9	4.1	5.5	3.9	1.8	1.6	0.2
4	5.5	3.9	5.7	4.6	1.6	1.1	0.5
5	5.5	3.5	5.2	3.6	2.0	1.6	0.4
6	7.0	4.9	6.9	5.0	2.1	1.9	0.2
7	4.2	2.8	4.5	3.0	1.4	1.5	-0.1
8	4.8	2.9	5.0	3.1	1.9	1.9	0.0
9	4.6	3.0	4.2	2.9	1.6	1.3	0.3

UNOP-PRE = Unoperated eye before surgery
UNOP-POST = Unoperated eye after surgery
OP-PRE = Operated eye before surgery
OP-POST = Operated eye after surgery
UNOP DIFF = Unop-pre - Unop-post
OP DIFF = Op-pre - Op-post
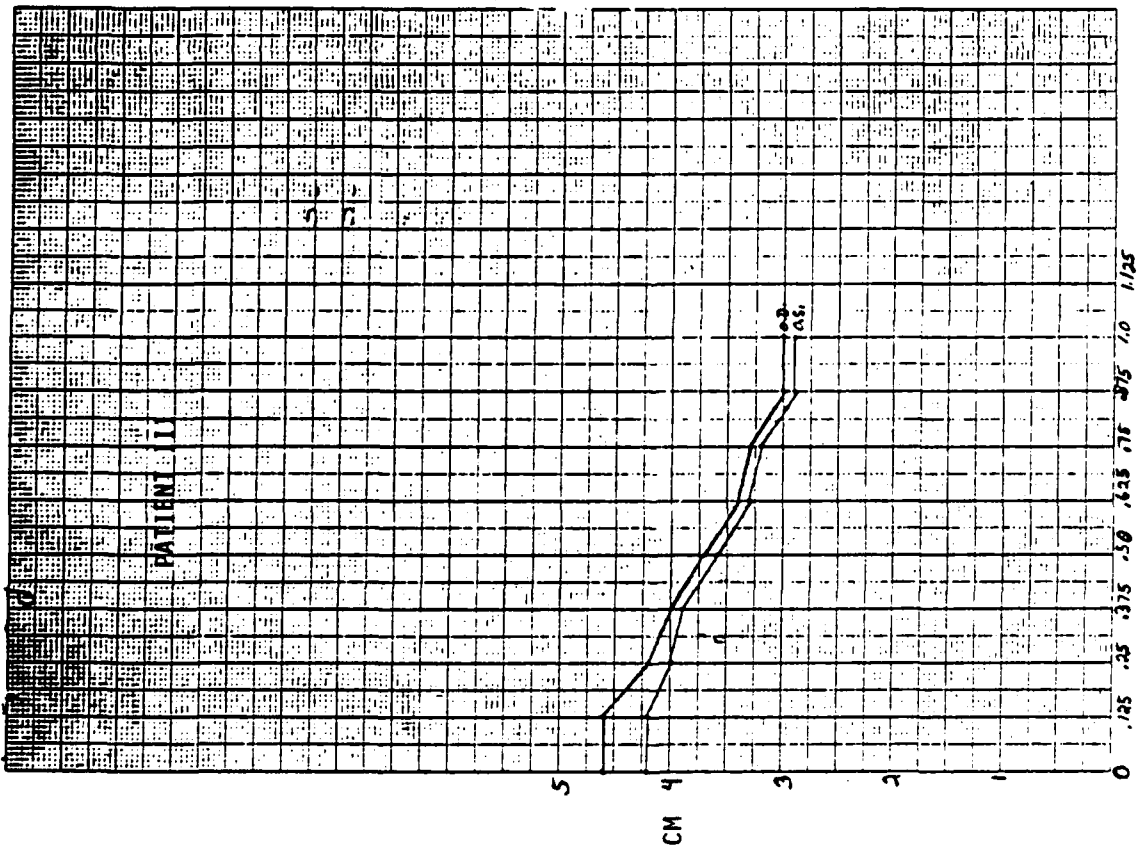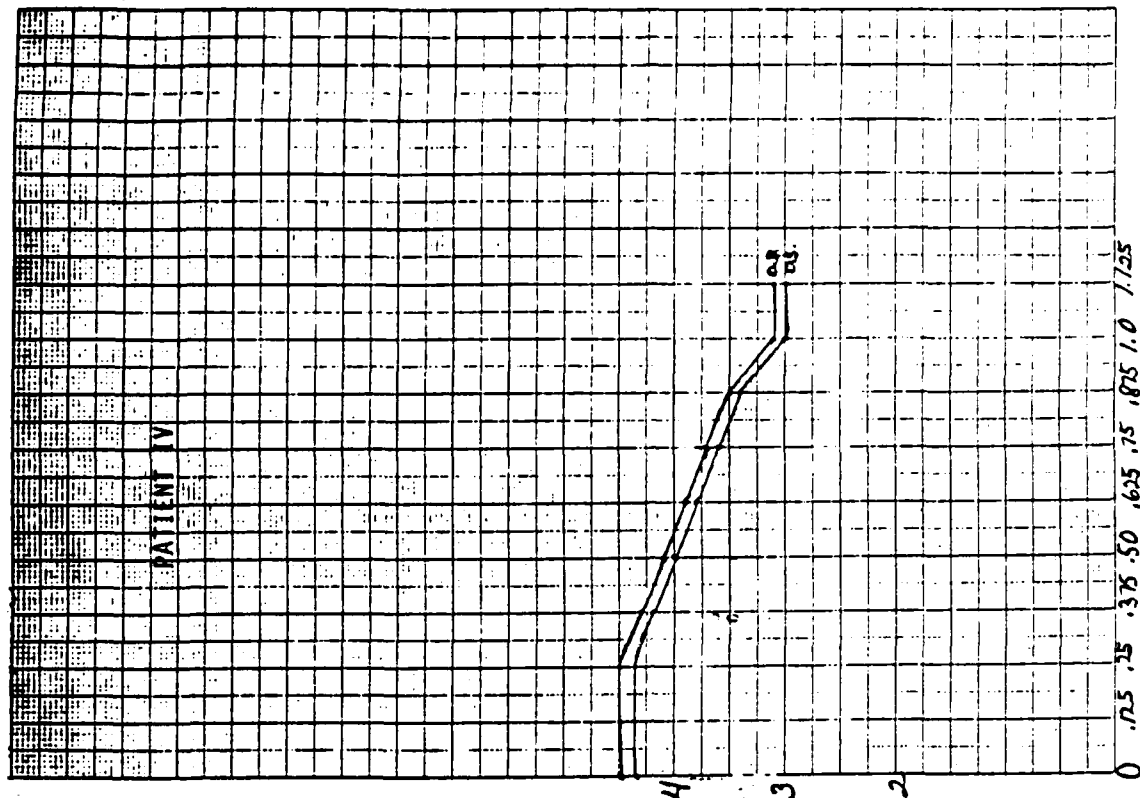UNOP-OP = Unop Diff - Op Diff

BASIC DATA AND DERIVED VARIABLES
THE T-STASTICTIC ONLY MAKES SENSE FOR UNOP-OP EYES

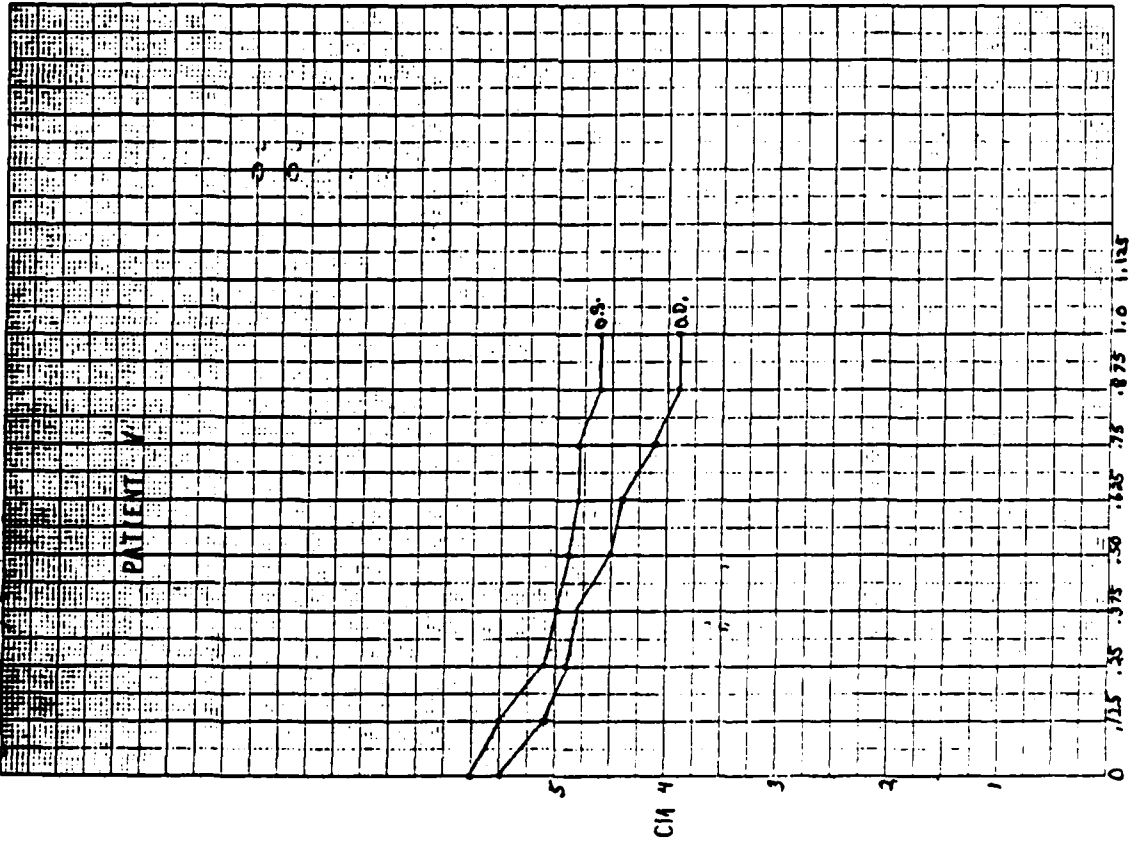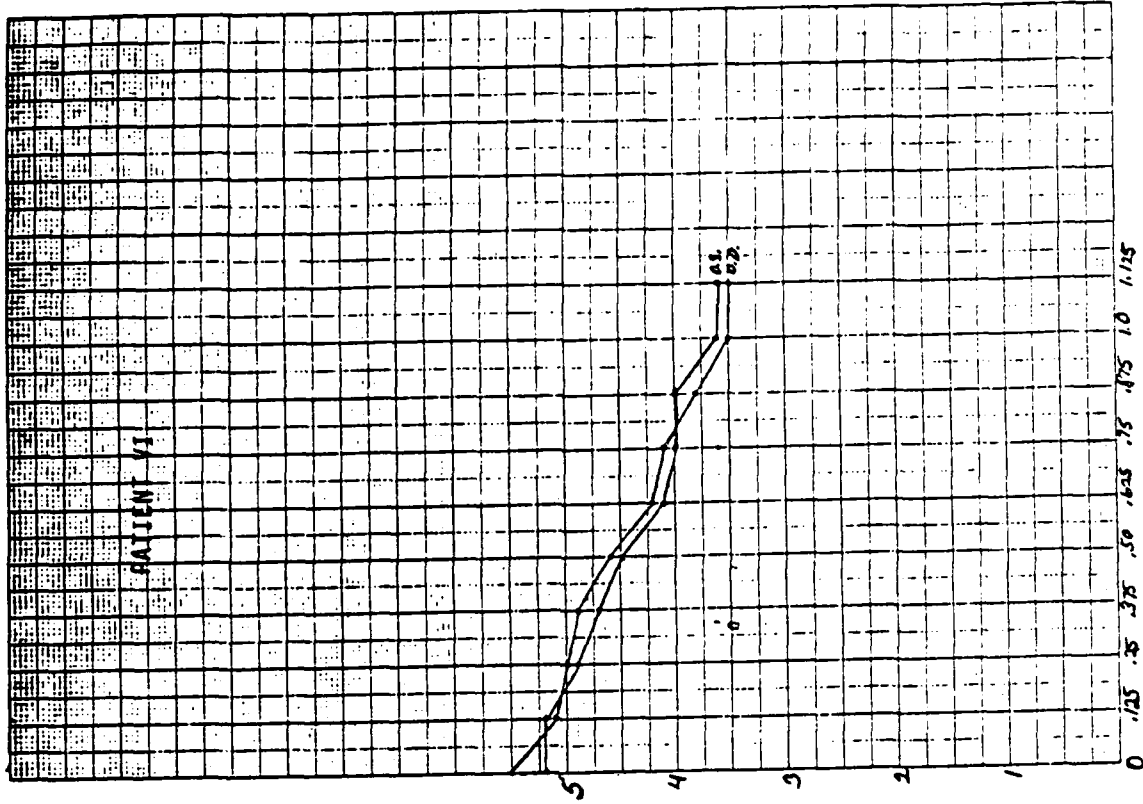| VARIABLE	LABEL	N	MEAN	STANDARD DEVIATION	STD ERROR OF MEAN	MIN. VALUE	MAX VALUE	RANGE	T
UNOP-OP	UNOP-DIFF-OP DIFF	9	0.1555	0.2186	0.0729	-0.1000	0.5000	0.6000	2.13
UNOP-PRE	Unoperated Pre	9	5.2111	0.8666	0.2889	4.2000	7.0000	2.8000	
UNOP-POST	Unoperated Post	9	3.4444	0.7248	0.2416	2.8000	4.9000	2.1000	
OP-POST	Operated Post	9	3.5444	0.8002	0.2667	2.8000	5.0000	2.2000	
OP-PRE	Operated Pre	9	5.1556	0.8233	0.2744	4.2000	6.9000	2.7000	
UNOPDIFF	Unoperated Pre and Post	9	1.7667	0.2784	0.0928	1.4000	2.1000	0.7000	
OP DIFF	Operated Pre and Post	9	1.6111	0.3407	0.1136	1.1000	2.2000	1.1000	

TABLE II

50-11

SECONDS

Patients I-IX represent graphs I-IX respectively.

50-12

PATIENT IV

PATIENT II

CM

SECONDS

50-13

PATIENT V3

O.S.
O.D.

O.D.

PATIENT V?

O.S.

O.D.

SECONDS

CI4

SECONDS

CM

50-15

SECONDS

CM
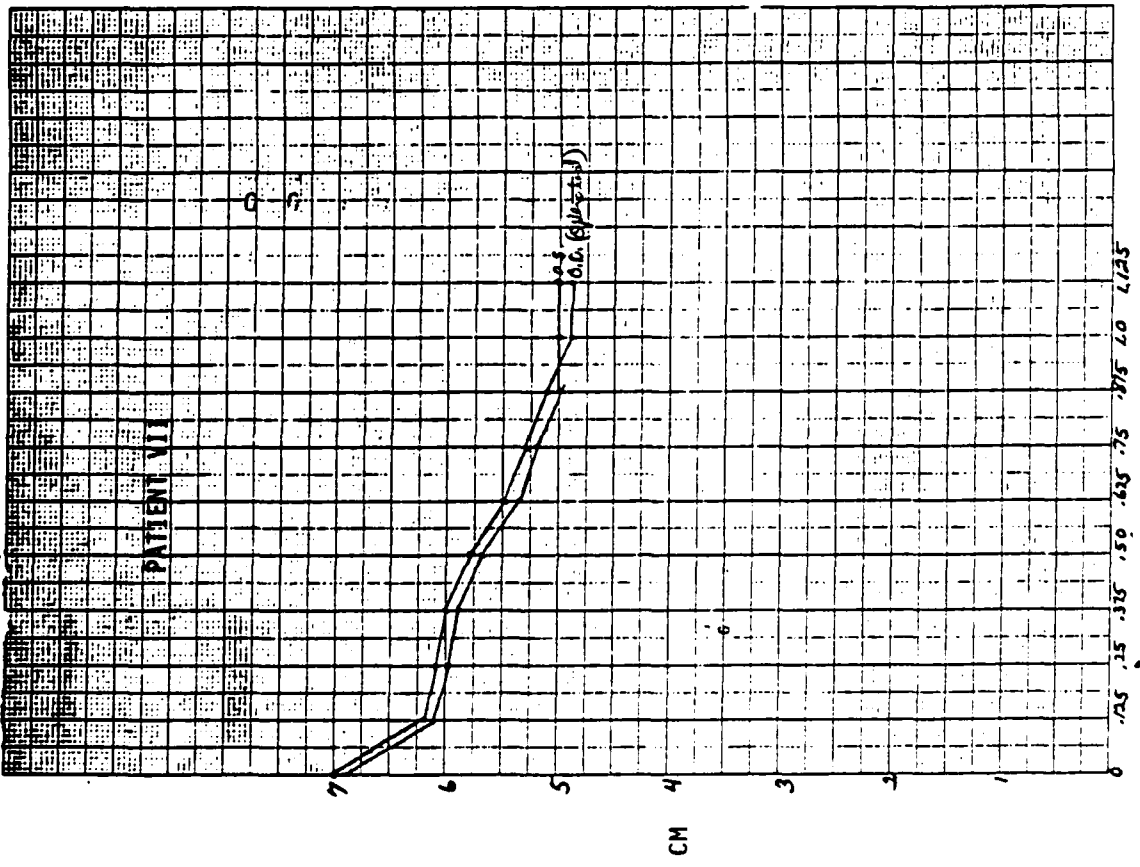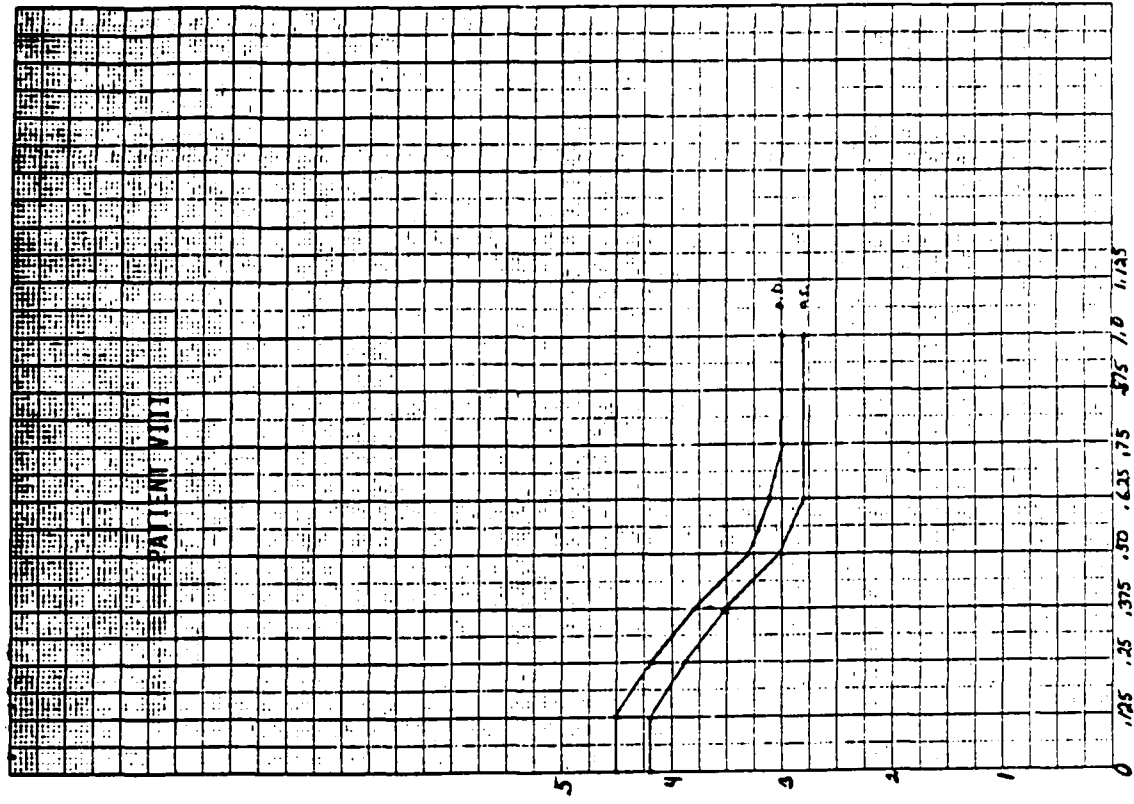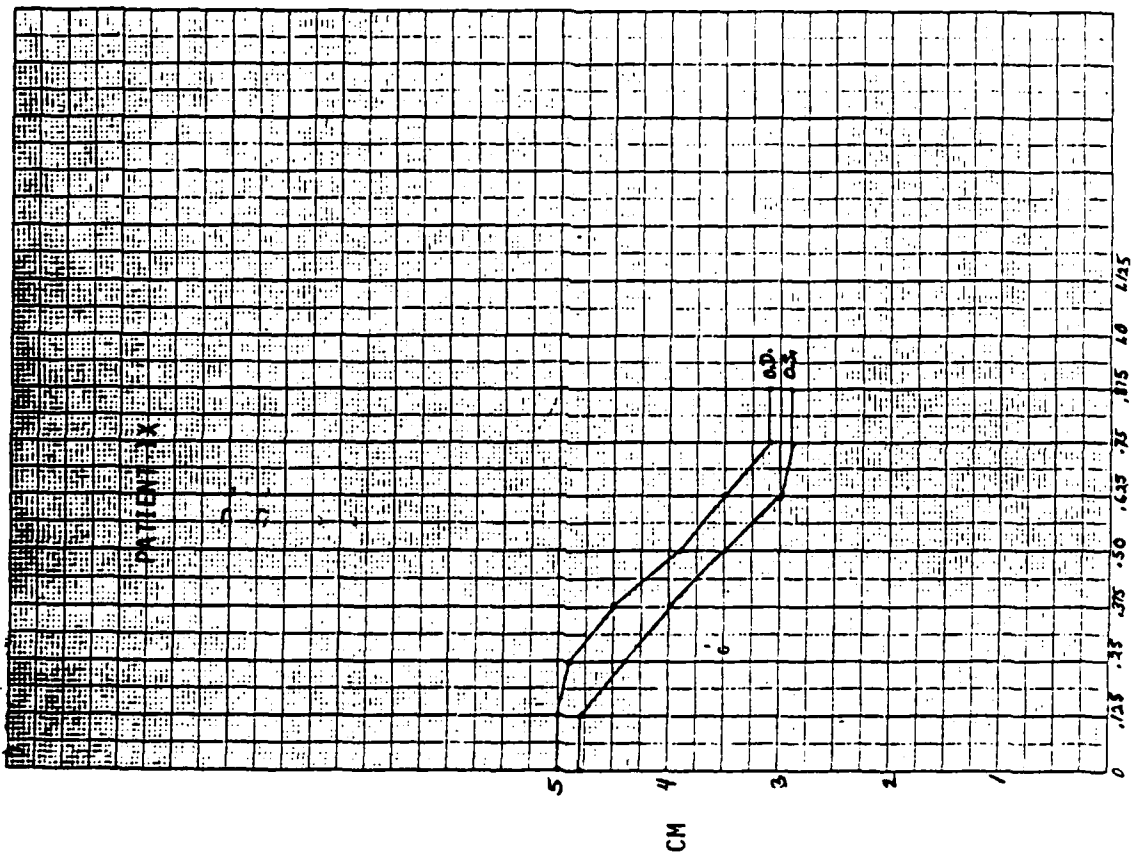
REFERENCES

Canavan, Y.M. & Archer, D.B., "Anterior Segment Consequences of Blunt Ocular Injury, British Journal of Ophthalmology. 1982, pp. 549-555.

Canavan, Y.M. & Archer, D.B., The Traumatized Eye, Transactions of the Ophthalmological Society of the United Kingdom. 1982 Vol. 102, pp. 79-84.

Cox, Terry A., M.D., Spontaneous Contractions of the Pupillary Sphincter in Traumatic Ophthalmoplegia, American Journal of Ophthalmology. 1986 Vol. 102. pp. 543-544.

Krieplstein, G.K., Ducanee, Z., and Leydhecker, W., Cataract Surgery: Types and Frequences of Complications. Albecht von Graefas Archir fur Klinische und experimentelle Ophthalmologie. 1980, Vol. 214, pp. 9-13.

Percival, S.P.B., F.R.C.S., Results After Intracapsular Extractions: The Atonic Pupil. Ophthalmic Surgery. 1977 Vol 8. pp. 138-143.

1987 USAF-UES SUMMER FACULTY RESEARCH PROGRAM/

GRADUATE STUDENT SUMMER SUPPORT PROGRAM

Sponsored by the

AIR FORCE OFFICE OF SCIENTIFIC RESEARCH

Conducted by the

Universal Energy Systems, Inc.

FINAL REPORT

LIQUID SCINTILLATION COUNTING WITH THE PACKARD 1500 ANALYZER

Prepared by:	Randal L. Mandock
Academic Rank:	Student
Department and	School of Mechanical Engineering (NE & HP Program)
University:	Georgia Institute of Technology
Research Location:	USAFOEHL/RZA Brooks AFB San Antonio TX 78235
USAF Researcher:	Amon J. Clay
Date:	28 Aug 87
Contract No:	F49620-85-C-0013

Liquid Scintillation Counting with the Packard 1500 Analyzer

by

Randal L. Mandock

ABSTRACT

Alpha and beta particles were detected with the Packard 1500 Liquid Scintillation Analyzer. Six tests of the EPA Radon-222 in water by liquid scintillation produced results which agreed with the known activities within the uncertainty when three regions were analyzed. The alpha activity measured for Pu-242 was consistently high, although the majority of the measurements taken in Region B agreed with the known activity within the uncertainty. The alpha activity measured for Am-241 agreed well with the known activity for every measurement in Region B. Measured tritium activities decreased due to color quenching as urine color progressed from light to dark. Background determination was found to be a key element when measuring low levels of activity.

ACKNOWLEDGEMENTS

I thank Mr Claude B Allen for his assistance in this and other projects which I was able to complete while here at OEHL. I acknowledge the support of Mr Clay, Lt Col Burr, Maj Maher and Hunter, Capt Adams, MSgt Moyes, and the RZA staff during my summer effort.

I wish to thank the Air Force Systems Command, the Air Force Office of Scientific Research, and OEHL/RZA for sponsorship of this research. Universal Energy Systems must be mentioned for its concern and help to me in all administrative and directional aspects of this program.

I. INTRODUCTION:

Recent technological advances in liquid scintillation detection of ionizing radiation have promoted the method to its present level of utilization at many laboratories which are in need of fast and dependable quantification of low level concentrations of radioactivity in a wide variety of media. The method is useful for tracer studies, radiological assessment, environmental monitoring, biomedical applications, and other biological monitoring tasks. Samples are immersed in a scintillation cocktail which is dense, transparent to specific visible wavelengths, surrounds and homogeneously distributes the sample, and is able to dissolve varied sample compositions. Computerized detectors now possess multichannel analysis capability with attendant hardware and software which enable technicians to perform radiochemical analyses that were formerly restricted to experienced chemists.

The Radioanalytical Branch of the USAF Occupational and Environmental Health Laboratory (OEHL) at Brooks Air Force Base analyzes environmental and biological samples for radioactive contamination on a routine basis. One year ago the Branch acquired a Packard 1500 Liquid Scintillation Analyzer to replace an aging unit. The Packard device is technologically sophisticated, requiring a substantial time investment for familiarization with its advanced performance characteristics. It is a computer-driven machine that is user compatible for the laboratory technician, but somewhat challenging to the protocol programmer. The normal workload of the laboratory staff prevented them from justifying

the time investment necessary to prepare the system for efficient utilization.

Several factors contributed to my assignment to the Radioanalytical Branch of OEHL. I have many years of data processing and analysis experience as well as an acquaintance with analytical radiochemistry. My most recent research interest has been collaboration with Bernd Kahn of Georgia Tech in the development of a new screening procedure for radium in drinking water. I used liquid scintillation counting as one among three methods of testing the procedure.

II. OBJECTIVES OF THE RESEARCH EFFORT:

The preliminary goals of the effort were five-fold: (1) Operation of the Packard 1500 Liquid Scintillation Analyzer to include basic scintillation counting theory and interrelationships of chemical, light, and color quenching. (2) Data reduction and interpretation. (3) Recommend Quality Control procedures to verify and maintain counting reliability and techniques. (4) Technique development to include Radon-222 in water by liquid scintillation, alpha particle spectral analysis, and the analysis of beta emitters. (5) Summary of accomplishments and recommendations.

III. PACKARD 1500 LIQUID SCINTILLATION ANALYZER OPERATION

This objective was continually being realized throughout the entire

51-5

research period, but primarily during the first three weeks of the effort. Approaches taken include: literature review, interaction with OEHL staff; personal communication with Packard researchers, sales representatives, and a district manager; review of Packard documentation; acquisition of supplementary Packard documentation; preliminary testing of system parameters.

This objective was realized when tests with actual samples produced interpretable, correct, and reproducible results.

IV. DATA REDUCTION AND INTERPRETATION:

Approaches taken here were determined by the nature of the testing procedures and the test results. The approach to the detection of Radon-222 in water was that of a Lockheed (EPA) Radon-222 procedure provided by OEHL staff. The approach to alpha and beta particle detection techniques was conventional, although data interpretation was enhanced by the multichannel analysis capability of the Packard unit.

V. RADON-222 IN WATER:

The EPA procedure was implemented with the Packard system. Preliminary tests were run in the Group Priostat mode in order to determine optimum counting region dimensions. Group Priostat provided hard copies of detected spectra from which final region specifications were made. Region A was chosen to range from 0 to 800 keV, Region B

from 220 to 800 keV, and Region C full spectrum (0 to 2000 keV).

Six tests were performed for verification and statistical precision. Region B produced results which agreed with the known activities (one-sigma limit of uncertainty) for two of the three samples tested, while Region C produced results which agreed with the remaining sample activity. However, all three regions produced results wherein the uncertainty associated with the average measured activities overlapped with the uncertainty associated with the known activities. In summary, the net result of the Radon-222 tests was reliable activity determination.

VI. ALPHA PARTICLE SPECTRAL ANALYSIS:

Spike tests were performed on two alpha emitters, Pu-242 and Am-241. On the basis of analysis of the Pu-242 spectrum, Region A was chosen to range from 100 to 300 keV, Region B from 150 to 400 keV, and Region C full spectrum. The measured activities were consistently too high, although for count times on the order of ten minutes, the majority of measured activities from Region B agreed with the spike activity to within two-sigma uncertainty. The following additional information was obtained from a 300 minute count. The photopeak was centered about the 208 keV channel. Since the maximum Pu-242 alpha energy is 4.9 MeV, the efficiency of energy determination for this nuclide is about 4 percent. This would be of concern if energy was the important parameter under consideration. However, activity is the parameter being sought. Therefore energy information is relegated to the status of a useful

guide for region setting and radionuclide identification. The peak

width was 80 keV at the zero cpm baseline and 35 keV at full width half

maximum. The range of energies under the peak was 160 to 240 keV.

According to the Am-241 spectrum, Region A was chosen to range from

100 to 300 keV, Region B from 150 to 400 keV, and Region C full

spectrum. All measured activities agreed with the spike activity to

within two-sigma uncertainty. The photopeak was centered about the 260

keV channel, about 5 percent of its maximum energy of 5.5 MeV. The peak

width was 88 keV at the zero cpm baseline and 45 keV at full width half

maximum. The range of energies under the peak was 208 to 304 keV.

VII. BETA EMITTER SPECTRAL ANALYSIS:

The beta emitters investigated were tritium and C-14. Tests were

run to determine the optimum water sample volume and scintillation

cocktail; the volume determined was then used in the analysis of

tritium-spiked urine samples.

Results of the tritium analysis generally agreed with expectations.

For optimum sample volumes of raw urine (1 and 2 ml) and optimum

scintillator cocktail (Beckman EP), measured activities decreased due to

color quenching as urine color progressed from light to dark. Distilled

urines for the optimum sample volume fluctuated about the known spike

activity and agreed with the spike to within two-sigma uncertainty.

Optimum sample volumes for C-14 were found to be 4 and 6 ml of

sample in 12 and 10 ml Beckman EP cocktail, respectively. Optimum

sample volumes were found for Packard Opti-Fluor cocktail to be 1 and 6

ml of sample, respectively.

VIII. RECOMMENDATIONS:

1. For production control purposes, particular protocols should be
dedicated to specific functions such as the following. (1) Protocol #1:
Single label H-3 protocol with quench curve. (2) Protocol #2: Single
label C-14 protocol with quench curve. (3) Protocol #3: Dual label
H-3/C-14 protocol with quench curves.

2. When making minor modifications to dedicated protocols, such as
changing the counting time or number of cycles, the dedicated protocol
should be copied to a nondedicated protocol. Desired changes may then
be incorporated into the new protocol.

3. Whenever possible, first vial background should be used, as it
provides the background values from which net counts are calculated.
Choosing first vial background results in the background subtraction
from all subsequent counts. Printed CPM's and DPM's will then be
corrected for background, regardless of the counting mode chosen.

4. Whenever possible, a background vial should be placed after the last
sample counted. The use of this background vial is especially important
when performing multiple counts per vial. Multiple counts per vial
result in the calculation of average count rates. A problem arises,
however, when one of the counts used in determining the average

background count is substantially higher than the others. This can occur for background counts that vary with time, e.g. counts which are affected by chemi- or photoluminescence. As an example, a test was run of 3 counts per vial for 25 minutes counting time each vial with first vial background, 2 samples, and a final background vial. Region C was set for full spectrum counting. The first background count for Region C was 56 cpm, the second 37 cpm, and the third 35 cpm. These resulted in an average background count of 43 cpm, far too high. The third count ended 75 minutes after the first count had begun; this third count was more representative of the true background count rate for the remaining samples than was the first background count rate. Adding 8 cpm to the count rates in Region C brought them in line with count rates from previous tests.

5. Multiple cycles should be run rather than multiple counts per vial whenever machine-calculated averages are not required. If machine averaging is desired, a background test should be run with multiple vials. Then a background value may be entered manually. Another alternative is to wait for suspected luminescence effects to die out; an hour may be adequate. Then count multiple vials per sample. Or the luminescence correction option may be used in conjunction with multiple vials per sample.

6. A useful flag for determining bad average background values is full spectrum monitoring in Region C. Full spectrum count rates should be approximately equal to or greater than windowed count rates, in general. When full spectrum count rates are consistently and substantially less

than windowed count rates, an incorrectly large average background subtraction is probably responsible.

7. Another useful flag is the last vial background vial suggested earlier in 4. When the average background value exceeds the count rate in a particular region, the count rate for that region is replaced with a zero. When a significant number of regions contain zero cpm for a multiply-counted last vial background, then an incorrectly large average background subtraction is probably the reason.

8. Suggested follow-on research might include spectral classification of other alpha and beta emitters, further development of the Radon-222 in water by liquid scintillation technique, further tests in the Full Spectrum DPM and Conventional DPM modes, and gamma emitter spectral classification.

1987 USAF-UES SUMMER FACULTY RESEARCH PROGRAM/

GRADUATE STUDENT SUMMER SUPPORT PROGRAM

Sponsored by the

AIR FORCE OFFICE OF SCIENTIFIC RESEARCH

Conducted by the

Universal Energy Systems, Inc.

De-embedding S-parameter Measurements Using

TSD Technique

Prepared by:	James W. Mattern
Academic Rank:	Graduate Student
Department and	Applied Physics and Electrical Engineering
University:	Oregon Graduate Center
Research Location:	AFWAL/AADM-2
	Wright-Patterson AFB OH 45433-6543
USAF Researcher:	Mark C. Calcatera
Date:	19 August 1987
Contract No:	F49620-85-C-0013

De-embedding S-parameter Measurements

Using TSD Technique

by

James W. Mattern

ABSTRACT

Scattering-parameter measurement of devices embedded in microstrip lines are de-embedded using the Thru-Short-Delay method. A computer algorithm was developed to calculate the error adjustment terms needed to adjust the error matrix supplied by the network analyzer. The results are new error terms that shift the measurement plane to device level. The algorithm was tested successfully by using a pair of 10 cm airlines with APC7 connectors to simulate a pair of arbitrary launchers.

ACKNOWLEDGEMENTS

I wish to thank the people at the Air Force Avionics Laboratory at Wright-Patterson AFB for their assistance in my research and preparation of this document.

The people in the Microwave Division were especially encouraging and influential. I wish to thank Mark Calcatera for his support and insight. I am greatful to the group of teams that allowed me to spend so much time on their equipment and especially Brian Kearns and Stu Labovitz for keeping my sanity.

Special thanks to Dr. Jim Whalen for steering me on course.

The kind assistance of John Archer of Varian Associates is greatly appreciated.

I.   INTRODUCTION:

De-embedding the correct S-parameters associated with a device, mounted on
microstrip lines has been a problem facing the microwave device design and
application community. Some members of industry have solved this problem, in
house, and have kept the solution proprietary.

With the current Department of Defense thrust to MMIC devices and designs,
the Avionics Laboratory has become particularly interested in the
de-embedding process.

At high frequencies (45MHz and greater) a network analyzer (HP8510A) is used
to send a electromagnetic continuous wave signal into a two port device
mounted on microstrip lines. The analyzer then returns values for the
voltage that is reflected and a value for the voltage transmitted. Both
these values are normalized by the incident voltage wave. These values are
called scattering parameters. S-parameters are taken from the input and from
the output. Each device has its own set. Each set represents a
characteristic family of S-parameters which can be used for comparison.
These values are used to determine the quality of the device performance. As
more devices are designed by design teams, access to and accuracy of these
parameters become very important for design evaluation. Device performance
can be predicted from these S-parameters.

In order to make these measurements the microstrip with the device must be mounted on a carrier and connected to the test ports by a launching system. Usually coaxial to microstrip mechanical connections are implemented by a step-down signal launcher. The HP8510A Network Analyzer can be calibrated to the ends of the coaxial cables but not down to the plane of the actual device. The process of de-embedding involves the mathematical process of shifting the measurements plane from the ends of the coax to the edges of the microstrip lines to which device bond wires are attached.

My experience in computer algorithm design, microwave circuit design, and mathematics made me a good choice to implement the TSD Algorithm.

II.   OBJECTIVES OF THE RESEARCH EFFORT:

The selection of a method for de-embedding the S-parameters of a device, mounted in microstrip line, an appropriate algorithm design to implement this method, and a few simple test cases by hand were the objectives of the research period.

The method chosen was the Thru-Short-Delay (TSD)[1]. This calibration is simple as it requires the microstrip characteristic impedance (Z0) to be 50 Ohms and constant for the frequency range of interest (45MHz to 18GHz). The standards themselves must be made with great care to prevent added air gaps, ceramic overhang and other problems that may introduce added capacitance or inductance. The short is required to be a highly reflective device. This method does not depend on the electrical length of the delay and thus is generally applicable to other test environments such as wave-guide and APC7 coaxial connectors.

The Algorithm was created from two sources. The published mathematical basis for the TSD Calibration algorithm[2] was provided and altered. The main change was the use of an assumption of a perfectly reflective device. New equations for error terms e_{11} and e_{22} in the 12-term, error model were derived. The algorithm was then programmed using the HP9000 series 320 computer in HP Basic 4.03. It is appropriate to insert TSD calibration as a routine in the 11863 Accuracy Enhancement PAC, provided with the HP8510A Network Analyzer.

The TSD calibration technique was coded, debugged, and tested using APC7 10 cm airlines with APC7 connectors to simulate a pair of launchers. Two APC7 shorts were used during TSD calibration. An APC7 THRU with known characteristics and the 20 dB Attenuator from the HP7mm Verification kit were used to verify the TSD algorithm.

III.

The full two port error correction routine for the HP8510A assumes a 12 term error model. These terms are determined using HP supplied standards: short, open, and sliding load. The conventional 12 term error matrix is then computed and stored using these standards for calibration with the test cable APC7 connector ends as reference planes.

The TSD method works in a similar manner. The Thru, Delay, and Short are measured and S-parameter data are collected, stored, and used to create error term adjustments. These error term adjustments may either be used in the complete TSD calibration or used to alter the original calibration error matrix and stored for use directly to calibrate measurements on the test device.

Adjusting the error term matrix was chosen as being the more general application since it would allow for real-time measurements[3]. The TSD error matrix is a ten term error matrix because the crosstalk error terms for microstrip are assured to be zero.

The error term flow diagram:
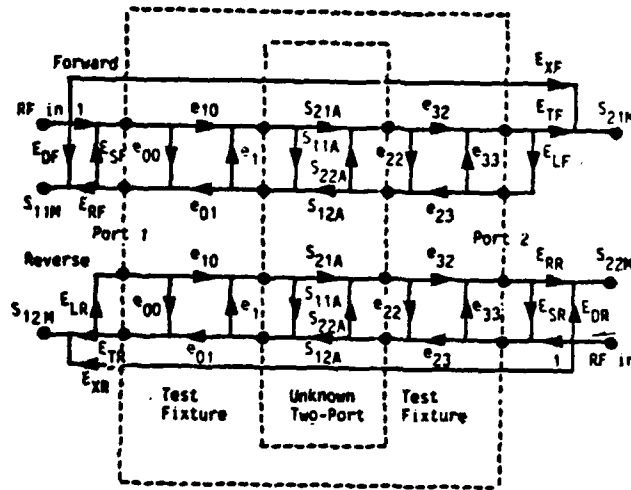
Due to the timing of the study of this TSD method, microstrip standards and launchers with good repeatable connections were not available. A computer language that is numerically sophisticated and handles complex matrix algebra was also unavailable. Thus, hand manipulation of the T matrices and the resulting equations became necessary to implement TSD.

The S matrix for any two-port device is given by:

$$S = \begin{bmatrix} S_{11} & S_{12} \\ S_{21} & S_{22} \end{bmatrix} \qquad (1)$$
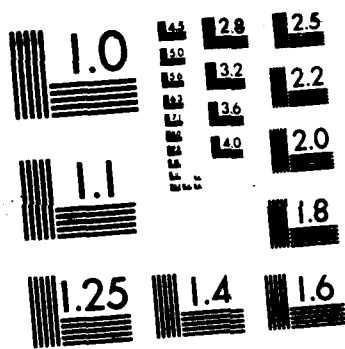
MICROCOPY RESOLUTION TEST CHART
NATIONAL BUREAU OF STANDARDS-1963-A

For cascading two or more matrices a T matrix is used. The T matrix and its inverse T^{-1} are given by:

$$T = \begin{bmatrix} \dfrac{S_{12}S_{21}-S_{11}S_{22}}{S_{21}} & \dfrac{S_{11}}{S_{21}} \\[2em] \dfrac{-S_{22}}{S_{21}} & \dfrac{1}{S_{21}} \end{bmatrix} \quad (2)$$

$$T^{-1} = \begin{bmatrix} \dfrac{1}{S_{12}} & \dfrac{-S_{11}}{S_{12}} \\[2em] \dfrac{S_{22}}{S_{12}} & \dfrac{S_{12}S_{21}-S_{11}S_{27}}{S_{12}} \end{bmatrix} \quad (3)$$

In order to solve for the error terms e_{00} and e_{33} it is necessary to solve the matrix equation.

$$[M][T_x] = [T_x][T_{ad}] \quad (4)$$

$$[T_y][N] = [T_{ad}][T_y] \quad (5)$$

Where

$[M]$ = $[T_{md}][T_{mt}]^{-1}$

$[T_{md}]$ = Measured T parameter matrix of the DELAY

$[T_{mt}]^{-1}$ = Measured T parameter inverse matrix of the THRU

$[T_{ad}]$ = Actual T matrix of a Delay element

$[T_x]$ = Network representing the left half of the THRU

$[T_y]$ = Network representing the right half of the THRU

$[N]$ = $[T_{mt}]^{-1}[T_{md}]$

Eliminating the electrical delay presented by $[T_{ad}]$ yields four equations:

$$M_{21} * \frac{X_{11}}{X_{21}} + (M_{22}-M_{11}) \frac{X_{11}}{X_{21}} - M_{12} = 0 \qquad (6)$$

$$M_{21} * \frac{X_{12}}{X_{22}} + (M_{22}-M_{11}) \frac{X_{12}}{X_{22}} - M_{12} = 0 \qquad (7)$$

$$M_{12} * \frac{Y_{11}}{Y_{12}} + (N_{22}-N_{11}) \frac{Y_{11}}{Y_{12}} - N_{21} = 0 \qquad (8)$$

$$M_{12} * \frac{Y_{21}}{Y_{22}} + (N_{22}-N_{11}) \frac{Y_{21}}{Y_{22}} - N_{21} = 0 \qquad (9)$$

The solutions to quadradic equations obtained by manipulating these four equations are defined by

$$\frac{X_{11}}{X_{21}} = e_{00} - \frac{e_{01}e_{10}}{e_{11}} = a \qquad (10)$$

$$\frac{X_{12}}{X_{22}} = e_{00} = b \qquad (11)$$

$$\frac{Y_{11}}{Y_{12}} = c = \frac{e_{23}e_{32}}{e_{22}} - e_{33} \qquad (12)$$

$$\frac{Y_{21}}{Y_{22}} = d = -e_{33} \qquad (13)$$

Since b and d represent terms for directivity error, they should be less than one. Thus, this is used as a test for root assignments.

The algorithm originally calls for a short that has merely high reflectivity. On the advice of Archer, (Ref 3) assume the short is perfect with a reflection coefficient equal to -1. This eliminates a possible uncertainty inherent in taking a square root of a complex number.

Equation 34 in [2]

$$e_{11} = \left[\frac{b-\Gamma_{mx}}{a-\Gamma_{mx}} \quad \frac{c-\Gamma_{my}}{d+\Gamma_{my}} \quad \frac{b-\Gamma_{m1}}{a-\Gamma_{m1}} \right]^{-\frac{1}{2}} \tag{14}$$

presents this problem.

However, by assuming a perfect short, Eq. 34 became

$$e_{11} = \frac{e_{00}-\Gamma_{mx}}{\Gamma_{mx}-e_{00}+b-a} \tag{15}$$

and

$$e_{22} = \frac{e_{33}-\Gamma_{my}}{\Gamma_{my}-e_{33}+c-d} \tag{16}$$

Where $\Gamma_{mx} = S_{11}$(Short); $\Gamma_{my} = S_{22}$(Short)

The set of equations used in the algorithm are repeated here

$$e_{00} = b \tag{17}$$

$$e_{33} = -d \tag{18}$$

$$e_{11} = e_{00} - \Gamma_{mx}/(\Gamma_{mx}-e_{00} + b-a) \tag{19}$$

$$e_{22} = e_{33} - \Gamma_{my}/(\Gamma_{my}-e_{33} + c-d) \tag{20}$$

$$e_{10}e_{01} = (b-a)e_{11} \tag{21}$$

$$e_{23}e_{32} = (c-d)e_{22} \tag{22}$$

$$e_{10}e_{32} = S_{21}(\text{measured thru}) \ (1-e_{11}e_{22}) \tag{23}$$

$$e_{23}e_{01} = S_{12}(\text{measured thru}) \ (1-e_{11}e_{22}) \tag{24}$$

By comparing the equations for the actual S-parameter corrections in the HP Accuracy Enhancement Program and the equations presented by Brubaker, it was shown by [3] that

$$EDF=e_{00} \qquad\qquad EDR=e_{33}$$

$$ESF=e_{11} \qquad\qquad ESR=e_{22}$$

$$ERF=e_{10}e_{01} \qquad\qquad ERR=e_{32}e_{23}$$

$$ETF=e_{32}e_{10} \qquad\qquad ETR=e_{23}e_{01}$$

$$ELF=e_{22} \qquad\qquad ELR=e_{11}$$

By doing so, Elsmore and Archer demonstrated that correction to the original error term matrix is possible by using these 12 relations:

$$EDF' = EDF + ERFe_{00}/(1-ESFe_{00}) \tag{25}$$

$$ERF' = ERFe_{10}e_{01}/(1-ESFe_{00})^2 \tag{26}$$

$$ESF' = e_{11} + ESFe_{10}e_{01}/(1-ESFe_{00}) \tag{27}$$

$$ELF' = e_{22} + EFLe_{32}^2{}_{23}/(1-ELFe_{33}) \tag{28}$$

$$ETF' = ETFe_{10}e_{32}/((1-ELFe_{33})(1-ESFe_{00})) \tag{29}$$

$$EDR' = EDR + ERRe_{33}/(1-ESRe_{33}) \tag{30}$$

$$ERR' = ESRe_{32}e_{23}/(1-ESRe_{33})^2 \tag{31}$$

$$ESR' = e_{22} + ESRe_{32}e_{23}/(1-ESRe_{33}) \tag{32}$$

$$ELF' = e_{11} + ELRe_{10}e_{01}/(1-ELRe_{00}) \tag{33}$$

$$ETR' = ETRe_{01}e_{23}/((1-ELRe_{00})(1-ESRe_{33})) \tag{34}$$

$$EXR' = EXR \tag{35}$$

$$EXF' = EXF \tag{36}$$

The Algorithm is thus completed by altering the original calibration error term matrix by the above set of equations. The modified error term matrix is then applied to obtain corrected S-parameters of the device with the reference planes shifted to the device location.

IV. CONCLUSION AND RECOMMENDATIONS

The TSD algorithm was verified by making a set of calculations by hand. The algorithm was tested by using a pair of 10 cm airlines with APC7 connectors to simulate a pair of transitions. One airline corresponded to the Left Hand Side (LHS) launcher represented by the matrix T_x. The other airline corresponded to the Right Hand Side (RHS) launcher represented by the matrix T_y. A pair of APC7 shorts were connected to the two airlines for the TSD short calibration. The two airlines were connected together for the TSD thru calibration. A third 10 cm airline with APC7 connectors was used for the TSD delay calibration. The TSD calibration was verified successfully by using a 10 cm airline, two short terminations and 20 dB attenuator from the APC7 Verification Kit. The de-embedded S-parameters measured using the TSD method agreed with the values provided by HP Device Characterization Data Sheet for the 20 dB Attenuator, within ±0.02 dB and ±0.3 degrees, averaged at all frequencies in the range of 2 to 18GHz (in 1GHz steps). At 13GHz, the error was 0.14dB and 2.0 degrees and 0.16 and 2.0 degrees for S21 and S12 respectively. These errors are within the HP uncertainty range. The agreement actually exceeded the uncertainties associated with the Verification Kit standard(s). The excellent agreement obtained provides the justification for stating that the TSD algorithm has been successfully implemented.

Since there were not standards available for microstrip line, the program could not be verified for microstrip lines. Therefore, I recommend the microstrip line standards be made and appropriate APC7-to-microstrip launchers be secured.

Repeatability of the TSD method is a problem. In microstrip the connection between APC7 and microstrip launcher and launcher to microstrip must be made many times. These connections are not presently accomplished in a manner that is easily repeatable. Selection of a launcher that makes easily repeatable connections must also be pursued.

Also, APC7 connectors should be hex-nut fasteners as application of constant torque is essential in the repeatability of these connections.

This method can be used to shift the reference plane of measurement to any device secured in microstrip, waveguide, or other propagation medium such as OS-50 semi-rigid coaxial cable. On-wafer device testing using the Cascade prober is also an application. Testing and adoption of the TSD method for each medium should be examined. For each medium, appropriate standards are required.

REFERENCES

1. Brubaker, D., Eisenberg, J.A., "Measure S-Parameters with the TSD Technique," Microwaves and RF, Nov. 85, pp. 97-101.

2. Brubaker, D., "TSD Calibration Algorithm," Microwaves and RF/TSD Math, Nov. 85, p. 101.

3. Archer, J., "Implementing the TSD Calibration Techniques," MSN & CT, May 1987, pp. 54-61.

4. Eismore, G., "De-embedded Measurements Using the HP8510 Microwave Network Analyzer," Hewlett Packard RF and Microwave Symposium, 1985.

1987 USAF-UES SUMMER FACULTY RESEARCH PROGRAM/GRADUATE STUDENT

SUMMER SUPPORT PROGRAM

Sponsored by the

AIR FORCE OFFICE OF SCIENTIFIC RESEARCH

Conducted by the

Universal Energy Systems, Inc.

FINAL REPORT

AN EXPERT SYSTEM FOR DIAGNOSIS AND REPAIR

OF ANALOG CIRCUITS

Prepared by :	Matthew B. McBeth
Academic Rank :	B.S. in Computer Science
Department and	Electrical Engineering
University :	Vanderbilt University
Research Location :	Sverdrup Tech. AEDC Tullahoma, TN
USAF Researcher :	Shirley Williams
Date:	10 AUG 87
Contract No :	F49620-85-C-0013

AN EXPERT SYSTEM FOR DIAGNOSIS AND REPAIR

OF ANALOG CIRCUITS

by

Matthew B. McBeth

ABSTRACT

The purpose for this research project is to study the use of artificial intelligence in the domains of electronic diagnosis and repair. This paper will describe a framework for building expert systems in such a domain. I will concentrate on an amplifier circuit board that is frequently used in data acquisition systems at Sverdrup Technology. The system under development is designed to aid the technicians in diagnosing and repairing the amplifier board down to the component level. This system will detect a potential fault and have the technician either adjust, check, or replace a component. It will then verify whether that was the problem and make a record of all repairs. This paper will also discuss the knowledge acquisition techniques used for the system, and the knowledge that was gained from each.

I. INTRODUCTION

The electronic systems of today are far from infallible and as long as that holds true there will have to be people around to fix them. A problem that electronic maintenance divisions, such as Sverdrup's, have with this is that when technicians retire, their knowledge goes with'them. Thus, every technician must learn on his own what the previous one spent a lifetime learning. With expert systems we have the promise of changing all that. By pooling what each technician knows into a knowledge base or rule base, their knowledge could be used for as long as needed. This concept is what expert systems are all about.

The maintenance and calibration division of Sverdrup tech. at Arnold Engineering Development Center has recently become interested in incorporating artificial intelligence in the diagnosis and repair of the equipment they work on. The Center for Intelligent Systems at Vanderbilt University is currently under contract by the USAF to perform research for Sverdrup to develop an expert diagnosis and repair system for analog circuits. With this project in mind, I was chosen to study the plausibility of a shallow knowledge rule-based system that could be compared to the deep knowledge system currently under development at Vanderbilt. I was chosen for my experience in rule-based programming and in building expert systems. Prior to the summer research project, I had developed a tutorial system and had worked in the distributed processing area of AI.

II. OBJECTIVES OF THE RESEARCH EFFORT

The major goal of the research effort was that of acquiring

knowledge. This was most important because an expert system can only be as expert as the knowledge that is in it and thus I decided to focus on this aspect of the project.

The other goal was to complete a shell for a system that the technicians could use in the repairing of a certain amplifier board that they often have problems with. This system is designed to be specific to that one circuit board, however the architecture could be used for many different circuits. For this to be completed the knowledge that was gathered must be converted to rules and a good graphics interface should be produced.

III. KNOWLEDGE ACQUISITION

The first approach I took toward gathering the knowledge was to interview the technician personally. I inquired about the general troubleshooting techniques he used on the amplifier board we were concentrating on. The obvious diagnosis were easy for him to relate to me, however to really get the expert knowledge he had I sat with him as he diagnosed several defective boards. The procedure we used for this was for him to try to repair each board and relate to me the reasons behind each step he would take. This approach was the most fruitful in gaining the technicians knowledge but there were times when he did not really know why he did some things. He usually would comment that that was just the way he had always done it. So I decided that I needed more than one persons knowledge on the diagnosing of this circuit. This prompted me to give the circuit diagram to a few colleagues at Vanderbilt who are experts in analog circuits. In doing this I could get a different approach to the

53-4

diagnosing of faults and perhaps fill in some of the gaps in the knowledge.

In the technicians case, I translated the knowledge he gave me into IF THEN rules written in English that would be translated into code later. The personnel at Vanderbilt have not yet completed their set of troubleshooting rules, but when they are completed they too will be translated into code.

IV. CODING THE KNOWLEDGE

The coding for this system was written in OPS83, a rule-based language for the PC. This was chosen because of its compatibility to the 'C' programming language. For the graphics interface to the user I used the Connell Scientific Graphics package, which also interfaces to 'C' and accesses the EGA board.

The Architecture for the system was based on the concept of grouping the rules into separate plans. Each plan was designed to diagnose a different problem that the board might have. After a few meetings with the technician, I found that he currently was using a DSE checkout station that ran tests on the board and gave an output for each test. In order to take advantage of this equipment already in use, we decided to use four of the tests from this system. These consisted of a test for gain output, zero output, input bias, and common mode rejection. The outputs given by these tests would then become the inputs to my expert system. Using these inputs, my system now had a starting place, or a hint of where to begin the diagnosing.

The system begins by taking the input and creating a working memory element that represents it, which is called a symptom. This symptom consists of slots that are filled as the troubleshooting is done. These slots contain the name of the test or plan for that symptom, its value, the current advice for the user, and a list of all repairs that have been done to this symptom. Each symptom has its own plan and these plans are executed in a predefined order.

The control for the system is handled by the elements on the control blackboard (Figure 1) which are the symptom, planner, and the tactician. As a troubleshooting session begins, the planner gets the first plan from the top of a preordered list. It then looks for a symptom whose name is the same, where upon control is given to the tactician. The other job of the planner is to change to a new plan when the tactician has found the problem of the prior symptom. Once the list of plans is exhausted, the system terminates and the user is put into the top level, read-eval-print loop of OPS83. Now back to the tactician, when it takes control it is informed what the current plan is and it monitors the rules that fire for that plan. When a problem is found, the tactician sets its flag to 'problem_found' and sends a script to be put into the message slot of the symptom. This message is then sent to the user advising him of the problem. The message will usually tell the technician one of two things, either take a measurement at a certain point and report the value or replace a part on the board. After this is done and the user has reported he is finished, the system will prompt him for a new output from the test currently being diagnosed. When the reading comes in, the symptoms value is updated and the tactician sets its flag to ready. This allows the current plan run again to verify that the problem is fixed. If the symptoms value is within the accepted limits then the tactician sets its

flag to 'problem_fixed' and control is given back to the planner. The code for the gain plan is included in the Appendix.

V. VARIOUS SPECIAL FEATURES

To further aid the technicians who would be using the system, I produced a graphical representation of the actual board they would be working on. It is displayed during the troubleshooting session and blinks the components that they need to check or replace. When the technicians have a question concerning the system, they may call up a help window by pressing a function key. This facility should be able to relate to him any information he needs to know. The next feature is probably the most important, it is the comment window. This will also be accessed by hitting a function key and be used by the technician to relate any information he feels is important. This information may be additional knowledge he has realized while using the system or problems that have occurred. Once the technician types this message in, it is written to a file that may be read by one of the programmers at Sverdrup. Thus the knowledge of the system may be expanded in this manner.

VII. RECOMMENDATIONS

The research done this summer has been partially implemented in the expert system previously described. This system appears to be a viable solution to the problem of diagnosing and repairing analog circuit boards and is quite easy to use, however the knowledge that is captured in the system must be expanded to get a greater level of expertise. This is the

main problem that plagues most expert systems that are being developed. In order to overcome this obstacle, more experts in the related field should be consulted and their knowledge be added to that which already exists. What this all boils down to is, that it doesn't matter how pretty the system is or how many bells and whistles you put into it, the system can only be as expert as the knowledge you put onto it. The extra features should be included in most systems but the attention must focus on the knowledge.

ACKNOWLEDGMENTS

Control Blackboard

Symptom

```
test (gain, zero, bias, cmr)
value (current value '11.0')
repair list
        replaced_U101
        trimmed_R120
message (current message being
            sent to user)
```
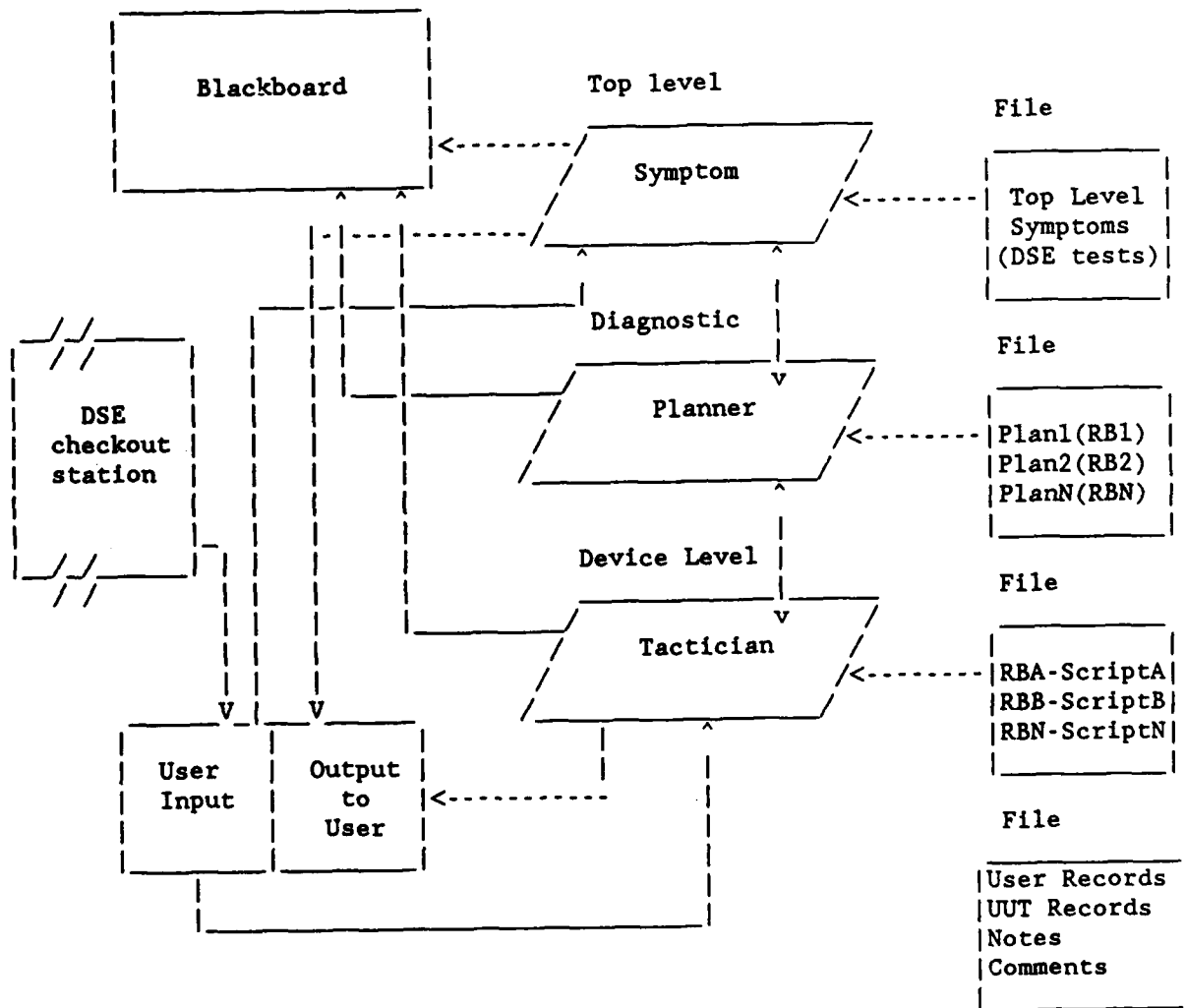
Planner

```
flag  (yes, no)
checklist (list of plans to
            execute)
results (current advice)
```

Tactician

```
flag (yes, no, problem_found
        problem_fixed)
current plan (gain, zero, bias, cmr)
```

Figure 1.

CONTROL LAYOUT

APPENDIX

```
--   RULE   BEGIN_PLAN
--
--   IF    there is a symptom in working mem.
--         and not a planner element.
--   THEN  draw the circuit board
--         create the wm (working memory) element planner
--         with the flag ready equal to yes
--         create the wm element tactic set its flag
--         to yes and initialize the current plan to gain.


rule begin_plan

{
   &1   (symptom ) ;
        (planner) ;
-->
        call dboard() ;
        make (planner ready=yes);
        make (tactic   ready=yes ;   cplan=gain) ;
} ;


--   RULE   CHANGE_TO_ZERO
--
--   IF    the planners flag is set to no
--         and the tactics flag is set to problem_fixed
--         and the last plan was the gain plan
--         and there is another symptom in wm
--   THEN  set the planners flag to yes
--         set the tactics flag to yes
--         and set the current plan to zero.


rule change_to_zero

{
   &1   (planner   ready=no) ;
   &2   (tactic    ready=problem_fixed; cplan=gain) ;
        (symptom) ;
-->
        modify &1 (ready=yes) ;
        modify &2 (ready=yes;   cplan=zero) ;

} ;



--   RULE   CHANGE_TO_BIAS
--
--   IF    the planners flag is set to no
--         and the tactics flag is set to problem_fixed
--         and the last plan was the gain zero
--         and there is another symptom in wm
--   THEN  set the planners flag to yes
--         set the tactics flag to yes
--         and set the current plan to bias.
```

```
rule change_to_bias
{
  &1  (planner  ready=no) ;
  &2  (tactic   ready=problem_fixed; cplan=zero) ;
      (symptom) ;
-->
      modify &1 (ready=yes) ;
      modify &2 (ready=yes;  cplan=bias) ;
} ;

--  RULE GAIN PLAN 1
--
--  IF   there is a symptom whose plan is gain
--       and whose value is greater than 8.9998 and less than 9.0002
--       and a tactic who is ready and has the current plan set to gain
--       and a planner who is ready
--  THEN set the planner to not ready
--       set the tactic to problem_fixed.

rule gp1
{
  &1  (symptom plan=gain;  (@.val > 8.9998 /\ @.val < 9.0002) ) ;
  &2  (tactic ready=yes; cplan=gain) ;
  &3  (planner ready=yes) ;
-->
      modify &3 (ready=no) ;
      modify &2 (ready=problem_fixed) ;
} ;
--  RULE  GAIN PLAN 2
--
--  IF   there is a symptom whose plan is gain
--       and whose value is greater than 8.97 and less than 9.03
--       and a tactic who is ready and has the current plan set to gain
--       and a planner who is ready
--  THEN set the symptom suggestion to gainpot
--       and the message to 'Adjust gain pot'
--       set the planners result to gainpot
--       set the tactic to problem_found.

rule gp2
{
  &1  (symptom plan=gain;  (@.val > 8.97 /\ @.val < 9.03)  );
  &2  (tactic  ready=yes; cplan=gain) ;
  &3  (planner ready=yes) ;
-->
      modify &1 (suggest=gainpot; mess=|Adjust gain pot | ) ;
      modify &3 (result=gain_pot) ;
      modify &2 (ready=problem_found) ;
};
--  RULE  GAIN PLAN 3A
--
--  IF   there is a symptom whose plan is gain
--       and whose value is greater than 7.5 and less than 8.98
--       and a tactic who is ready and has the current plan set to gain
--       and a planner who is ready
--  THEN set the symptom suggestion to R110
```

```
--          and the message to 'Add trim resistor here'
--          set the planners result to trim resistors
--          set the tactic to problem_found.

rule gp3A
{

   &1   (symptom plan=gain;  (@.val > 7.50 /\ @.val < 8.98)  );
   &2   (tactic  ready=yes; cplan=gain) ;
   &3   (planner ready=yes) ;
-->
        modify &1 (suggest=R110; mess=|Add trim resistor here |) ;
        modify &3 (result=trim_resistors) ;
        modify &2 (ready=problem_found) ;
};

--  RULE  GAIN PLAN 3B
--
--  IF   there is a symptom whose plan is gain
--          and whose value is greater than 9.03 and less than 10.5
--          and a tactic who is ready and has the current plan set to gain
--          and a planner who is ready
--  THEN set the symptom suggestion to R112
--          and the message to 'Add trim resistor here'
--          set the planners result to trim resistors
--          set the tactic to problem_found.

rule gp3B
{

   &1   (symptom plan=gain;  (@.val > 9.03 /\ @.val < 10.5)  );
   &2   (tactic  ready=yes; cplan=gain) ;
   &3   (planner ready=yes) ;
-->
        modify &1 (suggest=R112; mess=|Add trim resistor here |) ;
        modify &3 (result=trim_resistors) ;
        modify &2 (ready=problem_found) ;
};


--  RULE  GAIN PLAN 4
--
--  IF   there is a symptom whose plan is gain
--          and whose value is greater than -1.0 and less than 1.0
--          and a tactic who is ready and has the current plan set to gain
--          and a planner who is ready
--  THEN get input at U101 from user
--      IF   that reading is greater than -1.0 and less than 1.0
--          set the symptom suggestion to GAIN
--          and the message to 'replace GAIN chip'
--          set the planners result to gain chip
--          set the tactic to problem_found.
--      ELSE set the planner to check U101 output
--

rule gp4
```

```
{

  &1  (symptom plan=gain;  (@.val > -1.0 /\ @.val < 1.0) ) ;
  &2  (tactic  ready=yes; cplan=gain) ;
  &3  (planner ready=yes; result=||) ;
-->

  local &x : symbol, &y : symbol;

      &x=U101 ;
      &y=|What is the input at U101 | ;
      call draw_board(&x, &y, &reading) ;
      if (&reading > -1.0 /\ &reading < 1.0)
        {
        modify &1 (suggest=GAIN; mess=|Replace GAIN chip |) ;
        modify &3 (result=gain_chip) ;
        modify &2 (ready=problem_found) ;
        }
      else
        modify &3 (result=U101_output) ;

};

--  RULE  GAIN PLAN 5
--
--  IF    there is a symptom whose plan is gain
--        and whose value is greater than -1.0 and less than 1.0
--        and a tactic who is ready and has the current plan set to gain
--        and a planner who is ready and has a result of U101 output
--  THEN get output at U101 from user
--      IF   that reading is greater than -1.0 and less than 1.0
--           set the symptom suggestion to U101
--           and the message to 'replace opamp U101'
--           set the planners result to U101
--           set the tactic to problem_found.
--      ELSE set the planner to check U102 input
--

rule gp5
{

  &1  (symptom plan=gain;  (@.val > -1.0 /\ @.val < 1.0) ) ;
  &2  (tactic  ready=yes; cplan=gain) ;
  &3  (planner ready=yes; result=U101_output ) ;
-->
  local &x : symbol, &y : symbol;

      &x=U101 ;
      &y=|What is the output at U101 | ;
      call draw_board(&x, &y, &reading) ;
      if (&reading > -1.0 /\ &reading < 1.0)
        {
        modify &1 (suggest=U101; mess=|Replace opamp U101 |) ;
        modify &3 (result=U101) ;
        modify &2 (ready=problem_found) ;
        }
```

```
        else
            modify &3 (result=U102_input) ;

};


--   RULE   GAIN PLAN 6
--
--   IF    there is a symptom whose plan is gain
--         and whose value is greater than -1.0 and less than 1.0
--         and a tactic who is ready and has the current plan set to gain
--         and a planner who is ready and has a result of U102 input
--   THEN get input at U102 from user
--         IF    that reading is greater than -1.0 and less than 1.0
-- .               set the symptom suggestion to FILTER
--                 and the message to 'replace FILTER chip'
--               set the planners result to FILTER chip
--               set the tactic to problem_found.
--         ELSE set the planner to check U102 output
--


rule gp6
{

  &1   (symptom plan=gain;  (@.val > -1.0 /\ @.val < 1.0)) ;
  &2   (tactic  ready=yes; cplan=gain) ;
  &3   (planner ready=yes; result=U102_input ) ;
-->
  local &x : symbol, &y : symbol;

      &x=U102 ;
      &y=|What is the input at U102 | ;
      call draw_board(&x, &y, &reading) ;
      if (&reading > -1.0 /\ &reading < 1.0)
        {
          modify &1 (suggest=FILT; mess=|Replace FILTER chip |) ;
          modify &3 (result=filter_chip) ;
          modify &2 (ready=problem_found) ;
        }
      else
          modify &3 (result=U102_output) ;

};


--   RULE   GAIN PLAN 7
--
--   IF    there is a symptom whose plan is gain
--         and whose value is greater than -1.0 and less than 1.0
--         and a tactic who is ready and has the current plan set to gain
--         and a planner who is ready and has a result of U102 output
--   THEN get output at U102 from user
--         IF    that reading is greater than -1.0 and less than 1.0
--               set the symptom suggestion to U102
--               and the message to 'replace opamp U102'
--               set the planners result to U102
```

```
--          set the tactic to problem_found.
--     ELSE set the symptom suggestion to Q001
--          and the message to 'check fet switches'
--          set the planners result to Fet switches
--          set the tactic to problem_found.

rule gp7
{

  &1  (symptom plan=gain;  (@.val > -1.0 /\ @.val < 1.0) ) ;
  &2  (tactic  ready=yes; cplan=gain) ;
  &3  (planner ready=yes; result=U102_output ) ;
-->
  local &x : symbol, &y : symbol;

      &x=U102 ;
      &y=|What is the output at U102 | ;
      call draw_board(&x, &y, &reading) ;
      if (&reading > -1.0 /\ &reading < 1.0)
        {
         modify &1 (suggest=U102; mess=|Replace opamp U102 |) ;
         modify &3 (result=U102) ;
         modify &2 (ready=problem_found) ;
        }
      else
        {
         modify &1 (suggest=Q001; mess=|Check the FET switches |) ;
         modify &3 (result=Fet_switches) ;
         modify &2 (ready=problem_found) ;
        } ;

};

--    RULE  GAIN PLAN 8
--
--   IF    there is a symptom whose plan is gain
--         and the planner is ready
--         and the tactic is set to problem found
--   THEN tell user what action to take (contained in Symptom.mess)
--         ask the user what the new output is
--         set symptom.val to the new reading
--         add planner.result to the symptom.repairs list
--         increment the repair count by one
--         set the planner.result to a null value
--         set the tactic flag to ready.

rule gp8
{
  &1 (symptom plan=gain) ;
  &2 (planner ready=yes) ;
  &3 (tactic  ready=problem_found; cplan=gain) ;
-->
   local
     &x : symbol, &y : symbol ;

     &x = &1.suggest ;
```

```
&y = &1.mess ;
call draw_board(&x, &y, &reading) ;
&y = |What is the new output| ;
call out(&x, &y, &reading) ;
modify &1 (val=&reading; repairs[@.count]=&2.result ; count=@.count + 1) ;
modify &2 (result=||) ;
modify &3 (ready=yes) ;
} ;
```

REFERENCES

[1] Caviedes, J., Bourne, J., Brodersen, A., Osborne, P., Ross, A., Schaffer, J.D. and Bengtson, G., "A Meta-Level Architecture For Planning and Explanation in Repair Domains," Vanderbilt memo.

[2] Hofmann, M., Caviedes, J., Bourne, J., Beale, G. and Brodersen, A., "Building Expert Systems for Repair Domains," Expert Systems, The International Journal of Knowledge Engineering, 3(1):4-12, January, 1986.

[3] Osborne, P.H., "Meta-level Control Strategies for Intelligent Systems Repair," M.S. Thesis, Vanderbilt University, 1985.

[4] Bandler, J.W., Salama, A., "Fault Diagnosis of Analog Circuits," Proc. IEEE, 73(8):1279-1325, August, 1985.

[5] Hayes-Roth, F., Waterman, D.A. and Lenat, D.B., Building Expert Systems, Addison-Wesley, Reading, MA, 1983.

END

DATE

FILMED

5-88

DTIC